

Technical Report

TR-14-09

Revised edition

Radionuclide transport and dose calculations for the safety assessment SR-PSU

Svensk Kärnbränslehantering AB

October 2015

Svensk Kärnbränslehantering AB

Swedish Nuclear Fuel
and Waste Management Co

Box 250, SE-101 24 Stockholm
Phone +46 8 459 84 00



ISSN 1404-0344

SKB TR-14-09

ID 1442446

Revised edition

Radionuclide transport and dose calculations for the safety assessment SR-PSU

Svensk Kärnbränslehantering AB

October 2015

Preface

This report compiles radionuclide transport and dose calculations for the scenarios included in the long-term safety assessment of the SFR repository for short-lived low- and intermediate level waste in Forsmark. Calculations of radionuclide release and transport from the repository to the biosphere are presented together with corresponding radiation doses to humans and non-human biota. The report forms part of the SR-PSU safety assessment, which supports SKB's licence application to extend SFR.

The report is authored by Per-Gustav Åstrand (Facilia AB), Per-Anders Ekström (Facilia AB), Thomas Hjerpe (Facilia AB) and Sven Keesmann (SKB). The main author of Chapter 8 is Benedict Jaeschke (SKB). Many others who have contributed at specific stages of the work are acknowledged in Section 1.3.2. The report has been reviewed by Russell Alexander (Bedrock Geoscience, UK), Jordi Bruno (Amphos 21 Consulting S.L., Spain), Maria Lindgren (Kemakta Konsult AB) and Mike Thorne (only first edition) (Mike Thorne Ltd., UK). Fredrik Vahlund, the project manager for the safety assessment SR-PSU, is responsible for the safety analysis. Eva Andersson is the project manager in the licensing phase of SR-PSU (starting January 2015).

This report is a revised edition compared to the report published in December 2014. This revised edition of the Radionuclide transport report presents results with an updated (increased) inventory of Mo-93 (SKBdoc 1481419) taken into account. In addition to this, there was also an update in the inventory for the *high inventory calculation case*. Some minor errors in the previous calculations has also been corrected including 1) the probabilistic calculation for the silo releases which had been interrupted after 90% of the iterations, in the global warming calculation case, has now been run correctly and 2) estimation of collective dose, where a data handling mistake caused a minor error in the previous calculation. Also typographical errors, linguistic errors and ambiguities in the report text, found during the update, have been corrected.

The calculation of exposure of non-human biota has not been updated in this revised edition as the previous calculation showed that the exposure of non-human biota is well below the screening limits, and the increased inventory of Mo-93 is not large enough to change this conclusion.

October 2015

Fredrik Vahlund

Project leader SR-PSU

Eva Andersson

Project leader SR-PSU

Abstract

This report describes the modelling of radionuclide transport and dose calculation for the post-closure safety assessment SR-PSU. The post-closure safety assessment is part of SKB's licence application to extend the repository for short-lived low- and intermediate level waste, SFR. The role of SR-PSU in the application is to demonstrate post-closure safety of SFR. A set of scenarios is described in the **Main report**. These scenarios are identified to cover credible future evolutions of the SFR repository and its environs. In the current report, the radiological consequences of the different scenarios have been estimated to provide a basis for the subsequent risk evaluation in the **Main report**. It is hence difficult to draw conclusions on fulfilling requirements on radiological safety solely on the results given in this report. The results are summarised and discussed as far as possible in Chapter 10.

This report presents the models and compiles a description of the calculation cases discussing aspects of input data and results. The presentation of the modelling focuses on the near-field (repository) and far-field (geosphere) while the modelling of the biosphere (surface system) is described in more detail in Saetre et al. (2013).

Characteristic for the approach for radionuclide transport and dose calculations in this assessment is the full coupling of near-field, far-field and biosphere. In the previous assessment, annual doses were calculated from far-field releases by means of dose conversion factors, which had been obtained from peak dose responses of the biosphere model to constant releases of radionuclides to the biosphere. The present approach, presented in Chapter 2, accounts for the release history relative to the development of the surface system in the dose assessment. The treatment of uncertainties in the assessment in general, and in the implementation of calculation cases in particular, is also addressed in Chapter 2.

Chapter 3 presents the radionuclide inventory and the selection of the radionuclides to account for in the transport modelling and dose calculations. A larger number of radionuclides are explicitly taken into account than in previous assessments of SFR. This is due to that the decommissioning waste will contain new radionuclides compared with existing operational waste, and that a simpler screening of radionuclides is applied in this analysis, aiming at only excluding the clearly insignificant radionuclides from the modelling. The identification of the most significant radionuclides is then made in conjunction with the evaluation of the modelling results.

Chapter 4 describes the calculation cases according to the scenario category which they belong to, i.e. main scenario, less probable scenario, combined (less probable) scenarios or residual scenarios.

The following chapters discuss the obtained results, focusing on annual effective doses and respective contributions from waste vaults and dominating radionuclides for calculation cases of the main scenario (Chapter 5), of the less probable scenarios and two of their combinations (Chapter 6), and of residual scenarios (Chapter 7). The discussion of peak (mean) annual effective dose of a calculation case is of particular interest because of its relevance for the risk analysis in the **Main report**. In addition, radionuclide releases from the near-field and far-field are also discussed. The calculation results are in general compared with the *global warming calculation case* of the main scenario. The comparison of peak releases from the far-field of an analysed calculation case with the *global warming calculation case* illustrates in many cases the impact of specific assumptions of a calculation case. Statistics describing the distribution of annual effective doses are reported for all probabilistically assessed calculation cases.

Absorbed dose rates to non-human biota (a number of reference organisms in terrestrial, marine and limnic ecosystems) are reported in Chapter 8. Absorbed dose rates have been calculated for most calculation cases. The calculations were made deterministically, using site-data where possible; a short analysis of probabilistically derived results was also made, for comparison.

Chapter 9 provides the description of the models for the near-field, far-field and biosphere, putting most emphasis on the near-field and far-field as the biosphere model is described in details in Saetre et al. (2013).

Chapter 10 provides a summary of results and gives an overview for the calculation cases of peak annual effective doses, with statistics describing the variance, and of contributions from radionuclides and waste vaults to peak annual dose. Results of a calculation case assessing the collective dose and absorbed dose rates to non-human biota are also summarised.

The appendices compile complementary input data (radionuclide inventories, far-field flows), additional information and complementary results justifying the implementation of models and calculation cases, the mathematical model for transfers in the far-field, supporting information for the modelling of radionuclide transport through concrete barriers and a compilation of results of all calculation cases for all radionuclides (peak releases from the near-field, peak releases from the far-field, peak annual effective dose). The second last part of the appendix provides a sensitivity analysis based on the probabilistic calculations for the *global warming calculation case*. The last part of the appendix provides a glossary of the terms used in the report.

Sammanfattning

Denna rapport beskriver modellering av radionuklidtransport och dosberäkning för den långsiktiga säkerhetsanalysen SR-PSU. Analysen av säkerhet efter förslutning är en del av SKB:s licensansökan för att bygga ut slutförvaret för kortlivat låg- och medelaktivt avfall, SFR. SR-PSU:s roll i ansökan är att visa säkerheten efter förslutning för SFR. I huvudrapporten för SR-PSU (**Main report**) beskrivs ett antal scenarier som identifierats för att täcka in möjliga framtida utvecklingar av förvaret och dess omgivning. I den här rapporten, har de radiologiska konsekvenserna av de olika scenarierna uppskattats som ett underlag till den efterföljande riskutvärderingen i huvudrapporten för SR-PSU (**Main report**). Slutsatser avseende uppfyllande av krav rörande radiologisk säkerhet kan därför inte enbart dras direkt från resultaten i denna rapport. Resultaten sammanfattas och diskuteras så långt det är möjligt i kapitel 10.

Den här rapporten innehåller en beskrivning av modellerna, av beräkningsfallen för modellering av radionuklidtransport och dosberäkningar, samt en sammanställning beräkningsresultat. Presentationen av modelleringen fokuserar på närområdet (förvar) och fjärrområdet (geosfär) medan modellering av biosfären (ytnära system) beskrivs närmare i Saetre et al. (2013).

Karakteristiskt för den valda modelleringsapproachen är kopplingen av närområde, fjärrområde och biosfär i en sammanhängande modellkedja. I den föregående analysen beräknades doserna genom att skala det beräknade radionuklidutsläppet från geosfären med dosfaktorer. Dosfaktorerna (Landskapsdosfaktorer eller Ekosystemdosfaktorer) beräknades genom att ett enhetsutsläpp applicerades på en biosfärsmodell. Den nuvarande metoden, som beskrivs i kapitel 2, tar hänsyn till utsläppshistoriken i förhållande till utvecklingen av ytsystemet. Behandlingen av osäkerheter tas också upp i kapitel 2.

Kapitel 3 presenterar radionuklidinventariet och valet av radionuklider att ta hänsyn till i radionuklidtransport och dosberäkningen. Ett större antal radionuklider ingår i radionuklidtransport och dosberäkningen i denna analys jämfört med tidigare analyser av SFR. Detta beror på att avfall från avvecklingen av kärnkraftverken innehåller några nya radionuklider jämfört med befintligt driftavfall och att en enklare screening av radionuklider används i denna analys, med syftet att enbart identifiera och exkludera uppenbart icke-signifikanta radionuklider från modellering. Identifieringen av de mest signifikanta radionukliderna görs i samband med resultatutvärderingen.

Kapitel 4 beskriver beräkningsfallen utifrån de scenariokategorier som de tillhör, huvudscenariot, mindre troliga scenarier, kombinerade (mindre troliga) scenarier, eller restscenarier.

I de följande kapitlen diskuteras resultaten med fokus på den årliga effektiva dosen och bidragen från de olika förvarsdelarna och dominerande radionuklider för beräkningsfallen i huvudscenariot (kapitel 5), i de mindre sannolika scenarier och två av deras kombinationer (kapitel 6), och i restscenarierna (kapitel 7). Diskussion om maxvärden för den årliga effektiva dosen av särskilt intresse på grund av dess relevans för riskanalysen som görs i **Main report**. Förutom dosresultat diskuteras också utsläpp från närområdet och fjärrområdet. Beräkningsresultaten jämförs generellt med resultat från *beräkningsfallet med global uppvärmning* i huvudscenariot.

Absorberade doshastigheter till annan biota (ett antal referensorganismer i terrestra, marina och limniska ekosystem) presenteras i kapitel 8. Absorberade doshastigheter har beräknats för de flesta beräkningsfall. Beräkningarna utfördes deterministiskt och platsdata användes i största möjliga mån. En begränsad probabilistisk analys utfördes för jämförelse med de deterministiska resultaten.

I kapitel 9 ges en beskrivning av modellen för närområdet, fjärrområdet och biosfär. Eftersom biosfärsmodellen diskuteras i detalj i Saetre et al. (2013) så är endast en översiktlig beskrivning av den presenterad här.

I kapitel 10 ges en sammanfattning av resultaten. Den innehåller en översikt av maxvärden för årliga effektiva doser för de olika beräkningsfallen med statistik över variansen. Det ges också en sammanställning av bidrag från specifika radionuklider och förvarsdelar till maxvärdet för de årliga effektiva doserna, resultat för ett beräkningsfall som uppskattat kollektivdosen och absorberade doshastigheter till annan biota.

I bilagorna sammanställs, 1) kompletterande indata, 2) ytterligare information och kompletterande resultat som motiverar genomförandet av modeller och beräkningsfall, 3) detaljer kring den matematiska modellen för geosfären, 4) underlag för modellering av radionuklidtransport genom betongbarriärer och 5) en sammanställning av resultaten av alla beräkningsfall för alla radionuklider (maximalt utsläpp från närområdet, maximalt utsläpp från fjärrområdet och maximala årliga effektiva dosen). Den näst sista bilagan presenterar resultat från en känslighetsanalys baserad på de probabilistiska beräkningarna för *beräkningsfallet med global uppvärmning* i huvudscenariot. Slutligen presenteras också en ordlista med förklaringar till de begrepp som används i rapporten.

Contents

1	Introduction	13
1.1	Background	13
1.2	Report hierarchy in the SR-PSU safety assessment	14
1.3	This report	16
	1.3.1 Structure of the report	17
	1.3.2 Participating experts	18
1.4	Previous safety assessments	18
2	Assessment methodology and modelling approach	21
2.1	Future evolution	21
2.2	Scenarios	21
2.3	Calculation cases	23
2.4	Modelling approach	23
	2.4.1 Basic assumptions	26
	2.4.2 Handling of uncertainties	26
3	Radionuclide inventory and selection of radionuclides for transport modelling	29
3.1	Selection of radionuclides for the radionuclide transport and dose calculations	29
	3.1.1 Safety relevant radionuclides in the initial inventory	30
	3.1.2 Safety relevant progeny	31
	3.1.3 Selected radionuclides	31
	3.1.4 Comparison with previous assessments of SFR	31
3.2	Inventory and radiotoxicity over time	34
4	Description of the calculation cases	39
4.1	Calculation cases in the main scenario	39
	4.1.1 Global warming calculation case (CCM_GW)	40
	4.1.2 Early periglacial calculation case (CCM_EP)	45
	4.1.3 Timing of the releases calculation case (CCM_TR)	46
	4.1.4 Collective dose (CCM_CD)	47
4.2	Calculation cases for less probable scenarios	47
	4.2.1 High inventory calculation case (CCL_IH)	47
	4.2.2 High flow in the bedrock calculation case (CCL_FH)	48
	4.2.3 Accelerated concrete degradation calculation case (CCL_BC)	48
	4.2.4 Bentonite degradation calculation case (CCL_BB)	49
	4.2.5 Earthquake calculation case (CCL_EQ)	50
	4.2.6 High concentrations of complexing agents calculation case (CCL_CA)	50
	4.2.7 Wells downstream of the repository calculation case (CCL_WD)	51
	4.2.8 Intrusion wells calculation case (CCL_WI)	51
4.3	Calculation cases for residual scenarios	51
	4.3.1 Loss of barrier function calculation case – no sorption in the repository (CCR_B1)	52
	4.3.2 Loss of barrier function calculation case – no sorption in the bedrock (CCR_B2)	52
	4.3.3 Loss of barrier function calculation case – high water flow in the repository (CCR_B3)	52
	4.3.4 Changed repository redox conditions in SFR 1 calculation case (CCR_RX)	52
	4.3.5 Extended global warming calculation case (CCR_EX)	54
	4.3.6 Unclosed repository calculation case (CCR_UR)	54
	4.3.7 Glaciation and post-glacial conditions calculation case (CCR_GC)	54
4.4	Calculation cases for scenario combinations	56
	4.4.1 Scenario combination 1 calculation case (CCC_SC1)	56
	4.4.2 Scenario combination 2 calculation case (CCC_SC2)	56
4.5	Summary	56

5	Results for calculation cases in the main scenario	61
5.1	Global warming calculation cases	61
5.1.1	Global warming calculation case (CCM_GW)	61
5.1.2	Timing of the releases calculation case (CCM_TR)	70
5.2	Early periglacial calculation case (CCM_EP)	72
5.3	Collective dose (CCM_CD)	75
6	Results for calculation cases in less probable scenarios	77
6.1	High inventory calculation case (CCL_IH)	77
6.2	High flow in the bedrock calculation case (CCL_FH)	83
6.3	Accelerated concrete degradation calculation case (CCL_BC)	90
6.4	Bentonite degradation calculation case (CCL_BB)	96
6.5	Earthquake calculation case (CCL_EQ)	100
6.6	High concentrations of complexing agents calculation case (CCL_CA)	101
6.7	Wells downstream of the repository calculation case (CCL_WD)	108
6.8	Intrusion wells calculation case (CCL_WI)	112
6.9	Scenario combination 1 calculation case (CCC_SC1)	114
6.10	Scenario combination 2 calculation case (CCC_SC2)	116
7	Results for calculation cases in residual scenarios	119
7.1	Loss of barrier function calculation case – no sorption in the repository (CCR_B1)	119
7.2	Loss of barrier function calculation case – no sorption in the bedrock (CCR_B2)	122
7.3	Loss of barrier function calculation case – high water flow in the repository (CCR_B3)	126
7.4	Changed repository redox conditions in SFR 1 calculation case (CCR_RX)	131
7.5	Extended global warming calculation case (CCR_EX)	134
7.6	Unclosed repository calculation case (CCR_UR)	137
7.7	Glaciation and post-glacial conditions calculation case (CCR_GC)	138
8	Dose rates to non-human biota	141
8.1	Estimating dose rates to non-human biota across various scenarios	141
8.2	Reference organisms, site-specific parameters and site representative species	143
8.3	Overview of results	144
8.4	Results for the main scenario	146
8.4.1	Global warming calculation case	146
8.4.2	Early periglacial calculation case	155
8.4.3	Timing of the releases calculation case	157
8.5	Results for the less probable scenarios	159
8.5.1	High inventory calculation case	160
8.5.2	High flow in the bedrock calculation case	160
8.5.3	Accelerated concrete degradation calculation case	160
8.5.4	Bentonite degradation calculation case	161
8.5.5	Earthquake calculation case	164
8.5.6	High concentrations of complexing agents calculation case	164
8.6	Results for the residual scenarios	168
8.6.1	Loss of barrier function calculation case – no sorption in the repository	168
8.6.2	Loss of barrier function calculation case – no sorption in the bedrock	168
8.6.3	Loss of barrier function calculation case – high water flows in the repository	170
8.6.4	Changed repository redox conditions in SFR 1 calculation case	172
8.6.5	Extended global warming calculation case	172
8.7	Results for scenario combinations	175
8.7.1	Scenario combination 1 calculation case	175
8.7.2	Scenario combination 2 calculation case	175
8.8	Uncertainties in estimated dose rates	177

9	Models	181
9.1	Modelling concepts and tools	181
9.2	Coupling to hydrological modelling	183
9.3	Near-field models	184
9.3.1	Processes handled in the radionuclide transport calculations	185
9.3.2	Model discretisation	186
9.3.3	1BMA model	187
9.3.4	2BMA model	188
9.3.5	Silo model	190
9.3.6	BTF models	190
9.3.7	1BLA model	193
9.3.8	2–5BLA models	194
9.3.9	BRT model	194
9.3.10	Waste packages	196
9.3.11	Mathematical model description	198
9.4	Far-field model	200
9.4.1	Conceptual model	201
9.4.2	Processes handled in the RNT model	202
9.4.3	Mathematical model description	202
9.4.4	Far-field model discretisation	204
9.5	Biosphere model	205
9.5.1	Biosphere objects	205
9.5.2	Radionuclide transport model	206
9.5.3	Exposure of humans and non-human biota	209
10	Summary and conclusions	213
10.1	Calculation cases in the main scenario	213
10.2	Calculation cases in less probable scenarios	214
10.3	Exposure of non-human biota	214
10.4	Calculation cases in residual scenarios	214
10.5	Impact of parameter uncertainty	215
10.6	Dose contribution from different radionuclides and waste vaults	216
	References	219
	Appendix A Input data	223
	Appendix B Supporting calculations	235
	Appendix C Transfer coefficients for the far-field model.	241
	Appendix D Transport in fractured concrete	245
	Appendix E Result compilation	251
	Appendix F Sensitivity analysis	297
	Appendix G Glossary	303

1 Introduction

The aim of this report is to describe the radionuclide transport and dose calculations that have been undertaken to provide basis for the estimation of radiological risk in the safety assessment SR-PSU. This report describes in detail the modelling of radionuclide transport in the near- and far-field and compiles results from these calculations. The results are used in the risk assessment to verify that the extended SFR repository consisting of SFR 1 (existing SFR) and SFR 3 (extension) complies with the risk criteria designated by the regulator.

1.1 Background

The final repository for short-lived low- and intermediate-level radioactive waste, SFR, is located in Forsmark, see Figure 1-1. The SFR repository consists of a set of four rock chambers plus a concrete silo situated in rock at about 60 m depth beneath the sea floor. The radioactive waste deposited in SFR includes operational waste from Swedish nuclear power plants and from the interim storage facility for spent nuclear fuel, Clab, as well as radioactive waste from other industries, research institutions and medical care. In order to be able to also deposit decommissioning waste from the Swedish nuclear power plants, an extension of the repository, referred to as SFR 3, is planned¹. Additional disposal capacity is also needed for operational waste from nuclear power units in operation, since their operating life-time have been extended compared with what was originally planned.

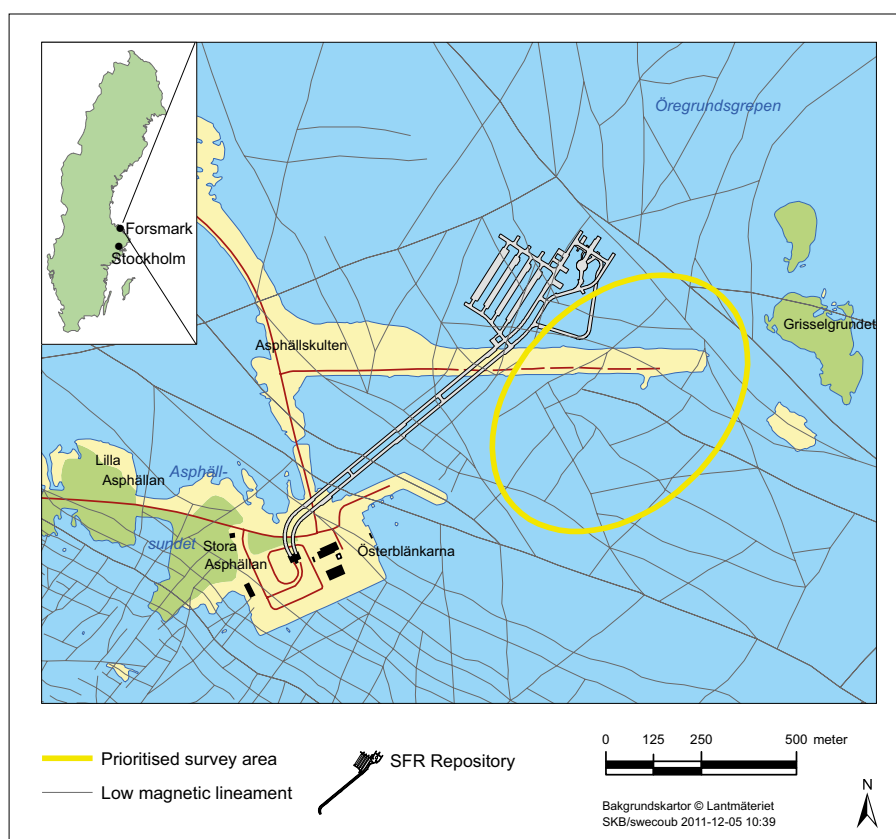


Figure 1-1. Location of the SFR repository (planned extension in the yellow circle).

¹ The extension is called SFR 3 since the name SFR 2 was used in a previous plan to build vaults adjacent to SFR 1 for disposal of reactor core components and internal parts. The current plan is to dispose of this waste in a separate repository.

The SFR repository includes waste vaults underground together with buildings above ground that host a number of technical installations. The existing facility SFR 1 comprises five waste vaults with a disposal capacity of approximately 63,000 m³. The extension SFR 3 will have a disposal capacity of 108,000 m³ in five new waste vaults plus one new vault for reactor pressure vessels from the nine boiling water reactors, see Figure 1-2.

As a part of the license application for the extension of SFR, the Swedish Nuclear Fuel and Waste Management Company (SKB) has performed the SR-PSU project (Safety Report – Project SFR Extension). The objective of SR-PSU is to assess the long-term radiological safety of the entire future SFR repository, i.e. both the existing SFR 1 and the planned SFR 3. SR-PSU is reported in a series of reports. The present report describes the calculations of radionuclide release and transport from the repository to the biosphere and the dose calculations that have been undertaken to provide a basis for estimation of radiological risk arising from the scenarios analysed in the safety assessment SR-PSU.

1.2 Report hierarchy in the SR-PSU safety assessment

The methodology for the long-term safety assessment comprises ten steps and is described in Chapter 2 of the **Main report**. While the **Main report** provides main conclusions central for the assessment, background information and calculations supporting the main conclusions are reported in supporting documents, so called Main references. The full titles of these reports together with the abbreviations by which they are identified in the following text (**abbreviated names in bold font**) together with short comments on the report contents are given in Figure 1-3 and Table 1-1.

There is also a large number of additional references which include both documents compiled within SR-PSU, but also documents compiled outside of the project, either by SKB or equivalent organisations as well as in the scientific literature. Additional publications and other documents are referenced in the usual manner.

A schematic illustration of the safety assessment documents is shown in Figure 1-3.

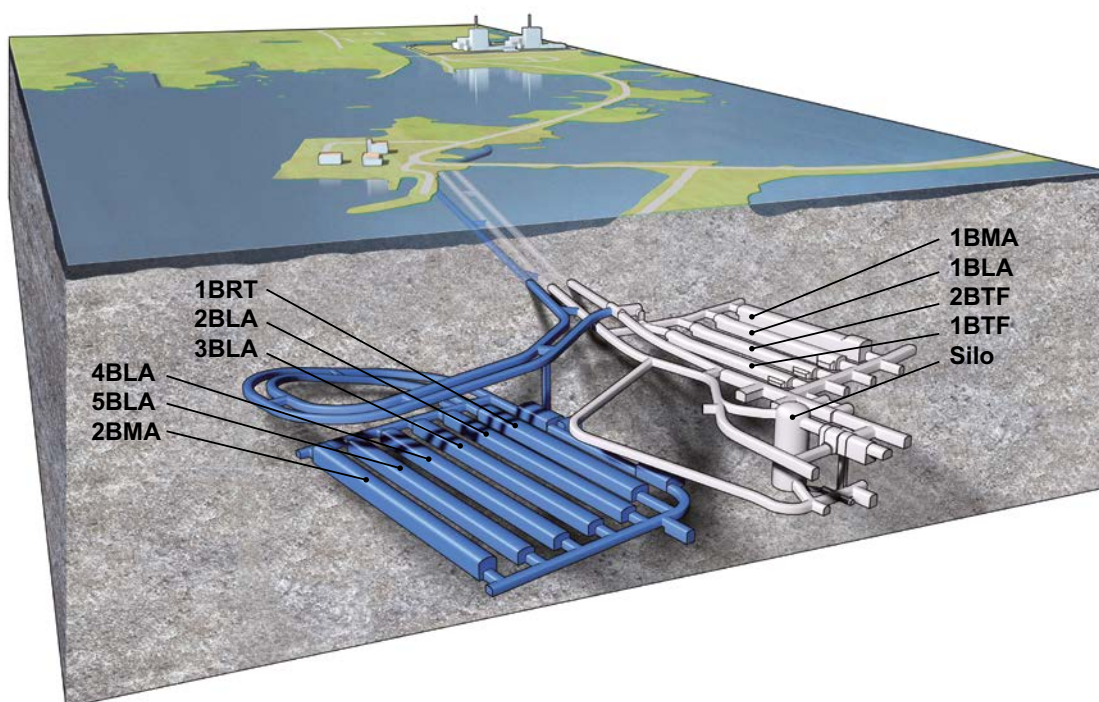


Figure 1-2. Schematic illustration of SFR. The grey part is the existing repository (SFR 1) and the blue part is the planned extension (SFR 3). The waste vaults in the figure are the silo for intermediate-level waste, 1–2BMA vaults for intermediate-level waste, 1–2BTF vaults for concrete tanks, 1–5BLA vaults for low-level waste and the BRT vault for reactor pressure vessels.

Table 1-1. Main report and Main references in the SR-PSU long term safety assessment.
All reports are available at www.skb.se

Abbreviation used when referenced in this report	Text in reference list	Comment on content
Main report	Main report, 2014. Safety analysis for SFR. Long-term safety. Main report for the safety assessment SR-PSU. SKB TR-14-01, Svensk Kärnbränslehantering AB.	This document is the main report of the SR-PSU long-term safety assessment for SFR. The report is part of SKB's licence application to extend and continue to operate SFR.
Barrier process report	Barrier process report, 2014. Engineered barrier process report for the safety assessment SR-PSU. SKB TR-14-04, Svensk Kärnbränslehantering AB.	Describes the current scientific understanding of the processes in the engineered barriers that have been identified in the FEP processing as potentially relevant for the long-term safety of the repository. Reasons are given in the process report as to why each process is handled a particular way in the safety assessment.
Biosphere synthesis report	Biosphere synthesis report, 2014. Biosphere synthesis report for the safety assessment SR-PSU. SKB TR-14-06, Svensk Kärnbränslehantering AB.	Describes the handling of the biosphere in the safety assessment. The report summarises site description and landscape evolution, FEP handling, exposure pathway analysis, the radionuclide model for the biosphere, included parameters, biosphere calculation cases and simulation results.
Climate report	Climate report, 2014. Climate and climate-related issues for the safety assessment SR-PSU. SKB TR-13-05, Svensk Kärnbränslehantering AB.	Describes the current scientific understanding of climate and climate-related processes that have been identified in the FEP processing as potentially relevant for the long-term safety of the repository. The report also describes the climate cases that are analysed in the safety assessment.
Data report	Data report, 2014. Data report for the safety assessment SR-PSU. SKB TR-14-10, Svensk Kärnbränslehantering AB.	Qualifies data and describes how data, including uncertainties, that are used in the safety assessment are quality assured.
FEP report	FEP report, 2014. FEP report for the safety assessment SR-PSU. SKB TR-14-07, Svensk Kärnbränslehantering AB.	Describes the establishment of a catalogue of features, events and processes (FEPs) that are of potential importance in assessing the long-term functioning of the repository.
FHA report	FHA report, 2014. Handling of future human actions in the safety assessment SR-PSU. SKB TR-14-08, Svensk Kärnbränslehantering AB.	Describes radiological consequences of future human actions (FHA) that are analysed separately from the main scenario, which is based on the reference evolution and less probable evolutions.
Geosphere process report	Geosphere process report, 2014. Geosphere process report for the safety assessment SR-PSU. SKB TR-14-05, Svensk Kärnbränslehantering AB.	Describes the current scientific understanding of the processes in the geosphere that have been identified in the FEP processing as potentially relevant for the long-term safety of the repository. Reasons are given in the process report as to why each process is handled a particular way in the safety assessment.
Initial state report	Initial state report, 2014. Initial state report for the safety assessment SR-PSU. SKB TR-14-02, Svensk Kärnbränslehantering AB.	Describes the conditions (state) prevailing in SFR after closure. The initial state is based on verified and documented properties of the repository and an assessment of the evolution during the period up to closure.
Input data report	Input data report, 2014. Input data report for the safety assessment SR-PSU. SKB TR-14-12, Svensk Kärnbränslehantering AB.	Describes the activities performed within the SR-PSU safety assessment and the input data used to perform these activities.
Model summary report	Model summary report, 2014. Model summary report for the safety assessment SR-PSU. SKB TR-14-11, Svensk Kärnbränslehantering AB.	Describes the calculation codes used in the assessment.
Radionuclide transport report	Radionuclide transport report, 2014. Radionuclide transport and dose calculations for the safety assessment SR-PSU. SKB TR-14-09, Svensk Kärnbränslehantering AB.	Describes the radionuclide transport calculations carried out for the purpose of demonstrating fulfilment of the criterion regarding radiological risk.
Waste process report	Waste process report, 2014. Waste form and packaging process report for the safety assessment SR-PSU. SKB TR-14-03, Svensk Kärnbränslehantering AB.	Describes the current scientific understanding of the processes in the waste and its packaging that have been identified in the FEP processing as potentially relevant for the long-term safety of the repository. Reasons are given in the process report as to why each process is handled in a particular way in the safety assessment.

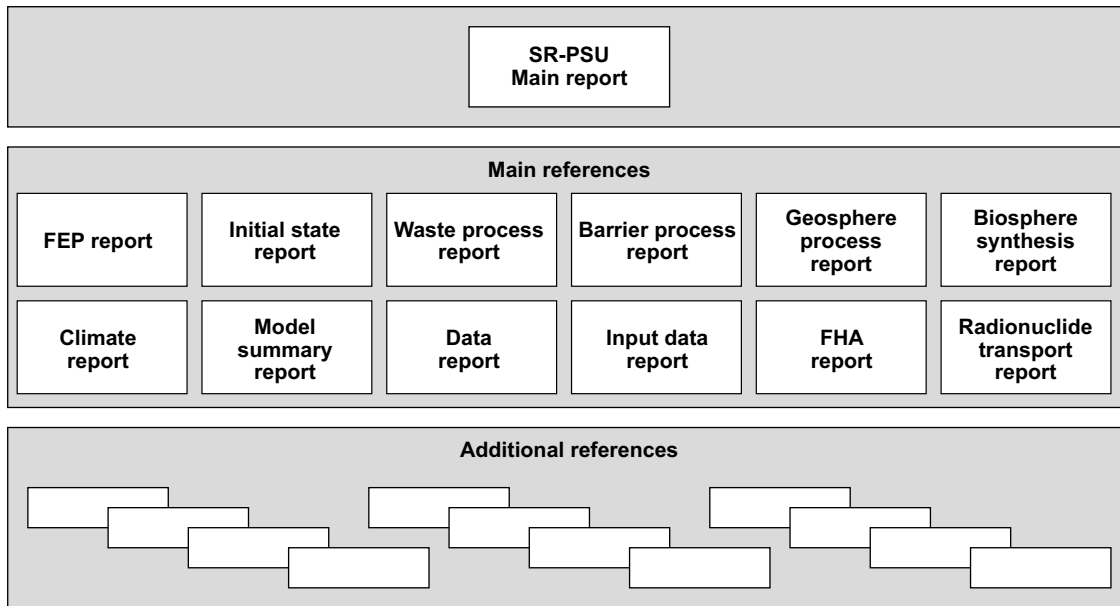


Figure 1-3. The hierarchy of the Main report, Main references and additional references in the SR-PSU long-term safety assessment. The additional references either support the Main report or any of the Main references.

1.3 This report

As stated above and as further elaborated in Chapter 2 of the **Main report**, the assessment methodology consists of ten steps. This report contributes to Step 9 – analysis of selected scenarios, which comprises the selection and description of calculation cases, radionuclide transport and dose calculations, and the evaluation of calculated doses against this particular regulatory criterion.

Radionuclide transport and dose calculations have been undertaken to provide a basis for estimation of radiological risk arising from the scenarios analysed in SR-PSU. The results are used in the risk assessment to show that the extended SFR repository complies with the risk criterion designated by the authorities (SSMFS 2008:37) and to show that there are no negative effects to be expected for plants and animals.

The radionuclide transport and dose modelling is performed with different models representing different parts of the disposal system; the near-field (repository), the far-field (geosphere) and the biosphere (surface system).

The modelling of radionuclide transport in the near-field and far-field is described in detail in this report. The results presented in this report focus on the annual doses to humans and the absorbed dose rates to non-human biota. The subsequent risk assessment is presented in Chapter 10 in the **Main report**. The radionuclide transport in the surface system and the dose calculations are described in detail in Saetre et al. (2013) and in the **Biosphere synthesis report**.

1.3.1 Structure of the report

This report contains descriptions of models, calculation cases and results from the radionuclide transport and dose calculations. The following is a brief description of the contents.

Chapter 1 – Introduction: This chapter gives the background and discusses the role of this report in SR-PSU.

Chapter 2 – Assessment methodology and modelling approach: This chapter describes the approach used in the modelling, discusses basic assumptions and the approach for handling of uncertainties.

Chapter 3 – Radionuclide inventory and selection of radionuclides for transport modelling: This chapter presents the radionuclide inventory used in the calculations and the initial selection performed to identify radionuclides potentially relevant for the long-term safety and hence needed to be considered in the modelling.

Chapter 4 – Description of calculation cases: This chapter gives a detailed description of the calculation cases used to evaluate the different scenarios.

Chapter 5 – Results for calculation cases in the main scenario: This chapter presents the results, i.e. activity releases from near-field, activity releases from the geosphere and annual doses in the calculation cases identified to be analysed for the main scenario.

Chapter 6 – Results for calculation cases in the less probable scenarios: This chapter presents the results, i.e. activity releases from near-field, activity releases from the geosphere, and annual doses in the calculation cases identified to be analysed for less probable scenarios.

Chapter 7 – Results for calculation cases in residual scenarios: This chapter presents the results, i.e. activity releases from near-field, activity releases from the geosphere and annual doses in the calculation cases identified to be analysed for residual scenarios.

Chapter 8 – Dose rates to non-human biota: This chapter presents the calculated dose rates to non-human biota.

Chapter 9 – Models: This chapter presents conceptual and mathematical models for the assessment of radionuclide transport in the near-field, geosphere and the biosphere as well as the calculation of doses to humans and dose rates to non-human biota.

Chapter 10 – Summary and conclusions: This chapter presents a summary of individual doses to humans, collective doses and exposure of non-human biota.

Appendix A, Input data: Description of how data and models have been handled to ensure the quality of the assessment. A more detailed description of the data is presented in the **Data report**, Grolander (2013), and in the **Input data report**.

Appendix B, Supporting calculations: Presentation of a set of calculations done to verify that the models and tools that were used produce correct results.

Appendix C, Transfer coefficients for the far-field model: Derivation of transfer coefficients for a compartment model of advection, dispersion and matrix diffusion in fractured rock.

Appendix D, Transport in fractured concrete: Investigation on the validity of a compartment model representing transport in fractured concrete walls.

Appendix E, Results compilation: Compilation of peak releases and doses for all calculation cases and radionuclides.

Appendix F, Sensitivity analysis: Determination of the sensitivity to parameter variation for a number of endpoints.

Appendix G, Glossary: Explanation of terms and abbreviations used in this report.

1.3.2 Participating experts

A number of people from various fields of expertise have been involved in the development of models and preparation of data for the radionuclide transport and dose calculations for SR-PSU. The most involved are listed below in alphabetical order:

Elena Abarca, Amphos 21 Consulting SL: near-field hydrology.
Eva Andersson, SKB: biosphere model and data.
Mikael Asperö, Kemakta Konsult AB: data handling.
Rodolfo Avila, Facilia AB: dose and risk assessment.
Sten Berglund, HydroResearch AB: hydrology and radionuclide transport.
Jenny Brandefelt, SKB: climate.
Per-Anders Ekström, Facilia AB: numerical modelling.
Sara Grolander, Grolander Miljökonsult AB: biosphere data handling.
Jordi Font, Amphos 21 Consulting SL: near-field hydrology.
Andres Idiart, Amphos 21 Consulting SL: near-field hydrology.
Benedict Jaeschke, SKB: non-human biota.
Thomas Hjerpe, Facilia AB: future human actions.
Sven Keesmann, SKB: radionuclide transport.
Klas Källström, SKB: near-field chemistry.
Maria Lindgren, Kemakta Konsult AB: near-field modelling and data handling.
Luis Manuel de Vries, Amphos 21 Consulting SL: near-field hydrology.
Jorge Molinero, Amphos 21 Consulting SL: near-field hydrology.
Teresita Morales, SKB: geochemistry.
Albert Nardi, Amphos 21 Consulting SL: near-field hydrology.
Sara Nordén, SKB: non-human biota.
Jens-Ove Näslund, SKB: climate.
Magnus Odén, SKB: far-field hydrogeology.
Peter Saetre, SKB: biosphere modelling.
Mona Sassner, DHI: surface hydrology.
Henrik von Schenk, SKB: near-field hydrology.
Patrik Sellin, SKB: engineered barriers.
Orlando Silva, Amphos 21 Consulting SL: near-field hydrology.
Graham Smith, GMS Abingdon Ltd: future human actions.
Fredrik Vahlund, SKB: project leader.
Patrik Vidstrand, SKB: far-field hydrogeology.
Kent Werner, EmpTec: hydrology for wells.
Ola Wessely, SKB: concrete barriers.
Marie Wiborgh, Kemakta Konsult AB: data handling.
Per-Gustav Åstrand, Facilia AB: numerical modelling.
Johan Öhman, Geosigma AB: far-field hydrogeology.

1.4 Previous safety assessments

In 1983, SKB (then SKBF) obtained a licence to build SFR 1 at the Forsmark Nuclear Power Plant. A final safety report, FSR, was submitted in 1987 as a basis for the application for a licence to commission SFR 1. SKB obtained a restricted operating licence in April 1988, conditional on providing certain supplementary accounts. On several occasions since then, safety assessments,

including quantitative radionuclide transport and dose calculations, have been performed. The work performed within the safety assessment SR-PSU can be seen as a continuation of this series of analyses. This section briefly describes some of the earlier assessments, focusing on the radionuclide transport and dose calculations. SAFE and SAR-08, described below, were both periodic safety reviews according to SSMFS 2008:1.

SAFE

The safety assessment conducted within the SAFE (Safety Assessment of Final Disposal of Operational Radioactive Waste) project was submitted to the regulatory authorities in 2001.

The NUCFLOW (Lindgren et al. 2001) code was used to represent the near-field at a very detailed level. This code allowed for a representation of waste and storage rooms in three dimensions.

The semi-analytical code FARF31 (Norman and Kjellbert 1990) was used for the far-field calculations. FARF31 calculates the transport of dissolved radionuclides through the fractured rock, the retention caused by interactions between the nuclides and the rock matrix, and radioactive chain decay.

The biosphere models (Karlsson et al. 2001) were based on models developed for the safety assessment for a spent fuel repository SR 97 (Bergström et al. 1999). Ecosystems included were: lakes, streams, agricultural land, peat bogs, coastal areas and wells. The models were parameterised with site-specific data. Changes in the biosphere as a consequence of land uplift were included. The approach allowed for taking into account accumulation of nuclides in marine sediments which are later used for agricultural purposes.

SAR-08

The most recent safety assessment for SFR, SAR-08 (SKB 2008), was submitted in 2008. In this study the assessment period for the quantitative analysis was extended to 100,000 years. In addition, the degradation of the engineered barriers during freezing, due to permafrost, was addressed as a potential consequence of future climate changes.

The Amber software (Thomson et al. 2008a) was used for the near-field and far-field calculations. The near-field model was essentially the same as the one used in SAFE. The far-field was here represented with a compartment model and the model was made to be equivalent to, and have the same parameterisation as, the code FARF31 used in SAFE.

The biosphere calculations were done using the Pandora tool (Åstrand et al. 2005). Supporting calculations were done with Ecolego (Bergström et al. 2008). A new C-14 model was developed for the SAR-08 project (Bergström et al. 2008). Earlier safety assessments for SFR had used the concentration ratio based approach, for uptake of radionuclides from soil to plants, for all elements including C-14. The new C-14 specific-activity based model was developed to enable a more realistic representation of C-14 uptake, taking photosynthesis into account.

SR-Site and other assessments for the spent nuclear fuel repository

SR-Site is the most recent safety assessment of the final repository for spent nuclear fuel, submitted to the regulatory authorities in 2011 (SKB 2011). The near-field of the spent-fuel repository and in particular its source term is fundamentally different from SFR due to the different nature of the disposed radioactive waste with spent fuel contained in copper canisters, which are embedded in bentonite clay. The far-field, however, representing radionuclide transport in fractured rock, though for different depths, is conceptually similar in many aspects. The aforementioned code FARF31 was also the main code applied for the assessment of the far-field in SR-Site. The biosphere model used in SR-PSU is to a large extent based on the biosphere model developed for SR-Site, although it has been further developed and adapted for SR-PSU. One important difference is the connection between geosphere and biosphere; in SR-Site a LDF-based (landscape-dose-conversion factors) approach was used i.e. dose-factors for a unit release were calculated with the biosphere model and those factors were applied to the releases to calculate dose. In SR-PSU the releases are fed directly to the biosphere model.

A detailed discussion of earlier approaches to the biosphere modelling can be found in the **Biosphere synthesis report**.

2 Assessment methodology and modelling approach

Chapter 2 in the **Main report** describes the methodology used in the safety assessment. The current chapter presents the part of the methodology that is directly related to radionuclide transport modelling. The main objective of the radionuclide transport calculations is to derive doses used in the evaluation of radiological risk for the safety assessment. To do that, the future evolution of the system needs to be defined (Section 2.1). As a description of the future evolution of the repository system is inherently associated with uncertainties, alternative scenarios need to be defined and included in the analysis (Section 2.2). Based on these scenarios, a number of calculation cases are defined (Section 2.3). Section 2.4 discusses the modelling approach, input data and uncertainties.

2.1 Future evolution

Pivotal for the post-closure safety assessment is a description of the evolution of the repository and its environs over the 100,000 year assessment period. As further discussed in Chapter 2 of the **Main report**, the evolution of the repository system will depend on the following.

- **The Initial state of the repository system.** The initial state is defined as the state of the repository system at closure. In order to describe the initial state, the reference design and evolution of the repository system during the operational phase need to be considered.
- **External conditions acting on the repository system after closure.** External processes include climate evolution and climate-related processes, for example permafrost, global warming, and shoreline displacement. Future human actions may also affect the future state of the repository.
- **Internal processes within the repository system.** Internal processes include thermal, hydraulic, mechanical and chemical processes that act in the repository system. Internal processes include, for example, groundwater flow and chemical degradation affecting the engineered barriers.

Based on a description of the future evolution, radiological impacts on humans and the environment can be estimated. This description, and associated uncertainties, are hence a key component in the post-closure safety assessment.

2.2 Scenarios

In the SR-PSU assessment, the evolution of the repository and its environs is described by the reference evolution. This reference evolution is based on likely processes and events relevant for the long-term safety and includes a range of the most probable future evolutions of the SFR repository system including uncertainties of importance. The reference evolution of the SFR repository and its environs is described in Chapter 6 of the **Main report**. Based on the reference evolution, scenarios are defined. These are based on the general advice in SSMFS 2008:21 which suggests that three categories of scenarios are used.

“The main scenario should be based on the probable evolution of external conditions and realistic, or where justified, pessimistic assumptions with respect to the internal conditions. It should comprise future external events which have a significant probability of occurrence or which cannot be shown to have a low probability of occurrence during the time covered in the safety assessment. Furthermore, it should be based, as far as possible, on credible assumptions with respect to internal conditions, including substantiated assumptions concerning the occurrence of manufacturing defects and other imperfections, and which allow for an analysis of the repository barrier functions (it is, for example, not sufficient to always base the analysis on leak-tight waste containers, even if this can be shown to be the most probable case). The main scenario should be used as the starting point for an analysis of the impact of uncertainties (see below), which means that the analysis of the main scenario also includes a number of calculation cases.”

Less probable scenarios should be prepared for the evaluation of scenario uncertainty (see also below). This includes variations of the main scenario with alternative sequences of events as well as scenarios that take into account the impact of future human activities such as damage inflicted on barriers. (Detriment to humans intruding into the repository is illustrated by residual scenarios, see below). The analysis of less probable scenarios should include analyses of such uncertainties that are not evaluated within the framework of the main scenario.

Residual scenarios should include sequences of events and conditions that are selected and studied independently of probabilities in order to, *inter alia*, illustrate the significance of individual barriers and barrier functions. The residual scenarios should also include cases to illustrate damage to humans intruding into the repository as well as cases to illustrate the consequences of an unclosed repository that is not monitored.”

From uncertainties in the Initial state, Internal processes and External conditions a number of scenarios can be defined. This is further discussed in Chapter 7 of the **Main report** and schematically displayed in Figure 2-1.

The main scenario is based on the probable evolution of external conditions and realistic, or where justified, *pessimistic assumptions with respect to the internal condition* and includes uncertainties in the Initial state, Internal processes and External conditions. Less probable scenarios are based on *uncertainties that are not evaluated within the framework of the main scenario* and address uncertainties that are deemed less probable, but more detrimental for the evolution of the repository and its environs than those included in the main scenario. Figure 2-1 also includes residual scenarios. For all scenarios, uncertainties in the dose estimate are addressed by different models for future human behaviour in order to assess an upper range of potential exposures.

The main objective of the radionuclide transport and dose calculations is to provide a quantitative assessment of radiological consequences, i.e. peak annual effective dose, for the defined scenarios which are to be represented by calculation cases. This is the basis to show compliance with regulatory requirements on radiological risk. To do so, estimates of scenario probabilities are required. The scenarios are thoroughly described in Chapter 7 of the **Main report** together with a discussion on the assigned scenario probabilities. The scenarios presented in the **Main report**, are together with the assigned probabilities summarised in Table 2-1. In Table 2-1, the scenario category *Scenario combinations* is introduced which combines less probable scenarios, see further Table 4-14 to Table 4-17.

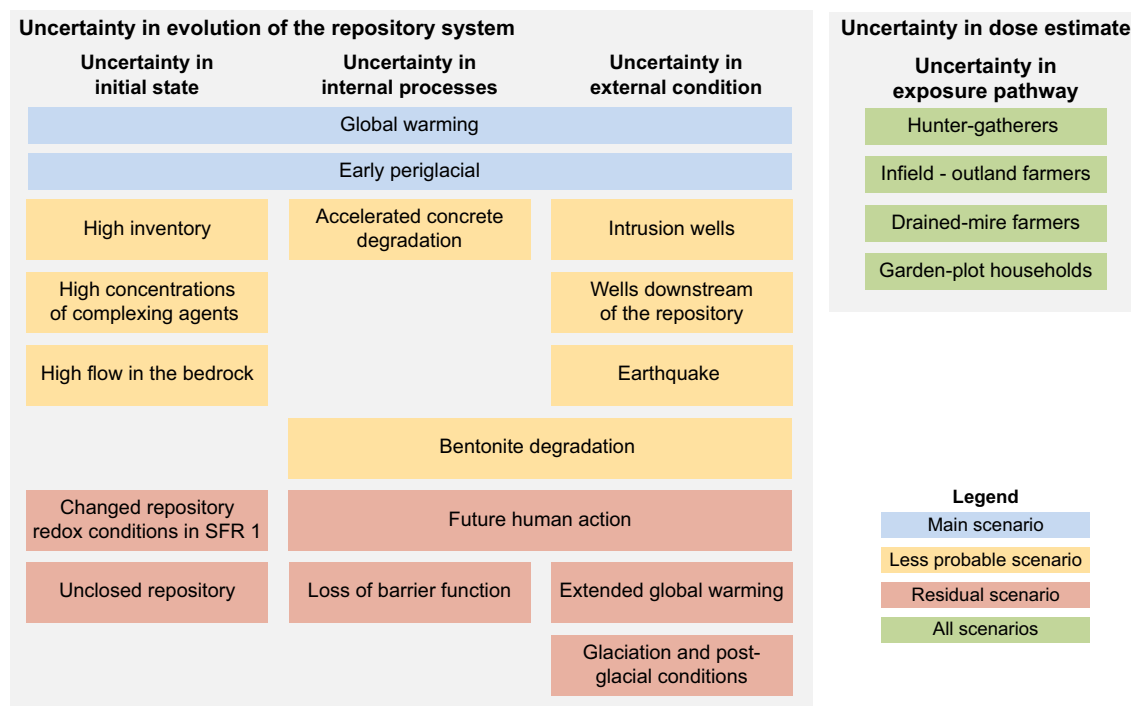


Figure 2-1. Illustration of scenarios and associated uncertainties.

Table 2-1. Summary of scenarios with probabilities and categories (the number in the brackets after the scenario name refers to the section in the Main report where it is presented in detail).

Scenario	Probability	Category
Global warming climate variant (7.4)	1	Main scenario
Early periglacial climate variant (7.4)	1	
High inventory scenario (7.6.1)	< 0.05	Less probable scenarios
High flow in the bedrock scenario (7.6.2)	< 0.1	
Accelerated concrete degradation scenario (7.6.3)	< 0.1	
Bentonite degradation scenario (7.6.4)	< 0.1	
Earthquake scenario (7.5.5)	10 ⁻⁶ /year	
High concentrations of complexing agents scenario (7.6.6)	< 0.1	
Wells downstream of the repository scenario (7.6.7)	0.13	
Intrusion wells scenario (7.6.8)	Silo Each waste vault in SFR 1 Each waste vault in SFR 3	
Loss of barrier function scenario – no sorption in the repository (7.7.1)		Residual scenarios
Loss of barrier function scenario – no sorption in the bedrock (7.7.2)		
Loss of barrier function scenario – high water flow (7.7.3)		
Changed repository redox conditions in SFR 1 scenario (7.7.4)		
Extended global warming scenario (7.7.5)		
Unclosed repository scenario (7.7.6)		
Future human action scenarios (7.7.7)		
Glaciation and post-glacial conditions scenario (7.7.8)		
Scenario combination 1 (7.8)	< 0.1×0.1	Scenario combinations
Scenario combination 2 (7.8)	< 0.1×0.1	

2.3 Calculation cases

A calculation case provides a parameterised model chain for the quantitative assessment of a scenario. A calculation case is not a unique representation of a scenario, because of intrinsic uncertainties in the scenario. The main scenario of the SR-PSU assessment is e.g. represented by four calculation cases addressing uncertainties in climate evolution (external condition), evolution of releases (internal processes) and to provide an alternative safety indicator (collective dose versus individual dose).

The scenarios, defined in Chapter 7 of the **Main report**, and associated calculation cases are presented in Figure 2-2. The global-warming variant of the main scenario is represented by three calculation cases whereas most other scenarios are only associated with one calculation case.

2.4 Modelling approach

Radionuclide transport and dose modelling are performed with a set of models representing different parts of the repository and its environs: the near-field (repository), the far-field (geosphere) and the surface system (biosphere).

The modelling of radionuclide transport in the near- and far-field is described in detail in this report. The radionuclide transport in the surface system and the dose calculations, however, are described in detail in Saetre et al. (2013).

Climate case	Scenario	Calculation case
Global warming	Main scenario	
	Global warming	CCM_GW, CCM_TR, CCM_CD
	Early periglacial	CCM_EP
Early periglacial	Less probable scenarios	
	High inventory	CCL_IH
	High flow in the bedrock	CCL_FH
	Accelerated concrete degradation	CCL_BC
	Bentonite degradation	CCL_BB
	Earthquake	CCL_EQ
	High concentrations of complexing agents	CCL_CA
Weichselian glacial cycle	Wells downstream of the repository	CCL_WD
	Intrusion wells	CCL_WI
Extended global warming	Residual scenarios	
	Loss of barrier function	CCR_B1, CCR_B2, CCR_B3
	Changed redox conditions in SFR 1	CCR_RX
	Extended global warming	CCR_EX
	Unclosed repository	CCR_UR
	Future human action	CCFHA1, CCFHA2, CCFHA3
	Glaciation and post-glaciation condition	CCR_GC
	Scenario combinations	
	Scenario combination 1	CCC_SC1
	Scenario combination 2	CCC_SC2
CCM_GW Global warming CC CCM_TR Timing of releases CC CCM_CD Collective dose CC CCM_EP Early periglacial CC		CCR_B1 Loss of barrier funct. CC - no sorption in the repository CCR_B2 Loss of barrier funct. CC - no sorption in the bedrock CCR_B3 Loss of barrier funct. CC - high water flow in the repository CCR_RX Changed repository redox conditions in SFR 1CC CCR_EX Extended global warming CC CCR_UR Unclosed repository CC CCFHA1 FHA CC - Exp. of on-site crew during a drilling event CCFHA2 FHA CC - Exp. during construction on drill. detritus landfill CCFHA3 FHA CC - Exp. due to cultivation on drill. detritus landfill CCR_GC Glacial and post-glacial conditions CC
CCL_IH High inventory CC CCL_FH High flow in the bedrock CC CCL_BC Accelerated concrete degradation CC CCL_BB Bentonite degradation CC CCL_EQ Earthquake CC CCL_CA High conc. of complexing agents CC CCL_WD Wells downstream of the repository CC CCL_WI Intrusion wells CC		CCC_SC1 Scenario combination 1 - CC CCC_SC2 Scenario combination 2 - CC

Figure 2-2. Scenarios and associated calculation cases (abbreviations: CC – calculation case, conc. – concentration, funct. – function, exp. – exposure, drill. – drilling).

The radionuclide transport calculations are carried out as dynamic calculations over the whole assessment period of 100,000 years during which transport conditions change due to barrier degradation, climate change and shoreline displacement. The dynamic radionuclide transport calculations are dependent on the hydrological and hydrogeological calculations which are carried out as steady-state calculations for a limited number of time-points representative of the respective environmental conditions, which imply changing boundary conditions for the calculations, for near-field (Abarca et al. 2013, 2014), geosphere (Odén et al. 2014) and biosphere (Werner et al. 2013) calculations. Water flow

related data are obtained from hydrogeological calculations at different points in time representing different stages of landscape development. During a transitional phase from one stage of landscape development to another, water flow related data are interpolated linearly in time between the data sets representing the initial and the final stage of the transition (see further details in Chapter 9 and in Saetre et al. 2013). The chosen approach is based on steady state hydrogeological calculations and gives the opportunity to study dynamic effects such as accumulation of radionuclides in bedrock and sediments during periods with low water-flow.

All calculations are performed with models implemented in the Ecolego tool, which is a tool for creating compartment models and performing deterministic and probabilistic simulations. The models for radionuclide transport and dose calculations are built using the compartment approach as described in detail in Section 9.1. Figure 2-3 shows conceptually the models and data used in the radionuclide transport and dose calculations; the data used in the radionuclide transport modelling is discussed further in Chapter 4 and the radionuclide transport models are discussed in Chapter 9. The model chain consists of models for the repository (waste and engineered barrier system) represented by the *near-field*, for the geosphere (geological barrier system) represented by the *far-field* and the surface ecosystems represented by the *biosphere*.

The main endpoints of the calculations presented in this report are the *annual effective doses*² to humans and *absorbed dose rates* to non-human biota. Furthermore, in the context of human exposure, “dose” refers to the effective dose, unless otherwise explicitly stated. The subsequent risk assessment is presented in Chapter 10 in the **Main report**.

The *annual effective dose* can be related to a risk criterion of 10^{-6} for a representative individual in the group exposed to the greatest risk (SSMFS 2008:37). The conversion from effective dose to risk is done using a detrimental adjusted nominal risk coefficient for cancer and hereditary effects for the whole population of 0.073 per Sievert, based on the 1990 Recommendations of the ICRP. It should be noted that a dose of 14 μ Sv corresponds to a risk of 10^{-6} without accounting for a probability (less than 100%) of the underlying scenario.

The regulation does not formulate a quantitative risk or dose criterion for non-human biota. The ERICA methodology, applied in the current assessment, proposes a screening dose rate at the ecosystem level of 10 μ Gy/h, (Beresford et al. 2007, Brown et al. 2008).

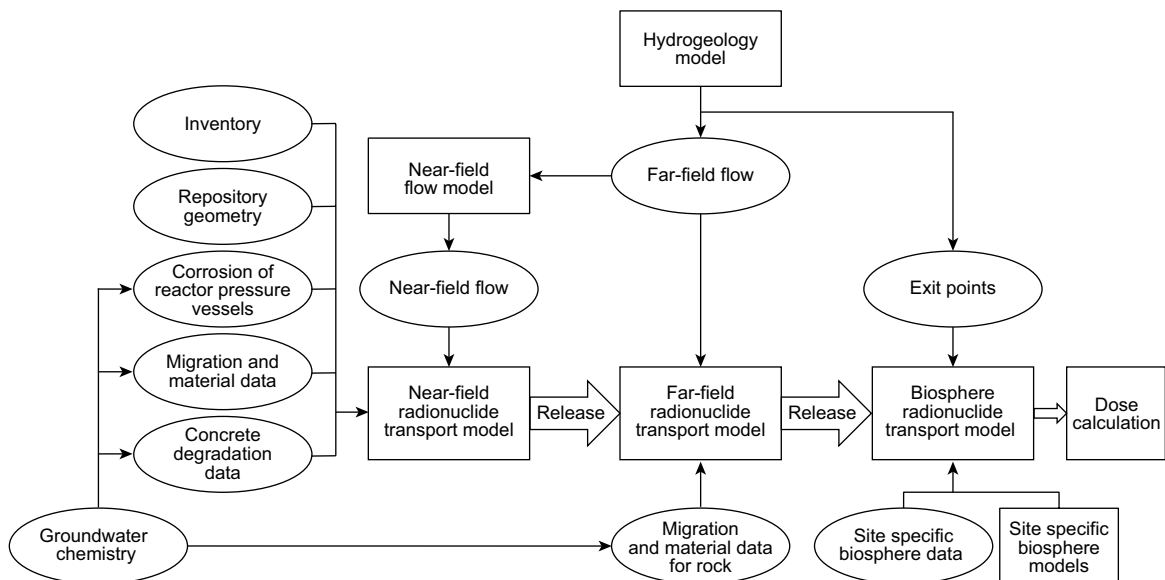


Figure 2-3. Models and data for the radionuclide transport and dose calculation. Boxes represent modelling activities and ovals represent data.

² In the present report, *annual effective dose* refers to the sum of the effective dose arising from external radiation within the period of one year, and the committed effective dose from the intake of radioactive substances within the same year.

2.4.1 Basic assumptions

This section briefly summarises basic and simplifying assumptions that are made throughout the radionuclide transport modelling process. It is assumed that maximum radiological consequences are not likely to be underestimated by the chosen approach, but tend to be overestimated. The following, pessimistic, simplifying assumptions have been made to facilitate the modelling and parameterisation.

- In the modelling, it is assumed that the saturation of the repository with water happens instantaneously following closure so that the repository is fully saturated with water during the whole calculation time frame (Chapter 12 in the **Initial state report**).
- Steel waste packaging will probably start to corrode during the operational phase (Chapter 12 in the **Initial state report**). Hence, the steel waste packages are assumed to be completely corroded instantaneously following repository closure and any potential limiting effect on radionuclide transport by the steel waste packaging is not taken into account.
- The potentially limiting effects of bitumen in bituminised waste, are not taken into account (Section 3.6, in the **Waste process report**).
- Radionuclides are assumed to be fully soluble in water, i.e. no solubility limitations are taken into account (Section 3.6, in the **Waste process report**).
- Potential sorption of radionuclides on corrosion products is not taken into account (Section 3.5.3, in the **Waste process report**).
- Potential sorption of radionuclides on various materials in the 1–5BLA vaults is not taken into account.

2.4.2 Handling of uncertainties

Handling of uncertainties is a key issue in any safety assessment. The regulatory guidelines for handling of uncertainties point out the following sources of uncertainties that should be handled in a safety assessment (SSMFS 2008:37).

Lack of knowledge and other uncertainties in the calculation presumptions (assumptions, models, data) are in this context denoted as uncertainties. These uncertainties can be classified as follows:

- *scenario uncertainty: uncertainty with respect to external and internal conditions in terms of type, degree and time sequence;*
- *system uncertainty: uncertainty as to the completeness of the description of the system of features, events and processes used in the analysis of both individual barrier performance and the performance of the repository as a whole;*
- *model uncertainty: uncertainty in the calculation models used in the analysis;*
- *parameter uncertainty: uncertainty in the parameter values (input data) used in the calculations;*
- *spatial variation in the parameters used to describe the barrier performance of the rock (primarily with respect to hydraulic, mechanical and chemical conditions).*

Scenario uncertainties

The analysis of features events and processes (FEPs) and their respective uncertainties results in a selection of scenarios to assess. The FEP analysis is presented in detail in the **FEP report** and the scenario selection is discussed in Chapter 7 in the **Main report**. The scenario uncertainties are not a topic of this report, but the bandwidth of calculation cases presented is first of all a consequence of this analysis³.

³ Fourteen scenarios, one variation of the main scenario and two scenario combinations are represented by 21 calculation cases of which 20 assess individual dose and one collective dose for a supra-regional and global population.

System uncertainties and model uncertainties

A model to be used in a safety assessment of a complex system such as the SFR will inevitably include simplified representations of the features of the repository, geosphere and biosphere, and of the processes acting within the system. It has to be determined that such simplifications do not lead to an underestimation of radiological risk. Cautious assumptions, as the basic assumptions presented in the previous section, are made when the real system is first conceptualised and then parameterised into a mathematical model. Sometimes it is not obvious whether a simplification leads to an underestimation of the dose or not; in this case, analysing several model alternatives may be a proper approach to bounding the uncertainty introduced into the model due to necessary simplifications. Examples of this type of analysis in the SR-PSU assessment address the impact of limited solubility in the source term and the start of radionuclide release with respect to the existence of submerged conditions at the exit points in the far-field (see Section 4.1 for case descriptions)⁴.

Parameter uncertainties and variations

The approach to quantification of the effects of uncertainties and variations in parameters is to propagate uncertainties in the parameter values through the model to obtain probability distributions of the assessment endpoints, i.e. in particular dose to humans. The uncertainty of a parameter is described by its probability distribution over its range of possible values.

Time-independent parameters

The propagation of parameter uncertainties is assessed by probabilistic Monte Carlo simulations applying Latin Hypercube sampling in the case of time-independent parameters. For each studied radionuclide, 100 to 1,000 simulations are carried out. Values of sampled parameters are drawn from the parameter range taking the probability distribution of the parameter into account. The probability distribution of time-independent parameters is described by (parameterised) standard probability distribution functions (PDF).

Time-dependent parameters

Some of the parameters used in the calculations are given as time-series values e.g. water flows interpolated from the steady-state values in the hydrological calculations. The uncertainties in time-dependent parameters are expressed by empirical probability distributions derived from modelling results. For example, for the advective travel time and flow-related transport resistance (F-factor) in the bedrock, a large number of possible pairs of parameter values are calculated from hydrogeological modelling. For these data, pairs of parameter values are sampled directly from datasets of correlated travel times and F-factors obtained from hydrogeological modelling (see also Appendix A).

Numerical uncertainties and code verification

There is a need to assess the contribution to the overall uncertainty from the numerical approximations and the accuracy of the numerical tools. This uncertainty is generally magnitudes smaller than the uncertainty introduced by the sources mentioned above (system, modelling and parameter uncertainties) so, when appropriate, numerical methods are used.

A number of comparisons of Ecolego with results from other tools have been done to confirm this (**Model summary report**). In the safety assessment SR-Site (Avila et al. 2010) a comparison of compartment models implemented in Ecolego and Simulink/Pandora (SKB 2010b) was performed. The results deviated not more than 1% for all considered cases between the two implementations. This accuracy is considered reasonable as different numerical methods are used in Simulink/Pandora and Ecolego so, the results cannot be expected to be exactly the same.

For the SR-PSU assessment, the compartmental far-field model implemented in Ecolego has been compared with the semi-analytical code FARF31. The results show good agreement, as presented in Appendix B.

⁴ Simplifying assumptions aim to not underestimate calculated peak dose. The related uncertainty is assessed by the definition of bounding cases, as e.g. the *timing of releases calculation case*.

3 Radionuclide inventory and selection of radionuclides for transport modelling

The waste and associated properties such as the radionuclide inventory are described in the **Initial state report**. The waste deposited in SFR mainly originates from the operation and decommissioning of the Swedish nuclear power plants and from the interim storage facility for spent nuclear fuel, Clab, but, SFR will also accommodate waste from industry, research institutions and medical care.

Most of the operational waste from nuclear power plants comes from decontamination of reactor water. This decontamination is mainly done by ion-exchange resins and particle filters that are later deposited in SFR. A smaller portion of the operational waste also originates from clothing, cloth, scrap and refuse.

The decommissioning waste consists primarily of contaminated steel; concrete and insulation materials from decommissioned nuclear plants and will mainly be deposited in the BLA waste vaults in SFR 3. Reactor pressure vessels from the nine Swedish boiling water reactors will also be deposited in a dedicated vault (BRT) in SFR 3.

In addition to the short-lived low- and intermediate-level waste being deposited in SFR, there are also plans to temporarily store waste intended to be deposited in the future repository for long-lived waste, SFL (described in SKBdoc 1412250). This additional inventory is taken into account in one of the calculation cases, *Abandoned unclosed repository* (CCR_UR), but is not considered in the following discussion for calculation cases referring to a repository closed following the current plans.

3.1 Selection of radionuclides for the radionuclide transport and dose calculations

The radionuclide inventory is given in the **Initial state report**. Not all radionuclides in the waste are relevant from a long-term safety perspective and so do not need to be included in the radionuclide transport and dose calculations. The criterion for including a radionuclide is basically that it cannot be ruled out that it has a non-negligible radiological impact when taking uncertainties into account.

The selection of relevant radionuclides is done in a consistent manner and is based on inventory, half-life and on the (shortest) time after the closure of the repository that a potential exposure may commence, taking the assessment context into account.

The screening of radionuclides with respect to their relevance in the long-term safety assessment is based on the concept of radiotoxicity, which serves to quantify and compare radiological impacts in a simplified way.

The radiotoxicity of a radionuclide inventory is hereby defined as the product of the disposed inventory and the dose conversion factor for ingestion (which is generally assessed to be the main route of exposure):

$$Rt^n(t) = DCC_{ing}^n A^n(t)$$

where:

$Rt^n(t)$ is the radiotoxicity for nuclide n at time t , [Sv],

$A^n(t)$ is the inventory of radionuclide n at time t , [Bq], and

DCC_{ing}^n is the ingestion dose coefficient for nuclide n and the short-lived progeny of radionuclide n , [Sv/Bq].

In other words, radiotoxicity is measured by the effective dose received from ingesting the whole inventory of the radionuclide. The dose coefficients derived from ICRP (1991, see SSMFS 2008:37), and taking short-lived progeny into account are reported in Grolander (2013).

3.1.1 Safety relevant radionuclides in the initial inventory

Radionuclides with a given inventory are selected for radionuclide transport calculations according to the two following criteria:

1. the half-life of a radionuclide is 10 years or longer, and
2. the radiotoxicity by ingestion of the inventory of the radionuclide at the time of repository closure exceeds 10 mSv.

Due to the first criterion, at least 10 half-lives will pass within a period of 100 years after closure, reducing the inventory of radionuclides with a half-life of less than 10 years by more than three orders of magnitude. The second criterion is a reasonably low screening limit to cut off radionuclides with negligible radiological impact compared with radiologically far more relevant radionuclides as can be seen in Figure 3-1.

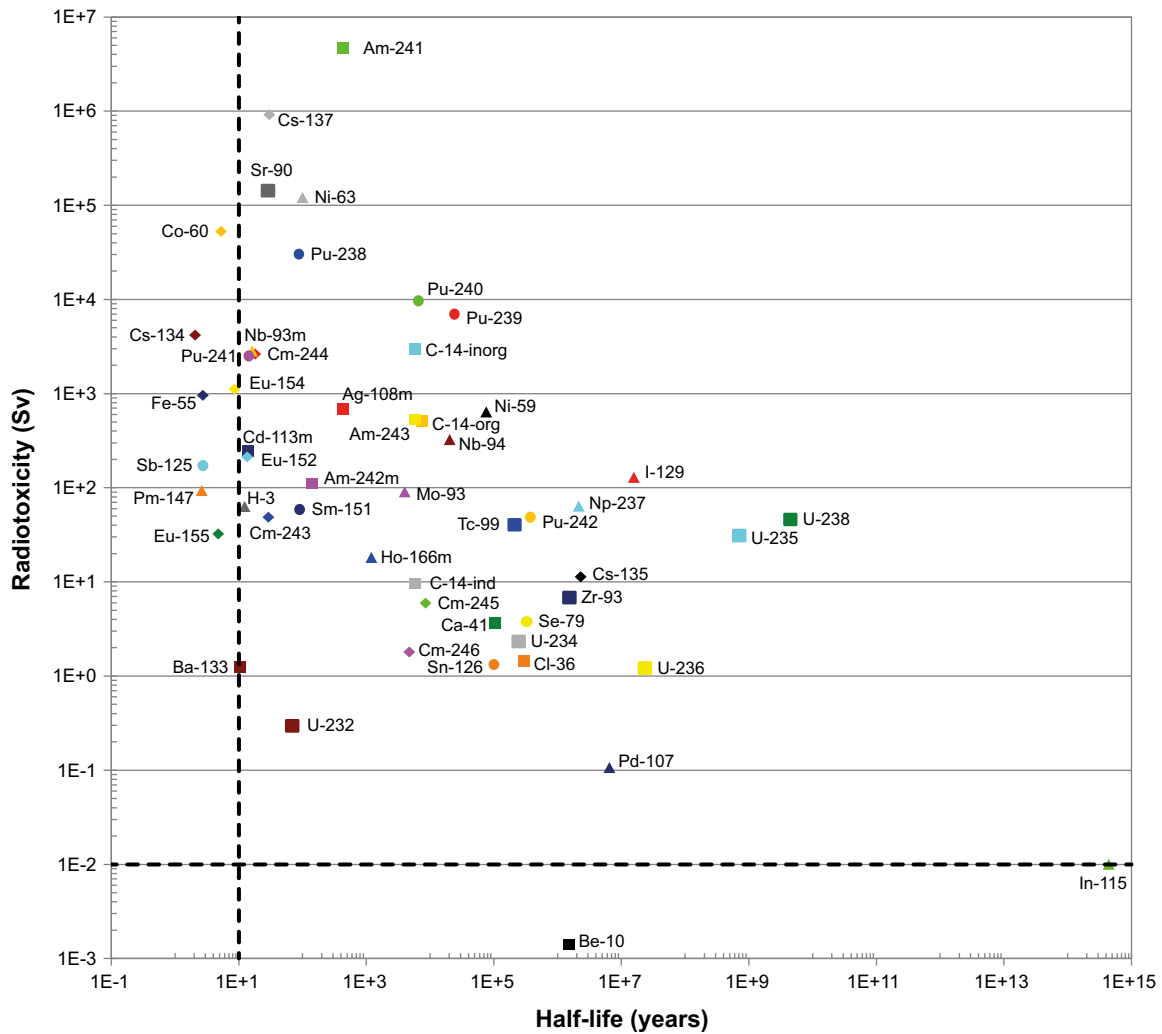


Figure 3-1. Initial radiotoxicity versus radionuclide half-lives. The vertical dashed line to the left at 10 years shows the limit of the selection criterion based on half-life. The horizontal line at 0.01 Sv shows the limit for the selection criterion due to radiotoxicity. Radionuclides selected by the criteria appear right of the vertical and above the horizontal dashed line. Different colours and shapes for radionuclide markers are used only to improve readability.

Figure 3-1 shows the initial radiotoxicity versus the half-life for each radionuclide together with a vertical and a horizontal line indicating the two above-mentioned selection criteria. An additional two radionuclides were screened out by the second criterion. Although the inventory of both will not decrease significantly in 100,000 years, Be-10, with an initial radiotoxicity of only about 2 mSv and In-115 with an initial radiotoxicity just below 10 mSv can be excluded. Thus, the radionuclides plotted below the horizontal dashed line in Figure 3-1 may be considered as less important with respect to a potential radiological impact. Those radionuclides above the dashed line and to the right of the vertical line in Figure 3-1 are included in the radionuclide transport calculations according to the two criteria given above. In addition, due to its relatively high radiotoxicity, Co-60 with a half-life of about five years is also included.

3.1.2 Safety relevant progeny

Regardless of the initial inventory, progeny have also to be considered for their safety relevance. The inventory of such “secondary radionuclides” results from ingrowth only or a combination of initial inventory and ingrowth. The radiotoxicity corresponding to this inventory can be assigned to secondary radionuclides in the same way as for primary radionuclides. The radiotoxicity might increase in time due to ingrowth by radioactive decay before finally reaching a peak value. Afterwards the radiotoxicity decreases again when the decay has a larger effect than ingrowth by decay of the parent nuclide.

The criterion for explicitly taking secondary radionuclides into account in the radionuclide transport calculations is that their half-life is longer than 100 days (in contrast to the half-life criterion in Section 3.1.1). Progeny with a half-life less than 100 days are not explicitly modelled in the transport calculations, but are considered in the dose calculation by calculating dose coefficients assuming that they are in secular equilibrium in the environment with their parent nuclides; see Grolander (2013) for details.

Figure 3-2 shows the radiotoxicity due to ingrowth only for progeny.

3.1.3 Selected radionuclides

Based on the discussions in Sections 3.1.1 and 3.1.2, the radionuclides to be included in the modelling, explicitly or implicitly, can be determined. Radionuclide decay chains included in the modelling are presented in Table 3-1 and additional single radionuclides (radionuclides not part of a decay chain) explicitly modelled in the radionuclide transport calculations are presented in Table 3-2.

3.1.4 Comparison with previous assessments of SFR

The post-closure safety of SFR has been assessed several times previously and the assessment of inventory and safety in the current context is based on this experience. The set of radionuclides considered in the inventory of the SR-PSU assessment is similar to the set of radionuclides considered in the assessment SAR-08. Only Ru-106 is now excluded, whereas Ca-41 and In-115 are newly included in inventories representing decommissioning waste. Comparing the inventories of the previous assessments with each other shows that no inventory was assigned to U-233 or to any Th isotope and its progeny in SAR-08, whereas this was done in the (previous) SAFE assessment.

Table 3-3 shows a comparison of which radionuclides were considered in the inventory and as safety relevant for the assessments SAFE (Lindgren et al. 2001) and SAR-08 (Thomson et al. 2008b) of SFR 1 and in SR-PSU for SFR 1 and SFR 3. The number of safety relevant radionuclides in both the SAFE and SAR-08 assessments is significantly lower.

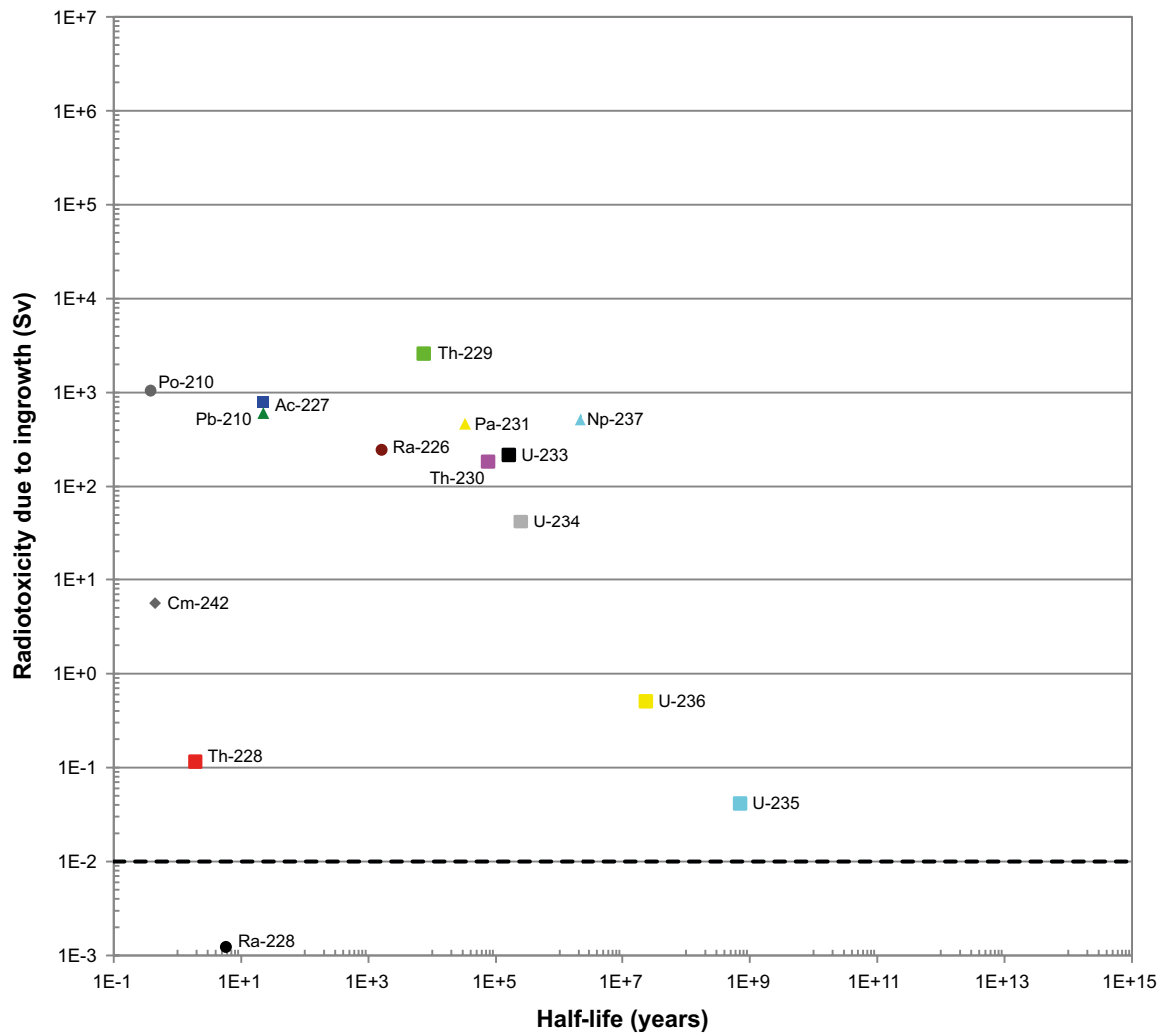


Figure 3-2. Ingrowth of radiotoxicity calculated as the difference between maximum and initial radiotoxicity. The horizontal dashed line at 0.01 Sv shows, for comparison, the limit for exclusion due to low radiotoxicity of parent radionuclides. Different colours and shapes for radionuclide markers are used only to improve readability.

Table 3-1. Radionuclide decay chains considered in the SR-PSU radionuclide transport calculations (black bold – explicitly modelled radionuclides of the initial inventory, black – explicitly modelled radionuclides that are not part of the initial inventory but where ingrowth is assumed, dark red – not explicitly modelled short-lived radionuclides accounted for in the dose calculations by summing the dose coefficient with the dose coefficient of the parent radionuclide assuming secular equilibrium, green – stable isotope.

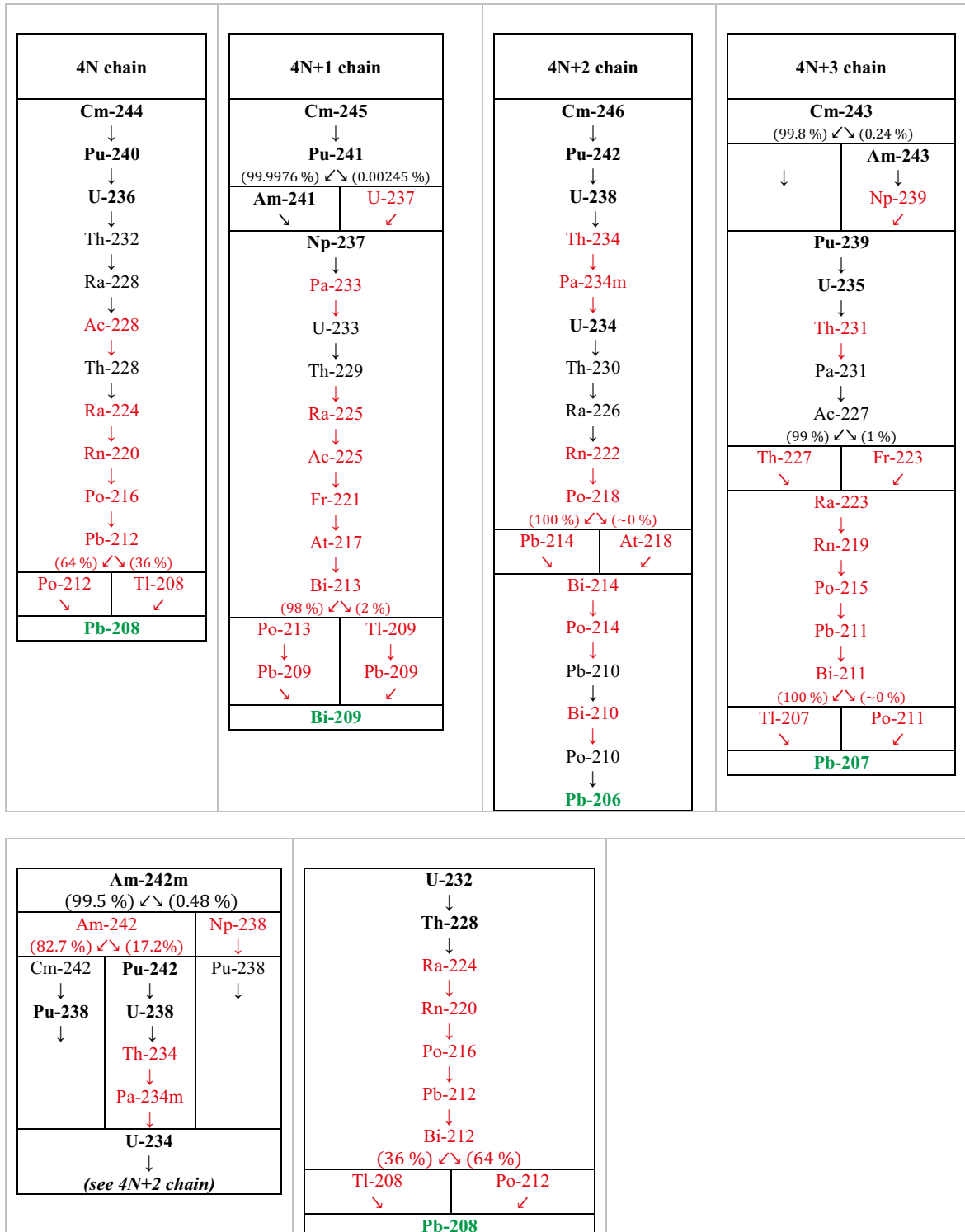


Table 3-1. Continued.

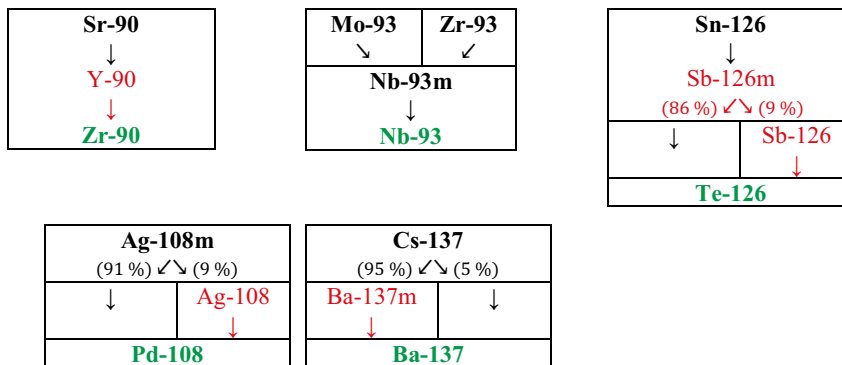


Table 3-2. Single radionuclides explicitly modelled in the SR-PSU radionuclide transport calculations.

Radionuclide	
H-3	Tc-99
C-14*	Pd-107
Cl-36	Cd-113m
Ca-41	I-129
Ni-59	Ba-133
Ni-63	Cs-135
Co-60	Sm-151
Se-79	Ho-166m
Nb-94	

* C-14 was included in the calculation in three forms: organic, inorganic and induced.

3.2 Inventory and radiotoxicity over time

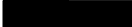




Initial amounts of radionuclides, and a summary of inventories for the different waste vaults, are listed in Table 3-16 of the **Initial state report**. The radionuclide inventory of each waste package type is given in the inventory report (SKB 2013, SKBdoc 1481419 (Mo-93)).

Figures 3-3 and 3-4 illustrate the decrease over time of activity relative to the total activity at repository closure, by waste vault and radionuclides, respectively. The activity in SFR is mainly located in the silo together with the two BMA waste vaults. Most of the radionuclide inventory in SFR is short-lived and the activity will have decayed to less than 2.5% of the initial activity within 1,000 years. The initial period is totally dominated by Ni-63. Ni-59 dominates the activity from about 1,000 years up to the end of the assessment period of 100,000 years.

Figures 3-5 and 3-6 show radiotoxicity for each waste vault and radionuclide over time for the whole inventory in SFR. During the first 4,000 years, the silo inventory contributes almost 100% of the total radiotoxicity; this is due to the amount of Am-241 stored in the silo. Radiotoxicity is dominated by actinides (Am-241 (first 4,000 years), Pu-239 (from 4,000 to about 75,000 years after closure), Th-229 (after 75,000 years after closure)) and decreases more slowly in the initial 1,000 years than the total activity, but falls to about 0.3% of its initial value after 10,000 years. The most significant aspect for the decrease of radiotoxicity is the effect of decay of Am-241 between about 1,000 and 5,000 years after closure.

Table 3-3. Comparison of relevance of radionuclides in the SFR assessments SAFE, SAR-08 and SR-PSU (Lindgren et al. 2001, Almkvist and Gordon 2007, Thomson et al. 2008b).

Radionuclide	SAFE	SAR-08	SR-PSU	Radionuclide	SAFE	SAR-08	SR-PSU
H-3	Green	Green	Green	Pb-210	Light Blue	Black	Green
Be-10	Light Blue	Light Blue	Light Blue	Po-210	Black	Black	Green
C-14	Green	Green	Green	Ra-226	Light Blue	Black	Green
Cl-36	Green	Green	Green	Ra-228	Black	Black	Green
Ca-41	Black	Black	Green	Ac-227	Light Blue	Black	Green
Fe-55	Light Blue	Light Blue	Light Blue	Th-228	Black	Black	Green
Co-60	Green	Green	Green	Th-229	Light Blue	Black	Green
Ni-59	Green	Green	Green	Th-230	Light Blue	Black	Green
Ni-63	Green	Green	Green	Th-232	Light Blue	Black	Black
Se-79	Green	Green	Green	Pa-231	Light Blue	Black	Green
Sr-90	Green	Green	Green	U-232	Green	Light Blue	Green
Zr-93	Green	Light Blue	Green	U-233	Light Blue	Black	Black
Nb-93m	Green	Light Blue	Green	U-234	Red	Light Blue	Green
Nb-94	Green	Green	Green	U-235	Red	Light Blue	Green
Mo-93	Green	Green	Green	U-236	Red	Light Blue	Green
Tc-99	Green	Green	Green	U-238	Red	Light Blue	Green
Ru-106	Light Blue	Light Blue	Black	Np-237	Red	Green	Green
Pd-107	Green	Light Blue	Green	Pu-238	Green	Light Blue	Green
Ag-108m	Green	Green	Green	Pu-239	Green	Green	Green
Cd-113m	Green	Light Blue	Green	Pu-240	Green	Green	Green
In-115	Black	Light Blue	Light Blue	Pu-241	Red	Light Blue	Green
Sn-126	Green	Green	Green	Pu-242	Red	Green	Green
Sb-125	Light Blue	Light Blue	Light Blue	Pu-244	Red	Light Blue	Black
I-129	Green	Green	Green	Am-241	Green	Green	Green
Cs-134	Light Blue	Light Blue	Light Blue	Am-242m	Red	Light Blue	Green
Cs-135	Green	Green	Green	Am-243	Red	Green	Green
Cs-137	Green	Green	Green	Cm-242	Black	Black	Black
Ba-133	Light Blue	Light Blue	Light Blue	Cm-243	Red	Light Blue	Green
Pm-147	Light Blue	Light Blue	Light Blue	Cm-244	Red	Light Blue	Green
Sm-151	Green	Light Blue	Green	Cm-245	Red	Light Blue	Green
Eu-152	Green	Light Blue	Green	Cm-246	Red	Light Blue	Green
Ho-166m	Green	Green	Green		Red	Light Blue	Green

-  Not included in the inventory.
-  Included in the inventory, but not in the assessment.
-  Implicitly included (inventory added to progeny inventory).
-  Included.
-  Included as progeny.

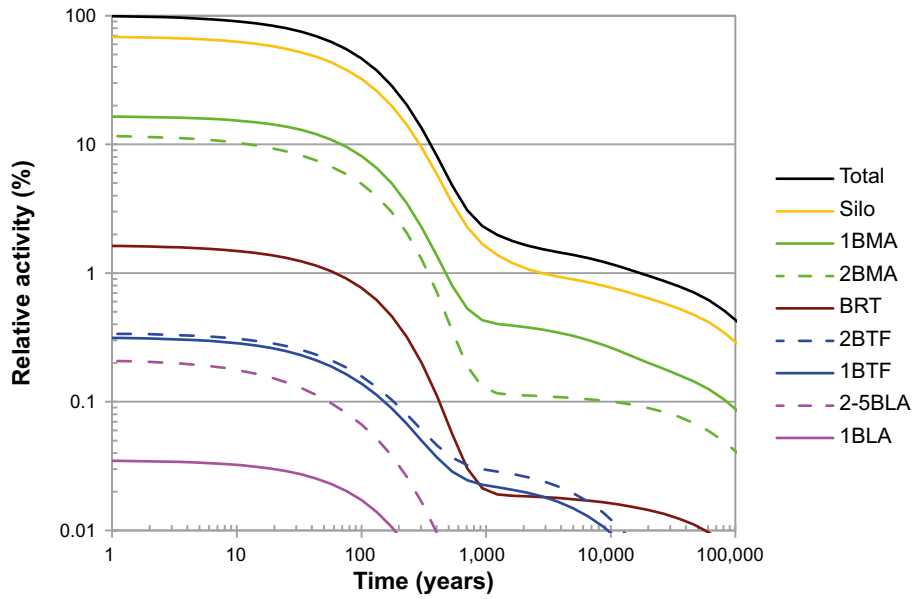


Figure 3-3. Contribution of waste vaults to the total activity as a function of time.

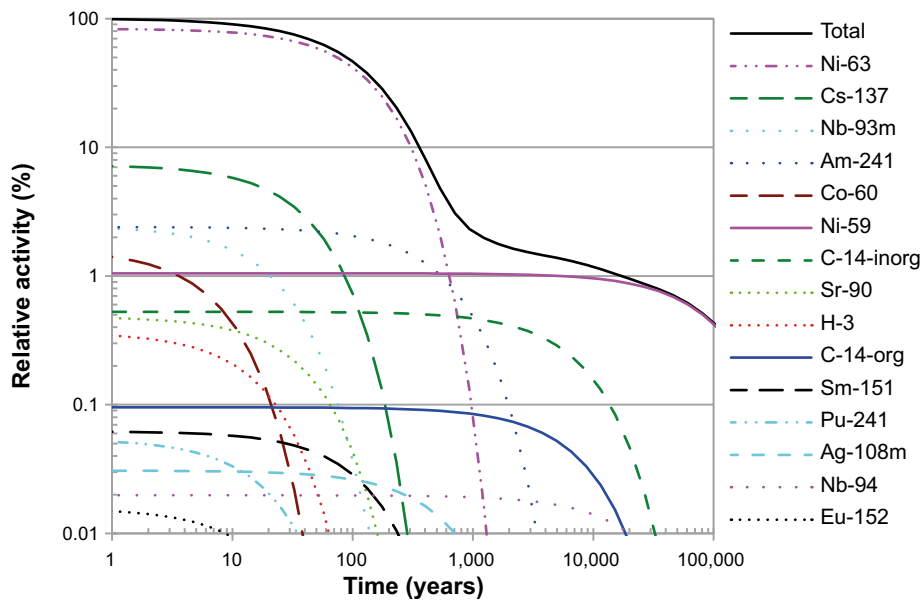


Figure 3-4. Contribution of dominant radionuclides to the total activity as a function of time.

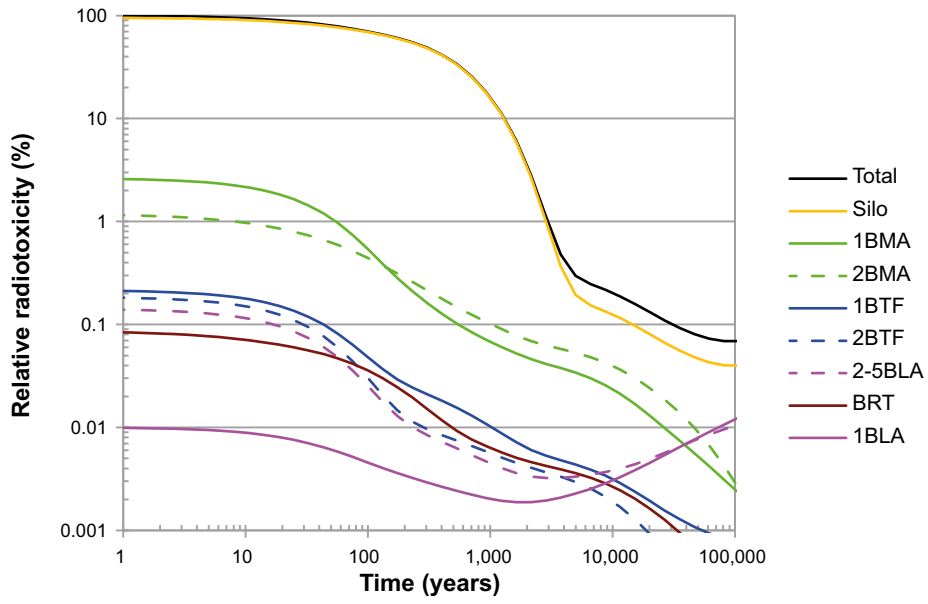


Figure 3-5. Contribution of waste vaults to the total radiotoxicity as a function of time.

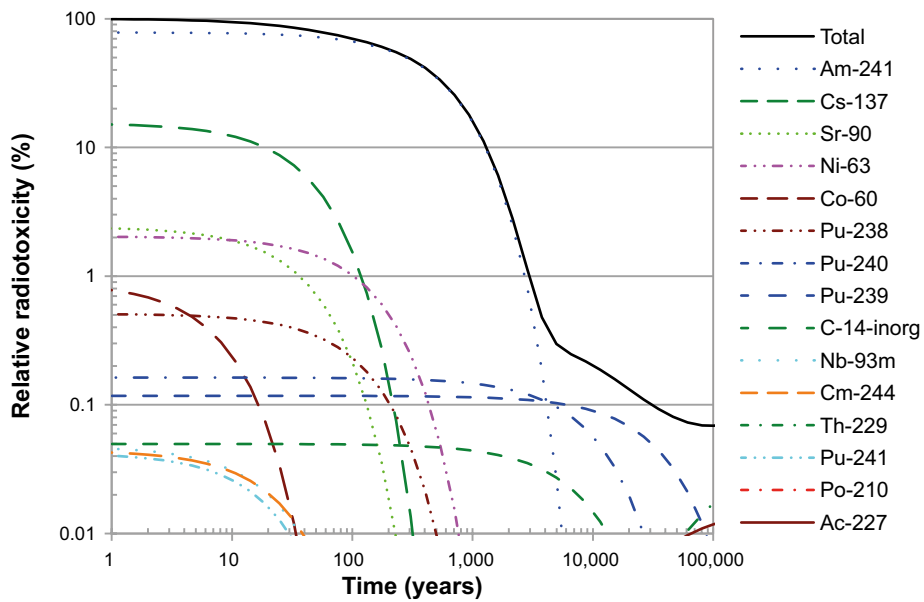


Figure 3-6. Contribution of the dominant radionuclides to the total radiotoxicity as a function of time.

4 Description of the calculation cases

Several calculation cases have been identified for analysing the selected scenarios in the safety assessment by means of radionuclide transport and dose calculations (see Section 2.3). The calculation cases were derived from FEP analysis and scenario selection (Chapter 3 and 7 in the **Main report**). The calculation cases are presented, in detail in this chapter, with a few exceptions. For the assessment of the surface ecosystems, the derivation of the so-called biosphere calculation cases (BCC) are described in the **Biosphere synthesis report**. The sub-model for the assessment of the biosphere in a calculation case is defined by an assigned BCC, which conforms to the specific boundary conditions assumed for the particular calculation case. The calculation cases related to future human actions are described in the **FHA report**, although note that the intrusion wells and drilled wells downstream of the repository scenarios are not treated as FHA scenarios but are instead included as less probable scenarios and described in this chapter.

In this chapter, the calculation cases in the main scenario, the less probable scenarios and residual scenarios are presented in detail (Sections 4.1, 4.2 and 4.3). Calculation cases for two combinations of less probable scenarios are presented in Section 4.4. Finally, in Section 4.5, a brief overview of all scenarios and calculation cases is presented.

4.1 Calculation cases in the main scenario

The main scenario is described in Section 7.4 in the **Main report**. Two variants of the main scenario are defined based on two of the climate cases included in the reference evolution: the *global warming climate case* and the *early periglacial climate case* (Section 7.4.1 in the **Main report** and the **Climate report**). Three calculation cases have primarily been identified to analyse the main scenario: the *global warming calculation case* (CCM_GW) and the *timing of the releases calculation case* (CCM_TR) for the assessment of the *global warming variant* of the main scenario, and the *early periglacial calculation case* (CCM_EP) for the assessment of the *early periglacial variant* of the main scenario. In addition to these three, the *collective dose calculation case* (CCM_CD) has been identified in order to provide an alternative safety indicator as requested by Swedish regulation. The assessment period for the calculation cases in the main scenario spans generally from the closure of the repository to 100,000 years into the future. These four calculation cases are described in the sections below.

As mentioned in Chapter 2, handling of uncertainties is of key importance for the safety assessment. Uncertainties are in most cases addressed by choosing pessimistic parameter values so that the estimated dose can be regarded as conservative when evaluated against the criteria for radiological risk. When it comes to radionuclide release, higher release rates are commonly regarded as more pessimistic than lower. However, in some situations this is not the case. An early start of radionuclide releases from the near-field results in an early release from the geosphere to the biosphere. During the first about 1,000 years of the assessment period, releases to the biosphere may be highly diluted with low radiological impact because of the submerged conditions of the exit points. Assuming a later onset of radionuclide releases might hence cause higher doses when the releases to the biosphere start only after the area covering the exit points has emerged from the sea when the potential dilution is much lower. It is, therefore, not obvious which timing of releases to the biosphere leads to higher peak doses and how significant the effect will be.

In order to investigate how these assumptions affect the estimated radiological risk, two calculation cases have been defined. In the *global warming calculation case* (CCM_GW) the radionuclide release does not begin until the conditions above SFR have changed to terrestrial. This is implemented by not activating any transport processes during the first 1,000 years. Prior to this, the only process affecting the size of the inventory is the radioactive decay and ingrowth of progeny.

In the *timing of the releases calculation case* (CCM_TR) the transport processes are modelled to begin immediately after closure, leading to an earlier release of radionuclides from the repository than in the *global warming calculation case* (see Section 4.1.3).

4.1.1 Global warming calculation case (CCM_GW)

The *global warming calculation case (CCM_GW)* is treated as the base case for the radionuclide transport and dose calculations in the present assessment. Many of the other calculation cases described in this chapter are modified variants of the *global warming calculation case*. Hence the description of the *global warming calculation case* is more detailed than the descriptions of the other calculation cases.

The *global warming calculation case* is based on the evolution of climate-related conditions in the *global warming climate case (Climate report)*. For radionuclide transport modelling, the evolution of climate-related conditions in the *global warming calculation case* has however been simplified. The simplified evolution, shown in Figure 4-1, contains four periods of the periglacial climate domain, as compared with ten periods in the *global warming climate case*. The total years 32,500, with periglacial climate domain in this simplified evolution is similar to the about 31,000 years for the *global warming climate case*. During these periods of periglacial climate domain, continuous permafrost down to and below repository depth is assumed.

Handling in the near-field model

In the modelling, the repository is assumed to be immediately saturated once it is closed. When the water comes into contact with the waste, radionuclides may dissolve. Dissolved radionuclides might then be transported, by diffusion and/or advection, out from the waste form, through the packaging and surrounding material and, finally, out from the repository.

During periods of periglacial climate conditions, it is assumed that there is no water flow in the near-field. Over time, as the concrete degrades, the sorption capacity may also be affected, hence different sorption partitioning coefficients, K_d values, are used for different waste vaults and for different time periods with various degradation states (Table 4-4). For the BLA vaults, sorption is not taken into account.

Radionuclide inventory

The best estimate inventory of radionuclides at repository closure is the base for the *global warming calculation*, see further Section 3.2.

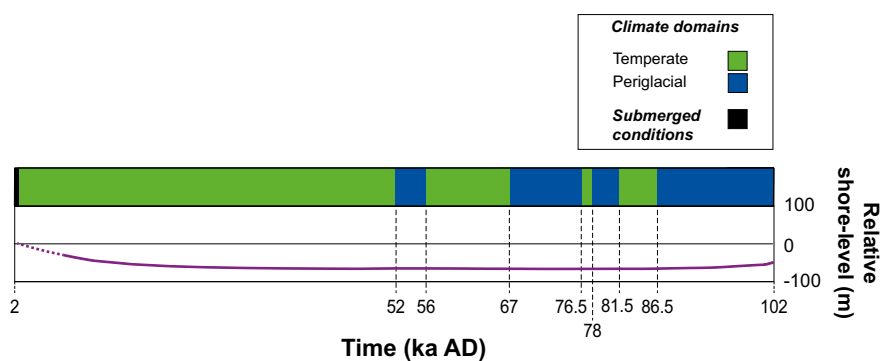


Figure 4-1. Simplified evolution of climate-related conditions at Forsmark as a time series of climate domains and submerged periods in the global warming variant of the main scenario, which was used in the *global warming calculation case*. The corresponding evolution in the *global warming climate case* is shown in Figure 4-3 in the *Climate report*.

Hydrology

The modelled groundwater flow through the repository is obtained from simulations of the near-field hydrology (Abarca et al 2013). These simulations have been performed for different degradation states. Over time, the concrete barriers degrade, from that of intact concrete to that of moderately degraded concrete, to that of severely degraded concrete and finally to that of completely degraded concrete (Chapter 10 in the Data report). Table 4-1 shows which near-field hydrogeological cases⁵ from Abaraca et al. (2013) that have been used for different time periods. The hydraulic conductivity for concrete barriers used in the hydrological calculations for the different degradation states are: intact concrete $K=8.3 \times 10^{-10}$ m/s, moderately degraded concrete $K=10^{-7}$ m/s, severely degraded concrete $K=10^{-5}$ m/s and completely degraded concrete $K=10^{-3}$ m/s. As explained before, no release during the first 1,000 years was assumed in this calculation case as one of two bounding cases to handle uncertainties (the other bounding case, with immediate onset of release, is described in Section 4.1.3). Also during permafrost, no flow is assumed to take place. For the two BMA vaults, the flow through the concrete barriers was modelled as fracture flow (see Appendix D) during periods with severely and completely degraded concrete. For other time periods and vaults, the concrete barriers were modelled as porous media.

Table 4-1. Progression of hydrological cases in the near-field over time in the *global warming calculation case*. No flow (black), moderately degraded concrete* $K=10^{-7}$ m/s (blue), severely degraded concrete $K=10^{-5}$ m/s (yellow), completely degraded concrete $K=10^{-3}$ m/s (orange) and base case used for BLA (green). "F" denotes fracture flow, see further Appendix D.

Time AD	2000–3000	3000–12,000	12,000–22,000	22,000–52,000	52,000–56,000	56,000–67,000	67,000–76,500	76,500–78,000	78,000–81,500	81,500–86,500	86,500–102,000
BMA	Black	Blue	Blue	Yellow	Black	Orange	Black	Orange	Black	Orange	Black
Silo	Black	Yellow	Yellow	Black	Black	Orange	Black	Orange	Black	Orange	Black
BTF, BRT	Black	Yellow	Orange	Orange	Black	Orange	Black	Orange	Black	Orange	Black
BLA	Black	Green	Green	Green	Black	Green	Black	Green	Black	Green	Black

* Conductivity values applies to concrete barriers, for other materials see Abarca et al. (2013).

Properties for cementitious materials

The diffusivities were handled in a corresponding way by assigning different D_e values for different time periods and for the different waste vaults. Values for different periods and vaults are presented in Table 4-2. The transitions between time periods were modelled as a gradual change over 100 years (but over 10 years for the first transition at 2100 AD). Note that the concrete in BRT was modelled as a stirred tank and hence D_e values were not used for the concrete.

The solid densities used for construction concrete and grout were 2,529 and 2,250 kg/m³, respectively.

The porosities were handled by assigning different values for the different time periods and vaults presented in Table 4-3.

⁵ The table shows the development due to the changes in hydraulic conductivity, it should also be noted that the water flow varies due to the changes in boundary conditions, during land rise. This is further described in Abarca et al. (2013).

Table 4-2. D_e values [m^2/s] for cementitious materials.

Time [years AD]	Construction concrete			Moulds/Tank Walls			Grout		
	1-2BMA*	Silo*	1-2BTF	1-2BMA	Silo	1-2BTF	1-2BMA	Silo	1-2BTF
2000–2100	3.50E–12	3.50E–12	3.50E–12	3.50E–12	3.50E–12	3.50E–12	3.50E–10	3.50E–10	3.50E–10
2100–2500	5.00E–12	1.00E–11	2.00E–11	2.00E–11	2.00E–11	5.00E–11	4.00E–10	3.50E–10	3.50E–10
2500–3000	5.00E–12	1.00E–11	2.00E–11	2.00E–11	2.00E–11	5.00E–11	4.00E–10	3.50E–10	3.50E–10
3000–12,000	5.00E–12	1.00E–11	2.00E–11	2.00E–11	2.00E–11	5.00E–11	4.00E–10	3.50E–10	3.50E–10
12,000–22,000	5.00E–12	5.00E–11	1.00E–10	5.00E–11	5.00E–11	2.00E–10	4.00E–10	5.00E–10	5.00E–10
22,000–52,000	1.00E–11	1.00E–10	5.00E–10	1.00E–10	1.00E–10	8.00E–10	5.00E–10	1.00E–09	1.00E–09
52,000–102,000	2.00E–10	1.00E–10	5.00E–10	5.00E–10	1.00E–10	8.00E–10	1.00E–09	1.00E–09	1.00E–09

* Probability density functions were used for construction concrete in 1-2BMA and the Silo (see the Data report), whereas single values were used for all other cementitious materials.

Table 4-3. Porosities for cementitious materials.

Time [years AD]	Construction concrete			Moulds/Tank Walls			Grout		
	1-2BMA	Silo	1-2BTF, BRT	1-2BMA	Silo	1-2BTF	1-2BMA	Silo	1-2BTF
2000–2100	0.11	0.11	0.11	0.11	0.11	0.11	0.3	0.3	0.2
2100–2500	0.14	0.11	0.11	0.14	0.11	0.11	0.4	0.3	0.2
2500–3000	0.14	0.16	0.11	0.14	0.11	0.11	0.4	0.3	0.2
3000–12,000	0.14	0.16	0.2	0.14	0.11	0.2	0.4	0.3	0.4
12,000–22,000	0.14	0.16	0.5	0.14	0.11	0.5	0.4	0.3	0.5
22,000–52,000	0.18	0.21	0.5	0.18	0.11	0.5	0.5	0.3	0.5
52,000–102,000	0.5	0.25	0.5	0.5	0.11	0.5	0.5	0.3	0.5

Properties for bentonite

Effective diffusivities for bentonite are presented in Table 7-5 in the **Data report** for neutral diffusing species, all anions and Cs (I). From that table, the highest values were, pessimistically, chosen for all radionuclides for both bentonite and sand-bentonite. The highest best estimate value of the porosity for bentonite from Table 7-4 in the **Data report** was used as a single value, i.e. 0.61. The porosity of sand-bentonite was 0.25. The solid densities for bentonite and sand-bentonite were 2,692 and 2,667 kg/m^3 , respectively.

Properties for macadam/crushed rock

The effective diffusivity, porosity and solid density for macadam/crushed rock were represented by single values $6 \times 10^{-10} m^2/s$, 0.3 and 2,700 kg/m^3 , respectively.

Sorption data

As the concrete degrades its sorption capacity is also affected, due to the pH evolution associated with cement leaching. Therefore, different K_d values are used for different waste vaults and different time periods (Table 4-4). For the BLA vaults, sorption is not considered. K_d values for bentonite and cement paste of different degradation states are presented in Tables 7-6 to 7-10 in the **Data report**. These values are to be multiplied with the factors in Table 4-5 in the present report to get the actual K_d value for various cementitious materials. According to the reference evolution on which the main scenario is based, see Chapters 6 and 7 in the **Main report**, redox conditions in the near-field become reducing shortly after closure.

Table 4-4. Time periods for different degradation states leading to different K_d values for concrete. Initially all cementitious materials are in the chemical degradation state I (dissolution of sodium and potassium hydroxides and the pH is higher than 12.5. Thereafter follows degradation state II (dissolution of portlandite pH≈12.5), degradation state IIIa (incongruent dissolution of CSH phases, presence of Ca-aluminates pH≈12) and degradation state IIIb (incongruent dissolution of CSH phases, absence of Ca-aluminates pH≈10.5).

Time AD	2000–4000	4000–7000	7000–22,000	22,000–34,000	34,000–58,000	58,000–102,000
BMA1	I	I	II	II	II	II
BMA2	I	I	II	II	II	II
Silo	I	I	I	I	II	II
BTF1	I	II	II	IIIa	IIIa	IIIb
BTF2	I	II	II	IIIa	IIIa	IIIb
BRT	I	II	II	IIIa	IIIa	IIIb

Table 4-5. Fraction of cement paste in construction concrete and grout (Table 7-12 in the Data report).

Material	Cement paste fraction
Construction concrete	0.219
Grout in silo	0.347
Grout in 1BMA	0.177
Grout in 2BMA	0.347
Grout in 1–2 BTF top	0.177
Grout in 1–2 BTF bottom	0.266

Due to presence of complexing agents, the K_d values were reduced with sorption reduction factors for the radionuclides affected. Concentration dependent reduction factors are given in Table 7-11a to 7-11c in the **Data report**. The concentrations of complexing agents are given in a dedicated reference report (Keith-Roach et al. 2014). The resulting reduction factors are described in the **Input data report** (Section AMF number 75).

Fractures

As the concrete barriers degrade, larger fractures may form. The modelling approach is adapted to account for larger fractures in the models for 1–2BMA. See Appendix D for details.

Handling in the far-field model

Results from an intermediate-flow case (bedrock case 1 in Odén et al. 2014) were selected to be used in the radionuclide transport calculations for the main scenario. The results used in the probabilistic radionuclide transport calculations are travel times and values of flow-related transport resistance⁶ that are used in pairs from the same realisations/particle tracks. These pairs of data are available for 2000 AD, 2500 AD, 3000 AD, 3500 AD, 5000 AD and 9000 AD. During permafrost, no flow is assumed to take place. Figures A-2 and A-3 in Appendix A display the hydrogeological data used in the calculation case.

K_d values are available for the three groundwater types that are selected to be representative for the main scenario; temperate saline, periglacial and late periglacial (Crawford 2013). In general, the lowest K_d value (from Table 8-7 in the Data report) was (pessimistically) selected to be used in the radionuclide transport calculations, except for some radionuclides that are sensitive to pH and redox conditions. The K_d values valid for environments with pH less than 10 were then selected (this concerns Np(IV), Pu(III/IV), Sn(IV) and U(IV)). For those elements where K_d values differ depending on their oxidation states, the K_d values for reducing conditions were applied (e.g. Np(IV) and Tc(IV)), since reducing conditions is expected to prevail in the main scenario.

⁶ The flow related transport resistance, F , is used to calculate the required input data on flow-wetted surface area, a_w , by dividing it by the travel time, t_w ($a_w = F/t_w$).

The interface between far-field and biosphere

Hydrogeological modelling of release locations in the landscape shows that, on average, more than 80% (and in most cases more than 90%) of the total potential releases from SFR 1 and SFR 3 would end up in biosphere object 157_2⁷ (**Biosphere synthesis report**). Hence, in the *global warming calculation case*, the entire releases are assumed to end up in biosphere object 157_2, radionuclides are then transported to other objects through water exchange or through water flow.

Handling in the biosphere model

The biosphere calculation case developed for the *global warming calculation case* is denoted BCC1. The development of the Forsmark landscape in BCC1 follows that of the *global warming climate case* where the climate is assumed to be temperate for the first 50,000 years (see Chapter 5 in the **Biosphere synthesis report**). In the *global warming climate case*, the annual average air temperature may increase by up to 3.7°C but will return to present conditions after about 25,000 years (**Climate report**). Ecosystem responses to the increased temperature (e.g. altered primary production or respiration) are uncertain (see Andersson (2010), Aquilonius (2010) and Löfgren (2010) for further discussion on potential ecosystem responses to warming). Therefore, the most reliable ecosystem data available for temperate conditions, i.e. site data under present conditions, are used for the entire assessment period for this calculation case. A simplifying assumption was made, in which temperate conditions are assumed in the biosphere also during the four periods of periglacial conditions. However, during these periods of periglacial climate conditions, agricultural activities cannot take place and therefore only a population of *Hunters and Gatherers* was assumed to be exposed to radionuclides originating from the repository (**Biosphere synthesis report**). The potential effects of shallow permafrost with taliks (unfrozen areas in the otherwise frozen landscape) are evaluated in the *early periglacial calculation case* (see Section 4.1.2).

Landscape development

Shoreline displacement occurs at Forsmark, and areas that are presently situated below the sea will gradually rise above sea-level. Biosphere object 157_2 that is currently a marine basin will in time be transformed into a wetland area. Radionuclides released during the submerged period reach all biosphere object basins in direct, or indirect, contact with basin 157_2, through lateral exchange of water.

However, as soon as the shoreline recedes from the area and biosphere object 157_2 emerges above sea-level radionuclides released to biosphere object 157_2 during the terrestrial stage will only reach biosphere objects in the surface water chain downstream from object 157_2 (namely 157_1 and 116, further described in the **Biosphere synthesis report**).

In this calculation case, the transport and fate of radionuclides are simultaneously simulated in multiple connected biosphere objects and each of these objects goes through a transition from a marine basin to a lake/wetland complex or a wetland area without an explicit lake stage.

Note that the continuous transport and fate of radionuclides is simulated in a landscape that is undisturbed by human inhabitants. However, once biosphere objects have emerged sufficiently above sea-level to prevent salt water intrusion, the consequences of draining and cultivating the lake-mire complex are also evaluated at each point in time by parallel simulations (conditioned on the state of the natural ecosystems), i.e. both natural and agricultural systems are evaluated at each time step.

Hydrological water fluxes

Hydrological water fluxes are modelled for future biosphere objects at three points in time: 3000 AD (submerged period for all objects), 5000 AD (terrestrial period, when objects are either lake-mire complexes or mires) and 11,000 AD (terrestrial period, all objects are mires). For each point in time, groundwater fluxes were simulated in a landscape based on a separate, stationary three-dimensional

⁷ A biosphere object is an area in the present and/or future landscape that potentially, at any time during the considered assessment period, could receive a discharge of radionuclide-containing groundwater associated with the repository, see further Section 9.5.

regolith map, with streams connecting water bodies on land (this approach used the landscape development model; Brydsten and Strömberg 2013). Present-day temperature and site data (with respect to precipitation, evaporation, and runoff) were used in the hydrological simulations for this calculation case. Hydrological modelling and parameter values are further described in Grolander (2013) and Werner et al. (2013).

Ecosystems

Ecosystem parameters are based on site data from lakes, wetlands and marine basins in the area, and applied to future ecosystems assuming present-day conditions concerning nutrients and temperature. Parameters are described further in Grolander (2013).

Exposed populations

The annual effective dose to a representative human is calculated for four different exposed populations, representing four variants of land-use. The four variants are: *hunters and gatherers* (H&G), *infield-outland farmers* (IO), *drained-mire farmers* (DM), and a *garden plot household* (GP). The different exposed populations are briefly described in Section 9.5 and further details are given in the **Biosphere synthesis report**. Dose rates to non-human biota are calculated for 11 marine, 13 limnic and 14 terrestrial organism types, two organism types living partly in marine and terrestrial ecosystems (combined habitats), and one organism type living partly in both limnic and terrestrial ecosystems (see Section 9.5).

4.1.2 Early periglacial calculation case (CCM_EP)

The *early periglacial calculation case* is based on the evolution of climate-related conditions in the *early periglacial climate case* (see Section 7.4.1 in the **Main report**). The evolution of climate-related conditions is identical in the *early periglacial climate case* and the *global warming climate case* during the complete assessment period except for the period of minimum insolation around 17,500 AD to 20,500 AD where the *early periglacial climate case* has a period of periglacial conditions with permafrost and the *global warming climate case* has temperate conditions. Since the climate-related conditions in both climate cases are identical beyond 20,500 AD, the *early periglacial calculation case* focuses on the time window from repository closure up to 20,500 AD. During the early periglacial period included in this calculation case, the entire modelled area is land, and the regolith layers are frozen. Therefore, discharge of deep groundwater, and hence also release of radionuclides, is restricted to taliks.

Prior to the start of the periglacial period (17,500 AD), the discharge is assumed to reach biosphere object 157_2 as in the *global warming calculation case*. For the periglacial period, results from hydrogeological modelling suggest that groundwater from the repositories may be discharged to wetlands North East of the present repository, and to large lakes formed in Öregrundsgrepen (Odén et al. 2014). Simulations of surface hydrology under periglacial conditions suggest that a discharge talik may be formed under a small wetland area (biosphere object 157_1 just north of the primary release area during periods of temperate conditions). Moreover, the deep lake of biosphere object 114, located in Öregrundsgrepen, will still be open, and is thus likely to be connected with a discharge talik (Bosson et al. 2013, Werner et al. 2013). In this calculation case, the entire release between 17,500 and 20,500 AD is directed in two separate variants of the calculation case to biosphere object 157_1 and to 114, respectively.

Hydrological calculations have been performed for periglacial as well as temperate conditions in SR-PSU (Odén et al. 2014). However, the near-field and far-field water fluxes for temperate conditions were used also for the calculation of doses from the taliks. This was considered justifiable as the hydrological calculations show that generally, during periglacial conditions, the vault flows are reduced, and the travel times and flow related resistance are increased (Odén et al. 2014). It is believed that the approach is cautious and that it can be ruled out with regard to the obtained peak dose, that a more realistic hydrological model for talik conditions could increase peak dose to a level close to or even above the peak dose of the *global warming calculation case*.

The *early periglacial calculation case* is combined with the biosphere calculation case BCC2 (details in the **Biosphere synthesis report**). The same biosphere model as in BCC1 was used for BCC2 but

parameter values and biosphere objects were altered for the periglacial period in BCC2 (biosphere objects 114 and 157_1). The water flow used in this case for the surface system were modelled for colder and drier climate conditions at both the wetland and the lake taliks (Grolander 2013, Werner et al. 2013). Ecosystem parameter values for primary production, and production of edible fish and crayfish are altered (compared with values applied in BCC1) to better reflect permafrost conditions; these values are based on literature data from colder environments (Grolander 2013). Effects of shoreline displacement and ecosystem succession are not considered for the periglacial period since at 17,500 AD, the effects of isostatic rebound are insignificant for the model area, although ecosystem succession due to infilling of lakes is very slow during periglacial conditions (Brydsten and Strömngren 2010) the periglacial period is too short to have any significant effect on the timing of lake infilling. For non-human biota, exposure is estimated for freshwater and terrestrial organisms. The same organisms as in BCC1 were assessed, with the exception that no limnic amphibians or mammals, and no trees, gastropods, amphibians or reptiles are assumed to occur (see Chapter 7 in the **Biosphere synthesis report** and Jaeschke et al. 2013).

During periglacial climate conditions, cultivation is not possible on drained mires due to permafrost, and dug wells will not yield any water in the frozen ground, hence the only exposed population considered in this calculation case is H&G.

4.1.3 Timing of the releases calculation case (CCM_TR)

As discussed in Section 4.1, in order to not underestimate the radiological consequence during later terrestrial periods, the *global warming calculation case* does not assume any releases for the initial mainly submerged period, up to 1,000 years after closure. The *timing of the releases calculation case* (CCM_TR), has been included to study the effect on the outcome of the safety assessment of assuming releases during the submerged period. Furthermore, this calculation case forms the basis for the calculation of collective doses (Section 4.1.4) as collective doses are to be calculated from releases during the first 1,000 years after closure of the repository.

In this calculation case, the release of radionuclides commences directly after closure. Table 4-6 shows the progression of near-field hydrological cases in the individual waste vaults that were used for different time periods. Apart from this, the models of the near-field, the far-field and the biosphere are handled as in the *global warming calculation case*. Together with the *global warming calculation case*, these two calculation cases cover the two bounding cases of possible outcomes.

Table 4-6. Progression of hydrological cases in the near-field in the *timing of the releases calculation case*. No flow (black), moderately degraded concrete* $K=10^{-7}$ m/s (blue), severely degraded concrete $K=10^{-5}$ m/s (yellow) and completely degraded concrete $K=10^{-3}$ m/s (orange) and base case used for BLA (green). "F" denotes fracture flow, see further Appendix D.

Time AD	2000–2500	2500–3000	3000–12,000	12,000–22,000	22,000–52,000	52,000–56,000	56,000–67,000	67,000–76,500	76,500–78,000	78,000–81,500	81,500–86,500	86,500–102,000
BMA	Blue	Blue	Blue	Blue	Yellow (F)	Black	Orange (F)	Black	Orange (F)	Black	Orange (F)	Black
Silo	Blue	Yellow	Yellow	Yellow	Yellow	Black	Orange	Black	Orange	Black	Orange	Black
BTF, BRT	Blue	Blue	Yellow	Orange	Orange	Black	Orange	Black	Orange	Black	Orange	Black
BLA	Green	Green	Green	Green	Green	Black	Green	Black	Green	Black	Green	Black

* Conductivity values applies to concrete barriers, for other materials see Abarca et al. (2013).

4.1.4 Collective dose (CCM_CD)

In addition to radiological risk, the regulations require collective dose to be calculated. The regulations (SSMFS 2008:37) specify that: “The collective dose, as a result of the expected outflow of radioactive substances over a period of 1,000 years after closure of a repository for spent nuclear fuel or nuclear waste shall be estimated as the sum, over 10,000 years, of the annual collective dose”. The *collective dose calculation case* is based on the geosphere releases from the *timing of releases calculation case*.

Two populations were selected for the calculations: the global population exposed to C-14 releases into the atmosphere, and the Baltic population affected by the release of radionuclides to the Baltic Sea via subsequent exposure due to ingestion of fish.

Collective dose to the global population

The complete (i.e. integrated over 50,000 years) collective dose commitment from C-14 was estimated by multiplying the total releases (from the *timing of releases calculation case*) of C-14 from all waste vaults during the first 1,000 years by a conversion factor of 109,000 manSv per PBq. This conversion factor has been used by UNSCEAR (2000) for estimating the complete collective dose commitment to the global population from releases of C-14 to the atmosphere. It has been calculated under the assumption that the future world population stabilises at 10^{10} people, and that the global inventory of stable carbon does not increase from its present value. Further, according to UNSCEAR (2000), collective doses following releases to soils or to surface oceans are about the same as those for atmospheric releases.

To estimate the incomplete collective dose commitment (i.e. the collective dose integrated over 10,000 years) the complete collective dose commitment was multiplied by 0.75. This is based on estimates (UNSCEAR 2000) that 75% of the complete dose commitment from a single release is delivered within 10,000 years. Estimations of collective dose commitments from C-14 releases made with several different models have given very similar results (UNSCEAR 2000). This consistency between model predictions has been attributed to the long half-life of C-14, relative to its rate of environmental transport, which makes the estimated dose commitments insensitive to the detailed structure of the models or to the values of the parameters used in them (see UNSCEAR 2000 and references therein).

Collective dose to the regional population

The whole Baltic Sea region is represented by a single compartment, with a volume of $2.1 \times 10^{13} \text{ m}^3$. The only radionuclide transport processes considered are the water retention time of the Baltic Sea (30 years), and radioactive decay and in-growth. The exposed population considered are the people in the Baltic region, assumed to consume the total amount of fish captured by commercial fishing ($8.5 \times 10^7 \text{ kg C/year}$). The collective effective dose is calculated using a truncation time at year 1,000 after closure, as recommended in the regulations, since the annual collective dose contribution decreases rapidly when the release ceases and only releases during the first 1,000 years after closure are to be taken into account.

4.2 Calculation cases for less probable scenarios

The less probable scenarios are summarised in Section 2.2 in this report and presented in detail in Section 7.6 in the **Main report**. The calculation cases identified to analyse the less probable scenarios are presented in the sections below. Unless stated otherwise, these calculation cases are variants of the *global warming calculation case*.

4.2.1 High inventory calculation case (CCL_IH)

The *high inventory calculation case* (CCL_IH) evaluates the dose from the *high inventory scenario*, which is selected to assess uncertainties associated with the inventory. The radionuclide inventory used in this calculation case is based on the best estimate radionuclide inventory, but including uncertainties. The 95th percentile values for each radionuclide in each waste vault are used to illustrate the influence of a higher inventory (Table 3-17 in the **Initial state report**).

Apart from this, the handling of the near-field, the far-field and the biosphere is identical to the *global warming calculation case*.

4.2.2 High flow in the bedrock calculation case (CCL_FH)

The *high flow in the bedrock calculation case* (CCL_FH) evaluates the dose from the *high flow in the bedrock scenario*, which is selected to assess uncertainties in the data used to describe the rock in the hydrogeological flow model.

For the *global warming calculation case*, hydrogeological data from bedrock case 1 (Odén et al. 2014) are selected, representing intermediate-flow through all waste vaults. In this calculation case, bedrock case 11 (Odén et al. 2014) is used for the radionuclide transport calculations in the geosphere, representing a case with higher water inflow into the waste vaults.

In the near-field, this case is implemented by scaling the water flux for each waste vault applied in the *global warming calculation case* with the scaling factors derived as the maximum quotient between the cross flow in all bedrock cases and the cross flow in the intermediate-flow case (bedrock case 1), see Figure 4-2.

Apart from this, the handling of the near-field, the far-field and the biosphere are identical to the *global warming calculation case* in the main scenario.

4.2.3 Accelerated concrete degradation calculation case (CCL_BC)

The *accelerated concrete degradation calculation case* (CCL_BC) evaluates the dose from the *accelerated concrete degradation scenario*, which is selected to assess uncertainties in concrete degradation processes.

In this calculation case, it is assumed that the hydraulic conductivity of the concrete increases earlier or to a greater extent than in the *global warming calculation case*. This results in the following effects:

- Earlier or greater increase in the water flow through the waste vaults. The same repository hydrological calculation cases as in the *global warming calculation case* are applicable, but apply to earlier time points, see Table 4-7.
- Earlier or greater increase in the diffusivities of the concrete barriers.
- Earlier or greater increase in the porosity.

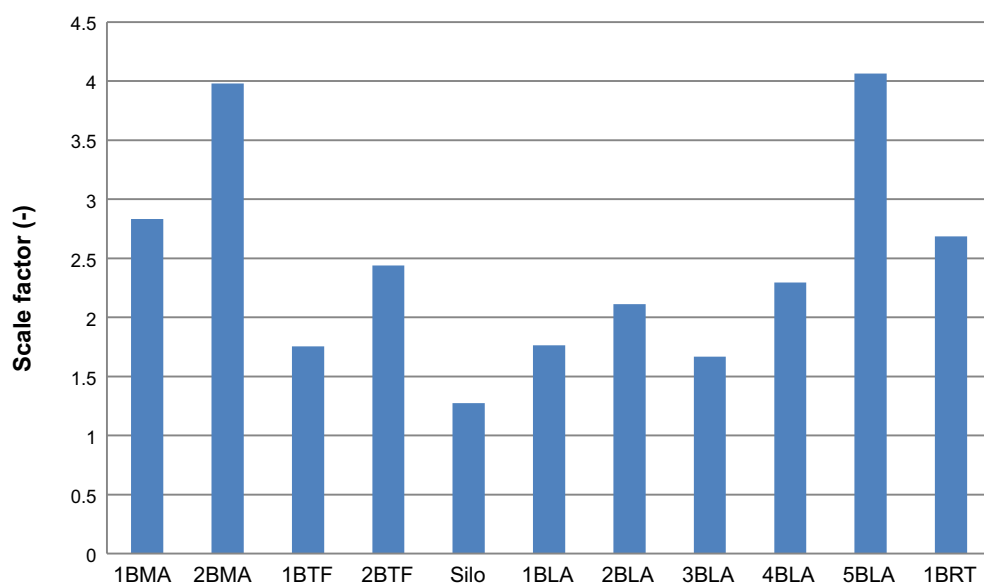


Figure 4-2. Scale factors for near-field flows for each waste vault, used in the *high flow in the bedrock calculation case*. The scaling factor for each waste vault is the maximum quotient between the cross flow in all bedrock cases and the cross flow in the intermediate-flow case used in the main scenario (all times ≥ 2500 AD).

The transitions between time periods were modelled as a gradual change over 100 years. The diffusivities and porosities for cementitious materials are given in Tables 4-8 and 4-9, respectively.

Apart from this, the handling of the near-field, the far-field and the biosphere are identical to the *global warming calculation case*.

Table 4-7. Progression of hydrological cases in the near-field over time in the *accelerated concrete degradation calculation case*. No flow (black), severely degraded concrete* $K=10^{-5}$ m/s (yellow) and completely degraded concrete $K=10^{-3}$ m/s (orange) and base case used for BLA (green). "F" denotes fracture flow, see further Appendix D.

Time AD	2000–3000	3000–22,000	22,000–52,000	52,000–56,000	56,000–67,000	67,000–76,500	76,500–78,000	78,000–81,500	81,500–86,500	86,500–102,000
BMA	Black	Yellow (F)	Orange (F)	Black	Orange (F)	Black	Orange (F)	Black	Orange (F)	Black
Silo	Black	Orange	Orange	Black	Orange	Black	Orange	Black	Orange	Black
BTF, BRT	Black	Orange	Orange	Black	Orange	Black	Orange	Black	Orange	Black
BLA	Black	Green	Green	Black	Green	Black	Green	Black	Green	Black

* Conductivity values applies to concrete barriers, for other materials see Abarca et al. (2013).

Table 4-8. D_e values [m^2/s] for cementitious materials used in the *accelerated concrete degradation calculation case*.

Time [years AD]	Construction concrete			Moulds/Tank Walls			Grout		
	1–2BMA	Silo	1–2BTF	1–2BMA	Silo	1–2BTF	1–2BMA	Silo	1–2BTF
2000–2100	3.50E–12	3.50E–12	3.50E–12	3.50E–12	3.50E–12	3.50E–12	3.50E–10	3.50E–10	3.50E–10
2100–2500	5.00E–12	1.00E–11	2.00E–11	2.00E–11	2.00E–11	5.00E–11	4.00E–10	3.50E–10	3.50E–10
2500–3000	5.00E–12	1.00E–11	2.00E–11	2.00E–11	2.00E–11	5.00E–11	4.00E–10	3.50E–10	3.50E–10
3000–12,000	5.00E–12	5.00E–11	1.00E–10	5.00E–11	5.00E–11	2.00E–10	4.00E–10	5.00E–10	5.00E–10
12,000–22,000	1.00E–11	1.00E–10	5.00E–10	1.00E–10	1.00E–10	8.00E–10	5.00E–10	1.00E–09	1.00E–09
22,000–102,000	2.00E–10	1.00E–10	5.00E–10	5.00E–10	1.00E–10	8.00E–10	1.00E–09	1.00E–09	1.00E–09

Table 4-9. Porosities [–] for cementitious materials used in the *accelerated concrete degradation calculation case*.

Time [years AD]	Construction concrete			Moulds/Tank Walls			Grout		
	1–2BMA	Silo	1–2BTF, BRT	1–2BMA	Silo	1–2BTF	1–2BMA	Silo	1–2BTF
2000–2100	0.11	0.11	0.11	0.11	0.11	0.11	0.3	0.3	0.2
2100–2500	0.14	0.11	0.11	0.14	0.11	0.11	0.4	0.3	0.2
2500–3000	0.14	0.16	0.11	0.14	0.11	0.11	0.4	0.3	0.2
3000–12,000	0.14	0.16	0.5	0.14	0.11	0.5	0.4	0.3	0.5
12,000–22,000	0.18	0.21	0.5	0.18	0.11	0.5	0.5	0.3	0.5
22,000–102,000	0.5	0.25	0.5	0.5	0.11	0.5	0.5	0.3	0.5

4.2.4 Bentonite degradation calculation case (CCL_BB)

The *bentonite degradation calculation case* (CCL_BB) evaluates the dose from the bentonite degradation scenario, which is selected to assess uncertainties in the consequences of extensive periglacial conditions in combination with uncertainties in the sealing properties of the bentonite.

In this calculation case, the hydraulic properties of the bentonite around the silo are assumed to deteriorate due to the formation of an ice-lens during a period of periglacial climate conditions with the consequences of higher water flow in the silo during a subsequent period of temperate climate conditions. A set of water-flux parameters has been calculated specifically for the ice-lens case in the detailed modelling of the near-field hydrology (Abarca et al. 2013). In this calculation case, radionuclide release calculations are performed using these specific water-fluxes.

The evolution of climate-related conditions is based on the *early periglacial calculation case*. The ice-lens is conservatively assumed to form during the first period of periglacial conditions in the *early periglacial calculation case*, i.e. the period between 17,500 and 20,500 AD. During this period of periglacial climate conditions, continuous permafrost is assumed to prevail. Furthermore, it is assumed that radionuclide releases from the repository to the geosphere and from the geosphere to the biosphere do not take place during this period. The potential effects of shallow permafrost with taliks are evaluated in the *early periglacial calculation case* (Section 4.1.2).

For the periods from 2000 AD to 17,500 AD and 20,500 AD to 102,000 AD, the handling of the near-field, the far-field and the biosphere are identical to the *global warming calculation case*.

4.2.5 Earthquake calculation case (CCL_EQ)

The *earthquake calculation case* (CCL_EQ) evaluates the dose from the *earthquake scenario*, which is selected since the occurrence of barrier damaging earthquakes cannot be ruled out.

This calculation case addresses only the silo and is based on the assumption that an earthquake damages the silo structure, leading to increased water flow through it. A deterministic simulation approach using best estimate values is applied in this calculation case due to the large number of calculations performed; a probabilistic approach would not have been feasible considering the available computational capacity.

The conditions in the geosphere are assumed to be adversely affected by an earthquake large enough to damage the silo structure. But such effects on the geosphere have not been quantified. Therefore, it is conservatively assumed that there will be no retardation of radionuclide transport in the geosphere in this calculation case.

Up to the time of the damage, radionuclide transport is assumed to occur in the same way as in the *global warming calculation case*. After the earthquake event, the concrete barriers in the silo are assumed to have failed, and the water flow increases. The increased water flow through the silo arising from concrete barrier damage was analysed in the safety analysis SAFE. With bentonite as a flow barrier, the increased flow of water is relatively small, 1 m³/year (Holmén and Stigsson 2001).

The dose calculations are repeated, using the same biosphere model as in the *global warming calculation case*, assuming an earthquake at different time points (every 100th year) from closure of the repository up to the end of the assessment period at 102,000 AD.

4.2.6 High concentrations of complexing agents calculation case (CCL_CA)

The *high concentrations of complexing agents calculation case* (CCL_CA) evaluates the dose from the *high concentrations of complexing agents scenario*, which is selected to assess uncertainties in the amounts of complexing agents and cellulose in the repository.

In the calculations, the concrete sorption reduction factor used was increased by a factor of 10 compared with the *global warming calculation case*. This factor was chosen because reduction factors are estimated to increase by a factor of 10 with each 10-fold increase in the concentration of complexing agent above the indicated no-effect level given in the **Data report**. Increased sorption reduction factors were applied to all waste vaults where complexing agents and cellulose are, or could be, disposed. The waste vaults, 1BLA and 2–5BLA, where sorption is not included in the model, are not affected by this calculation case.

Apart from this, the handling of the near-field, the far-field and the biosphere are identical to the *global warming calculation case*.

4.2.7 Wells downstream of the repository calculation case (CCL_WD)

The *wells downstream of the repository calculation case (CCL_WD)* evaluates the dose from the *wells downstream of the repository scenario*. Although the area in the direct vicinity of the repository is not the most likely location for a well, one in this area cannot be ruled out as future human behaviour cannot be predicted with certainty. No consideration is given to constraints that would arise from considering the current placement of wells, and they are assumed to be possible in the *wells downstream of the repository scenario*.

This calculation case focuses on wells drilled downstream of the repository, close enough to be affected by potential releases. Consequences from direct intrusion wells are addressed below in the *intrusion wells calculation case* (Section 4.2.8). Due to the position of the shoreline, it is not relevant to consider these wells before 2500 AD .

Wells downstream of the repository can attract a certain amount of water containing radionuclides from the repository. A so called *well interaction area* has been delineated, i.e. the area (or rather, volume) with the highest density of groundwater flow pathways for radionuclides from the repository within a depth interval from 10 to 80 m below the present-day sea level. For the *well interaction area*, an estimate in the analysis is that a water-supply well in this area can attract some 10% of a radionuclide discharge from the repository (see Werner et al. 2013 for details).

The concentrations of radionuclides in drinking and irrigation water are calculated by dividing the amount of radionuclides that reach the well by the amount of water drawn from the well.

The handling of the near-field, the far-field and the biosphere are identical to the *global warming calculation case* with the exception that in the biosphere modelling, drilled wells have been identified as a calculation case (BCC5), where dose to the most exposed group is only calculated for a *garden plot household*.

4.2.8 Intrusion wells calculation case (CCL_WI)

The *intrusion wells calculation case (CCL_WI)* evaluates the dose from the *intrusion wells scenario*. Although the area above the repository is not the most likely place for a well, a future well in this area cannot be ruled out as future human habits cannot be predicted with certainty. Wells for drinking water can be drilled into the repository at the earliest when the shoreline has passed the repository and the place is high enough above sea level to avoid sea water intruding into the well. It is assumed that wells can be drilled into the repository when the shoreline has passed the entire footprint of the repository, at 3000 AD. The concentrations of radionuclides in an intrusion well are assumed to be equal to the pore water concentrations in the backfill. In waste vaults lacking backfill (BLA), the concentrations are assumed to be equal to the concentrations in free water in the vault. Dose to humans due to radionuclides in the intrusion well water are estimated in the same way as for the *wells downstream of the repository calculation case*.

In this calculation case, as well as in the *global warming calculation case*, retention is not considered in the BLA vaults. This is a cautious assumption for most radionuclides, but not necessarily for some long-lived radionuclides for which progeny might increase the radiotoxicity in the system . For example, U-238 and U-235 have highly radiotoxic progeny that will grow-in to significant levels on timescales of tens of thousands of years. Variants of the calculation case focus therefore on uncertainties in the retention properties in IBLA, to find a bounding case for the possible consequences of a situation with significant ingrowth. These calculations were performed with lower releases of radionuclides from the near-field. The underlying processes that most likely lead to lower releases are sorption and possibly solubility limitation (for uranium).

4.3 Calculation cases for residual scenarios

The residual scenarios are summarised in Section 2.2 in this report and presented in details in Section 7.7 in the **Main report**. The calculation cases identified to analyse the residual scenarios are presented in the sections below. Unless stated otherwise, these calculation cases are variants of the *global warming calculation case*.

4.3.1 Loss of barrier function calculation case – no sorption in the repository (CCR_B1)

The *loss of barrier function calculation case – no sorption in the repository* (CCR_B1) evaluates the dose from the *loss of barrier function scenario – no sorption in the repository*, which is selected to illustrate the importance of sorption in the repository.

In this calculation case, it is assumed that radionuclides do not sorb in the repository, which is implemented by setting all sorption partitioning coefficients, K_d values, for all materials in the near-field to zero.

Apart from this, the handling of the near-field, the far-field and the biosphere is identical to the *global warming calculation case*.

4.3.2 Loss of barrier function calculation case – no sorption in the bedrock (CCR_B2)

The *loss of barrier function calculation case – no sorption in the bedrock* (CCR_B2) evaluates the dose from the *loss of barrier function scenario – no sorption in the bedrock*, which is selected to illustrate the importance of sorption in the rock.

In this calculation case, it is assumed that radionuclides do not sorb in the bedrock, which is implemented by setting all sorption partitioning coefficients, K_d values, in the far-field to zero.

Apart from this, the handling of the near-field, the far-field and the biosphere are identical to the *global warming calculation case*.

4.3.3 Loss of barrier function calculation case – high water flow in the repository (CCR_B3)

The *loss of barrier function calculation case – high water flow in the repository* (CCR_B3) evaluates the dose from the *loss of barrier function scenario – high water flow in the repository*, which is selected to illustrate the importance of the engineered barriers capability to limit the water flow through the part of the waste vaults containing waste.

In this calculation case, the near-field water-flows from the “no barriers” case in the hydrological calculations (Abarca et al. 2013) were used during the whole assessment period. In addition, the diffusivities and porosities for the most degraded concrete were used (i.e. same values as was used in last time period in Tables 4-2 and 4-3).

Apart from this, the handling of the near-field, the far-field and the biosphere are identical to the *global warming calculation case*.

4.3.4 Changed repository redox conditions in SFR 1 calculation case (CCR_RX)

The *changed repository redox conditions in SFR 1 calculation case* (CCR_RX) evaluates the dose from the *changed repository redox conditions in SFR 1 scenario*, which is selected to show the importance of maintained reducing conditions.

Sorption of many elements, such as Np, Pa, Pu, Se, Tc and U, is sensitive to the redox conditions. Due to changes in speciation, sorption of these elements under oxidising conditions can differ considerably from sorption under reducing conditions. In the *global warming calculation case*, the chemical conditions in the repository are reducing.

This calculation case assumes oxidising conditions in the repository, modelled by applying alternative sorption partition coefficients, K_d values, for the redox-sensitive elements Np, Pa, Se, Tc, U and Pu in the near-field (cementitious materials, bentonite, sand-bentonite and macadam/crushed rock). K_d values for Np(V), Pa(V), Se(VI), Tc(VII) and U(VI) were used. For plutonium, the oxidation state with the lowest K_d values was chosen. Tables 4-10, 4-11, and 4-12 show K_d values for oxidising conditions (this calculation case) and reducing conditions (the *global warming calculation case*) for cement paste,

bentonite and macadam/crushed rock, respectively. As is evident from the selected values shown in the tables, sorption of all these elements (except for selenium on cement) is the same or lower under oxidising conditions.

Apart from this, the handling of the near-field, the far-field and the biosphere are identical to the *global warming calculation case*.

Table 4-10. K_d values for hydrated cement paste (These values are to be multiplied with the fraction of cement paste in cementitious material from Table 4-5 to get the actual K_d value for various cementitious materials) for oxidising and reducing conditions (excerpt from Table 7-7 to 7-10 in the Data report, upper and lower limits of the distributions are also given in the Data report).

Element and oxidation state used for oxidising conditions	K_d [m ³ /kg]	Element and oxidation state used for reducing conditions	K_d [m ³ /kg]
<i>Changed repository redox conditions in SFR 1 scenario</i>		<i>Main scenario</i>	
Np(V)	0.1	Np(IV)	30
Pa(V)	10	Pa(IV)	30
Pu(V)	0.1	Pu(IV)	5 a)
Se(VI)	3×10 ⁻³ b)	Se(-II)	0
Tc(VII)	1×10 ⁻³	Tc(IV)	3
U(VI)	2 c)	U(IV)	30

a) 30 in degradation state IIIa and IIIb, b) 0 in degradation state IIIb, c) 30 in degradation step 2, IIIa and IIIb.

Table 4-11. K_d values for bentonite for oxidising and reducing conditions (excerpt from Table 7-6 in the Data report, upper and lower limits of the distributions are also given in the Data report).

Element and oxidation state used for oxidising conditions	K_d [m ³ /kg]	Element and oxidation state used for reducing conditions	K_d [m ³ /kg]
<i>Changed repository redox conditions in SFR 1 scenario</i>		<i>Main scenario</i>	
Np(V)	0.02	Np(IV)	63
Pa(V)	3	Pa(IV)	3
Pu(V)	0.02	Pu(III)	61
Se(VI)	0	Se(-II)	0
Tc(VII)	0	Tc(IV)	63
U(VI)	3	U(IV)	63

Table 4-12. K_d values (best estimate) for macadam/crushed rock for oxidising and reducing conditions (excerpt from Table 8-7 in the Data report, upper and lower limits of the distributions are also given in the Data report).

Element and oxidation state used for oxidising conditions	K_d [m ³ /kg]	Element and oxidation state used for reducing conditions	K_d [m ³ /kg]
<i>Changed repository redox conditions in SFR 1 scenario</i>		<i>Main scenario</i>	
Np(V)	4.1×10 ⁻⁴	Np(IV)	4.1×10 ⁻⁴
Pa(V)	5.9×10 ⁻²	Pa(V)	5.9×10 ⁻²
Pu(III/IV)	1.5×10 ⁻⁵	Pu(IV)	1.5×10 ⁻⁵
Se(VI)	0	Se(-II)	0
Tc(VII)	0	Tc(IV)	5.3×10 ⁻²
U(VI)	1.1×10 ⁻⁴	U(IV)	1.1×10 ⁻⁴

4.3.5 Extended global warming calculation case (CCR_EX)

The *extended global warming calculation case* (CCR_EX) evaluates the dose from the *extended global warming scenario*, which is selected to analyse the effect of future global sea-level rise and the potential influence on the surface systems of the warmer and wetter climate conditions expected in the *global warming climate case*.

In this calculation case, temperate climate conditions are assumed during the entire assessment period. The near-field and far-field models are handled similarly to the *global warming calculation case* in the main scenario, with the exceptions that no periods of periglacial climate domain are included. Also the transport pathways in the near-field and far-field are not expected to be affected by the surface climate, hence, the entire release is assumed to occur in biosphere object 157_2 as in the *global warming calculation case*.

The biosphere calculation case BCC3 *extended global warming* (Section 7.4.3 in the **Biosphere synthesis report**) for warmer and wetter climate conditions, is applied as the biosphere model in this calculation case. Assumptions on human behaviour and land-use are identical to the *global warming calculation case* in the main scenario.

4.3.6 Unclosed repository calculation case (CCR_UR)

The *unclosed repository calculation case* (CCR_UR) evaluates the dose from the *unclosed repository scenario*, which is selected since according to the regulations (SSM 2008:21), it is required to define and analyse a scenario that illustrates the consequences of an unclosed repository that is not monitored. As this calculation case is highly simplified and pessimistic, it was considered appropriate to apply only deterministic calculations.

In this calculation case, it is assumed that the repository is abandoned without being properly closed and sealed. The repository will become filled with water within a few years. However, since the groundwater that is pumped out of the repository today is relatively saline, it is not likely that the water volume that fills the repository will be used as a water supply as long as the repository is situated near the sea. On the other hand, it is not unreasonable to assume that the influx of meteoric water and limited remixing due to the difference in salinity and temperature could lead to the formation of a fresh water pool near the tunnel opening. Viewed over an extended period, fresh water could seep down into the repository and replace the saline water present there today with potable water. Hence, exposure to humans in this calculation case is assumed to occur when using water from the tunnel entrance as drinking water; this is the only considered exposure pathway in this calculation case. During the first 100 years it is assumed that knowledge of the hazard of the repository is preserved, therefore, doses are calculated from 100 years and onward after the repository has been abandoned.

Two variants of radionuclide inventories are considered: one is the inventory disposed of in SFR (same as in the *global warming calculation case*), the other includes waste intended for the SFL repository that is brought into SFR for interim storage (SKBdoc 1412250). The possible decrease of the radionuclide inventory due to release from the repository is not taken into account in this calculation case.

4.3.7 Glaciation and post-glacial conditions calculation case (CCR_GC)

The *glaciation and post-glacial conditions calculation case* evaluates the dose from the glaciation and post-glacial conditions scenario, which is selected to study the radiological consequences, from SFR, of a glaciation in the Forsmark region. The scenario is based on the ice-sheet development as described in the Weichselian glacial cycle climate case (**Climate report**, Section 4.4).

The first glacial period in the Weichselian glacial cycle climate case, which occurs between 59,600 AD and 68,200 AD, is chosen for the evaluation of the evolution of the repository and its environs in the glaciation and post-glacial conditions scenario. This glacial period is followed by a period of submerged conditions from 68,200 to 76,200 AD, in accordance with the climate case. During the remaining part of the assessment period, temperate climate conditions are assumed.

Based on the Weichselian glacial cycle climate case, continuous permafrost at repository depth is assumed to exist prior to the ice sheet advance over the site at 59,600 AD. Thus, no groundwater flow in the waste vaults is assumed during the passage of the advancing ice front over the repository. The permafrost remains at repository depth until 63,900 AD, when it has thawed. This is the starting point of the calculation case. No transport of radionuclides out of the repository is assumed to occur prior to this time. Thus, the radionuclide inventory in SFR at the starting point of this calculation case is determined by the inventory at closure and the radioactive decay and ingrowth that has occurred prior to 63,900 AD.

During the latter part of the glacial period, 63,900 AD to 68,200 AD, when the bedrock is unfrozen, radionuclides are transported from SFR to the Baltic Sea. Due to the isostatic depression of the bedrock at SFR, a substantial water depth is assumed in this part of the Baltic Sea. Therefore the radionuclides are assumed to spread over a larger part of the Baltic resulting in no accumulation of radionuclides in the sediments in the Forsmark area during this period in the calculation case.

The period from 63,900 AD, when the bedrock has thawed, until the deglaciation of Forsmark at 68,200 AD, has been divided into three parts with respect to groundwater flow, see Table 4-13. During these three parts, the groundwater flow is taken as one, two and three times, respectively, the groundwater flow in temperate terrestrial periods of the *loss of barrier function calculation case – high water flow in the repository* (Section 4.3.3).

During the 8,000 year submerged period following the glacial period, radionuclides transported out of SFR to the Baltic Sea are assumed to accumulate in the sediments above SFR. The period of the calculation case representing the submerged period after deglaciation and the transition to temperate terrestrial conditions, 68,200 AD to 76,200 AD is modelled (for the landscape development in the biosphere) in this calculation case based on the period from 5000 BC to 3000 AD in the *Weichselian glacial cycle climate case*.

Table 4-13. Summary of the glaciation and post-glacial conditions calculation case (1x, 2x etc. in the rightmost column denotes the scale factor used on the flow from the loss of barrier function calculation case – high water flows in the repository).

Time period	Climate domain above repository	Prevailing conditions at repository depth	Ice sheet surface gradients	Duration of period (years)	Groundwater flow as compared to temperate terrestrial conditions
Ice sheet advance over Forsmark 59,600–61,600 AD	Glacial	Frozen bedrock and no groundwater flow	High	2,000	No flow at repository depth
Continued ice sheet growth 61,600–63,900 AD	Glacial	Frozen bedrock and no groundwater flow	Intermediate to low	2,300	No flow at repository depth
Thawed bedrock conditions 63,900–66,200 AD	Glacial	Thawed bedrock with groundwater flow	Very low (comparable to non-glaciated conditions)	2,300	1x
Ice-sheet deglaciation 66,200–67,200 AD	Glacial	Thawed bedrock with groundwater flow	Low	1,000	2x
Deglaciation of the Forsmark site 67,200–68,200 AD	Glacial	Thawed bedrock with groundwater flow	Intermediate	1,000	3x
Submerged conditions above repository 68,200–76,200 AD	Temperate climate domain, but submerged conditions	Thawed bedrock with groundwater flow	–	8,000	0.2x
Terrestrial conditions above repository 76,200–102,000 AD	Temperate	Thawed bedrock with groundwater flow	–	25,800	1x

The subsequent temperate period is cautiously assumed to last until the end of the assessment period and the biosphere is modelled in the same way as for temperate periods in the main scenario. During this period, the near-field flow is based on the temperate terrestrial periods of the *loss of barrier function calculation case – high water flows in the repository*, as the barriers are assumed to be fully degraded by the glaciation. These flows are further scaled with the scale factors given in Table 4-13 (rightmost column).

In order not to underestimate the chemical and tectonic effects of a glaciation on the geosphere, the releases from the near-field are directed directly to the biosphere, i.e. to biosphere object 157_2 as in BCC1.

The landscape development in the *glaciation and post glacial calculation case* is identical to the global warming variant up to the first glaciation. At the end of the glaciation, the shoreline is assumed to be identical to the shoreline in Forsmark at 5000 BC with submerged conditions. Thereafter the landscape development is assumed to evolve as the development after the Weichselian glaciation. The biosphere calculation case BCC4 is applied for the submerged period.

4.4 Calculation cases for scenario combinations

In addition to the less probable scenarios, combinations of the less probable scenarios are clearly possible. In order to illustrate this, two scenario combinations have been generated, these are summarised in Section 2.2 in this report and presented in more details in the **Main report**, Section 7.8. The two calculation cases identified to analyse the scenario combinations are presented below.

4.4.1 Scenario combination 1 calculation case (CCC_SC1)

The *scenario combination 1 calculation case* evaluates the dose from the *scenario combination 1*. The calculation case combines the two calculation cases *high flow in the bedrock calculation case* and the *accelerated concrete degradation calculation case*, described in Section 4.2.2 and Section 4.2.3, respectively.

4.4.2 Scenario combination 2 calculation case (CCC_SC2)

Scenario combination 2 calculation case evaluates the dose from the *scenario combination 2*. The calculation case combines the two calculation cases *high flow in the bedrock calculation case* and the *high concentrations of complexing agents calculation case*, described in Section 4.2.2 and Section 4.2.6, respectively.

4.5 Summary

The calculation cases identified for the main scenario, for less probable scenarios, for residual scenarios and for the scenario combinations are summarised in Table 4-14 to 4-17. The tables include a short description of differences in the applied data sets with respect to the *global warming calculation case*, considered as the base case.

Table 4-14. Summary of the calculation cases identified for analysing the main scenario (the number in the brackets after a calculation case name refers to the section where it is presented in detail). Base case data refers to the *global warming calculation case (CCM_GW)*.

Calculation case	Brief description
CCM_GW Global warming calculation case (Section 4.1.2)	This case, considered as the base case, is defined to assess the <i>global warming climate variant of the main scenario</i> . It is assumed that the radionuclide releases do not begin until 1,000 years after closure of the repository. near-field: base case data far-field: base case data biosphere: base case data (BCC1)
CCM_EP Early periglacial calculation case (Section 4.1.2)	This case is defined to assess the <i>early periglacial climate variant of the main scenario</i> . It differs from the <i>global warming calculation case</i> during the period between 17,500 AD and 20,500 AD in which periglacial climate conditions are assumed, with releases of radionuclides restricted to taliks. near-field: base case data far-field: base case data biosphere: talik case during early periglacial period (BCC2)
CCM_TR Timing of the releases calculation case (Section 4.1.3)	In this case, the radionuclide release is assumed to commence directly after closure of the repository. near-field: immediate onset of releases from the near-field far-field: base case data biosphere: base case data
CCM_CD Collective dose (Section 4.1.4)	This case is defined to evaluate collective doses for a population in the Baltic region affected by the release of radionuclides to the Baltic Sea and for the global population exposed by C-14 releases to the atmosphere. near-field: immediate onset of releases from the near-field far-field: base case data biosphere: alternative geosphere–biosphere interface and dose models

Table 4-15. Summary of the calculation cases identified for analysing the less probable scenarios (the number in the brackets after a calculation case name refers to the section where it is presented in detail).

Calculation case	Brief description
CCL_IH High inventory calculation case (Section 4.2.1)	In this case a radionuclide inventory with higher activity than the best estimate inventory is applied. near-field: radionuclide inventories as 95 th percentile of their distribution of uncertainty far-field: base case data biosphere: base case data
CCL_FH High flow in the bedrock calculation case (Section 4.2.2)	This case applies higher water flows in bedrock and waste vaults. near-field: higher water flows by scaling far-field: higher water flows (bedrock case 11 in Odén et al. 2014) biosphere: base case data
CCL_BC Accelerated concrete degradation calculation case (Section 4.2.3)	In this case it is assumed that the hydraulic conductivity, diffusivity and porosity of the concrete increases earlier or to a greater extent than in the global warming calculation case. near-field: accelerated increase of water flows far-field: base case data biosphere: base case data
CCL_BB Bentonite degradation calculation case (Section 4.2.4)	In this case, the hydraulic properties of the bentonite around the silo are assumed to deteriorate due to the formation of an ice-lens during a period of periglacial climate conditions, with the consequence of higher water flow in the silo during a subsequent period of temperate climate conditions. near-field: after early periglacial period without flows onset of water flows for deteriorated bentonite conditions far-field: base case data biosphere: base case data

Table 4-15. Continued

Calculation case		Brief description
CCL_EQ	Earthquake calculation case (Section 4.2.5)	This case assumes increased water flows due to an earthquake damaging the silo structure. near-field: onset of water flows calculated specifically for the silo with earthquake damage far-field: excluded from the model chain (bypassed) biosphere: base case data; dose derived as maximum from all individually evaluated earthquake events
CCL_CA	High concentrations of complexing agents calculation case (Section 4.2.6)	In this case, concentrations of complexing agents higher than in the <i>global warming calculation case</i> are assumed, implemented in the calculations by increasing the concrete sorption reduction factor. near-field: reduced K_d values far-field: base case data biosphere: base case data
CCL_WD	Wells downstream of the repository calculation case (Section 4.2.7)	This case considers wells drilled into rock that are located downstream of and close enough to the repository that they are affected by potential releases from the repository. near-field: base case data far-field: base case data biosphere: garden plot land use with alternative well locations
CCL_WI	Intrusion wells calculation case (Section 4.2.8)	This case assumes that a well is drilled in the bedrock straight down into the waste vaults. near-field: base case data far-field: not included in the calculations biosphere: garden plot land use with alternative well locations

Table 4-16. Summary of the calculation cases identified for analysing the scenario combinations (the number in the brackets after a calculation case name refers to the section where it is presented in detail).

Calculation case		Brief description
CCC_SC1	Scenario combination 1 calculation case (Section 4.4.1)	The calculation case combines the two calculation cases <i>high flow in the bedrock calculation case</i> and the <i>accelerated concrete degradation calculation case</i> . This case applies higher water flows in bedrock and waste vaults. The hydraulic conductivity, diffusivity and porosity of the concrete increases earlier or to a greater extent than in the <i>global warming calculation case</i> . near-field: accelerated increase of water flows (see CCL_BC) and higher water flows by scaling (see CCL_FH) far-field: higher water flows (see CCL_FH) biosphere: base case data
CCC_SC2	Scenario combination 2 calculation case (Section 4.4.2)	The calculation case combines the two calculation cases <i>high flow in the bedrock calculation case</i> and the <i>high concentrations of complexing agents calculation case</i> . This case applies higher water flows in bedrock and waste vaults. Augmented concentrations of complexing agents are implemented by increasing the concrete sorption reduction factor with respect to the <i>global warming calculation case</i> . near-field: higher water flows by scaling (see CCL_FH), reduced K_d values (see CCL_CA) far-field: higher water flows (see CCL_FH) biosphere: base case data

Table 4-17. Summary of the calculation cases identified for analysing the residual scenarios (the section number or report in the brackets after a calculation case name refers to where it is presented in detail).

Calculation case	Brief description
CCR_B1	<p>Loss of barrier function calculation case – no sorption in the repository (Section 4.3.1)</p> <p>In this calculation case, it is postulated that radionuclides are not sorbed in the repository, which is implemented by setting sorption partitioning coefficients for all materials in the near-field to zero.</p> <p>near-field: zero K_d values far-field: base case data biosphere: base case data</p>
CCR_B2	<p>Loss of barrier function calculation case – no sorption in the bedrock (Section 4.3.2)</p> <p>In this calculation case, it is postulated that no sorption of radionuclides occur in the bedrock, which is implemented by setting all sorption partitioning coefficients in the far-field to zero.</p> <p>near-field: base case data far-field: zero K_d values biosphere: base case data</p>
CCR_B3	<p>Loss of barrier function calculation case – high water flows in the repository (Section 4.3.3)</p> <p>This case demonstrates the importance of the engineered barriers in the repository to limit the water flow by applying near-field water flows, porosities and diffusivities of the “no barriers” flow case.</p> <p>near-field: “no barriers” water-flow case far-field: base case data biosphere: base case data</p>
CCR_RX	<p>Changed repository redox conditions in SFR 1 calculation case (Section 4.3.4)</p> <p>This case assumes oxidising conditions in the repository for the redox-sensitive elements. An alternative set of sorption partitioning coefficients in the near-field is used for Tc, Pu, U, Np, Pa and Se.</p> <p>near-field: K_d values for oxidising conditions for redox-sensitive elements far-field: base case data biosphere: base case data</p>
CCR_EX	<p>Extended global warming calculation case (Section 4.3.5)</p> <p>In this case it is assumed that temperate climate conditions prevail during the entire assessment period (i.e. no periods of periglacial climate conditions).</p> <p>near-field: base case data far-field: base case data biosphere: BCC3</p>
CCR_UR	<p>Unclosed repository calculation case (Section 4.3.6)</p> <p>In this case it is assumed that the repository is abandoned without being closed and sealed and future humans use water from the tunnel entrance as drinking water.</p> <p>near-field: base case data in simplified stirred tank model far-field: not applicable biosphere: ingestion of drinking water only</p>
CCR_GC	<p>Glacial and post-glacial conditions calculation case (Section 4.3.7)</p> <p>This calculation case studies the potential consequences of glaciations, assessing the consequences of melt water flow during deglaciation and of deteriorated technical and geological barriers thereafter.</p> <p>near-field: no transport until year 59,600 AD, upscaled water flows for melt water flushing, water flows for completely degraded barriers thereafter far-field: not applied biosphere: BCC4, BCC1</p>
CCFHA1	<p>Exposure of the on-site crew during the drilling event (see FHA report)</p> <p>In this case, drilling into the waste vaults brings radioactive material to the surface in the drill detritus. Doses are evaluated for workers at the drill site.</p> <p>near-field: homogenous distribution of radionuclides and materials per waste vault far-field: not applicable biosphere: irradiation (from core detritus), dust inhalation and inadvertent ingestion of core detritus</p>
CCFHA2	<p>Exposure during construction on drilling detritus landfill (see FHA report)</p> <p>In this case, drilling into the waste vaults brings radioactive material to the surface in the drill detritus which is disposed of in a shallow uncovered landfill at the drill site. Doses are evaluated for a worker during construction on this landfill.</p> <p>near-field: homogenous distribution of radionuclides and materials per waste vault far-field: not applicable biosphere: irradiation (from ground and attached soil), dust inhalation and inadvertent soil ingestion</p>
CCFHA3	<p>Exposure due to cultivation on drilling detritus landfill (see FHA report)</p> <p>In this case, drilling into the waste vaults brings radioactive material to the surface in the drill detritus which is disposed of in a shallow uncovered landfill at the drill site. Doses are evaluated for a member of a family using the contaminated landfill as a garden plot for cultivating vegetables.</p> <p>near-field: homogenous distribution of radionuclides and materials per waste vault far-field: not applicable biosphere: garden plot land use with detritus inventory distributed in the soil</p>

5 Results for calculation cases in the main scenario

This chapter presents results for the calculation cases in the main scenario (Section 4.1).

Four calculation cases were identified for the analysis of the main scenario: the *global warming calculation case* (CCM_GW), the *timing of the releases calculation case* (CCM_TR), the *early periglacial calculation case* (CCM_EP) and the *collective dose calculation case* (CCM_CD). Generally, a period of 100,000 years is simulated starting from the closure of the repository (~ 2075 AD). Output is generated every 50 years of simulated time.

Monte Carlo simulations with Latin-hypercube sampling (McKay et al. 1979) were performed using 100 iterations for the near-field and far-field. The data set from these calculations was used as input to Monte Carlo simulation of the biosphere and dose calculations, using 1,000 iterations. Each realisation of a set of input parameters for the near-field and far-field is matched with 10 realisations of input parameter sets for the biosphere resulting in 1,000 input parameter sets for the entire modelling chain.

Radiotoxicity of releases, i.e. mean releases from the near-field and from the far-field transformed to (ingestion) radiotoxicity are presented for the most dominant radionuclides, with respect to radiotoxicity.

Annual effective doses for humans are calculated for representative individuals of four exposed populations, each associated with a unique variant of land-use: H&G, IO, DM and GP exposed groups. Details of the approach for calculations of doses to humans can be found in Section 9.5 and in Saetre et al. (2013).

Exposure to these representative individuals is considered in several potentially contaminated biosphere objects. The maximum dose across all land-use variants and biosphere objects at each point of time is the most important presented time-dependent performance indicator for a calculation case. The maximum over time of this maximum dose defines peak dose, which is the quantity carried on to the risk assessment,

A listing of results comprising peak release from the near-field and far-field and peak doses including time of occurrence for all radionuclides can be found in Appendix E. The doses derived in the calculation cases have subsequently been used for estimating the radiological risks associated with the repository. Quantification of risks is presented in Chapter 10 of the **Main report**.

5.1 Global warming calculation cases

Two calculation cases are identified for analysing the *global warming variant* of the main scenario. These two calculation cases are the *global warming calculation case* (described in Section 4.1.1) and the *timing of the releases calculation case* (described in Section 4.1.3). Results from these two calculation cases are presented below.

5.1.1 Global warming calculation case (CCM_GW)

In CCM_GW, releases of radionuclides from the repository begin after the conditions above SFR have changed to terrestrial. This assumption ensures that there are no releases during the initial submerged state of the potential exit points in the near-surface environment; any such releases would be diluted in the sea with low radiological impact. This assumption is implemented in this calculation case by not activating any transport processes during the first 1,000 years.

Releases

The arithmetic mean of releases from the near-field and the far-field of 100 simulation runs with randomly sampled input parameters is discussed below. For many radionuclides, the radiotoxicity

of the releases from the near-field is highest shortly after the release is initiated (3000 AD) and declines as the repository becomes gradually depleted of activity, by radioactive decay and release (Figure 5-1). The rates of release vary as a function of depletion in individual waste vaults, changes in the near-field hydrology and degradation of the engineered barriers. For vaults with engineered barriers, the peak is delayed due to the barriers and, this can be seen e.g. for the peak release of C-14-org which is mainly deposited in the silo and 1BMA vaults, which both have relatively effective barriers. For progeny (e.g. Po-210) the releases increase with time, as the initial inventories of these radionuclides are small compared with the activity from in-growth due to radioactive decay of the parent radionuclides.

At 22,000 AD there is a distinct increase in the radiotoxicity of the near-field releases, as both the water fluxes and the effective diffusivity in the 1BMA and 2BMA vaults increase due to degradation of the engineered barriers. At 52,000 AD there is another increase of diffusivity and water fluxes, however this time coincides with the first period of periglacial conditions and the resulting increase in the radiotoxicity of the near-field releases becomes visible only after this first periglacial period.

Figure 5-2 shows the radiotoxicity of the releases from the far-field. For most radionuclides the geosphere causes a smoothing of the initial peak release, this applies e.g. to U-235, U-238 and Tc-99. For short-lived radionuclides with high sorption, the geosphere also causes a significant reduction of the steady-state release, due to the relatively long residence-time in the geosphere, during which the radionuclides undergo radioactive decay. For progeny e.g. Pa-231, Ac-227 and Ra-226 the effect of the geosphere is the opposite, the progeny have time to grow-in during the delay of parent nuclides in the geosphere. For Ni-59, the far-field has a small transport limiting effect. Mo-93 shows up in Figures 5-1 and 5-2 as one of the less important of the top 15 dominating radionuclides with respect to releases; however, Mo-93 dominates the peak annual dose in this calculation case, see Table 5-1 or Figure 5-4 below.

Annual doses

Time series of the maximum annual effective doses (across all biosphere objects and exposed groups) are presented in Figure 5-3. In the same figure, annual effective doses for different exposed groups are also shown for biosphere object 157_2, for which the peak annual effective dose is observed. For periods of periglacial conditions doses are only relevant for the exposed group *H&G*. The same figure also includes a dashed line at 14 μSv , which is the annual effective dose that corresponds to the annual risk constraint of 10^{-6} for a representative individual in the group exposed to the greatest risk (SSMFS 2008:37).

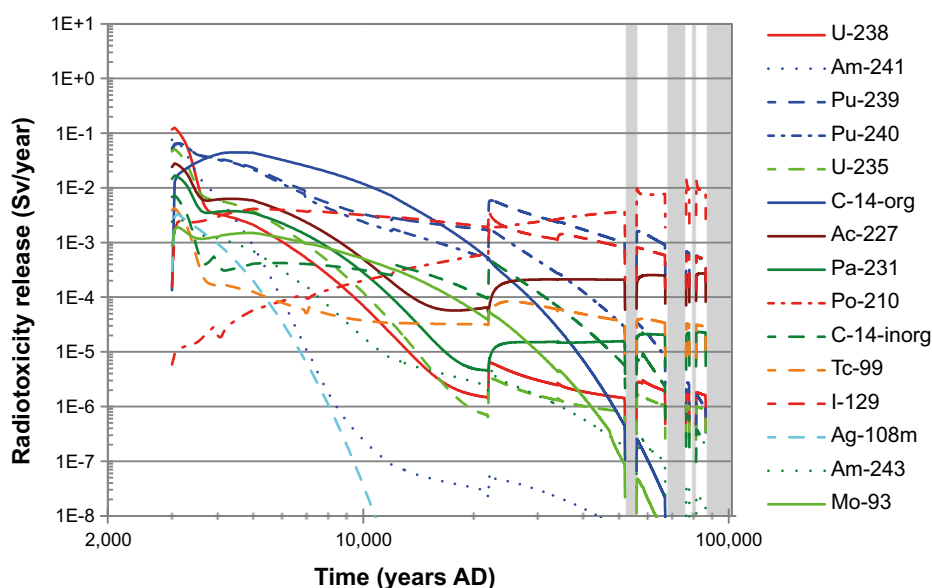


Figure 5-1. Arithmetic mean of the radiotoxicity of releases from the near-field for the 15 dominating radionuclides in the **global warming calculation case (CCM_GW)**. The unshaded areas correspond to temperate climatic conditions and the grey shaded areas to periglacial conditions with continuous permafrost.

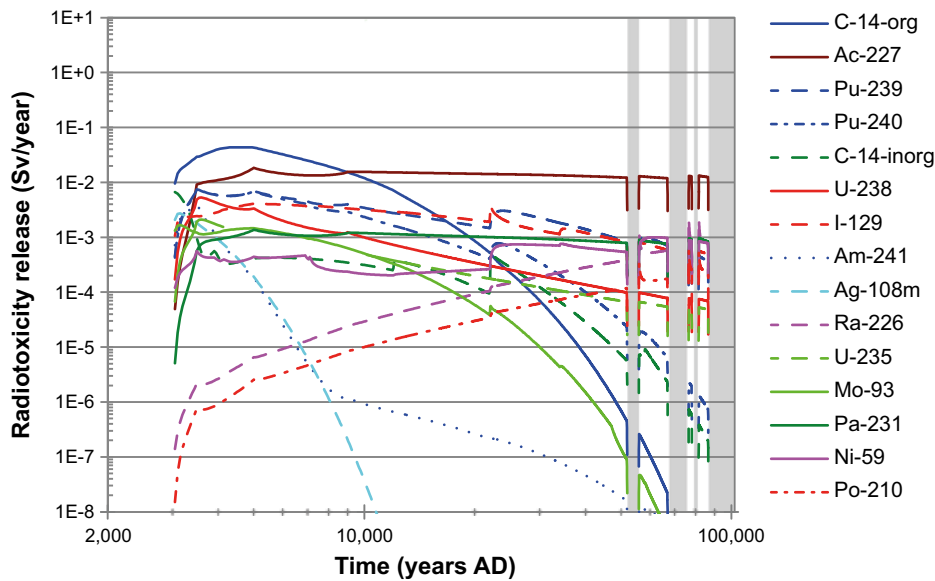


Figure 5-2. Arithmetic mean of the radiotoxicity of releases from the far-field for the 15 dominating radionuclides in the **global warming calculation case (CCM_GW)**. The unshaded areas correspond to temperate climatic conditions and the grey shaded areas to periglacial conditions with continuous permafrost.

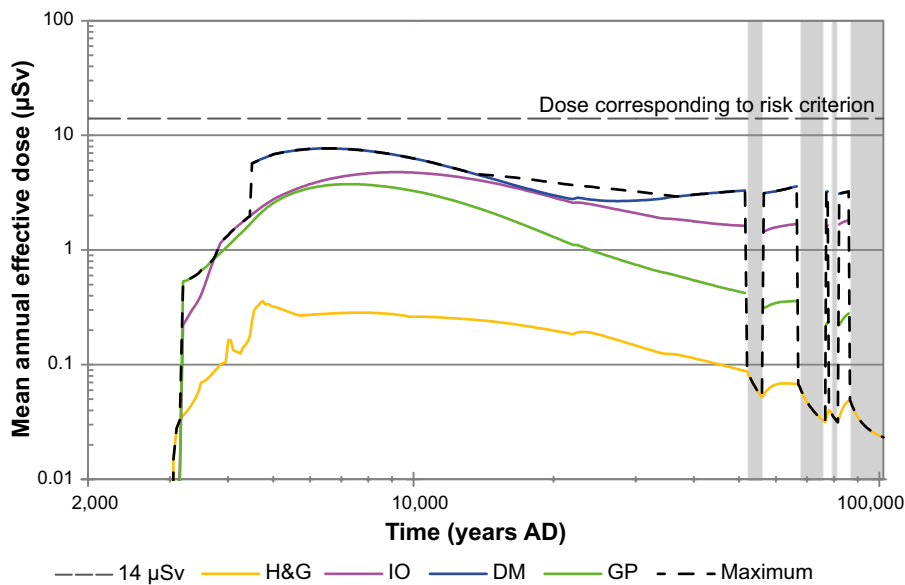


Figure 5-3. Arithmetic mean of the annual effective dose for the different exposed groups in object 157_2 and maximum annual effective dose across all exposed groups and biosphere objects for the **global warming calculation case (CCM_GW)**. The unshaded areas correspond to temperate climatic conditions and the grey shaded areas to periglacial conditions with continuous permafrost.

The dynamics of the maximum annual dose curve (Figure 5-3) reflects the dynamics of radionuclide releases from the repository, as well as the development of the surface system. The peak annual dose occurs about 6500 AD, this is 3,450 years after the releases begin. This delay is due to the retention of radionuclides in the engineered barriers and the geosphere. Large amounts of the mobile C-14-org is stored in the silo and BMA, and the engineered barriers of these vaults delay the onset of the release also for this mobile radionuclide. The less mobile radionuclides from these vaults do not contribute significantly to the dose at this early time-point, due to the very large delay of these radionuclides in the engineered barriers. The contribution to peak dose from U-238 and U-235 comes from the BLA vault where the delay is mainly due to the geosphere.

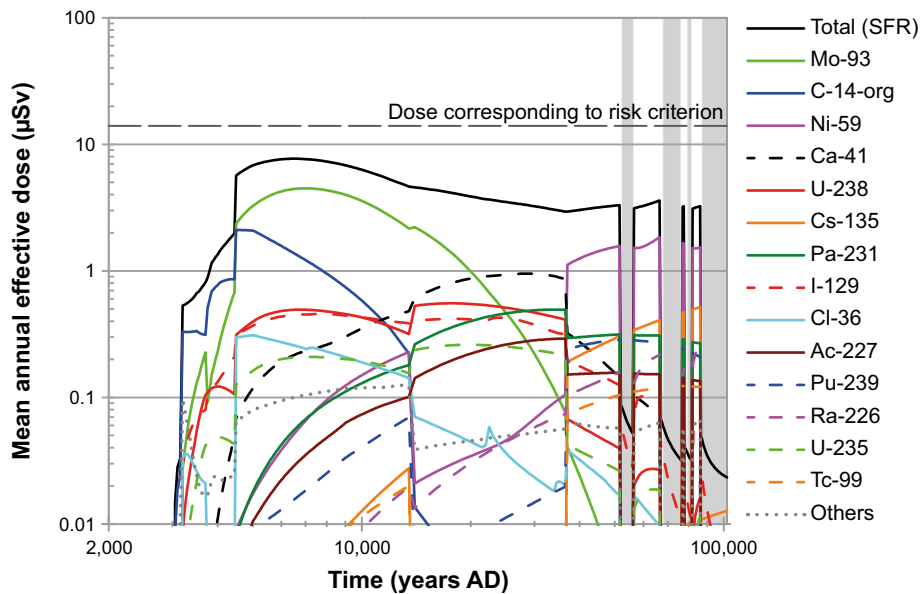


Figure 5-4. Arithmetic mean of the annual effective dose to the most exposed group for releases from the entire repository in the *global warming calculation case (CCM_GW)*. The unshaded areas correspond to temperate climatic conditions and the grey shaded areas to periglacial conditions with continuous permafrost.

Table 5-1. Peak annual dose (and related data) to a representative individual of the most exposed group obtained for the *global warming calculation case (CCM_GW)*.

Annual dose (µSv)	Year (AD)	Contribution from waste vault (%)	Contribution from radionuclides (%)	Exposed group (biosphere object)
7.7	6500	Silo (45.3)	Mo-93 (57.7)	Drained-mire farmers
		1BMA (15.8)	C-14-org (17.9)	(Object 157_2)
		1BLA (11.9)	U-238 (6.4)	
		2BMA (8.4)	I-129 (5.8)	
		2BTF (5.0)	Cl-36 (3.3)	
		BRT (4.2)	Ca-41 (2.8)	
		1BTF (4.1)	U-235 (2.7)	
		2BLA (1.4)	Others (4.1)	
		5BLA (1.4)		
		3BLA (1.3)		
		4BLA (1.3)		

The peak annual dose is observed for the *DM* exposed group (7.7 µSv) in biosphere object 157_2, which is receiving the releases directly from the geosphere. The major exposure pathway for this group is ingestion of food originating from cultivation on drained land where radionuclides have accumulated since the start of the release. Thereafter, the annual doses during temperate periods only slightly decrease until the first period of periglacial conditions and then slightly increase again during the subsequent temperate period. Hence, after the point in time when the peak annual dose is observed, there is only a small variation of the maximum annual dose. One exception is for the periods of periglacial conditions when much lower doses are observed because agriculture is deemed unlikely and extraction of groundwater from a well is impossible under these conditions. It can also be noted that the exposure of *H&G* under periglacial periods only decreases slowly, in spite of the interruption of releases from the near-field and the far-field. This indicates that dose contributing radionuclides (e.g. I-129) that have accumulated in regolith layers deplete only slowly in the biosphere during these periods.

During an interim period after the peak dose, which is defined by *DM* cultivating biosphere object 157_2, the maximum annual dose (across all biosphere objects and exposed groups) is defined by *DM* cultivating the down-stream biosphere object 157_1, see Figure 5-3. This object 157_1 has a lake stage before becoming a mire, and cultivation of the thick peat layer that develops in the lake basin yields a higher dose than in the upstream object due to accumulation of radionuclides retained in, or adsorbed to, organic matter (e.g. Mo-93, Ca-41 and U-238), see Figure 5-4.

The peak annual dose is presented in Table 5-1 for the exposed population with the highest doses (*DM*). The peak annual dose is dominated by a few radionuclides that have a high mobility in the near-field and the far-field but accumulate in peat layers in the biosphere. Those are Mo-93, organic C-14, U-238, I-129, Cl-36, Ca-41 and U-235, which together contribute almost 97% of the peak annual dose.

The main contribution from waste vaults to the peak annual dose for the *DM* exposed group comes from the silo, 1BMA, 1BLA, 2BMA and 2BTF, which together contribute to about 90% of the total annual dose (Figure 5-5). The peak annual dose due to exposure from releases from all waste vaults together occurs at year 6500 AD, whereas the point in time when the peak contributions from the individual vaults occur spread across a period of more than 60,000 years from 4800 AD with 0.52 µSv from 2BTF to 66,500 AD with 1.77 µSv from 1BMA, as seen in Table 5-2. A summary of peak annual dose from each of the waste vaults is given in Table 5-2. These are presented together with the time of occurrence and exposed group, location and the most contributing radionuclide.

Table 5-2. Peak contributions to annual dose and the time at which the peak is observed for releases from individual waste vaults and from the entire repository in the *global warming calculation case*. The radionuclides with the highest contribution to the peak are indicated.

Waste vault	Annual dose (µSv)	Year (AD)	Biosphere Object	Exposed group	Most contributing radionuclide (%)
Silo	3.55	7200	157_2	DM	Mo-93 (49.2)
1BMA	1.77	66,500	157_2	DM	Ni-59 (65.4)
1BLA	1.34	24,000	157_1	DM	U-238 (30.5)
1BTF	0.42	4950	157_2	DM	Mo-93 (68.5)
2BTF	0.52	4800	157_2	DM	Mo-93 (74.0)
BRT	0.37	5450	157_2	DM	Mo-93 (98.7)
2BMA	0.88	10,500	157_2	DM	Mo-93 (68.8)
2BLA	0.11	21,000	157_1	DM	Ca-41 (39.1)
3BLA	0.10	6050	157_2	DM	Mo-93 (43.3)
4BLA	0.12	20,000	157_1	DM	Ca-41 (39.9)
5BLA	0.13	22,500	157_1	DM	Ca-41 (34.8)
Total SFR	7.69	6500	157_2	DM	Mo-93 (57.7)

Figure 5-6 to Figure 5-10 show the mean annual doses to the most exposed group over the entire simulation period due to releases from the waste vaults silo, 1BMA, 1BLA, 2BMA and 2BTF respectively. The total dose and the contributions from main radionuclides are presented. The silo, which contains the majority of the radionuclide content, contributes only 45% of the peak annual dose (at year 6500 AD) demonstrating the significance of the engineered barrier system in delaying the release of radionuclides until a substantial amount of decay has occurred. For the silo, the main contribution to the peak annual dose comes from Mo-93 and organic C-14, followed by I-129 and Cl-36. The peak annual dose for only 1BMA is dominated by Ni-59, Cs-135, Pu-239 and Tc-99. However, the contribution to the total peak annual dose (at 6500 AD) from 1BMA is also dominated by Mo-93 and C-14-org. For 1BLA, U-238, U-235 and its progeny (Pa-231 and Ac-227) together with Mo-93 are the radionuclides that contribute most to the peak annual dose (at 6500 AD). The dose contribution of Ca-41 shown in Figure 5-4 and Figure 5-9 comes mainly from the concrete decommissioning waste in 2BMA, but 2BMA also has a large contribution from Mo-93 at the time of peak annual dose (6500 AD). The dose from 2BTF is also dominated by Mo-93 which is the only radionuclide that contributes substantially from all of these five waste vaults, with contributions to the peak annual dose (at year 6500 AD) as follows: silo (21%), 1BMA (7%), 2BMA (6%), 2BTF (3%) and 1BLA (3%).

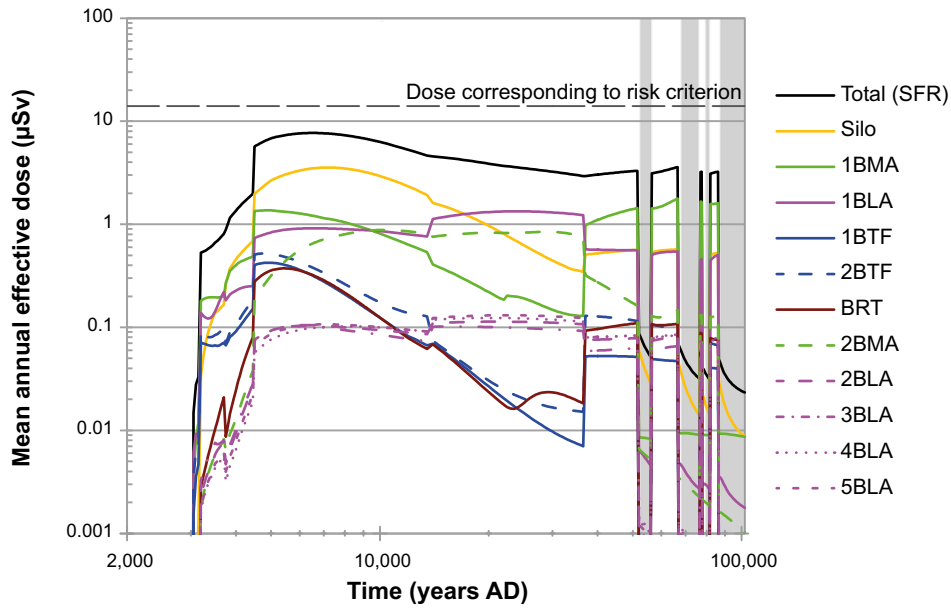


Figure 5-5. Arithmetic mean of the annual effective dose to the most exposed group, for releases from the entire repository and contributions from the individual waste vaults, in the **global warming calculation case** (CCM_GW). The unshaded areas correspond to temperate climatic conditions and the grey shaded areas to periglacial conditions with continuous permafrost.

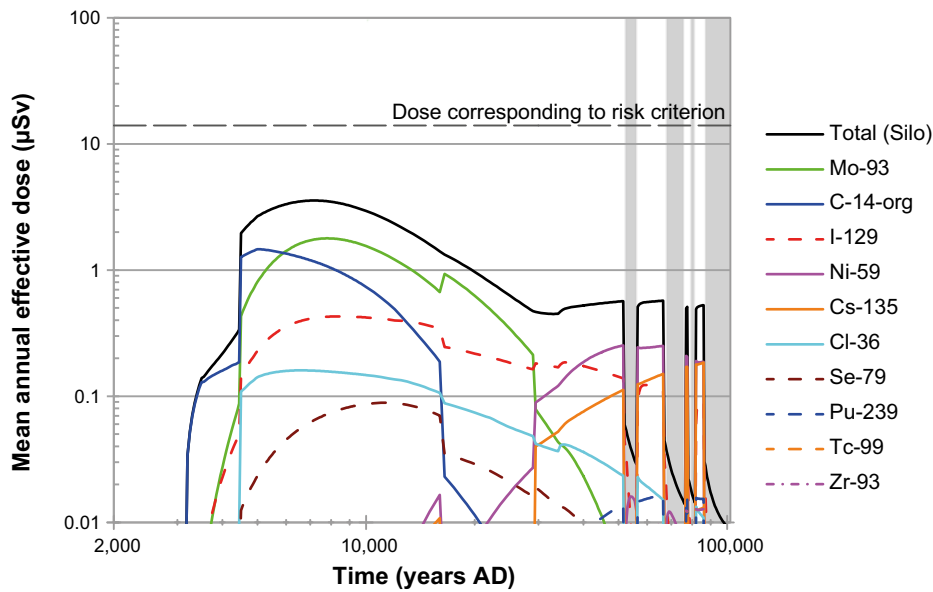


Figure 5-6. Arithmetic mean of the annual effective dose to the most exposed group for releases from the **Silo** in the **global warming calculation case** (CCM_GW). The unshaded areas correspond to temperate climatic conditions and the grey shaded areas to periglacial conditions with continuous permafrost.

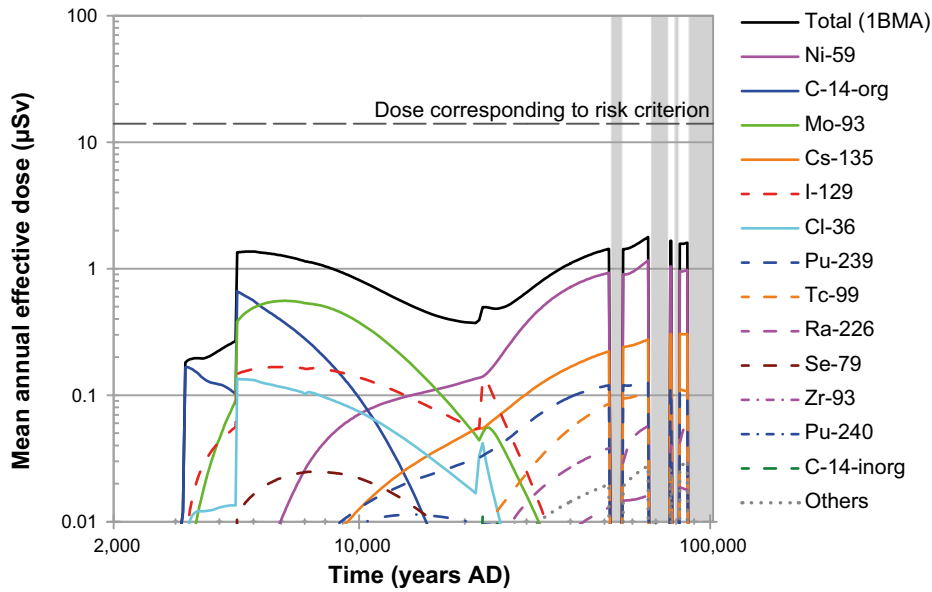


Figure 5-7. Arithmetic mean of the annual effective dose to the most exposed group for releases from **IBMA** in the **global warming calculation case (CCM_GW)**. The unshaded areas correspond to temperate climatic conditions and the grey shaded areas to periglacial conditions with continuous permafrost.

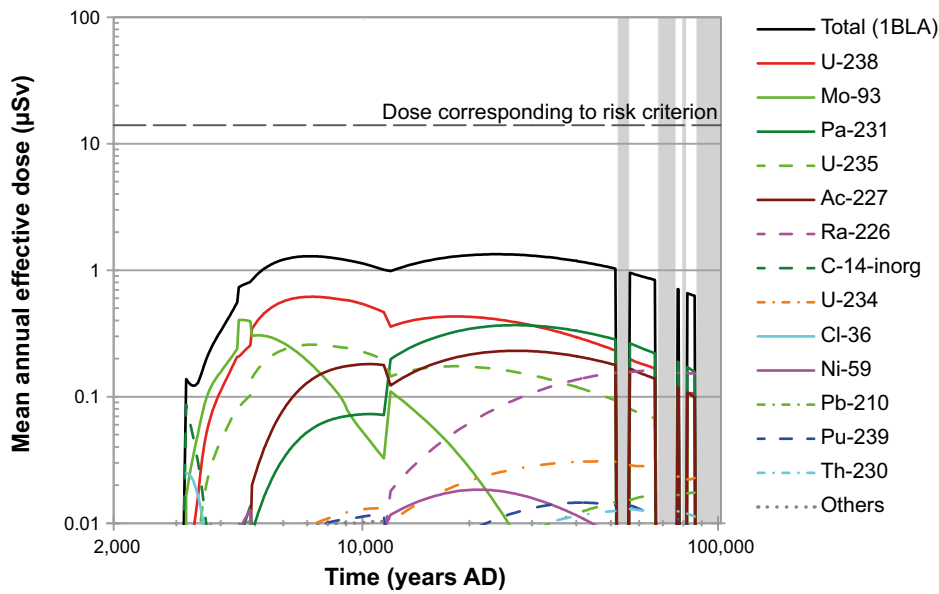


Figure 5-8. Arithmetic mean of the annual dose to the most exposed group for releases from **1BLA** in the **global warming calculation case (CCM_GW)**. The unshaded areas correspond to temperate climatic conditions and the grey shaded areas to periglacial conditions with continuous permafrost.

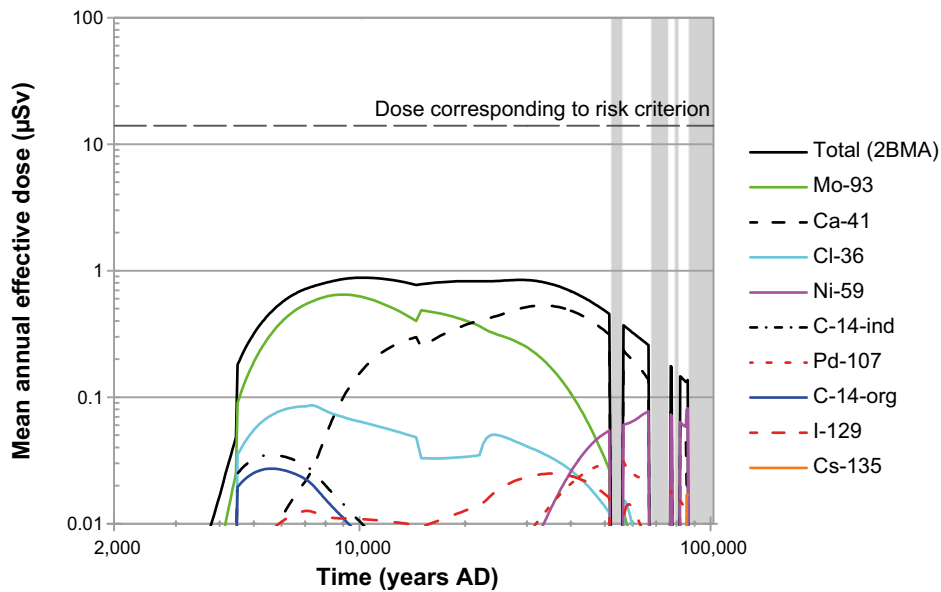


Figure 5-9. Arithmetic mean of the annual dose to the most exposed group for releases from **2BMA** in the **global warming calculation case (CCM_GW)**. The unshaded areas correspond to temperate climatic conditions and the grey shaded areas to periglacial conditions with continuous permafrost.

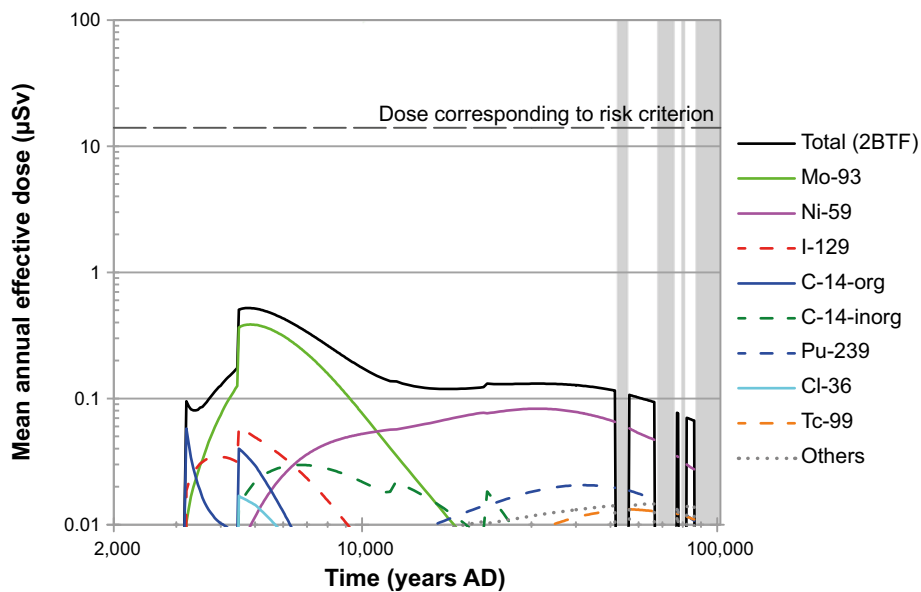


Figure 5-10. Arithmetic mean of the annual dose to the most exposed group for releases from **2BTF** in the **global warming calculation case (CCM_GW)**. The unshaded areas correspond to temperate climatic conditions and the grey shaded areas to periglacial conditions with continuous permafrost.

Impact of parameter uncertainty

The results presented above are arithmetic mean values of the annual effective doses derived from the probabilistic (Monte Carlo) simulations. From the same probabilistic results, other relevant statistics have been derived, such as the median and different percentiles of the annual dose distribution at each time point. These statistical values provide an estimate of the uncertainties of the calculated doses with respect to the uncertainties of input parameters in the calculation case. The different statistical values obtained are presented in Figure 5-11, including the arithmetic mean, median, and 5th and 95th percentiles of the maximum annual dose.

In Figure 5-11, the arithmetic mean of the annual dose at a specific point in time is defined by the dose distribution of the exposed group that receives the maximum dose. Since the most exposed group shifts over time, the uncertainty will change due to the fact that exposure from different radionuclides, biosphere objects and exposure scenarios involve different uncertainties. It can be specifically noted, that the uncertainty (i.e. the bandwidth of the distribution of annual dose) increases when the maximum dose defining biosphere object switches from *DM* in biosphere object 157_2 (into which radionuclides are discharged) to *DM* in the (downstream) biosphere object 157_1 around 15,000 AD. This can be expected as the potential number of compartments and parameters affecting the results increase with transport length. In addition, the uncertainty or variation in input parameters is different for different biosphere objects. The parameters that contribute most to the uncertainty are further discussed in Appendix F.

Uncertainty related to sample size

The limited number of iterations in the Monte Carlo simulations has an impact on the robustness of the result. Repeating the sampling does not result in exactly the same parameter sample values and hence statistics of the result such as the mean (annual dose) will not obtain exactly the same value. To evaluate the robustness of the arithmetic mean a 95% confidence interval of the mean of the annual dose to the *DM* exposed group in biosphere object 157_2 has been calculated, see Figure 5-12. The confidence interval is calculated using a bootstrap function (DiCiccio and Efron 1996) resulting from the sample of size 1,000 (Efron and Tibishirani 1993). This analysis shows that the uncertainty of the mean due to Monte-Carlo sampling (Figure 5-12) is small compared with the uncertainty caused by the overall parameter uncertainty (Figure 5-11). Moreover, the upper boundary for the 95% confidence interval (8.2 μSv) of the peak mean annual dose is less than 10% higher than the peak mean annual dose (7.7 μSv) used in the assessment (Table 5-1).

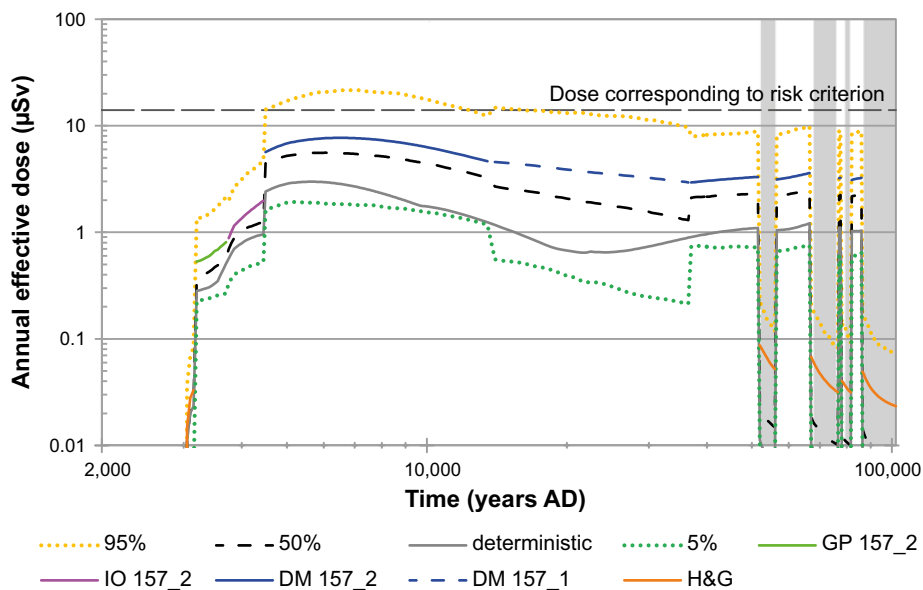


Figure 5-11. Arithmetic mean, median, 5th and 95th percentiles of the annual dose to the most exposed group from SFR in the **global warming calculation case (CCM_GW)**. The group receiving the highest dose shifts over time, and for clarity doses to other groups are not displayed in the figure. The dose from deterministic calculations is displayed as a reference. The unshaded areas correspond to temperate climatic conditions and the grey shaded areas to periglacial conditions with continuous permafrost.

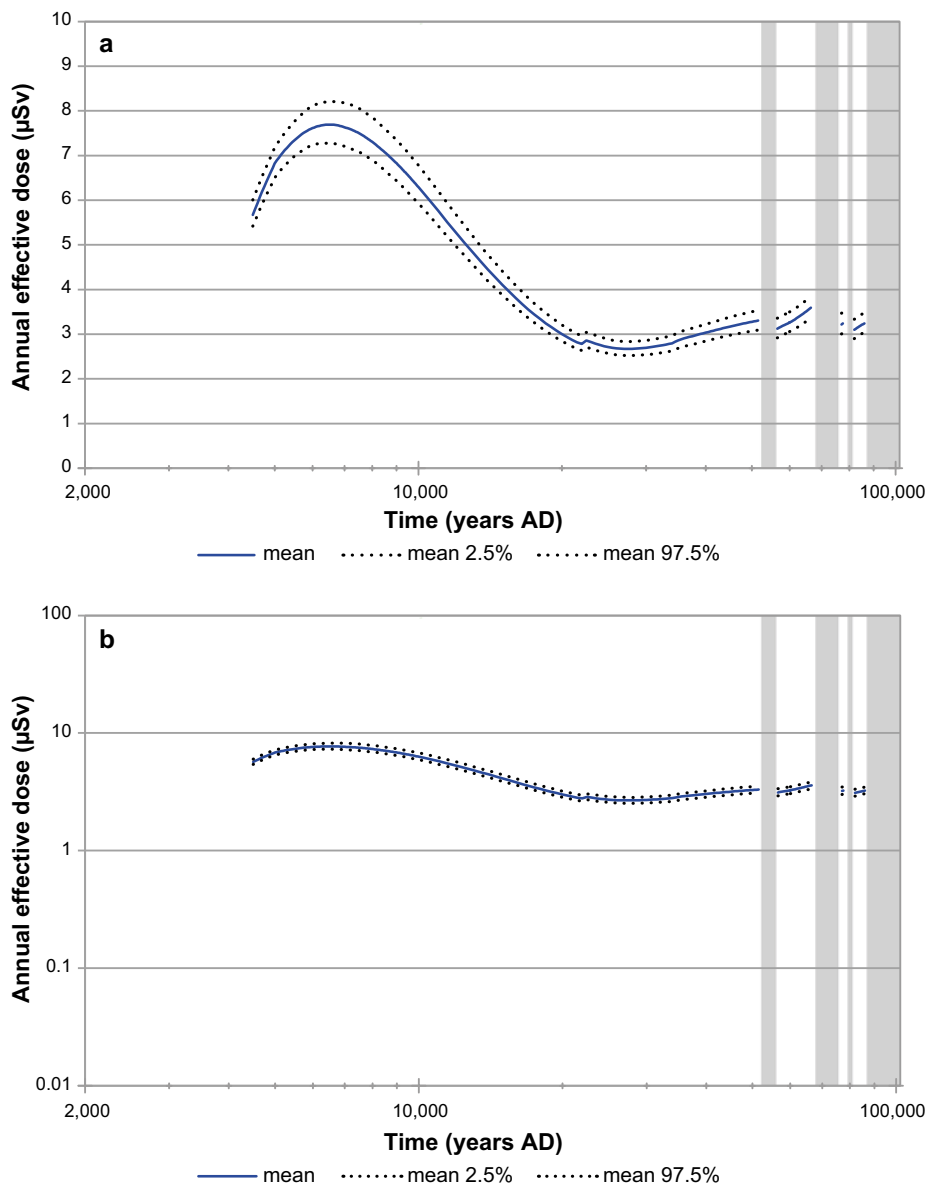


Figure 5-12. Arithmetic mean and 95% confidence interval of the mean of the annual dose to the DM exposed group in biosphere object 157_2 in the **global warming calculation case (CCM_GW)**. The unshaded areas correspond to temperate climatic conditions and the grey shaded areas to periglacial conditions with continuous permafrost. The lower figure is shown in logarithmic scale (as in the previous figures, e.g. Figure 5-11). The upper figure is shown in linear scale, needed to show the difference.

5.1.2 Timing of the releases calculation case (CCM_TR)

The *timing of the releases calculation case (CCM_TR)* is the second calculation case for the *global warming variant* of the main scenario identified for the assessment of individual dose. The release is assumed to start right at the beginning of the assessment period. This calculation case has been carried out with the purpose of studying the effect on the outcome of the safety assessment of assuming releases during the submerged period, and to provide input to the calculation of collective doses (Section 5.3).

Releases

The releases in this calculation case, and hence the radiotoxicity, differ considerably from the *global warming calculation case* with respect to short-lived radionuclides such as Ni-63, Cs-137 and Ag-108m (compare Figure 5-1 and Figure 5-13). However, the effect of an instant release of short-lived radionuclides is not significant for the total radiotoxicity released from the far-field (Figure 5-14) or for the peak annual doses, see results below.

Annual doses

The peak annual dose resulting from *timing of the releases calculation case* (Table 5-3) is similar to that for the *global warming calculation case* (Table 5-1). The doses are slightly higher (about 6%) due to accumulation of Mo-93 in sediments during the submerged period.

Figure 5-15 illustrates dose during the first 1,000 years. Due to submerged conditions during this period the only exposed groups are *H&G* and *GP* (the latter by fertilising the soil with contaminated marine macrophytes). Doses due to early releases are mainly caused by organic C-14.

Table 5-3. Peak annual dose (and related data) to a representative individual of the most exposed group obtained for the *timing of the releases calculation case* (CCM_TR).

Annual dose (µSv)	Year (AD)	Contribution from waste vault (%)	Contribution from radionuclides (%)	Exposed group (biosphere object)
8.2	6000	Silo (45.8) 1BMA (16.1) 2BMA (9.9) 1BLA (9.3) 2BTF (5.2) BRT (4.3) 1BTF (4.3) 5BLA (1.3) 2BLA (1.3) 3BLA (1.3) 4BLA (1.2)	Mo-93 (61.4) C-14-org (17.9) I-129 (5.6) U-238 (4.7) Cl-36 (3.2) Ca-41 (2.6) U-235 (2.0) Others (2.7)	Drained-mire farmers (Object 157_2)

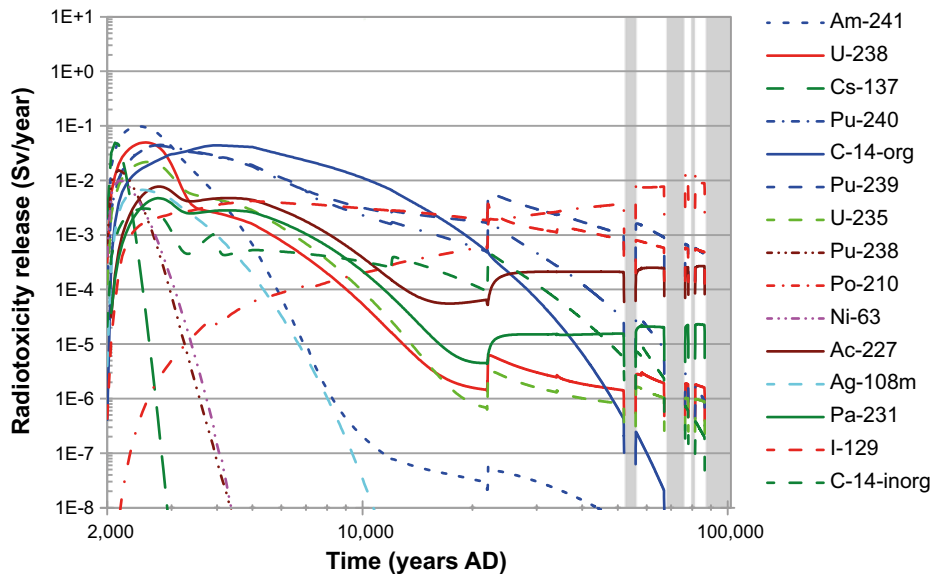


Figure 5-13. Arithmetic mean of the radiotoxicity of releases from the near-field for the 15 dominating radionuclides in the *timing of the releases calculation case* (CCM_TR). The unshaded areas correspond to temperate climatic conditions and the grey shaded areas to periglacial conditions with continuous permafrost.

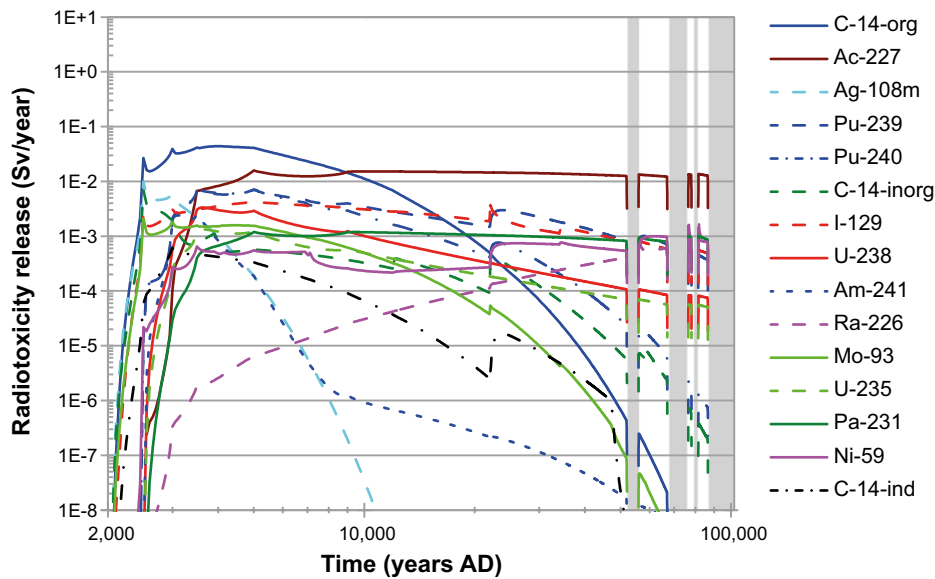


Figure 5-14. Arithmetic mean of the radiotoxicity of releases from the far-field for the 15 dominating radionuclides in the **timing of the releases calculation case** (CCM_TR). The unshaded areas correspond to temperate climatic conditions and the grey shaded areas to periglacial conditions with continuous permafrost.

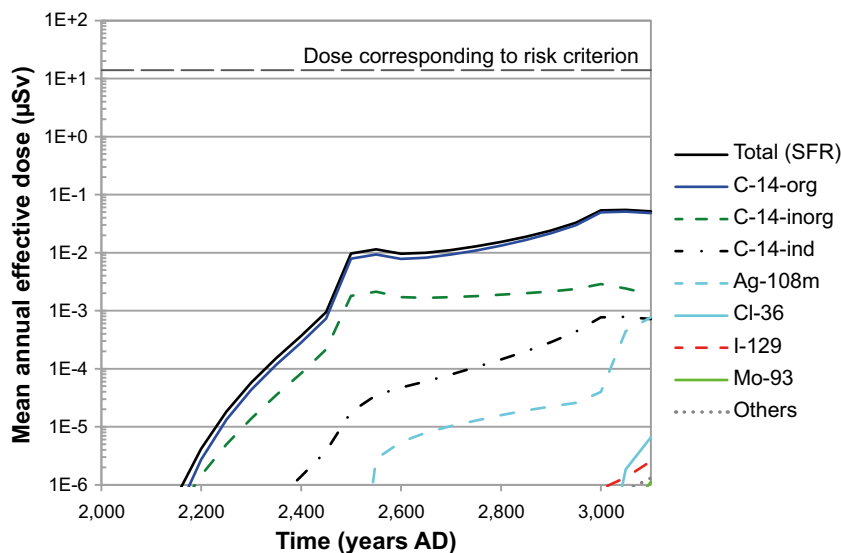


Figure 5-15. Arithmetic mean of the total annual dose during the submerged period in the **timing of the releases calculation case** (CCM_TR). The highest exposure during this period occurs for H&G.

5.2 Early periglacial calculation case (CCM_EP)

The *early periglacial calculation case* of the main scenario does not differ from the *global warming calculation case* except for a period of periglacial conditions with shallow permafrost in Forsmark during a period of minimum insolation around 17,500 AD to 20,500 AD. The identified *early periglacial calculation case* (CCM_EP) thus focuses on the period 17,500 AD to 20,500 AD (see Section 4.1.2).

Due to the similarities with the *global warming variant* of the main scenario beyond the end of the early periglacial period at 20,500 AD, it is sufficient to analyse the *early periglacial variant* with a calculation case that ends at 20,500 AD. Since the results in this calculation case up to 17,500 AD are identical with the results in the *global warming calculation case*, the discussion below addresses only the period of periglacial conditions.

During the periglacial period, discharge of deep groundwater, and hence releases of radionuclides, will be restricted to taliks, which are unfrozen areas in the otherwise frozen landscape. Simulations of surface hydrology under periglacial conditions (Bosson et al. 2010, Werner et al. 2013) suggest that a discharge talik may be formed under a small wetland area (biosphere object 157_1 just north of the primary release area during periods of temperate conditions). Moreover, the deep lake of biosphere object 114, located in Öregrundsgrepen, will still be open, and is thus likely to be connected with a discharge talik (Bosson et al. 2013, Werner et al. 2013), see Section 4.1.2. In this calculation case, the entire release between 17,500 and 20,500 AD is directed to biosphere object 157_1 or to 114.

Releases

As discussed in Chapter 4, the releases were quantitatively taken to be the same (as amount over time) as for the temperate conditions of the *global warming calculation case*, but were directed to the mire talik (biosphere object 157_1) and the lake talik (biosphere object 114) in two variants of the calculation case.

Annual doses

The results show that the peak annual doses are much lower for the variant where the releases are directed to biosphere object 114 (lake talik) than for the variant where the releases are directed to biosphere object 157_1 (mire talik). A summary of the results is presented in Figure 5-16, Figure 5-17 and Table 5-4. It is assumed that *H&G* is the only potentially exposed group since cultivation is not deemed possible under such climate conditions. The same land use assumption was made for the dose calculation during periglacial conditions after 50,000 years in the *global warming calculation case*. However, in the *early periglacial calculation case*, releases during the early periglacial period can take place, whereas in the *global warming calculation case* there are no releases during periglacial periods. Taking this into account, and the fact that in the *early periglacial calculation case* permafrost conditions occur earlier than in the *global warming calculation case*, it is reasonable to expect that doses during periglacial conditions will be higher in the *early periglacial calculation case* than in the *global warming calculation case*. The results obtained confirm this, as the doses in the *early periglacial calculation case* are roughly three times higher than in the periglacial periods of the *global warming calculation case* (compare Figure 5-16 with Figure 5-3). The peak values of the total dose in the periglacial period (17,500–20,500 AD) of the *early periglacial calculation case* are well below the peak values of the total dose for the temperate period.

Table 5-4. Peak annual dose (and related data) to a representative individual of the most exposed group in biosphere object 157_1 and 114 obtained for the periglacial period (17,500-20,500AD) of the early periglacial calculation case (CCM_EP).

Annual dose (µSv)	Year (AD)	Contribution from waste vault (%)	Contribution from radionuclides (%)	Exposed group (biosphere object)
0.28	17,800	Silo (59.4)	I-129 (71.7)	Hunters and gatherers (Object 157_1)
		1BMA (16.6)	Ca-41 (7.9)	
		1BLA (9.5)	Mo-93 (7.8)	
		2BMA (8.1)	Ac-227 (3.8)	
		1BTF (1.3)	U-235 (2.9)	
		5BLA (1.1)	U-238 (2.8)	
		4BLA (1.0)	Pa-231 (1.1)	
		2BLA (0.9)	Others (1.9)	
		3BLA (0.8)		
		2BTF (0.8)		
		BRT (0.2)		
		0.00061	18,500	
2BTF (8.1%)	C-14-inorg (10.7%)			
1BTF (2.6%)	Others (0.5%)			
1BMA (1.9%)				
2BMA (0.8%)				
BRT (0.0%)				
1-5BLA (0.0)				

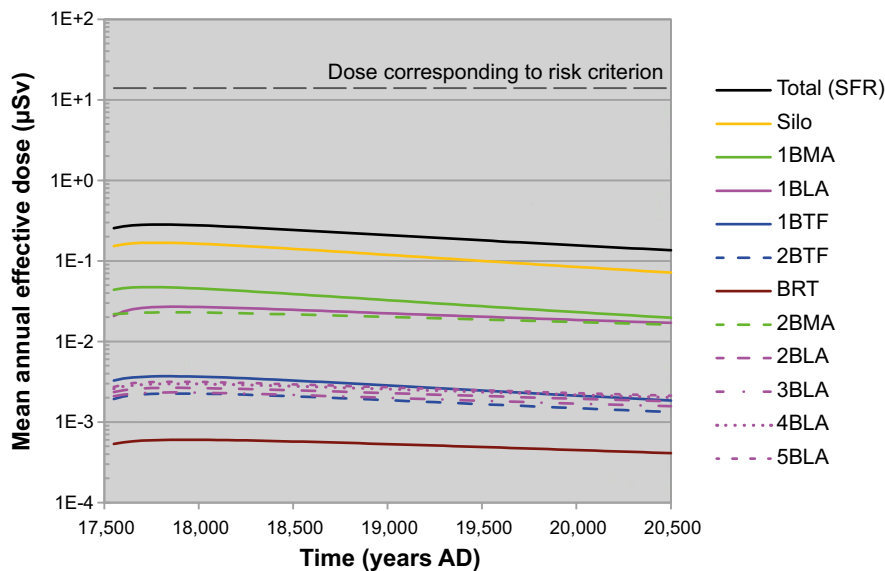


Figure 5-16. Arithmetic mean of the annual dose to the exposed group H&G in biosphere object 157_1. Doses are shown for releases from each and all waste vaults in SFR in the *early periglacial calculation case (CCM_EP)*.

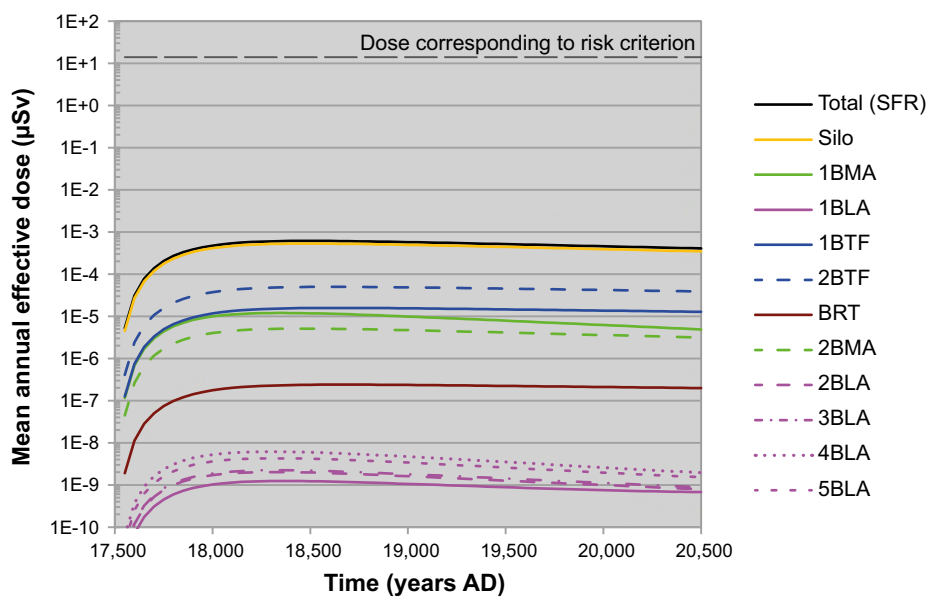


Figure 5-17. Arithmetic mean of the annual dose to H&G in biosphere object 114. Doses are shown for releases from each and all waste vaults in SFR in the *early periglacial calculation case (CCM_EP)*.

The peak annual dose assuming a mire talik in biosphere object 157_1 is nearly 460 times higher than the peak dose that occurs approximately 1,000 years later assuming a lake talik in biosphere object 114, see Figures 5-18 and 5-19. In the mire talik case, the exposure to radionuclides is mainly due to accumulation of I-129 in the surface peat and edible mire vegetation, whereas exposure related to the lake talik case is the result of consuming fish with a relatively high activity concentration of C-14 (originating from the silo) (Table 5-4).

Impact of parameter uncertainty

The values of the different statistics obtained for the *early periglacial calculation case* are presented in Figure 5-20, including the arithmetic mean, median, and 5th and 95th percentiles of the maximum annual effective dose at each point in time. As the exposed group is the same over this time interval there is no significant shift in the bandwidth of the uncertainty.

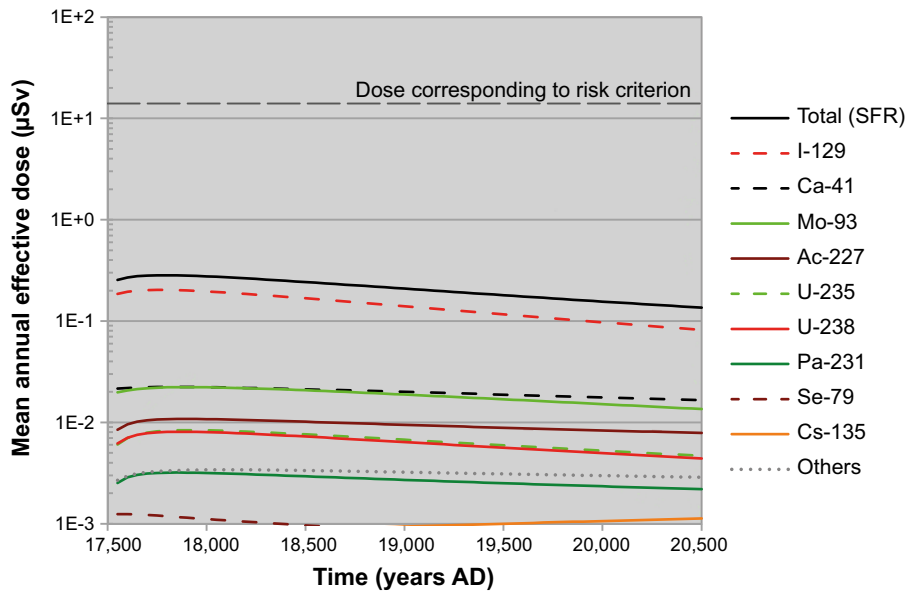


Figure 5-18. Arithmetic mean of the annual dose to H&G in biosphere object 157_1 for releases from all waste vaults in SFR in the *early periglacial calculation case (CCM_EP)*.

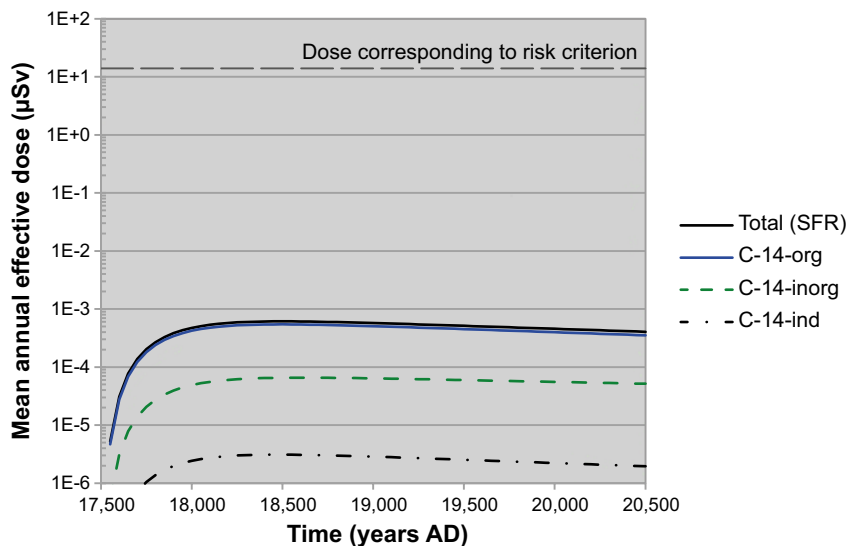


Figure 5-19. Arithmetic mean of the annual dose to H&G in biosphere object 114 for releases from all waste vaults in SFR in the *early periglacial calculation case (CCM_EP)*.

5.3 Collective dose (CCM_CD)

The *collective dose calculation case (CCM_CD)* has been identified in order to provide an alternative safety indicator as requested by Swedish regulations. Calculations to estimate the collective dose during a period of 10,000 years have been performed, focusing on potential releases during the first 1,000 years after closure of the repository. The calculation case is described in Section 4.1.4. Collective doses are calculated using the releases from the geosphere obtained for the *timing of the releases calculation case* which begins directly after repository closure.

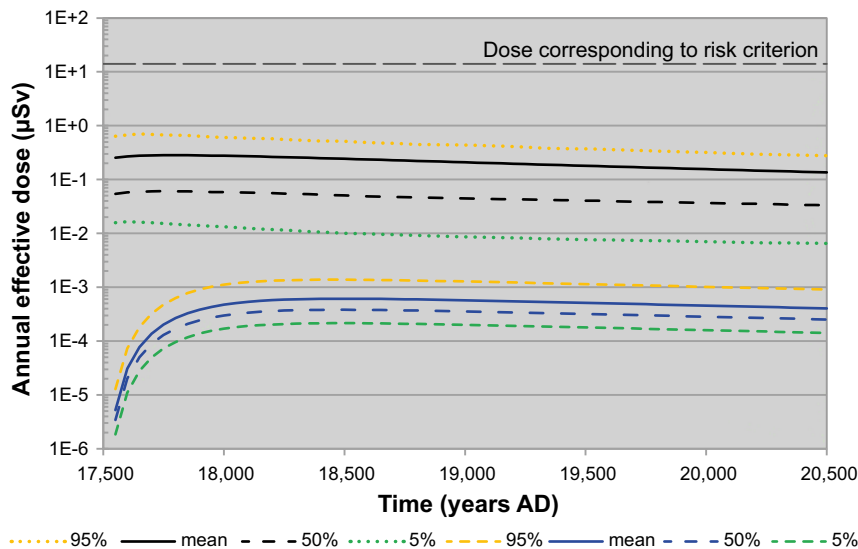


Figure 5-20. Arithmetic mean, median, 5th and 95th percentiles of the annual dose to a representative individual of the most exposed group (H&G) in the **early periglacial calculation case**. Black curves correspond to dose for exposed group in biosphere object 157_1 and blue curves corresponds to dose for exposed group in object 114.

Doses

The collective dose was calculated for two populations: 1) for the global population due to C-14 releases to the atmosphere, which yielded a value of 2.5 manSv and 2) for the Baltic Sea population due to radionuclide releases to the Baltic Sea and subsequent exposure of the population by ingestion of fish, which yielded a value of about 0.15 manSv, with a 96% contribution from C-14 and a 3% contribution from Ag-108m (Table 5-5).

Since these calculations are based on releases during the first 1,000 years after closure, there is a potential contribution from short-lived radionuclides to the collective dose for the Baltic population. However, the contributions from short-lived radionuclides are insignificant for the total dose (Table 5-5).

Table 5-5. Collective doses for the Baltic region obtained in the collective dose calculation case.

Radionuclide	Collective dose (manSv)
C-14-org	1.3×10^{-1}
C-14-inorg	1.9×10^{-2}
Ag-108m	4.9×10^{-3}
C-14-ind	1.3×10^{-3}
Se-79	5.2×10^{-4}
I-129	2.9×10^{-5}
Others	$< 1 \times 10^{-5}$
Total	0.15

6 Results for calculation cases in less probable scenarios

This chapter presents results of calculation cases in less probable scenarios and combined scenarios that are described in Sections 4.2 and 4.4. As in Chapter 5, it presents results for the radionuclides contributing significantly to dose, for releases from individual waste vaults, and annual effective doses caused by releases from the entire repository. Results of calculation cases in less probable scenarios are compared in particular with results of the *global warming calculation case* with regard to peak mean annual dose and the structure of contributions from waste vaults and dominating radionuclides. Additionally, peak releases from the far-field of some calculation cases are graphically compared with those of the *global warming calculation case* to analyse system performance. Appendix E provides a compilation of results including those for less significant radionuclides; the listed data comprise peak releases from the near-field and the far-field and peak doses including time of occurrence of the peaks.

All calculation cases in less probable scenarios but one are carried out as probabilistic calculations in the same way as the calculation cases in the main scenario (Chapter 5). The *earthquake calculation case* (CCL_EQ) is the single one which is carried out in a deterministic manner (as the calculation for this case is repeated for earthquake occurrences at 1,000 time points, a probabilistic treatment would not have been feasible, due to calculation time and data volume).

6.1 High inventory calculation case (CCL_IH)

The *high inventory calculation case* (CCL_IH) is described in Section 4.2.1. The inventory of a radionuclide for this scenario is derived as the 95th percentile of its distribution of inventory activity; the high inventory is presented and compared with the best estimate inventory in Appendix A (Table A-2). The uncertainty of the inventory depends on the radionuclide and the waste type as, for the latter, the methods to determine the inventory differ from waste type to waste type (SKB 2013).

Releases

Figure 6-1 shows a comparison of peak releases from the far-field in the *high inventory calculation case* (CCL_IH) with the *global warming calculation case* (CCM_GW). As can be seen in Figure 6-1, the releases of Ag-108 (22-fold increased initial inventory), Se-79 (50), Zr-93 (20), Nb-93m (progeny of Mo-93 (2) and Zr-93 (20)), Am-241 (12) and Sn-126 (28) are significantly higher than in the *global warming calculation case* due to the significantly increased inventory. This is due to the large uncertainties concerning the inventory of these radionuclides (or parent nuclides) as indicated within brackets. See Table A-2 in Appendix A for the ratios of high radionuclide inventories and best estimate inventories.

It can be derived from Figure 6-1 and the data in Table A-2, Appendix A, that the release to the biosphere is not proportional to the total inventory of a radionuclide. It also depends on the waste package types with different inventories and their release properties as addressed in Chapter 9.

Annual doses

Time series of annual effective doses for different exposed groups in biosphere object 157_2, of the maximum dose over all biosphere objects and of the maximum dose for the *global warming calculation case* are presented in Figure 6-2. The evolution of the annual dose for the exposed groups and the maximum dose are similar to the calculation cases of the *global warming calculation case* with the level elevated by about a factor of two. This holds particularly for the peak dose of 17.7 μSv compared with 7.7 μSv in the *global warming calculation case*, Table 6-1 and Table 5-1, which occurs about 1,000 years later at 7500 AD than in the *global warming calculation case*.

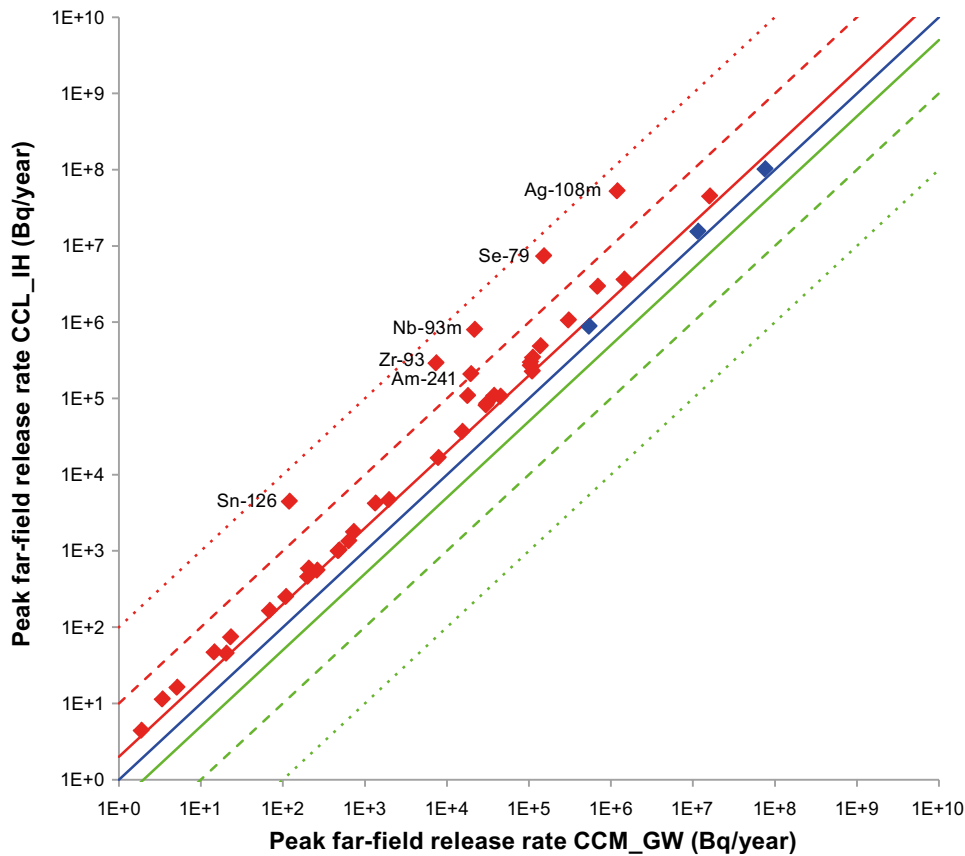


Figure 6-1. Comparison of peak releases from the far-field in the **high inventory calculation case** compared to the **global warming calculation case**. Dots on the blue line on the diagonal represent radionuclides for which the calculated releases in the current calculation case and the case CCM_GW are the same. At the solid red line the calculated releases are twice as high as in the case CCM_GW, at the dashed red line the calculated releases are ten times as high as in the case CCM_GW and at the dotted red line the calculated releases are one hundred times the case CCM_GW. In the same way the green lines represents 0.5 times, 0.1 times and 0.01 times the calculated releases of case CCM_GW.

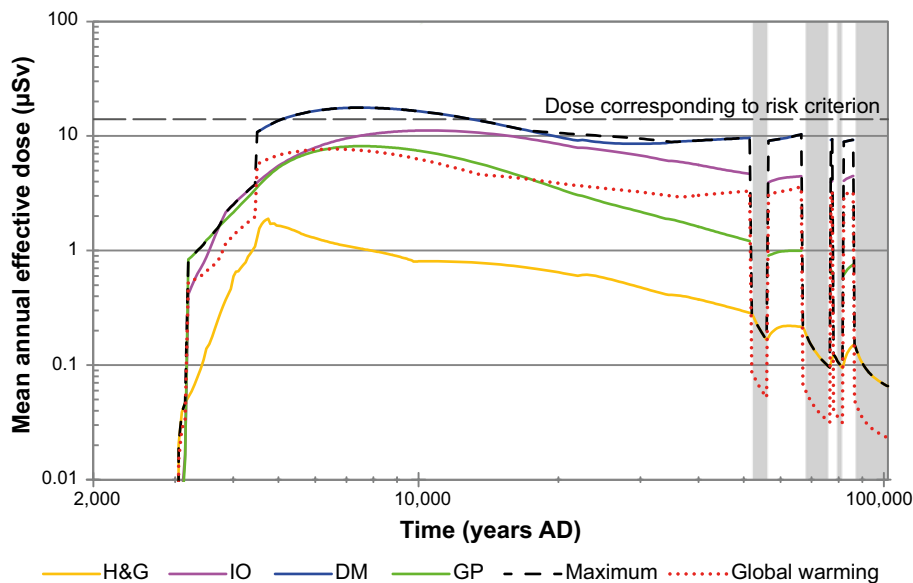


Figure 6-2. Arithmetic mean of annual effective dose for different exposed groups in biosphere object 157_2 and the maximum across all exposed groups and biosphere objects, shown for the **high inventory calculation case**). The maximum annual effective dose of the **global warming calculation case** is shown for comparison. The unshaded areas correspond to temperate climatic conditions and the grey shaded areas to periglacial conditions with continuous permafrost.

Peak annual effective dose and contributions from waste vaults and radionuclides are presented in Table 6-1. The main difference in radionuclide contributions compared with the *global warming calculation case* is the increase for Se-79 due to a 50-fold increase of its inventory; see Table A-2 (Appendix A).

Table 6-1. Peak annual effective dose to a representative individual of the most exposed group obtained for the *high inventory calculation case*.

Annual dose (µSv)	Year (AD)	Contribution from waste vault (%)	Contribution from radionuclides (%)	Exposed group (biosphere object)
17.7	7500	Silo (52.3)	Mo-93 (47.3)	Drained-mire farmers (Object 157_2)
		1BMA (13.7)	Se-79 (15.1)	
		1BLA (11.2)	C-14-org (8.4)	
		2BMA (9.0)	I-129 (7.7)	
		2BTF (2.9)	U-238 (5.8)	
		1BTF (2.5)	Cl-36 (4.6)	
		5BLA (1.8)	Ca-41 (3.7)	
		2BLA (1.7)	U-235 (2.9)	
		4BLA (1.7)	Ni-59 (1.5)	
		3BLA (1.6)	Pa-231 (1.1)	
		BRT (1.5)	Others (2.0)	

The reason for the later occurring peak dose compared with the *global warming calculation case* is a different inventory distribution, with a relative increase in dose contribution from the silo in the higher inventory, (see Figure 5-5 and 6-3). The higher retention capacity of the silo barriers leads to the time shift of the peak dose. A summary of peak contributions, including time of occurrence, most exposed group, location and the most contributing radionuclide from the waste vault, from the individual waste vaults and the entire repository is given in Table 6-2. Figure 6-3 shows the evolution of waste vault contributions to annual dose over time.

Table 6-2. Peak annual dose and the time at which the peak is observed for releases from individual waste vaults and from the entire repository in the *high inventory calculation case (CCL_IH)*. Indicated is also the location, where the peak dose occurs, the exposed group and the most contributing radionuclide.

Waste vault	Annual dose (µSv)	Year (AD)	Biosphere Object	Exposed group	Most contributing radionuclide (%)
Silo	9.30	7950	157_2	DM	Mo-93 (40.7)
1BMA	5.07	66,500	157_2	DM	Ni-59 (66.3)
1BLA	3.06	24,500	157_1	DM	U-238 (28.2)
1BTF	0.79	4800	157_2	DM	Mo-93 (49.2)
2BTF	0.82	4800	157_2	DM	Mo-93 (61.5)
BRT	0.38	5450	157_2	DM	Mo-93 (98.6)
2BMA	3.19	30,000	157_1	DM	Ca-41 (66.6)
2BLA	0.33	26,500	157_1	DM	Ca-41 (30.6)
3BLA	0.32	5750	157_2	DM	Mo-93 (45.9)
4BLA	0.35	23,500	157_1	DM	Ca-41 (33.4)
5BLA	0.38	26,000	157_1	DM	Ca-41 (28.4)
Total SFR	17.69	7500	157_2	DM	Mo-93 (47.3)

The main contribution to the peak annual dose occurring for the DM exposed group in biosphere object 157_2 comes from the silo, 1BMA, 1BLA, 2BMA and 2BTF which together contribute almost 90%.

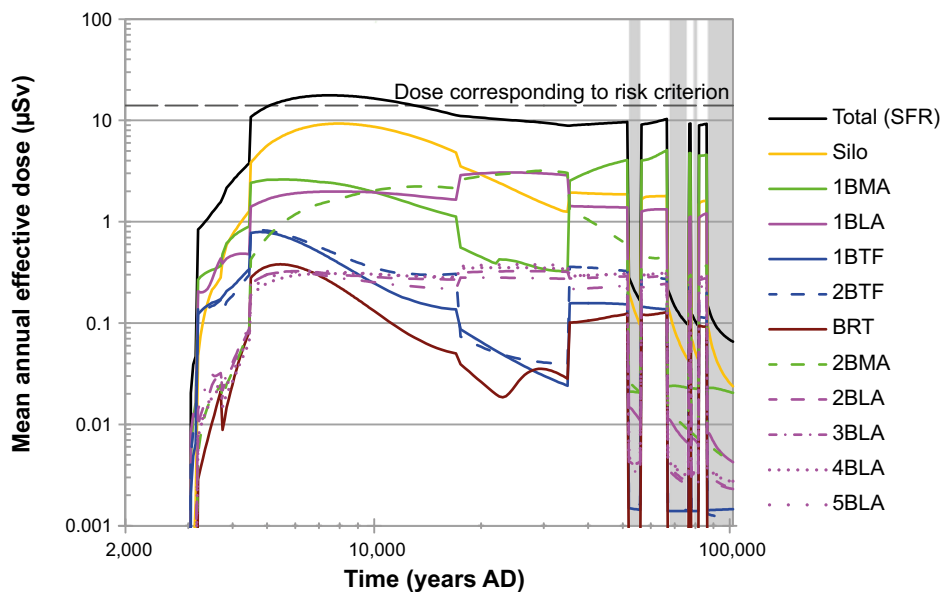


Figure 6-3. Arithmetic mean of the annual effective dose to the most exposed group for releases from the entire repository and contributions from the individual waste vaults in the **high inventory calculation case (CCL_IH)**. The unshaded areas correspond to temperate climatic conditions and the grey shaded areas to periglacial conditions with continuous permafrost.

Due to the uncertainty of inventories of activation products in the decommissioning waste (SKBdoc 1427105), the inventory of Ca-41, which is largely employed in 2BMA, is three times higher in the *high inventory calculation case* than in the main scenario (Table A-2 in Appendix A).

The relative contributions to annual dose in the high inventory scenario are similar to those obtained for the global warming variant of the main scenario, with the differences discussed below. Time series of annual doses from waste vault specific releases are presented for the five most contributing waste vaults in Figure 6-5 to Figure 6-9.

The contribution to total dose from specific radionuclides is shown in Figure 6-4. As in the *global warming calculation case*, the initial period is here also dominated by C-14-org.

For the silo (Figure 6-5), Mo-93, Se-79, C-14-org, I-129 and Cl-36 are the most contributing radionuclides to the peak dose at 7500 AD. Ni-59 is the dominating radionuclide after 35,000 AD during temperate climate conditions; during periglacial conditions, the dose (which is decreasing due to interrupted releases from the near-field) is dominated by I-129. The high relevance of Se-79 (particularly in biosphere object 157_2 about 10,000 AD) is due to its higher relative increase in inventory. This is the most prominent difference with respect to the *global warming calculation case*.

For 1BMA (Figure 6-6), the highest contributions until 10,000 AD originate from the same radionuclides as for the silo, Mo-93, Se-79, organic C-14, I-129 and Cl-36. From 16,000 AD, Ni-59 becomes more important. The build-up of dose due to Ni-59 lasts until the end of the second period of the temperate domain, when a peak annual dose of 5 µSv for the release from the 1BMA vault is reached at 66,500 AD, dominated by Ni-59 (66%), Zr-93 (11%) and Cs-135 (9%).

In the case of 1BLA (Figure 6-7), the peak dose occurring in biosphere object 157_2 (around 7000 AD) is close to the peak dose defined by biosphere object 157_1 only at 24,000 AD. The peak in object 157_1 is only slightly higher than the earlier in object 157_2. In biosphere object 157_2, the main contributions up to 10,000 AD are due to U-238, U-235, Ac-227 and Mo-93; progeny of U-235, Pa-231 and Ac-227, become increasingly more important over time. The peak in biosphere object 157_1 at 24,000 AD, is dominated by U-238 and progeny of U-235. The accumulation capacity of a thicker peat layer in biosphere object 157_1 allows for the build-up of inventories of long-lived actinides which are released from 1BLA and which explain the evolution of dose in this object.

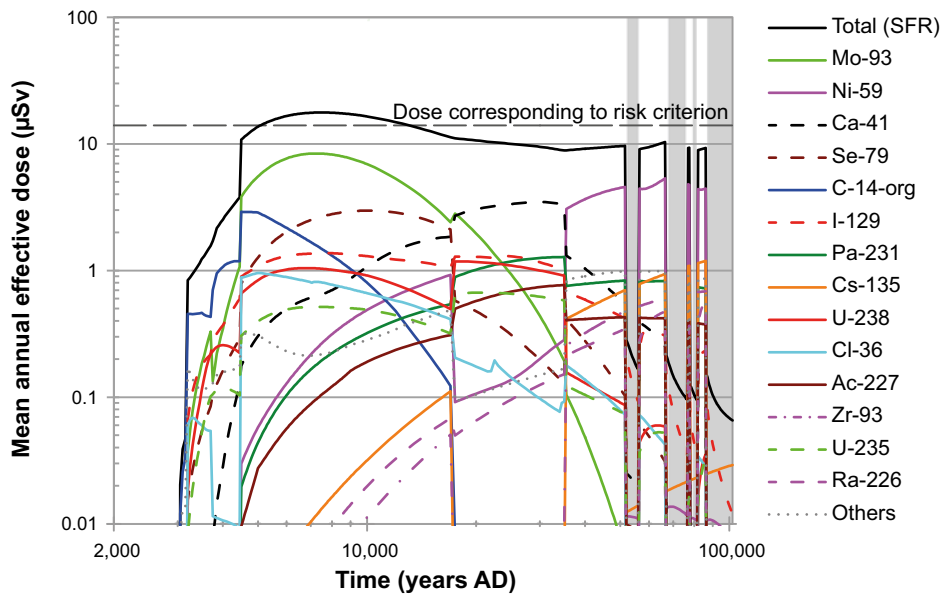


Figure 6-4. Arithmetic mean of the annual effective dose to the most exposed group and respective radionuclide contributions, shown for releases from the entire repository in the **high inventory calculation case** (CCL_IH). The unshaded areas correspond to temperate climatic conditions and the grey shaded areas to periglacial conditions with continuous permafrost.

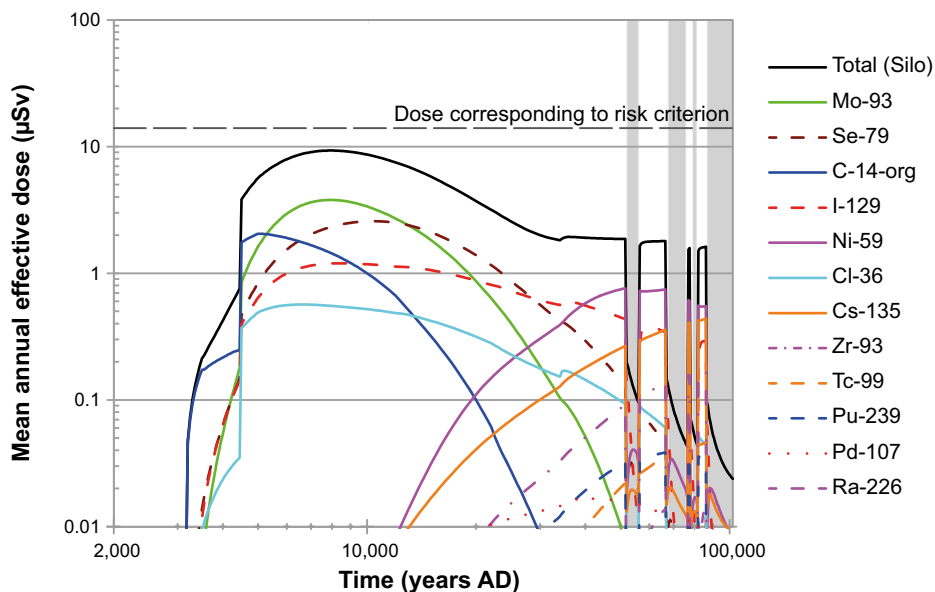


Figure 6-5. Arithmetic mean of the annual effective dose to the most exposed group, shown for releases from the silo in the **high inventory calculation case** (CCL_IH). The unshaded areas correspond to temperate climatic conditions and the grey shaded areas to periglacial conditions with continuous permafrost.

For 2BMA (Figure 6-8), Mo-93 contributes the most followed by Cl-36 and Ca-41 until about 15,000 AD. After this, dose is dominated by Ca-41 and Mo-93 until about 50,000 AD, when Ni-59 becomes dominating.

In the case of 2BTF (Figure 6-9), Mo-93 dominates the peak dose, with relevant but far lower contributions from I-129 and Se-79. After 20,000 AD the dose is dominated by Ni-59.

As in the *global warming variant*, Mo-93 is the only radionuclide that contributes from all waste vaults substantially to the peak dose of the entire release at 7500 AD. The contribution from Mo-93 to the peak dose (at 7500 AD) is as follows: silo (21%), 2BMA (6%), 1BMA (4%), 1BLA (2%) and 2BTF (1%).

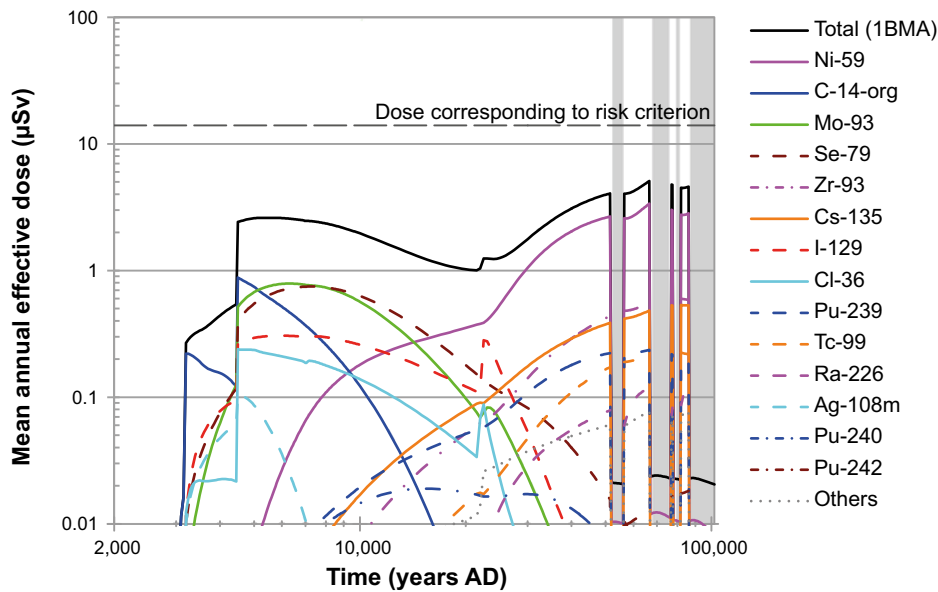


Figure 6-6. Arithmetic mean of the annual effective dose to the most exposed group, shown for releases from **1BMA** in the **high inventory calculation case (CCL_IH)**. The unshaded areas correspond to temperate climatic conditions and the grey shaded areas to periglacial conditions with continuous permafrost.

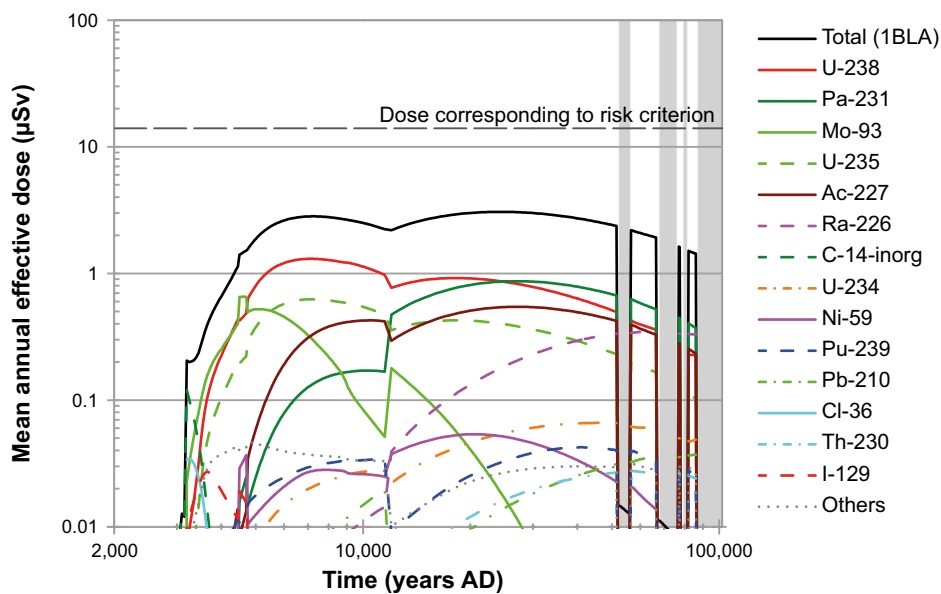


Figure 6-7. Arithmetic mean of the annual effective dose to the most exposed group, shown for releases from **1BLA** in the **high inventory calculation case (CCL_IH)**. The unshaded areas correspond to temperate climatic conditions and the grey shaded areas to periglacial conditions with continuous permafrost.

Impact of parameter uncertainty

In addition to the arithmetic mean value presented above, statistics such as the median and different percentiles of the annual dose distribution at each time point have been obtained from the probabilistic calculations. These statistics are used to provide a better understanding of the uncertainties associated with calculated doses. In Figure 6-10, arithmetic mean, median, and 5th and 95th percentiles of the maximum total dose at each point in time are presented. The time evolution of the statistics is similar to the *global warming calculation case*, although on a level increased by about a factor of two.

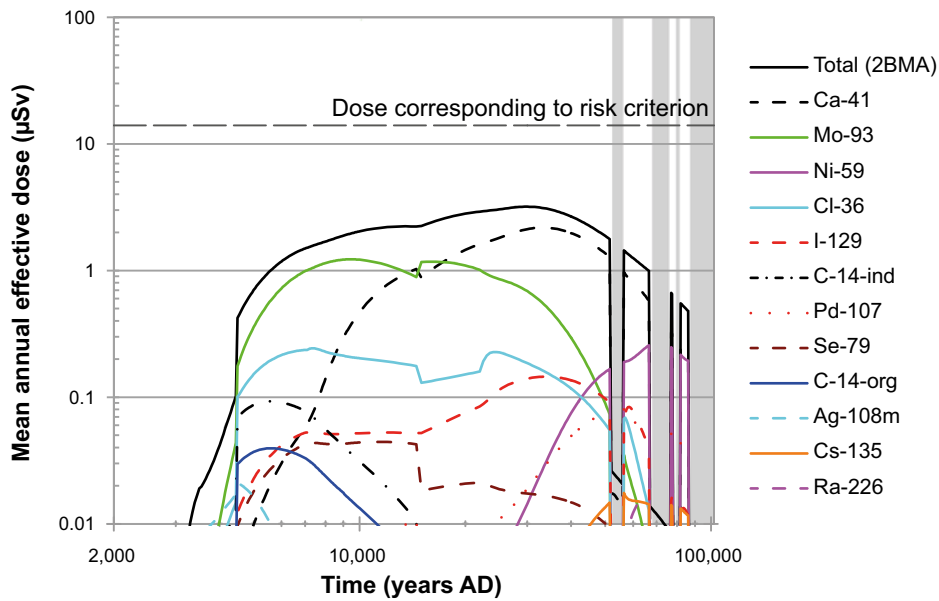


Figure 6-8. Arithmetic mean of the annual effective dose to the most exposed group, shown for releases from 2BMA in the **high inventory calculation case (CCL_IH)**. The unshaded areas correspond to temperate climatic conditions and the grey shaded areas to periglacial conditions with continuous permafrost.

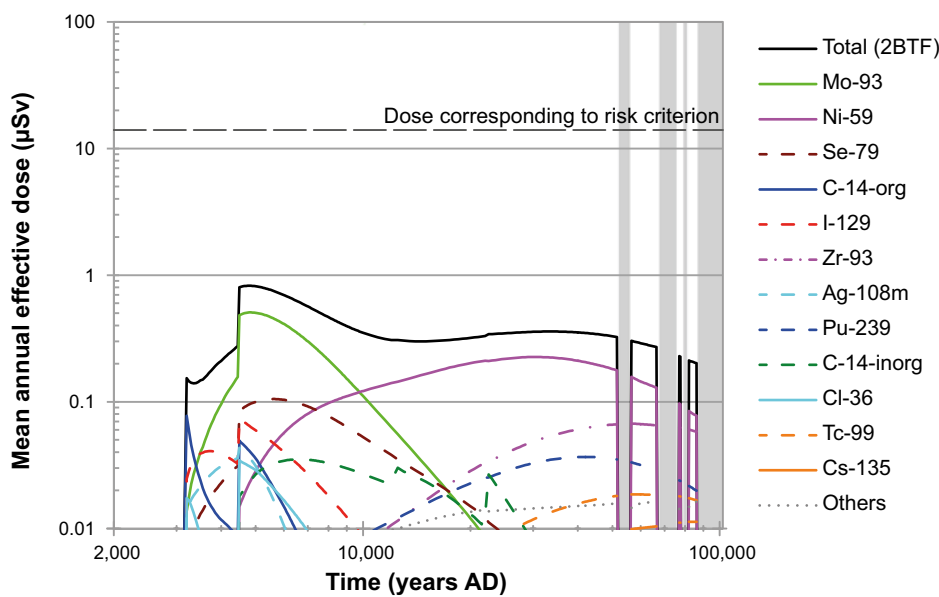


Figure 6-9. Arithmetic mean of the annual effective dose to the most exposed group, shown for releases from 2BTF in the **high inventory calculation case (CCL_IH)**. The unshaded areas correspond to temperate climatic conditions and the grey shaded areas to periglacial conditions with continuous permafrost.

6.2 High flow in the bedrock calculation case (CCL_FH)

The *high flow in the bedrock calculation case (CCL_FH)* is described in Section 4.2.2. This calculation case is based on a scenario with water flows in the bedrock that are higher than in the *global warming calculation case*. Due to this increased flow in the bedrock also the flow in the waste vaults is assumed to be larger than in the *global warming calculation case*. Figure 4-2 illustrates the relative increase in water flow through waste vaults for this calculation case compared to the *global warming calculation case*.

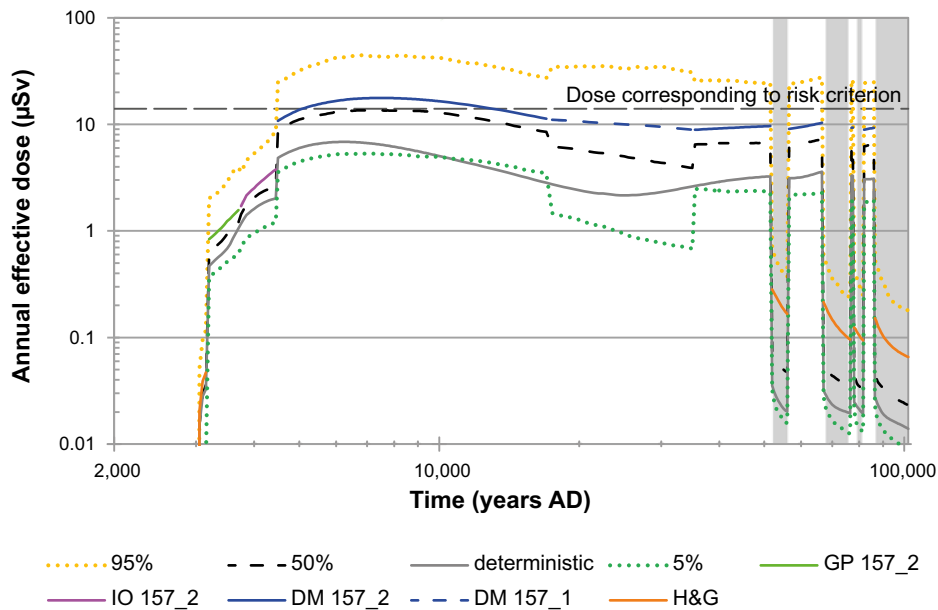


Figure 6-10. Arithmetic mean, median, 5th and 95th percentiles of the annual dose to a representative individual of the most exposed group from SFR in the **high inventory calculation case (CCL_IH)**. The unshaded areas correspond to temperate climatic conditions and the grey shaded areas to periglacial conditions with continuous permafrost.

Releases

Figure 6-11 shows a comparison of peak releases from the far-field in the *high flow in bedrock case* (CCL_IH) with the *global warming calculation case* (CCM_GW). As can be seen, the variation in the bedrock properties and the induced impact on waste vault flow has a minor effect on the releases. This points to the efficiency of the flow barriers in the repository as, for example, the BMA vaults' hydraulic cage diverts flow and the bentonite barrier of the silo blocks it.

Annual doses

The time series of annual effective dose for different exposed groups in biosphere object 157_2, of the maximum dose over all biosphere objects and of the maximum dose for the *high flow in the bedrock calculation case* is presented in Figure 6-12. The peak annual dose is obtained 250 years earlier than in the *global warming calculation case*. The shorter transport time is consistent with higher groundwater flow in the vaults and the geosphere.

The peak annual dose of 9.7 µSv (Table 6-3) is 26% higher than in the *global warming calculation case* with a 7.7 µSv peak dose (Table 5-1). The radionuclides contributing most to the peak annual dose are the same as in the *global warming calculation case*.

The peak annual dose due to exposure for releases from the entire repository occurs at year 6250 AD, (Table 6-3). A summary of peak contributions from the individual waste vaults is given in Table 6-4, including the timing of peak contributions as well as the most exposed group, location and the most contributing radionuclide in the waste vault release.

The main contributions to the peak annual dose come from the silo, 1BMA, 1BLA, 2BMA and 2BTF, which together contribute about 87% to the peak annual dose (Figure 6-13). The relative contributions from the waste vaults to peak annual dose are similar to the *global warming calculation case* and also the dynamics of the *high flow in the bedrock calculation case* are similar to the *global warming calculation case*. After the peak dose at 6250 AD only small variations in the maximum doses during the whole simulation period of 100,000 years (apart for periglacial periods) are observed (Figure 6-13). Figure 6-13 shows radionuclide contributions to maximum annual dose due to releases from all waste vaults, while Figures 6-15 to 6-19 show maximum annual doses due the release of radionuclides from the most contributing waste vaults individually, i.e. silo, 1BMA, 1BLA, 2BMA and 2BTF, respectively.

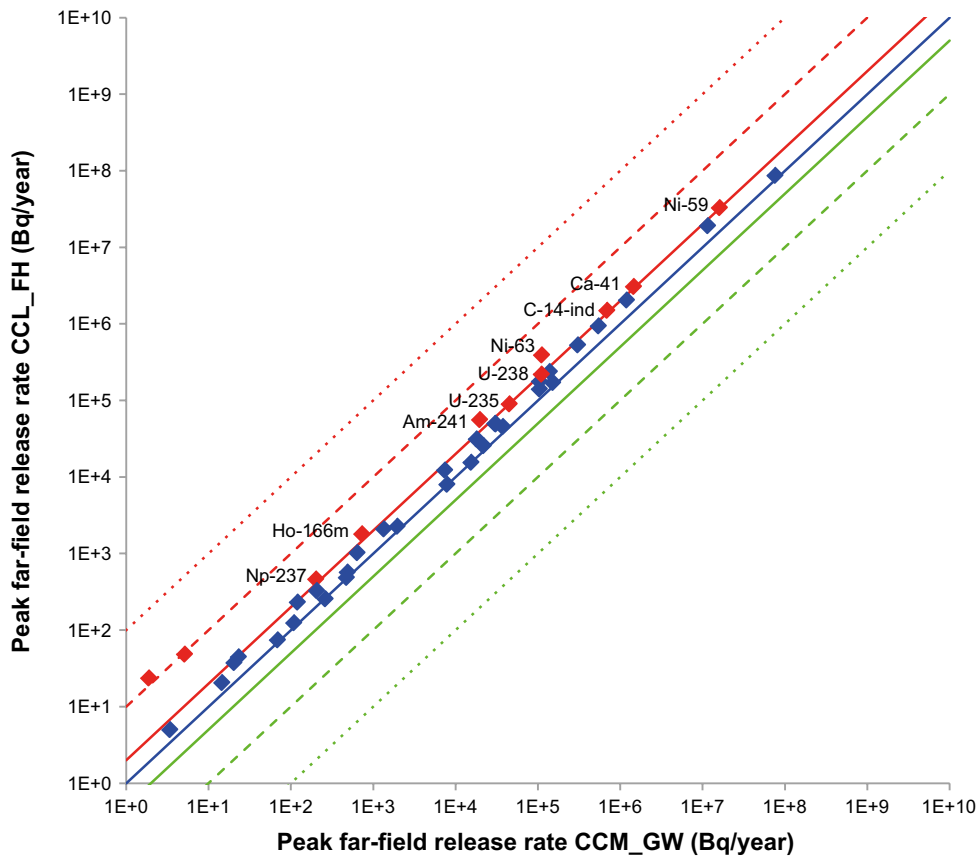


Figure 6-11. Comparison of peak releases from the far-field in the **high flow in the bedrock calculation case** with the **global warming calculation case**. Dots on the blue line on the diagonal represents radionuclides for which the calculated releases in the current calculation case and CCL_GW are the same. At the solid red line the calculated releases are twice as high as in CCL_GW, at the dashed red line the calculated releases are ten times as high as in CCL_GW and at the dotted red line the calculated releases are one hundred times the **global warming calculation case**. In the same way the green lines represents 0.5 times, 0.1 times and 0.01 times the CCL_GW releases.

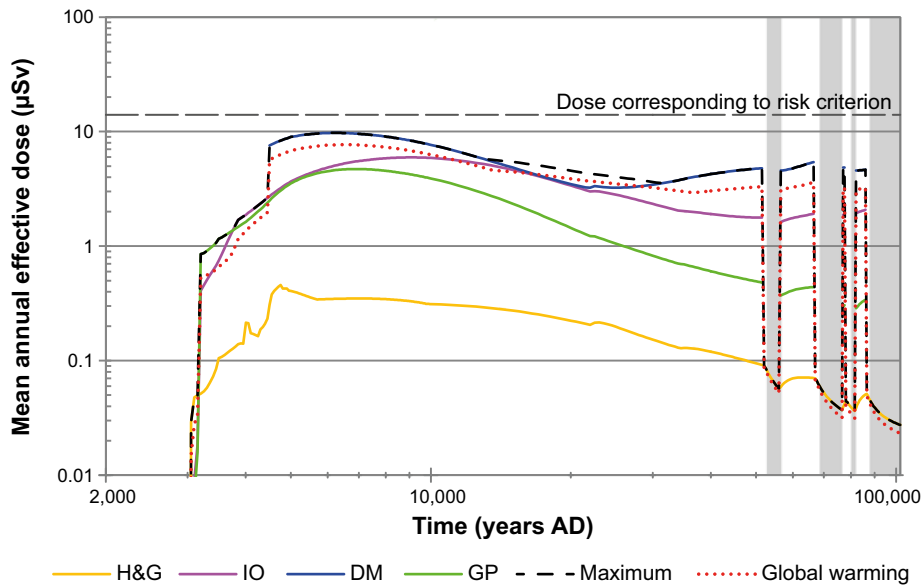


Figure 6-12. Arithmetic mean of annual dose for exposed groups in biosphere object 157_2 and the maximum across exposed groups and biosphere objects in the **high flow in the bedrock calculation case**. Maximum dose for the **global warming calculation case** is also shown for comparison. The unshaded areas correspond to temperate climatic conditions and the grey shaded areas to periglacial conditions with continuous permafrost.

Table 6-3. Peak annual effective dose to a representative individual of the most exposed group obtained for the *high flow in the bedrock calculation case (CCL_FH)*.

Annual dose (µSv)	Year (AD)	Contribution from waste vault (%)	Contribution from radionuclides (%)	Exposed group (biosphere object)
9.7	6250	Silo (44.3)	Mo-93 (58.1)	Drained-mire farmers
		1BMA (14.7)	C-14-org (17.4)	(Object 157_2)
		1BLA (11.8)	U-238 (6.6)	
		2BMA (11.6)	I-129 (5.4)	
		2BTF (4.7)	Cl-36 (3.1)	
		BRT (3.9)	U-235 (2.9)	
		1BTF (3.8)	Ca-41 (2.7)	
		4BLA (1.4)	Others (3.8)	
		5BLA (1.3)		
		2BLA (1.2)		
		3BLA (1.2)		

Table 6-4. Peak annual dose and the time at which the peak is observed for releases from individual waste vaults and from the entire repository occurrence in the *high flow in the bedrock calculation case (CCL_FH)*. Indicated is also the location, where the dose due to the contribution occurs, the most exposed group and the most contributing radionuclide.

Waste vault	Annual dose (µSv)	Year (AD)	Biosphere object	Exposed group	Most contributing radionuclide (%)
Silo	4.45	7050	157_2	DM	Mo-93 (49.8)
1BMA	3.25	66,500	157_2	DM	Ni-59 (71.8)
1BLA	1.54	6600	157_2	GP	U-238 (49.7)
1BTF	0.51	4750	157_2	DM	Mo-93 (69.4)
2BTF	0.67	4650	157_2	DM	Mo-93 (72.7)
BRT	0.51	4950	157_2	DM	Mo-93 (98.6)
2BMA	1.36	9200	157_2	DM	Mo-93 (75.0)
2BLA	0.12	5400	157_2	DM	Mo-93 (45.7)
3BLA	0.12	5400	157_2	DM	Mo-93 (45.4)
4BLA	0.16	23,000	157_1	DM	Ca-41 (29.7)
5BLA	0.15	24,000	157_1	DM	Ca-41 (31.5)
Total SFR	9.74	6250	157_2	DM	Mo-93 (58.1)

The radionuclide contributions to the annual doses vary between waste vaults, mainly due to different radionuclide inventories. The dominating radionuclides contributing to the peak doses due to waste vault releases are the same as in the *global warming calculation case*. Comparing the results with the *global warming calculation case* in Section 5.1.1 shows no significant differences in the two cases and indicates that the dose is rather insensitive to the increased water flow, at least for the waste vaults with engineered barriers.

Impact of parameter uncertainty

In addition to the arithmetic mean values presented above, statistics such as the median and different percentiles of the annual dose distribution at each time point have been obtained. These statistics are used to provide a better understanding of the uncertainties associated with calculated doses. In Figure 6-20, arithmetic mean, median, and 5th and 95th percentiles of the maximum total dose at each point in time are presented. The temporal evolution of the statistics is similar to the *global warming calculation case*, with the doses increased by about 25%.

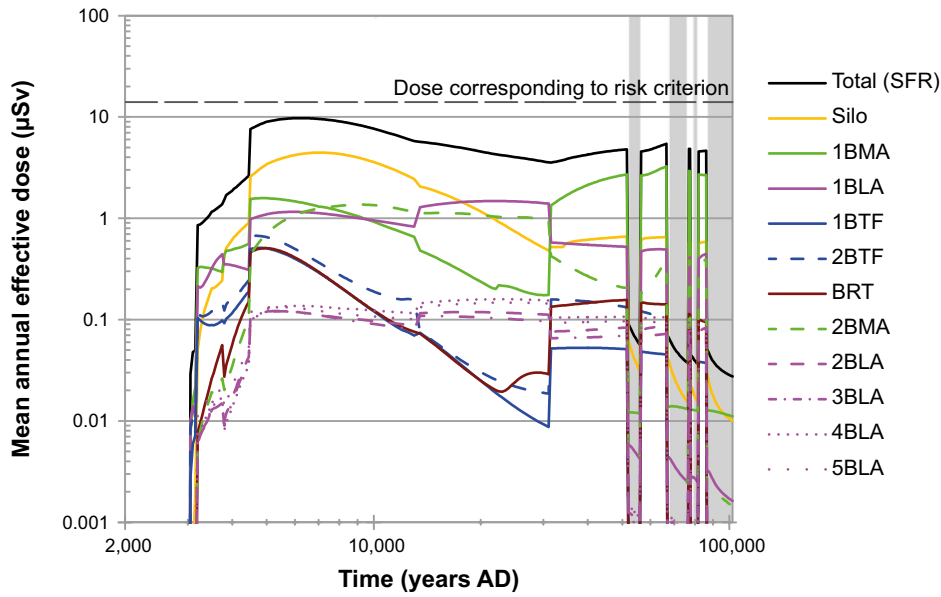


Figure 6-13. Arithmetic mean of the annual dose to the most exposed group for releases from the entire repository and contributions from the individual waste vaults in the **high flow in the bedrock calculation case (CCL_FH)**. The unshaded areas correspond to temperate climatic conditions and the grey shaded areas to periglacial conditions with continuous permafrost.

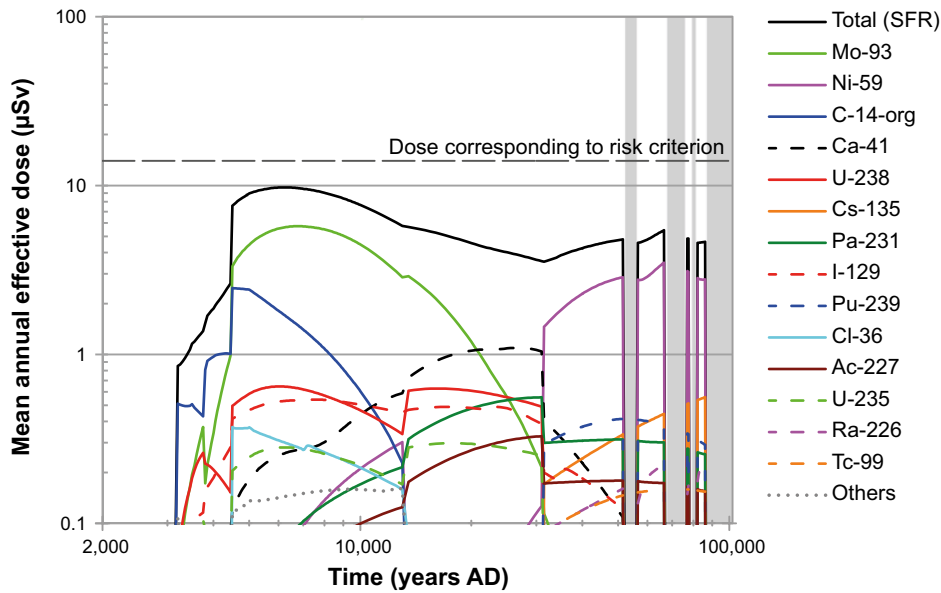


Figure 6-14. Arithmetic mean of the annual effective dose to the most exposed group and respective contributions from radionuclides, shown for releases from the entire repository in the **high flow in the bedrock calculation case (CCL_FH)**. The unshaded areas correspond to temperate climatic conditions and the grey shaded areas to periglacial conditions with continuous permafrost.

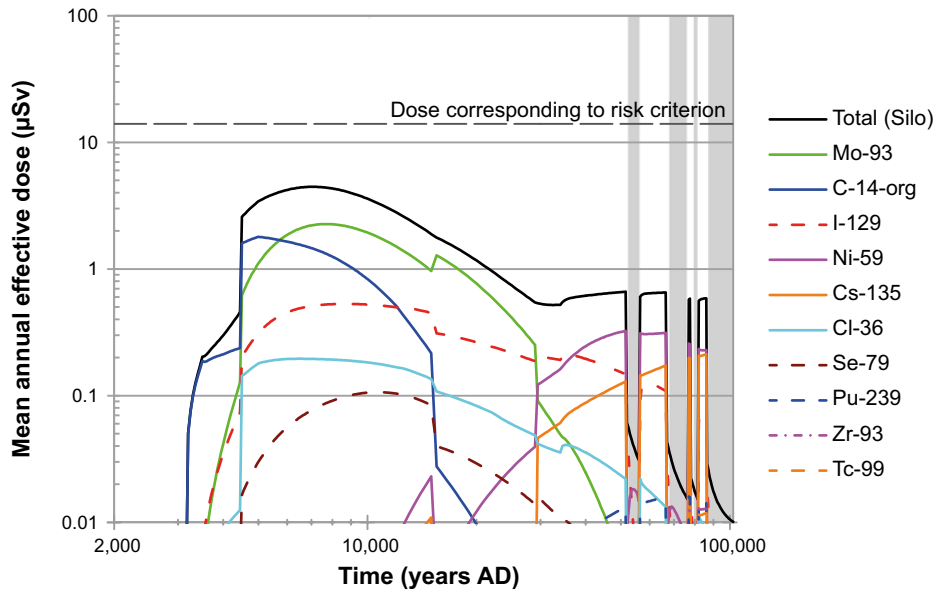


Figure 6-15. Arithmetic mean of the annual dose to the most exposed group, shown for releases from the silo in the **high flow in the bedrock calculation case (CCL_FH)**. The unshaded areas correspond to temperate climatic conditions and the grey shaded areas to periglacial conditions with continuous permafrost.

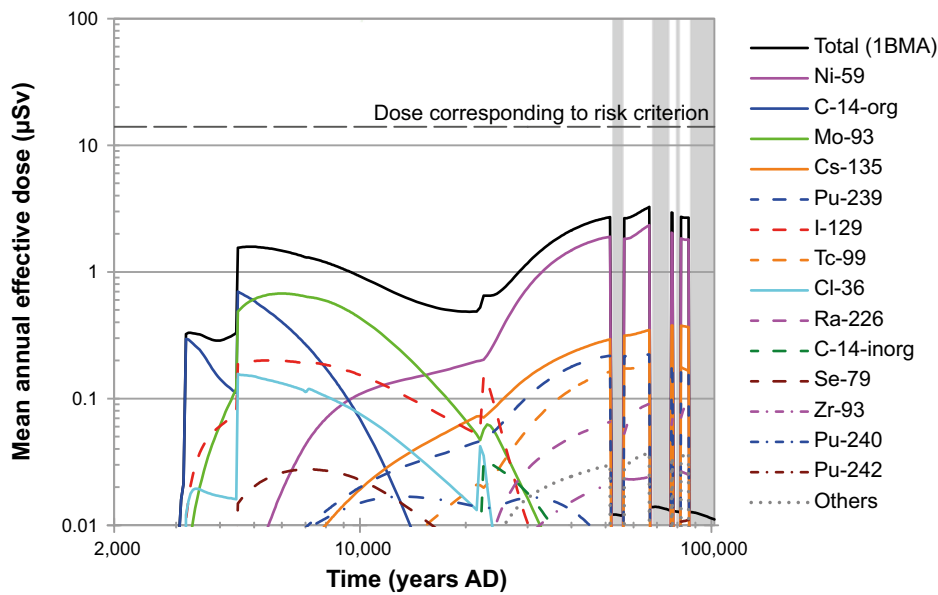


Figure 6-16. Arithmetic mean of the annual dose to the most exposed group, shown for releases from **IBMA** in the **high flow in the bedrock calculation case (CCL_FH)**. The unshaded areas correspond to temperate climatic conditions and the grey shaded areas to periglacial conditions with continuous permafrost.

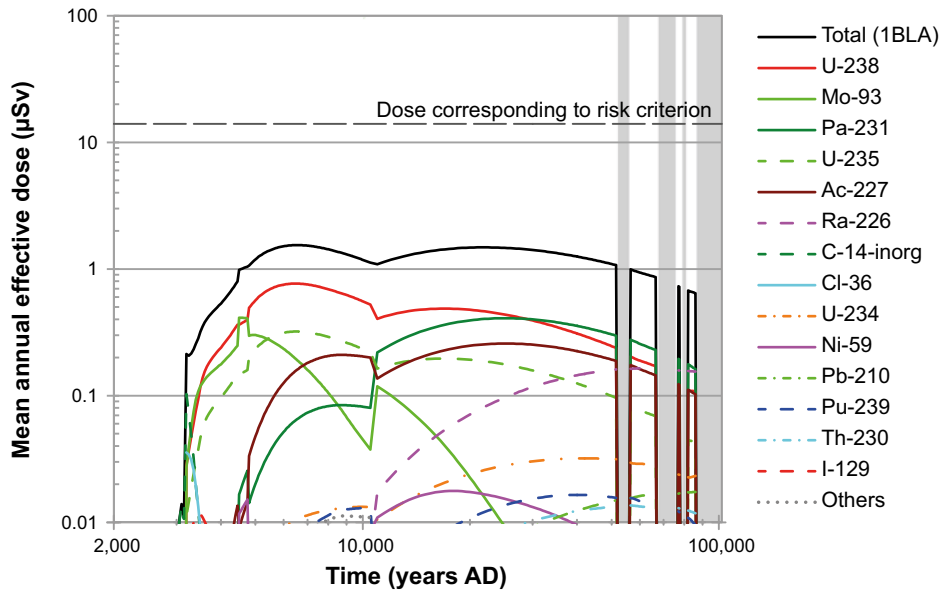


Figure 6-17. Arithmetic mean of the annual dose to the most exposed group, shown for releases from 1BLA in the **high flow in the bedrock calculation case (CCL_FH)**. The unshaded areas correspond to temperate climatic conditions and the grey shaded areas to periglacial conditions with continuous permafrost.

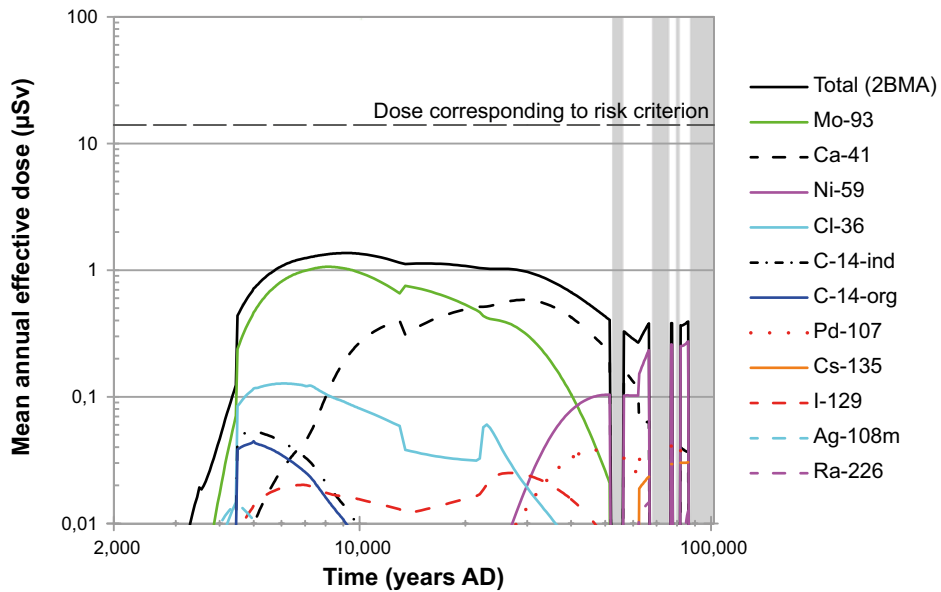


Figure 6-18. Arithmetic mean of the annual dose to the most exposed group, shown for releases from 2BMA in the **high flow in the bedrock calculation case (CCL_FH)**. The unshaded areas correspond to temperate climatic conditions and the grey shaded areas to periglacial conditions with continuous permafrost.

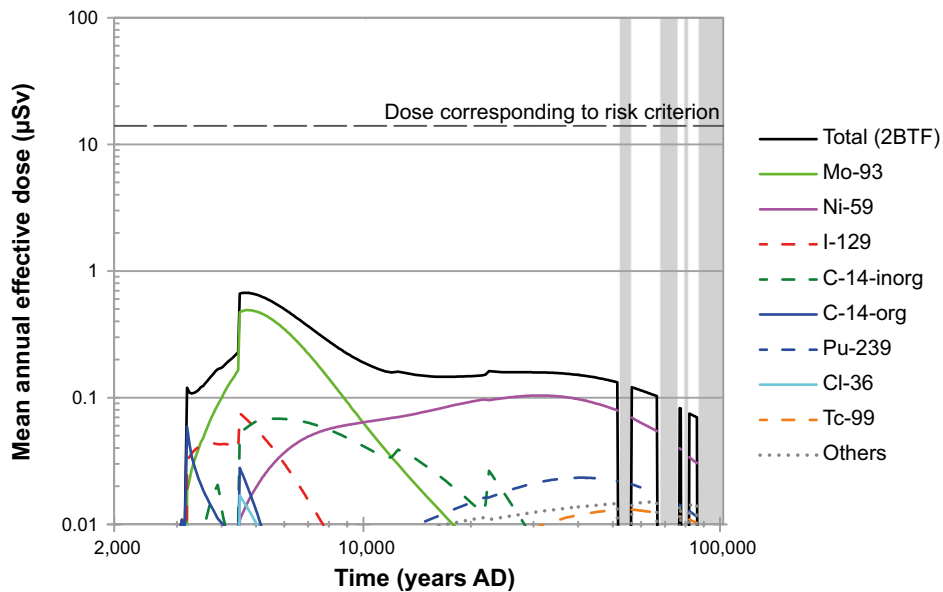


Figure 6-19. Arithmetic mean of the annual dose to the most exposed group, shown for releases from 2BTF in the **high flow in the bedrock calculation case (CCL_FH)**. The unshaded areas correspond to temperate climatic conditions and the grey shaded areas to periglacial conditions with continuous permafrost.

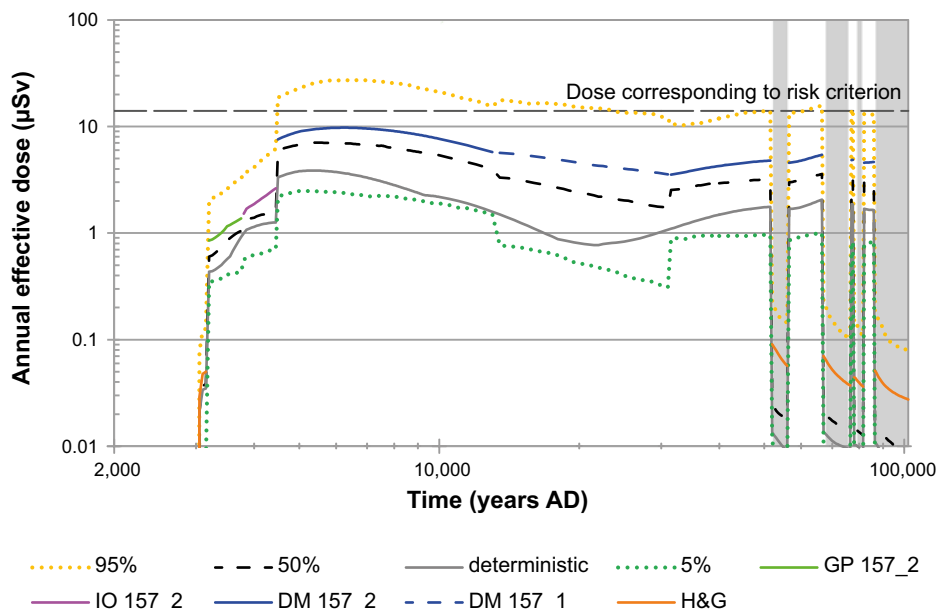


Figure 6-20. Arithmetic mean, median (50th percentile), 5th and 95th percentiles of the annual dose to a representative individual of the most exposed group in the **high flow in the bedrock calculation case (CCL_FH)**. The unshaded areas correspond to temperate climatic conditions and the grey shaded areas to periglacial conditions with continuous permafrost.

6.3 Accelerated concrete degradation calculation case (CCL_BC)

The *accelerated concrete degradation calculation case (CCL_BC)* is described in Section 4.2.3. In this calculation case, the hydraulic conductivity of the concrete increases considerably earlier or to a greater extent than in the *global warming calculation case*. Apart from this, the handling of the near-field, the far-field and the biosphere are identical to the *global warming calculation case*.

Releases

Figure 6-21 compares peak releases from the far-field of the *accelerated concrete degradation calculation case* with the *global warming calculation case*, and Figure 6-22 shows the evolution of far-field releases for important radionuclides over time. The main difference from the *global warming calculation case* is slightly higher releases from the beginning. This is due to higher water flow through the 1BMA and 2BMA concrete barriers. The increase of releases around 22,000 AD occurs for a similar reason as in the *global warming calculation case*, but here the degradation of BMA barriers progresses from a severe to a complete state of degradation. Peak releases are not affected by the degradation at 22,000 AD as the rise in releases at this time point is not large enough to reach up to the peak release that occurs much earlier.

Annual doses

Time series of annual effective dose to groups exposed in biosphere object 157_2 and the maximum annual effective dose for the corresponding calculation case are presented in Figure 6-23. The peak dose is obtained 950 years earlier than in the *global warming calculation case* (increased by less than 40%) and also 700 years earlier than in the *high flow in the bedrock calculation case*. The earlier peak is consistent with faster transport in and accelerated release from the near-field.

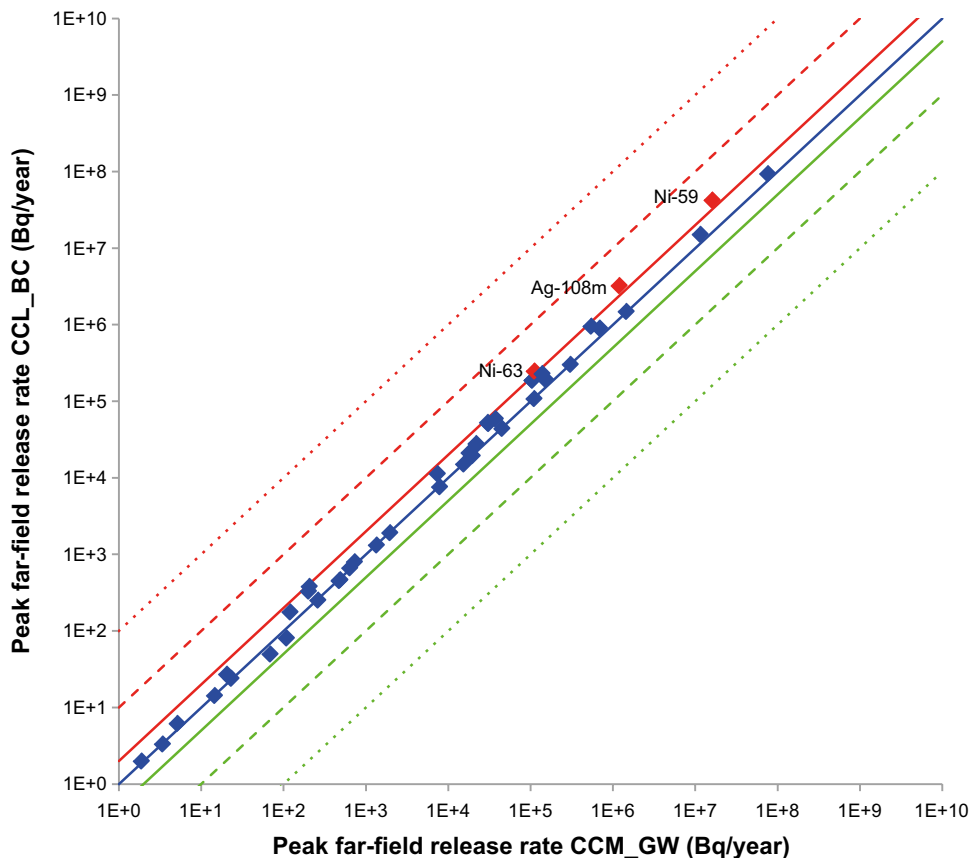


Figure 6-21. Comparison of peak releases from the far-field in the *accelerated concrete degradation calculation case* (CCL_BC) with the *global warming calculation case* (CCM_GW). Dots on the blue line on the diagonal represent radionuclides for which the calculated releases in the current calculation case and CCM_GW are the same. At the solid red line the calculated releases are twice as high as in CCM_GW, at the dashed red line the calculated releases are ten times as high as in CCM_GW and at the dotted red line the calculated releases are one hundred times the base case. In the same way the green lines represents 0.5 times, 0.1 times and 0.01 times the CCM_GW releases.

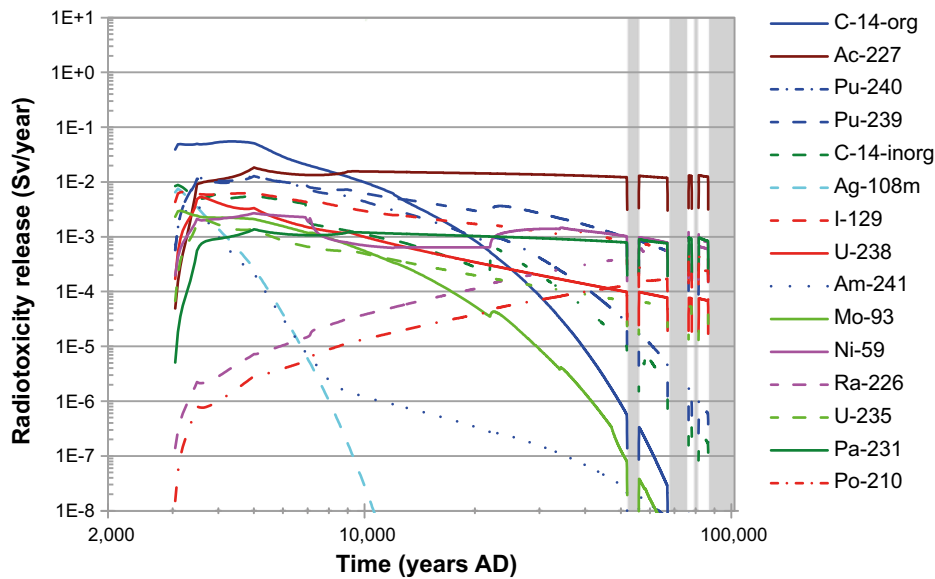


Figure 6-22. Radiotoxicity of releases from the far-field for the 15 most contributing radionuclides in the accelerated concrete degradation calculation case (CCL_BC). The unshaded areas correspond to temperate climatic conditions and the grey shaded areas to periglacial conditions with continuous permafrost.

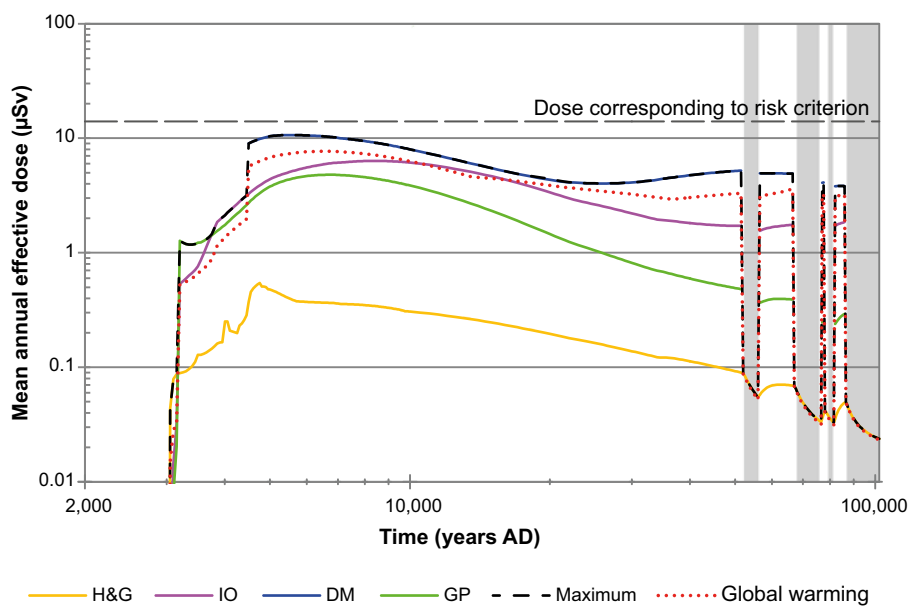


Figure 6-23. Arithmetic mean of the annual dose for different exposed groups in biosphere object 157_2 and maximum dose across all exposed groups and biosphere objects, shown for the accelerated concrete degradation calculation case (CCL_BC). The unshaded areas correspond to temperate climatic conditions and the grey shaded areas to periglacial conditions with continuous permafrost.

Peak annual dose and peak waste vault contributions to maximum dose, see Table 6-5 and Table 6-6, are about 40% higher than for the global warming calculation case. The dominating radionuclides are practically the same as in the global warming calculation case. A small increase in the contribution from Ni-59 and inorganic C-14 to peak dose is due to faster transport in the concrete barriers and concrete waste packaging.

The main contribution to the peak values of the total doses for the DM exposed group comes from waste vaults 1BMA, silo, 2BMA, 1BLA and 2BTF, which together contribute almost 90% of the total dose.

The order of the contributions from the vaults is different from the *global warming calculation case*, with 1BLA and silo having a lower relative contribution in this scenario. This is due to enhanced releases from 1BMA and 2BMA, which have concrete flow barriers. The silo is only negligibly affected by the accelerated concrete degradation, as the bentonite barrier stays intact. The increase of the releases from the far-field due to releases from 1BMA, 2BMA and the silo this scenario is lower in comparison with the *high flow in bedrock scenario* (Section 6.2).

Table 6-5. Peak annual dose to a representative individual of the most exposed group obtained for the accelerated concrete degradation calculation case (CCL_BC).

Annual dose (µSv)	Year (AD)	Contribution from waste vault (%)	Contribution from radionuclides (%)	Exposed group (biosphere object)
10.6	5550	1BMA (33.6)	Mo-93 (59.8)	Drained-mire farmers (Object 157_2)
		Silo (33.6)	C-14-org (17.0)	
		2BMA (8.8)	I-129 (6.4)	
		1BLA (8.4)	U-238 (4.3)	
		2BTF (4.8)	Cl-36 (4.0)	
		1BTF (3.8)	C-14-inorg (2.3)	
		BRT (3.5)	U-235 (1.8)	
		2BLA (1.0)	Ca-41 (1.6)	
		3BLA (1.0)	Ni-59 (1.3)	
		5BLA (0.9)	Others (1.5)	
		4BLA (0.8)		

Table 6-6. Peak annual dose and the time at which the peak is observed for releases from individual waste vaults and from the entire repository in the accelerated concrete degradation calculation case (CCL_BC). The value given for each waste vaults is the sum of values obtained for all released radionuclides. The radionuclides with the highest contribution to the peak doses are indicated.

Waste vault	Annual dose (µSv)	Year (AD)	Biosphere object	Exposed group	Most contributing radionuclide (%)
Silo	3.9	6850	157_2	DM	Mo-93 (50.9)
1BMA	4.2	4800	157_2	DM	Mo-93 (47.7)
1BLA	1.3	24,000	157_1	DM	U-238 (30.5)
1BTF	0.43	5000	157_2	DM	Mo-93 (67.5)
2BTF	0.56	4800	157_2	DM	Mo-93 (70.3)
BRT	0.37	5450	157_2	DM	Mo-93 (98.7)
2BMA	1.6	9350	157_2	DM	Mo-93 (75.6)
2BLA	0.11	21,000	157_1	DM	Ca-41 (39.1)
3BLA	0.10	6050	157_2	DM	Mo-93 (43.3)
4BLA	0.12	20,000	157_1	DM	Ca-41 (39.9)
5BLA	0.13	22,500	157_1	DM	Ca-41 (34.8)
Total SFR 1	10.6	5550	157_2	DM	Mo-93 (59.8)

The radionuclide contributions to the dose vary between the five most contributing waste vaults (1BMA, silo, 1BLA, 2BMA and BRT). This is dictated by differences in the inventory of dose dominating radionuclides in each vault and the different properties of the barriers (see Table 6-6). In this calculation case, the relative contributions from the most dose dominating radionuclides are similar to the ones for the *global warming calculation case*, though peak dose is reached 950 years earlier and is about 40% higher than in the *global warming calculation case*.

Figure 6-24 shows temporal variation in vault contributions to maximum annual dose and Figure 6-25 the radionuclide contributions. Apart from the described shifts in time, the evolution of annual effective dose in this calculation case follows the same pattern as in the *global warming calculation case*.

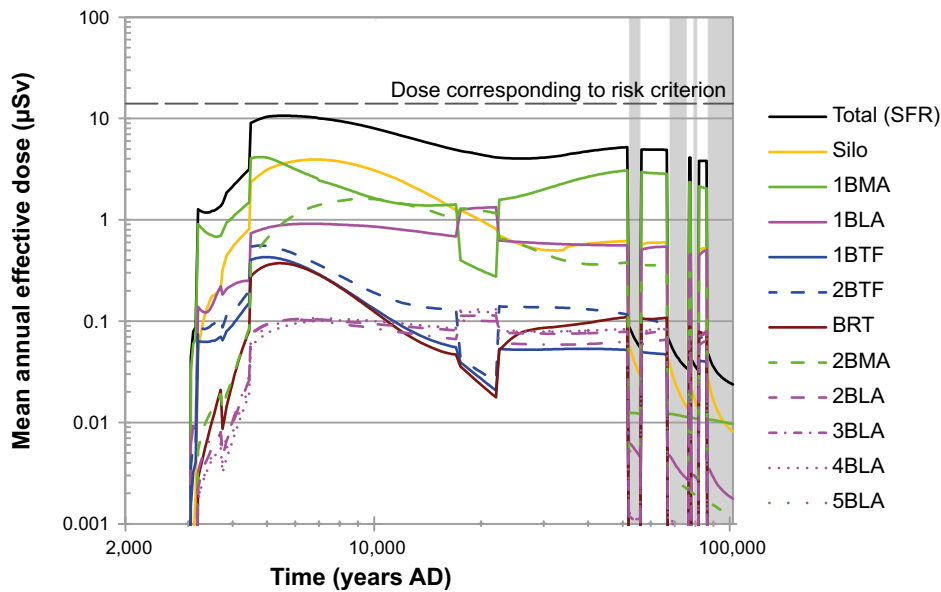


Figure 6-24. Arithmetic mean of the annual dose to the most exposed group for releases from the entire repository and contributions from the individual waste vaults in the **accelerated concrete degradation calculation case (CCL_BC)**. The unshaded areas correspond to temperate climatic conditions and the grey shaded areas to periglacial conditions with continuous permafrost.

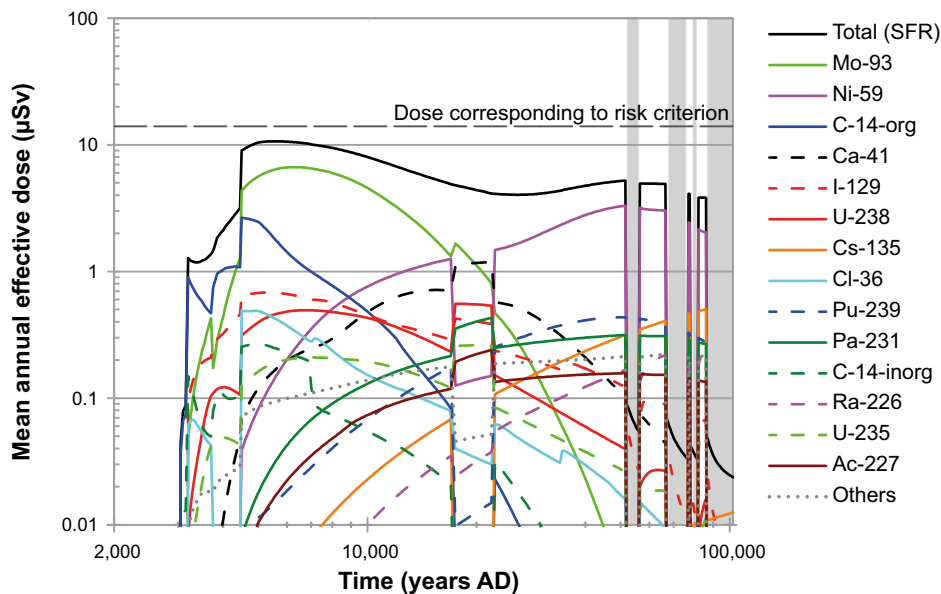


Figure 6-25. Arithmetic mean of the annual effective dose to the most exposed group and respective radionuclide contributions, shown for releases from the entire repository in the **accelerated concrete degradation calculation case (CCL_BC)**. The unshaded areas correspond to temperate climatic conditions and the grey shaded areas to periglacial conditions with continuous permafrost.

After the peak dose at 5550 AD, there is only weak variation in the maximum dose during the whole simulation period, except for periods of the periglacial domain.

Figure 6-26 to Figure 6-30 show the mean annual dose to the most exposed group over the entire simulation period due to releases from waste vaults 1BMA, silo, 2BMA, 1BLA and 2BTF, respectively. The maximum annual dose and the contributions of main radionuclides are presented.

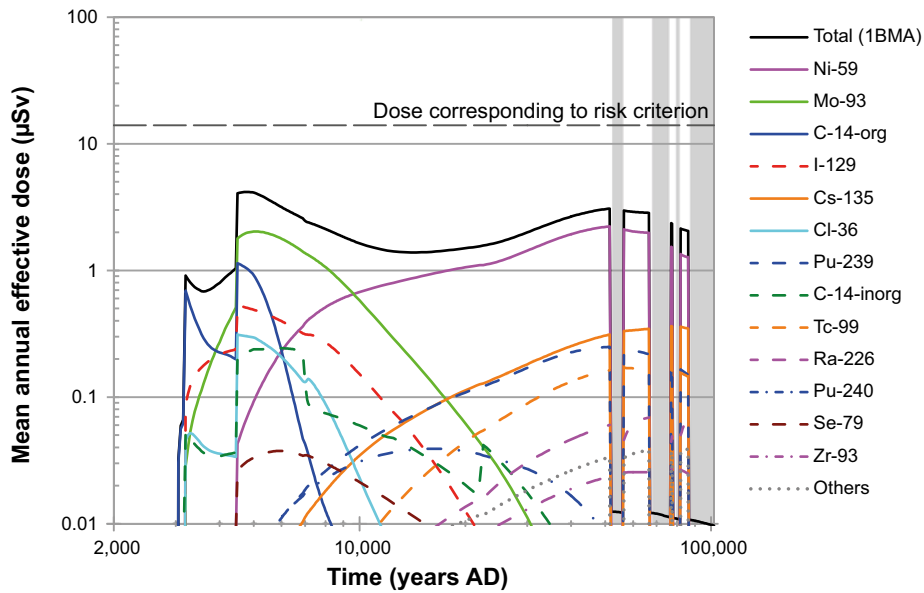


Figure 6-26. Arithmetic mean of the annual dose to the most exposed group, shown for releases from **1BMA** in the **accelerated concrete degradation calculation case**. The unshaded areas correspond to temperate climatic conditions and the grey shaded areas to periglacial conditions with continuous permafrost.

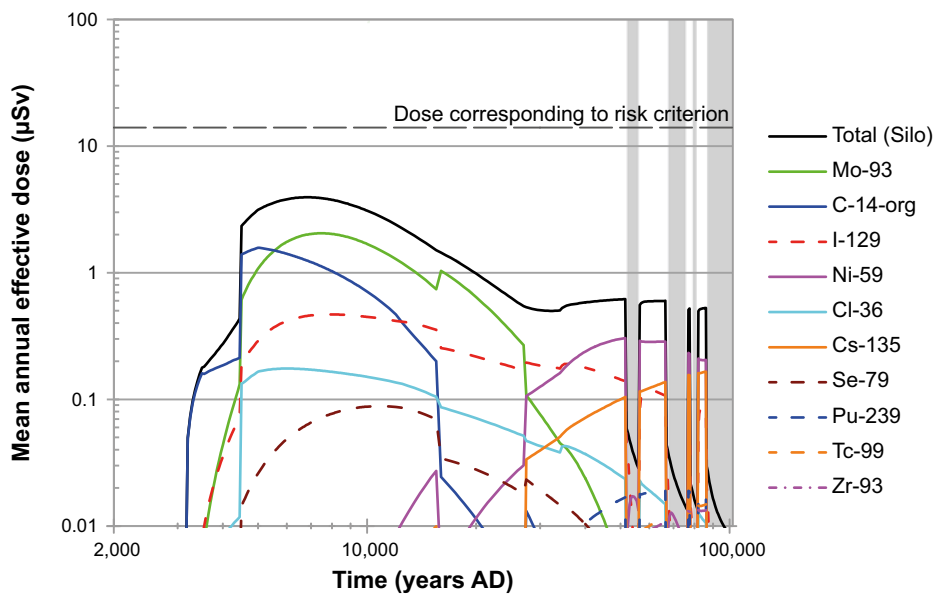


Figure 6-27. Arithmetic mean of the annual dose to the most exposed group, shown for releases from the **Silo** in the **accelerated concrete degradation calculation case**. The unshaded areas correspond to temperate climatic conditions and the grey shaded areas to periglacial conditions with continuous permafrost.

Impact of parameter uncertainty

In addition to the arithmetic mean values presented above, statistics such as the median and different percentiles of the annual dose distribution at each time point have been obtained from the probabilistic calculations. These statistics are used to provide a better understanding of the uncertainties associated with calculated doses. In Figure 6-31, arithmetic mean, median, and 5th and 95th percentiles of the maximum total dose at each point in time are presented. The time evolution of the statistics is different from the *global warming calculation case* as maximum dose is defined by object 157_1 during a much shorter period and, hence, the period with increased uncertainty bandwidth is short in comparison to the corresponding period in the *global warming calculation case*.

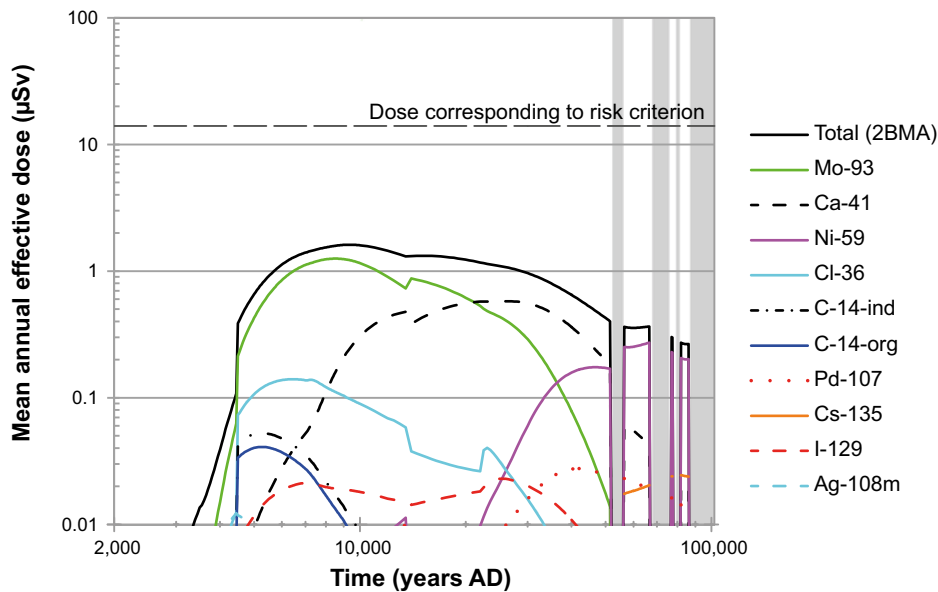


Figure 6-28. Arithmetic mean of the annual dose to the most exposed group, shown for releases from **2BMA** in the **accelerated concrete degradation calculation case**. The unshaded areas correspond to temperate climatic conditions and the grey shaded areas to periglacial conditions with continuous permafrost.

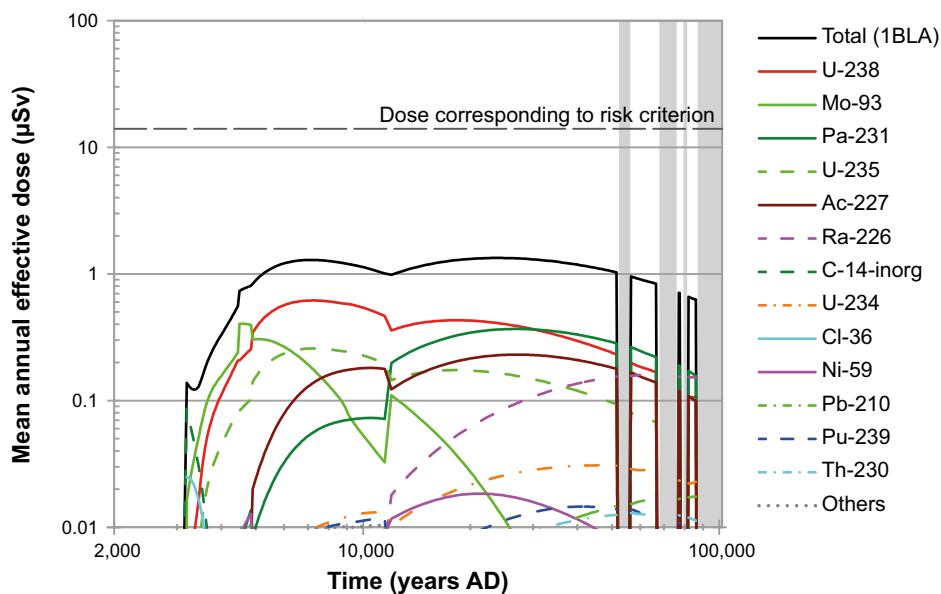


Figure 6-29. Arithmetic mean of the annual dose to the most exposed group, shown for releases from **1BLA** in the **accelerated concrete degradation calculation case**. The unshaded areas correspond to temperate climatic conditions and the grey shaded areas to periglacial conditions with continuous permafrost.

6.4 Bentonite degradation calculation case (CCL_BB)

The *bentonite degradation calculation case (CCL_BB)* is described in Section 4.2.4. In this calculation case, the bentonite as part of the engineered barrier system of the silo degrades due to the formation of an ice-lens during an early periglacial period prevailing from 17,500 AD to 20,500 AD with the consequence of increased water flow in this part of the vaults. For other internal and external conditions, the same assumptions are made as for the *global warming calculation case*.

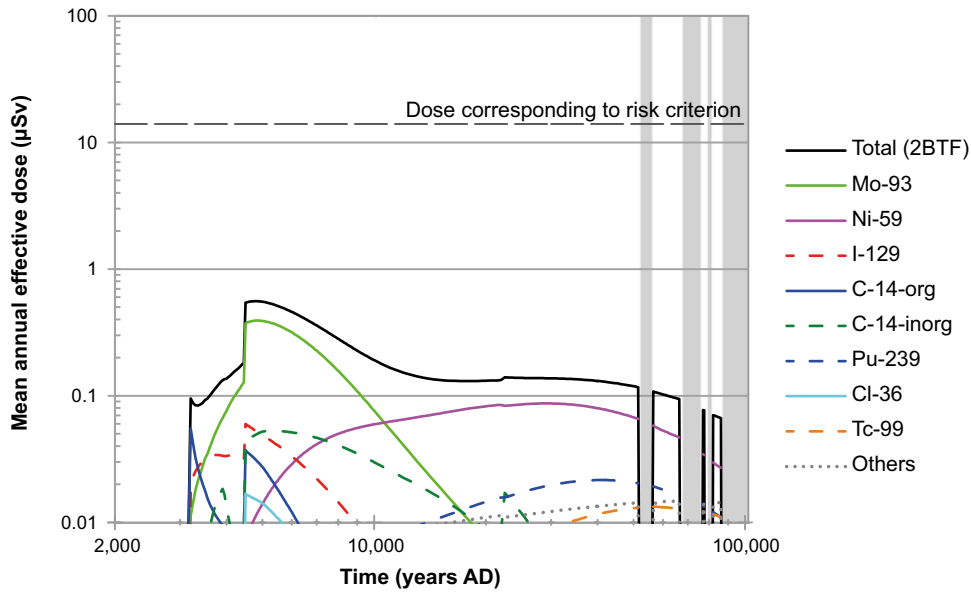


Figure 6-30. Arithmetic mean of the annual dose to the most exposed group, shown for releases from 2BTF in the accelerated concrete degradation calculation case. The unshaded areas correspond to temperate climatic conditions and the grey shaded areas to periglacial conditions with continuous permafrost.

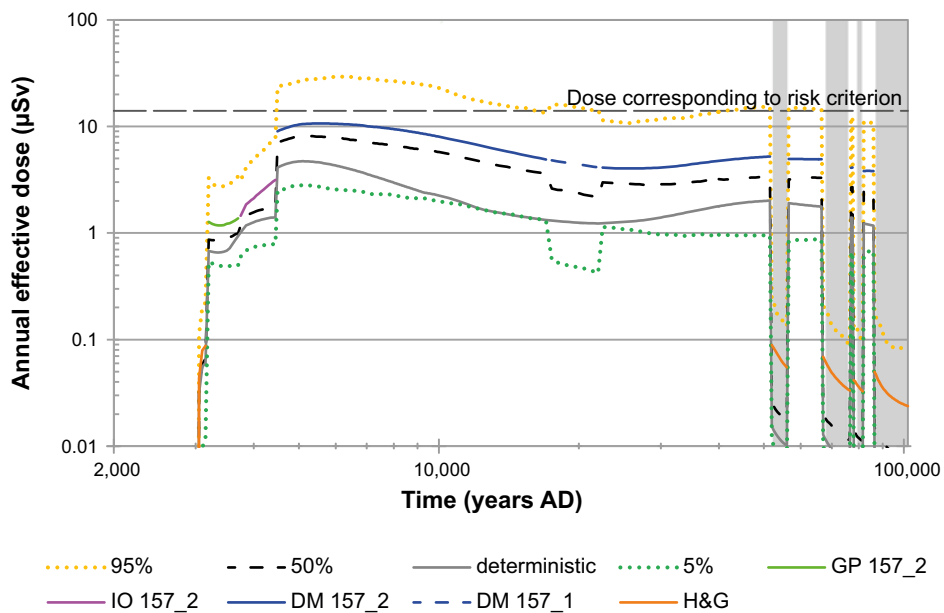


Figure 6-31. Arithmetic mean, median, 5th and 95th percentiles of the annual dose to the most exposed group in the accelerated concrete degradation calculation case. The unshaded areas correspond to temperate climatic conditions and the grey shaded areas to periglacial conditions with continuous permafrost.

Releases

The evolution of releases from the near-field and the far-field over time, as indicated in Figure 6-32 and Figure 6-33 respectively, indicate an increase at the beginning of the second temperate period at 20,500 AD. This is due to the increased water flows in the silo, after the bentonite barrier has been damaged by freezing during permafrost. Freezing occurs after 6500 AD, when peak dose is reached in the *global warming calculation case* (Table 5-2). Peak releases are, for most safety relevant radionuclides, not significantly affected when compared with the *global warming calculation case* as the increase in release at 20,500 is not large enough to cause releases as large as those at 6500 AD.

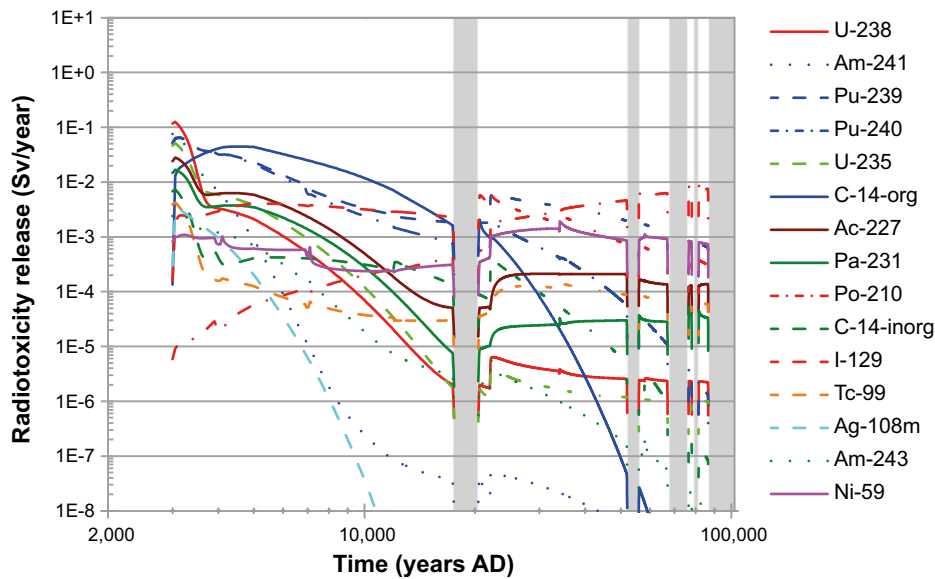


Figure 6-32. Radiotoxicity of releases from the near-field for the 15 most dominating radionuclides in the bentonite degradation calculation case (CCL_BB). The unshaded areas correspond to temperate climatic conditions and the grey shaded areas to periglacial conditions with continuous permafrost.

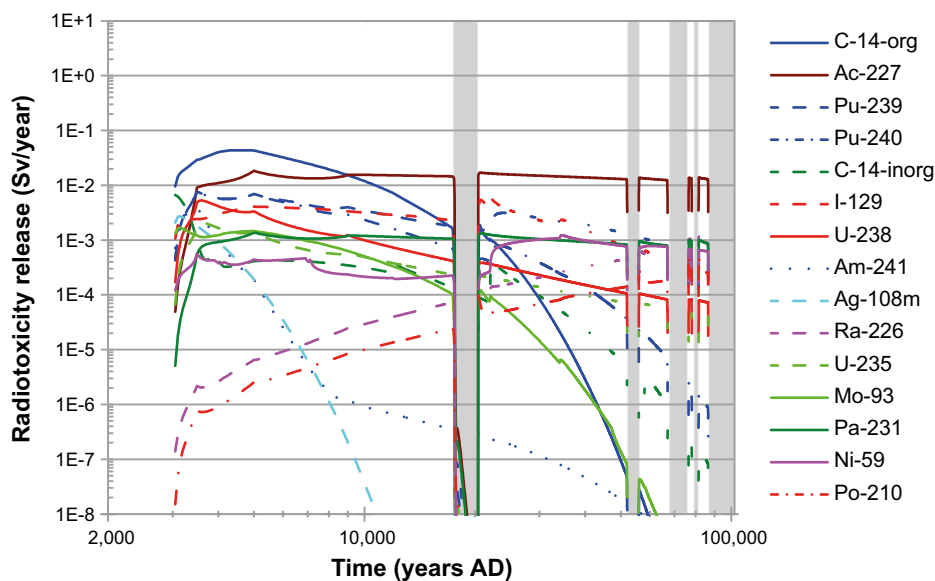


Figure 6-33. Radiotoxicity of releases from the far-field for the 15 most dominating radionuclides in the bentonite degradation calculation case (CCL_BB). The unshaded areas correspond to temperate climatic conditions and the grey shaded areas to periglacial conditions with continuous permafrost.

It should be noted that transport does not occur during the early periglacial period in the near-field and the far-field, assuming that all transport processes are inhibited in the repository and the geosphere by the permafrost. However, ingrowth of progeny of e.g. U-238 continues during permafrost. This results in an elevated release of, for example, Po-210 at 20,500 AD when the permafrost thaws, as compared with the global warming calculation case.

Annual doses

Time series of annual effective doses to the exposed groups in biosphere object 157_2 and the maximum annual effective dose are presented in Figure 6-34, and the contribution of individual radionuclides to the total dose is displayed in Figure 6-35.

Until the start of the early periglacial period, the set-up and results of this calculation case are identical to the *global warming calculation case*. Hence the peak annual dose for this calculation case coincides with the peak of the *global warming calculation case* as the accelerated release of radionuclides after the early periglacial period does not cause a higher dose than during the initial temperate period.

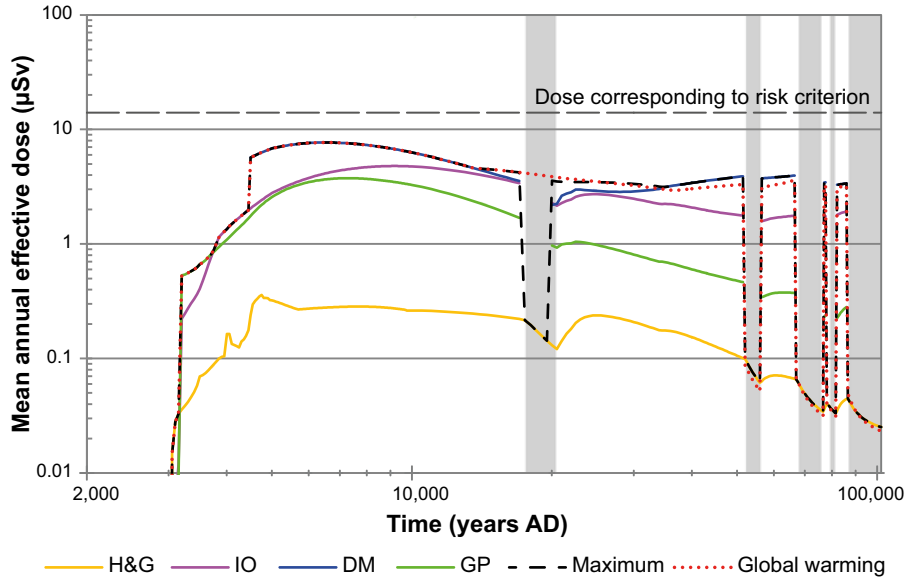


Figure 6-34. Arithmetic mean of the annual effective dose for different exposed groups in biosphere object 157_2 and maximum annual dose across biosphere objects and exposed groups, shown for the **bentonite degradation calculation case**. Maximum annual dose of the **global warming calculation case** is also shown for comparison. The unshaded areas correspond to temperate climatic conditions and the grey shaded areas to periglacial conditions with continuous permafrost.

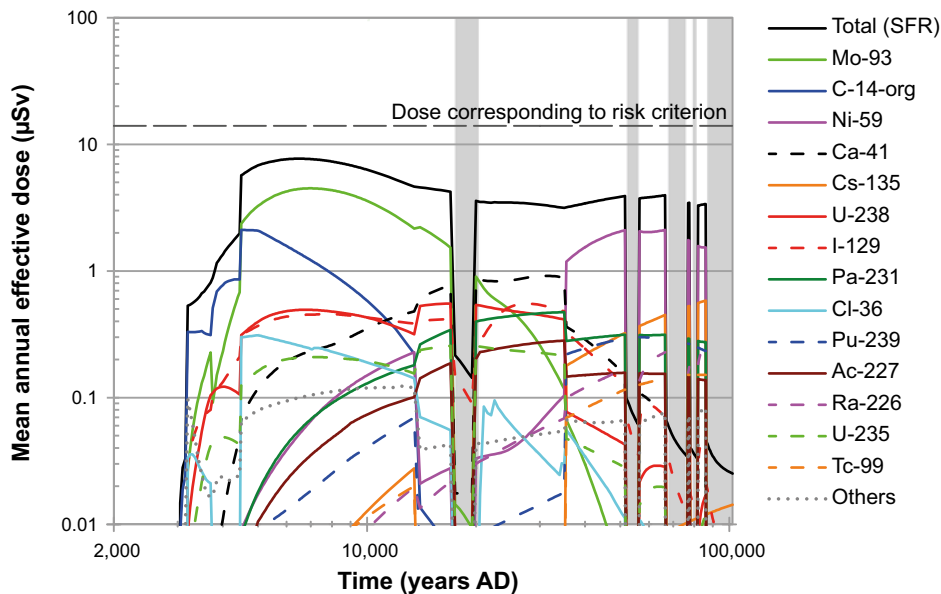


Figure 6-35. Arithmetic mean of the annual effective dose to the most exposed group, shown for releases from the entire repository in the **bentonite degradation calculation case (CCL_BB)**. The unshaded areas correspond to temperate climatic conditions and the grey shaded areas to periglacial conditions with continuous permafrost.

6.5 Earthquake calculation case (CCL_EQ)

The *earthquake calculation case* (CCL_EQ) is described in Section 4.2.5. The effect of increased water flow due to an earthquake damaging the structure of the silo is analysed in this scenario. Note that in this calculation case only doses that result from a release of radionuclides from the silo are analysed. Moreover, parameter values were not sampled, and the calculations were repeated assuming an earthquake to happen every 100 years, starting from repository closure until the end of the assessment period.

Annual doses

The annual effective doses to the exposed groups are presented in Figure 6-36 as a function of time. For all evaluated earthquake events, the highest dose to an exposed group is plotted in the figure for each point in time, irrespective of when the earthquake occurred. The peak dose of 27 μSv for this scenario occurring at 4550 AD, Table 6-7, is due to an earthquake at 2100 AD. The delay between this earthquake and the peak dose is primarily caused by the time it takes for the area to emerge sufficiently above sea level to allow drainage and cultivation of the land. The peak dose of this scenario is about 3.5 times higher than the peak dose of 7.7 μSv in the *global warming calculation case*.

Table 6-7. Peak annual dose to a representative individual of the most exposed group obtained for the earthquake calculation case.

Annual dose (μSv)	Year (AD)	Earthquake event (AD)	Contribution from radionuclides (%)	Exposed group (biosphere object)
27	4550	2100	Mo-93 (71.1) C-14-inorg (9.0) Ni-59 (7.4) I-129 (5.4) C-14-org (2.5) Pu-240 (1.6) Pu-239 (1.4) Others (1.5)	Drained-mire farmers (Object 157_2)

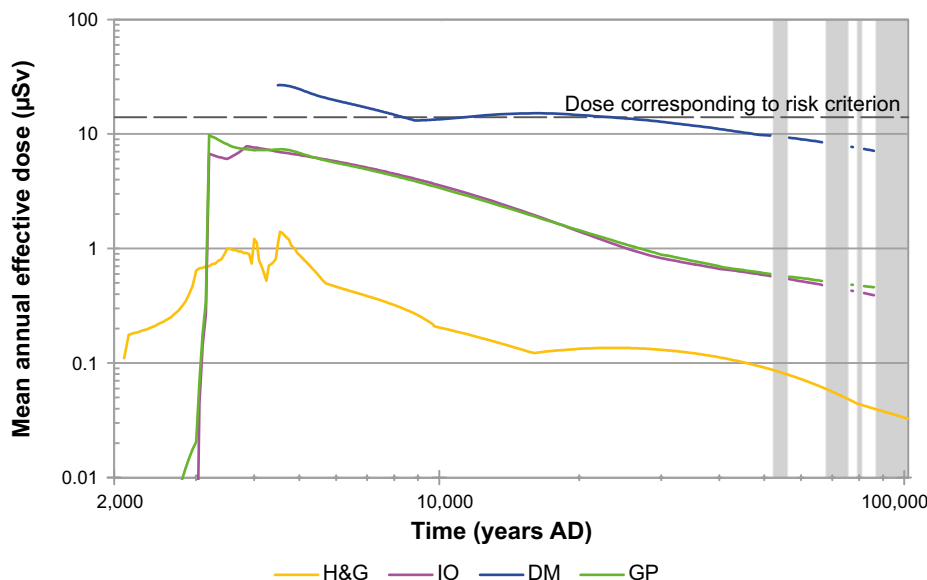


Figure 6-36. Annual dose for exposed groups in biosphere object 157_2 in the *earthquake calculation case*. Horizontal axis reflects time that dose occurs, irrespective of when the earthquake occurred. The unshaded areas correspond to temperate climatic conditions and the grey shaded areas to periglacial conditions with continuous permafrost.

Figure 6-37 shows contributions of the most significant radionuclides to maximum annual dose. Mo-39, inorganic C-14 and Ni-59 are the most important radionuclides contributing to the peak dose, Table 6-7. The highest dose from a single radionuclide is generated by Ni-59, which dominates the dose after 9000 AD, Figure 6-37.

6.6 High concentrations of complexing agents calculation case (CCL_CA)

The *high concentrations of complexing agents calculation case (CCL_CA)* is described in Section 4.2.6. It accounts for uncertainties in the amount of complexing agents and cellulose in the repository. Higher sorption reduction factors than in the *global warming calculation case* are applied to reflect chemical conditions with higher concentrations of complexing agents, see Chapter 7 in the **Data report**. Only radionuclides whose sorption properties are potentially affected by organic complexing agents are attributed the reduction factor for the partitioning coefficient in waste vaults actually containing organic complexing agents (1BMA, silo, 2BMA, 1BTF and 2BTF). The waste vaults, 1BLA and 2-5BLA, where sorption is not included in the model, are not affected by this calculation case. For other internal conditions and for all external conditions the same assumptions as for the *global warming calculation case*.

Releases

Figure 6-38 compares peak releases from the geosphere of the *high concentrations of complexing agents calculation case* to the *global warming calculation case*. The figure shows a significant increase of the peak release for Ni-59. The relatively small changes in radionuclide release for radionuclides other than Ni-59 can be attributed to the fact that these are dominated by non- or weakly-sorbing radionuclides or by radionuclides whose sorption properties are not affected by the presence of complexing agents. Therefore, the changes in K_d values have a rather limited impact. Even for strongly sorbing actinides, decreased K_d values increase the release from the far-field only moderately because of a still significant sorption capacity on cementitious material under the influence of organic complexing agents.

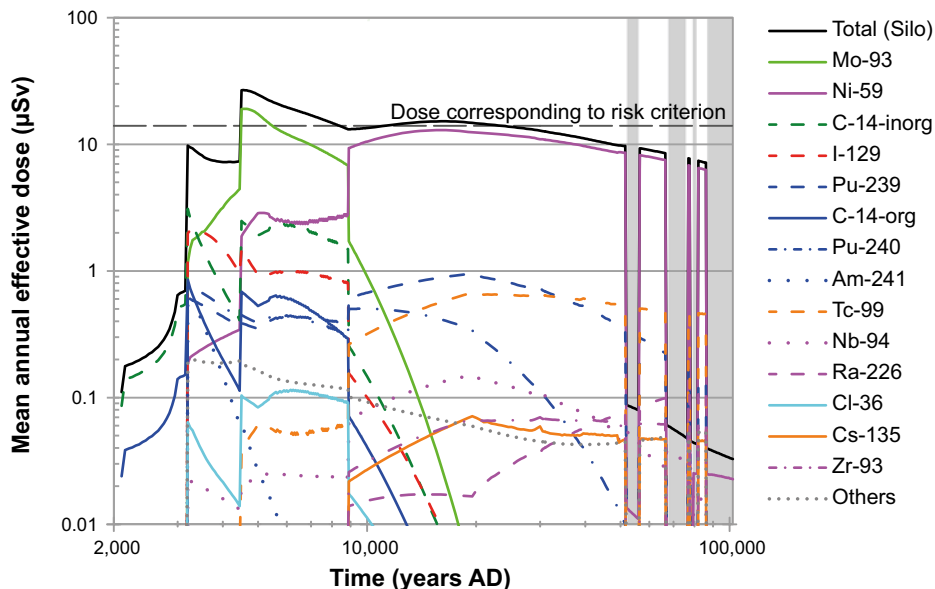


Figure 6-37. The annual dose to the most exposed group and respective contributions from radionuclides in biosphere object 157_2 for releases from the repository in the *earthquake calculation case*. Note that only the *silo* is included in this calculation case (see text). The unshaded areas correspond to temperate climatic conditions and the grey shaded areas to periglacial conditions with continuous permafrost.

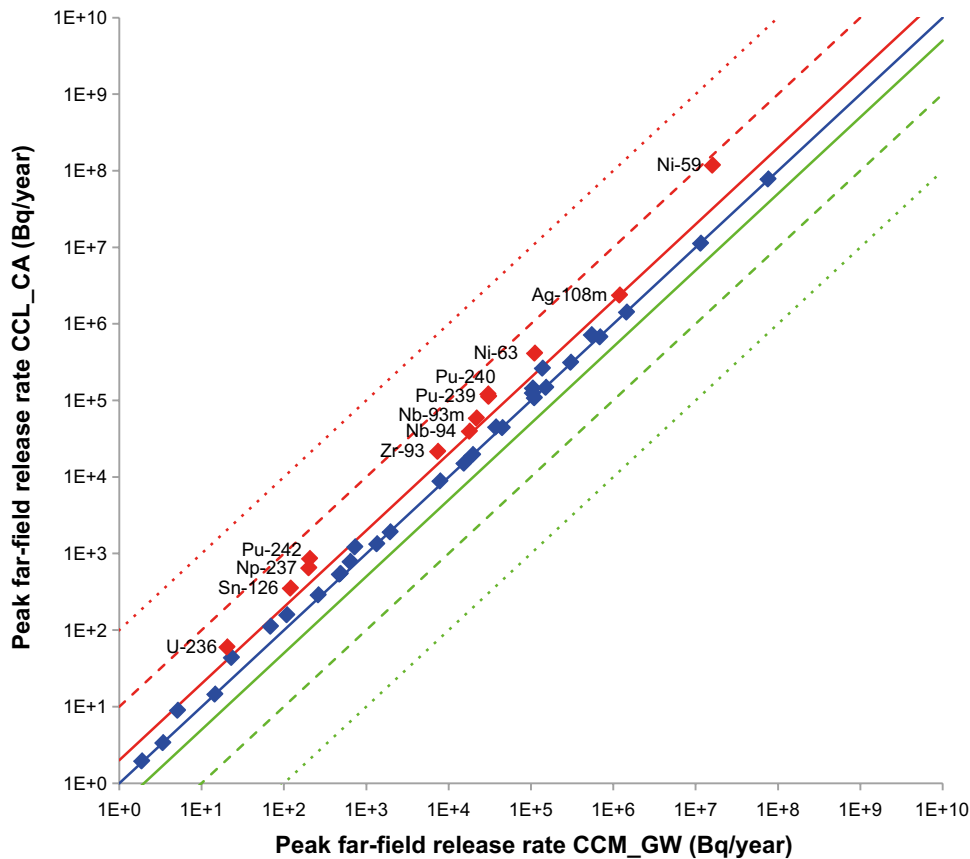


Figure 6-38. Comparison of peak releases from the far-field in the **high concentrations of complexing agents calculation case (CCL_CA)** with the **global warming calculation case (CCL_GW)**. Dots on the blue line on the diagonal represents radionuclides for which the calculated releases in the current calculation case and CCL_GW are the same. At the solid red line the calculated releases are twice as high as in CCL_GW, at the dashed red line the calculated releases are ten times as high as in CCL_GW and at the dotted red line the calculated releases are one hundred times CCL_GW. In the same way the green lines represents 0.5 times, 0.1 times and 0.01 times CCL_GW releases.

Annual doses

Time series of annual effective doses to the exposed groups in biosphere object 157_2 and the maximum annual effective dose are presented in Figure 6-39, and compared with the maximum dose for the *global warming calculation case*. The peak annual effective dose is presented in Table 6-8, together with the year of occurrence, the contributions from the waste vaults and most safety relevant radionuclides, as well as the information of the exposed group for which the peak annual dose occurs and in which of the biosphere objects. The peak annual effective dose is reached, compared with the previously discussed cases, much later, at 44,500 AD, which is late in the first period of the temperate domain. The peak dose is less than a factor 2 higher than in the *global warming calculation case*, 10.7 μ Sv compared to 7.7 μ Sv. After the peak, the maximum dose shows a moderate decrease until the end of the simulation during temperate periods. During periglacial periods, the level of exposure is significantly lower because of the same conceptual assumptions on exposed groups as in previously discussed calculation cases.

Peak contributions from waste vaults are documented in Table 6-9 and the time evolution of waste vault contributions to the maximum dose in Figure 6-40. The contribution of individual radionuclides to the total dose is displayed in Figure 6-41.

The main contribution to the peak dose comes from 1BMA and the silo, which together contribute about 82% to the peak annual dose. The radionuclide contributions to the doses vary between five waste vaults (1BMA, silo, 2BMA, 2BTF and 1BTF) that, in this scenario, are assumed to have

higher concentrations of complexing agents than in the *global warming calculation case*. The vault, that is most affected, is 1BMA because of the large quantities of cellulose deposited therein, see the **Initial state report**. This is despite the fact that the quantity of cellulose in the 1BLA vault is four times higher than in the 1BMA vault, but this has no effect as sorption is not accounted for in 1BLA. Therefore releases and annual dose from 1BLA are the same as in the *global warming calculation case*, see Figure 5-8.

The late and increased peak is due to Ni-59 which is subject, in this calculation case as a conservative approach, to enhanced complexation and is the most important radionuclide in this calculation case. This is clearly seen in Figure 6-42 to Figure 6-46 in which the temporal variation of the annual effective dose and contributions of dominating radionuclides are shown for the five waste vaults having higher concentrations of complexing agents. The radionuclides that dominate the peak dose in the *global warming calculation case* (Mo-93, C-14-org, U-238, I-129, Cl-36 and U-235) are not subject to decreased retardation due to increased levels of complexing agents.

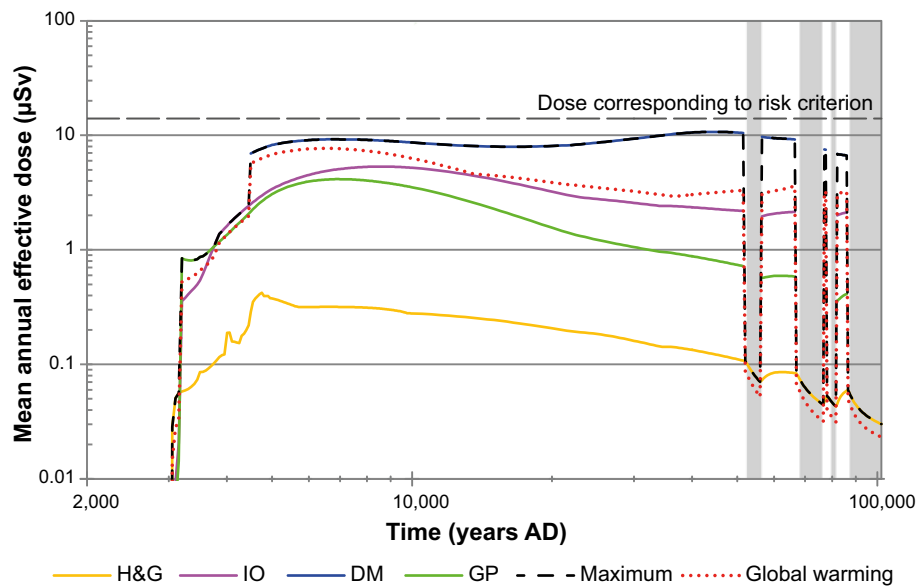


Figure 6-39. Arithmetic mean of annual dose for exposed groups in biosphere object 157_2 and the maximum for all biosphere objects in the **high concentrations of complexing agents calculation case**. Maximum dose for the **global warming calculation case** is also shown for comparison. The unshaded areas correspond to temperate climatic conditions and the grey shaded areas to periglacial conditions with continuous permafrost.

Table 6-8. Peak annual effective dose to a representative individual of the most exposed group obtained for the **high concentrations of complexing agents calculation case**.

Annual dose [µSv]	Year [AD]	Contribution from waste vault (%)	Contribution from radionuclides (%)	Exposed group (biosphere object)
10.7	44,500	1BMA (46.5)	Ni-59 (75.7)	Drained-mire farmers (Object 157_2)
		Silo (36.1)	Pu-239 (8.5)	
		2BMA (6.1)	Pa-231 (2.9)	
		1BLA (5.2)	Cs-135 (2.4)	
		2BTF (1.6)	Ca-41 (2.0)	
		BRT (1.0)	Tc-99 (1.7)	
		1BTF (0.9)	Ra-226 (1.5)	
		4BLA (0.8)	Ac-227 (1.5)	
		5BLA (0.8)	I-129 (1.4)	
		2BLA (0.7)	Others (2.5)	
		3BLA (0.6)		

Table 6-9. Peak annual dose and the time at which the peak is observed for releases from individual waste vaults and from the entire repository in the *high concentration of complexing agents calculation case (CCL_CA)*. The radionuclides with the highest contribution to the waste vault contributions are indicated.

Waste vault	Annual dose (μSv)	Year (AD)	Biosphere object	Exposed group	Most contributing radionuclide (%)
Silo	3.9	45,500	157_2	DM	Ni-59 (75.7)
1BMA	5.0	44,000	157_2	DM	Ni-59 (79.3)
1BLA	1.3	24,000	157_1	DM	U-238 (30.5)
1BTF	0.43	4950	157_2	DM	Mo-93 (67.3)
2BTF	0.53	4850	157_2	DM	Mo-93 (72.0)
BRT	0.37	5450	157_2	DM	Mo-93 (98.7)
2BMA	0.92	11,000	157_2	DM	Mo-93 (61.8)
2BLA	0.11	21,000	157_1	DM	Ca-41 (39.1)
3BLA	0.10	6050	157_2	DM	Mo-93 (43.3)
4BLA	0.12	20,000	157_1	DM	Ca-41 (39.9)
5BLA	0.13	22,500	157_1	DM	Ca-41 (34.8)
Total SFR 1	10.7	44,500	157_2	DM	Ni-59 (75.7)

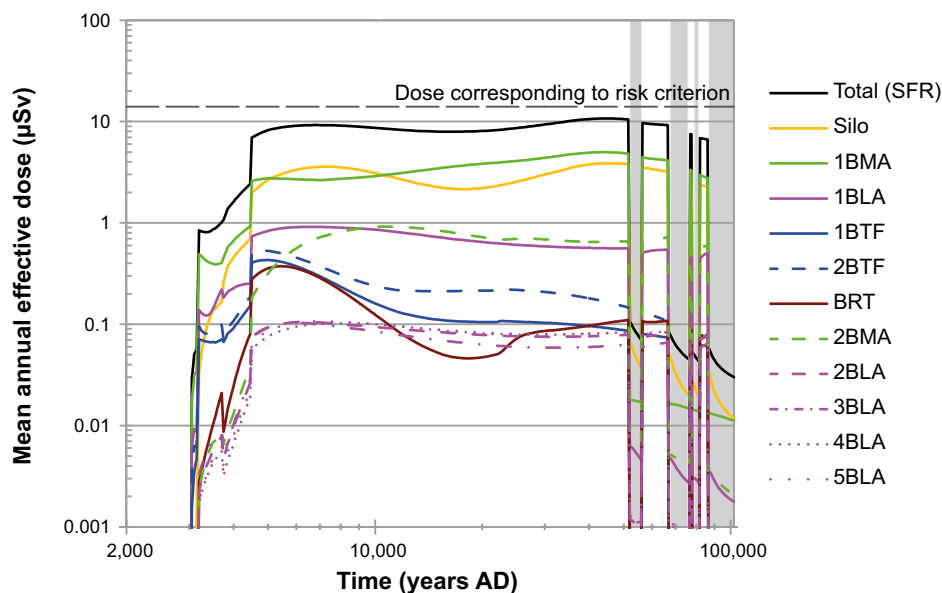


Figure 6-40. Arithmetic mean of the annual dose to the most exposed group for releases from the entire repository and contributions from the individual waste vaults in the *high concentrations of complexing agents calculation case (CCL_CA)*. The unshaded areas correspond to temperate climatic conditions and the grey shaded areas to periglacial conditions with continuous permafrost.

The increased release of Ni-59 over a long period of time is regarded as cautiously estimated, since depletion of complexing agents by advective transport from the waste vaults is not taken into account and also the assumption that retention of nickel is affected by organic complexing agents must be considered very pessimistic.

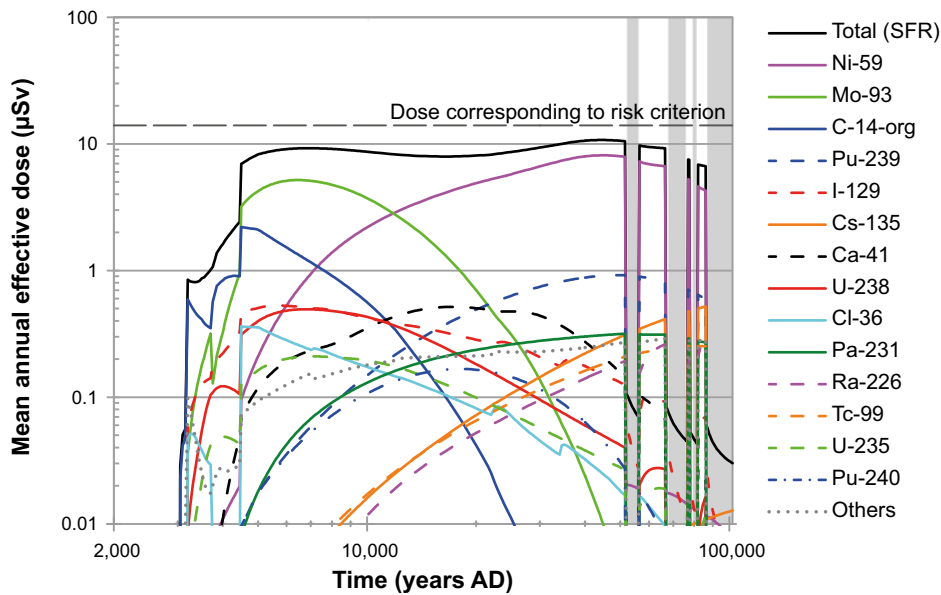


Figure 6-41. Arithmetic mean of the annual dose to the most exposed group and respective radionuclide contributions, shown for releases from the entire repository in the **high concentrations of complexing agents calculation case (CCL_CA)**. The unshaded areas correspond to temperate climatic conditions and the grey shaded areas to periglacial conditions with continuous permafrost.

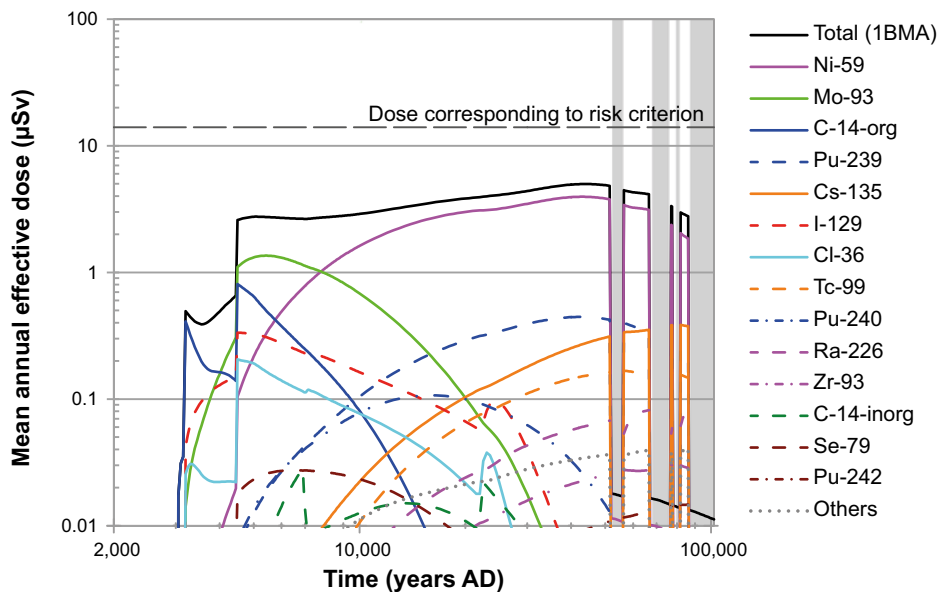


Figure 6-42. Arithmetic mean of the annual dose to the most exposed group, shown for releases from **1BMA** in the **high concentrations of complexing agents calculation case (CCL_CA)**. The unshaded areas correspond to temperate climatic conditions and the grey shaded areas to periglacial conditions with continuous permafrost.

Impact of parameter uncertainty

In addition to the arithmetic mean values presented above, statistics such as the median and different percentiles of the annual dose distribution at each time point have been calculated. These statistics are used to provide a better understanding of the uncertainties associated with calculated doses. In Figure 6-47, arithmetic mean, median, and 5th and 95th percentiles of the maximum total dose at each point in time are presented. The time evolution of the statistics is different from the *global warming calculation case* as maximum dose is always defined by biosphere object 157_2, whereas, in an interim period, it is defined by biosphere object 157_1 in the *global warming calculation case*.

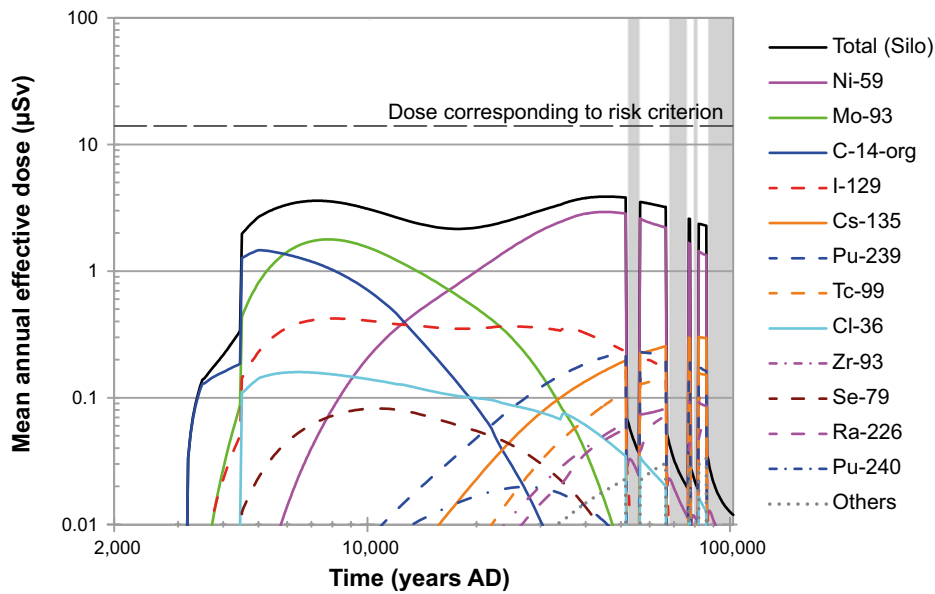


Figure 6-43. Arithmetic mean of the annual dose to the most exposed group, shown for releases from the silo in the high concentrations of complexing agents calculation case (CCL_CA). The unshaded areas correspond to temperate climatic conditions and the grey shaded areas to periglacial conditions with continuous permafrost.

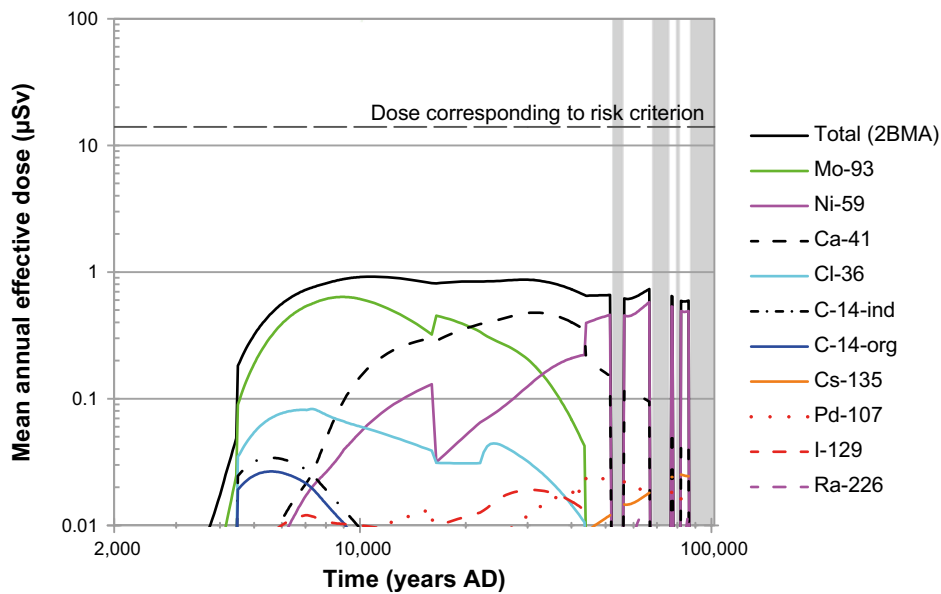


Figure 6-44. Arithmetic mean of the annual dose to the most exposed group, shown for releases from 2BMA in the high concentrations of complexing agents calculation case (CCL_CA). The unshaded areas correspond to temperate climatic conditions and the grey shaded areas to periglacial conditions with continuous permafrost.

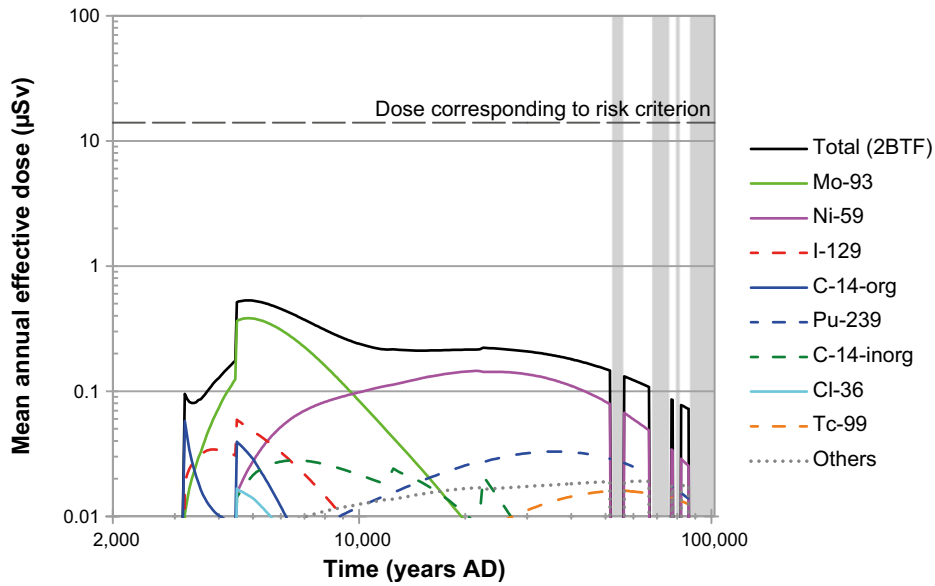


Figure 6-45. Arithmetic mean of the annual dose to the most exposed group, shown for releases from 2BTf in the **high concentrations of complexing agents calculation case (CCL_CA)**. The unshaded areas correspond to temperate climatic conditions and the grey shaded areas to periglacial conditions with continuous permafrost.

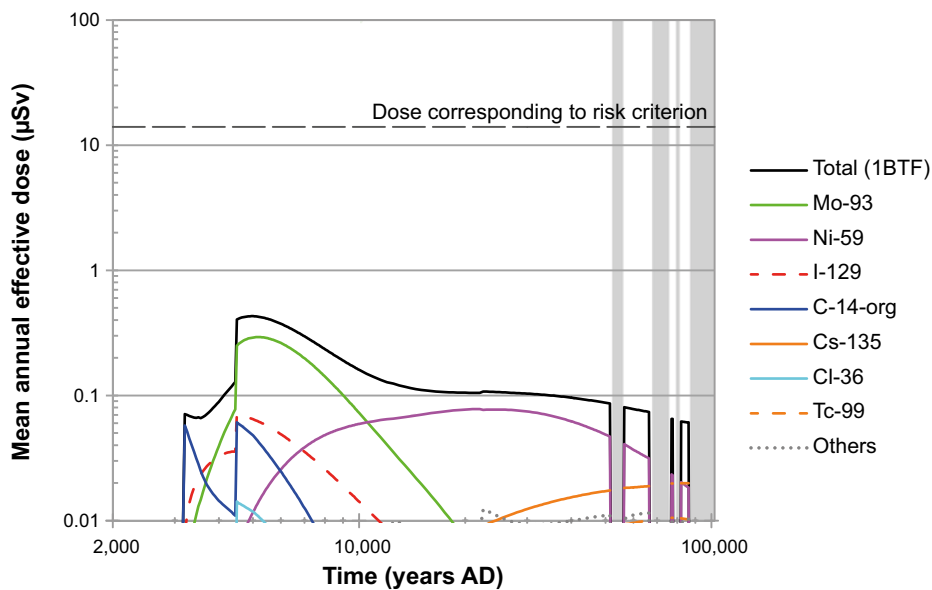


Figure 6-46. Arithmetic mean of the annual dose to the most exposed group, shown for releases from 1BTf in the **high concentrations of complexing agents calculation case (CCL_CA)**. The unshaded areas correspond to temperate climatic conditions and the grey shaded areas to periglacial conditions with continuous permafrost.

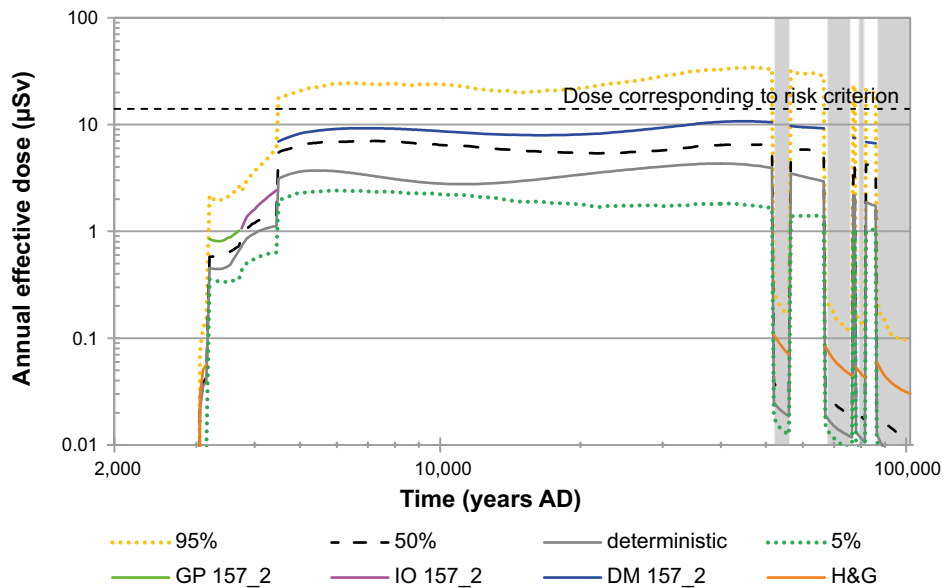


Figure 6-47. Arithmetic mean, median, 5th and 95th percentiles of the annual dose to a representative individual of the most exposed group from SFR in the **high concentrations of complexing agents case (CCL_CA)**. The unshaded areas correspond to temperate climatic conditions and the grey shaded areas to periglacial conditions with continuous permafrost.

6.7 Wells downstream of the repository calculation case (CCL_WD)

The *wells downstream of the repository calculation case* is described in Section 4.2.7. The objective of this calculation case is to assess the radiological consequences of a water-supply well downstream of the repository, but which is close enough so that it can be affected by a release from the repository. This is considered possible after 2500 AD. It is assumed that a well (of unlimited life-time) in the so-called *well interaction area* captures 10% of the radionuclide releases from each waste vault (Section 6.4.5 in Werner et al. 2013). The calculation case is based on waste vault releases of the *global warming calculation case*. Doses are calculated for the *GP* exposed group.

Annual doses

Table 6-10 shows the peak annual dose and the dose contributions from the waste vaults. The releases from the near-field, and the far-field, in this scenario, are the same as in the *global warming calculation case*. Temporal variance in the annual effective dose and the contributions from waste vaults are shown in Figure 6-48. Figure 6-49 shows contributions from radionuclides to annual dose due to releases from the entire repository. Additionally, Figures 6-50, 6-51 and 6-52 provide this information for the most contributing waste vaults 1BLA, 1BMA and silo, respectively.

For all waste vaults, a moderately decreasing trend in the doses is observed after the peak dose.

The results show that Ac-227 contributes most to the peak dose; the most relevant exposure pathway is ingestion of well water. The major part of Ac-227 in the well water is due to releases from 1BLA. Radionuclides of the decay-chains $4n$, $4n+2$ and $4n+3$ (Table 3-1) contribute more than 60% to the peak annual dose.

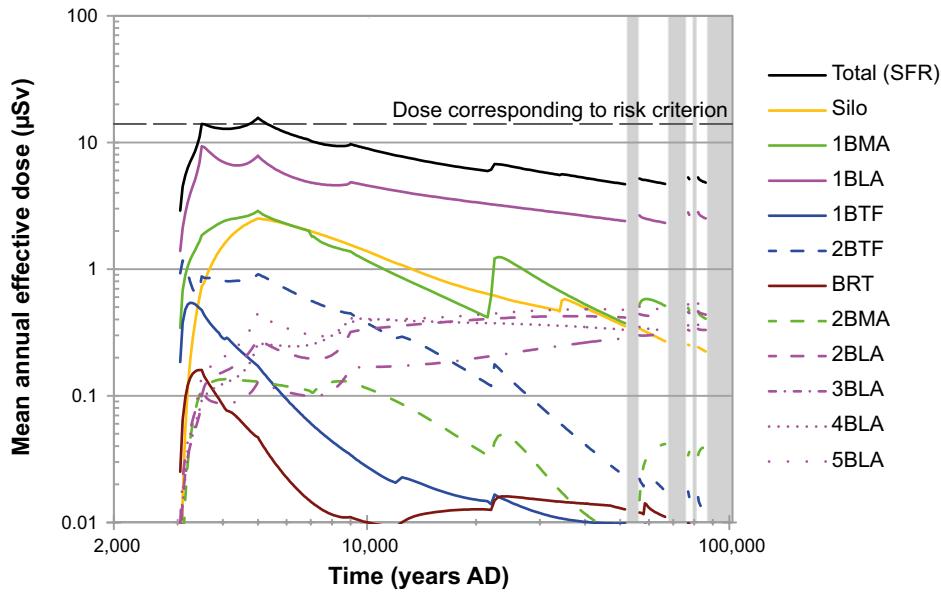


Figure 6-48. Arithmetic mean of the annual dose to the most exposed group for releases from the entire repository and contributions from the individual waste vaults in the **wells downstream of the repository calculation case**. The unshaded areas correspond to temperate climatic conditions and the grey shaded areas to periglacial conditions with continuous permafrost.

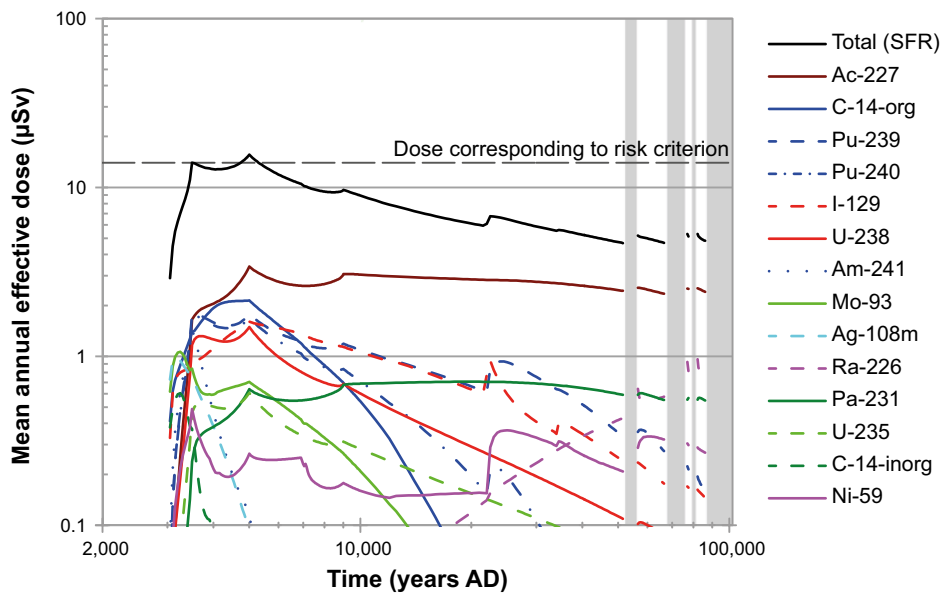


Figure 6-49. Arithmetic mean of the annual dose for the garden plot household exposed group, shown for releases from the entire repository in the **wells downstream of the repository calculation case (CCL_WD)**. The unshaded areas correspond to temperate climatic conditions and the grey shaded areas to periglacial conditions with continuous permafrost.

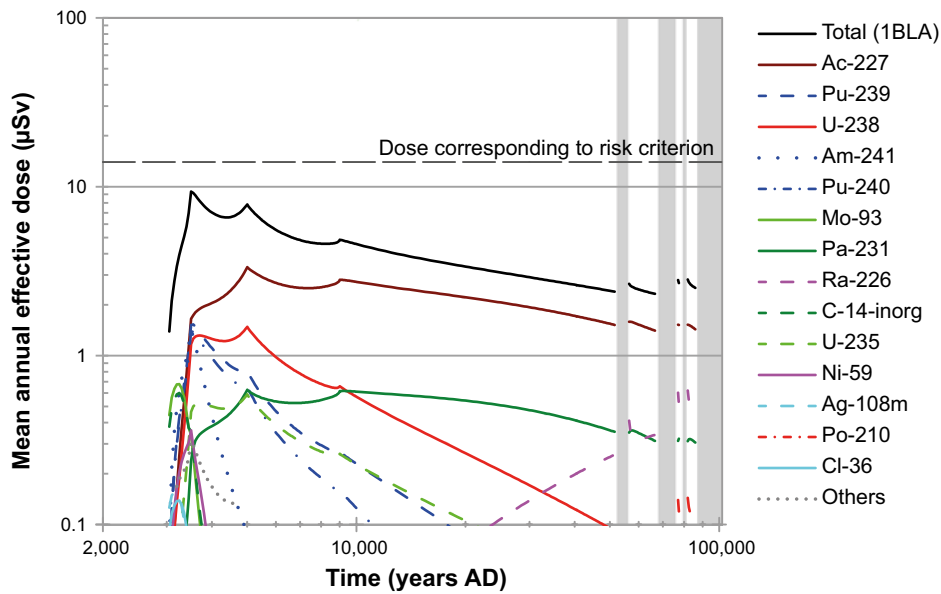


Figure 6-50. Arithmetic mean of the annual dose for the garden plot household exposed group shown for from 1BLA in the wells downstream of the repository calculation case (CCL_WD). The unshaded areas correspond to temperate climatic conditions and the grey shaded areas to periglacial conditions with continuous permafrost.

Table 6-10. Peak value of the annual dose to a representative individual of the most exposed group obtained for the wells downstream the repository calculation case (CCL_WD).

Annual dose (µSv)	Year (AD)	Contribution from waste vault (%)	Contribution from radionuclides (%)	Exposed group
16	5000	1BLA (50.2)	Ac-227 (21.8)	GP
		1BMA (18.4)	C-14-org (13.7)	
		Silo (16.0)	Pu-239 (11.5)	
		2BTF (5.8)	Pu-240 (10.9)	
		5BLA (2.9)	I-129 (10.3)	
		2BLA (1.8)	U-238 (9.5)	
		4BLA (1.8)	Mo-93 (4.5)	
		1BTF (1.1)	Pa-231 (4.1)	
		3BLA (0.8)	U-235 (3.9)	
		2BMA (0.8)	Ca-41 (1.9)	
		BRT (0.3)	Ni-59 (1.7)	
			Se-79 (1.2)	
			Others (5.1)	

Impact of parameter uncertainty

The values of the different statistics obtained in the calculation are presented in Figure 6-53 including the arithmetic mean, median, and 5th and 95th percentiles of the maximum total dose at each point in time. The uncertainty is largely due to geosphere transport properties of decay products of U-238 and U-235.

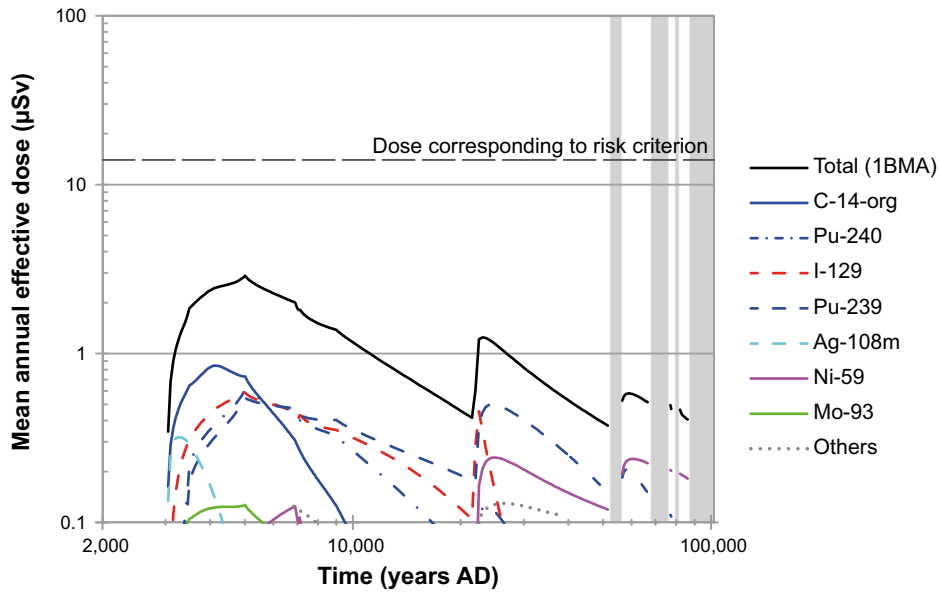


Figure 6-51. Arithmetic mean of the annual dose for the garden plot household exposed group, shown for releases from **IBMA** in the wells downstream of the repository calculation case (CCL_WD). The unshaded areas correspond to temperate climatic conditions and the grey shaded areas to periglacial conditions with continuous permafrost.

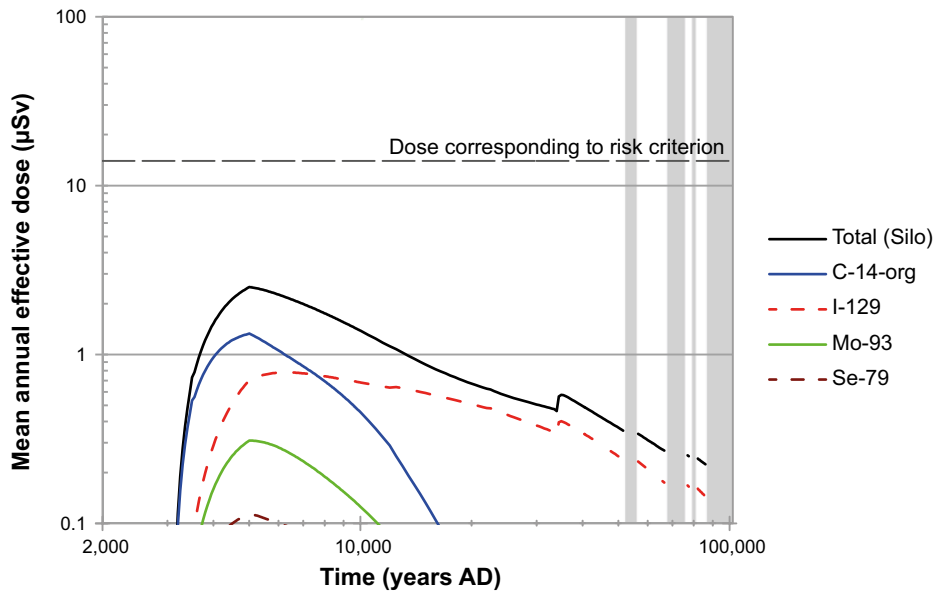


Figure 6-52. Arithmetic mean of the annual dose for the garden plot household exposed group, shown for releases from the **silo** in the wells downstream of the repository calculation case (CCL_WD). The unshaded areas correspond to temperate climatic conditions and the grey shaded areas to periglacial conditions with continuous permafrost.

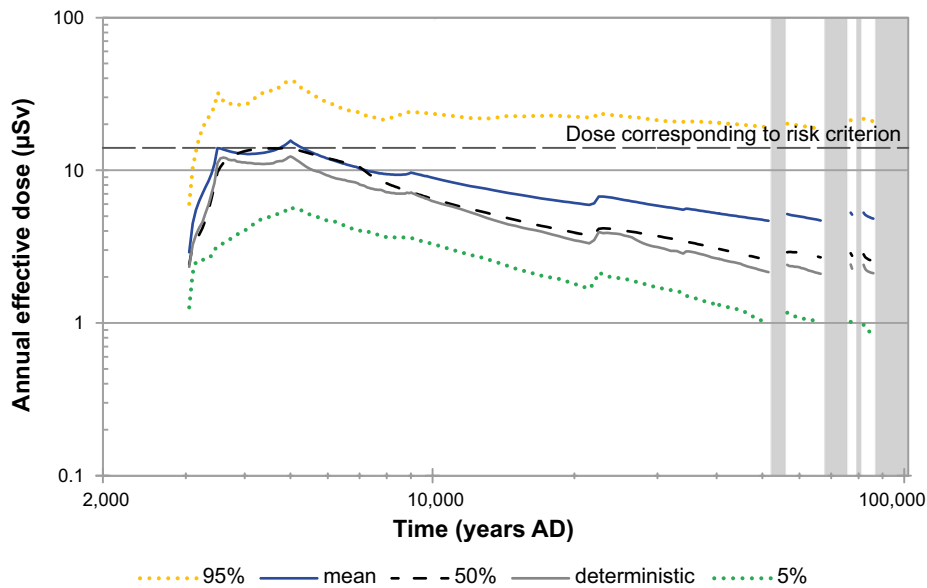


Figure 6-53. Arithmetic mean, median, 5th and 95th percentiles of the annual dose to a representative individual of the most exposed group in the wells downstream of the repository calculation case (CCL_WD). The unshaded areas correspond to temperate climatic conditions and the grey shaded areas to periglacial conditions with continuous permafrost.

6.8 Intrusion wells calculation case (CCL_WI)

The *intrusion wells calculation case* is described in Section 4.2.8. The objective of the case is to assess the radiological consequences of a water-supply well which is drilled directly into one of the waste vaults; each waste vault represents a variant for the case. The inventory of the near field evolves as in the *global warming calculation case*. For the present calculation case, assumptions made for near-field releases in the *global warming calculation case* might not be cautious, as a slower rate of radionuclide migration from the near-field would lead to a higher rate of radioactive ingrowth in the vaults. Variants of the calculation case with increased residence times, address the impact of radioactive ingrowth; these variants are applied only for the 1BLA vault, which is the vault with the highest annual dose in the *intrusion wells calculation case*. Doses are calculated for the GP exposed group as in the *wells downstream of the repository calculation case*.

Annual doses

Table 6-11 reports the peak values of annual doses, as well as the radionuclide contribution for each waste vault. The peak annual doses caused by the individual waste vaults vary within a range of 40 µSv for BRT to 4,500 µSv for 1BLA. Figure 6-54 shows the temporal evolution of annual doses for each waste vault.

Initially (at 3000 AD) the dose is dominated by 1BLA. However the inventory in 1BLA is quickly depleted as radionuclides are released. It should be noted that the high consequences from 1BLA are also related to the fact that the 1BLA model has no separate compartments for waste and void space. Hence, a full mixing of nuclides is assumed to take place immediately at 3000 AD. This is not the case for the other vaults.

Variants with alternative transport properties for 1BLA

In the 1BLA-vaults retention of radionuclides is not accounted for. This leads to high initial concentrations and transport of radionuclides. Such an assumption is normally conservative as more short-lived radionuclides will contribute to the dose. For radionuclide decay-chains where the total radiotoxicity increases with time, this might not be true. For these cases, assuming the radionuclide transport rate was lower, doses might be higher if a well is drilled at a late stage.

Table 6-11. Peak annual effective dose, for each waste vault, to a representative individual of the potentially most exposed group obtained for the intrusion wells calculation case.

SFR 1			
Waste vault	Annual dose [μ Sv]	Year [AD]	Contributions from radionuclides (%)
Silo	1,406	4450	C-14-org (59.9), I-129 (23.9), Mo-93 (10.6), Se-79 (3.4), Cl-36 (1.1) and Others (1.1)
1BMA	1,474	4100	Pu-240 (34.0), Pu-239 (28.6), C-14-org (22.2), I-129 (7.7), Ag-108m (2.5), Mo-93 (1.6), Se-79 (1.1) and Others (2.3)
1BLA	4,524	3050	U-238 (30.3), Am-241 (17.8), Pu-239 (13.6), Pu-240 (12.8), U-235 (12.1), Ac-227 (6.5), Pa-231 (4.0), Tc-99 (1.0) and Others (1.9)
1BTF	145	3250	C-14-org (36.6), I-129 (34.0), Ag-108m (13.3), Mo-93 (11.3), Cs-135 (2.6), Cl-36 (1.0) and Others (1.2)
2BTF	194	3850	Pu-240 (40.6), Pu-239 (33.5), I-129 (9.0), C-14-org (5.0), Mo-93 (4.9), Ag-108m (2.9), Ni-59 (2.3) and Others (1.8)
SFR 3			
Waste vault	Annual dose [μ Sv]	Year [AD]	Contributions from radionuclides (%)
2BMA	73	86,000	Po-210 (84.4), Ni-59 (10.6), Ra-226 (3.4) and Others (1.6)
2BLA	923	3450	Pu-239 (29.8), Pu-240 (28.4), Am-241 (18.7), U-235 (6.9), Ac-227 (5.2), U-238 (3.9), Pa-231 (3.1), Am-243 (1.5) and Others (2.7)
3BLA	897	3400	Pu-239 (29.4), Pu-240 (28.1), Am-241 (19.9), U-235 (6.8), Ac-227 (4.9), U-238 (3.8), Pa-231 (3.0), Am-243 (1.4) and Others (2.6)
4BLA	749	3550	Pu-239 (30.5), Pu-240 (28.9), Am-241 (16.3), U-235 (7.1), Ac-227 (5.7), U-238 (4.0), Pa-231 (3.4), Am-243 (1.5) and Others (2.7)
5BLA	982	3550	Pu-239 (30.5), Pu-240 (28.9), Am-241 (16.3), U-235 (7.1), Ac-227 (5.7), U-238 (4.0), Pa-231 (3.4), Am-243 (1.5) and Others (2.7)
BRT	39	3250	Ag-108m (63.4), Mo-93 (26.9), Ni-59 (5.8), Pu-240 (2.0), Pu-239 (1.5) and Others (0.4)

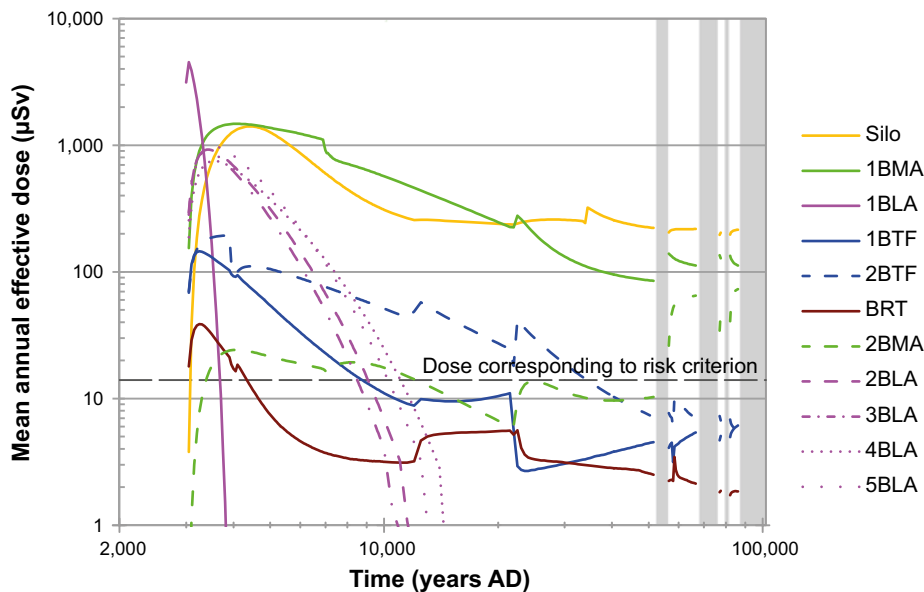


Figure 6-54. Arithmetic mean of the annual effective dose for the garden plot household exposed group, shown for the individual waste vaults in the intrusion wells calculation case (CCL_WI). The unshaded areas correspond to temperate climatic conditions and the grey shaded areas to periglacial conditions with continuous permafrost.

To estimate the possible consequences of higher residence time, variants of the calculation case with alternative transport properties for 1BLA were investigated. The alternative transport properties are sorption and/or solubility limits. As the model for 1BLA is very simple the implementation of this has been done by reducing the water flow, with 1–4 magnitudes, to increase the residence time and scaling the resulting concentrations with the same factor, to obtain the corresponding radionuclide concentration in the water. Figure 6-55 shows the resulting doses which are lower than in the main case for intrusion wells. However, the doses are dominated by progeny of U-235 (Ac-227 and Pa-231) and U-238 (Po-210) in the two variants with the highest residence times. Figure 6-56 shows the radionuclides that contribute most to the dose, in the variant with three magnitudes higher residence time which gives the highest dose in the far future when progeny dominates the doses.

6.9 Scenario combination 1 calculation case (CCC_SC1)

The *scenario combination 1 calculation case*, described in Section 4.4.1, addresses the combination of scenarios *high flow in the bedrock scenario* and *accelerated concrete degradation scenario*.

Figure 6-57 shows the temporal evolution of annual doses for the calculation case and Table 6-12 reports the information related to peak dose. The peak dose of 15.5 μSv is about 5 μSv higher than in the corresponding calculation cases for the single scenarios and occurs 550 years later than in the *accelerated concrete degradation calculation case* and 150 years earlier than in the *high flow in the bedrock calculation case*. The most dose dominating radionuclides are similar in both the single scenario cases and in the combined case with Mo-93 and C-14-org contributing about 77% to peak dose. Remarkably, the silo contributes only about 29%, whereas it contributes about 34% and 44% in the single scenario cases, but 2BMA contributes 24% in the combined scenario but not more than 12% in the single scenarios, this can be expected as the releases from 1BMA and 2BMA are significantly affected by both accelerated concrete degradation and complexing agents, while the releases from the silo are not significantly affected by the concrete degradation. The contribution of 1BMA (27%) is between 15% and 34% of the single scenarios.

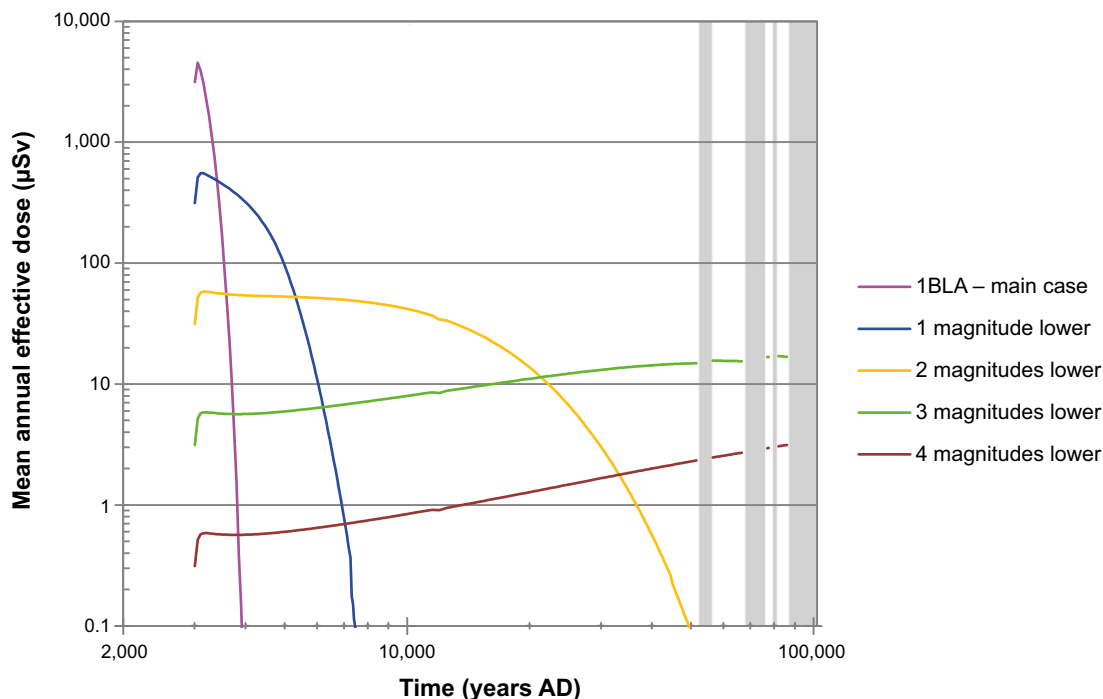


Figure 6-55. Arithmetic mean of the annual effective dose for the garden plot household exposed group, shown for the variants of the **intrusion wells calculation case** with alternative transport properties where 1 to 4 orders of magnitude lower activity concentrations in the water is assumed.

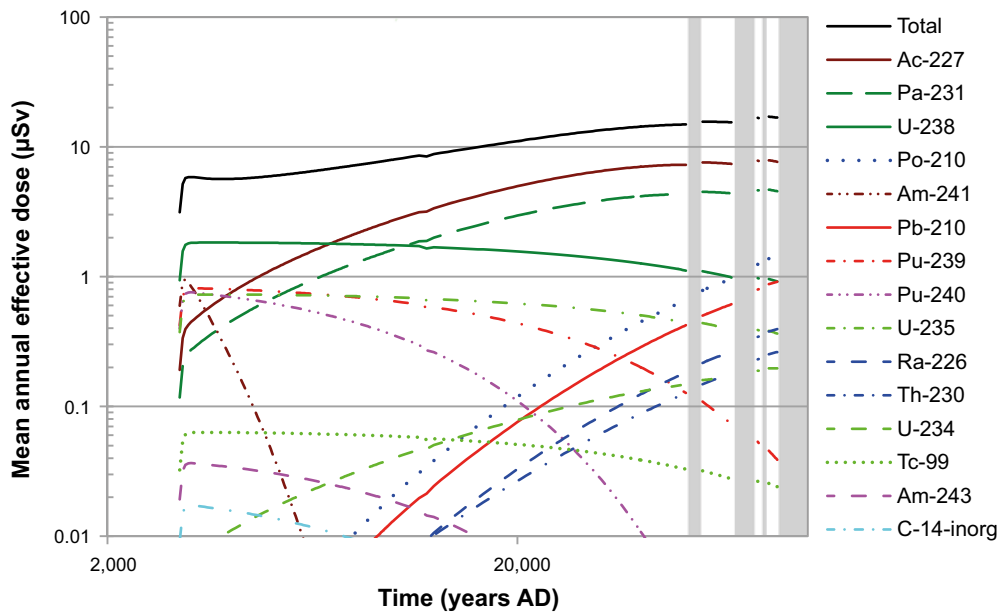


Figure 6-56. Arithmetic mean of the annual effective dose for the garden plot household exposed group, shown for the radionuclides that contribute most to the dose in the **intrusion wells calculation case** with alternative transport properties where 3 orders of magnitude lower activity concentration in the water is assumed.

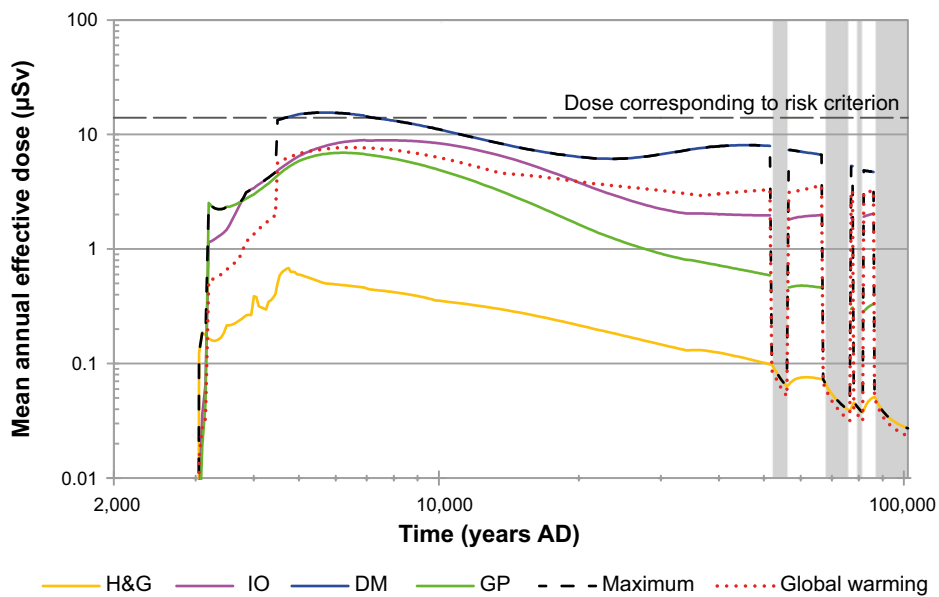


Figure 6-57. Arithmetic mean of annual dose for exposed groups in biosphere object 157_2 and the maximum for all biosphere objects in the **scenario combination 1 calculation case**. Maximum annual effective dose for the **global warming calculation case** is also shown for comparison. The unshaded areas correspond to temperate climatic conditions and the grey shaded areas to periglacial conditions with continuous permafrost.

Table 6-12. Peak annual dose to a representative individual of the most exposed group obtained for scenario combination 1 calculation case.

Annual dose [μ Sv]	Year [AD]	Contribution from waste vault (%)	Contribution from radionuclide (%)	Exposed group (biosphere object)
15.5	5700	Silo (29.1)	Mo-93 (66.3)	Drained-mire farmer (Object 157_2)
		1BMA (26.8)	C-14-org (10.3)	
		2BMA (23.8)	I-129 (5.2)	
		1BLA (7.4)	U-238 (4.1)	
		2BTF (3.8)	C-14-inorg (3.9)	
		1BTF (2.9)	Ni-59 (2.6)	
		BRT (2.9)	Cl-36 (2.3)	
		4BLA (0.9)	Ca-41 (1.8)	
		5BLA (0.9)	U-235 (1.8)	
		2BLA (0.8)	Others (1.7)	
		3BLA (0.8)		

6.10 Scenario combination 2 calculation case (CCC_SC2)

The *scenario combination 2 calculation case*, described in Section 4.4.2, addresses the combination of scenarios *high flow in the bedrock calculation case* and *high concentrations of complexing agents calculation case*.

Figure 6-58 shows the time evolution of annual doses for the calculation case and Table 6-13 summarises the information relating to peak dose. The results for this combination of scenarios are comparable to the outcomes for the *high concentration of complexing agents calculation case*. The peak dose of 13.3 μ Sv occurs late at 40,000 AD but is still 4,500 years earlier than in the *high concentration of complexing agents calculation case* and is 25% higher. Contributions from waste vaults and radionuclides are similar to those in the *high concentration of complexing agents calculation case*. Radionuclide contributions are clearly dominated by Ni-59 (nearly 80%), whereas 1BMA dominates for the waste vaults; the 1BMA vault and the silo are together responsible for more than 80% of the peak dose at 40,000 AD. Dose contributions from both 1BMA and the silo have increased significantly (at 40,000 AD). The contribution from 1BMA increases significantly due to both higher bedrock flow and complexing agents, while the increase in releases from the silo is less sensitive to the higher bedrock flow.

Table 6-13. Peak annual dose to a representative individual of the most exposed group obtained for the scenario combination 2 calculation case.

Annual dose [μ Sv]	Year [AD]	Contribution from waste vault (%)	Contribution from radionuclide (%)	Exposed group (biosphere object)	
13.3	40,000	1BMA (50.2)	Ni-59 (78.0)	Drained-mire farmer (Object 157_2)	
		Silo (32.0)	Pu-239 (8.4)		
		2BMA (8.0)	Pa-231 (2.3)		
		1BLA (4.1)	Cs-135 (1.9)		
		2BTF (1.3)	Ca-41 (1.7)		
		BRT (1.1)	Tc-99 (1.5)		
		4BLA (0.8)	I-129 (1.4)		
		5BLA (0.7)	Ac-227 (1.3)		
		1BTF (0.7)	Ra-226 (1.1)		
		2BLA (0.6)	Others (2.4)		
		3BLA (0.5)			

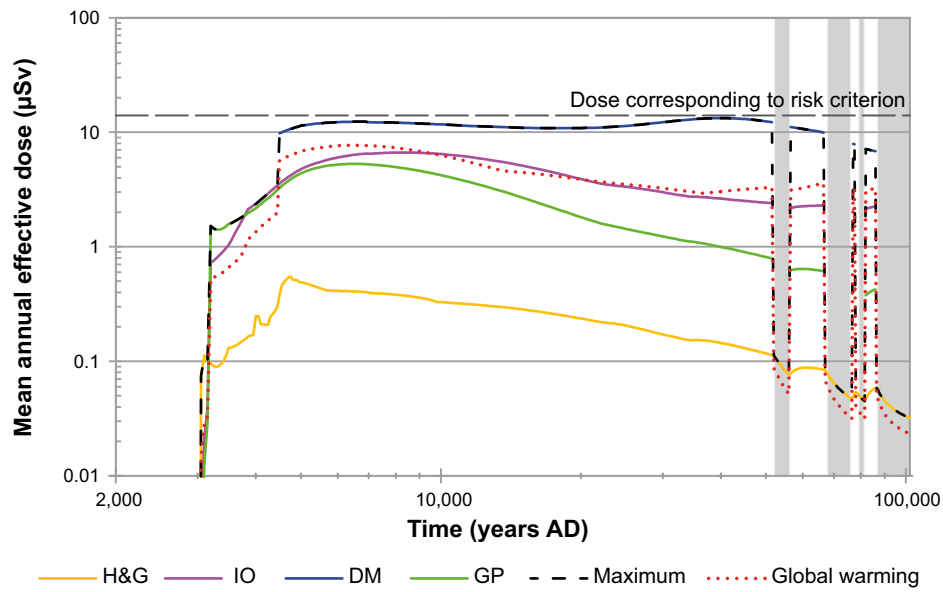


Figure 6-58. Arithmetic mean of annual dose for exposed groups in biosphere object 157_2 and the maximum across biosphere objects and exposed groups in the **scenario combination 2 calculation case**. Maximum dose for the **global warming calculation case** is also shown for comparison. The unshaded areas correspond to temperate climatic conditions and the grey shaded areas to periglacial conditions with continuous permafrost.

7 Results for calculation cases in residual scenarios

This chapter presents results from calculation cases for residual scenarios which are described in Section 4.3. It presents results for the radionuclides contributing significantly to dose, and cumulative results from all radionuclides. Appendix E provides a more complete compilation of results including those for less significant radionuclides.

7.1 Loss of barrier function calculation case – no sorption in the repository (CCR_B1)

The *loss of barrier function calculation case – no sorption in the repository* is described in Section 4.3.1. The objective of this case is to illustrate the importance of sorption in the near-field, which is dominated by sorption on cement. In this calculation case, radionuclides do not sorb in the near-field, i.e. K_d values for the near-field are set to zero. Other internal and external conditions are assumed to be the same as in the *global warming calculation case*.

Releases

Figure 7-1 shows a comparison of peak releases from the far-field in the *loss of barrier function calculation case – no sorption in the repository* (CCR_B1) with the *global warming calculation case* (CCM_GW).

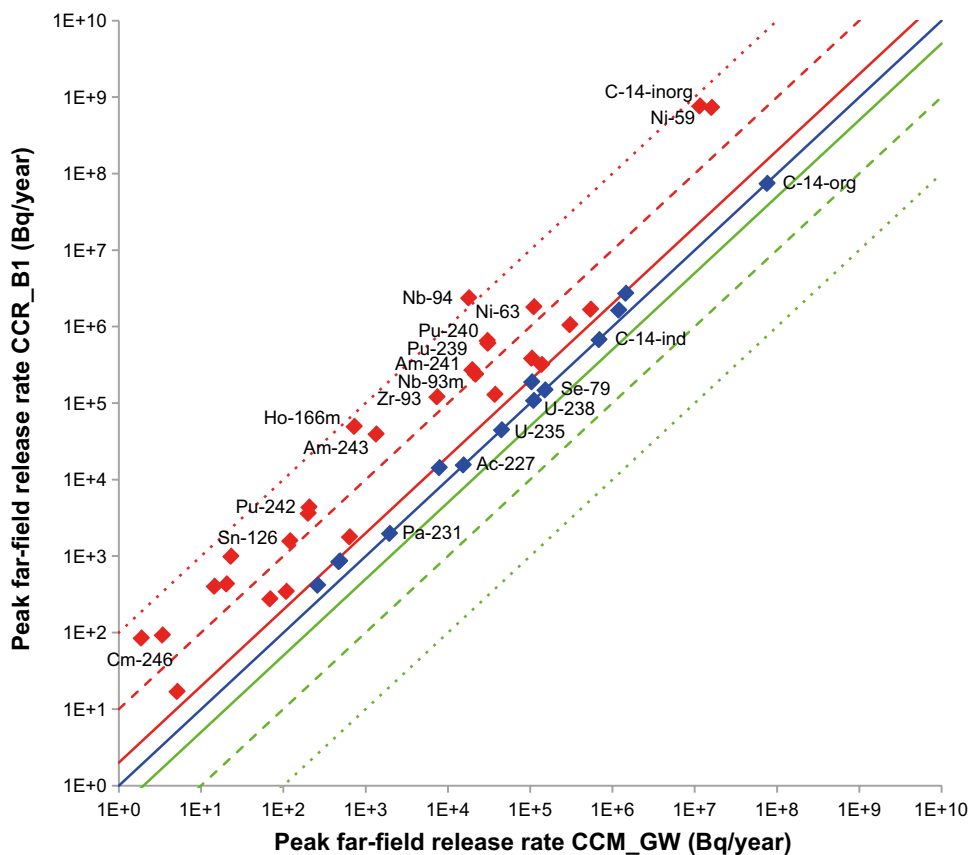


Figure 7-1. Comparison of peak releases from the far-field in the *loss of barrier function calculation case – no sorption in the repository* (CCR_B1) with the *global warming calculation case* (CCM_GW). Dots on the blue line on the diagonal represents radionuclides for which the calculated releases in the current calculation case and the CCM_GW are the same. At the solid red line the calculated releases are twice as high as in CCM_GW and at the dashed red line the calculated releases are ten times as high as in CCM_GW and at the dotted red line the calculated releases are one hundred times the CCM_GW value. In the same way, the green lines represents 0.5 times, 0.1 times and 0.01 times the CCM_GW releases.

The relevance of the chemical barriers in the near-field for most radionuclides is obvious. An exception is U-235 with progeny (Ac-227 and Pa-231) and U-238, as a consequence of neglect of any form of retardation in the near-field for these parent radionuclides in 1BLA in the *global warming calculation case*. Also C-14-ind, C-14-org and Se-79 are unaffected in this calculation case as they are not sorbing (or very weakly sorbing) in the near-field.

Annual doses

Temporal variation of annual effective doses to the exposed groups in biosphere object 157_2 and the maximum annual effective dose are presented in Figure 7-2, and compared with the maximum dose of the *global warming calculation case*. Peak dose and related data are reported in Table 7-1 and peak contributions from waste vaults in Table 7-2. Figures 7-3 and 7-4 present the contributions of waste vaults and radionuclides, respectively, to maximum dose.

Table 7-1. Peak annual dose to a representative individual of the most exposed group obtained for the loss of barrier function calculation case – no sorption in the repository (CCR_B1).

Annual dose (µSv)	Year (AD)	Contribution from waste vault (%)	Contribution from radionuclides (%)	Exposed group (biosphere object)
41.4	25,000	Silo (62.2)	Ni-59 (77.3)	Drained-mire farmers (Object 157_2)
		1BMA (25.4)	Pu-239 (12.3)	
		2BMA (8.1)	Pu-240 (2.8)	
		1BLA (1.5)	Tc-99 (1.0)	
		BRT (0.9)	Ca-41 (1.1)	
		1BTF (0.8)	Tc-99 (1.0)	
		2BTF (0.6)	Mo-93 (1.0)	
		5BLA (0.2)	Others (5.0)	
		4BLA (0.2)		
		2BLA (0.2)		
		3BLA (0.1)		

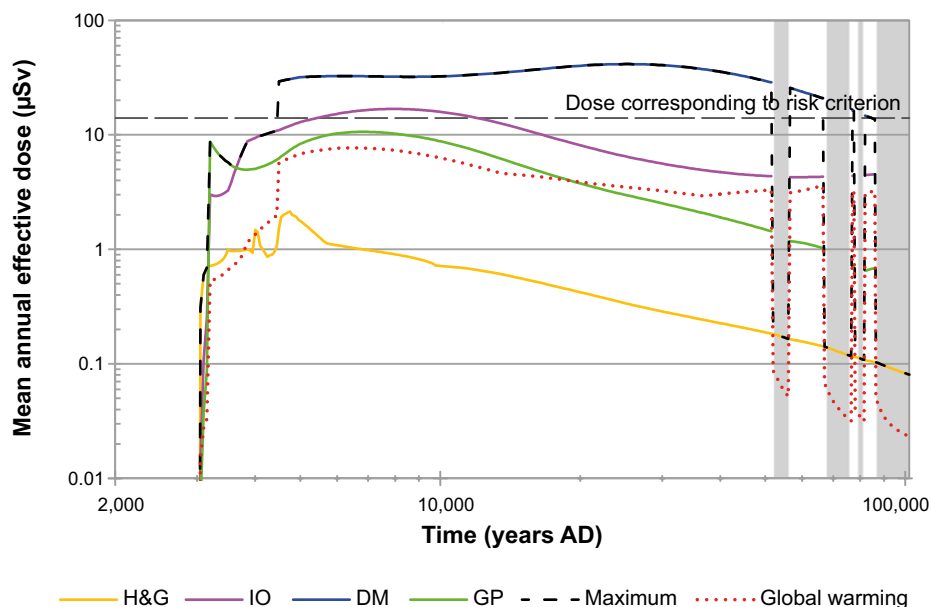


Figure 7-2. Arithmetic mean of annual dose for the different exposed groups in object 157_2 and maximum dose across exposed groups and biosphere objects. Values are shown for the loss of barrier function calculation case – no sorption in the repository (CCR_B1). The unshaded areas correspond to temperate climatic conditions and the grey shaded areas to periglacial conditions with continuous permafrost.

The peak dose of 41.4 μSv is about five times higher than the peak dose for the *global warming calculation case* and occurs nearly 20,000 years later. As for other calculation cases with lower retardation of radionuclides in the near-field, the relative dose contributions from the silo, 1BMA and 2BMA become more important. The silo and 1BMA contribute 87% to the peak dose and 2BMA with another 8%. The radionuclides Ni-59, Pu-239 and Pu-240, less mobile radionuclides in calculation cases of the main scenario, account for 92% of the peak dose. It is worth noting that the increase of contributions from strongly sorbing radionuclides (to peak dose) is relatively higher than the total increase of peak dose, hence the strongly sorbing radionuclides Ni-59 and Pu-239 become the most dose contributing ones in this calculation case. These results highlight that sorption in the near-field contributes significantly to the safety function of retardation.

Table 7-2. Peak annual dose and the time at which the peak is observed for releases from individual waste vaults and from the entire repository in the *loss of barrier function calculation case – no sorption in the repository (CCR_B1)*. The radionuclides with the highest contribution to the peak doses are indicated.

Waste vault	Annual dose (μSv)	Year (AD)	Biosphere object	Exposed group	Most contributing radionuclide (%)
Silo	26.1	28,000	157_2	DM	Ni-59 (78.4)
1BMA	12.3	4500	157_2	DM	C-14-inorg (65.0)
1BLA	1.3	24,000	157_1	DM	U-238 (30.5)
1BTF	1.5	4500	157_2	DM	C-14-inorg (54.3)
2BTF	2.9	3200	157_2	GP	C-14-inorg (95.5)
BRT	0.66	4800	157_2	DM	Mo-93 (87.6)
2BMA	3.6	7900	157_2	DM	Mo-93 (65.5)
2BLA	0.11	21,000	157_1	DM	Ca-41 (39.1)
3BLA	0.10	6050	157_2	DM	Mo-93 (43.3)
4BLA	0.12	20,000	157_1	DM	Ca-41 (39.9)
5BLA	0.13	22,500	157_1	DM	Ca-41 (34.8)
Total SFR	41.5	25,000	157_2	DM	Ni-59 (77.3)

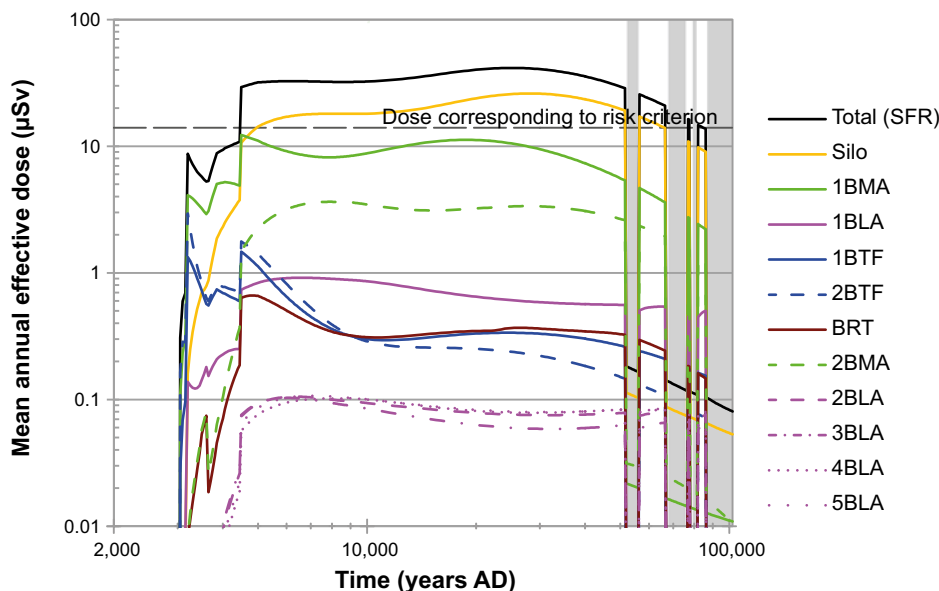


Figure 7-3. Arithmetic mean of the annual dose to the most exposed group for releases from the entire repository and contributions from the individual waste vaults in the *loss of barrier function calculation case – no sorption in the repository*. The unshaded areas correspond to temperate climatic conditions and the grey shaded areas to periglacial conditions with continuous permafrost.

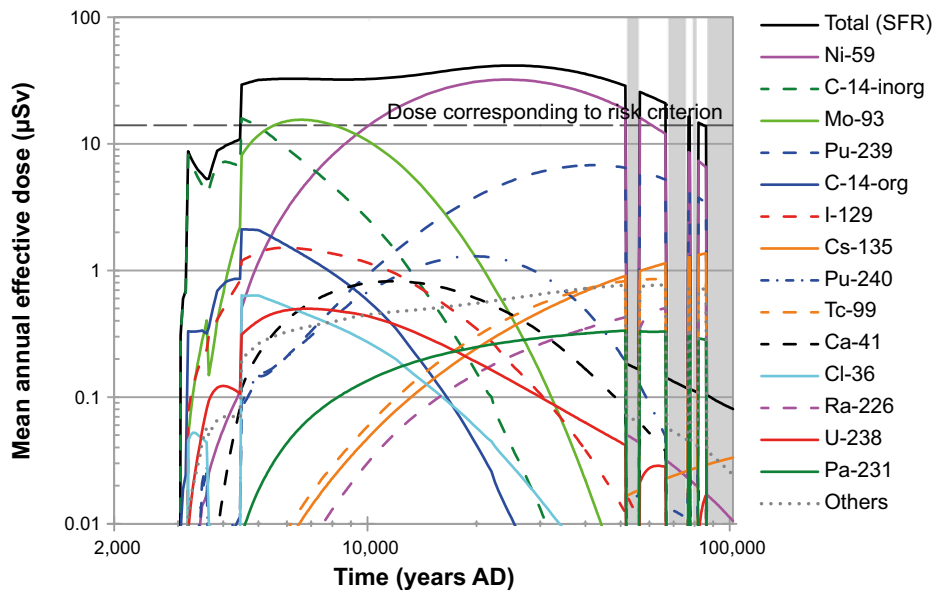


Figure 7-4. Arithmetic mean of the annual dose to the most exposed group and respective radionuclide contributions, shown for releases from the entire repository in the **loss of barrier function calculation case** – no sorption in the repository. The unshaded areas correspond to temperate climatic conditions and the grey shaded areas to periglacial conditions with continuous permafrost.

Impact of parameter uncertainty

The values of the different statistics obtained in the calculation are presented in Figure 7-5, including the arithmetic mean, median, and 5th and 95th percentiles of the maximum annual dose at each point in time. The variation here is lower than in the *global warming calculation case* as the large variation of near-field releases due to variation in K_d values in cement is not included here.

7.2 Loss of barrier function calculation case – no sorption in the bedrock (CCR_B2)

The *loss of barrier function calculation case – no sorption in the bedrock (CCR_B2)* is described in Section 4.3.2. The objective of this case is to illustrate the importance of sorption of radionuclides in the geosphere. It is assumed that radionuclides do not sorb in the bedrock, i.e. K_d values for the far-field are set to zero. Other internal and external conditions are assumed to be the same as in the *global warming calculation case*.

Releases

Figure 7-6 shows a comparison of peak releases from the far-field in the loss of barrier function scenario – no sorption in the bedrock (CCR_B2) with the *global warming calculation case* (CCM_GW).

The relevance of the far-field as a sorption barrier for many radionuclides can be seen from the figure. Here, there is less in-growth of progeny because of the shorter residence-time in the bedrock of radionuclides compared with the *global warming calculation case*. In Figure 7-6 it can be seen how the release from the far-field of e.g. Ra-226 decreases when the residence time of U-238 in the geosphere is shorter.

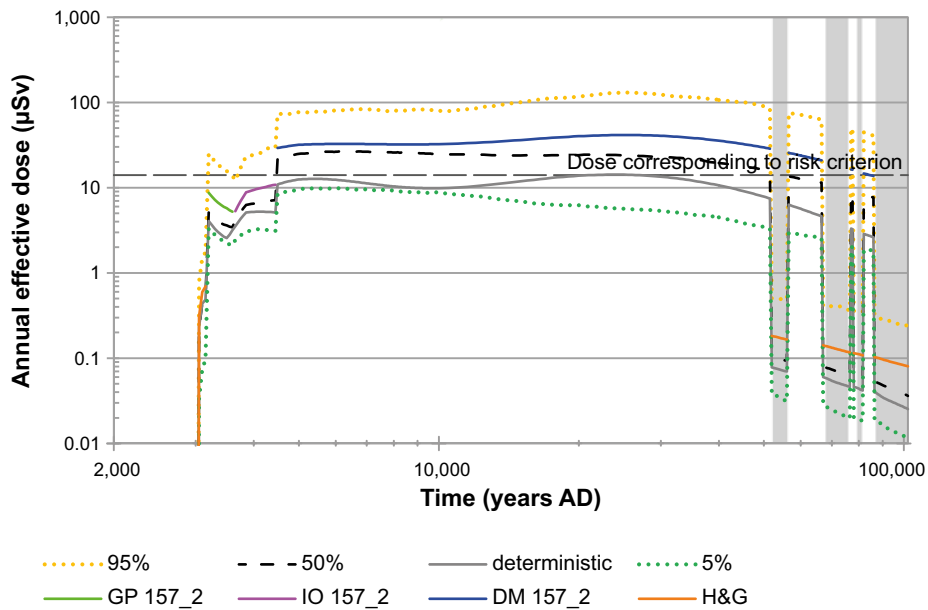


Figure 7-5. Arithmetic mean, median, 5th and 95th percentiles of the annual dose to a representative individual of the most exposed group from the entire repository in the **loss of barrier function calculation case** – no sorption in the repository. The unshaded areas correspond to temperate climatic conditions and the grey shaded areas to periglacial conditions with continuous permafrost.

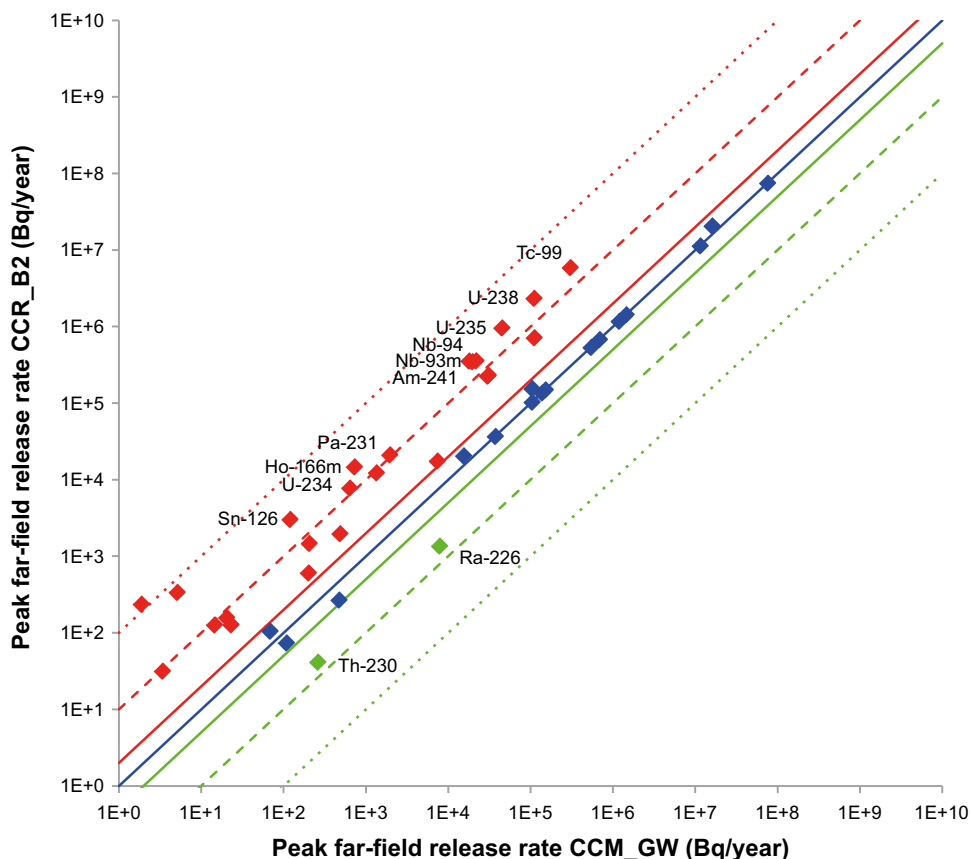


Figure 7-6. Comparison of peak releases from the far-field in the **loss of barrier function calculation case** – no sorption in the bedrock (CCR_B2) with the **global warming calculation case** (CCM_GW). Dots on the blue line on the diagonal represent radionuclides for which the calculated releases in the current calculation case and the CCM_GW are the same. At the solid red line the calculated releases are twice as high as in the CCM_GW, at the dashed red line the calculated releases are ten times as high as in the CCM_GW and at the dotted red line the calculated releases are one hundred times the CCM_GW value. In the same way, the green lines represent 0.5 times, 0.1 times and 0.01 times the CCM_GW releases.

Annual doses

Temporal variation in annual effective doses to the exposed groups in biosphere object 157_2 and the maximum annual effective dose are presented in Figure 7-7, and compared with the maximum dose of the *global warming calculation case*. Peak dose and related data are reported in Table 7-3, and peak contributions from waste vaults in Table 7-4. Figure 7-8 and Figure 7-9 present the contribution of waste vaults and radionuclides, respectively, to maximum dose.

The peak dose is about 35% higher than the estimate for the *global warming calculation case* and is observed 400 years earlier. The 1–5BLA waste vaults contribute more to the peak dose, which is significantly different from the *global warming calculation case*. U-238 originating from 1BLA contributes about 15% to the peak dose, which is a significant increase of the contribution of this radionuclide, compared to the *global warming calculation case*, where its contribution is 6.4%. Comparison with the *loss of barrier function scenario – no sorption in the repository calculation case* shows that sorption in the far-field is relevant but less important for the mitigation of exposure than sorption in the near-field.

Table 7-3. Peak annual dose to a representative individual of the most exposed group obtained for the *loss of barrier function calculation case – no sorption in the bedrock (CCR_B2)*.

Annual dose (µSv)	Year (AD)	Contribution from waste vault (%)	Contribution from radionuclides (%)	Exposed group (biosphere object)
10.4	6100	Silo (32.4)	Mo-93 (41.3)	Drained-mire farmers (Object 157_2)
		1BLA (22.6)	U-238 (15.3)	
		1BMA (12.2)	C-14-org (14.7)	
		2BMA (5.6)	U-235 (10.5)	
		3BLA (4.4)	I-129 (4.2)	
		2BTF (4.3)	Pa-231 (3.9)	
		2BLA (4.2)	Cl-36 (2.6)	
		5BLA (3.9)	Ac-227 (2.0)	
		4BLA (3.8)	Ca-41 (1.9)	
		BRT (3.4)	Others (3.7)	
		1BTF (2.5)		

Table 7-4. Peak annual dose and the time at which the peak is observed for releases from individual waste vaults and from the entire repository in the *loss of barrier function calculation case – no sorption in the bedrock (CCR_B2)*. The value given for each waste vault is the sum of values obtained for all released radionuclides. The radionuclides with the highest contribution to the peak doses are indicated.

Waste vault	Annual dose (µSv)	Year (AD)	Biosphere object	Exposed group	Most contributing radionuclide (%)
Silo	3.6	7150	157_2	DM	Mo-93 (48.9)
1BMA	2.1	66,500	157_2	DM	Ni-59 (62.8)
1BLA	3.8	5250	157_2	GP	U-238 (54.1)
1BTF	0.43	4950	157_2	DM	Mo-93 (68.2)
2BTF	0.53	4800	157_2	DM	Mo-93 (71.8)
BRT	0.38	5450	157_2	DM	Mo-93 (95.8)
2BMA	0.88	10,500	157_2	DM	Mo-93 (68.7)
2BLA	0.54	17,000	157_1	DM	Pa-231 (30.4)
3BLA	0.54	16,500	157_1	DM	Pa-231 (30.2)
4BLA	0.54	17,500	157_1	DM	Pa-231 (30.3)
5BLA	0.54	17,000	157_1	DM	Pa-231 (30.2)
Total SFR	10.4	6100	157_2	DM	Mo-93 (41.3)

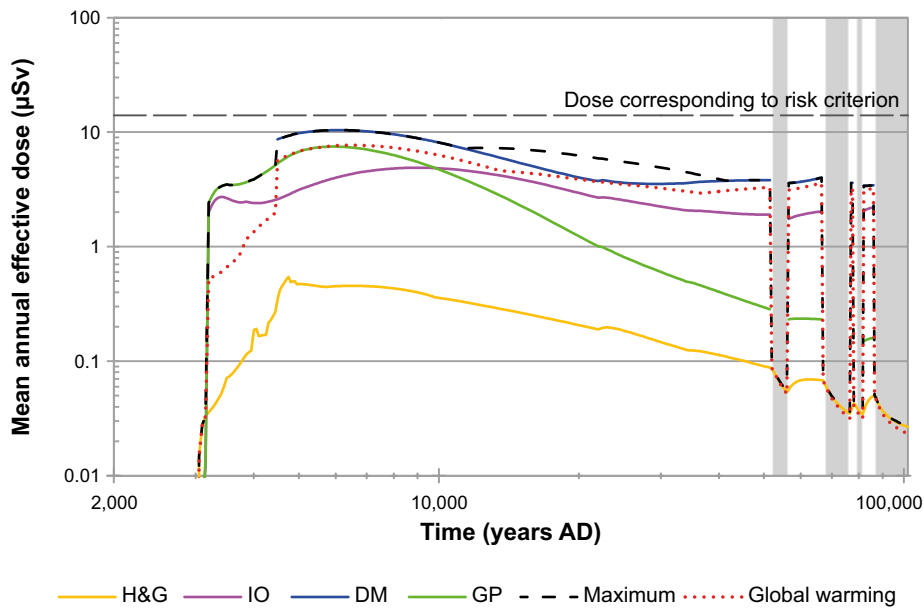


Figure 7-7. Arithmetic mean annual dose for the different exposed groups in object 157_2 and maximum annual dose, shown for the **loss of barrier function calculation case** – no sorption in the bedrock (CCR_B2). The unshaded areas correspond to temperate climatic conditions and the grey shaded areas to periglacial conditions with continuous permafrost.

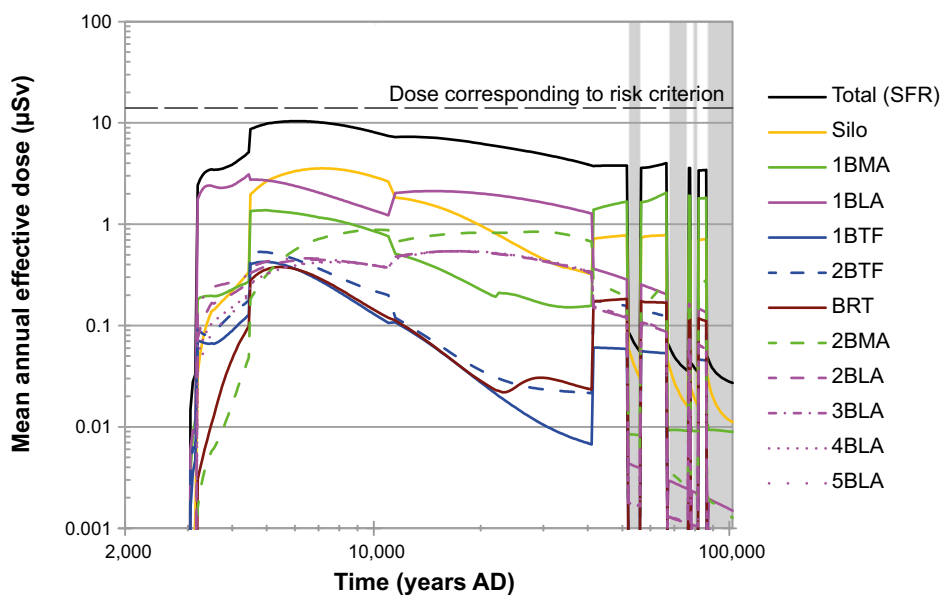


Figure 7-8. Arithmetic mean of the annual dose to the most exposed group for releases from the entire repository and contributions from the individual waste vaults in the **loss of barrier function calculation case** – no sorption in the bedrock (CCR_B2). The unshaded areas correspond to temperate climatic conditions and the grey shaded areas to periglacial conditions with continuous permafrost.

Impact of parameter uncertainty

The values of the different statistics obtained in the calculation are presented in Figure 7-10, including the arithmetic mean, median, and 5th and 95th percentiles of the maximum total dose at each point in time. Switching the maximum dose defining biosphere object changes abruptly the bandwidth between 5th and 95th percentile as in the *global warming calculation case*.

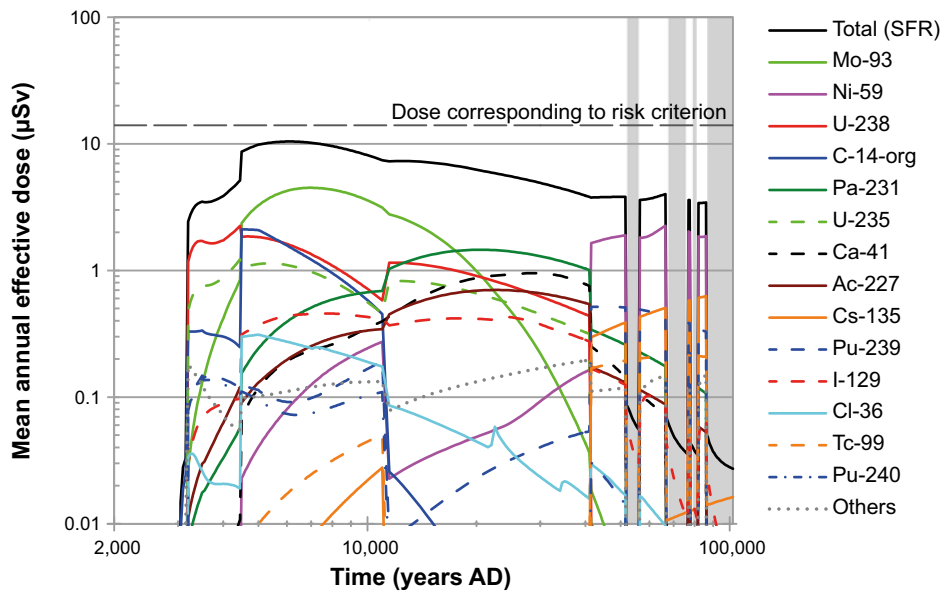


Figure 7-9. Arithmetic mean of the annual dose to the most exposed group, shown for releases from the entire repository in the **loss of barrier function calculation case** – no sorption in the bedrock (CCR_B2). The unshaded areas correspond to temperate climatic conditions and the grey shaded areas to periglacial conditions with continuous permafrost.

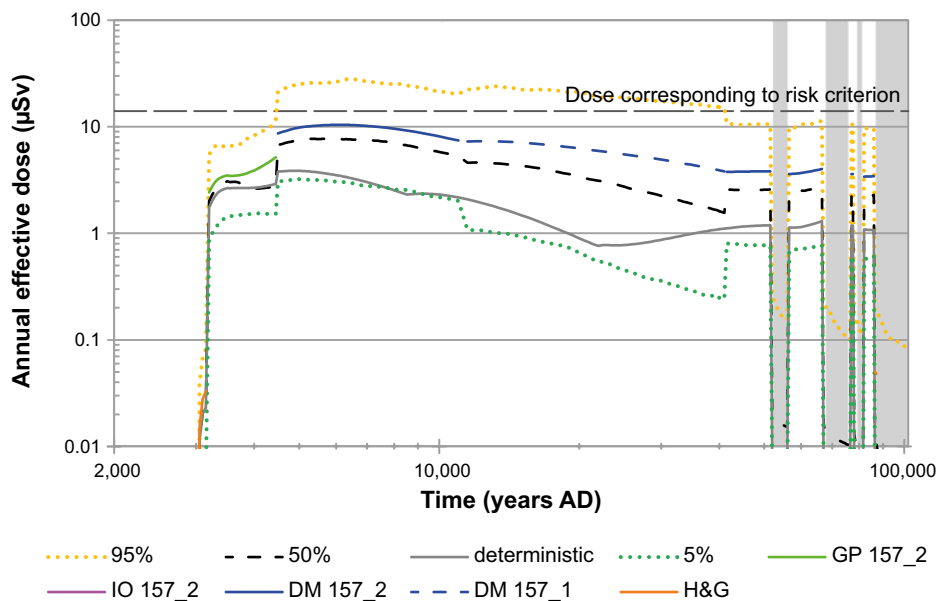


Figure 7-10. Arithmetic mean, median, 5th and 95th percentiles of the annual dose to a representative individual of the most exposed group from SFR in the **loss of barrier function calculation case** – no sorption in the bedrock (CCR_B2). The unshaded areas correspond to temperate climatic conditions and the grey shaded areas to periglacial conditions with continuous permafrost.

7.3 Loss of barrier function calculation case – high water flow in the repository (CCR_B3)

The *loss of barrier function scenario – high water flow in the repository* is described in Section 4.3.3.

Near-field water flow from the hydrological case of “no barriers” (Abarca et al. 2013), with, from the outset, completely degraded concrete and bentonite barriers, are applied in this calculation case.

The groundwater flow is calculated assuming no resistance to flow due to concrete and bentonite barriers in the vault structures and tunnel closure plugs. Furthermore, porosities and diffusivities for completely degraded concrete are applied in this calculation case. Other internal and external conditions are assumed to be the same as in the *global warming calculation case*.

Releases

Figure 7-11 shows a comparison of peak releases to the biosphere in the *loss of barrier function calculation case – high water flow in the repository (CCR_B3)* with the *global warming calculation case (CCM_GW)*.

The comparison indicates the high relevance of hydraulic barriers in the near-field for the safety of the repository.

Annual doses

Temporal variation in annual effective doses to the exposed groups in biosphere object 157_2 and the maximum annual effective dose are presented in Figure 7-12, and compared with the maximum dose of the *global warming calculation case*. Peak dose and related data are reported in Table 7-5. Figure 7-13 and Figure 7-14 present the contribution of waste vaults and radionuclides, respectively, to maximum dose.

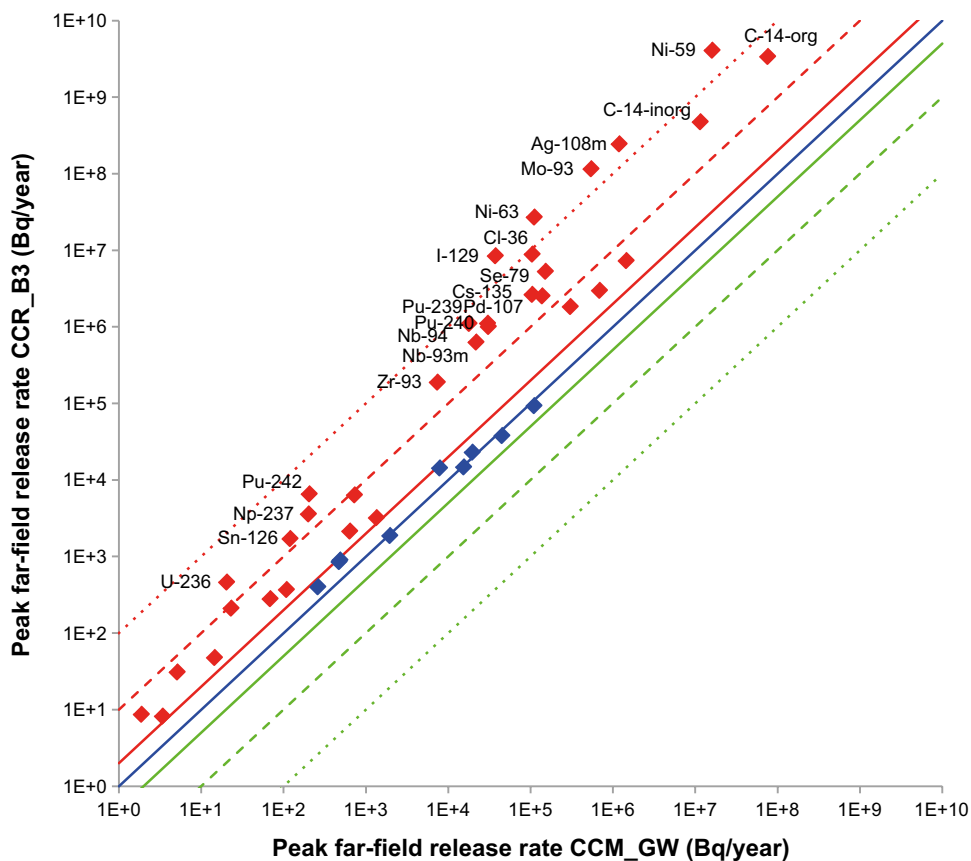


Figure 7-11. Comparison of peak releases to the biosphere in the *loss of barrier function calculation case – high water flow in the repository (CCR_B3)* with the *global warming calculation case (CCM_GW)*. Dots on the blue line on the diagonal represent radionuclides for which the calculated releases in the current calculation case and the CCM_GW are the same. At the solid red line the calculated releases are twice as high as in the CCM_GW, at the dashed red line the calculated releases are ten times as high as in the CCM_GW and at the dotted red line the calculated releases are one hundred times the CCM_GW value. In the same way, the green lines represent 0.5 times, 0.1 times and 0.01 times the CCM_GW releases.

The peak dose in this calculation case is almost one order of magnitude higher than the in the *global warming calculation case*. Some of the radionuclides, i.e. Mo-93, inorganic C-14 and I-129, that contribute significantly to the peak dose in this case are also relevant in the *global warming calculation case*. However, Ni-59, which starts to be important for the dose later in the main scenario, contributes significantly in this case already at 4650 AD. These results demonstrate that the hydraulic barriers in the near-field are important for the long-term safety of the repository.

Table 7-5. Peak annual dose to a representative individual of the most exposed group obtained for the loss of barrier function calculation case – high water flow in the repository (CCR_B3).

Annual dose (µSv)	Year (AD)	Contribution from waste vault (%)	Contribution from radionuclides (%)	Exposed group (biosphere object)
69	4650	Silo (73.3)	Mo-93 (72.2)	Drained-mire farmers (Object 157_2)
		1BMA (13.2)	C-14-inorg (13.1)	
		2BMA (9.7)	Ni-59 (6.6)	
		2BTF (1.1)	I-129 (4.8)	
		1BLA (1.0)	Others (3.3)	
		1BTF (0.9)		
		BRT (0.3)		
		2BLA (0.2)		
		3BLA (0.2)		
		4BLA (0.1)		
		5BLA (0.1)		

A summary of peak contributions to mean annual dose for individual waste vaults and the entire repository is presented in Table 7-6. Together with peak contributions to dose, the times of their occurrence and the exposed group, location and the radionuclide contributing most to dose are reported.

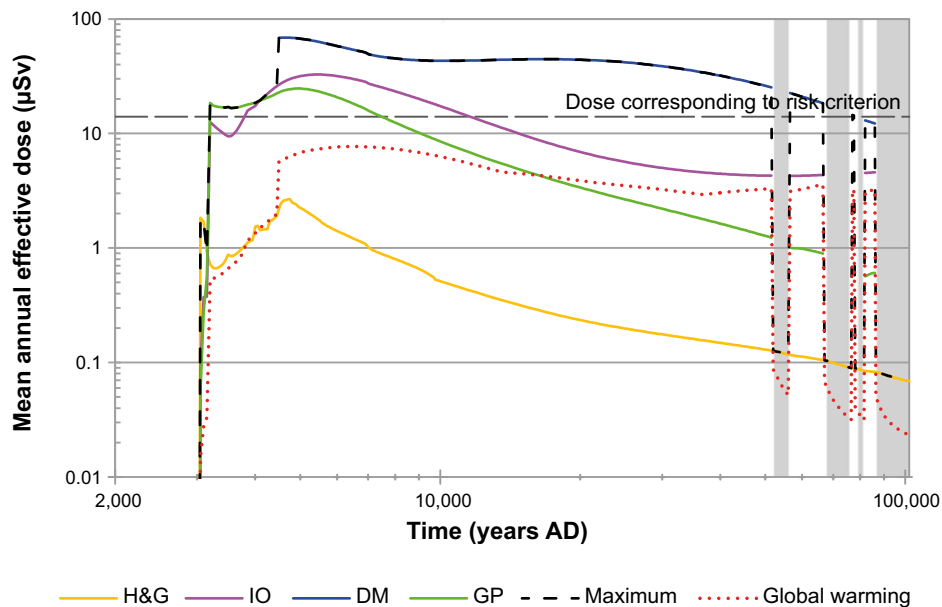


Figure 7-12. Arithmetic mean of the total (across all radionuclides and waste vaults) annual dose for the different exposed groups in object 157_2 and maximum across all exposed groups and biosphere objects. Values are shown for the loss of barrier function calculation case – high water flow in the repository (CCR_B3). The unshaded areas correspond to temperate climatic conditions and the grey shaded areas to periglacial conditions with continuous permafrost.

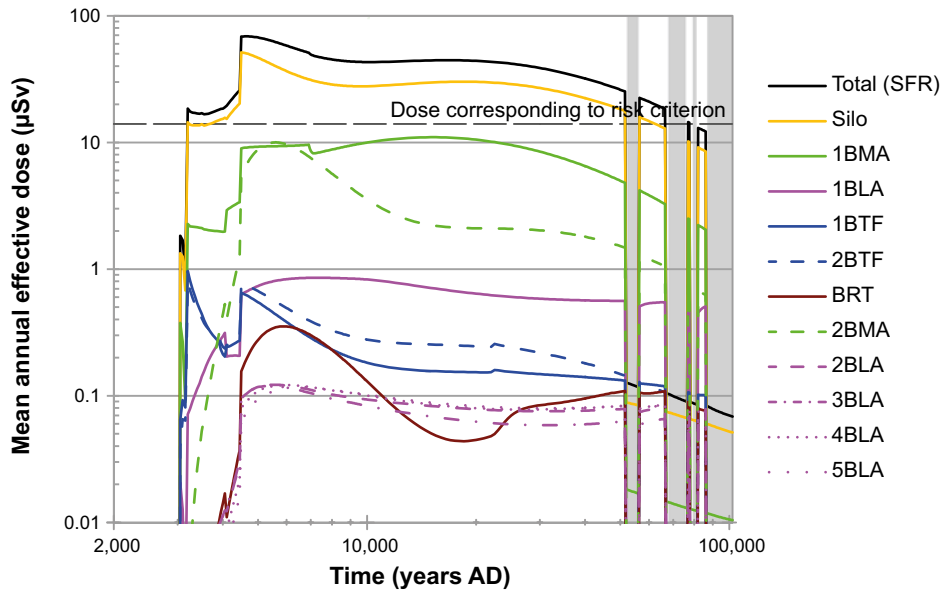


Figure 7-13. Arithmetic mean of the annual dose to the most exposed group for releases from the entire repository and contributions from the individual waste vaults in the **loss of barrier function calculation case** – high water flow in the repository (CCR_B3). The unshaded areas correspond to temperate climatic conditions and the grey shaded areas to periglacial conditions with continuous permafrost.

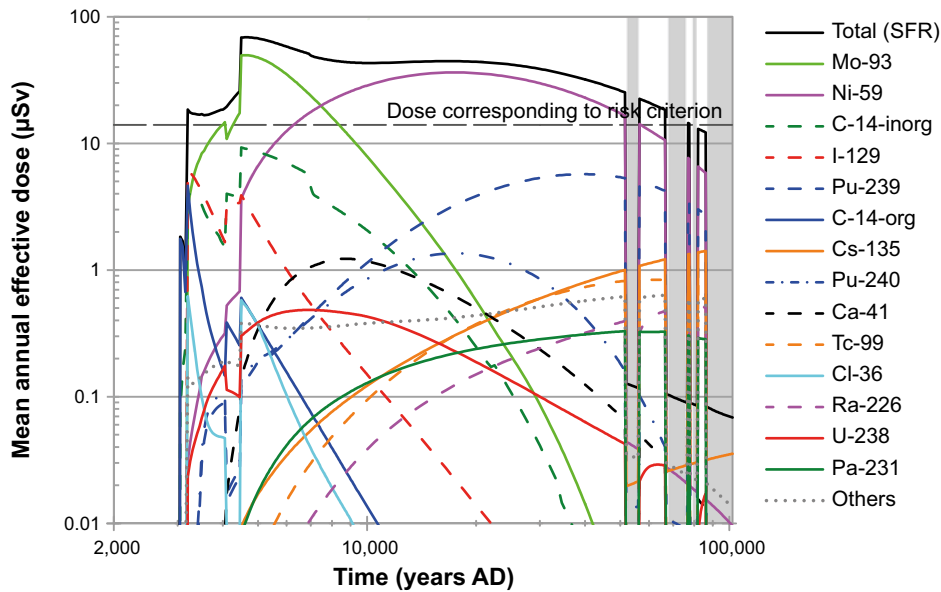


Figure 7-14. Arithmetic mean of the annual dose to the most exposed group and respective radionuclide contributions, shown for releases from the entire repository in the **loss of barrier function calculation case** – high water flow in the repository (CCR_B3). The unshaded areas correspond to temperate climatic conditions and the grey shaded areas to periglacial conditions with continuous permafrost.

Compared with the *global warming calculation case*, the largest relative increase in contribution to the annual dose comes from the silo, 1BMA and 2BMA. This points again to the importance of the hydraulic barriers in these vaults.

Table 7-6. Peak annual dose and the time at which the peak is observed for releases from individual waste vaults and from the entire repository in the *loss of barrier function calculation case – high water flow in the repository (CCR_B3)*. The radionuclides with the highest contribution to the peak doses are indicated.

Waste vault	Annual dose (μSv)	Year (AD)	Biosphere object	Exposed group	Most contributing radionuclide (%)
Silo	51.4	4500	157_2	DM	Mo-93 (66.6)
1BMA	11.0	15,000	157_2	DM	Ni-59 (85.1)
1BLA	1.3	24,500	157_1	DM	U-238 (30.5)
1BTF	0.96	3200	157_2	GP	C-14-inorg (77.1)
2BTF	0.80	3200	157_2	GP	C-14-inorg (74.7)
BRT	0.35	5900	157_2	DM	Mo-93 (99.0)
2BMA	10.0	5600	157_2	DM	Mo-93 (88.6)
2BLA	0.12	5550	157_2	DM	Mo-93 (46.8)
3BLA	0.12	5400	157_2	DM	Mo-93 (49.7)
4BLA	0.12	18,000	157_1	DM	Ca-41 (40.7)
5BLA	0.13	21,500	157_1	DM	Ca-41 (35.6)
Total SFR	68.8	4650	157_2	DM	Mo-93 (72.2)

Impact of parameter uncertainty

The values of the different statistics obtained in the calculation are presented in Figure 7-15, including the arithmetic mean, median, and 5th and 95th percentiles of the maximum total dose at each point in time. A switch between biosphere objects defining maximum dose is not observed and the temporal evolution of the statistics is similar to the case *loss of barrier function calculation case – no sorption in the repository*.

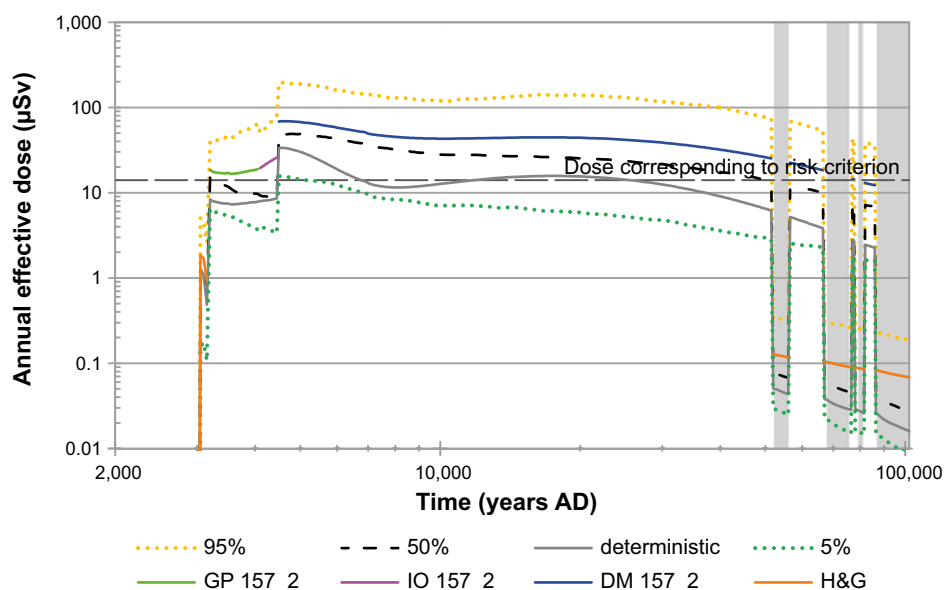


Figure 7-15. Arithmetic mean, median, 5th and 95th percentiles of the annual dose to a representative individual of the most exposed group in the *loss of barrier function calculation case – high water flow in the repository (CCR_B3)*. The unshaded areas correspond to temperate climatic conditions and the grey shaded areas to periglacial conditions with continuous permafrost.

7.4 Changed repository redox conditions in SFR 1 calculation case (CCR_RX)

The *changed repository redox conditions in SFR 1 calculation case* is described in Section 4.3.4. In this case, an alternative set of K_d values is used for redox-sensitive elements in SFR 1. SFR 3 is not considered in this calculation case, as the main purpose of this residual calculation case is to address questions from the regulatory authorities in connection with the SAR-08 safety assessment of SFR 1 (see also Chapter 7 in the **Main report**). Other internal and external conditions are assumed to be the same as in the *global warming calculation case*.

Releases

As stated above, changed redox-conditions lead to changed sorption behaviour of redox-sensitive nuclides. Although U is a redox-sensitive species found as U(IV) under normal near-field conditions but might oxidise to U(VI) under more oxidising conditions, the out-flux of and dose from U-238 and U-235 do not change in this calculation case. This is due to the fact that the main releases of these nuclides come from 1BLA, where sorption is not taken into account in the assessment. The flux of Se-79 out of the repository decreases under oxidising conditions due to assumption that selenide, Se(-II), does not sorb upon cement minerals whereas selenate, Se(VI), does. The flux of U-236 (progeny of Pu-240) also increases since it is included in the Pu-240 decay chain. The release of Np-237 progeny U-233 and Th-229 out of the repository decreases in this calculation case compared with the *global warming calculation case* due to the shorter retention time of Np-237 in the near-field (Figure 7-16).

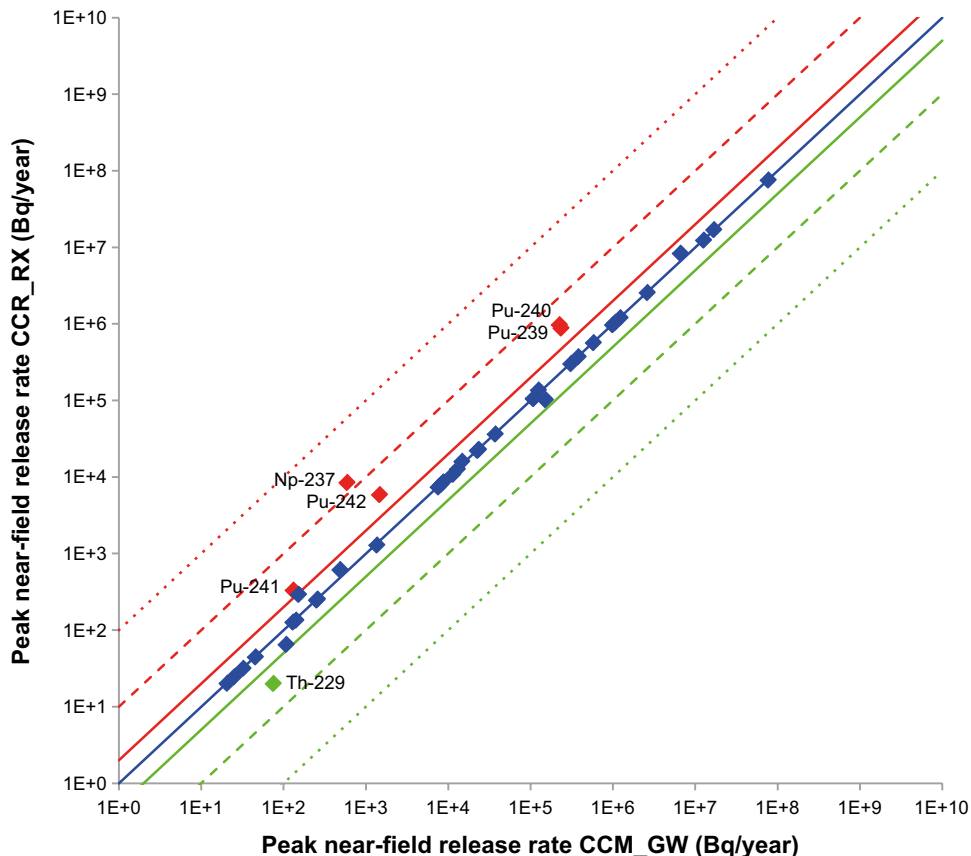


Figure 7-16. Comparison of peak releases from the near-field in *changed repository redox conditions in SFR 1 calculation case (CCR_RX)* with the *global warming calculation case (CCM_GW)*. Dots at the blue line on the diagonal represent radionuclides for which the calculated releases in the current calculation case and CCM_GW are the same. At the solid red line the calculated releases are twice as high as in the CCM_GW, at the dashed red line the calculated releases are ten times as high as in CCM_GW and at the dotted red line the calculated releases are one hundred times the CCM_GW value. In the same way, the green lines represent 0.5 times, 0.1 times and 0.01 times CCM_GW releases.

Annual doses

Temporal variation in annual effective doses to the exposed groups in biosphere object 157_2 and the maximum annual effective dose are presented in Figure 7-17, and compared with the maximum dose for the *global warming calculation case*. Peak dose and related data are reported in Table 7-7 and peak contributions from waste vaults in Table 7-8. Figure 7-18 and Figure 7-19 present the contribution of waste vaults and radionuclides, respectively, to maximum dose.

The peak dose obtained for this calculation case (7.4 μSv) is 1.1 μSv higher than the dose contribution from SFR1 (6.3 μSv) to the peak dose in the *global warming calculation case* (Table 5-1). In addition, the peak dose occurs about 45,000 years later in this calculation case and has a different set of contributing radionuclides, but a comparable distribution with respect to contributions from the waste vaults. The late peak is due to the long-lasting build-up of dose from Pu-239 dominating after 15,000 AD and exceeding after 30,000 AD the peak contribution from Mo-93. The Pu-239 dose reaches a maximum after 50,000 AD, at which point the main contributing radionuclides of the *global warming calculation case* Mo-93 and C-14 have largely decayed. At about 30,000 AD Ni-59 and Tc-99 becomes the second and third main contributors to dose.

Table 7-7. Peak value (and related data) of the annual dose to a representative individual of the most exposed group obtained for releases from SFR 1 for the *changed repository redox conditions in SFR 1 calculation case*.

Annual dose (μSv)	Year (AD)	Contribution from waste vault (%)	Contribution from radionuclides (%)	Exposed group (biosphere object)
7.4	51,500	Silo (59.4)	Pu-239 (53.8)	Drained-mire farmers (Object 157_2)
		1BMA (29.1)	Ni-59 (18.8)	
		1BLA (7.5)	Tc-99 (11.0)	
		1BTF (2.1)	Cs-135 (3.8)	
		2BTF (1.9)	Pa-231 (3.0)	
			Ra-226 (2.0)	
			I-129 (1.8)	
			Pu-240 (1.6)	
			Ac-227 (1.3)	
			Pu-242 (1.2)	
			Others (1.8)	

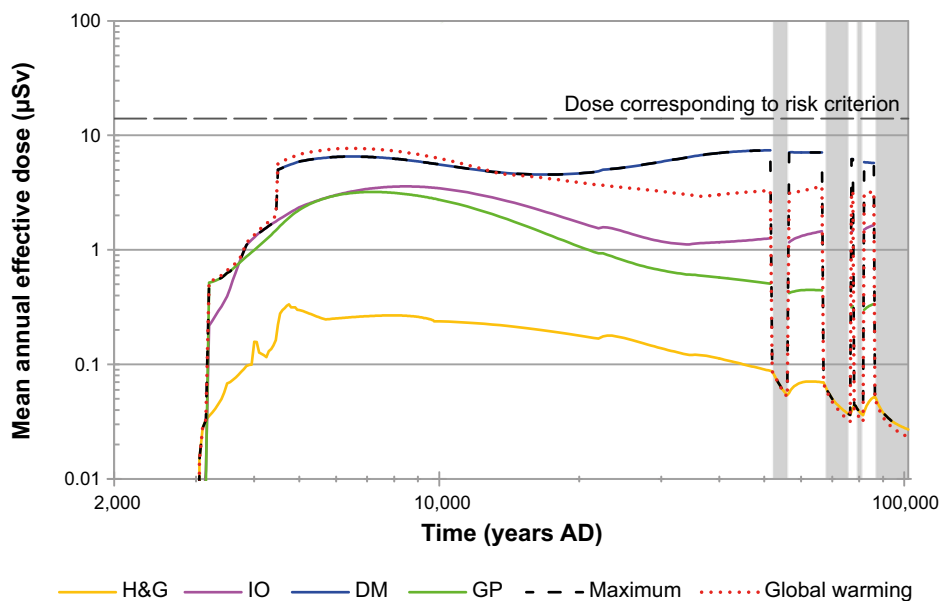


Figure 7-17. Arithmetic mean of the annual effective dose for the different exposed groups in object 157_2 and maximum dose across all exposed groups and biosphere objects, shown for the *changed repository redox conditions in SFR 1 calculation case*. The unshaded areas correspond to temperate climatic conditions and the grey shaded areas to periglacial conditions with continuous permafrost.

Table 7-8. Peak contributions to mean annual doses and times at which the peak is observed for releases from waste vaults and the entire SFR 1 repository in the *changed repository redox conditions in SFR 1 calculation case*. The radionuclides with the highest contribution to the peak doses are indicated.

Waste vault	Annual dose (μSv)	Year (AD)	Biosphere object	Exposed group	Most contributing radionuclide (%)
Silo	4.4	50,500	157_2	DM	Pu-239 (30.5)
1BMA	2.3	66,500	157_2	DM	Ni-59 (55.6)
1BLA	1.3	24,000	157_1	DM	U-238 (30.5)
1BTF	0.43	4900	157_2	DM	Mo-93 (68.1)
2BTF	0.53	4800	157_2	DM	Mo-93 (73.3)
Total SFR 1	7.4	51,500	157_2	DM	Pu-239 (53.8)

Table 7-9. Peak contributions of radionuclides to annual effective dose for the *global warming calculation case (CCM_GW)* compared with the *changed repository redox conditions in SFR 1 calculation case (CCR_RX)*. Indicated is also the time of occurrence for the peak contributions in both cases.

Radionuclide	CCM_GW Annual dose (μSv)	Year (AD)	CCR_RX Annual dose (μSv)	Year (AD)	CCR_RX/CCM_GW Quotient (μSv/μSv)
Se-79	0.06	10,000	0.04	11,500	0.74
Tc-99	0.12	77,000	0.85	66,500	6.94
U-233	0.00	86,000	0.02	86,000	6.45
U-234	0.04	51,500	0.04	49,500	0.93
U-235	0.34	7250	0.33	7000	0.96
U-236	0.00	47,500	0.00	42,500	2.59
U-238	0.81	7050	0.8	6950	0.99
Np-237	0.00	86,000	0.03	86,000	11.91
Pu-239	0.28	51,500	4.02	47,500	14.13
Pu-240	0.04	18,000	0.63	21,000	16.37
Pu-242	0.01	86,000	0.13	86,000	10.01

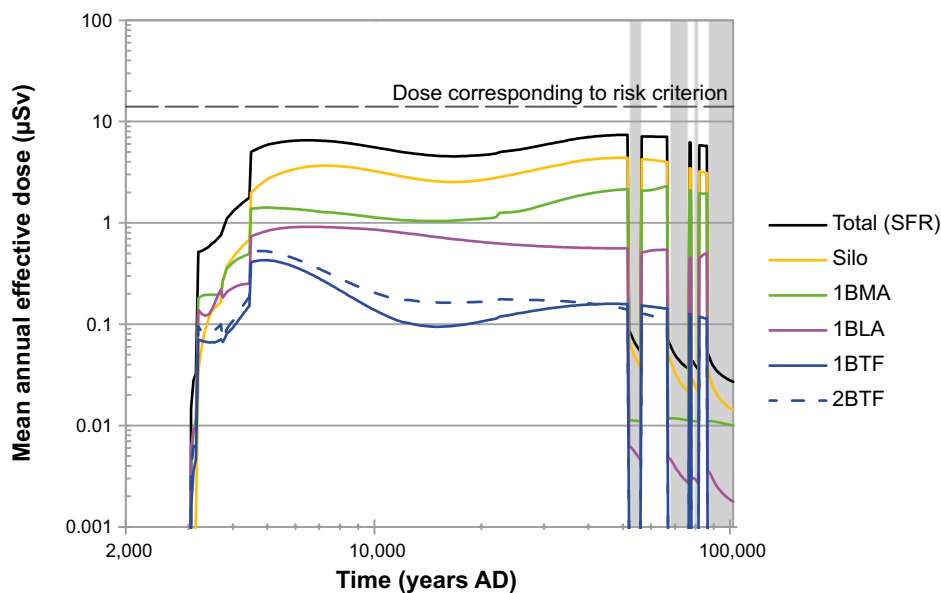


Figure 7-18. Arithmetic mean of the annual dose to the most exposed group for releases from the entire SFR 1 and contributions from the individual waste vaults in the *changed repository redox conditions in SFR 1 calculation case (CCR_RX)*. The unshaded areas correspond to temperate climatic conditions and the grey shaded areas to periglacial conditions with continuous permafrost.

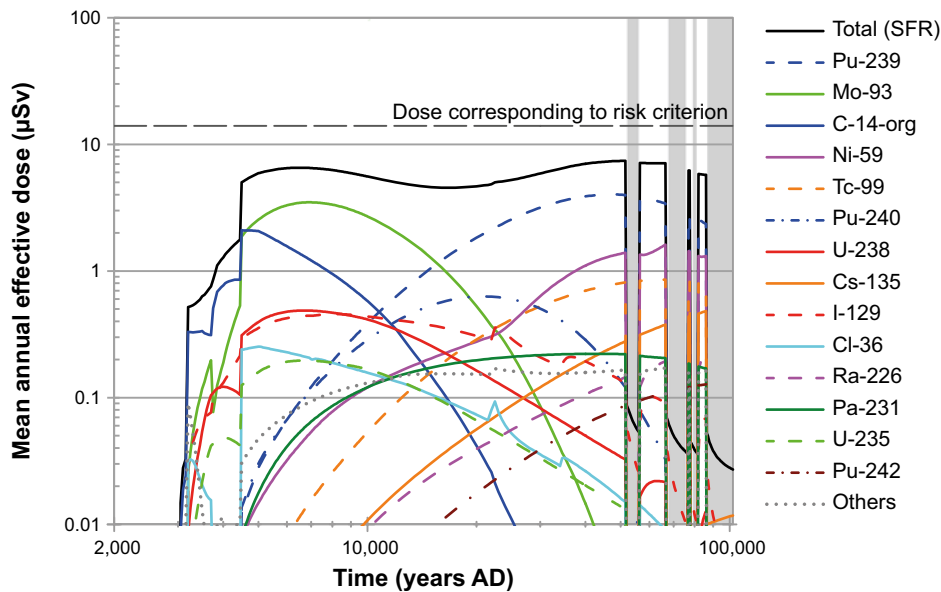


Figure 7-19. Arithmetic mean of the annual dose to the most exposed group and respective radionuclide contributions, shown for releases from entire SFR 1 in the **changed repository redox conditions in SFR 1 calculation case (CCR_RX)**. The unshaded areas correspond to temperate climatic conditions and the grey shaded areas to periglacial conditions with continuous permafrost.

Impact of parameter uncertainty

The values of the different statistics obtained in the calculation are presented in Figure 7-20, including the arithmetic mean, median, and 5th and 95th percentiles of the maximum total dose at each point in time. A switch between biosphere objects defining maximum dose is not observed and the temporal evolution of the statistics is similar to the case *loss of barrier function calculation case* – no sorption in the repository with doses being half an order of magnitude lower.

7.5 Extended global warming calculation case (CCR_EX)

The *extended global warming calculation case* is described in Section 4.3.5. In this calculation case, temperate climate conditions prevail during the entire simulation period of 100,000 years and rates of precipitation are higher than in the *global warming calculation case*.

Releases

Figure 7-21 shows the temporal variation in radiotoxicity releases from the geosphere for the most significant radionuclides. The releases are very similar to those in the *global warming calculation case* with the exception that there are no interruptions by periods of periglacial conditions. However, this does not affect the peak dose that occurs at year 6500 AD before the first periglacial period in the *global warming calculation case*. Instead the result in this case is affected solely by conditions in the biosphere.

Annual doses

Time series of annual effective doses to the exposed groups in biosphere object 157_2 and the maximum annual effective dose are presented in Figure 7-22, and compared with the maximum dose of the *global warming calculation case*. Peak dose and related data are reported in Table 7-10 and peak contributions from waste vaults in Table 7-11. Figures 7-23 and 7-24 present the contributions of waste vaults and radionuclides, respectively, to maximum dose.

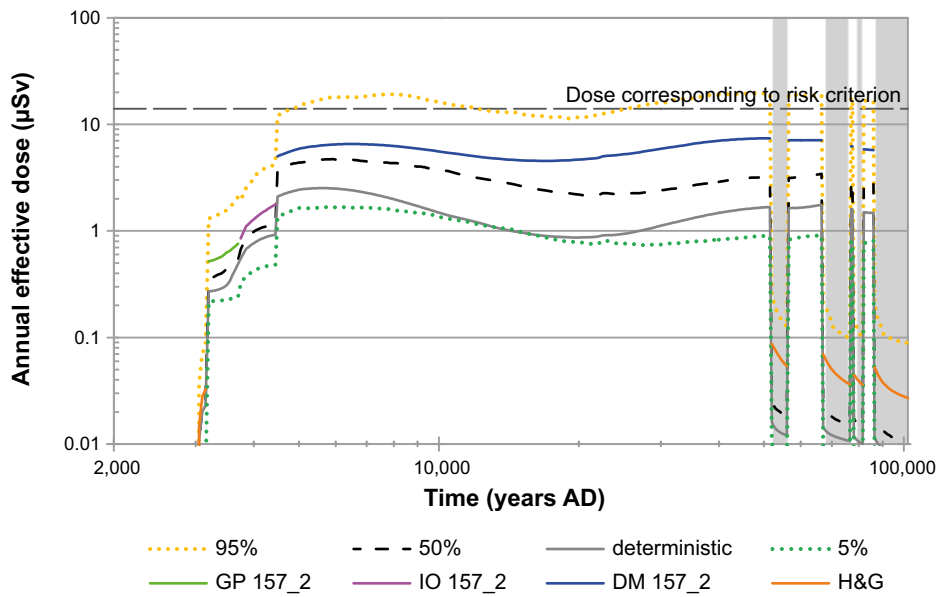


Figure 7-20. Arithmetic mean, median, 5th and 95th percentiles of the annual dose to a representative individual of the most exposed group in the **changed repository redox conditions in SFR 1 calculation case (CCR_RX)**. The unshaded areas correspond to temperate climatic conditions and the grey shaded areas to periglacial conditions with continuous permafrost.

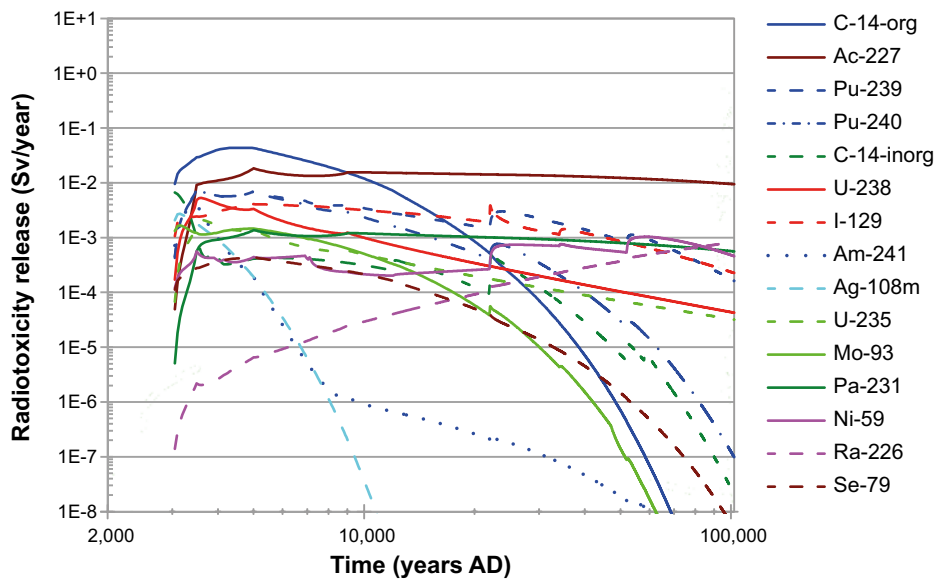


Figure 7-21. Radiotoxicity of the releases to the biosphere for the 15 most dominating radionuclides in the **extended global warming calculation case**.

The higher precipitation in the *extended global calculation warming case* leads to an increased horizontal flow of groundwater resulting in faster transport and larger dilution of radionuclides in surface water and surface peat (see the **Biosphere synthesis report** and Grolander 2013). This explains why the peak dose is slightly lower (7.0 µSv) in the *extended global warming calculation case* compared with the *global warming calculation case*.

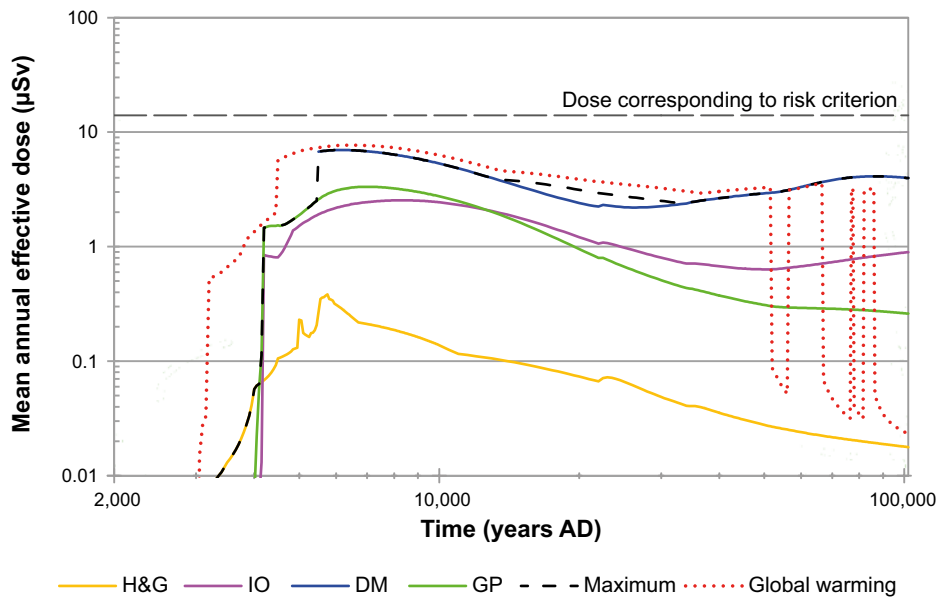


Figure 7-22. Arithmetic mean of annual dose for the different exposed groups in object 157_2 and maximum dose across exposed groups and biosphere objects shown for the extended global warming calculation case (CCR_EX).

Table 7-10. Peak annual dose to a representative individual of the most exposed group obtained for the extended global warming calculation case (CCR_EX).

Annual dose (µSv)	Year (AD)	Contribution from waste vault (%)	Contribution from radionuclides (%)	Exposed group (biosphere object)
7.0	6150	Silo (45.2)	Mo-93 (54.3)	Drained-mire farmers (Object 157_2)
		1BMA (16.5)	C-14-org (22.1)	
		1BLA (11.9)	U-238 (6.5)	
		2BMA (7.5)	I-129 (5.7)	
		2BTF (5.3)	Cl-36 (3.4)	
		1BTF (4.4)	U-235 (2.7)	
		BRT (4.3)	Ca-41 (2.4)	
		2BLA (1.3)	Others (2.9)	
		5BLA (1.3)		
		3BLA (1.3)		
		4BLA (1.2)		

Table 7-11. Peak annual dose and the time at which the peak is observed for releases from individual waste vaults and from the entire repository in the extended global warming calculation case. The radionuclide with the highest contribution is indicated.

Waste vault	Annual dose (µSv)	Year (AD)	Biosphere object	Exposed group	Most contributing radionuclide (%)
Silo	3.2	6850	157_2	DM	Mo-93 (45.6)
1BMA	2.3	84,000	157_2	DM	Ni-59 (68.2)
1BLA	1.2	29,000	157_1	DM	Pa-231 (28.1)
1BTF	0.36	5500	157_2	DM	Mo-93 (69.2)
2BTF	0.42	5500	157_2	DM	Mo-93 (72.3)
BRT	0.32	5600	157_2	DM	Mo-93 (98.6)
2BMA	0.74	9800	157_2	DM	Mo-93 (70.5)
2BLA	0.09	6200	157_2	DM	Mo-93 (40.1)
3BLA	0.09	6050	157_2	DM	Mo-93 (43.0)
4BLA	0.09	15,000	157_1	DM	Ca-41 (39.9)
5BLA	0.09	36,000	157_1	DM	Ac-227 (23.0)
Total SFR	7.0	6150	157_2	DM	Mo-93 (54.3)

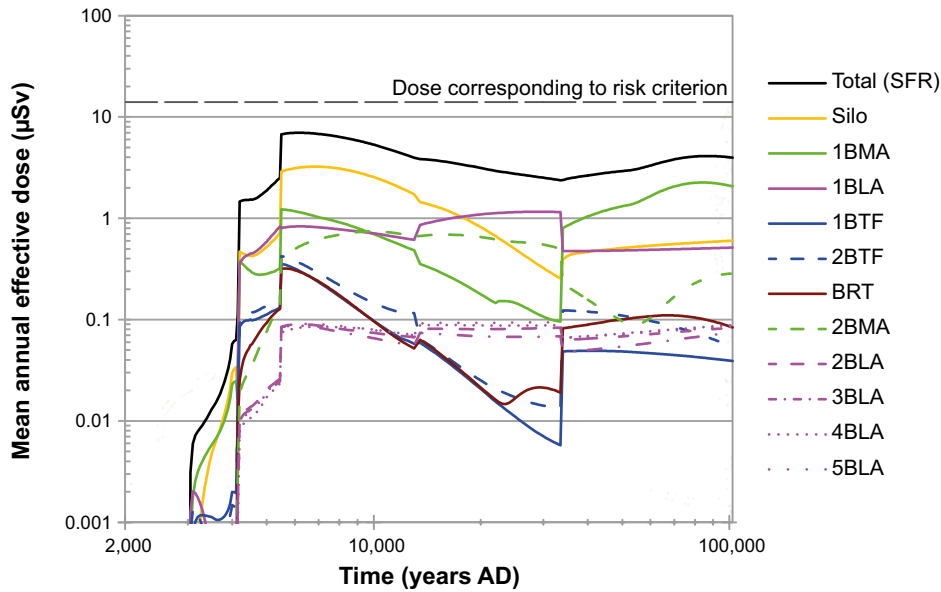


Figure 7-23. Arithmetic mean of the annual dose to the most exposed group due to releases from waste vaults and the entire repository in the *extended global warming calculation case (CCR_EX)*.

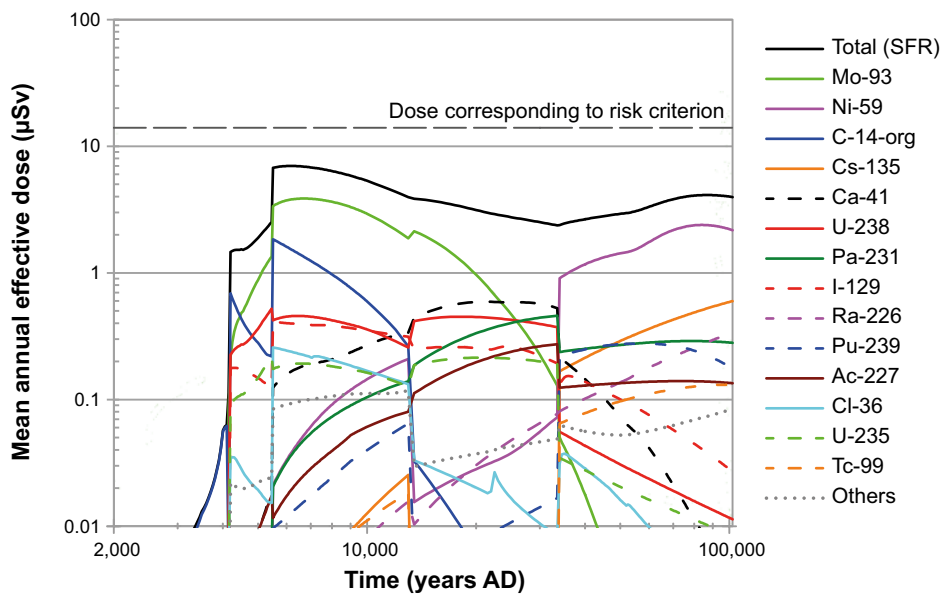


Figure 7-24. Arithmetic mean of the annual dose to the most exposed group and respective contributions of most important radionuclides in the *extended global warming calculation case (CCR_EX)*.

Impact of parameter uncertainty

The values of the different statistics obtained in the calculation are presented in Figure 7-25, including the arithmetic mean, median, and 5th and 95th percentiles of the maximum total dose at each point in time. Switching the maximum dose defining biosphere object changes abruptly the bandwidth between 5th and 95th percentile.

7.6 Unclosed repository calculation case (CCR_UR)

The *unclosed repository calculation case* is described in Section 4.3.6. In this calculation case, it is assumed that, following completion of waste disposal, the repository is neither closed nor monitored.

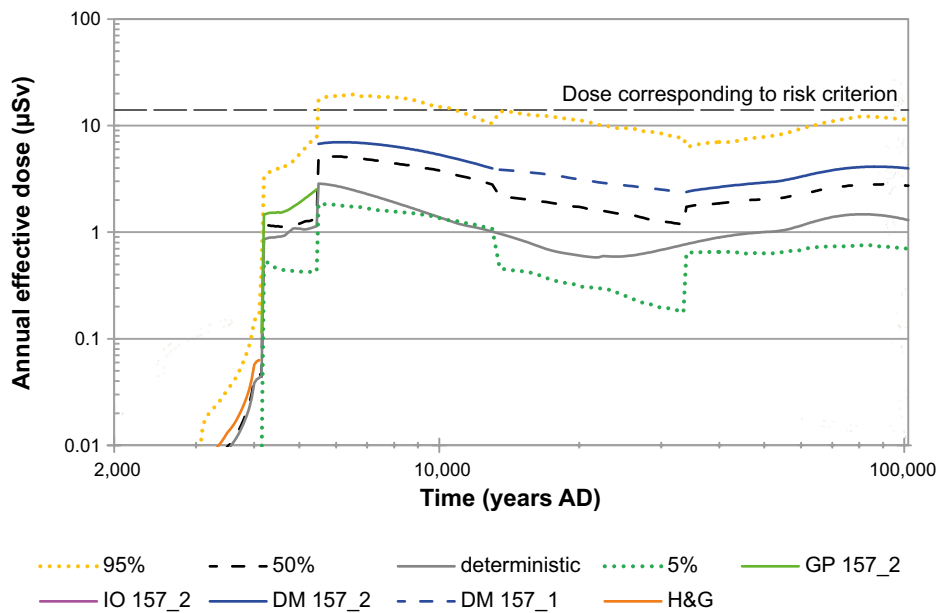


Figure 7-25. Arithmetic mean, median, 5th and 95th percentiles of the annual dose to a representative individual of the most exposed group in the *extended global warming calculation case (CCR_EX)*.

Two different inventories are considered for the assessment: one is the inventory disposed in SFR and the other includes SFL waste that is intended to be temporarily stored in SFR. The calculation of radionuclide concentrations at the tunnel entrance are performed deterministically and the only exposure pathway considered is drinking water directly from the tunnel entrance.

The results of the peak annual doses from ingestion of water are in the order of 13 mSv if only the SFR inventory is considered and in the order of 550 mSv if the inventory of SFL waste that is intended to be temporarily stored in SFR is included in the total inventory, Table 7-12.

Table 7-12. Annual dose to a representative individual exposed by water ingestion obtained for the *unclosed repository calculation case (CCR_UR)* 100 years after the unclosed repository has been abandoned.

Case	Annual dose [mSv]	Contribution from radionuclides (%)
Considering only inventory disposed in SFR	13.3	Cs-137 (63.3), Ni-63 (28.1), Sr-90 (3.3), Am-241 (2.4)
Considering also the inventory of SFL waste that is intended to be temporarily stored in SFR	548	Ni-63 (91.3), C-14-ind (5.1), Cs-137 (1.6), Mo-93 (1.1)

7.7 Glaciation and post-glacial conditions calculation case (CCR_GC)

The *glaciation and post-glacial conditions calculation case* is described in Section 4.3.7.

The temporal variation in annual effective doses are presented in Figure 7-26, and compared with the maximum dose for the *global warming calculation case*. Figure 7-27 and Figure 7-28 show the contributions from waste vaults and radionuclides, respectively. The peak annual effective dose is reported in Table 7-13, together with the year of occurrence, the contributions from the waste vaults and the most relevant radionuclides, as well as the exposed group for which the peak annual dose occurs and in which biosphere object.

Following uplift above sea level, *DM* receives the maximum dose which peaks at 2.8 μSv close to the end of the assessment period (Table 7-13, Figure 7-26). The silo and the 1-2BMA vault contribute more than 95% to peak dose. Contributions from the BLA vaults are insignificant, their contribution is below 0.05% each. The dominating radionuclide is Ni-59, contributing more than 75% to peak dose, with another 15% contributed by Ra-226 and Pu-239.

Table 7-13. Peak annual dose to a representative individual of the most exposed group obtained for the *glacial and post-glacial conditions calculation case*.

Annual dose [μSv]	Year [AD]	Contribution from waste vault (%)	Contribution from radionuclide (%)	Exposed group (biosphere object)
2.8	96,400	Silo (50.6)	Ni-59 (77.6)	Drained-mire farmer (Object 157_2)
		1BMA (30.9)	Ra-226 (8.2)	
		2BMA (13.6)	Pu-239 (7.2)	
		BRT (3.0)	Tc-99 (2.2)	
		1BTF (1.4)	Others (4.8)	
		2BTF (0.6)		
		1BLA (0.0)		
		2BLA (0.0)		
		3BLA (0.0)		
		4BLA (0.0)		
		5BLA (0.0)		

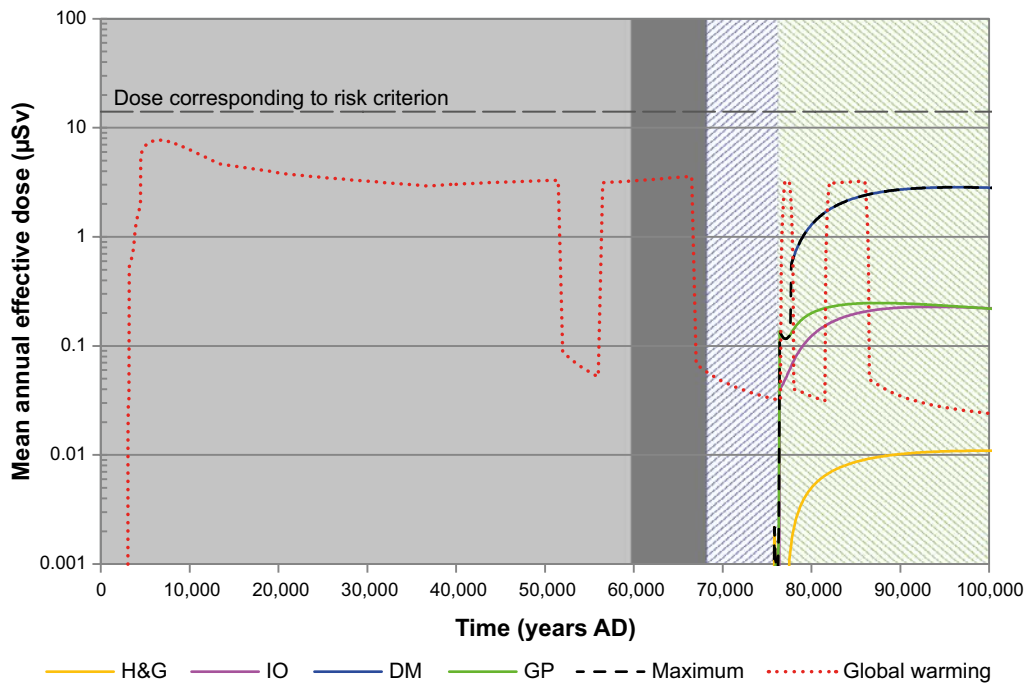


Figure 7-26. Arithmetic mean of annual dose for exposed groups in biosphere object 157_2 and the maximum for all biosphere objects in the *glaciation and post-glacial conditions calculation case*. Maximum dose for the *global warming calculation case* is also shown for comparison. The grey shaded area indicates temperate and periglacial conditions without radionuclide releases to the biosphere, dark grey indicates glacial conditions. The hatched areas indicate temperate conditions, blue for submerged and green for terrestrial periods.

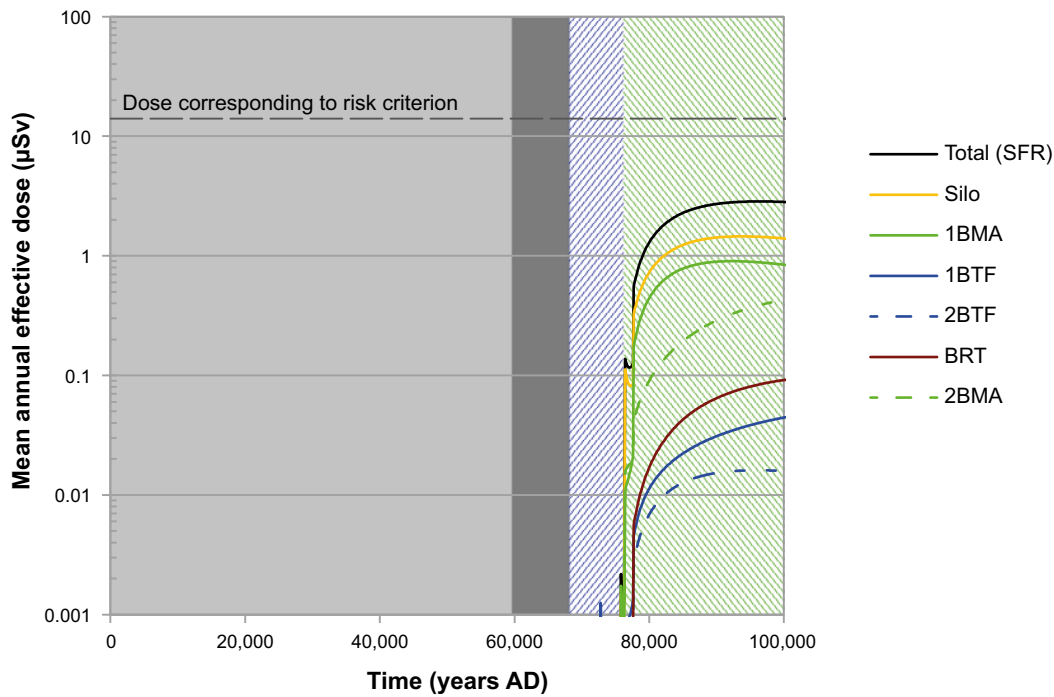


Figure 7-27. Arithmetic mean of the annual dose to the most exposed group for releases from the entire repository and contributions from the individual waste vaults in the **glaciation and post-glacial conditions calculation case (CCR_GC)**. The grey shaded area indicates temperate and periglacial conditions without radionuclide releases to the biosphere, dark grey indicates glacial conditions. The hatched areas indicate temperate conditions, blue for submerged and green for terrestrial periods.

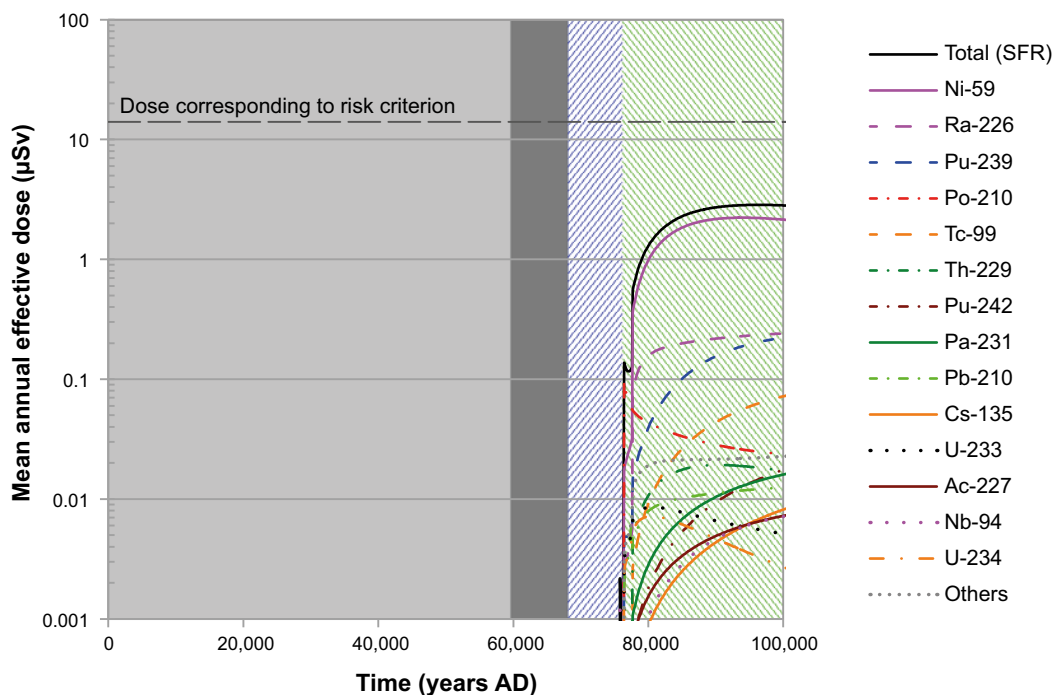


Figure 7-28. Arithmetic mean of the annual dose to the most exposed group and respective radionuclide contributions, shown for releases from the entire repository in the **glaciation and post-glacial conditions calculation case (CCR_GC)**. The grey shaded area indicates temperate and periglacial conditions without radionuclide releases to the biosphere, dark grey indicates glacial conditions. The hatched areas indicate temperate conditions, blue for submerged and green for terrestrial periods.

8 Dose rates to non-human biota

8.1 Estimating dose rates to non-human biota across various scenarios

Exposures of non-human biota to ionising radiation from radionuclides originating from the SFR repository have been estimated by calculating absorbed dose rates, according to the method described in Saetre et al. (2013). Described here are 3 calculation cases for the main scenario, 6 calculation cases for less probable scenarios, 5 calculation cases for residual scenarios and 2 calculation cases for the calculation case combinations. The calculation cases analysed for non-human biota are listed in Table 8.1 with the main results, whereas a description of the calculation cases is given in Chapter 4. The majority of results presented in this chapter are from deterministic calculations, but probabilistic calculations have also been analysed and summarised (see Section 8.8) in order to investigate the uncertainty associated with the deterministic results. As mentioned in the preface to this report there has been an update to the estimate of the radionuclide inventory in SFR after the first edition of this report, and the calculation of doses to humans have been updated. However an update of calculations of exposure of non-human biota (presented in this chapter) has not been updated with this new inventory, as the previous calculation showed that the exposure of non-human biota is well below the screening limits and the increased inventory is not large enough to change this conclusion. The inventory used for calculations presented in the previous edition of this report, and still used for calculations of exposure of non-human biota presented in this chapter, is presented in Table A-5 and Table A-6 in Appendix A.

Radiation exposures of plants and animals living in the biosphere objects are the result of external exposure (i.e. radiation from water, sediment or soil), and from internal exposure (i.e. from radionuclide uptake or intake). Both external and internal exposure directly depend on the activity concentrations in the environmental media, and thus temporal and spatial variations in dose rates for any organism group are expected to roughly follow those of the environmental media. The radioactivity released from the repository is a mixture of different radionuclides and their impacts on biota differ, depending on their half-lives, decay modes (mirrored by the dose conversion coefficients; Grolander et al. 2013), and their availability for uptake in biota (described by *Concentration Ratios*, CR; Grolander et al. 2013). The radionuclide with the highest environmental concentration, does not always dominate the exposure, as is evident in the following sections.

As described in Chapter 2 in the **Main report**, the dose assessment results have been interpreted with respect to the ERICA screening dose rate ($10 \mu\text{Gy h}^{-1}$). Consideration is also given to relevant ICRP Derived Consideration Reference Levels (DCRLs), where these are more restrictive than the generic ERICA screening value. The ICRP DCRLs are recommended as benchmarks against which acceptability, in terms of environmental impacts of planned activities, should be gauged (ICRP 2014). There is no ICRP DCRL available for either Phytoplankton (simple plants and bacteria) or Zooplankton (typically made up of crustaceans and insect larvae) and direct comparison is therefore not possible, however, these organisms are acknowledged to be less radiosensitive than the likes of mammals and pine trees (Harrison and Anderson 1996, Whicker and Schulz 1982) and use of the ERICA screening value for dose rate evaluation is therefore considered to be conservative.

The ecosystem types included in the safety assessment were Marine (sea; while the site is in fact brackish, the ecosystem has been assumed to be equivalent to marine conditions. Functionally, this only affects the assemblage of organism types considered), freshwater (lake/stream) and terrestrial (wetland). Agricultural ecosystems were not considered relevant in the analysis as discussed in SKB (2014). Some organism types (e.g. Soil invertebrate) were included in the terrestrial ecosystem, where un-drained wetland ecosystems are clearly inaccurate as a habitat; however, the use of such organism types in a wetland has been maintained in this assessment to give a conservative assessment for such organism types that may exist in surrounding non-wetland terrestrial ecosystems.

The highest total dose rates were always found in the biosphere object where radionuclides from the repository reach the biosphere directly from the geosphere, i.e. biosphere object 157_2. Therefore, analysis has concentrated on the exposure of non-human biota in this biosphere object (the exception

is in the *early periglacial climate variant* of the main scenario where radionuclide transfer to biosphere object 157_2 would not occur under periglacial conditions). For the calculation cases in the main scenario, exposure in the downstream biosphere object 157_1 has also been presented to identify the potential impact on organisms from radionuclides that are transferred through surface water to an object that is not a direct recipient of radionuclides from the repository via the geosphere.

Table 8-1. Summary of information relating to the maximum dose rates found in non-human biota in the calculation cases for the main scenario, less probable scenarios, residual scenarios and scenario combinations. For each calculation case, data for the relevant ecosystems (MA = Marine; FW = Freshwater; TE = Terrestrial) in primary source object 157_2 (unless specified) are given.

Calculation case	Ecosystem	Organism type	Time (year AD)	Maximum dose rate ($\mu\text{Gy/h}$)	Percentage internal dose rate (%)	Key radionuclide (contribution to dose rate)
Main scenario						
Global warming calculation case	MA	(Wading) bird	4250	5.2E-3	100	C-14 (org) (98%)
	FW	Bird	4500	7.1E-3	100	C-14 (org) (98%)
	TE	Lichen & bryophytes	7000	3.3E-3	100	U-238 (66%)
Early periglacial calculation case (object 157_1)	MA	No marine ecosystem in assessment period				
	FW	Zooplankton	17,850	2.7E-3	100	Pa-231 (81%)
	TE	Detritivorous invert.	17,850	1.4E-3	98	Pa-231 (79%)
Timing of the releases calculation case	MA	(Wading) bird	4250	5.2E-3	100	C-14 (org) (98%)
	FW	Bird	4300	7.0E-3	100	C-14 (org) (98%)
	TE	Lichen & bryophytes	7400	2.7E-3	100	U-238 (66%)
Less probable scenarios						
High inventory calculation case	MA	(Wading) bird	4250	6.5E-3	100	C-14 (org) (93%)
	FW	Zooplankton	8400	2.9E-2	100	Se-79 (65%)
	TE	Detritivorous invert.	5250	9.0E-3	68	Pa-231 (43%)
High flow in the bedrock and calculation case	MA	(Wading) bird	4250	6.2E-3	100	C-14 (org) (97%)
	FW	Bird	4350	8.5E-3	100	C-14 (org) (97%)
	TE	Lichen & bryophytes	6300	4.1E-3	99	U-238 (66%)
Accelerated concrete degradation calculation case	MA	(Wading) bird	4250	7.0E-3	100	C-14 (org) (92%)
	FW	Bird	4350	9.6E-3	100	C-14 (org) (92%)
	TE	Lichen & bryophytes	6950	3.3E-3	100	U-238 (66%)
Bentonite degradation calculation case	MA	(Wading) bird	4250	5.2E-3	100	C-14 (org) (98%)
	FW	Bird	4500	7.1E-3	100	C-14 (org) (98%)
	TE	Lichen & bryophytes	7000	3.3E-3	100	U-238 (66%)
Earthquake calculation case	MA	(Wading) bird	4250	6.9E-2	No data, see Section 8.5.5	
	FW	Bird	4350	9.2E-2		
	TE	Bird Egg	4350	6.4E-3		
High concentration of complexing agents calculation case	MA	(Wading) bird	4250	5.5E-3	100	C-14 (org) (98%)
	FW	Bird	4350	7.4E-3	100	C-14 (org) (98%)
	TE	Lichen & bryophytes	7050	3.4E-3	100	Pa-231 (66%)
Residual scenarios						
Loss of barrier function calculation case – no sorption in the repository	MA	(Wading) bird	4250	4.6E-2	100	C-14 (inorg) (89%)
	FW	Bird	4300	6.2E-2	100	C-14 (inorg) (89%)
	TE	Bird Egg	4650	3.9E-3	98	C-14 (inorg) (53%)
Loss of barrier function calculation case – no sorption in the bedrock	MA	(Wading) bird	4250	5.2E-3	100	C-14 (org) (98%)
	FW	Zooplankton	6150	2.1E-2	100	Pa-231 (78%)
	TE	Lichen & bryophytes	5350	1.5E-2	100	U-238 (60%)
Loss of barrier function calculation case – high water flows in the repository	MA	(Wading) bird	4250	2.0E-2	100	C-14 (inorg) (92%)
	FW	Vascular plant	31,500	3.2E-2	100	Pu-239 (73%)
	TE	Bird Egg	4200	5.7E-3	93	I-129 (64%)
Changed repository redox conditions in SFR 1 calculation case	MA	(Wading) bird	4250	5.1E-3	100	C-14 (org) (100%)
	FW	Vascular plant	52,000	1.7E-2	100	Pu-239 (92%)
	TE	Lichen & bryophytes	7050	3.3E-3	100	U-238 (66%)
Extended global warming calculation case	MA	(Wading) bird	5250	5.4E-3	100	C-14 (org) (98%)
	FW	Bird	5300	6.4E-3	100	C-14 (org) (98%)
	TE	Lichen & bryophytes	6600	1.7E-3	100	U-238 (65%)

Table 8-1. Continued.

Calculation case	Ecosystem	Organism type	Time (year AD)	Maximum dose rate ($\mu\text{Gy/h}$)	Percentage internal dose rate (%)	Key radionuclide (contribution to dose rate)
Scenario combinations						
Scenario combination 1 calculation case	MA	(Wading) bird	4250	8.6E-3	100	C-14 (org) (82%)
	FW	Bird	4300	1.1E-2	100	C-14 (org) (82%)
	TE	Lichen & bryophytes	6250	4.2E-3	99	U-238 (65%)
Scenario combination 2 calculation case	MA	(Wading) bird	4250	6.3E-3	100	C-14 (org) (97%)
	FW	Zooplankton	37,000	9.1E-3	100	Ni-59 (90%)
	TE	Lichen & bryophytes	6300	4.2E-3	99	U-238 (65%)

Attention should be paid to the assessment duration⁸, as it may vary between and within calculation cases. In some calculation cases, the assessment duration in one ecosystem type (marine, freshwater, terrestrial) may extend for a longer period compared with that in other calculation cases. The time periods when different ecosystems are present in the two biosphere objects 157_2 and 157_1 are presented in Table 8-2. The biosphere object 157_2 evolves directly from a marine bay into a wetland (terrestrial) and therefore has no defined freshwater stage, but since surface water in mire areas is an important habitat for water-dwelling organisms, exposure of limnic organisms to radiation in this object has been estimated from radionuclides in the upper peat and corresponding pore water.

Table 8-2. Time periods when marine, freshwater and terrestrial ecosystems are present in the biosphere objects 157_2 and 157_1.

Biosphere object	Ecosystem		
	Marine	Freshwater	Terrestrial
157_2	Start –> 4276 AD	4276 AD –> end	2501 AD –> end
157_1	Start –> 4493 AD	4493 AD –> end*	4001 AD –> end

* The freshwater lake stage of object 157_1 ends at 5700 AD, but a stream remains in the object for which exposure of non-human biota is assessed.

8.2 Reference organisms, site-specific parameters and site representative species

Following from the methodology used in a previous assessment of effects on non-human biota from a repository for spent nuclear fuel and high-level waste (Jaeschke et al. 2013), a limited number of reference organisms from the ERICA (radiological risk assessment) tool were used to represent the diversity of organisms at the site (Brown et al. 2008). Instead of attempting to incorporate the variation within, and across, all organism types, the reference organisms used in ERICA have specific characteristics (geometry, habitat residence, concentration ratio of radionuclides, etc.) that have been selected to represent a broad category of organisms. These reference organisms are given a capitalised name to distinguish them as a hypothetical “average” (or with conservatively selected characteristics relevant for assessment purposes) organism of that type. The ERICA reference organisms are shown in Table 8-3. Of the reference organisms available, the marine reference organisms: ‘Reptile’ and ‘Sea anemones or true corals’ (colony and polyp), which are not relevant to the conditions at Forsmark today or in the future, have been excluded from the assessment.

⁸ When comparing dose rates across ecosystems, objects or calculation cases, it is important to compare at the same time point (where such comparisons are applicable), so as not to erroneously conclude that one system is more highly exposed than another, for example, because an increasing (or decreasing) trend is followed for a longer period.

Table 8-3. ERICA reference organisms in terrestrial, freshwater and marine ecosystems.

Terrestrial	Freshwater	Marine
Amphibian	Amphibian	(Wading) bird
Bird	Benthic fish	Benthic fish
Bird egg	Bird	Benthic mollusc
Detritivorous invertebrate	Bivalve mollusc	Crustacean
Flying insects	Crustacean	Macroalgae
Gastropod	Gastropod	Mammal
Grasses and Herbs	Insect larvae	Pelagic fish
Lichen and bryophytes	Mammal	Phytoplankton
Mammal (Deer)	Pelagic fish	Polychaete worm
Mammal (Rat)	Phytoplankton	Reptile *
Reptile	Vascular plant	Sea anemones or true corals – colony *
Shrub	Zooplankton	Sea anemones or true corals – polyp *
Soil Invertebrate (worm)		Vascular plant
Tree		Zooplankton

* Not relevant for the conditions at Forsmark today or in the future.

Further recommendations from Jaeschke et al. (2013) were the use of site-specific CR data (where available, from an extensive site characterisation programme at Forsmark (Tröjbom et al. 2013)), organism residence is biased towards soil/sediment habitats (where appropriate), and the use of split residence for organisms that may spend significant parts of their lives in more than one ecosystem. Four site-specific ‘representative species’ have also been modelled to better represent the diversity of organisms found at the site (SKB 2014). Microphytobenthos are photosynthetic cyanobacteria and microalgae that grow on the sediment in freshwater lakes. The individual organisms are similar to the pelagic phytoplankton, but exist as a dense community on the lake-bottom, where they may be more exposed to sediment-borne contaminants. The representative species Microphytobenthos is mapped in the model with the same geometry and CR values as phytoplankton, but existing entirely ‘on sediment’. Furthermore, two marine species and one freshwater species are identified as living for significant periods of their lives on land; all three species feed in the aquatic ecosystems but are exposed externally from terrestrial ecosystems (soil and air). The species identified were a marine bird (Scientific name: *Arenaria interpres*; English name: ruddy turnstone; Swedish name: roskarl), a marine mammal (Scientific name: *Lutra lutra*; English name: European otter; Swedish name: utter), and a freshwater bird (Scientific name: *Chlidonias niger*; English name: black tern; Swedish name: svarttärna). Dose rates were proportioned *ad hoc* using data from the relevant reference organisms in each ecosystem, according to the species’ specific residence times in each ecosystem. These species with residence split over two ecosystems are analysed separately to the rest of the *global warming calculation case*, in Section 8.4.1.

8.3 Overview of results

The maximum dose rate calculated was in freshwater Bird in the *earthquake calculation case* at 4350 AD (Table 8-1); dose rates of the same order of magnitude ($10^{-2} \mu\text{Gy h}^{-1}$) were found in seven calculation cases:

- *high inventory calculation case*,
- *earthquake calculation case*,
- *loss of barrier function calculation case – no sorption in the repository*,
- *loss of barrier function calculation case – no sorption in the bedrock*,
- *loss of barrier function calculation case – high water flow in the repository*,
- *changed repository redox conditions in SFR 1 calculation case, and the*
- *scenario combination 2 calculation case (that combines the high flow in the bedrock calculation case and high concentration of complexing agents calculation case).*

The highest dose rates were typically found in the freshwater ecosystem. Since all estimated dose rates are well below the screening values that were adopted (discussed in Section 8.1), it was concluded that the repository would not affect biodiversity or sustainable use of biological resources in the Forsmark area.

In all the calculation cases the highest dose rates overall were found in the primary source biosphere object 157_2, except the *early periglacial calculation case*, where exposures in biosphere object 157_2 were not relevant. Exposures to non-human biota in the *global warming calculation case* are analysed in both biosphere objects 157_2 and 157_1; in all other cases the analysis focusses only on the more-exposed object. In the *early periglacial calculation case*, the analysis focuses on the biosphere objects where taliks may exist that allow transfer of radionuclides to the surface, i.e. biosphere objects 157_1 and 114.

In the marine ecosystem, dose rates in organisms increased rapidly before beginning to level off; the gradually decreasing exchange of water with outer basins (caused by land uplift) meant that dose rates to organisms did not reach a stable levels, but continued to increase until the point in time where the sea withdrew completely from the object (~ 4250 AD in most calculation cases). The maximum dose rates in marine organisms were thus found at the end of the marine assessment period.

In freshwater and terrestrial ecosystems, for most organisms, results in most calculation cases followed the pattern of the *global warming calculation case*: with a well-defined peak either at the very beginning, or after just a few thousand years, before decreasing gradually over the rest of the assessment period. In the terrestrial ecosystem, the maximum dose rate for the most exposed organism of each calculation case occurred towards the beginning of the assessment period, during the peak in dose rates, described above. In the freshwater environment, the patterns of dose rate, across the various scenarios, fit into one of three categories that can be identified by the type of organism that received the highest dose rate. In scenarios where Bird was the most exposed organism type, the peak (described above) was evident in most organism types, and represented the maximum dose rates for all freshwater organism types. In scenarios where Vascular plant was the most exposed freshwater organism type, the peak in dose rates was less pronounced (in the *changed repository redox conditions calculation case*) or non-existent (in the *loss of barrier function calculation case – high water flow in the repository*), and instead of decreasing after the peak, dose rates for vascular plants continued to increase until ~ 30,000–50,000 AD. In scenarios where Zooplankton was the most exposed freshwater organism type, the dose rate pattern included a significant peak in the *loss of barrier function calculation case – no sorption in the bedrock* and *high inventory calculation case*, in the remaining cases (*early periglacial calculation case* and the *calculation case combination 2*) the dose rates increased for longer, with the highest dose rate occurring later.

The *earthquake calculation case* gave the highest dose rates. The calculation cases investigating differences in the near-field conditions (the *loss of barrier function calculation case – high water flow in the repository* and the *loss of barrier function calculation case – no sorption in the repository*) also resulted in higher exposures than did other cases. Lowest exposures were seen in the *early periglacial calculation case*.

Internal sources of radiation dominated the dose rates to the most exposed organisms in all calculation cases (Table 8-1). No trend was seen with regards to habitat (in/on water vs. in/on sediment; in air vs. in/on soil), due to the largely internal exposure. If dose rates were more affected by external sources, higher doses in soil/sediment habitats than those in water/air would be expected.

C-14 dominated the dose rate to the most exposed marine organisms in all calculation cases. C-14 was a key radionuclide in the freshwater ecosystem in most calculation cases, but in some scenarios other radionuclides were dominant (Pa-231 in the *early periglacial calculation case* and the *loss of barrier function calculation case – no sorption in the bedrock*; Pu-239 in the *loss of barrier function calculation case – high water flow in the repository* and the *changed repository redox conditions in SFR 1 calculation case*; Se-79 in the *high inventory calculation case*; and Ni-59 in *scenario combination 2 calculation case*). In the terrestrial ecosystem, U-238 was the key radionuclide in the most exposed organisms in most calculation cases, with the exception of a few cases where dose rates to the most exposed organism were dominated by Pa-231 (*early periglacial calculation case*, *high inventory calculation case* and *high concentration of complexing agents calculation case*), C-14 (*loss of barrier function calculation case – no sorption in the repository*), and I-129 (*loss of barrier function calculation case – high water flows in the repository*).

Probabilistic assessments, discussed in Section 8.8, used sampling of probability density functions (PDFs) to investigate the implications of uncertainties in parameter values used in the simulations. In the most exposed organisms, the dose rate at the 95% confidence level was still well below the screening dose rate. In the probabilistic assessment, the most exposed organism types differed in some scenarios, compared with those identified in the deterministic assessment; in some calculation cases, the most exposed organism type was from a different ecosystem, reflecting the similar magnitude of dose rates calculated in freshwater and terrestrial ecosystems under certain scenarios.

8.4 Results for the main scenario

The main scenario is described in detail in Section 7.4 in the **Main report**, and its calculation cases are summarised in Section 4.1. The assessment of the main scenario comprises the assessment of its two variants, the *global warming climate variant* and the *early periglacial climate variant*. The first variant is assessed evaluating two calculation cases (the *global warming calculation case* and the *timing of the releases calculation case*), the second variant by a single calculation case (the *early periglacial calculation case*). An overview of the key results obtained for the main scenario is presented below.

8.4.1 Global warming calculation case

In the *global warming calculation case* the radionuclides from the repository reach the biosphere about one thousand years after repository closure. At that time, part of the main recipient object (157_2) is evolving from a marine bay into a mire, and exposures of marine and terrestrial (wetland) organisms has been estimated. The object has no defined freshwater stage, but since surface water in mire areas is an important habitat for water-dwelling organisms, radiological exposure to freshwater organisms has been estimated from the environmental concentrations of radionuclides in the upper peat and corresponding pore water.

The estimated dose rates to most exposed organisms are similar in the terrestrial and freshwater ecosystems and approximately one order of magnitude lower for marine organisms. The dose rates are all well below the screening value of $10 \mu\text{Gy h}^{-1}$.

Marine ecosystem

Since the simulated objects are only marine areas during the initial time period, the simulated period for marine ecosystems was short compared with that applicable to freshwater and terrestrial ecosystems, and the exposure pattern seen for freshwater and terrestrial ecosystems (initial peak followed by a somewhat more stable long term phase) was not evident for the marine ecosystems. Instead, only the initial stage of what has been described as the peak phase (as seen in terrestrial and freshwater ecosystems) can be seen in the simulation period. Marine organisms received dose rates more than three orders of magnitude lower than the screening dose rate, with the highest dose rate occurring in the (Wading) bird at $5.2 \times 10^{-3} \mu\text{Gy h}^{-1}$ (Figure 8-1). The least exposed organism (Phytoplankton) received maximum dose rates of the order of $10^{-5} \mu\text{Gy h}^{-1}$. The dose rates for all organism types, except Phytoplankton, followed each other closely and the difference between most and least exposed was approximately one order of magnitude. The most exposed marine organism type, in both biosphere objects 157_1 and 157_2, was the (Wading) bird, which has been conservatively assumed to live in the water. The most exposed benthic organism was the Benthic fish (max dose rate: $2.5 \times 10^{-3} \mu\text{Gy h}^{-1}$), living on the seafloor, where doses from radionuclides in the sediment are expected; however dose rates were dominated by internal sources of radiation (99.5%), further highlighting the general unimportance of external sources in this assessment. Organisms living in biosphere object 157_2 received higher dose rates than their equivalents living in biosphere object 157_1 (Figure 8-1); the remaining part of this section thus concentrates on dose rates to organisms in the more-exposed biosphere object 157_2.

Phytoplankton, which was the most exposed organism type in the dose rate assessment to non-human biota from a repository for spent nuclear fuel (Jaeschke et al. 2013), in the present assessment received the lowest exposure of any organism type throughout the whole simulation period by a significant margin (Figure 8-1). The gap between the dose rate for Phytoplankton and the others decreased during the simulation but was still about one order of magnitude at the end of the period.

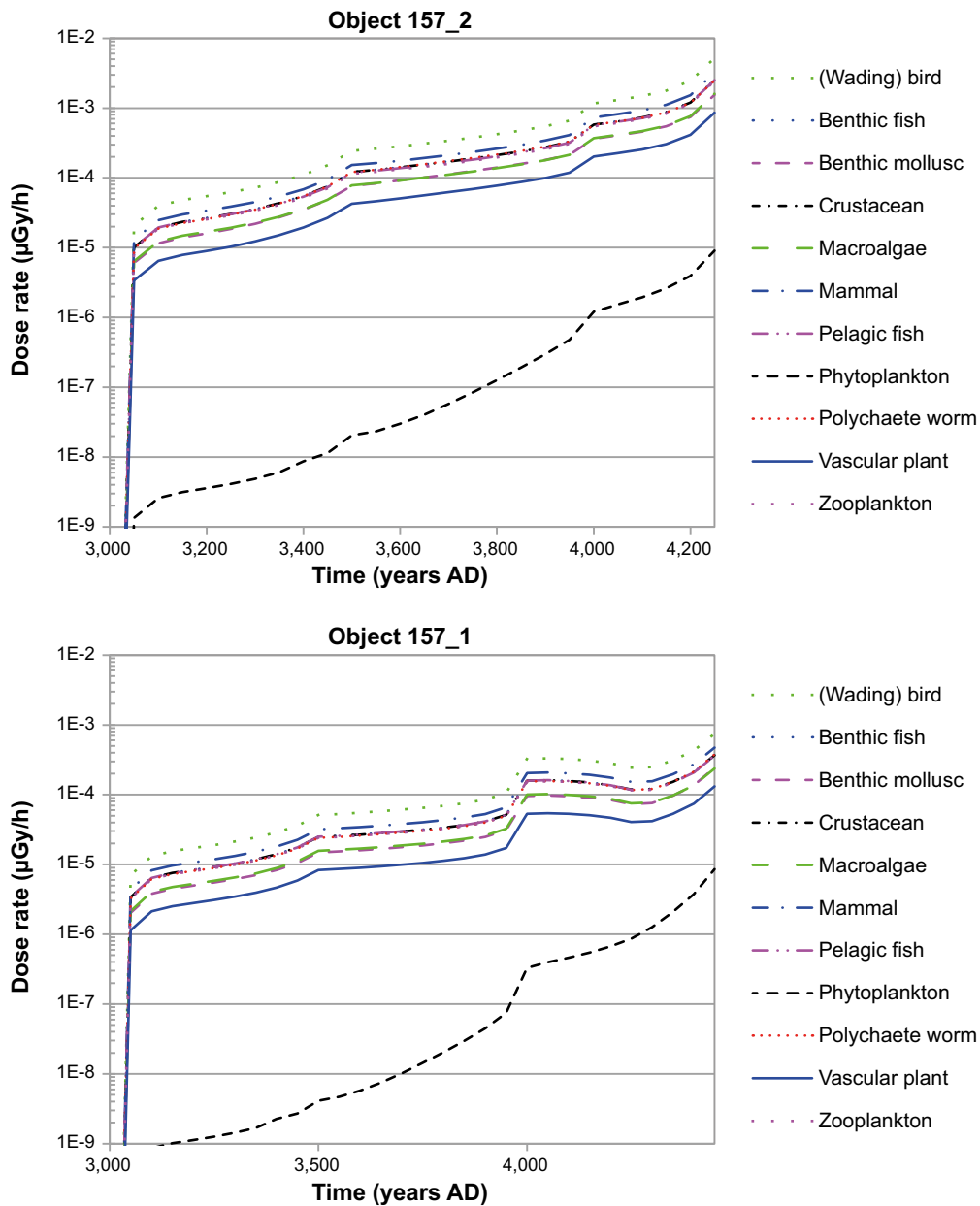


Figure 8-1. Dose rates to non-human biota in the marine ecosystem, in the **global warming calculation case**. *N.b. the dose rates are several orders of magnitude lower than the screening dose rate ($1E+1 \mu\text{Gy/h}$) which cannot be seen on this figure.*

The large gap in dose rates indicates a major difference in exposure for the Phytoplankton compared with all other organism types. The much lower dose rates to Phytoplankton, compared to other organisms in this assessment, were due to the very small size of the organism; thus an increased proportion of the high-energy beta emission from internal sources can escape without contributing to dose rate. The lower dose rates in Phytoplankton in this assessment, compared with the assessment of a repository for spent nuclear fuel, are due to the domination of high-energy beta-emitting radionuclides in the present assessment, whereas radionuclides originating from the spent nuclear fuel contained a higher proportion of alpha and low-energy beta emitters that do not escape the very small-sized Phytoplankton, contributing more effectively to dose.

As the marine component of the assessment focuses only on very early stages of release from the repository, the dominating radionuclide was C-14 for all organisms except Phytoplankton (Figure 8-2). Due to weak sorption, C-14 reaches the biosphere relatively rapidly from the repository, and having a half-life of $\sim 5,700$ years makes it a major dose contributor in the early period of the assessment. The total dose rates were very similar in all organisms (except Phytoplankton) due to the

similar exposures from C-14 which dominated the contribution for the marine organisms (due to similar C-14 concentrations in sea water in the two objects, see Figure 8-3 for environmental concentrations of the key radionuclides in water in biosphere object 157_1 and 157_2). C-14 is present as three different forms in the repository; organic, inorganic or induced (C-14-org, C-14-inorg and C-14-ind, respectively) although in the biosphere, all C-14 from the repository is assumed to have been oxidised to inorganic C and thus is available for bioaccumulation through carbon fixation by primary producers. Exposure came predominantly from organic carbon sources in the repository but also somewhat from carbon in inorganic form. For the (Wading) bird, Ag-108m and Se-79 were the next largest contributors to dose rates, but their contributions to dose rates were insignificant compared with that from C-14 (and therefore not visible in figure 8-2).

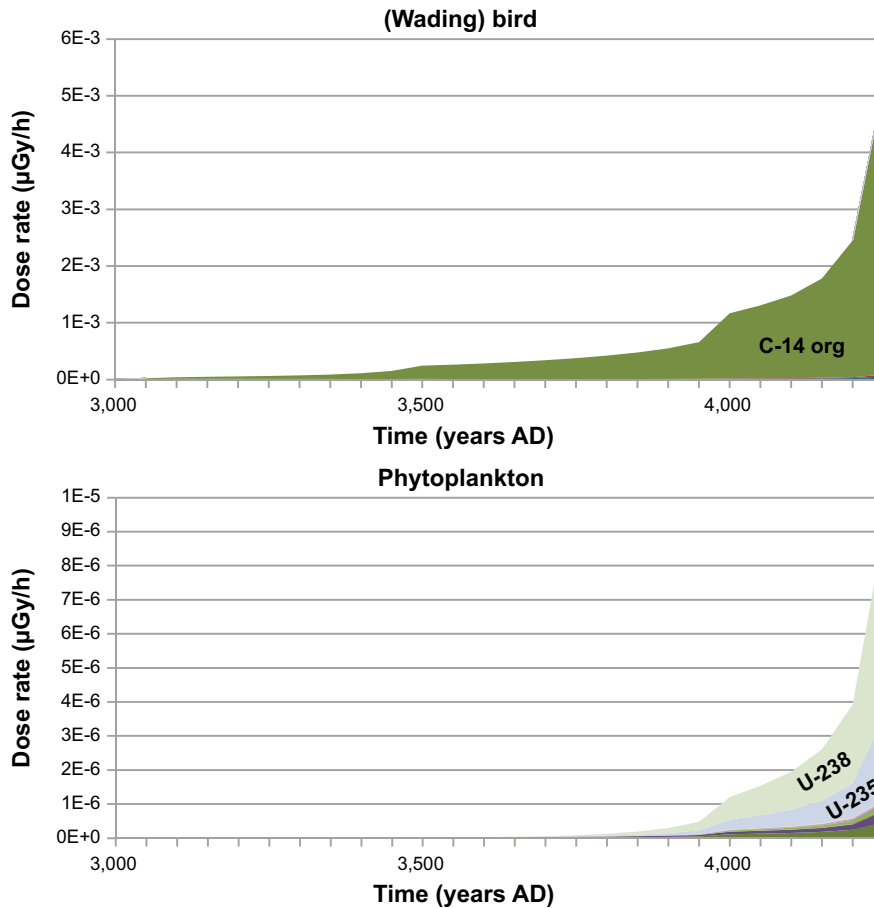


Figure 8-2. Contribution from radionuclides to dose rates in the most exposed organism, (Wading) bird (top) in object 157_2 marine ecosystem, in the **global warming calculation case**. For contrast, contribution from radionuclides to dose rates in Phytoplankton are shown (bottom). Radionuclides with significant contribution to total dose rate are labelled and the colouring is consistent across all panels.

Freshwater ecosystem

The most exposed freshwater organism type in biosphere objects 157_1 and 157_2 was the Bird, with a maximum dose rate of $7.1 \times 10^{-3} \mu\text{Gy h}^{-1}$ (Figure 8-4); this was more than three orders of magnitude lower than the screening dose rate. A peak in dose rates, in many organisms, was seen at about 7000 AD (Figure 8-4). Some organisms, such as the Bird and Mammal received high doses rates from C-14 at the very beginning of the assessment period, causing the highest dose rates of

the whole assessment; however, as the concentration of C-14 in the environmental media decreased, these dose rates dropped dramatically. By approximately 15,000 AD, these organism types had become the least exposed. For the majority of the assessment period, Zooplankton was the most exposed organism type.

Dose rates to organisms were higher in biosphere object 157_2 than their equivalents in object 157_1 throughout the assessment, albeit by less than a factor of ten; the remaining part of this section concentrates on dose rates to organisms in the more-exposed object 157_2. Higher exposures were seen during the peak phase in 157_2 than 157_1; however, as the contributions of radionuclides changed, exposures in 157_1 became closer to those in 157_2 in the longer term.

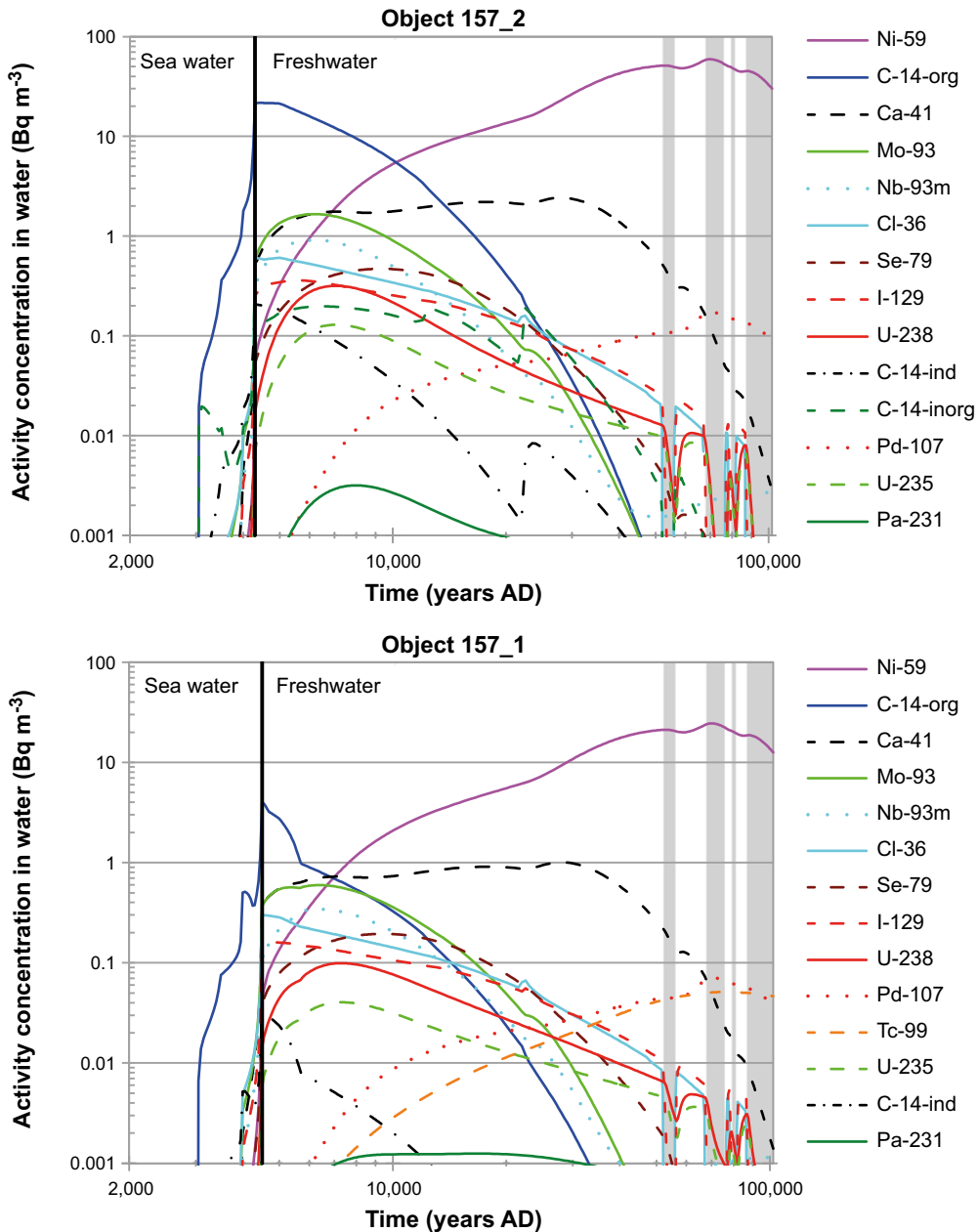


Figure 8-3. Environmental concentrations in sea water (times up to the black line) and freshwater (times beyond the black line) used in the non-human biota dose assessment, for the biosphere objects 157_2 (top) and 157_1 (bottom) in the **global warming calculation case**. The key of radionuclides is shown in descending order of contribution for 14 radionuclides.

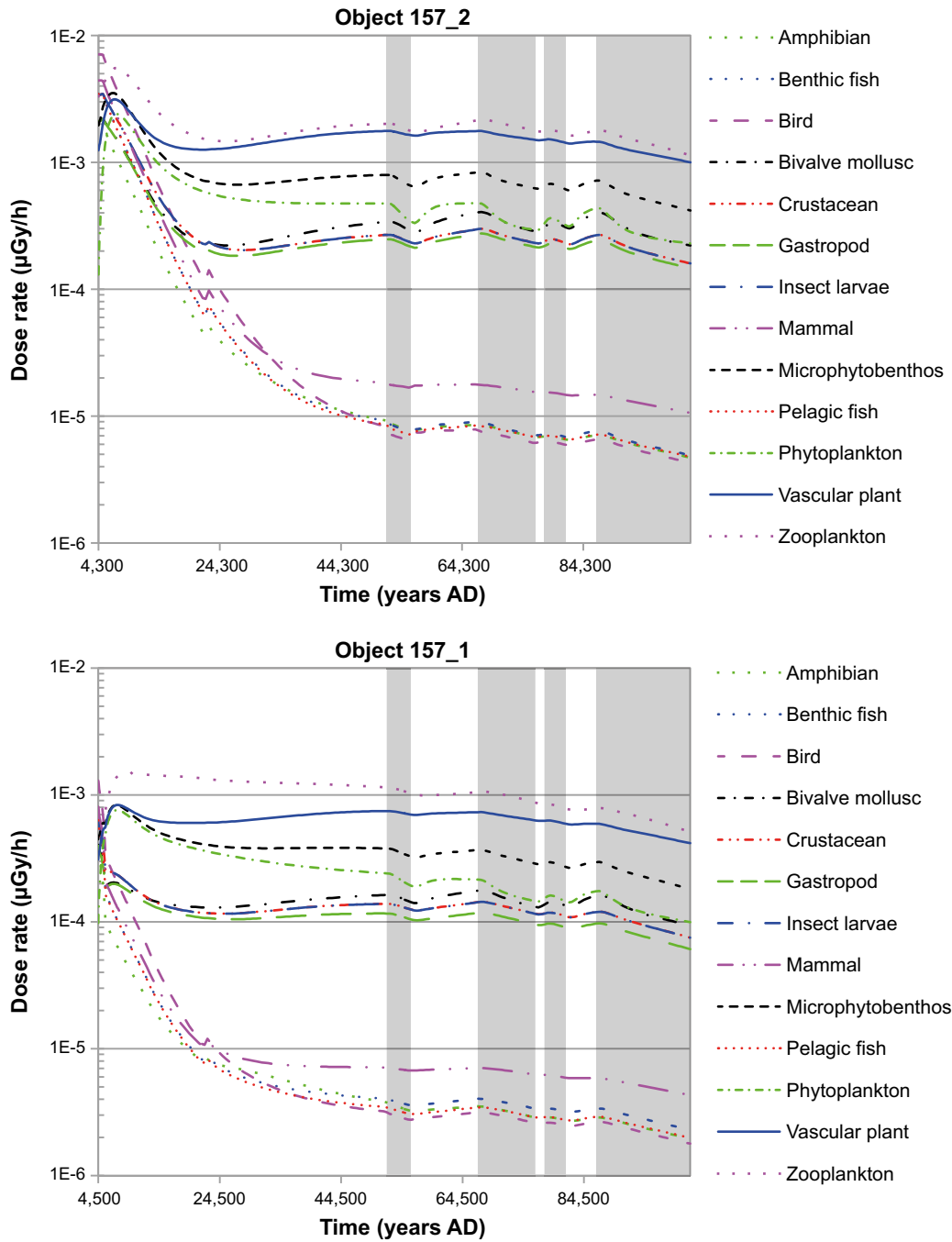


Figure 8-4. Dose rates in non-human biota in the freshwater ecosystem, in the **global warming calculation case**. Grey-shaded areas indicate periglacial periods. N.b. the dose rates are several orders of magnitude lower than the screening dose rate ($1E+1 \mu\text{Gy/h}$) which cannot be seen on this figure.

At the very beginning of the assessment, C-14 can be seen to contribute significantly to dose rates (Figure 8-5); however, exposure from C-14 drops rapidly as the concentration in water decreases, due to its relatively short half-life of $\sim 5,700$ years. Longer-lived radionuclides were responsible for dose rates in organisms that were most exposed over the later phase of the assessment. Pa-231 contributed significantly to dose rates during both the peak and long-term phases, particularly in Zooplankton (Figure 8-5). The environmental concentration of this radionuclide is relatively low (see Figure 8-3), but the dominating contribution to exposure is due to its high-energy alpha emission, and its relatively high CR (especially for Zooplankton and primary producers). Contributions from Ni-59 increased during the assessment period, becoming significant contributors to dose in the longer term (Figure 8-5). Ni-59 is the dominating radionuclide in surface water during most of the simulated

period (see Figure 8-3) and the concentration is higher than maximum concentrations for uranium isotopes at the peak, but its relatively low dose conversion coefficient results in somewhat lower dose rates. Significant radionuclides during the peak phase in Microphytobenthos were U-238, U-235 and C-14, but the importance of these, relative to other radionuclides, decreased over the assessment period, becoming much less significant in the longer term (Figure 8-5).

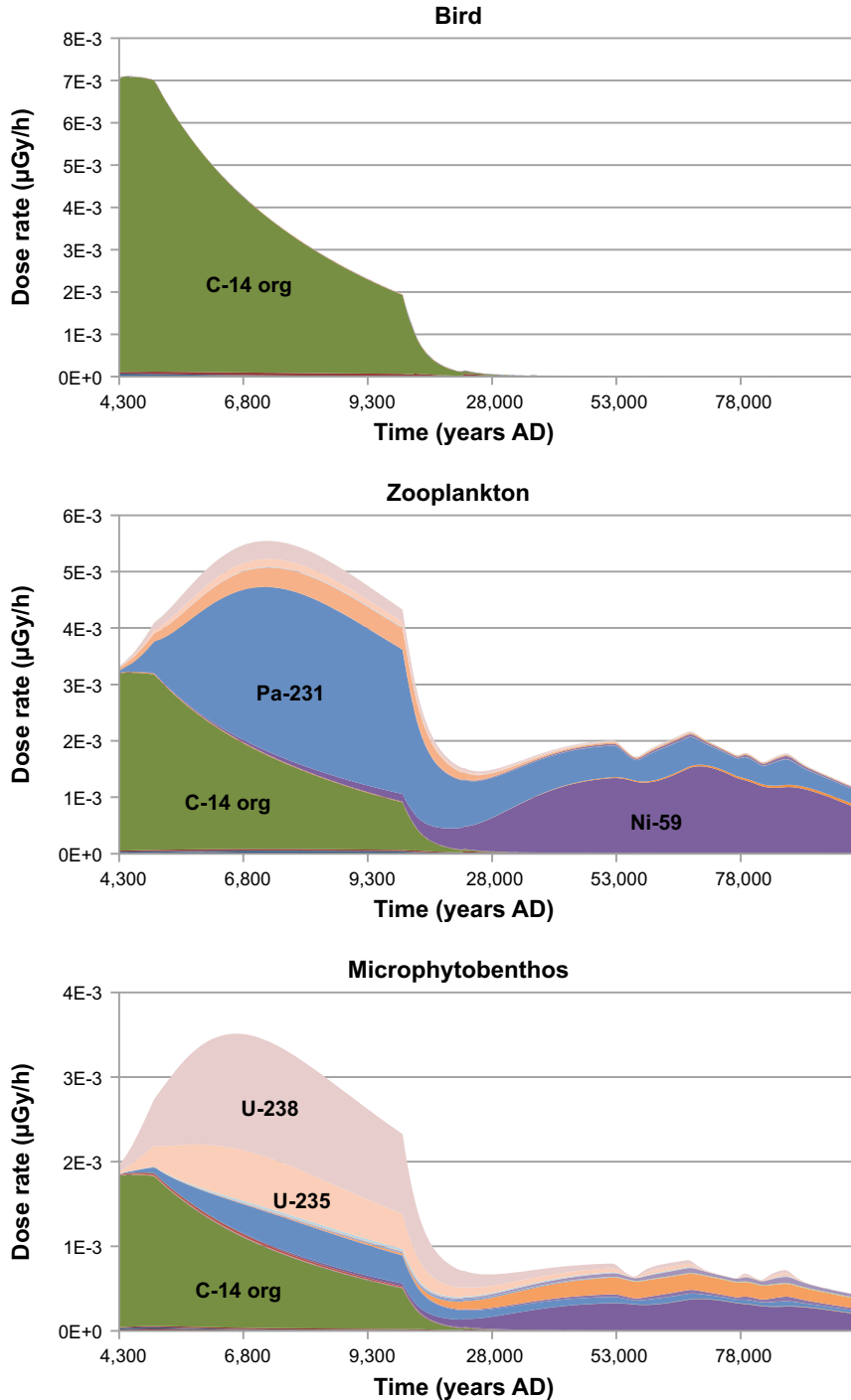


Figure 8-5. Contribution from radionuclides to dose rates in selected organism types in the freshwater ecosystem, in the **global warming calculation case**. Organism types represent the most exposed organism in the scenario (top; Bird); a long-term highly exposed organism (middle; Zooplankton); and, for contrast, a highly exposed benthic organism (bottom; Microphytobenthos). Radionuclides with significant contribution to total dose rate are labelled and the colouring is consistent across all panels.

Terrestrial ecosystem

The highest dose rate seen in any terrestrial organism was $3.3 \times 10^{-3} \mu\text{Gy h}^{-1}$ (Lichen & Bryophytes), more than three orders of magnitude lower than the screening dose rate (Figure 8-6); the lowest dose rates were approximately a further order of magnitude lower. A peak, that reaches its maximum at ~ 7000 AD, was seen, similar to that observed in the freshwater ecosystem. The most exposed organisms in the longer term were Lichen & bryophytes and Detritivorous invertebrate. The most exposed higher plant throughout the assessment was the Tree.

Dose rates in Lichen & bryophytes, Detritivorous invertebrate, and Tree (for contrast), in biosphere object 157_2 decreased markedly at several points (after 52,000 AD) before returning to its previous trending line (Figure 8-6), due to predicted periglacial periods when the inflow of radionuclides from the geosphere halts as groundwater discharge is prevented. This pattern is less pronounced in the downstream object 157_1, where the source of radionuclides is the surface water flow from object 157_2. This source declines gradually as radionuclides are washed out from the upstream object, but does not halt abruptly with the onset of permafrost. Once the periglacial period passes, the supply of radionuclides from the repository, through groundwater transport, resumes.

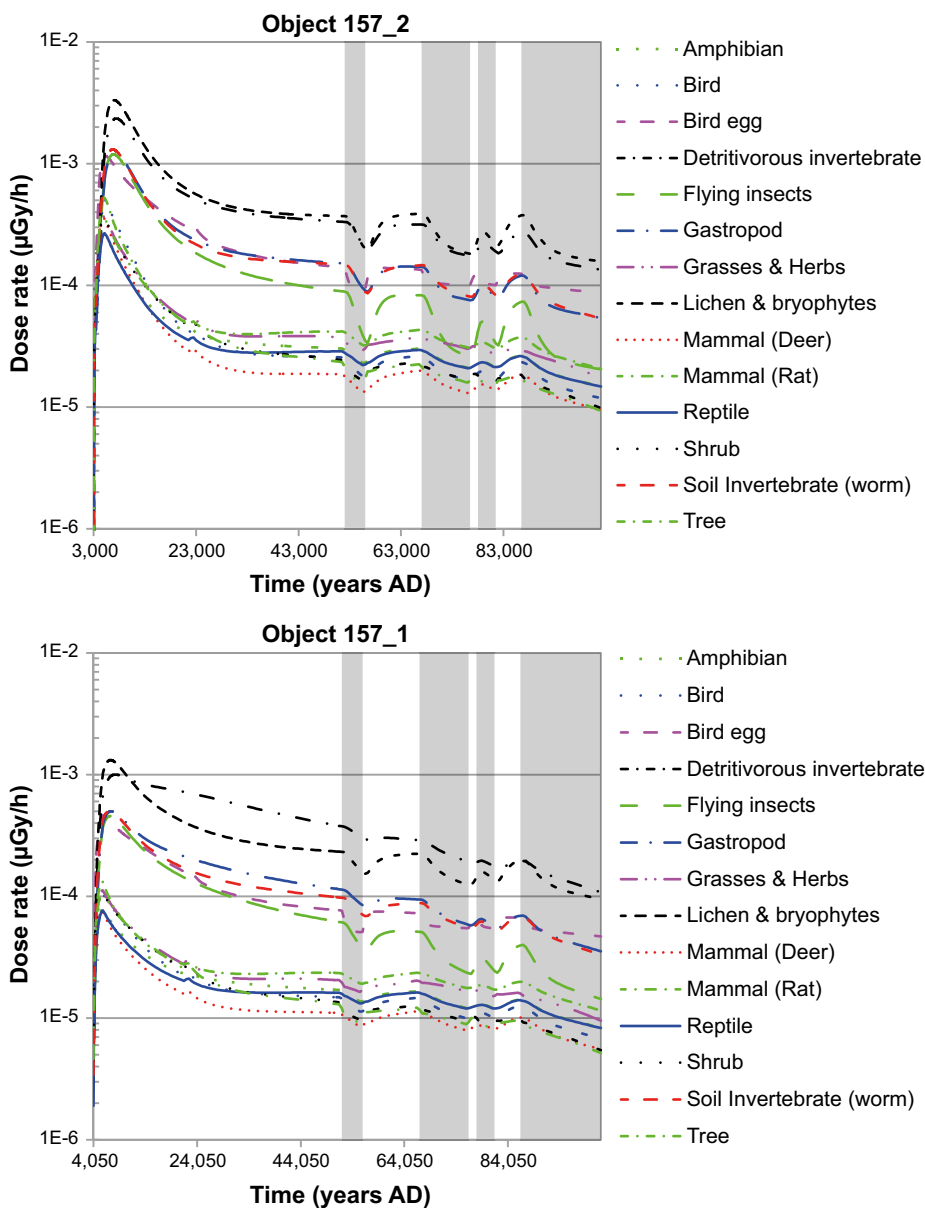


Figure 8-6. Dose rates in non-human biota in the terrestrial ecosystem, in the **global warming calculation case**. N.b. the dose rates are several orders of magnitude lower than the screening dose rate ($1E+1 \mu\text{Gy/h}$) which cannot be seen on this figure.

Dose rates in biosphere object 157_2 were higher than those in the equivalent organisms in object 157_1 (by less than a factor of ten); the remaining part of this section thus concentrates on dose rates to organisms in the more-exposed object 157_2.

Lichen & Bryophytes received the highest dose rates in the analysis both in the peak phase and in the longer term. In the peak phase, exposure was dominated by U-238 and U-235 (Figure 8-7). This was expected since these radionuclides have relatively high concentrations in surface peat during the initial simulation period (see Figure 8-8). Small troughs (short-term temporary decreases) in the dose rates from U-238 and U-235 are seen (at ~ 53,000–59,000 AD and 68,500–84,500 AD), during the simulated periglacial conditions when no radionuclides are discharged to the biosphere.

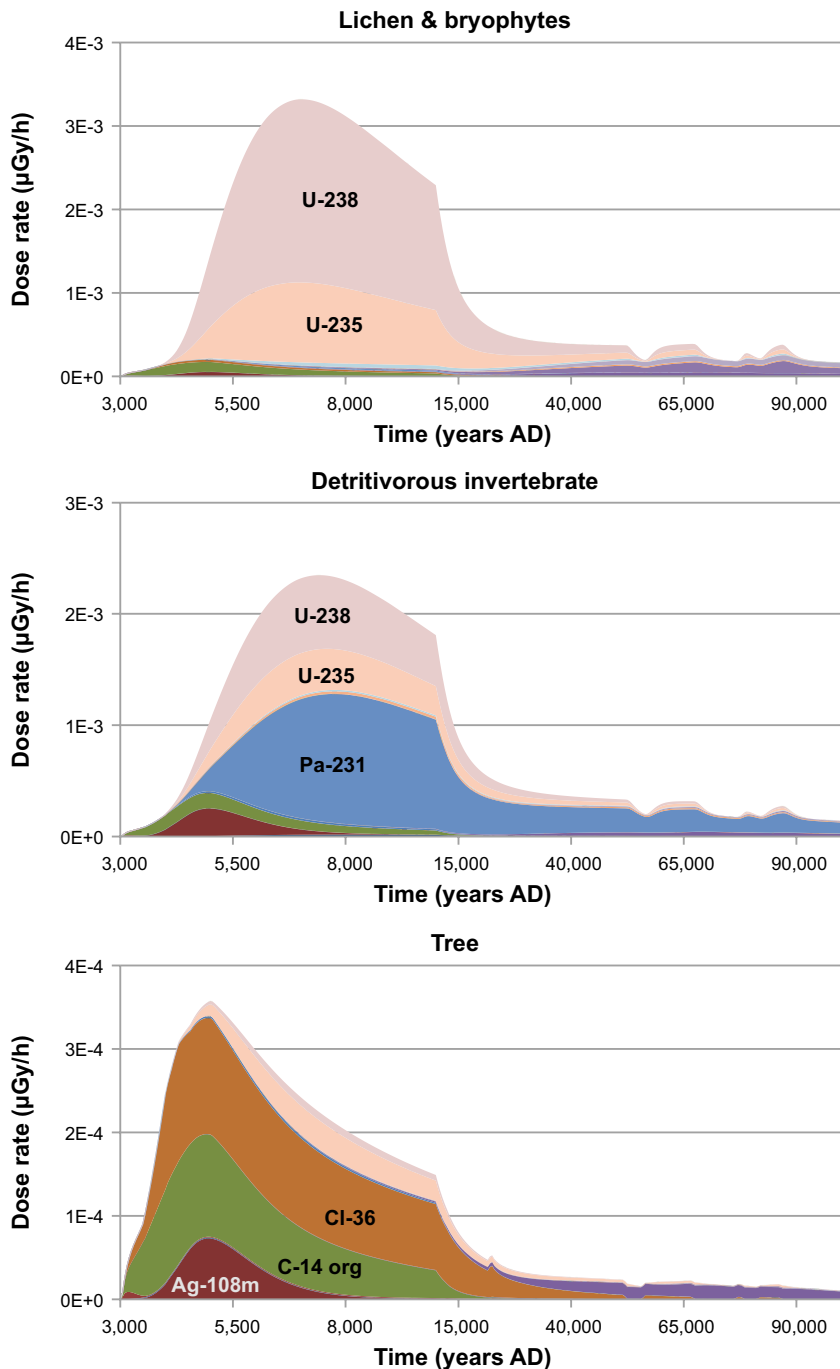


Figure 8-7. Contribution from radionuclides to dose rates in selected organism types in the terrestrial ecosystem, in the **global warming calculation case**. Organism types represent the most exposed organism in the scenario (top; Lichen & bryophytes) and, for contrast, a highly exposed burrowing organism (middle; Detritivorous invertebrate), and a highly exposed higher plant (bottom; Tree). Radionuclides with significant contribution to total dose rate are labelled and the colouring is consistent across all panels.

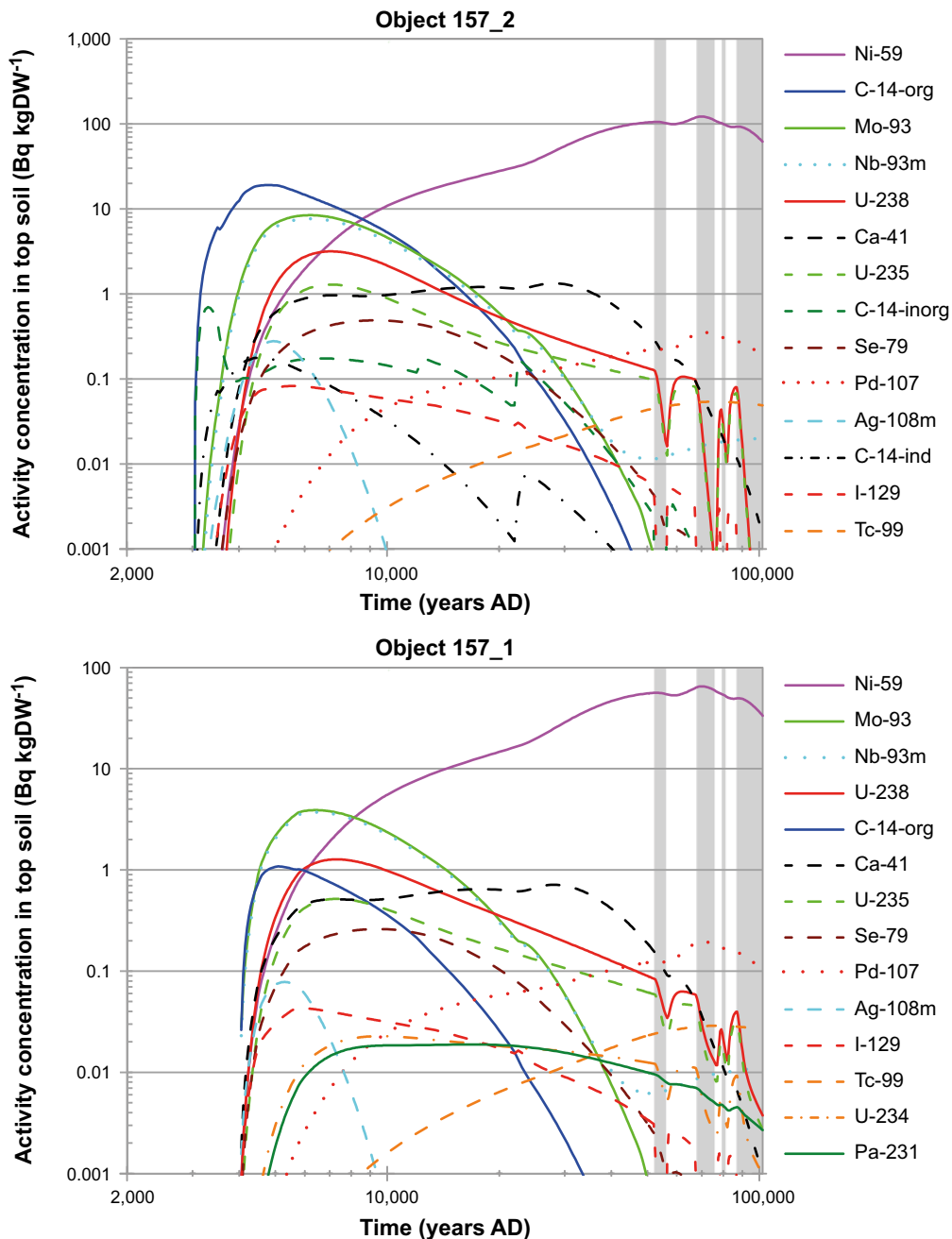


Figure 8-8. Environmental concentrations in used in the non-human biota dose assessment, for the biosphere objects 157_2 (top) and 157_1 (bottom) in the **global warming calculation case**. The key of radionuclides is shown in descending order of contribution.

Detritivorous Invertebrate demonstrated a similar pattern to the other terrestrial organisms, with highest exposure during the peak phase and a slightly lower exposure in the longer term. Dose contributions in both objects were attributable to Pa-231, U-238, and U-235 (Figure 8-7); the increased dose rate from Pa-231 in Detritivorous invertebrate (living in soil) compared to Lichen & bryophytes (living on trees, modelled as in air) highlights the difference in exposure with regards to proximity to contaminated soils, implicit in the CR values.

The predominant radionuclide contributing to dose in Tree throughout the assessment period was Cl-36 (Figure 8-7), giving dose rates approximately 100 times higher than the next highest contributing radionuclide, U-235. The dominance of Cl-36, despite its low concentration in peat, was due to a very high CR (in higher plants) and relatively high dose coefficient (for internal beta and gamma radiation).

Representative species, multiple habitat residence and the impact of external exposure

An organism that resides in multiple contaminated ecosystems may receive higher dose rates than predicted using the reference criteria, i.e. using a single reference habitat. It is potentially possible that, through the combination of exposures from two environments, an organism could receive a dose rate higher than it could otherwise achieve if inhabiting a single environment exclusively. This could occur when dose rates are dominated by internal sources in one environment, and by external sources in the other, and thus the combination of the highest exposures of each environment could lead to an overall higher dose rate.

Two marine species and one freshwater species identified at the site to inhabit terrestrial ecosystems were selected for further assessment. These three species reside in the terrestrial environment for a proportion of their life, but feed entirely from their respective aquatic habitats; thus, internal exposure remained entirely related to the organisms' reference ecosystem, whereas external exposure would be divided between terrestrial and aquatic environments. Combined exposures are only assessed for periods where dose rate assessments exist in both ecosystems simultaneously.

The 'marine' bird, ruddy turnstone, was considered to receive all external exposure from the terrestrial ecosystem whereas the mammal, European otter, was considered to spend ~40% of its time in water (the estimation in SKB (2014) was that it spends ~30% on water and 10% in water, this has conservatively been adjusted to 40% in water). The time period where marine and terrestrial ecosystems were present simultaneously was identified (3000–4250 AD), and exposure from these two ecosystems was combined during this period. Since internal exposures dominated terrestrial dose rates, the additional contribution from terrestrial external exposure of these marine representative species is rather low, so the total dose rates to the representative species follow those of the marine reference organism so closely as to be indiscernible in Figure 8-9. From ~ 3700 AD dose rates to both representative species (ruddy turnstone and European otter) became higher than either of those to the corresponding reference organisms, albeit by a very small degree (i.e. in the region of 1% greater dose rate over the more exposed corresponding reference organism). Although the differences in dose rate were small in these specific cases, it indicates that the use of reference organisms could underestimate dose rates to some marine organisms that spend some time in the terrestrial ecosystem.

The representative species, black tern, is a freshwater bird that was assumed to spend 60% of its time on land and 40% of its time in water and its external exposure was proportioned accordingly. Since internal exposures dominated terrestrial dose rates, the additional contribution from terrestrial external exposure of the black tern is rather low, so the total dose rates to the representative species follow those of the freshwater reference bird very closely (Figure 8-10). The black tern had higher dose rates than the freshwater reference bird throughout the assessment period. The black tern had higher dose rates than the terrestrial reference bird, when the doses from C-14 in the freshwater environment were highest, lasting until 34,000 AD (Figure 8-10); thereafter the black tern received lower dose rates than terrestrial reference bird. Until 34,000 AD, the black tern received higher doses than either reference bird; around 33,000 AD the black tern received dose rates approximately 10% higher than either reference organism. Thus, this split-residence species also highlights the potential for underestimation of dose rates (albeit by a small degree in respects to the assessment) to species that receive doses from radionuclides in more than one ecosystem.

The screening dose rate remains more than three orders of magnitude higher than any of the dose rates to representative species (ruddy turnstone, European otter and black tern); furthermore, some other organism types received higher dose rates than these representative species (Table 8-1; Lichen & bryophytes). Therefore no additional risk is identified to these representative species over that calculated for the *global warming calculation case*, when using reference organisms. However, this assessment identifies the potential for higher dose rates as a result of split residence in two (or more) ecosystems.

8.4.2 Early periglacial calculation case

The *early periglacial calculation case* models the specific phenomenon known as a talik that may occur during a periglacial period, where an area of unfrozen ground exists, typically beneath a lake. This calculation case is thus highly limited in space and time. Two biosphere objects have been identified as possible sites of through-taliks where radionuclides from the repository may reach the biosphere, namely object 157_1 and 114 (**Biosphere synthesis report**). Biosphere

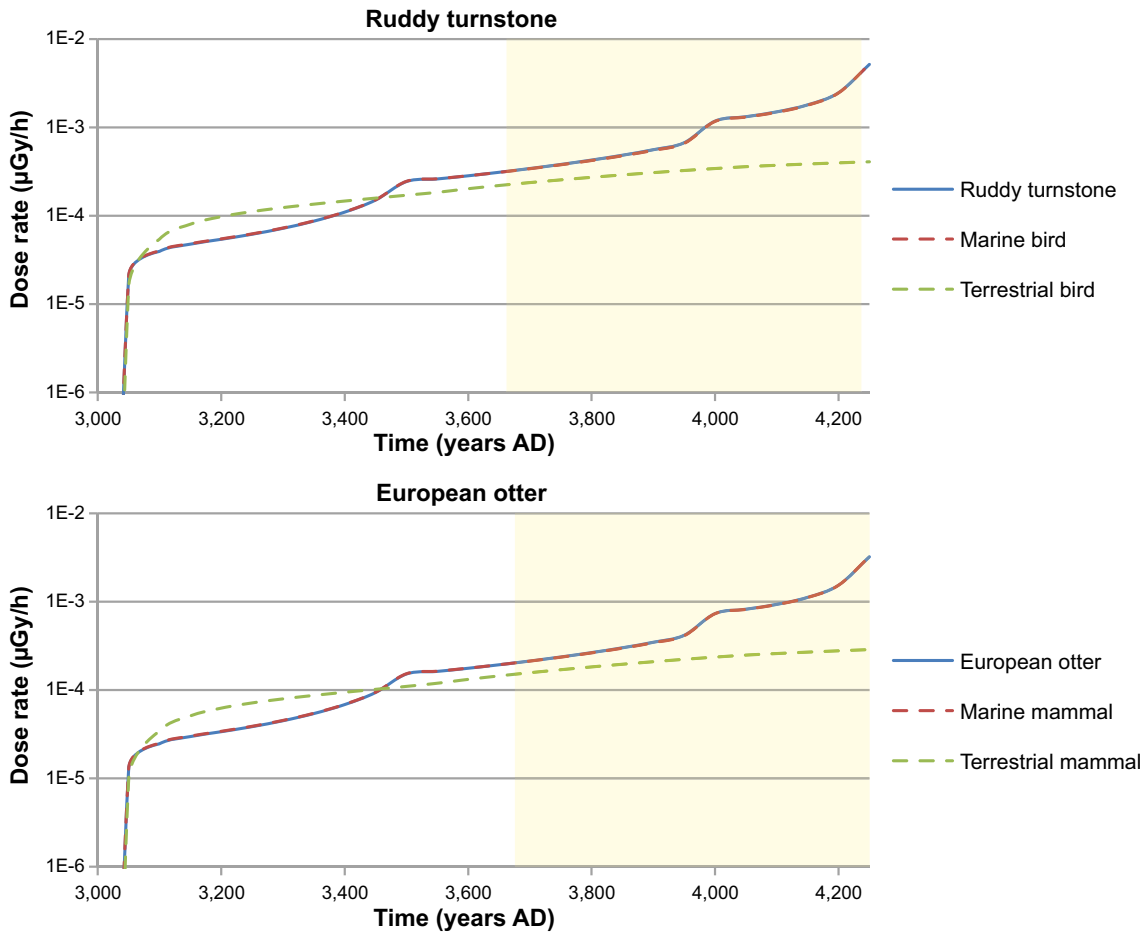


Figure 8-9. Dose rates to two representative species of bird (top; ruddy turnstone) and mammal (bottom; European otter), living in both marine and terrestrial ecosystems (solid blue line). Dashed lines indicate the dose rate to the equivalent reference organism living solely in the terrestrial (red) and marine (green) ecosystems. Yellow shaded areas indicate the time period where the dose rate to the representative species is higher than that to either of the corresponding reference organisms. N.b. the dose rates are several orders of magnitude lower than the screening dose rate ($1E+1 \mu\text{Gy/h}$) which cannot be seen on this figure.

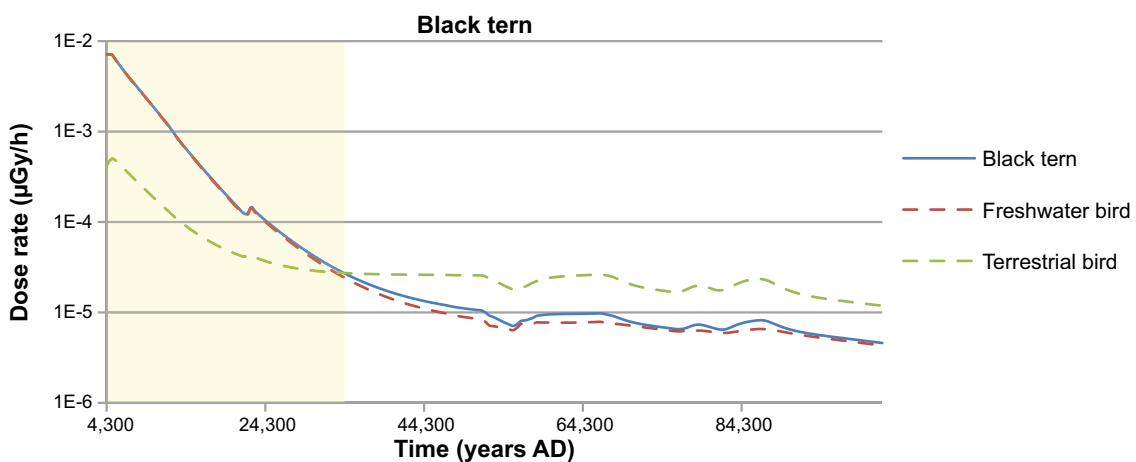


Figure 8-10. Dose rates to a representative species of bird (black tern) living in both freshwater and terrestrial ecosystems (solid blue line). Dashed lines indicate the dose rate to the equivalent reference organism living solely in the terrestrial (red) and freshwater (green) ecosystems. The yellow shaded area indicates the time period where the dose rate to the representative species is higher than that to either of the corresponding reference organisms. N.b. the dose rates are several orders of magnitude lower than the screening dose rate ($1E+1 \mu\text{Gy/h}$) which cannot be seen on this figure.

object 157_1 is a lake basin down-stream object 157_2. At the start of the *early periglacial period* (17,500–20,500 AD) it has been filled with peat and is an arctic mire drained by a stream. Object 114 is a relatively large lake the eastern part of the investigation area (Bosson et al. 2010, Werner et al. 2013). The areas of open water are surrounded by peatlands, but the accumulation of radionuclides in these areas is insignificant, as the discharged of deep groundwater is restricted to the lake parts and flooding is limited during this period. The water balances of both objects are presented in Grolander (2013).

Another important aspect to keep in mind when comparing the exposure from these two objects calculation case is that radionuclide release into object 157_2 starts at 3000 AD, resulting in a radionuclide inventory in the downstream object 157_1 already when the talik occurs. Object 114 is situated outside the simulated drainage area during temperate climate conditions, but during periglacial conditions groundwater flow changes, and release from the repository enter this object for the first time. Due to the cold climate, organism assemblages are not the same as those under the *global warming calculation case* and have been estimated, with some insight from data from the Greenland Analogue Surface Project (GRASP; Clarhäll 2011). In such ecosystems, it has been determined that freshwater ecosystems would lack amphibians and mammals, and terrestrial ecosystems lack trees, gastropods, amphibians and reptiles. While such organisms may be found in small numbers in cold areas that border temperate areas, we have used assemblages representative of the general periglacial environment.

Figure 8-11 shows the dose rates over time for all considered organism types in freshwater and terrestrial ecosystems. In biosphere object 157_1, maximum dose rates in this case were slightly higher than those in the *global warming calculation case* (Fresh water ecosystem: $2.7 \times 10^{-3} \mu\text{Gyh}^{-1}$ compared with $1.5 \times 10^{-3} \mu\text{Gyh}^{-1}$ in the *global warming calculation case*, Terrestrial ecosystem: $1.4 \times 10^{-3} \mu\text{Gyh}^{-1}$ compared with $1.3 \times 10^{-3} \mu\text{Gyh}^{-1}$ in the *global warming calculation case*). No radionuclides reached object 114 in the *global warming calculation case*. The most exposed freshwater organism in object 114 in the *early periglacial calculation case* achieved a dose rate no higher than $2.6 \times 10^{-6} \mu\text{Gyh}^{-1}$, three orders of magnitude lower than the maximum dose rates found in the *global warming calculation case*, and nearly seven orders of magnitude lower than the screening dose rate.

The organism type most exposed in the *early periglacial calculation case* differed from the *global warming calculation case*, with Bird and Detritivorous invertebrate achieving the highest dose rates in 157_1 freshwater and terrestrial ecosystems, respectively; whereas in the *global warming calculation case*, in object 157_1, Zooplankton and Lichen & byrophytes were the most exposed organisms in freshwater and terrestrial ecosystems, respectively. The difference in most exposed organism is due to the different environmental concentrations of radionuclides that occurred as a result of the reduced transfer of radionuclides through permafrost in the *early periglacial calculation case*. As in the *global warming calculation case*, internally incorporated radionuclides dominated the exposures of all of the most exposed organisms.

When comparing the same organism types, at the same time periods, between the *early periglacial calculation case* and the *global warming calculation case* the pattern of radionuclides contributing to dose rate in organisms in object 157_1 were approximately the same. The radiation exposure of object 114 freshwater Bird in the *early periglacial calculation case* was dominated by C-14, which is similar to the object 157_2 freshwater Bird in the *global warming calculation case* at the same time period.

8.4.3 Timing of the releases calculation case

In the *timing of the releases calculation case*, the release of radionuclides from the repository is assumed to start immediately after repository closure at 2050 AD whereas the release of radionuclides in the *global warming calculation case* was assumed to be delayed approximately 1,000 years. In both calculation cases, the main recipient biosphere object (157_2) was a marine bay at the beginning of the simulation period. As the marine stage was longer in the *timing of release calculation case* higher exposure of marine organisms to radiation may be expected, compared with the *global warming calculation case*. However, as the dose dominating radionuclide in the marine period was C-14, which accumulates insignificantly in open water, there was no significant difference in the maximum dose rates for the most exposed marine organism (Table 8-1).

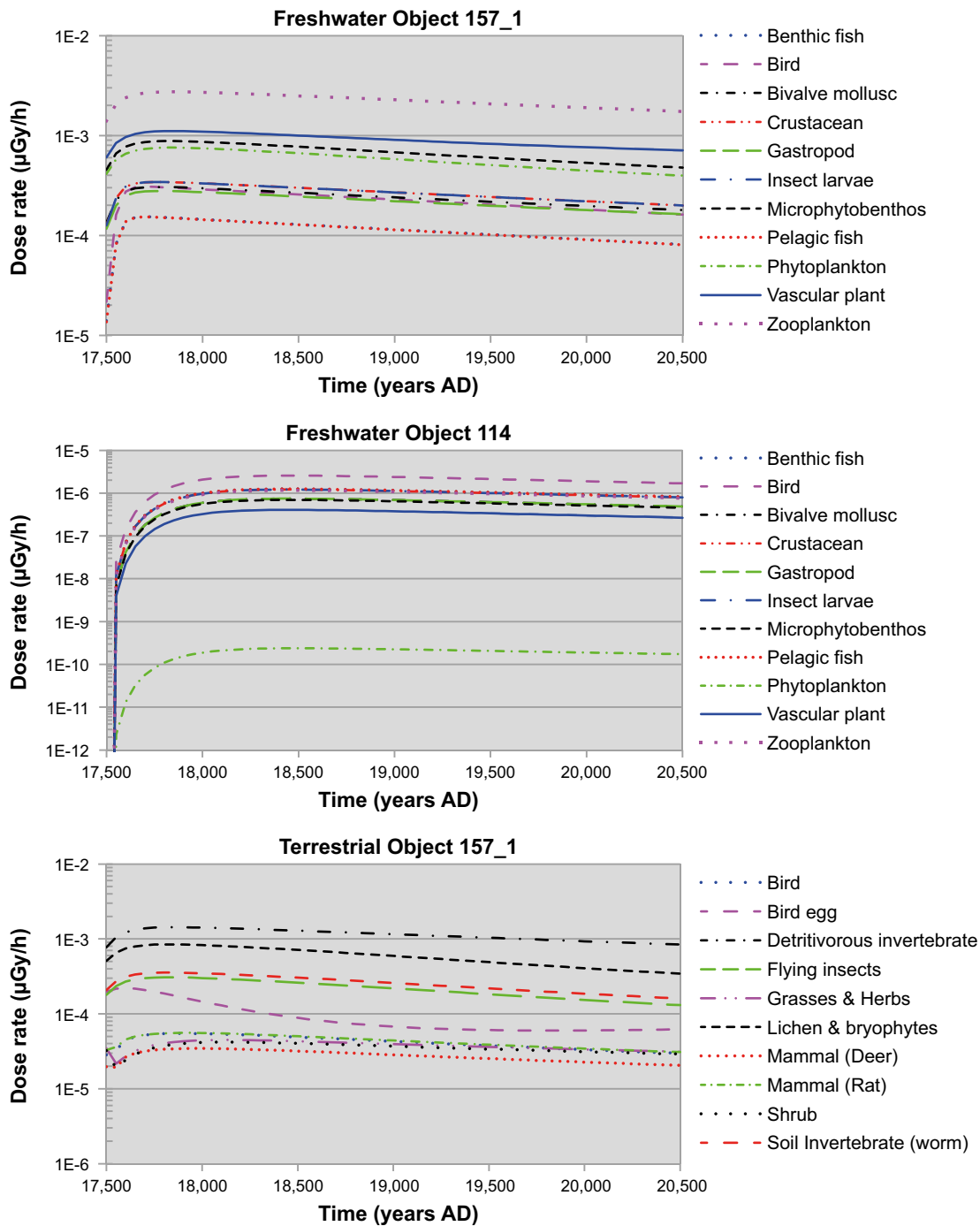


Figure 8-11. Dose rates in non-human biota in freshwater (in biosphere object 157_1, top; and object 114, middle) and terrestrial (bottom) ecosystems, in the *early periglacial calculation case*. Grey shaded areas indicate periglacial periods. N.b. the dose rates are several orders of magnitude lower than the screening dose rate ($1E+1 \mu\text{Gy/h}$) which cannot be seen on this figure.

Exposures in freshwater and terrestrial ecosystems were slightly lower in this calculation case compared with the *global warming calculation case* (Table 8-1). Figure 8-12 shows the dose rates over time for all considered organism types in marine, freshwater and terrestrial ecosystems. The details regarding the maximum exposures in the *timing of releases calculation case* mirrored the *global warming calculation case* closely, with the same organism types and biosphere objects, and similar peak dose rate times, and internal radionuclide contributions (Table 8-1); the pattern of radionuclides contributing to dose rate were virtually identical between the *timing of the releases calculation case* and the *global warming calculation case*.

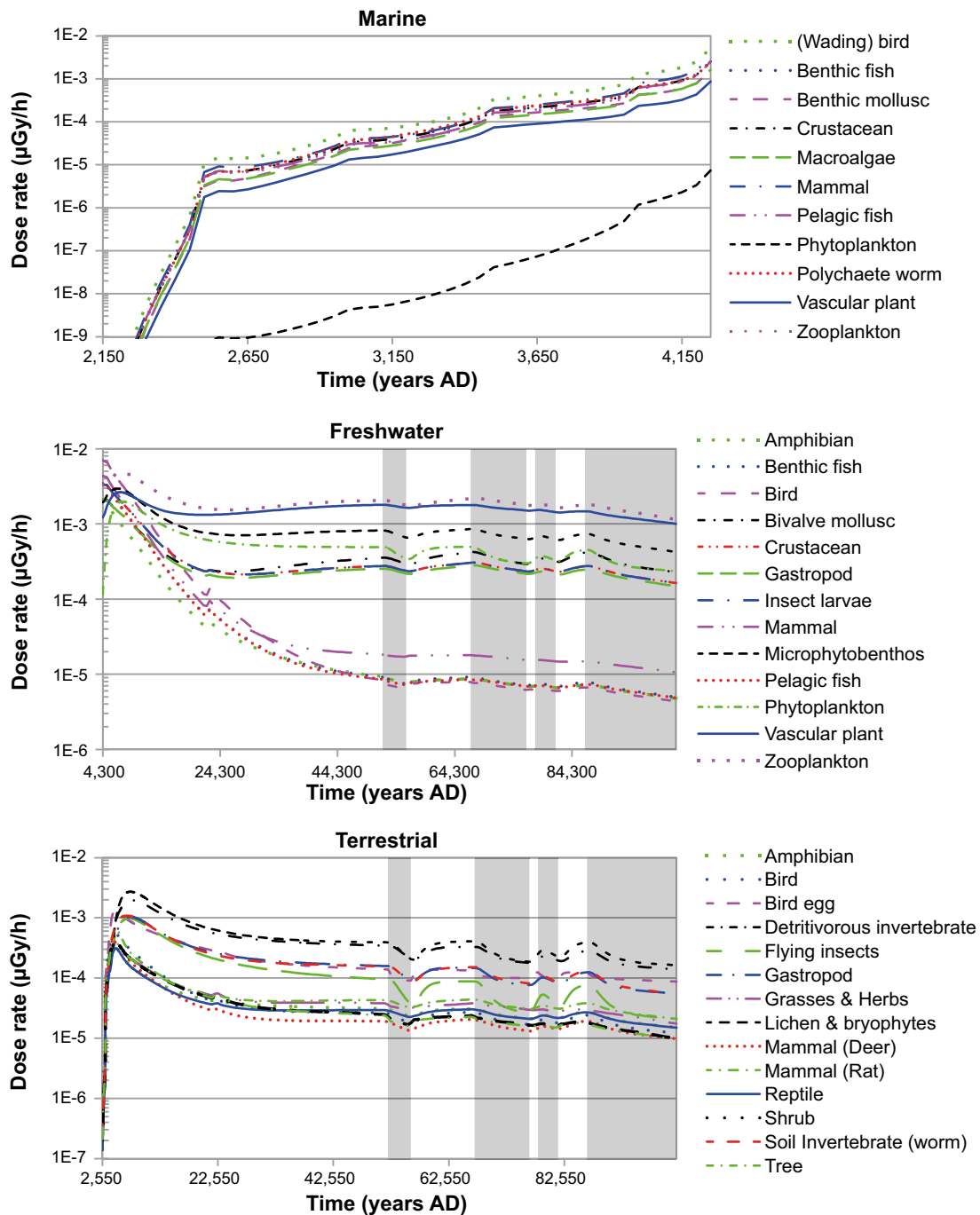


Figure 8-12. Dose rates in non-human biota in the marine (top), freshwater (middle) and terrestrial (bottom) ecosystems, in the *timing of releases calculation case*. Grey shaded areas indicate periglacial periods. *N.b.* the dose rates are several orders of magnitude lower than the screening dose rate ($1\text{E}+1 \mu\text{Gy/h}$) which cannot be seen on this figure.

8.5 Results for the less probable scenarios

The less probable scenarios are summarised in Section 4.2 and described in details in the **Main report**, Section 7.6. The assessment of the less probable scenarios comprises six calculation cases for non-human biota; the key results obtained for these calculation cases are presented below.

8.5.1 High inventory calculation case

The temporal release of radionuclides from the repository and the successive changes in the biosphere is the same as for the *global warming calculation case*. Figure 8-13 shows the dose rates over time for all considered organism types in marine, freshwater and terrestrial ecosystems in the *high inventory calculation case*. The dose rates experienced by organisms in the *high inventory calculation case* closely reflected the patterns seen in the *global warming calculation case*, though higher in all organisms, in all ecosystems throughout the assessment, than the equivalents in the *global warming calculation case* (Table 8-1; Marine ecosystems: $6.5 \times 10^{-3} \mu\text{Gyh}^{-1}$; Freshwater ecosystems: $2.9 \times 10^{-2} \mu\text{Gyh}^{-1}$; Terrestrial ecosystems: $9.0 \times 10^{-3} \mu\text{Gyh}^{-1}$). The maximum exposures in this calculation case occurred at roughly similar times as in the *global warming calculation case*, though a little later in the freshwater ecosystem, and a little earlier in the terrestrial ecosystem (Table 8-1). In the freshwater and terrestrial ecosystems the most exposed organism types (Zooplankton and Detritivorous invertebrate, respectively) were different from those in the *global warming calculation case* (Table 8-1). The most exposed marine organism in the *high inventory calculation case* was the (Wading) bird as in the *global warming calculation case*. The differences in maximally-exposed organism type were due to the different proportion of radionuclides contributing to dose rates. In the freshwater environment, higher concentrations of Se-79 in the *high inventory calculation case* than the *global warming calculation case* led to higher dose rates in Zooplankton. In the terrestrial ecosystem, a high concentration of Ag-108m in the soil in this calculation case contributed significantly to the total dose rate. While C-14 was the most influential radionuclide in the marine (Wading) bird in this calculation case, as in the *global warming calculation case*, the relative influence on total dose rate is slightly lower (93%, compared with 98% in the *global warming calculation case*), indicating a small increase in dose contribution from other radionuclides resulting from the *high inventory calculation case*. This calculation case indicates that a change in inventory could not only increase the exposure of organisms in the environment, but could also change the principal target and mode of exposure.

8.5.2 High flow in the bedrock calculation case

The temporal release of radionuclides from the repository and the successive changes in the biosphere is the same as for the *global warming calculation case*. Figure 8-14 shows the dose rates over time for all considered organism types in marine, freshwater and terrestrial ecosystems in the *high flow in the bedrock calculation case*. The dose rates experienced by organisms in the *high flow in the bedrock calculation case* closely reflected the patterns seen in the *global warming calculation case*. In each ecosystem, the most exposed organism types were the same as those in the *global warming calculation case*. Maximum dose rates to the most exposed organisms in the *high flow in the bedrock calculation case*, compared with the *global warming calculation case*, were marginally higher in all ecosystems (Table 8-1; Marine ecosystems: $6.2 \times 10^{-3} \mu\text{Gyh}^{-1}$; Freshwater ecosystem: $8.5 \times 10^{-3} \mu\text{Gyh}^{-1}$; Terrestrial ecosystem: $4.1 \times 10^{-3} \mu\text{Gyh}^{-1}$) and, in the freshwater and terrestrial ecosystems, occurred slightly sooner (Table 8-1). The details regarding the maximum exposures in this calculation case reflected the *global warming calculation case* closely, with the same organism types, key radionuclides, and internal radionuclide contributions (Table 8-1).

8.5.3 Accelerated concrete degradation calculation case

The temporal release of radionuclides from the repository and the successive changes in the biosphere is the same as for the *global warming calculation case*. Figure 8-15 shows the dose rates over time for all considered organism types in marine, freshwater and terrestrial ecosystems in the *accelerated concrete degradation calculation case*. The dose rates experienced by organisms in the *accelerated concrete degradation calculation case* closely reflected the patterns seen in the *global warming calculation case*. In each ecosystem, the most exposed organism types were the same as those in the *global warming calculation case*. Maximum dose rates to the most exposed organisms in the *accelerated concrete degradation calculation case*, compared with the *global warming calculation case*, were marginally higher in aquatic ecosystems (Table 8-1; Marine ecosystem: $7.0 \times 10^{-3} \mu\text{Gyh}^{-1}$; Freshwater ecosystem: $9.6 \times 10^{-3} \mu\text{Gyh}^{-1}$). The dose rates to the most exposed organism in the Terrestrial ecosystem in this case followed those of the *global warming calculation case* very closely. The details regarding the maximum exposures in this calculation case reflected the *global warming calculation case* closely, with the same organism types, key radionuclides, and similar peak dose rate times, and internal radionuclide contributions (Table 8-1).

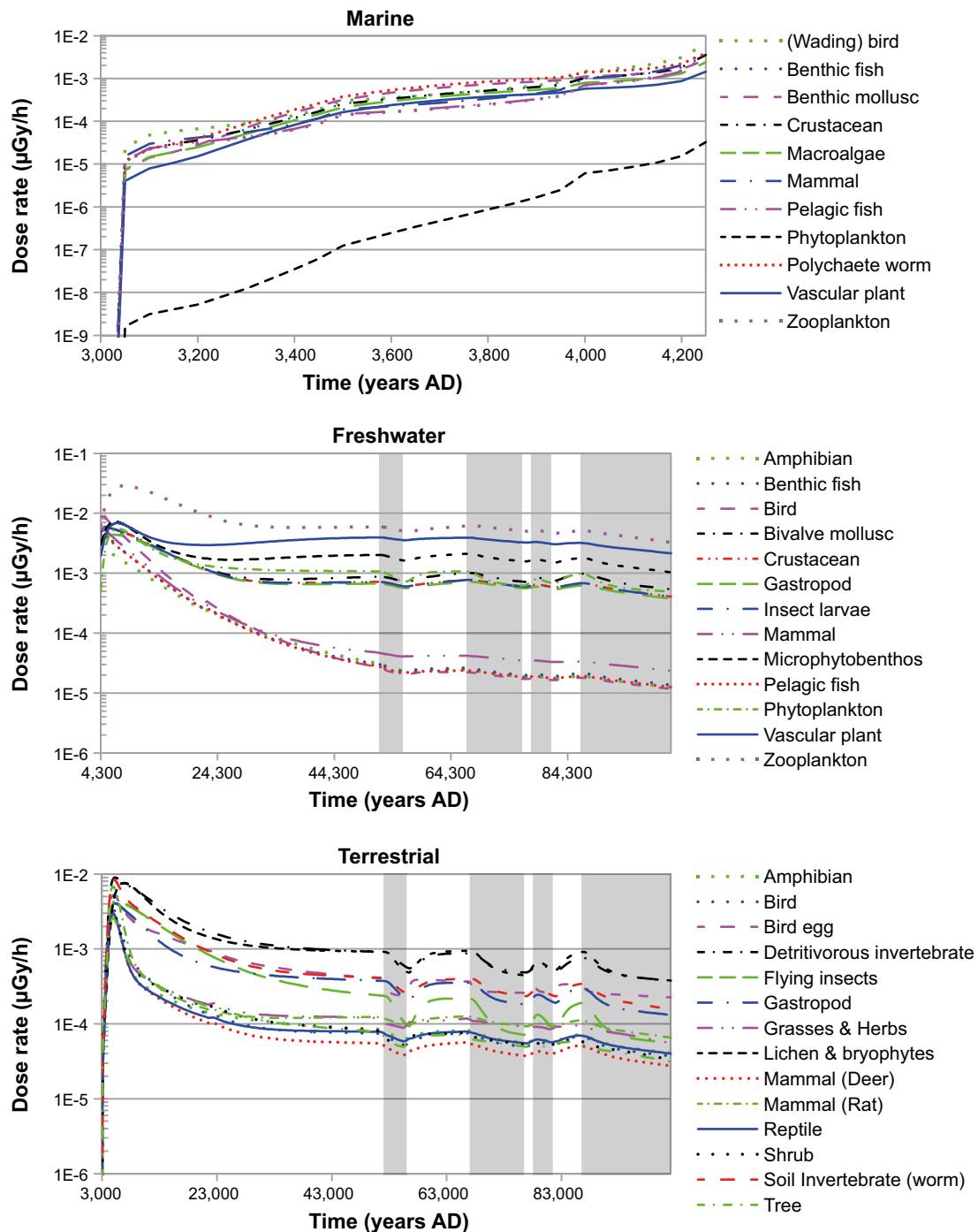


Figure 8-13. Dose rates in non-human biota in the marine (top), freshwater (middle) and terrestrial (bottom) ecosystems, in the **high inventory calculation case**. Grey shaded areas indicate periglacial periods. *N.b.* the dose rates are several orders of magnitude lower than the screening dose rate ($1E+1 \mu\text{Gy/h}$) which cannot be seen on this figure.

8.5.4 Bentonite degradation calculation case

The temporal release of radionuclides from the repository and the successive changes in the biosphere is the same as for the *global warming calculation case*. Figure 8-16 shows the dose rates over time for all considered organism types in marine, freshwater and terrestrial ecosystems in the *bentonite degradation calculation case*. The dose rates experienced by organisms in the *bentonite degradation calculation case* broadly reflected the patterns seen in the *global warming calculation case*. A brief drop in dose rates by as much as an order of magnitude was seen in several organism types in the freshwater and terrestrial ecosystems of object 157_2 at 17,500 AD, due to significant

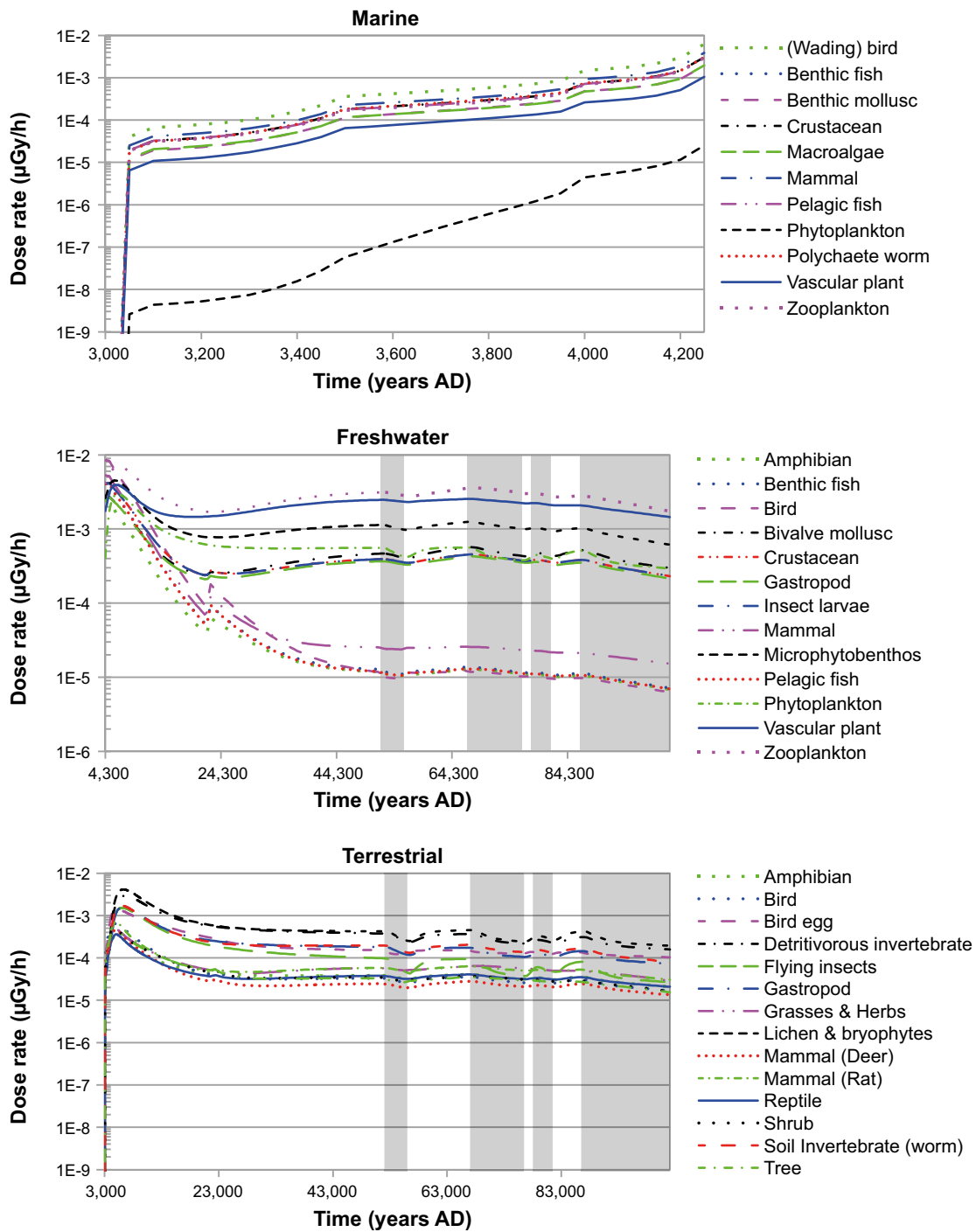


Figure 8-14. Dose rates in non-human biota in the marine (top), freshwater (middle) and terrestrial (bottom) ecosystems, in the **high flow in the bedrock** calculation case. Grey shaded areas indicate periglacial periods. N.b. the dose rates are several orders of magnitude lower than the screening dose rate ($1\text{E}+1 \mu\text{Gy/h}$) which cannot be seen on this figure.

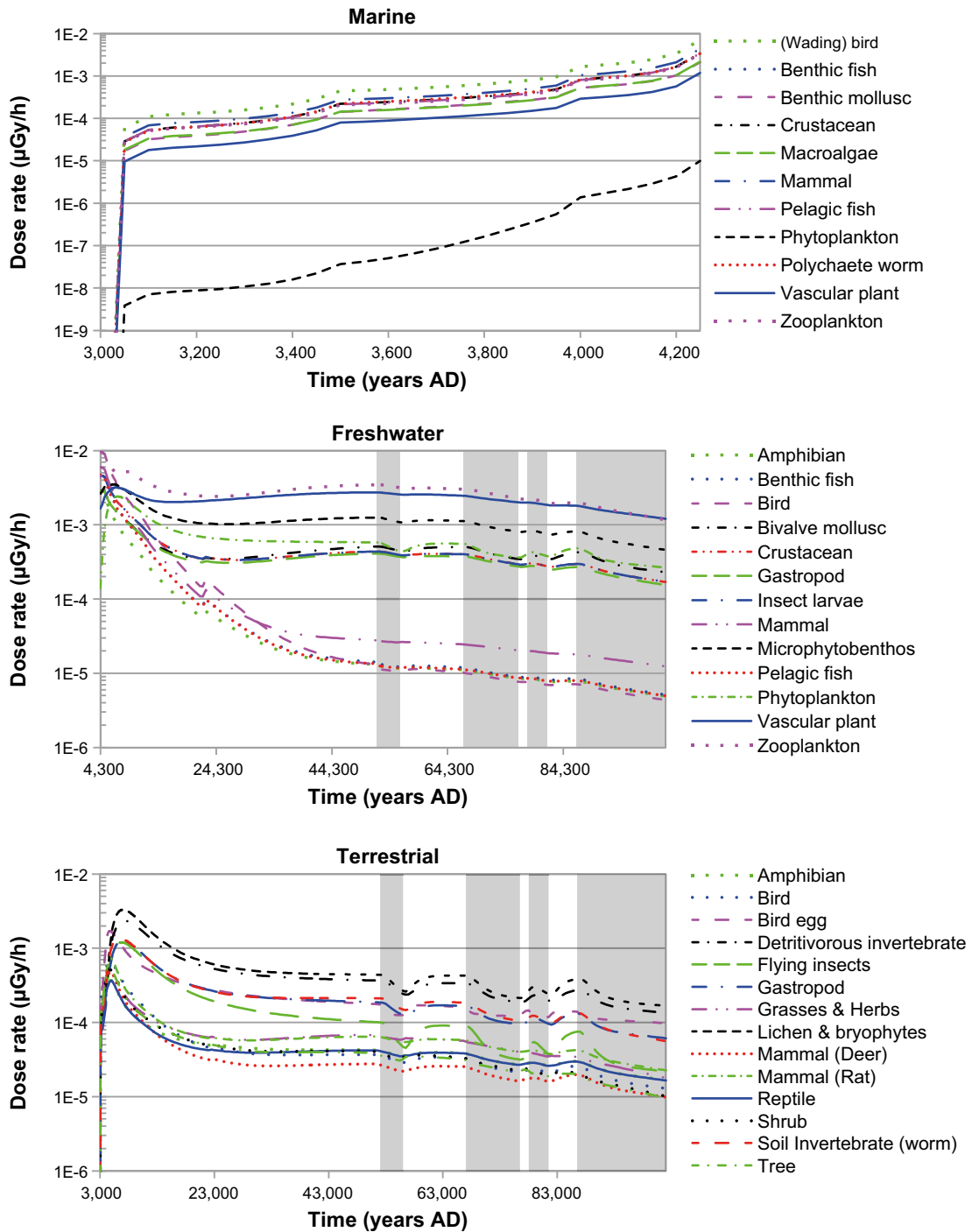


Figure 8-15. Dose rates in non-human biota in the marine (top), freshwater (middle) and terrestrial (bottom) ecosystems, in the *accelerated concrete degradation calculation case*. Grey shaded areas indicate periglacial periods. N.b. the dose rates are several orders of magnitude lower than the screening dose rate ($1\text{E}+1 \mu\text{Gy/h}$) which cannot be seen on this figure.

drops in environmental concentrations of C-14, Cl-36 and I-129, due to periglacial conditions that limit water flow to the surface. Further smaller drops in dose rate were seen after 52,000 AD due to periglacial conditions, as per the *global warming calculation case*.

In each ecosystem, the most exposed organism types were the same as those in the *global warming calculation case*. Maximum dose rates to the most exposed organisms in the *bentonite degradation calculation case* were virtually the same as those in the *global warming calculation case* in all ecosystems (Table 8-1; Marine ecosystem: $5.2 \times 10^{-3} \mu\text{Gyh}^{-1}$; Freshwater ecosystem: $7.1 \times 10^{-3} \mu\text{Gyh}^{-1}$; Terrestrial ecosystem: $3.3 \times 10^{-3} \mu\text{Gyh}^{-1}$). The details regarding the maximum exposures in this calculation reflected the *global warming calculation case* precisely, with the same organism types, key radionuclides, peak dose rate times, and internal radionuclide contributions (Table 8-1).

8.5.5 Earthquake calculation case

The *earthquake calculation case* is calculated differently from the other analyses, see description in Section 4.2.5. In addition, results regarding internal/external exposures or contributing radionuclides were not produced in the calculations for this calculation case. Figure 8-17 shows the dose rates over time for all considered organism types in marine, freshwater and terrestrial ecosystems in the *earthquake calculation case*. The dose rates experienced by organisms in the *earthquake calculation case* indicate some significant differences from those in the *global warming calculation case*, with much higher dose rates overall and different patterns over time. Maximum dose rates in each ecosystem were the highest of all calculation cases, with the most exposed organisms receiving dose rates of more than $10^{-2} \mu\text{Gyh}^{-1}$ in aquatic ecosystems (Table 8-1; Marine: $6.9 \times 10^{-2} \mu\text{Gyh}^{-1}$; Freshwater: $9.2 \times 10^{-2} \mu\text{Gyh}^{-1}$). Dose rates in terrestrial ecosystems were higher than in the *global warming calculation case*, but only by a factor of ~ 2 (Table 8-1; $6.4 \times 10^{-3} \mu\text{Gyh}^{-1}$). The maximum dose rates in marine, freshwater and terrestrial ecosystems were 31, 8.8 and 2.5 times larger, respectively, than in the *global warming calculation case*. The most exposed organism in the terrestrial ecosystem (Bird egg) was different from that in the *global warming calculation case*. Relative to the *global warming calculation case*, peak dose rates occurred earlier in the terrestrial ecosystem, and at approximately the same time in the freshwater ecosystem; the dose rates in the marine ecosystem continued to rise throughout the assessment period, as in the *global warming calculation case*, achieving the maximum dose rate at the end of the period. The highest dose rates of this calculation case, despite being highest of the whole assessment, were still over two factors of ten lower than the screening dose rate, and therefore do not represent a concern.

8.5.6 High concentrations of complexing agents calculation case

The temporal release of radionuclides from the repository and the successive changes in the biosphere is the same as for the *global warming calculation case*. Figure 8-18 shows the dose rates over time for all considered organism types in marine, freshwater and terrestrial ecosystems in the *high concentrations of complexing agents calculation case*. The dose rates experienced by organisms in the *high concentrations of complexing agents calculation case* were nearly identical to those in the *global warming calculation case*, throughout the assessment period.

The maximal dose rates were slightly higher than those in the *global warming calculation case* (Table 8-1; Marine: $5.5 \times 10^{-3} \mu\text{Gyh}^{-1}$; Freshwater: $7.4 \times 10^{-3} \mu\text{Gyh}^{-1}$; Terrestrial: $3.4 \times 10^{-3} \mu\text{Gyh}^{-1}$). The details regarding the maximum exposures in this calculation case reflected the *global warming calculation case* closely, with the same organism types, and internal radionuclide contributions, and similar peak dose rate times (Table 8-1). Key radionuclides were the same for the two most exposed aquatic organisms, but in the terrestrial environment, the most exposed organism (Lichen & byrophytes) received dose mostly from Pa-231, instead of U-238 as in the *global warming calculation case*.

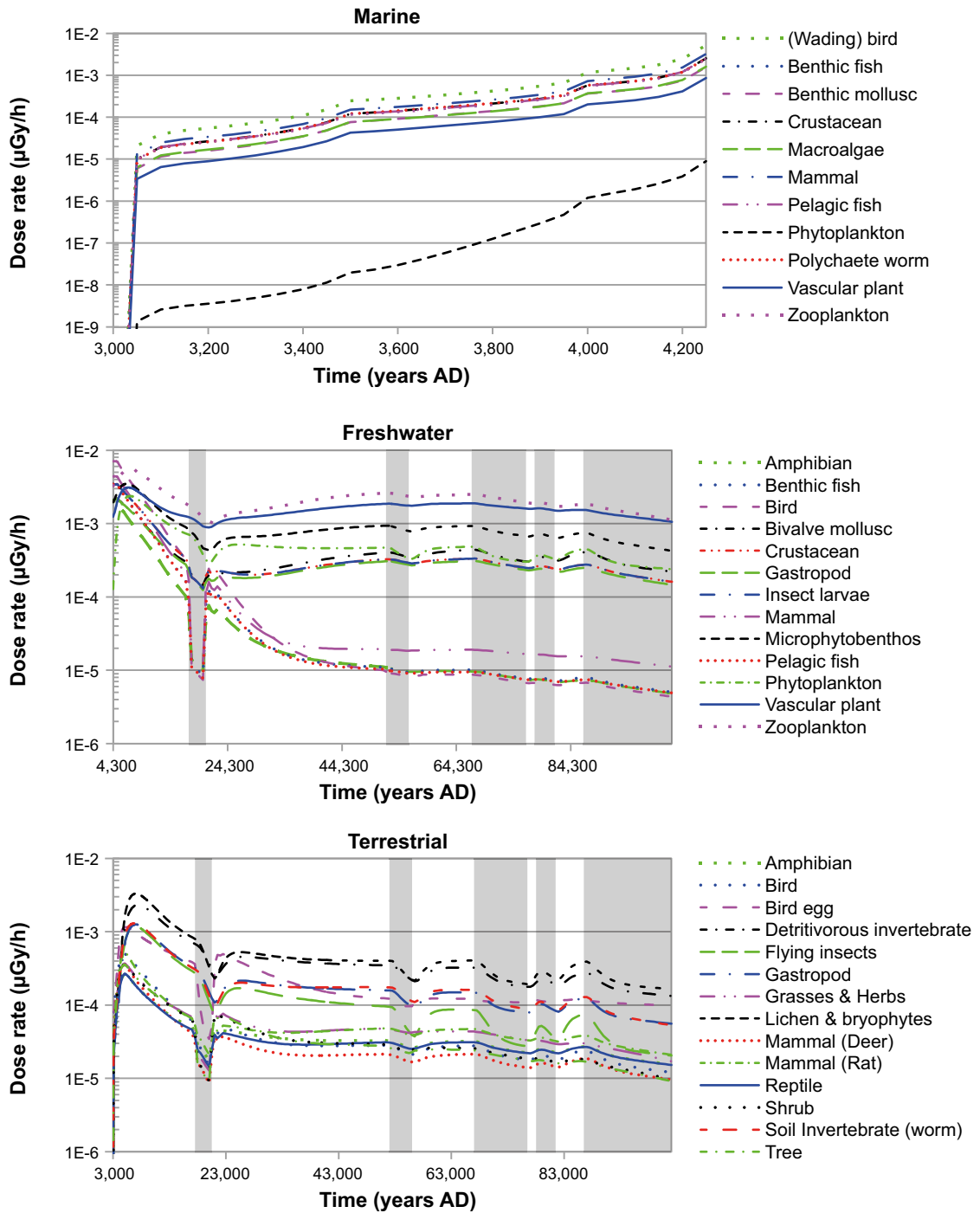


Figure 8-16. Dose rates in non-human biota in the marine (top), freshwater (middle) and terrestrial (bottom) ecosystems, in the **bentonite degradation calculation case**. Grey shaded areas indicate periglacial periods. *N.b.* the dose rates are several orders of magnitude lower than the screening dose rate ($1E+1 \mu\text{Gy/h}$) which cannot be seen on this figure.

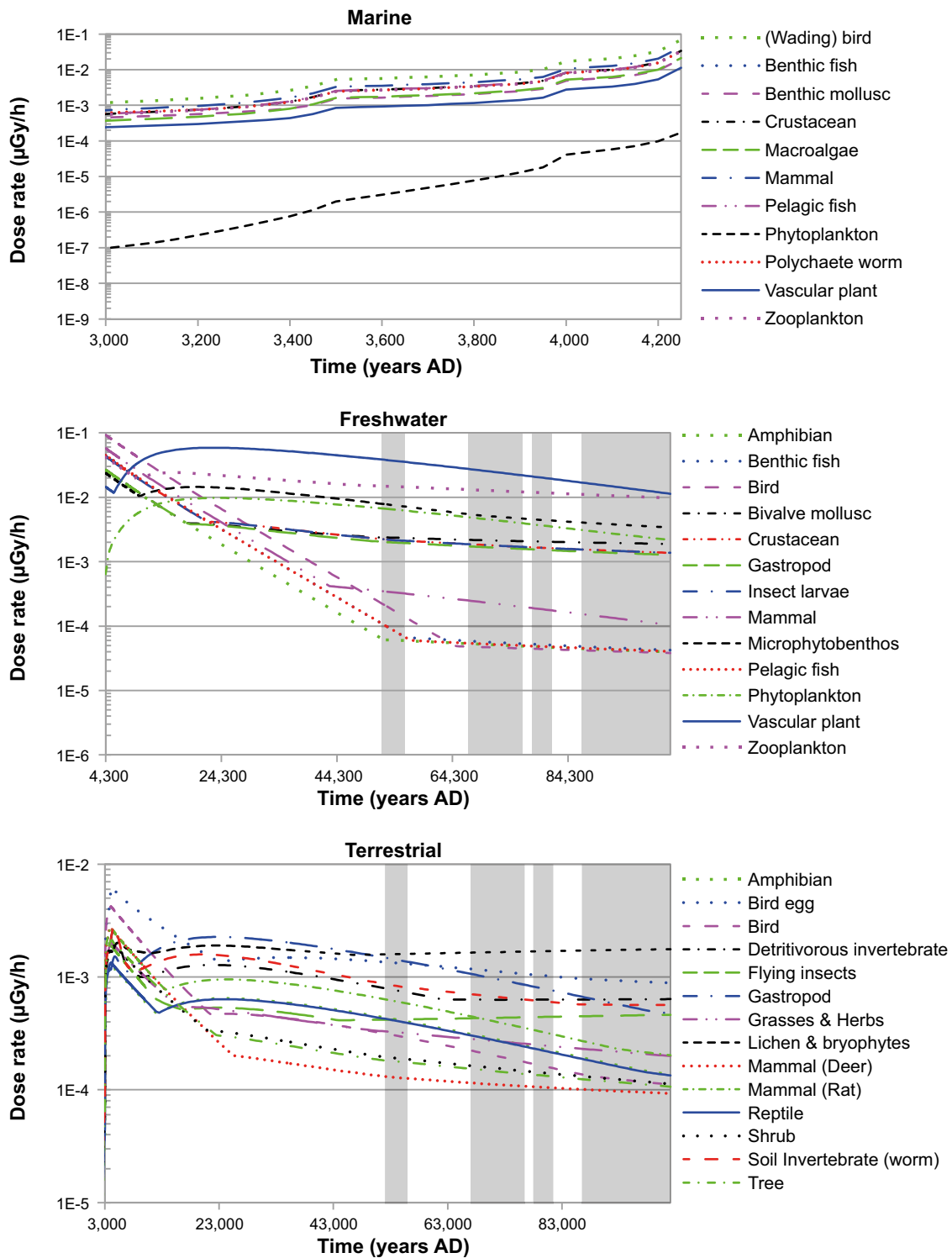


Figure 8-17. Dose rates in non-human biota in the marine (top), freshwater (middle) and terrestrial (bottom) ecosystems, in the **earthquake calculation case**. Grey shaded areas indicate periglacial periods. N.b. the dose rates are several orders of magnitude lower than the screening dose rate ($1\text{E}+1 \mu\text{Gy/h}$) which cannot be seen on this figure.

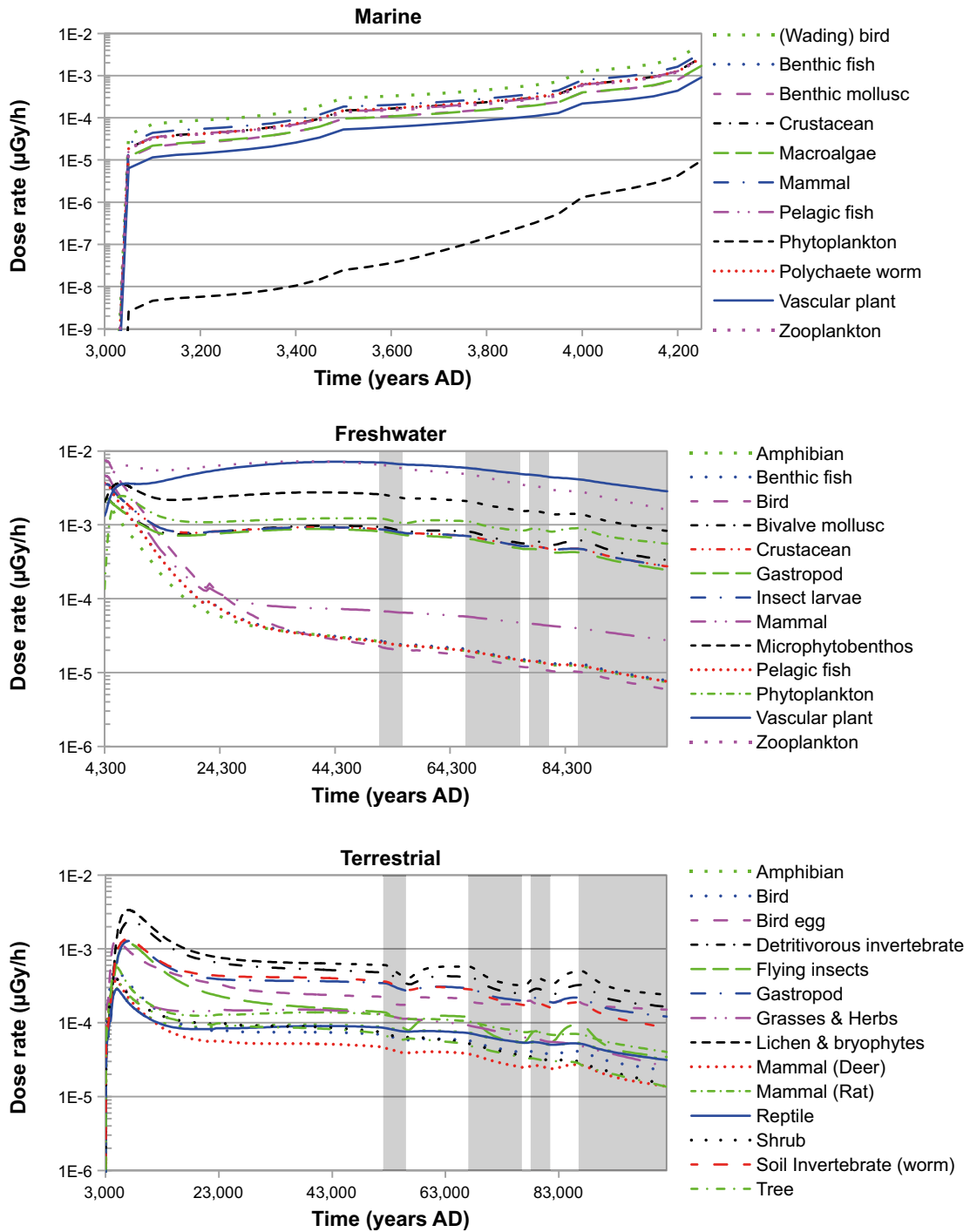


Figure 8-18. Dose rates in non-human biota in the marine (top), freshwater (middle) and terrestrial (bottom) ecosystems, in the **high concentrations of complexing agents calculation case**. Grey shaded areas indicate periglacial periods. N.b. the dose rates are several orders of magnitude lower than the screening dose rate ($1E+1 \mu\text{Gy/h}$) which cannot be seen on this figure.

8.6 Results for the residual scenarios

The residual scenarios are summarised in Section 4.3 and described in details in Section 7.7 in the **Main report**. The assessment of the residual scenarios comprises five calculation cases for non-human biota; the key results obtained for these calculation cases are presented below.

8.6.1 Loss of barrier function calculation case – no sorption in the repository

The temporal release of radionuclides from the repository and the successive changes in the biosphere is the same as for the *global warming calculation case*. Figure 8-19 shows the dose rates over time for all considered organism types in marine, freshwater and terrestrial ecosystems in the *loss of barrier function calculation case – no sorption in the repository*. The dose rates experienced by marine and terrestrial organisms in the *loss of barrier function calculation case – no sorption in the repository* reflected the patterns seen in the *global warming calculation case*. In the freshwater ecosystem, the pattern of exposures in the *loss of barrier function calculation case – no sorption in the repository* diverged significantly from that of the *global warming calculation case* in several organism types. Instead of experiencing a peak at ~ 7000 AD as in the *global warming calculation case*, Vascular plant, Zooplankton, Zooplankton, Microphytobenthos, and Phytoplankton experienced steadily increasing dose rates until later in the assessment period, due to large increases in environmental concentrations of Ni-59 and Pu-239, which led to maximum dose rates in some organisms occurring later, after 25,000 AD. However, in the freshwater ecosystem, it was the high concentration of C-14 at the beginning that led to the highest dose rates overall, in Bird. Once the C-14 concentrations decreased, the dose rate dropped dramatically and the Bird became the least exposed organism in the ecosystem by 33,000 AD. Maximum dose rates to the most exposed organisms in the *loss of barrier function calculation case – no sorption in the repository*, compared with the *global warming calculation case*, were significantly higher in aquatic ecosystems (Table 8-1; Marine: $4.6 \times 10^{-2} \mu\text{Gyh}^{-1}$; Freshwater: $6.2 \times 10^{-2} \mu\text{Gyh}^{-1}$) and somewhat higher in the terrestrial ecosystem (Table 8-1; $3.9 \times 10^{-3} \mu\text{Gyh}^{-1}$). The most exposed aquatic organism types in this case were the same as for the *global warming calculation case* (Bird); however the Bird egg was the most exposed terrestrial organism type, in contrast to the *global warming calculation case*. Some details regarding the maximum exposures of this calculation case reflected those of the *global warming calculation case* closely, with the same or similar peak dose rate times, and internal radionuclide contributions (Table 8-1). In all ecosystems, the dose rate to the most exposed organisms was dominated by the inorganic form of C-14, as opposed to the organic form that dominated exposures in the *global warming calculation case*, reflecting the lack of sorption of inorganic carbon in the *loss of barrier function calculation case – no sorption in the repository*. The small temporary drops in dose rates in terrestrial ecosystems due to periglacial conditions as seen in the *global warming calculation case* appeared greatly reduced or absent in the *loss of barrier function calculation case – no sorption in the repository* as the dose rates are dominated by radionuclides that are more strongly retarded in the environment, and thus environments retain a higher concentration of radionuclides and are not so affected by the change in water flows resulting from periglacial conditions.

8.6.2 Loss of barrier function calculation case – no sorption in the bedrock

The temporal release of radionuclides from the repository and the successive changes in the biosphere is the same as for the *global warming calculation case*. Figure 8-20 shows the dose rates over time for all considered organism types in marine, freshwater and terrestrial ecosystems in the *loss of barrier function calculation case – no sorption in the bedrock*. The dose rates experienced by organisms in the *loss of barrier function calculation case – no sorption in the bedrock* closely reflected the patterns seen in the *global warming calculation case*, but because of the lack of sorption in the bedrock in this calculation case, the exposure peaks seen in the freshwater and terrestrial ecosystems were larger and occurred sooner than those in the *global warming calculation case*. In marine and terrestrial ecosystems, the most exposed organism types were the same as those in the *global warming calculation case*, however in the freshwater ecosystem, the most exposed organism was Zooplankton. Maximum dose rates to the most exposed organisms in the *loss of barrier function calculation case – no sorption in the bedrock*, compared with the *global warming calculation case*, were approximately equal in the marine ecosystem (Table 8-1; Marine:

$5.2 \times 10^{-3} \mu\text{Gy/h}^{-1}$), but were significantly larger in the other two ecosystems (Table 8-1; Freshwater: $2.1 \times 10^{-2} \mu\text{Gy/h}^{-1}$; Terrestrial: $1.5 \times 10^{-2} \mu\text{Gy/h}^{-1}$). Key radionuclides for the most exposed organisms in the marine and terrestrial ecosystems were the same as in the *global warming calculation case*, whereas in the freshwater ecosystem, high exposures from Pa-231 dominated the dose rate to Zooplankton. Internal radionuclide contributions were approximately the same as in the *global warming calculation case* for the most exposed organisms of all ecosystems (Table 8-1).

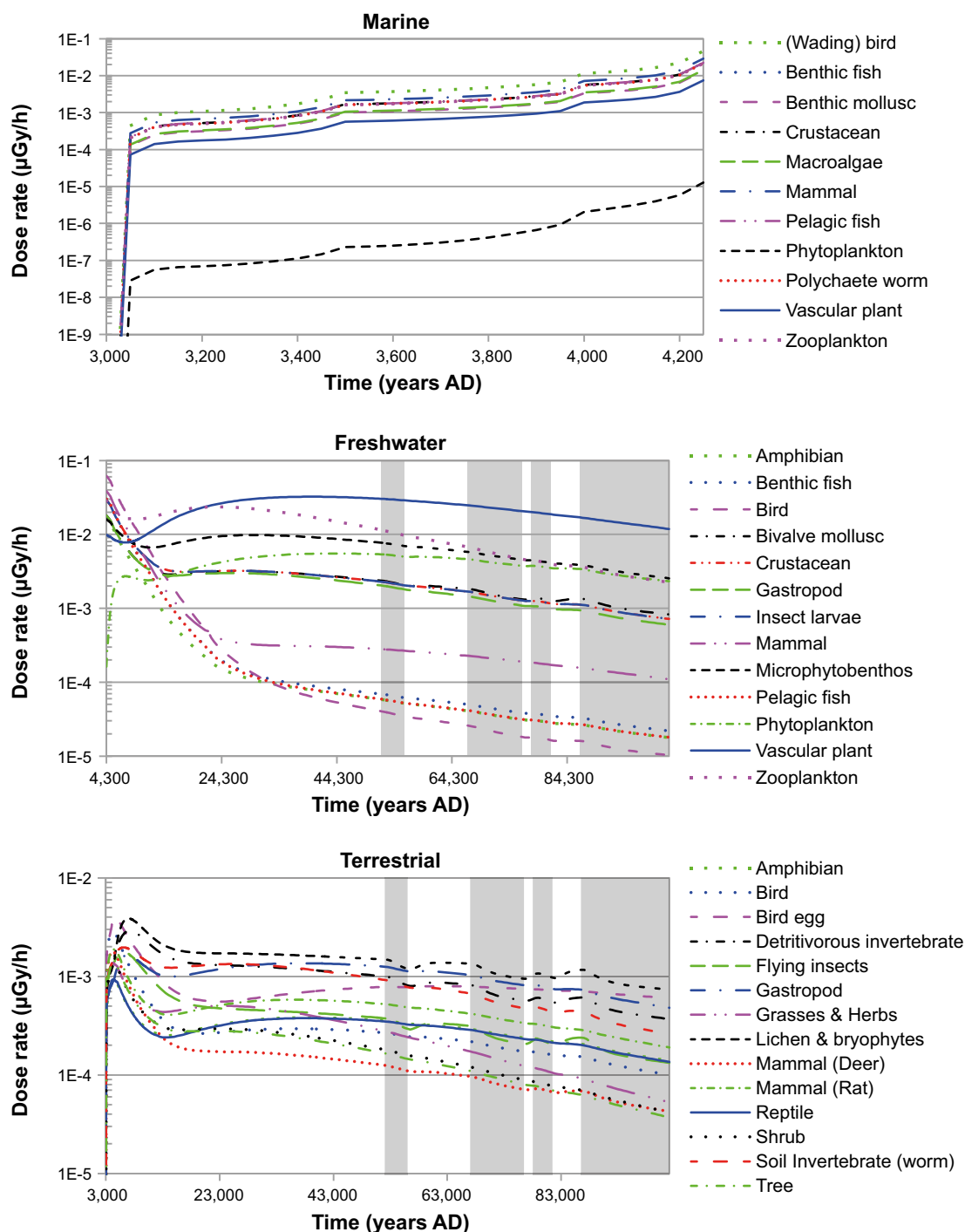


Figure 8-19. Dose rates in non-human biota in the marine (top), freshwater (middle) and terrestrial (bottom) ecosystems, in the *loss of barrier function calculation case* – no sorption in the repository. Grey shaded areas indicate periglacial periods. N.b. the dose rates are several orders of magnitude lower than the screening dose rate ($1E+1 \mu\text{Gy/h}$) which cannot be seen on this figure.

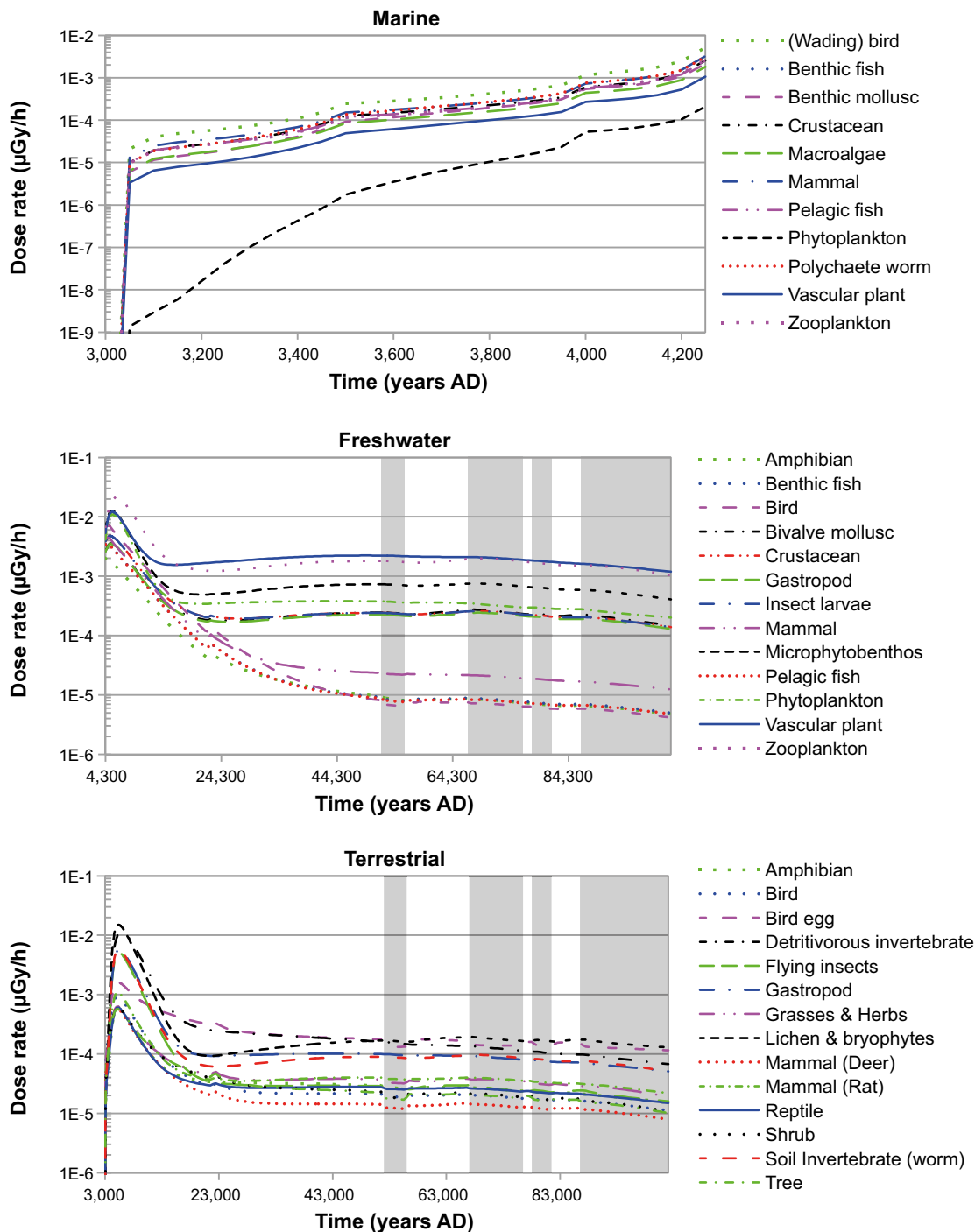


Figure 8-20. Dose rates in non-human biota in the marine (top), freshwater (middle) and terrestrial (bottom) ecosystems, in the **loss of barrier function calculation case** – no sorption in the bedrock. Grey shaded areas indicate periglacial periods. N.b. the dose rates are several orders of magnitude lower than the screening dose rate ($1E+1 \mu\text{Gy/h}$) which cannot be seen on this figure.

8.6.3 Loss of barrier function calculation case – high water flows in the repository

The temporal release of radionuclides from the repository and the successive changes in the biosphere is the same as for the *global warming calculation case*. Figure 8-21 shows the dose rates over time for all considered organism types in marine, freshwater and terrestrial ecosystems in the *loss of barrier function calculation case – high water flows in the repository*. The patterns of exposure experienced by marine and terrestrial organisms in the *loss of barrier function calculation case – high water flows in the repository* broadly resembled those seen in the *global warming*

calculation case. However, the marine organisms experienced a small peak of exposure at the beginning of the assessment period that was not seen in the *global warming calculation case*, though the maximum dose rate in the marine ecosystem still occurred at the end of the assessment period. Similarly to the most exposed organism in the *loss of barrier function calculation case – no sorption in the repository*, the predominant radionuclide was inorganic C-14, unlike the organic form that dominated exposures in the *global warming calculation case*. In the freshwater ecosystem, the pattern of exposures in the *loss of barrier function calculation case – high water flows in the repository* diverged significantly from that of the *global warming calculation case*.

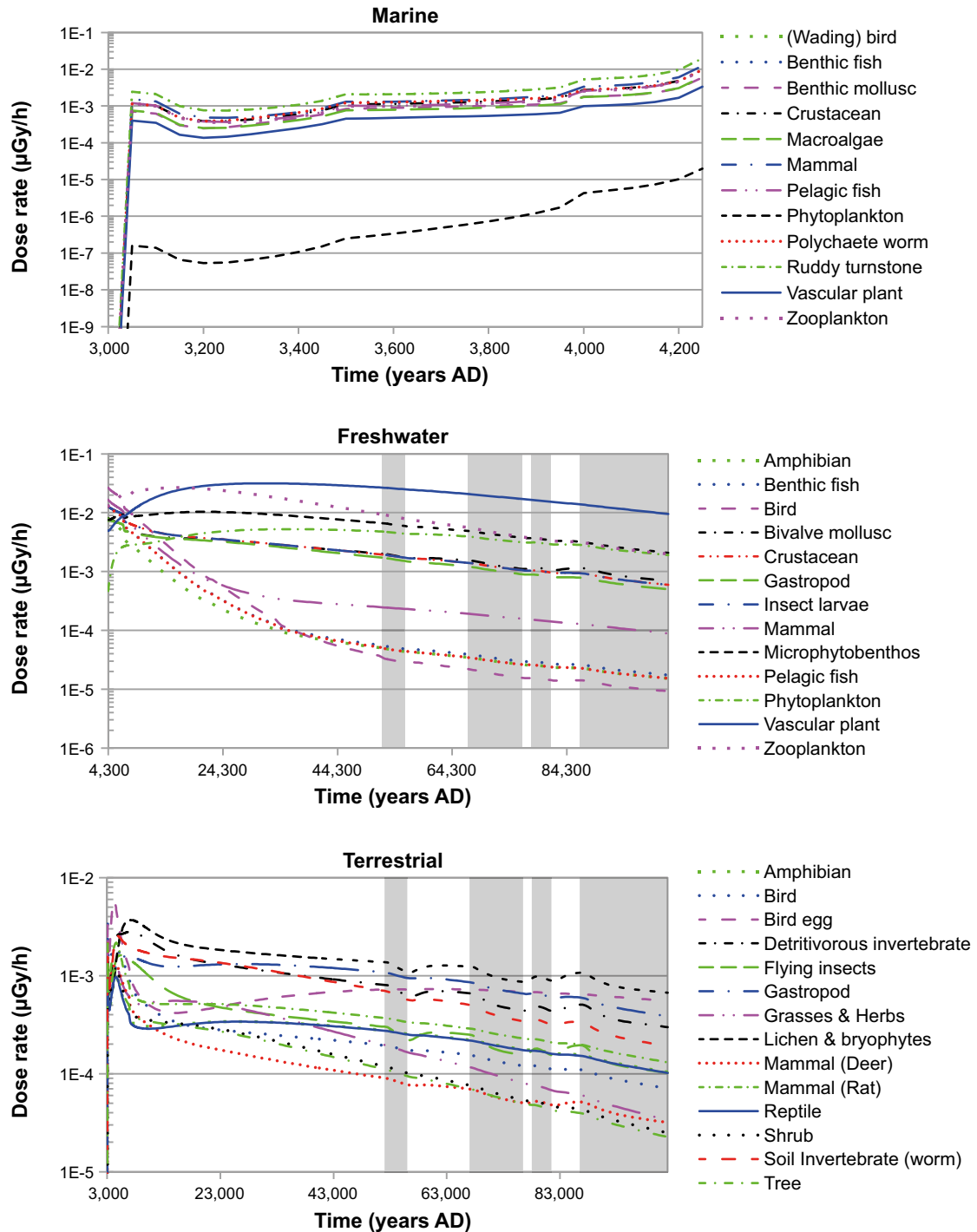


Figure 8-21. Dose rates in non-human biota in the marine (top), freshwater (middle) and terrestrial (bottom) ecosystems, in the *loss of barrier function calculation case – high water flows in the repository*. Grey shaded areas indicate periglacial periods. N.b. the dose rates are several orders of magnitude lower than the screening dose rate ($1\text{E}+1 \mu\text{Gy/h}$) which cannot be seen on this figure.

Instead of experiencing a peak at ~ 7000 AD, Vascular plant, Zooplankton, Microphytobenthos, and Phytoplankton experienced steadily increasing dose rates until later in the assessment period, due to large increases in environmental concentrations of Pu-239, which led to maximum dose rates occurring later. Consequently, the maximum dose rate to freshwater organisms, found in Vascular plant (unlike the *global warming calculation case*), occurred at 31,500 AD, and was dominated by exposure from Pu-239. In the terrestrial ecosystem, the Bird egg was the most exposed 'organism' type (in contrast to the *global warming calculation case*), which received a higher proportion of dose from I-129 than the most exposed organism in the *global warming calculation case*. In the marine ecosystem, the most exposed organism type was the same as those in the *global warming calculation case*.

Maximum dose rates to the most exposed organisms in the *loss of barrier function calculation case – high water flows in the repository*, compared with the *global warming calculation case*, were significantly higher in aquatic ecosystems (Table 8-1; Marine: $2.0 \times 10^{-2} \mu\text{Gyh}^{-1}$; Freshwater: $3.2 \times 10^{-2} \mu\text{Gyh}^{-1}$) and slightly higher in the terrestrial ecosystem (Table 8-1; $5.7 \times 10^{-3} \mu\text{Gyh}^{-1}$). The details regarding the maximum exposures in the terrestrial ecosystem of this calculation case reflected those of the *global warming calculation case* closely, with the same organism type, key radionuclide, and similar peak dose rate time, and internal radionuclide contributions. The small temporary drops in dose rates in terrestrial ecosystems due to periglacial conditions as seen in the *global warming calculation case* appeared greatly reduced or absent in the *loss of barrier function calculation case – no sorption in the repository* as the dose rates are dominated by radionuclides that are more strongly retarded in the environment, and thus environments retain a higher concentration of radionuclides and are not so affected by the change in water flows resulting from periglacial conditions.

8.6.4 Changed repository redox conditions in SFR 1 calculation case

The temporal release of radionuclides from the repository and the successive changes in the biosphere is the same as for the *global warming calculation case*. Figure 8-22 shows the dose rates over time for all considered organism types in marine, freshwater and terrestrial ecosystems in the *changed repository redox conditions in SFR 1 calculation case*. The pattern of radioactive exposures of organisms in the marine and terrestrial ecosystems were very similar, in the *changed repository redox conditions in SFR 1 calculation case*, to those in the *global warming calculation case*; maximum dose rates (Table 8-1; Marine: $5.1 \times 10^{-3} \mu\text{Gyh}^{-1}$; Terrestrial: $3.3 \times 10^{-3} \mu\text{Gyh}^{-1}$), most exposed organism type, time of maximum dose rate, key radionuclides, and internal contributions were all nearly identical to those of the *global warming calculation case*. The troughs in dose rates in terrestrial ecosystems during periglacial periods as seen in the *global warming calculation case* appeared greatly reduced in the *changed repository redox conditions in SFR 1 calculation case* as the dose rates are dominated by radionuclides that are otherwise more strongly retarded in the environment. The release of the redox sensitive radionuclides, from the repository, through the geosphere, to the biosphere, is sufficiently rapid that a significant inventory of such radionuclides exists in the biosphere before the reduction of flow during periglacial periods. Therefore, the change in flow conditions during periglacial times is effectively of little impact to the resulting dose rates. In the freshwater ecosystem, significant differences in radioactive exposure were seen between the *changed repository redox conditions in SFR 1 calculation case* and the *global warming calculation case*. The maximum dose rate to the most exposed freshwater organism in the *changed repository redox conditions in SFR 1 calculation case* was significantly higher (Table 8-1; $1.7 \times 10^{-2} \mu\text{Gyh}^{-1}$). Moreover, the maximum dose rate was recorded in a different organism type (Vascular plant), later in the assessment period (52,000 AD) and with a different key radionuclide, Pu-239; this was due to the increased mobilisation of plutonium from the repository under the changed redox conditions (Section 7.4), leading to high environmental concentrations of this radionuclide.

8.6.5 Extended global warming calculation case

The *extended global warming calculation case* involves a period of increased warming over that simulated in the *global warming calculation case*, leading to an increased sea-level due to polar melting that counteracts the uplift at the site. In this calculation case, it is assumed that the shore level at Forsmark remains in the same position as today until about 3000 AD; after this time the land progression continues as predicted under the *global warming calculation case* (except 1,000 years delayed). The main recipient biosphere object (157_2) was a marine bay for 1,000 years longer than in the *global warming calculation case*, and therefore this case could also potentially result in higher exposure of marine organisms to radiation, compared with the *global warming calculation case*.

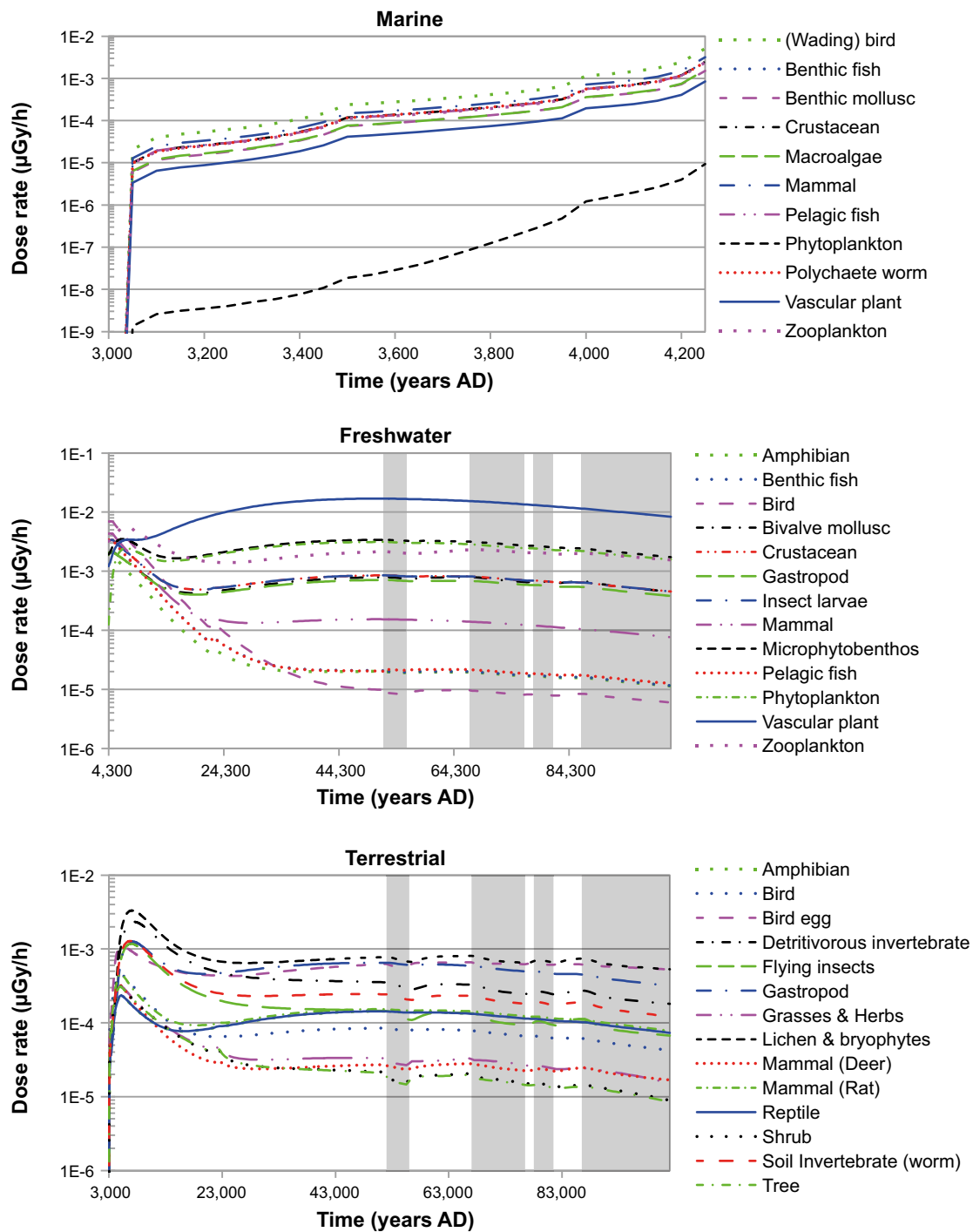


Figure 8-22. Dose rates in non-human biota in the marine (top), freshwater (middle) and terrestrial (bottom) ecosystems, in the *changed repository redox conditions in SFR 1 calculation case*. Grey shaded areas indicate periglacial periods. N.b. the dose rates are several orders of magnitude lower than the screening dose rate ($1E+1 \mu\text{Gy/h}$) which cannot be seen on this figure.

Comparing maximum dose rates for the most exposed marine organism, with the *global warming calculation case*, the difference was minor ($5.4 \times 10^{-4} \mu\text{Gy h}^{-1}$). As the dose rates to marine organisms increased throughout the assessment period, the maximum dose rate recorded in marine organisms in this calculation case was found at the end of marine period, like that in the *global warming calculation case*, only 1,000 years later. Exposures in freshwater and terrestrial ecosystems were lower in this scenario compared with the *global warming calculation case* (Freshwater: $6.4 \times 10^{-3} \mu\text{Gy h}^{-1}$, and Terrestrial: $1.7 \times 10^{-3} \mu\text{Gy h}^{-1}$). The maximum dose rate in the *extended global warming calculation case* occurred slightly later for the freshwater ecosystem and slightly earlier for the terrestrial ecosystem compared with in the *global warming calculation case*. Figure 8-23

shows the dose rates over time for all considered organism types in marine, freshwater and terrestrial ecosystems in the *extended global warming calculation case*. The modelled climate for the *extended global warming calculation case* includes no periglacial periods; therefore, unlike the *global warming calculation case*, no drops in dose rate as a result of periglacial periods were seen in the terrestrial ecosystem.

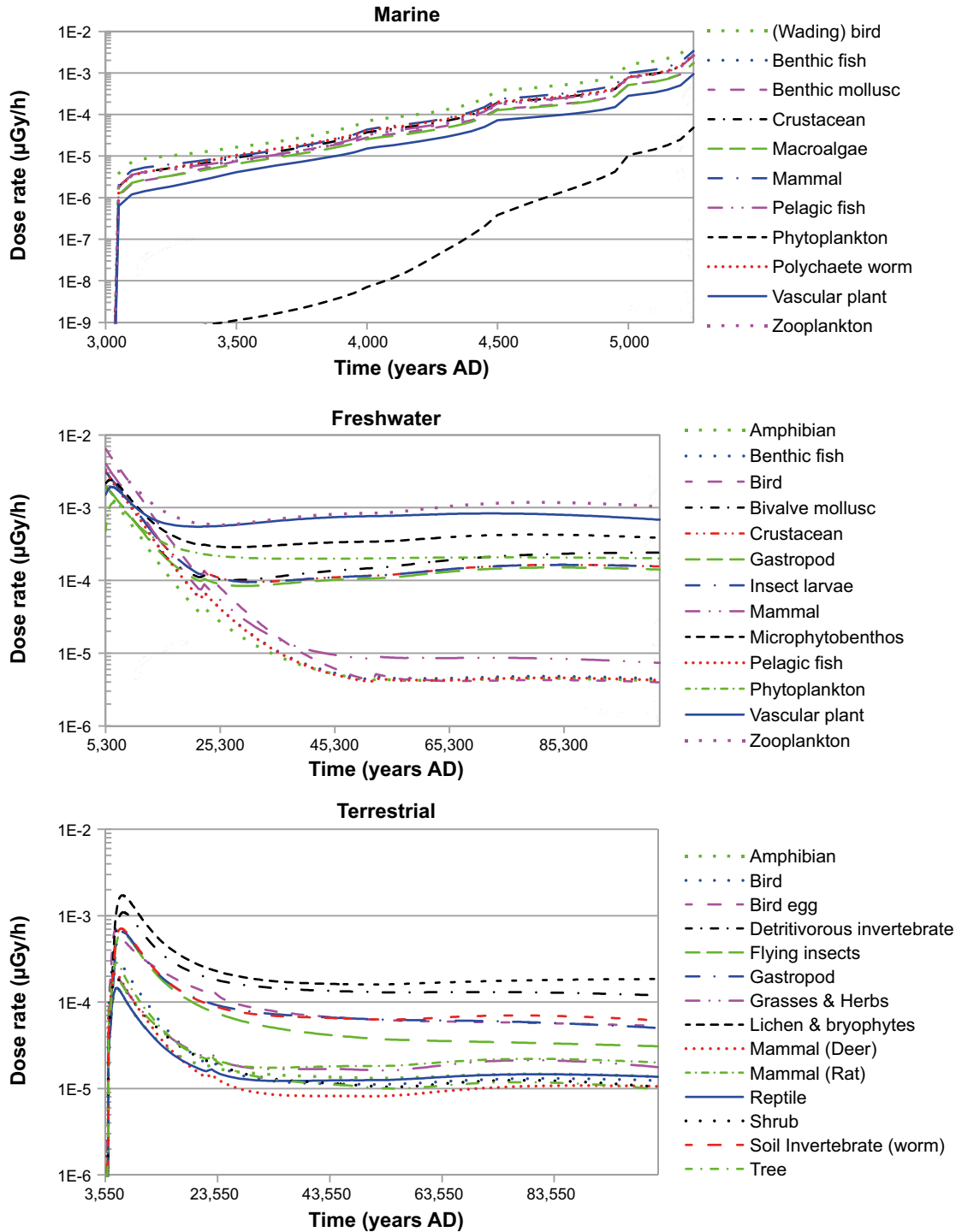


Figure 8-23. Dose rates in non-human biota in the marine (top), freshwater (middle) and terrestrial (bottom) ecosystems, in the *extended global warming calculation case*. No periglacial conditions exist throughout this assessment. N.b. the dose rates are several orders of magnitude lower than the screening dose rate ($1E+1 \mu\text{Gy/h}$) which cannot be seen on this figure.

The *extended global warming calculation case* reflected the *global warming calculation case* closely regarding the maximum dose rates in each ecosystem, with the same organism types and biosphere objects, and internal radionuclide contributions (Table 8-1). The pattern of radionuclides contributing to dose rate in the most exposed organisms of each ecosystem was the same in the *extended global warming calculation case* and the *global warming calculation case*.

8.7 Results for scenario combinations

The calculation cases for scenario combinations are summarised in Section 4.4 and described in detail in the **Main report**, Section 7.8. The assessment of the calculation case combinations comprises two calculation cases; the key results obtained for these cases are presented below.

8.7.1 Scenario combination 1 calculation case

The temporal release of radionuclides from the repository and the successive changes in the biosphere is the same as for the *global warming calculation case*. This calculation case, *scenario combination 1 calculation case*, combines elements from the *high flow in the bedrock calculation case* and the *accelerated concrete degradation calculation case*. Figure 8-24 shows the dose rates over time for all considered organism types in marine, freshwater and terrestrial ecosystems in the *scenario combination 1 calculation case*. The dose rates experienced by organisms in the *scenario combination 1 calculation case* closely reflected the patterns seen in the *global warming calculation case*.

In each ecosystem, the most exposed organism types were the same as those in the *global warming calculation case*. Maximum dose rates to the most exposed organisms in the *scenario combination 1 calculation case*, compared with the *global warming calculation case*, were slightly higher in all ecosystems (Table 8-1; Marine ecosystems: $8.6 \times 10^{-3} \mu\text{Gyh}^{-1}$; Freshwater ecosystem: $1.1 \times 10^{-2} \mu\text{Gyh}^{-1}$; Terrestrial ecosystem: $4.2 \times 10^{-3} \mu\text{Gyh}^{-1}$) and, in the freshwater and terrestrial ecosystems, occurred slightly sooner (Table 8-1). The details regarding the maximum exposures in this case reflected the *global warming calculation case* closely, with the same organism types, key radionuclides, and internal radionuclide contributions (Table 8-1). The decreased contribution of organic C-14 in the most exposed aquatic organisms reflects the small increase in concentration of inorganic C-14. The troughs in dose rates in terrestrial ecosystems during periglacial periods as seen in the *global warming calculation case* also appeared in the *scenario combination 1 calculation case*.

8.7.2 Scenario combination 2 calculation case

The temporal release of radionuclides from the repository and the successive changes in the biosphere is the same as for the *global warming calculation case*. This *scenario combination 2 calculation case* combines elements from the *high flow in the bedrock calculation case* and the *high concentrations of complexing agents calculation case*. Figure 8-25 shows the dose rates over time for all considered organism types in marine, freshwater and terrestrial ecosystems in the *scenario combination 2 calculation case*.

The dose rates experienced by marine and terrestrial organisms in the *scenario combination 2 calculation case* reflected the patterns seen in the *global warming calculation case*. In the freshwater ecosystem, the pattern of exposures in the calculation case *scenario combination 2 calculation case* diverged significantly from that of the *global warming calculation case* in several organism types: instead of experiencing a peak at ~ 7000 AD as in the *global warming calculation case*, Zooplankton and Vascular plant experienced a small increase in dose rates until later in the assessment period, following environmental concentrations of Ni-59, which led to the maximum dose rate occurring later, at 37,000 AD. Maximum dose rates to the most exposed organisms in the *scenario combination 2 calculation case*, compared with the *global warming calculation case*, were slightly higher in all ecosystems (Table 8-1; Marine: $6.3 \times 10^{-3} \mu\text{Gyh}^{-1}$; Freshwater: $9.1 \times 10^{-3} \mu\text{Gyh}^{-1}$; Terrestrial: $4.2 \times 10^{-3} \mu\text{Gyh}^{-1}$). The most exposed organisms of the marine and terrestrial ecosystems were the same as for the *global warming calculation case*; however Zooplankton was the most exposed freshwater organism type, in contrast to the *global warming calculation case*. For marine and terrestrial

ecosystems, some details regarding the maximum exposures of this calculation case reflected those of the *global warming calculation case* closely, with the same or similar peak dose rate times, and internal radionuclide contributions (Table 8-1). The troughs in dose rates in terrestrial ecosystems during periglacial periods as seen in the *global warming calculation case* also appeared in the *scenario combination 2 calculation case*.

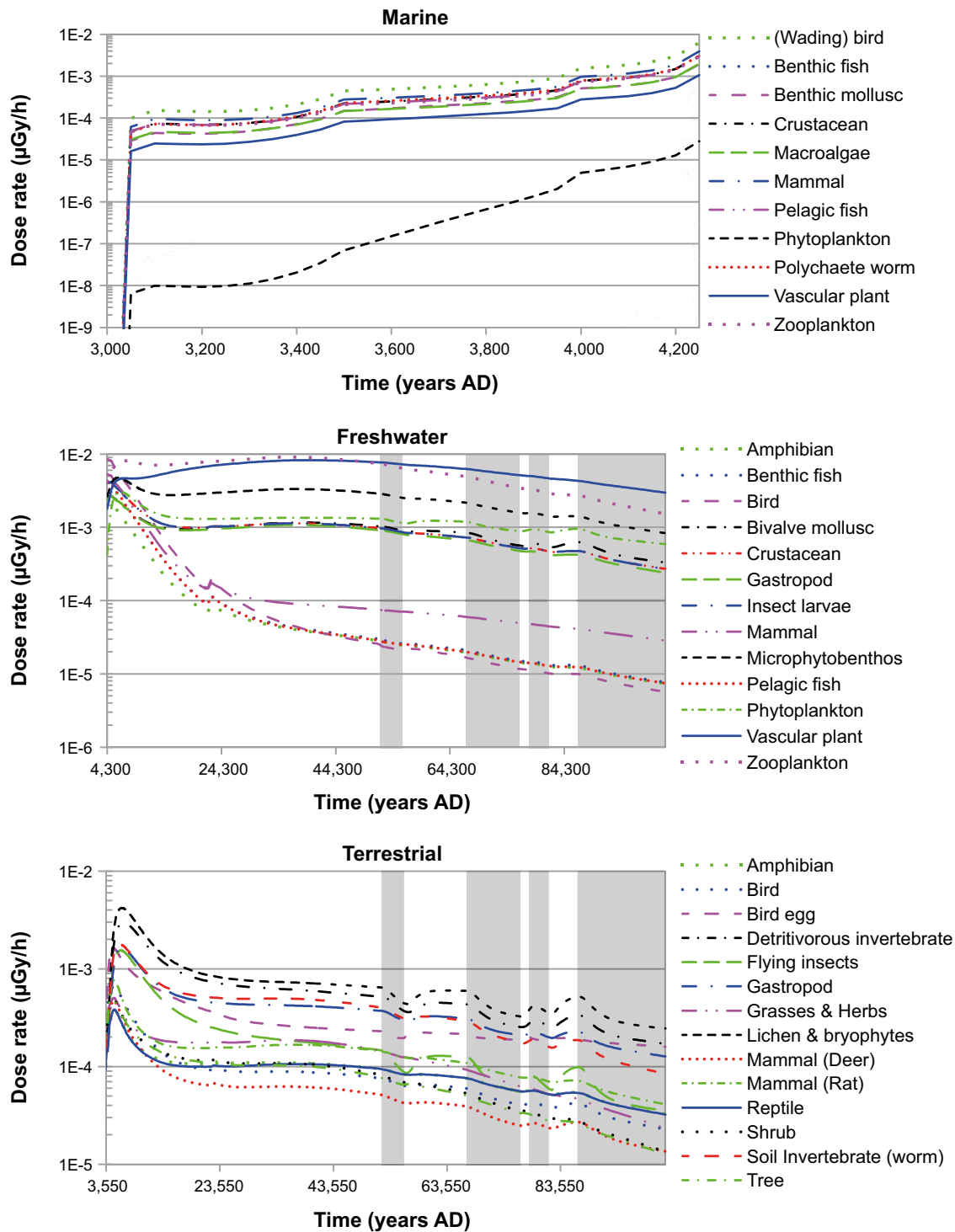


Figure 8-24. Dose rates in non-human biota in the marine (top), freshwater (middle) and terrestrial (bottom) ecosystems, in the calculation case *scenario combination 1 calculation case*. Grey shaded areas indicate periglacial periods. N.b. the dose rates are several orders of magnitude lower than the screening dose rate ($1\text{E}+1 \mu\text{Gy/h}$) which cannot be seen on this figure.

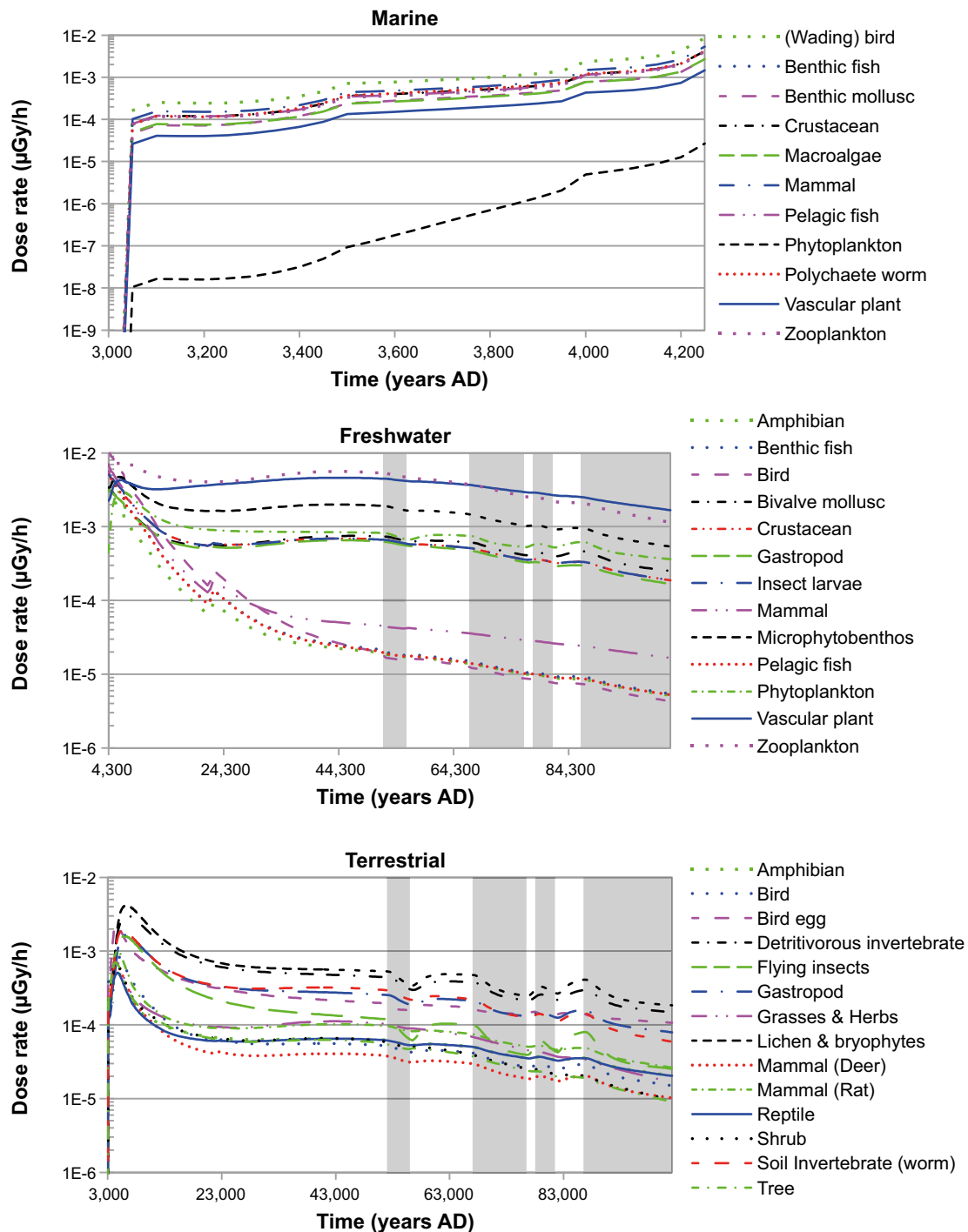


Figure 8-25. Dose rates in non-human biota in the marine (top), freshwater (middle) and terrestrial (bottom) ecosystems, in the calculation case **scenario combination 2 calculation case**. Grey shaded areas indicate periglacial periods. N.b. the dose rates are several orders of magnitude lower than the screening dose rate ($1E+1 \mu\text{Gy/h}$) which cannot be seen on this figure.

8.8 Uncertainties in estimated dose rates

The sections above have discussed the results of simulations where parameters were fixed at values expected to be typical for Forsmark (i.e. deterministic simulations with best estimates). This section focuses on estimates of dose rates that incorporate parameter uncertainty; in these simulations, parameter sets ($n=1,000$) have been sampled from parameter probability density functions (PDF), and are referred to as probabilistic simulations.

A comparison between LDFs (i.e. annual doses to humans for a unit release rate simulation) derived deterministically and probabilistically has been performed for 55 radionuclides (**Biosphere synthesis report**, Chapter 10), and the mean values from probabilistic simulation were always equal to or higher than the LDF values from the deterministic simulation (on average 2.5 times higher). The difference between the mean values from probabilistic simulations and the corresponding deterministic values can, to a large extent, be explained by the skewed distributions of the most influencing parameters. That is, the partitioning coefficients for sorption (K_d) for surface peat and soils and the plant/soil concentration ratios (CR) all had log-normal PDFs, and consequently the average parameter value from a random sample was higher than the geometric mean, which was used as the “best-estimate” for these parameters. Both of these parameters increase apparent radionuclide concentrations in the environment and food consumed by humans, and thus a higher LDF is to be expected from a probabilistic simulation. A similar analysis of dose rates to non-human biota was performed for four radionuclides (C-14, Cl-36, Mo-93 and Ni-59), and the mean from probabilistic simulations was 2–5 times higher than the best estimate of the dose rates for each of the radionuclides.

For the probabilistic simulated dose rates to non-human biota, the 90% confidence interval varied over time (as seen in Figure 8-26); the 95% and 5% limits of this interval are presented for the most exposed organisms in each scenario, in Table 8-4. The 95% confidence values (highest range of dose rates) of a few calculation cases (*loss of barrier function calculation case – no sorption in the repository* and the *loss of barrier function calculation case – high water flows in the repository*) approach the screening value (within a factor of ten). However, the highest dose rate determined at 95% confidence (for freshwater Vascular plant in the *loss of barrier function calculation case – no sorption in the repository*, see Figure 8-26) remained >5 times lower than the screening dose rate ($10 \mu\text{Gyh}^{-1}$), indicating that there is no significant risk to biota populations at the site.

The largest 90% confidence intervals were nearly always seen in primary producers, i.e. Lichen & bryophytes, Vascular plants, Phytoplankton, etc, with a spread of as much as three orders of magnitude. According to the analysis of parameter uncertainty in the **Biosphere synthesis report**, CR of the exposed organism dominated dose rate uncertainty (for Cl-36, Mo-93 and Ni-59). It is a reasonable assumption that this is true also for all other radionuclides (except C-14 and H-3 for which this parameter is not used) and the results found here reflect the generally wide parameter probability density functions (PDFs) used for CR for primary producers.

In some calculation cases, the most exposed organism type, and sometimes also ecosystem type, differed between deterministic and probabilistic calculations, reflecting the similar magnitude of dose rates calculated in freshwater and terrestrial ecosystems under certain scenarios. In the deterministic calculations, the freshwater ecosystem demonstrated the highest overall dose rates, in all calculation cases, and this is largely reflected in the probabilistic calculations, with the exception of *loss of barrier function calculation case – no sorption in the bedrock* where the terrestrial organism type Lichen & bryophytes received the highest dose rate. In the probabilistic calculations, when highest dose rates were found in the freshwater ecosystem, Vascular plant was always the most exposed organism, with the exception of the *high inventory calculation case*, where Zooplankton was the most exposed. The higher exposures to Vascular plant in the freshwater ecosystem determined in the probabilistic calculations contrasts with the result from the deterministic calculations, where Zooplankton or Bird were more often the most exposed freshwater organism type.

In all calculation cases, the mean probabilistic dose rate was as much as an order of magnitude higher than the dose rate from the corresponding deterministic calculation. However, both probabilistic and deterministic results were all well below screening dose rate.

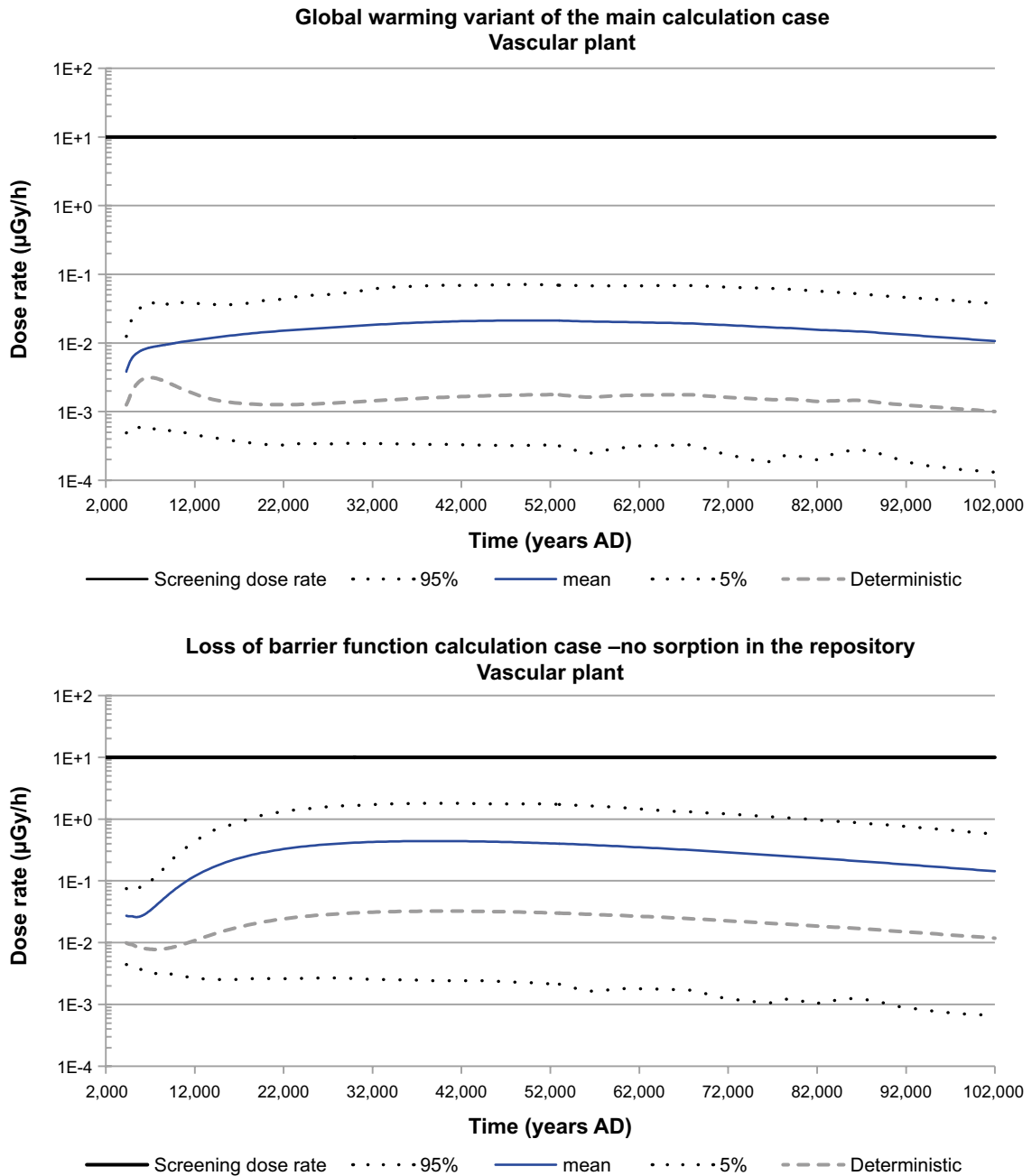


Figure 8-26. Dose rates of the probabilistic assessment for the most exposed organism in the **global warming calculation case** (top; the **global warming calculation case Vascular plant**) and for the calculation case resulting in highest dose rate across all calculation cases (bottom; the **loss of barrier function calculation case – no sorption in the repository Vascular plant**). The mean, and 5th and 95th percentiles from the probabilistic simulations are presented together with their corresponding deterministic assessment (grey dashed line) and the applied screening dose rate for non-human biota (black solid line).

Table 8-4. Dose rates from probabilistic simulations of each calculation case. The most exposed organism with respect to mean dose rate is presented; mean dose rates shown are the maximum value over the entire simulation period. The limits for the 90% confidence interval (at the time of peak mean dose rate) indicate the degree of uncertainty involved. For comparison, the most exposed organism data for each calculation case, from the deterministic assessment, are shown in blue. TE = terrestrial, FW = freshwater. Data is taken from object 157_2 unless otherwise stated.

Calculation case	Most exposed organism	Ecosystem	90% confidence interval ($\mu\text{Gy}\cdot\text{h}^{-1}$)		Mean dose rate ($\mu\text{Gy}\cdot\text{h}^{-1}$)
			5%	95%	
Main scenario					
Global warming calculation case	Vascular plant	FW	3.2E-4	7.1E-2	2.1E-2
	Bird	FW			7.1E-3
Early periglacial calculation case (Object 157_1)	Vascular plant	FW	1.1E-4	2.6E-2	7.5E-3
	Zooplankton	FW			2.7E-3
Timing of the releases calculation case	Vascular plant	FW	3.4E-4	7.8E-2	2.2E-2
	Bird	FW			7.0E-3
Less probable scenarios					
High inventory calculation case	Zooplankton	FW	5.2E-4	1.6E-1	3.8E-2
	Zooplankton	FW			2.9E-2
High flow in the bedrock calculation case	Vascular plant	FW	4.2E-4	1.1E-1	3.2E-2
	Bird	FW			8.5E-3
Accelerated concrete degradation calculation case	Vascular plant	FW	4.4E-4	1.2E-1	3.4E-2
	Bird	FW			9.6E-3
Bentonite degradation calculation case	Vascular plant	FW	3.5E-4	8.1E-2	2.3E-2
	Bird	FW			7.1E-3
High concentrations of complexing agents calculation case	Vascular plant	FW	7.8E-4	2.6E-1	7.4E-2
	Bird	FW			7.4E-3
Residual scenarios					
Loss of barrier function calculation case – no sorption in the repository	Vascular plant	FW	2.4E-3	1.8E+0	4.4E-1
	Bird	FW			6.2E-2
Loss of barrier function calculation case – no sorption in the bedrock	Lichen & bryophytes	TE	6.2E-4	3.3E-1	7.5E-2
	Zooplankton	FW			2.1E-2
Loss of barrier function calculation case – high water flows in the repository	Vascular plant	FW	2.2E-3	1.5E+0	4.2E-1
	Vascular plant	FW			3.2E-2
Changed repository redox conditions in SFR 1 calculation case	Vascular plant	FW	6.5E-4	9.8E-1	2.8E-1
	Vascular plant	FW			1.7E-2
Extended global warming calculation case	Vascular plant	FW	1.4E-4	4.0E-2	1.0E-2
	Bird	FW			6.4E-3
Calculation case combination					
Scenario combination 2 calculation case	Vascular plant	FW	9.3E-4	3.4E-1	9.7E-2
	Zooplankton	FW			9.1E-3
Scenario combination 1 calculation case	Vascular plant	FW	6.4E-4	2.1E-1	5.7E-2
	Bird	FW			1.1E-2

9 Models

This chapter presents the radionuclide transport (RNT) modelling concept and models representing different parts of the repository and its environs, the near-field (repository), the far-field (geosphere) and the biosphere (surface system) developed for the SR-PSU assessment.

The near-field and far-field models are presented in detail here and in appendices B, C and D, whereas the biosphere model is only briefly presented. The near-field models of SFR 1 vaults are based on the SAR-08 assessment and additional background material can be found in Thomson et al. (2008a). New models had to be set up for SFR 3 vaults using a similar approach. As the previously used far-field code (FARF31) does not represent time varying transport conditions, the model was re-implemented in Ecolego with this additional feature, see also Appendix C. This allowed establishing Ecolego as a common platform for all performance assessment models of the SR-PSU assessment. A more detailed presentation of the biosphere model can be found in Saetre et al. (2013) and in the **Biosphere synthesis report**.

9.1 Modelling concepts and tools

Compartment models

The radionuclide transport models (near-field, far-field and biosphere) are built using the compartmental approach. In compartment modelling, the modelled system is divided into compartments with homogenous properties, where in each compartment the nuclides are assumed to be fully mixed. This simplification reflects the uncertainty in the description of the system and its future evolution, but the level of spatial resolution represented by the compartmental structure has to be chosen appropriately; to avoid overestimation of dilution (by mixture) and underestimation of possible peak radiological impacts. This is further discussed in appendices B and C.

A compartment is assumed to be a homogeneous entity of the modelled system with its own properties and own sub-model-state. The state of a compartment (i.e. the radionuclide inventory) depends on local processes (e.g. radioactive decay) and exchange processes with connected compartments (e.g. advective and diffusive transport.) and with sources and sinks.

The concepts “transfer” and “transfer coefficient” are used here to describe these exchange processes being defined as:

- **Transfer** Tr_{ij} [Bq/year]: The flux of radionuclides from the source compartment i of the transfer to the target compartment j .
- **Transfer coefficient** TC_{ij} [1/year]: The factor of proportionality between the transfer Tr_{ij} and the radionuclide inventory A_i^n of the source compartment i . The transfer coefficient can be applied for transfers depending linearly on the inventory of the source compartment. I.e. $Tr_{ij} = TC_{ij} A_i^n$. The linear model is applied for most transfer processes in SR-PSU. One exception is solubility limited transport, which is discussed in Appendix B.

The rate of change of a compartment’s inventory can be described by the following equation.

$$\dot{A}_i^n = \sum_{j \in N_i} Tr_{ji}^n - \sum_{j \in N_i} Tr_{ij}^n + \sum_{p \in P_n} Br_p^n \lambda^n A_i^p - \lambda^n A_i^n + r_i^n \quad \text{Equation 9-1}$$

where

A_i^n = inventory of radionuclide n in compartment i , [Bq],

\dot{A}_i^n = change rate (first time derivative) of A_i^n , [Bq/yr],

A_i^p = inventory of parent nuclide p in compartment i , [Bq],

N_i = set of indices of compartments connected to compartment i , [-],

P_n = set of indices of parents of radionuclide n , [-],

Tr_{ij}^n = transfer for nuclide n from compartment i to j , [Bq year⁻¹],

λ^n = decay rate of nuclide n [year⁻¹],

Br_p^n = branching ratio from parent nuclide p to radionuclide n , [-],

r_i^n = sink/source term for radionuclide n in compartment i , [Bq year⁻¹].

Capacity and retardation

The sorption of radionuclides is dependent on a number of physical and chemical processes described in the process reports for SR-PSU (**Waste process report, Barrier process report, Geosphere process report**). These processes are taken into account by a simplified linear model for the partitioning of radionuclides dissolved in the water and sorbed to the matrix of the porous medium. In this model the partitioning coefficient, K_d , is defined as the ratio of the quantity of the radionuclide sorbed per unit mass of porous medium to the amount remaining in solution at equilibrium.

The concepts of capacity [m^3] and retardation-factor [-] have been used in this work to simplify the mathematical expressions used in the models and report.

The *capacity* [m^3] of a compartment is defined as:

$$\text{Capacity} = \text{Volume}(\phi + (1 - \phi)K_d\rho_{part}) \quad \text{Equation 9-2}$$

where:

ϕ = porosity of the material in the compartment. [-],

K_d = solid-liquid partitioning coefficient [m^3/kg],

ρ_{part} = particle density of the media in the compartment [kg/m^3].

In some cases it is more practical to use bulk density instead of particle density.

Capacity for bulk density is derived from capacity for particle density by the substitution:

$$\rho_{part} = \frac{\rho_{bulk}}{(1 - \phi)} \quad \text{Equation 9-3}$$

$$\text{Capacity} = \text{Volume}(\phi + K_d\rho_{bulk}) \quad \text{Equation 9-4}$$

where:

ρ_{bulk} = bulk density of the medium in the compartment [kg/m^3].

Retardation factor, R , is defined as:

$$R = 1 + \frac{K_d\rho_{bulk}}{\phi} \quad \text{Equation 9-5}$$

Hence:

$$\text{Capacity} = \text{Volume} \phi R \quad \text{Equation 9-6}$$

The pore water concentration of a radionuclide in a compartment is obtained by dividing the total amount of the radionuclide in the compartment by the capacity of the compartment. This is used when describing advective and diffusive transfers (Sections 9.3 and 9.4)

Solubility limits

Solubility limits could have a large retarding effect on the release of some nuclides, e.g. Ni-59. This effect is however, pessimistically, not taken into account in the radionuclide transport calculations. The effect is studied in a supporting calculation, described in Appendix B.

Spatial resolution

The compartmental approach provides a simple and transparent model for the transport of radionuclides from the waste packages in the repository vaults, via the barriers and the bedrock to the surface ecosystems. However, the number and size of the compartments must be chosen with care such that the representation is detailed enough for the assessment context.

The transport properties are assumed to be constant within each compartment. A homogenous region in the modelled system can often be represented with one single compartment. However if the distribution of radionuclides within one such region cannot be assumed to be homogenous, the approach is to represent the region with several sub compartments. The latter applies particularly to the concrete walls in the repository and to the bedrock. The effect of dividing the concrete barriers into a varying number of compartments is analysed in Appendix B. The compartment modelling approach to transport in the geosphere is described in detail in Appendix C.

The Ecolego software

Ecolego is the software that was used for the implementation of the radionuclide transport models in SR-PSU. It is a software tool for creating compartment models allowing deterministic and probabilistic simulations as well as performing sensitivity analyses.

The software is used by means of a graphical user interface for defining and running the models. It facilitates the quality management process by offering reporting capabilities and the possibility to provide input data by suitably structured Microsoft Excel spreadsheets.

Further information on Ecolego can be found in the **Model summary report**.

9.2 Coupling to hydrological modelling

A large number of parameters are used in the radionuclide transport calculations, many of them derived from dedicated process modelling performed specifically for SR-PSU. The Assessment Model Flow Chart (**Main report**, Appendix G) visualises the (conceptual) interdependence of models applied for the SR-PSU assessment.

Of special importance and challenge is the coupling between hydrological modelling tasks and radionuclide transport modelling. The flowchart in Figure 9-1 sketches the main data flows between the hydrological modelling tasks and the radionuclide transport modelling.

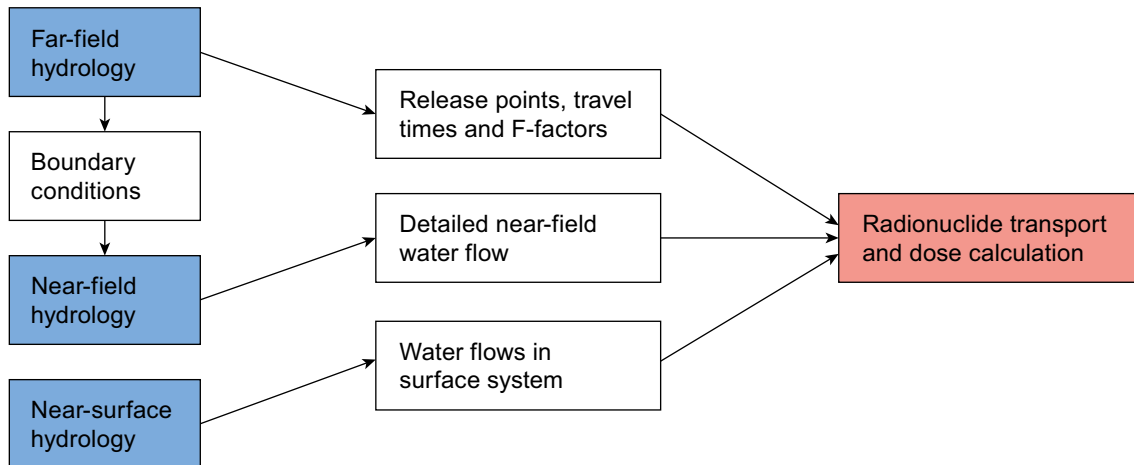


Figure 9-1. Concept for the assessment of hydrological conditions and their consideration in radionuclide transport for the safety assessment of SR-PSU Blue boxes represents hydro-modelling tasks, white boxes represents data transfer between models and the red box represents the radionuclide transport modelling task.

9.3 Near-field models

Figure 9-2. shows the layout of the extended SFR. The upper grey part shows the existing SFR (SFR 1) and the blue part shows the extension (SFR 3).

In radionuclide transport modelling, a sub-model has been developed for each of the 11 waste vaults.

The engineered concrete and bentonite barriers of the near-field limit the release of radionuclides by reducing the water flow through the waste packages and by introducing high radionuclide sorption capacity, mainly in the cementitious materials. These are explicitly represented by a number of compartments in the radionuclide transport model.

The access tunnels and tunnel plugs are of importance for long-term safety; however, they are not explicitly represented in the radionuclide transport model. Instead, their impact on radionuclide transport is considered through their effect on water flow. As the plugs represent flow resistances, they also affect the water flow in the vaults. Calculations of water flow in the near-field have been performed using the calculation tool Comsol Multiphysics (Abarca et al. 2013) on the geometry depicted in Figure 9-3. The calculated water flow through barriers and waste has then been used in the radionuclide transport models as input data.

Control volumes and compartments

Control volumes (Abarca et al. 2013) are defined to evaluate the annual water balance in the vault volume including the calculation of (directional) annual water flows through its bounding surfaces. The annual water flow is transferred from the hydrological calculations to the radionuclide transport calculations. Annual water flow is assigned to the bounding surfaces of the control volumes in such a way that the flow is in balance for each control volume.

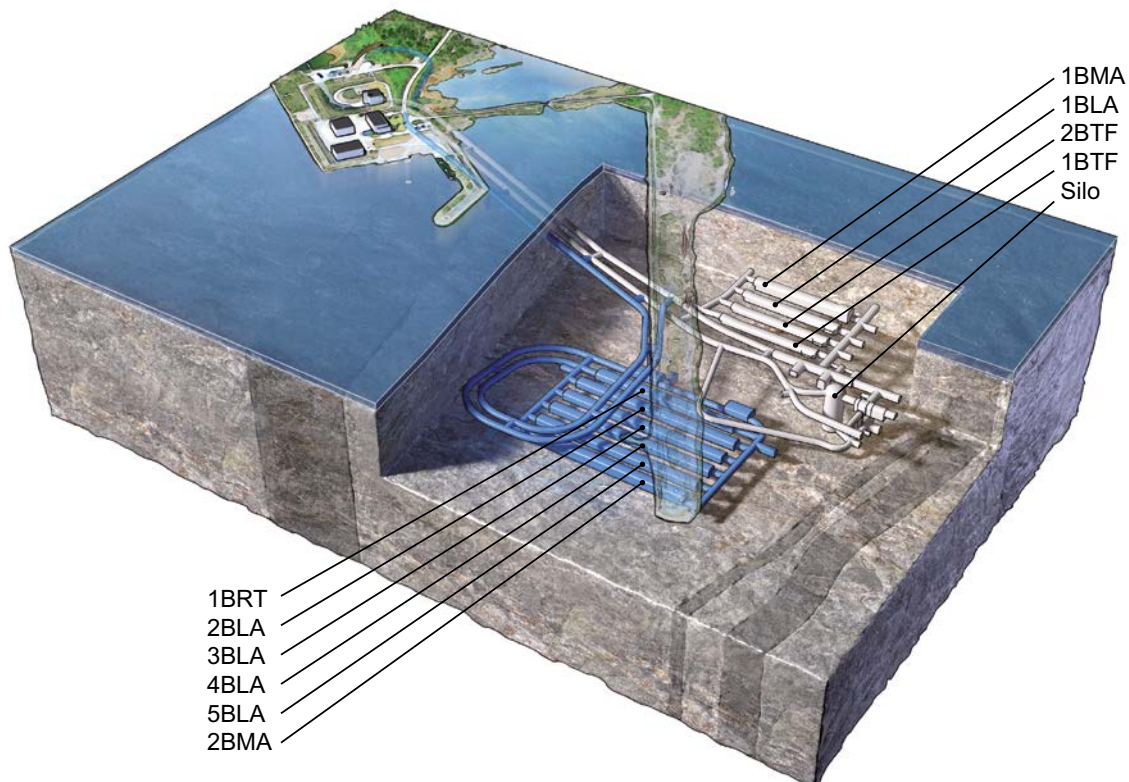


Figure 9-2. The existing SFR (SFR 1) in grey and the extension (SFR 3) in blue with access tunnels. The waste vaults in the figure are the silo for intermediate-level waste, 1 and 2BMA vaults for intermediate-level waste, 1–2BTF vaults for concrete tanks with intermediate-level waste with low activity levels, 1BLA and 2–5BLA vaults for low-level waste and the 1BRT vault for reactor pressure vessels.

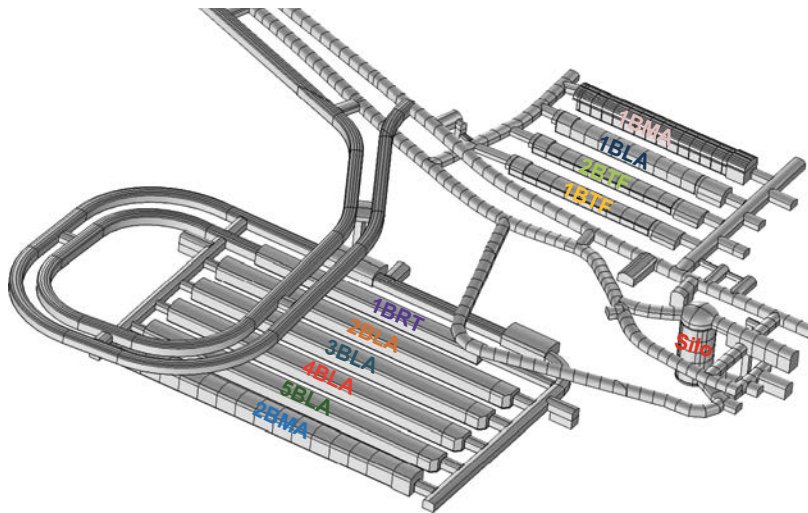


Figure 9-3. CAD representation of the geometry of SFR 1 (on the upper right) and SFR 3 (on the lower left) as imported into the hydrological model. (Abarca et al. 2013).

A control volume is either represented by a single or by a group of compartments. Barriers separating sections of the repository from each other are, in some cases partitioned between the control volumes that represent the respective sections. In this case, the part of a control volume representing the barrier is modelled with 5 compartments in a line along the flow direction. Additionally, the waste domain is generally represented with more detail in the radionuclide transport model than in the hydrological model, where the waste domain is represented as a homogenous porous medium.

In the case of the 1BMA vault, for example, 77 control volumes are represented by 617 compartments.

9.3.1 Processes handled in the radionuclide transport calculations

A large number of physical and chemical processes have been identified and analysed in the near-field of SFR, see the **Waste process report** and the **Barrier process report**. However, only a few of them are relevant for radionuclide transport modelling.

The main near-field processes of relevance for radionuclide transport modelling are the following.

Radioactive decay and in-growth

Radioactive decay and in-growth are well known physical processes with a very exact mathematical description. These processes are explicitly included in the modelling by means of rates for decay and in-growth proportional to the inventory of the corresponding radionuclide or its parent, respectively, and parameterised with decay constants and branching ratios (see Equation 9-1 and Appendix A).

Advection

Advection is explicitly included in the RNT modelling. The water flow between control volumes simulated in the near-field hydrological model is used, together with volumes and sorption data for waste vaults, to calculate the retention and advective transport of radionuclides in the RNT model. The control volumes and their surfaces are mapped to compartments or groups of compartments. As the water flow is calculated for various degradation states of the concrete barriers and cementitious materials in the waste, the modelling implicitly takes the expected degradation of the barriers over time into account. A possible future occurrence of larger fractures in the concrete barriers in 1BMA and 2BMA is also considered in the models, by assuming advective transfer directly through the barriers, i.e. without taking sorption in the barriers into account (Appendix D).

Diffusion

Diffusion is explicitly included in the model equations. The calculation takes into account the material specific effective diffusivities, as well as the porosities and compartmental geometries (transport lengths and cross section areas) of the waste packages and barriers. The effective diffusivities are increased over time to describe a gradual degradation of the concrete barriers. Diffusive resistance is, pessimistically, neglected for bitumen-solidified wastes. No diffusion resistance is taken into account for the concrete structure in the BRT vault, as this structure is modelled as a stirred tank.

Dispersion

Dispersion, as discussed here, refers to dispersive effects caused by the pore-structure of the material.

In contrast to diffusion, dispersion is not represented explicitly in the model, (see discussion in Appendix D). The coarse spatial resolution of the compartmental structure introduces a dispersive effect with respect to radionuclide transport in the system. This numerical dispersion is assumed to be larger than the physical dispersion, hence there is no need for a specific dispersion term in the model equations.

Sorption

Sorption (on an immobile solid phase) has a retarding effect on both advective and diffusive transport of radionuclides. Sorption on near-field materials is explicitly included in the radionuclide transport modelling using a linear approach, based on element-specific K_d values. The K_d is treated as a dynamic entity that changes with time. The change with time is determined by the expected changes of chemical conditions for example Eh and pH of the system.

Solubility limits

Solubility limits are, pessimistically, not considered in the main calculation cases. However, the effect of solubility limits has been investigated in specific supporting calculations, see Appendix B.

Speciation

Speciation of radionuclides is considered by the use of pre-calculated time-dependent sorption coefficients. These are determined based on chemical conditions that are assumed to change with time.

Corrosion

The reactor pressure vessels in the BRT vault contain radionuclides produced as a result of neutron activation of the steel during the operation of the reactor. During this time, the surface of the vessels is also contaminated by radionuclides present in the reactor water. The surface contamination is assumed to dissolve in the surrounding pore water directly after closure of the repository, whereas the fraction of the radionuclides that originates from neutron activation is assumed to be released congruently with the corrosion products as the steel corrodes. The corrosion rate of the steel in the reactor pressure vessels changes with time. The change with time is determined by the expected change of pH in the vault.

9.3.2 Model discretisation

Compartments of the RNT model of the near-field coincide with control volumes of the near-field hydrological model (or sub volumes thereof). The flow (of aqueous solution) from one compartment to another is determined by calculating the flow across the surfaces of the control volumes. The subdivision of control volumes into several compartments for achieving a finer resolution in the radionuclide transport applies particularly to the concrete walls of the models of the BMA vaults and the silo. The subdivision of the concrete walls is done to avoid the large numerical dispersion that would result from representing the walls with only one compartment each. In the radionuclide transport model all outer walls were represented by five compartments each. The determination of a sufficient number of wall-compartments is discussed further in Appendix B.

9.3.3 1BMA model

The existing waste vault for intermediate-level waste (1BMA) contains almost 20% of the total activity in SFR (as can be seen in Figure 3-3). The waste vault consists of a concrete structure with 15 sections separated by concrete walls. Each section contains several waste packages. At closure, the concrete structure will be covered with a lid and concrete slabs, so that the waste will be completely encased in concrete barriers. The waste packages in 1BMA are embedded in grout. A detailed description of 1BMA is given in the **Initial state report**.

For 1BMA, a discretisation has been chosen to allow each of the 15 sections to be represented separately. For each section, the model also includes four compartments for the backfill (with the exception of Sections 14 and 15, which are only surrounded by 3 such compartments, as each of these two sections covers only one half of a vault cross section, sharing a common inner boundary). The backfill in each end of the vault is also each represented in the model by a compartment. Figure 9-4 shows the separation into control volumes of 1BMA used in the water flow calculations.

Figure 9-5 shows a schematic view of the discretisation of the 1BMA model in the RNT model. The blue arrows represent advective transfers. The yellow arrows represent diffusion. (Vertical flows are not shown in the figure.) Each advective transfer corresponds to a water flow delivered from the hydrological calculations. In the RNT model, the outer walls of each section (black in the figure) were represented with five compartments each. Also the waste packages within each section were modelled with more detail; five types of model waste packages were chosen to represent the larger number of actual waste packages.

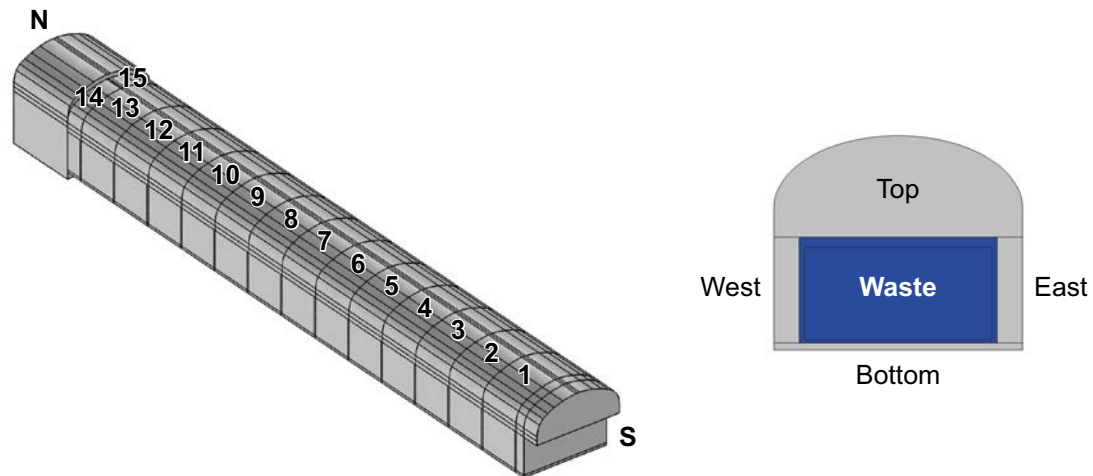


Figure 9-4. Control volumes for 1BMA in the hydrological model (Abarca et al. 2013).

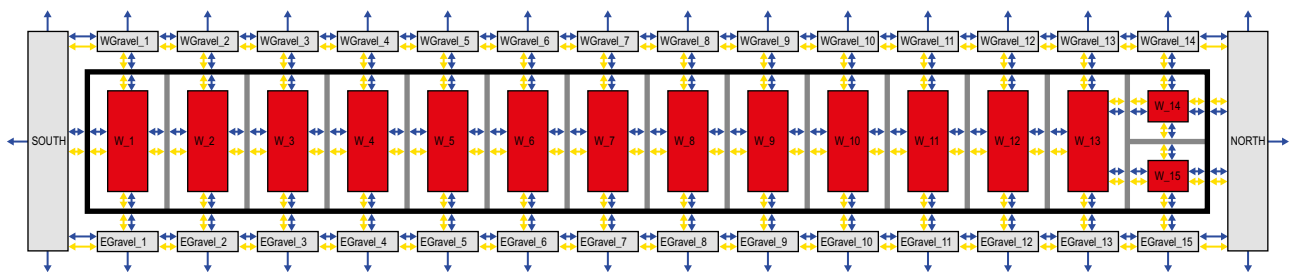


Figure 9-5. Schematic view of how 1BMA is represented in the radionuclide transport model. The figure shows a horizontal cross section of the model (i.e. compartments above and below the waste compartment are not shown). Blue arrows represent the water flows used in the radionuclide transport model. Yellow arrows represent diffusive transport in the model. Each red box in the figure represents several waste packages in the model.

Figure 9-6 shows conceptually the processes in the waste, backfill and barriers considered in the radionuclide transport model. The types of model waste packages are selected in such a way that the important characteristics of the many different types of real waste deposited in the repository can be modelled in appropriate detail (see Section 9.3.10).

Five different types of model waste packages are used to represent the waste in 1BMA. These are: cement-solidified or concrete embedded waste in concrete moulds, cement-solidified or concrete embedded waste in steel moulds, cement-solidified or concrete embedded waste in steel drums, bitumen-solidified waste in steel moulds, and bitumen-solidified waste in steel drums.

9.3.4 2BMA model

In 2BMA, the radioactive waste is stored in free-standing concrete caissons. These will be filled with waste packages, which will then be grouted. As they are filled with waste, the caissons are closed with a concrete lid. The space outside the caissons is backfilled with macadam. A detailed description of 2BMA is given in the **Initial state report**.

In the radionuclide transport model, a discretisation where the 14 caissons are represented separately has been selected. For each caisson, the model also includes a compartment for macadam backfill surrounding the caisson. The macadam backfill in the ends of the vaults is also represented by one compartment for each end. Figure 9-7 shows the separation into control volumes of 2BMA used in the water flow calculations. Figure 9-8 shows the different components (waste, backfill and barriers) and processes included in the radionuclide transport model.

The waste packages inside each caisson are handled as three different types of model waste packages that each represents a larger number of real waste packages (see Section 9.3.10).

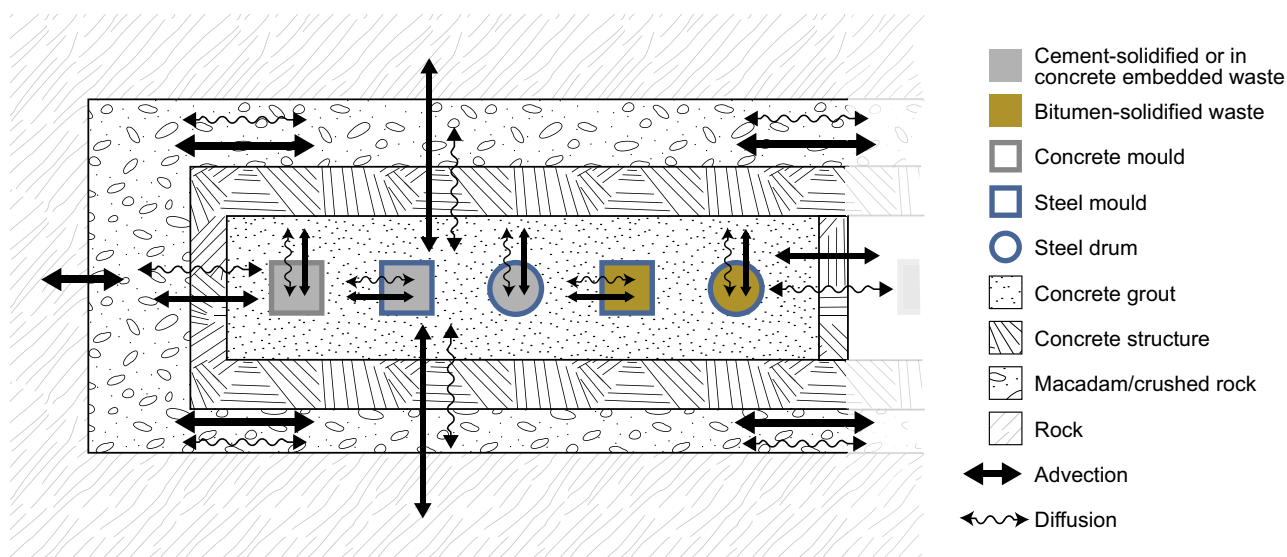


Figure 9-6. Conceptual model of one of the sections of 1BMA in the radionuclide transport model. Innermost in the picture, the five different types of model-waste packages used in the radionuclide transport modelling are shown. From the left: waste package with cement-solidified or concrete embedded waste in concrete moulds, cement-solidified or concrete embedded waste in steel moulds, cement-solidified or concrete embedded waste in steel drums, bitumen-solidified waste in steel moulds, and bitumen-solidified waste in steel drums (figure modified from Lindgren et al. 2001).

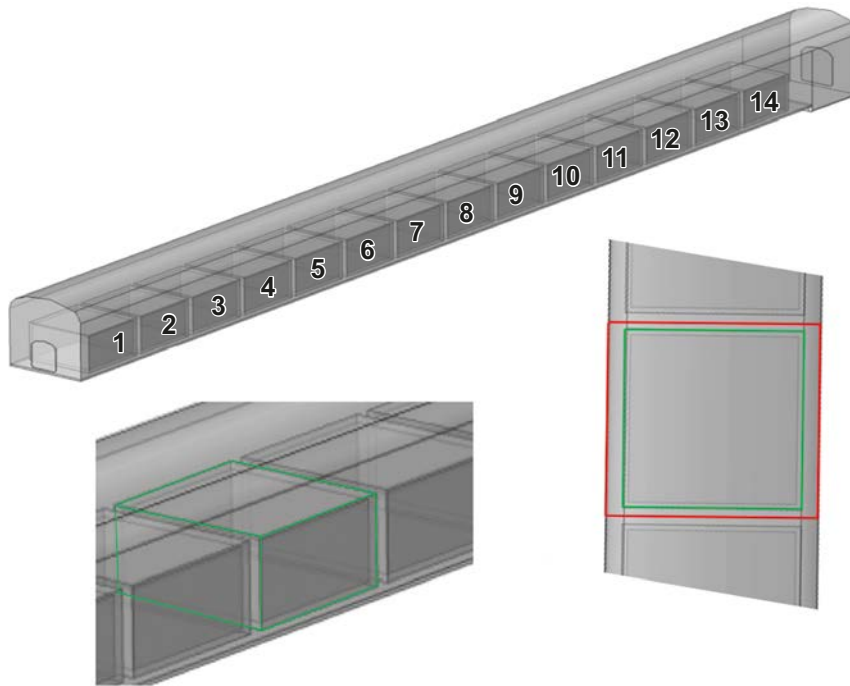


Figure 9-7. The division of 2BMA into control volumes in the hydrological model (Abarca et al. 2013). The green wire frame marks one of the cassettes. The red wire frame in the plan view delimits one cassette and surrounding backfill as one of the 14 sections modelled in the RNT model.

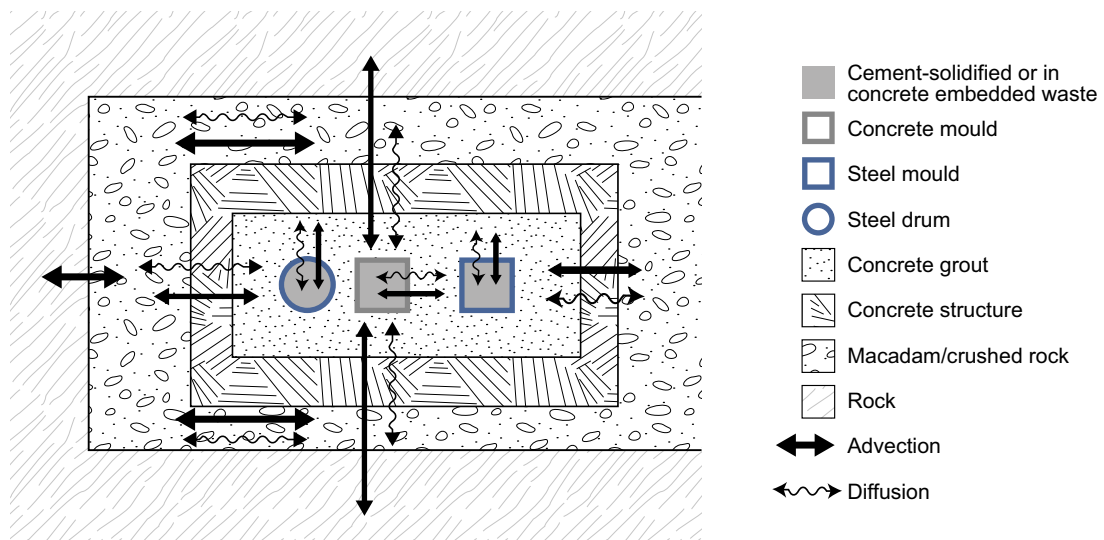


Figure 9-8. Conceptual model of 2BMA (the figure corresponds to one of the 14 modelled sections) in the radionuclide transport model. The figure shows the different types of model-waste packages used in the modelling of radionuclide transport. From the left: cement-solidified or concrete embedded waste in steel drums, cement-solidified or concrete embedded waste in concrete moulds, cement-solidified or concrete embedded waste in steel moulds (figure modified from Lindgren et al. 2001).

9.3.5 Silo model

The silo contains most of the activity in SFR (almost 70%, as can be seen in Figure 3-3), and it therefore has the most sophisticated barrier systems. The silo consists of a cylindrical rock cavern within which a cylinder of reinforced concrete has been built. Inside this concrete cylinder are a number of shafts separated by thinner concrete walls. These shafts are filled with waste packages that are grouted. The outer wall of the silo is completely surrounded by bentonite, creating a barrier to advective flow between the silo and the rock. The lower part of the silo consists of a slab of reinforced concrete founded on a bed of sand mixed with bentonite. The top of the silo will also be a slab of concrete covered with a layer of sand-bentonite. The empty space above the silo will be filled with crushed rock. A detailed description of the silo is given in the **Initial state report**.

For the silo, a level of detail for control volumes has been chosen where the vertical shafts are grouped in nine control volumes (as shown in Figure 9-9, right). Vertically, the silo is divided in 8 layers: 5 layers representing the waste domain, one layer each for sand/bentonite at the top and bottom, and one layer of backfill at the top of the silo. Figure 9-10 shows conceptually how different processes in the waste, backfill and barriers are modelled in the model of radionuclide transport.

Three types of waste packages are used to represent the waste in the silo: cement-solidified or concrete embedded waste in concrete moulds, cement-solidified or concrete embedded waste in steel packaging (moulds and drums), bitumen-solidified waste in steel packaging (moulds and drums).

9.3.6 BTF models

The repositories 1BTF and 2BTF have been designed primarily for concrete tanks. In addition, 1BTF also contains waste drums and a reactor tank lid. Most of the waste in 2BTF is in concrete tanks of the same type as those in 1BTF. In addition to this, 2BTF also contains 18 steel containers.

The 1BTF and 2BTF vaults have a concrete floor and space between the waste packages; rock walls and the floor are grouted with concrete. A lid of concrete is placed on top of the waste. The remaining empty space is backfilled with crushed rock. A detailed description of 1–2BTF is given in the **Initial state report**.

For 1BTF and 2BTF, the waste domain is divided into 10 sections, each consisting of three control volumes, for the bottom, the waste and the top domains; as shown in Figure 9-11. An additional discretisation of the concrete constructions and waste is made in the radionuclide transport model. The conceptual descriptions of radionuclide transport modelling for 1BTF and 2BTF are presented in Figure 9-12 and Figure 9-13, respectively.

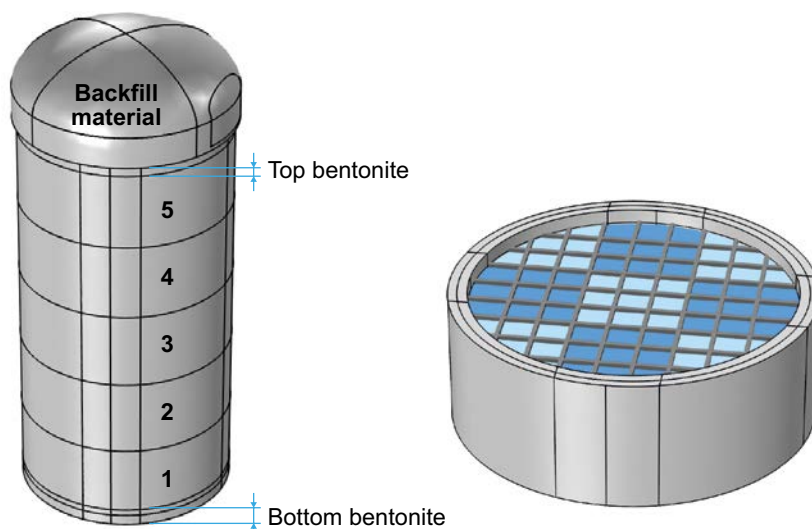


Figure 9-9. Control volumes in the silo model (Abarca et al. 2013).

Four types of model waste packages are used in the model of 1BTF: Concrete tanks with dewatered ion exchange resins, cement-solidified or concrete embedded waste in concrete moulds, ash drums and a reactor tank lid. Two types of model waste packages are used in the model of 2BTF: Concrete tanks with dewatered ion exchange resins and waste in steel containers.

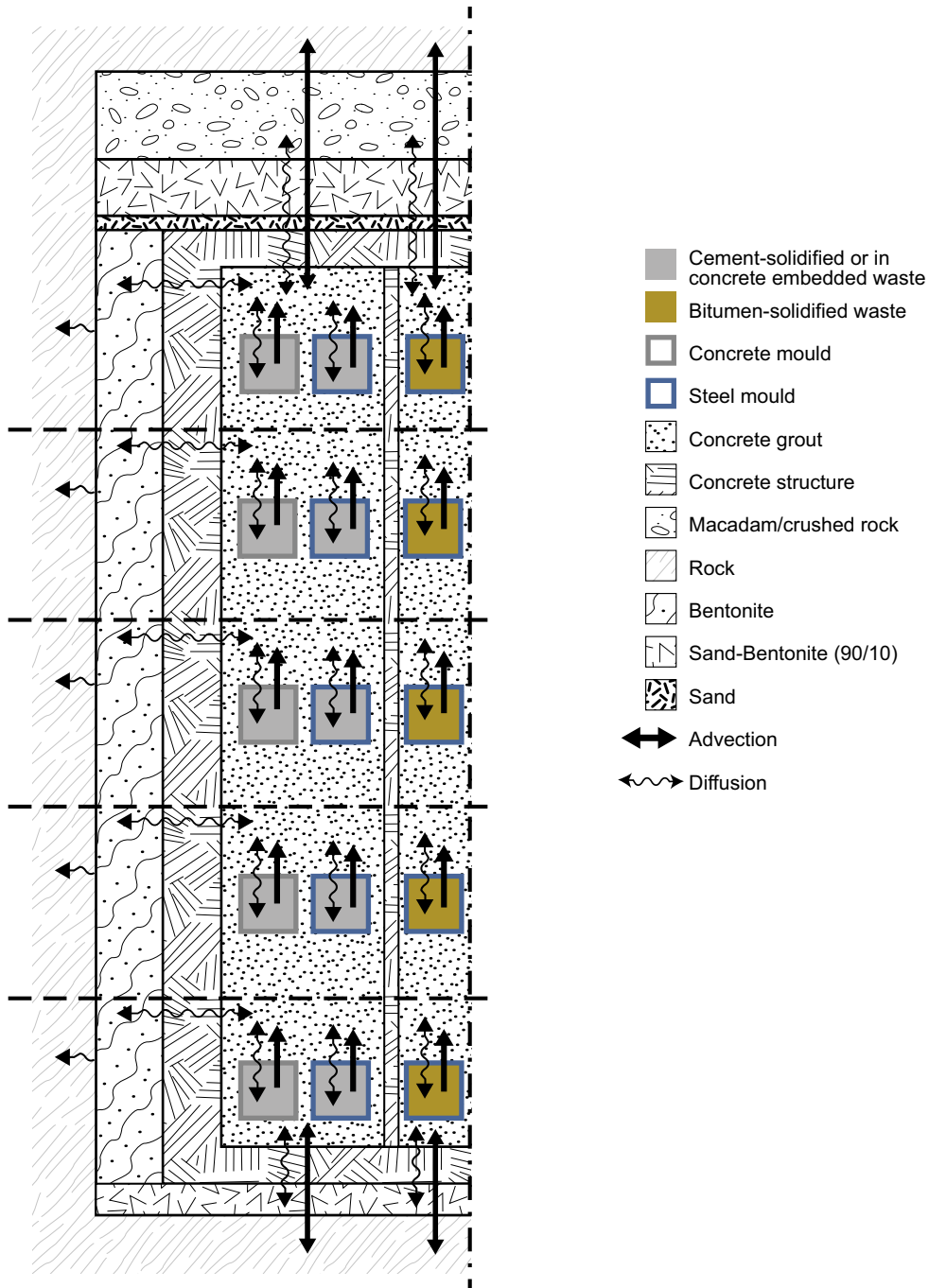


Figure 9-10. Conceptual model of the silo in the radionuclide transport model. The figure shows the three different types of model-waste packages used in the radionuclide transport modelling. From the left: cement-solidified or concrete embedded waste in concrete moulds, cement-solidified or concrete embedded waste in steel packaging and bitumen-solidified waste in steel packaging (figure modified from Lindgren et al. 2001).

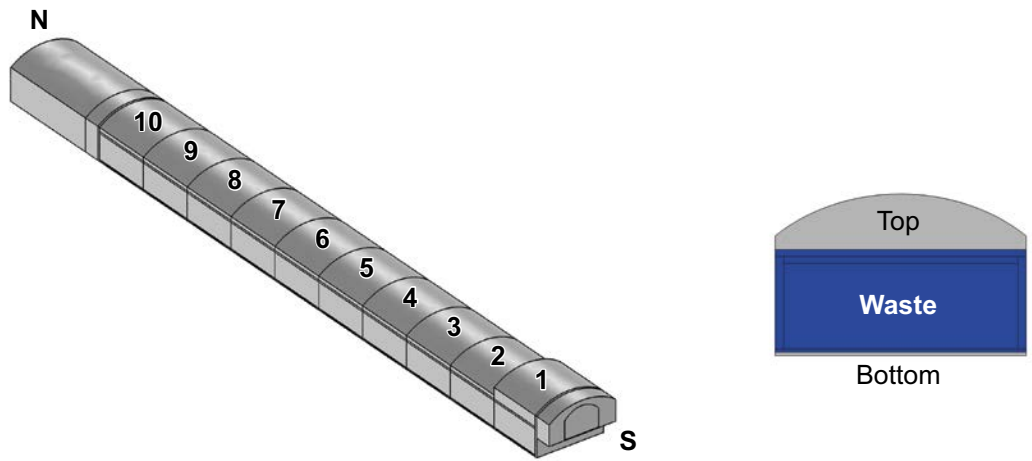


Figure 9-11. Control volumes for the BTF vaults (Abarca et al. 2013).

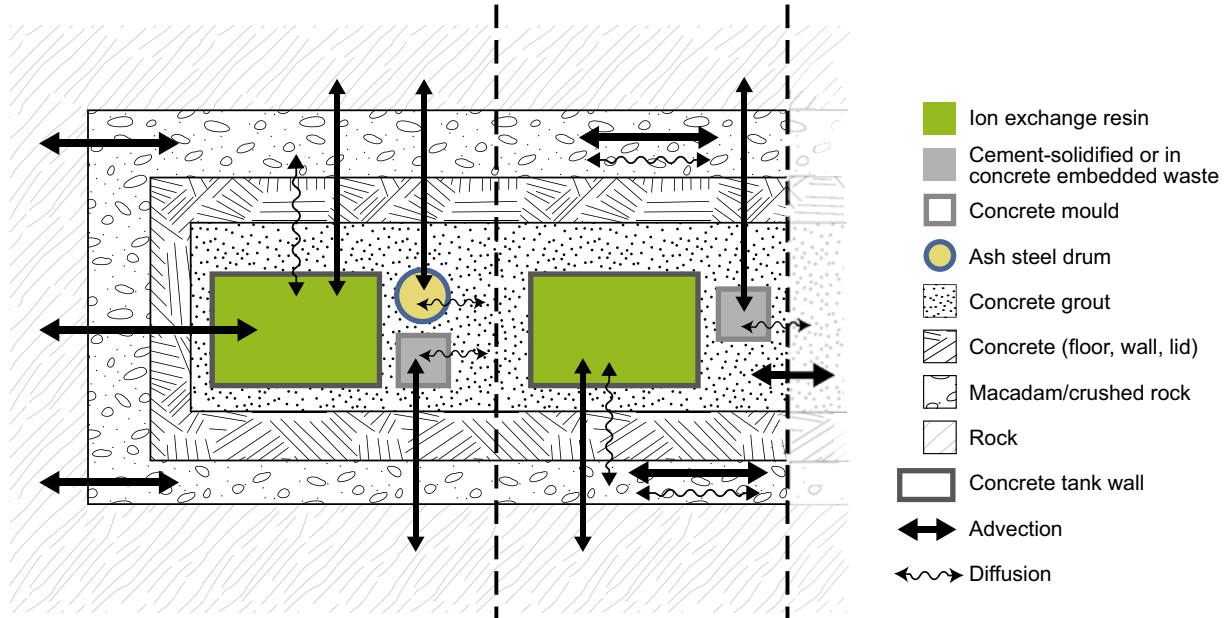


Figure 9-12. Conceptual model of 1BTF in the radionuclide transport calculations. The figure shows the three different types of model-waste packages used in the radionuclide transport model: concrete tanks, ash drums, and cement-solidified or concrete embedded waste in concrete moulds. In the model, there is also a reactor tank lid (not shown in the figure) (figure modified from Lindgren et al. 2001).

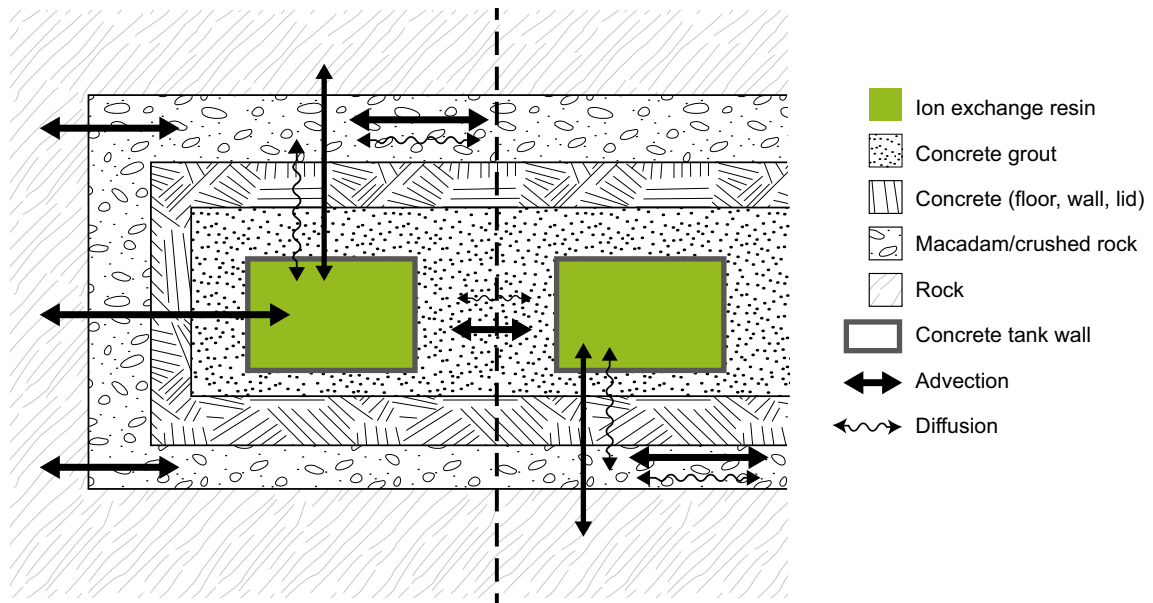


Figure 9-13. Conceptual model of 2BTF in the radionuclide transport calculations. This model contains concrete tanks and a few steel containers (not shown in the picture), figure from Lindgren et al. (2001).

9.3.7 1BLA model

In 1BLA, most of the waste is placed in ISO-containers directly on a concrete floor. A small part of the waste is placed in drums. No backfill or grouting is used in the 1BLA. A detailed description of 1BLA is given in the **Initial state report**.

For 1BLA, a discretisation with 10 sections in the waste domain was made in the radionuclide transport model. The control volumes of 1BLA are shown in Figure 9-14 and the conceptual description of the radionuclide transport modelling is presented in Figure 9-15. Possible sorption that could occur in, for example, the concrete floor is not taken into account in the modelling of radionuclide transport.

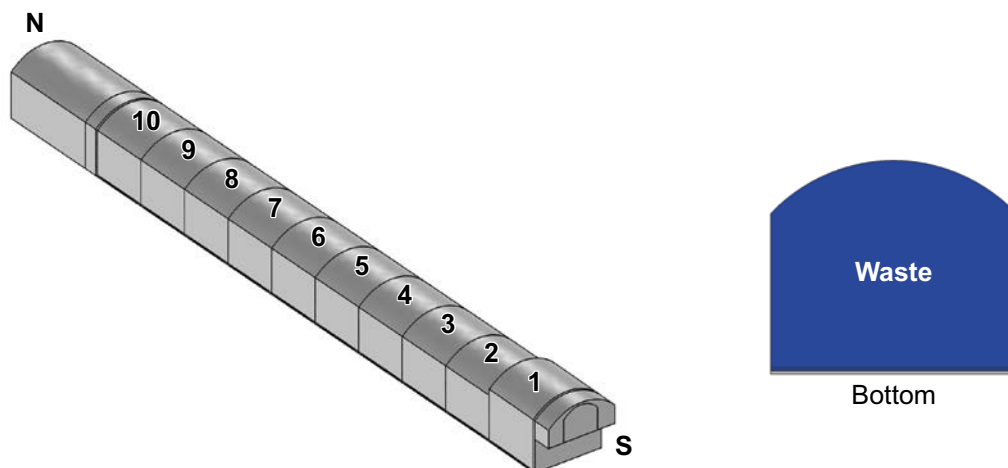


Figure 9-14. Control volumes for 1BLA (Abarca et al. 2013)

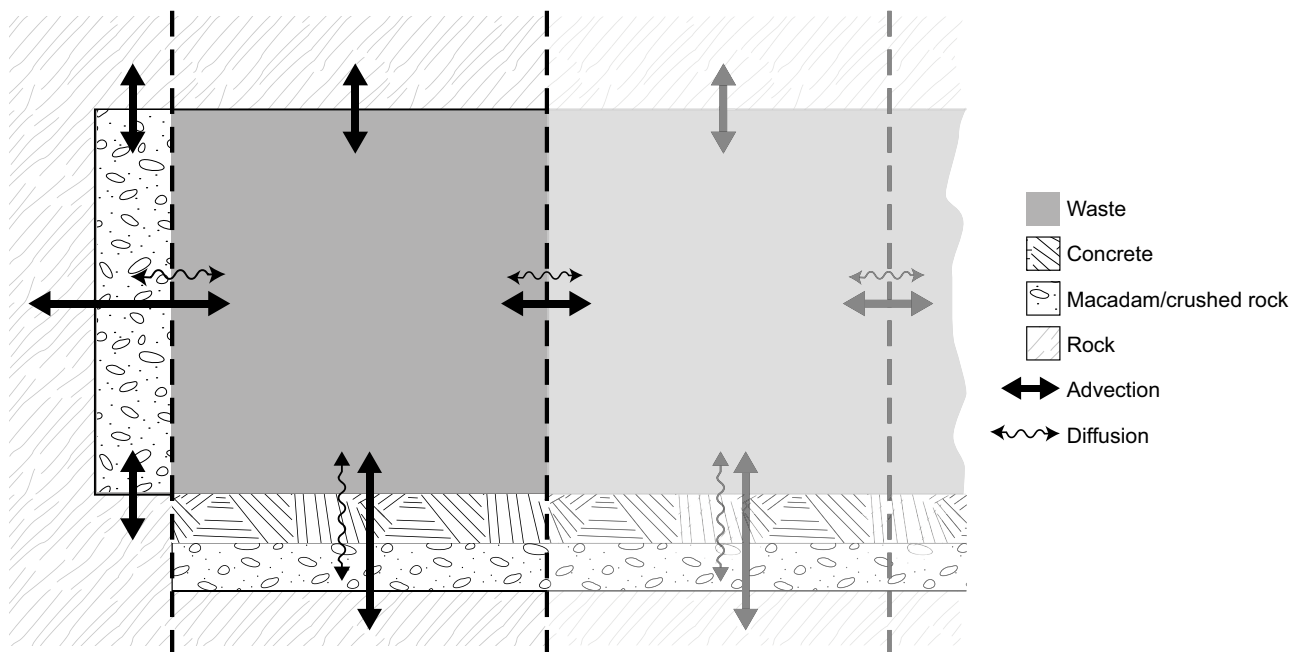


Figure 9-15. Conceptual model of 1BLA in the radionuclide transport calculation. In this model, no detailed division of waste packages is made. The concrete floor under the waste is represented in the model, without taking account of its potential sorption capacity (figure modified from Lindgren et al. 2001).

9.3.8 2–5BLA models

In 2–5BLA, the waste is emplaced in ISO-containers that are placed directly on a concrete floor. No backfilling or grouting is planned for 2–5BLA.

The vaults 2–5BLA will contain mainly low-level decommissioning waste. A detailed description of 2–5BLA is given in the **Initial state report**.

The models for the vaults 2–5BLA are conceptually identical, though they differ with respect to the parameterisation of transfers due to slightly different flows from the hydrologic model. 2–5BLA are waste vaults similar to 1BLA, but for 2–5BLA, a simpler discretisation than the one used for 1BLA was chosen⁹. Only two compartments are used in the model, one representing the waste, and one representing the void above the waste (see Figure 9-16 and Figure 9-17). Possible sorption that could occur in, for example, the concrete floor is not taken into account in the modelling of radionuclide transport.

9.3.9 BRT model

In the waste vault for reactor pressure vessels (BRT), nine reactor pressure vessels from boiling water reactors will be placed. The reactor pressure vessels will be embedded in concrete. The vault will be backfilled with macadam. A detailed description of BRT is given in the **Initial state report**.

The control volumes of BRT are shown in Figure 9-18.

The conceptual description in radionuclide transport modelling is presented in Figure 9-19.

In the model for the BRT vault, the reactor pressure vessels are represented by one compartment each. In addition, there are two more compartments in the model: one representing the concrete structure surrounding the reactor pressure vessels, and one representing the backfill.

The surface contamination on the reactor pressure vessel is assumed to dissolve and be released to the surrounding concrete structure immediately at saturation.

⁹ The design of the models for 2–5BLA was performed later in the project than the design of the models for 1BLA, experience from the 1BLA model showed that a more detailed discretisation does not significantly alter the calculated radionuclide transport.

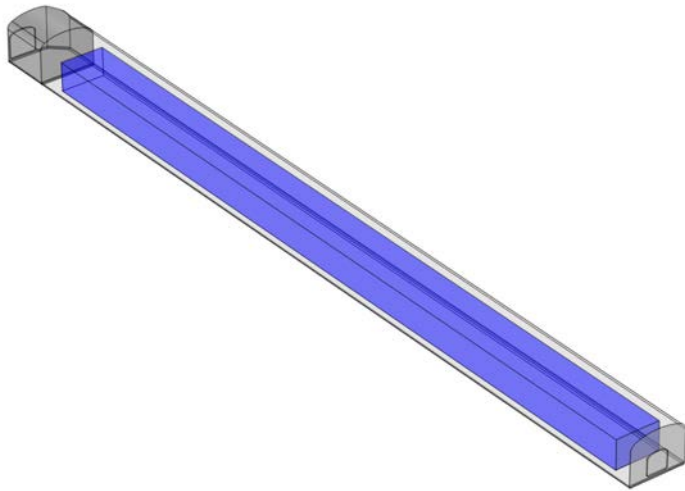


Figure 9-16. Control volumes of a vault of 2-5BLA type. The control volume representing the waste domain is coloured in blue while the surrounding void space is shaded in light grey. The loading area (dark grey) is not represented by compartments in the radionuclide transport model; its presence is accounted for by its impact on water flow (modified from Abarca et al. 2013).

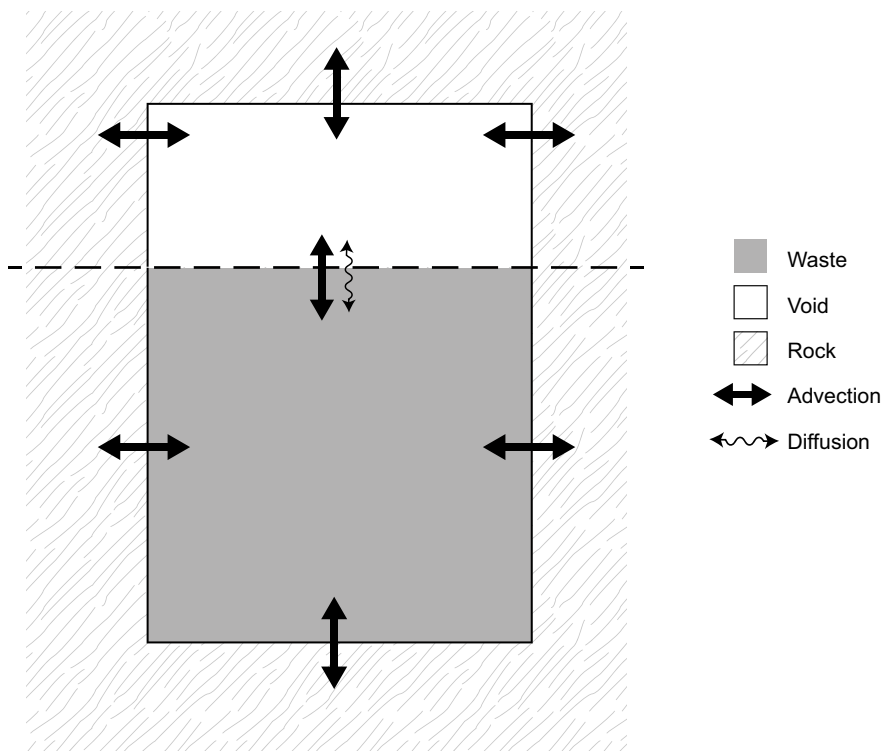


Figure 9-17. Conceptual model of 2-5BLA in the radionuclide transport calculation.

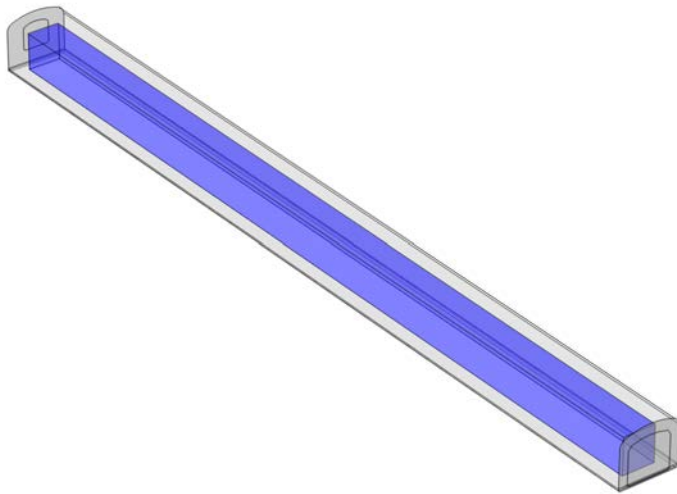


Figure 9-18. Control volumes of the BRT vault with the control volume for the waste domain coloured in blue and the surrounding backfill and concrete shaded in light grey. In the radionuclide transport model the waste domain was further divided into nine compartments each representing one of the pressure vessels (Abarca et al. 2013).

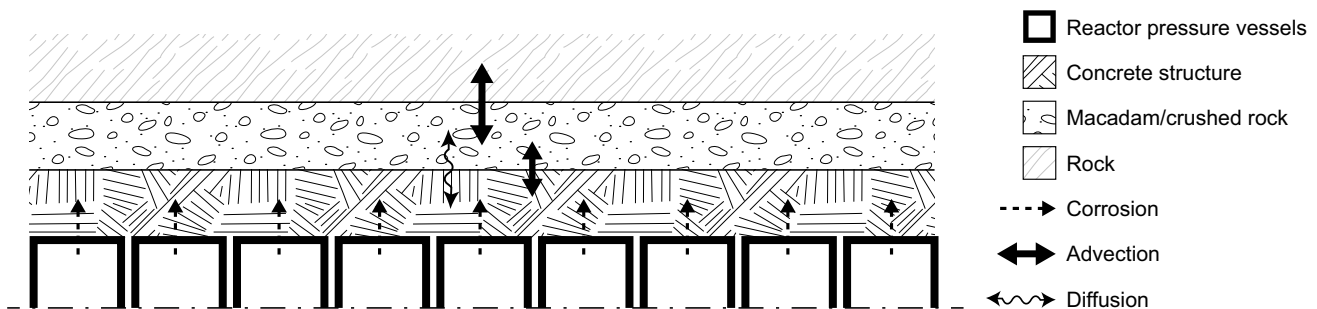


Figure 9-19. Conceptual model of radionuclide transport in the BRT vault. The nine reactor pressure vessels in the waste domain are represented by one compartment each; macadam/crushed rock and the concrete structure are also each represented by a single compartment.

For the induced fraction of the activity, the slow corrosion rate is expected to lead to an important delay in radionuclide release. This delay is expected to be significant for long term safety, and is therefore included in the modelling. The release of induced radionuclides to the surrounding concrete structure is considered to take place congruently with the release of corrosion products of the steel in the reactor pressure vessels (see also Section 9.3.11).

It should be noted that no diffusive resistance is taken into account for the concrete structure, it is modelled as a stirred tank.

9.3.10 Waste packages

Every waste type that is to be disposed in SFR has an approved waste type description (**Initial state report**). These waste type descriptions are also the basis for the estimation of material amounts and radionuclide inventory in the radionuclide transport model. However, it has not been considered necessary to model each waste type with its own model in the radionuclide transport model. Instead a simplified approach is used as described below.

In the near-field hydrological model, the waste packages are not resolved in detail, but rather the interior of the waste domain is assumed to be homogeneous. However, in the near-field radionuclide transport model, the waste packages are represented with more detail in some of the vaults.

In the model for the BRT vault, all the waste “packages” (i.e. the nine reactor pressure vessels) are represented individually, with one compartment each.

The model of the 1BLA vault consists of one single section, modelled as a stirred tank.

In the models of the 2–5BLA vaults each section is modelled as a stirred tank.

For the 1–2BMA, 1–2BTF and silo models, the waste packages are represented in more detail, although still in a simplified way, as it would not be feasible to represent each single waste package separately in the model. There are also more than 50 types of waste packages, which would be difficult and unnecessary in the present context to represent by a dedicated model each. However, as many of the package types are similar, the chosen approach is to group similar package types into one group and represent each of the groups with one representative model waste package type. The representation of waste packages for the 1–2BMA, 1–2BTF and silo models is described below.

Cement-solidified or concrete embedded waste in concrete moulds

This model waste package is represented using three compartments, two for the interior with cement-solidified or concrete embedded waste and one for the concrete mould. These waste packages comprise cement solidified ion-exchange resins and sludge in concrete moulds (BMA and silo), concrete embedded trash and scrap metal in concrete moulds (BMA and silo) and cement-solidified evaporate concentrate in concrete moulds (BMA) from operational waste (**Initial state report**, Table 3-4), and concrete embedded trash and scrap metal in concrete moulds (BMA) from decommissioning waste (**Initial state report**, Table 3-5).

Cement-solidified or concrete embedded waste in steel moulds

This model waste package is represented with two compartments for the interior with cement-solidified or concrete embedded waste. The steel casing is not accounted for in the modelling. These waste packages comprise cement-solidified sludge and ion-exchange resins in steel moulds (silo), cement-solidified ion-exchange resins in steel moulds (BMA and silo) and concrete embedded trash and scrap metal in steel moulds (BMA and silo) from operational waste (**Initial state report**, Table 3-4). These waste packages also comprise cement-solidified ion-exchange resins in steel moulds (silo), concrete embedded trash and scrap metal in steel moulds (BMA) and concrete embedded trash and scrap metal, concrete and sand in tetramoulds (BMA) from decommissioning waste (**Initial state report**, Table 3-5).

Cement-solidified or concrete embedded waste in steel drums

This model waste package is represented with two compartments for the interior with cement conditioned waste, the steel casing is not accounted for in the modelling. These waste packages comprise cement-solidified ion-exchange resins in steel drums (silo), concrete embedded ashes (BTF), trash and scrap metal (BMA) in steel drums from operational waste (**Initial state report**, Table 3-4), and concrete embedded ash in steel drums (BMA) from decommissioning waste (**Initial state report**, Table 3-5).

Bitumen-solidified waste in steel moulds

This model waste package is represented with only one compartment for the interior with bitumen conditioned waste, the steel casing was not accounted for in the modelling. No transport limiting effects are accounted for in this waste type. These waste packages comprise bitumen solidified ion-exchange resins in steel moulds (BMA and silo) from operational and decommissioning waste (**Initial state report**, Tables 3-4 and 3-5).

Bitumen-solidified waste in steel drums

This model waste package is represented with only one compartment for the interior with bitumen-solidified waste, the steel casing is not accounted for in the modelling. No transport limiting effects are accounted for in this waste type. These waste packages comprise bitumen-solidified ion-exchange resins in steel drums (BMA and silo) from operational waste (**Initial state report**, Table 3-4).

Concrete tanks with dewatered ion exchange resins

This model waste package is represented with two compartments, one for the interior with ion-exchange resins and one for the concrete tank walls. These waste packages comprise only the de-watered ion-exchange resins in the concrete tank (BTF) from operational waste (**Initial state report**, Table 3-4).

Solute advection and diffusion in waste packages

Diffusion is accounted for between all parts of the waste packages as well as to/from the surrounding media.

Due to the lack of detailed water flow data in the interior of the waste domains, a simplified approach is taken to estimate the water flow through the waste packages. For grouted waste packages in 1-2BTF, silo and 1-2BMA, all the water flowing into the waste domain is also assumed to flow through the waste packages.

9.3.11 Mathematical model description

All the near-field models take into account advective transport, diffusive transport, decay and ingrowth of radionuclides. The model for the BRT vault also takes into account corrosion induced radionuclide release. Supporting calculations (Appendix B) for 1BMA also take into account solubility limits.

The mathematical description of decay and ingrowth is shown in Equation 9-1. The transfer coefficients used to represent other processes in the models are presented below.

Advection

The advective transfer coefficient between compartments is expressed as:

$$TC_{adv_{ij}}^n = \frac{q_{ij}}{Capacity_i^n} \quad \text{Equation 9-7}$$

where:

$TC_{adv_{ij}}^n$ = advective transfer coefficient for nuclide n from compartment i to j [year^{-1}],

q_{ij} = water flow from compartment i to compartment j [m^3/year],

$Capacity_i^n$ = capacity for nuclide n in compartment i [m^3] (Equation 9-2).

Diffusion

The diffusive transfer between compartments is expressed as a combination of a forward and a backward diffusive transfer:

$$TC_{diff_{ij}}^n = \frac{1}{0.5(res_i + res_j)Capacity_i^n} \quad \text{Equation 9-8}$$

where:

$TC_{diff_{ij}}^n$ = diffusive transfer coefficient for nuclide n from compartment i to j . [year^{-1}],

res_i = diffusive resistance of compartment i ,

$Capacity_i^n$ = capacity for nuclide n in compartment i . [m^3] (Equation 9-2).

Diffusive resistance for a compartment is defined as:

$$res = \frac{L}{AD_e} \quad \text{Equation 9-9}$$

where:

res = diffusive resistance, [year/m^3],

L = length of compartment in assumed direction of diffusion [m],

A = cross sectional area of compartment perpendicular to flow [m^2],

D_e = effective diffusivity for the porous medium in the compartment. [m^2/year].

The resulting diffusive net transport $t_{ij}^{diff,net}$ from compartment i to j is driven by the difference in concentration in both compartments:

$$t_{ij}^{diff,net} = \frac{1}{0.5(res_i + res_j)} \left(\frac{A_i}{Capacity_i} - \frac{A_j}{Capacity_j} \right) \quad \text{Equation 9-10}$$

where:

A_i = Activity in compartment i [Bq].

A waste compartment in a near-field model can represent multiple physical waste packages in the repository. In this case the expression for the diffusive resistance of the model compartment becomes:

$$res = \frac{L}{NAD_e} \quad \text{Equation 9-11}$$

Where:

N = the actual number of waste packages represented by the compartment.

Diffusion into bedrock

The equivalent water flow, Q_{eq} , is used for representing the diffusive transport of radionuclides from the near-field into the far-field, i.e. out from near-field compartments that are in contact with the far-field (host rock). This flow transports dissolved radionuclides, with concentrations equal to the concentrations in the compartment from where releases to the far-field take place. The value of Q_{eq} [m³/y] depends on the size of the contact area, the water flux (Darcy velocity), the flow porosity and the diffusivity as follows (Abarca et al. 2014, Neretnieks et al. 1987):

$$Q_{eq} = A_w \phi_{rock} \sqrt{\frac{4D_w}{\pi t_{res}}} \quad \text{Equation 9-12}$$

where:

A_w = contact area between the compartment and rock [m²],

ϕ_{rock} = flow porosity in rock [-],

D_w = diffusivity of the nuclides in water [m²/year],

t_{res} = residence time of the rock pore water in contact with the compartment [year].

$$t_{res} = \frac{\epsilon_{rock} Length}{DarcyVelocity} \quad \text{Equation 9-13}$$

where:

$Length$ = the length over which the flowing water is in contact with the compartment [m],

$DarcyVelocity$ = the Darcy velocity of water in the rock [m/year].

Corrosion induced radionuclide release

The expressions below describe the yearly release of radionuclides from the steel with a rate corresponding to the amount of nuclides in a thin layer of the steel corroding each year. The reactor pressure vessel is assumed to corrode from both sides.

Radionuclides embedded in the steel are released congruently with corrosion products as the metal corrodes. The transfer is modelled with the following expressions for alkaline (Equation 9-14 and Equation 9-16) and non-alkaline (Equation 9-15 and Equation 9-17) conditions:

$$TC_{corr} = \frac{dec.V1}{\max(1, corrosionTime1 - time)} \quad \text{Equation 9-14}$$

$dec.V1 = 1$ if $time < corrosionTimeOffset$, else $dec.V1 = 0$

$$TC_{corr} = \frac{dec.V2}{\max(1, corrosionTime2 + corrosionTimeOffset - time)} \quad \text{Equation 9-15}$$

$dec.V2 = 1$ if $time \geq corrosionTimeOffset$, else $dec.V2 = 0$

where:

TC_{corr} = transfer coefficient representing release due to corrosion [1/year].

$corrosionTime1$ = time needed for all the steel to corrode under (1) alkaline conditions

$corrosionTime2$ and (2) non-alkaline conditions [year].

$corrosionTimeOffset$ = delay for the start of the corrosion for non-alkaline conditions [year].

$time$ = current time in simulation [year].

Further,

$$corrosionTime1 = \frac{x_{steel}}{2 corrosionRate1} \quad \text{Equation 9-16}$$

$$corrosionTime2 = \frac{x_{steel}}{2 corrosionRate2} \quad \text{Equation 9-17}$$

where:

x_{steel} = steel thickness.

$corrosionRate1$ = corrosion rate for alkaline conditions [m/year].

$corrosionRate2$ = corrosion rate for non-alkaline conditions [m/year].

In the model two logic statement or decision variables ($dec.V1$ and $dec.V2$) are used, that determine which corrosion rate to use at a specific time point. Note that the corrosion rate increases significantly when alkaline conditions end. When the reactor pressure vessel is fully corroded, the denominator in Equation 9-14 and Equation 9-15 becomes 1. This is done in order to prevent errors in the model resulting from division by zero or negative transfer coefficients.

9.4 Far-field model

The conceptual hydrogeological model is shown in Figure 9-20. The model extends approximately 1.5 km in the horizontal directions and 1.1 km in the vertical direction. The geometry of the geosphere is not explicitly considered in the RNT model. The geometry is implicitly represented in the results from the hydrogeological calculations for the geosphere used in the RNT model.

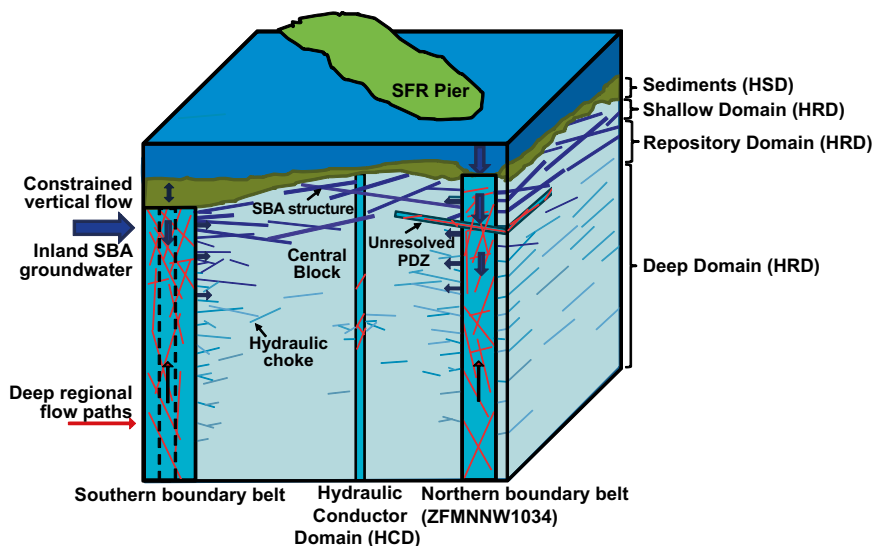


Figure 9-20. Conceptual view of the SFR geosphere used in the hydrogeological modelling. The horizontal and vertical dimensions of this illustration are approximately 1.5 km and 1.1 km, respectively (Odén et al. 2014).

Hydrogeological calculations for the geosphere are performed with the code DarcyTools (Odén et al. 2014). This calculation results in a flow field used for particle tracking from which advective travel-times, t_w , and flow related transport resistance, F , from the different waste vaults of the repository to the biosphere are obtained. These are used in the compartmental RNT model.

The advective travel-time is calculated without taking retardation into account and hence does not directly represent the migration rate of a radionuclide in the geosphere. The retardation of radionuclides is due to two main retardation mechanisms, which are considered in the radionuclide transport modelling: 1) radionuclides in the fracture network enter the internal porous network of the rock matrix by diffusion, and 2) radionuclides are removed from the aqueous phase by sorption.

9.4.1 Conceptual model

The RNT model solves the transport equations along one-dimensional path lines (conceptualised as stream tubes) based on a dual porosity description with advection–dispersion in the mobile phase (flowing water along the rock fracture) and diffusion into the immobile pore water in the rock matrix, where also sorption is considered.

Figure 9-21 shows a schematic view of the discretisation of the geosphere in the radionuclide transport model. Solid blue arrows represent advective transport, dashed blue arrows represent dispersion, and yellow arrows represent diffusion.

In the modelling for SR-PSU, the geosphere is implemented as a compartment model in which the flow wetted area, a_w , is used as a parameter. In the simplified case of a uniform fracture of width W , length L and aperture b , $a_w = 2WL/(Wb)$, the flow related transport resistance, F , is used to calculate flow-wetted surface area, a_w , by dividing it by the travel time, t_w ($a_w = F/t_w$).

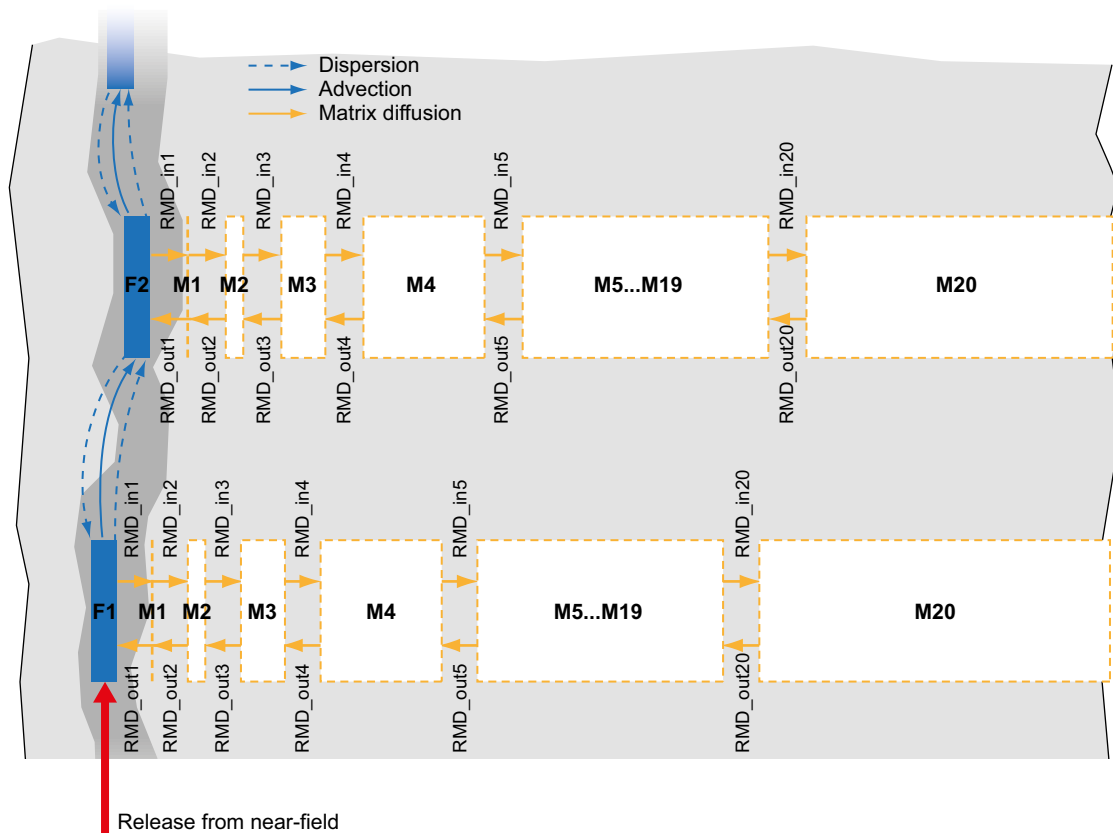


Figure 9-21. Conceptual model of the geosphere. A total of 420 compartments are used in the model. The blue boxes represent the compartments in the model used to represent water-bearing fractures (advection), and the white boxes represent compartments used to represent the rock matrix (diffusion). Solid blue arrows represent advection, dashed blue arrows represent dispersion, and yellow arrows represent diffusion (figure modified from Thomson et al. 2008a).

9.4.2 Processes handled in the RNT model

A large number of physical and chemical processes are identified and analysed for the geosphere of SFR, see the **Geosphere process report**, however only a few of them are relevant for radionuclide transport modelling.

The main radionuclide-transport-related processes identified in the geosphere are:

- Radioactive decay and ingrowth.
- Advection.
- Dispersion.
- Rock matrix diffusion.
- Sorption.

Radioactive decay and ingrowth are included in the modelling described by nuclide-specific decay constants and branching ratios (see Equation 9-1). Sorption in the rock matrix is included in the model, however sorption in the fractures (on e.g. fracture minerals) is, pessimistically, omitted in the model. Advection, dispersion, rock matrix diffusion and sorption in the geosphere are discussed below.

Advective flow

The hydrogeological calculations for the geosphere are performed as steady state calculations for a number of time-points (Odén et al. 2014). The temporal evolution of the groundwater flow used in the radionuclide transport calculations is obtained from an interpolation in time of the results of these simulations.

Dispersion

Dispersion along the individual flow paths is modelled by means of a dispersion term in the RNT model. This term is expressed through the dimensionless Peclet number that quantifies the ratio between advective and dispersive transport (see Equation 9-21).

Rock-matrix diffusion

The exchange between advective transport process in the fracture and the diffusive process in the confining rock matrix is included in the radionuclide transport model. A finite penetration depth for radionuclides, based on fracture half-spacing, is assumed in the model. Matrix diffusion is caused by random movement of radionuclides, which, in the presence of concentration gradients, causes a net movement of a solute. It is assumed here that the pore space of the matrix is connected over distances of possible penetration depth into the matrix, i.e. the matrix is modelled as a continuous porous medium. Thus, it is the fracture half-spacing that governs the penetration depth. Diffusion of a few centimetres into the rock matrix leads to a relevant retardation of radionuclide releases to the surface environment. After entering the pore system of the rock matrix, the solutes may sorb on the extensive pore surfaces. It is important to note that matrix diffusion extends the residence time in the rock, even for radionuclides that do not sorb on the rock matrix.

Sorption

Sorption in the rock matrix is included in the model, whereas sorption in the fractures (on e.g. fracture minerals) is, pessimistically, omitted. Sorption on the rock matrix is modelled using a linear equilibrium approach, based on element (species) specific K_d values, in the same way as for the near-field models (see Section 9.3).

9.4.3 Mathematical model description

The radionuclide transport model for the geosphere was built using the compartment approach. The model is a two-dimensional model of fractured rock, which takes into account advection and dispersion in the main direction of water flow. Diffusion and sorption in the rock matrix are also taken into account. Radionuclide decay and in-growth are considered for all model compartments.

The advantage of using a compartment model, instead of a semi-analytical model such as e.g. FARF31, is that flow parameters can be allowed to vary in space and time. In the modelling for SR-PSU presented here, the water flow varies in time, although it is kept constant in space.

A dual porosity model for radionuclide transport in fractured rock is derived in Norman and Kjellbert (1990). The governing equations are:

$$\frac{\partial C_f^n}{\partial t} = -v \frac{\partial C_f^n}{\partial z} + D \frac{\partial^2 C_f^n}{\partial z^2} - \lambda^n C_f^n + \lambda^n C_f^p + a_w D_e \left. \frac{\partial C_m^n}{\partial x} \right|_{x=0} \quad \text{Equation 9-18}$$

$$\frac{\partial C_m^n}{\partial t} = + \frac{D_e}{R_m^n} \frac{\partial^2 C_m^n}{\partial x^2} - \lambda^n C_m^n + \frac{R_m^p}{R_m^n} \lambda^n C_m^p \quad \text{Equation 9-19}$$

where

C_f^n = the concentration of radionuclide n in the fracture [Bq/m³],

C_f^p = the concentration of parent radionuclide p in the fracture [Bq/m³],

C_m^n = the concentration of radionuclide n in the matrix pore-water [Bq/m³],

C_m^p = the concentration of parent radionuclide p in the matrix pore-water [Bq/m³],

t = time [year],

v = velocity of water in the water bearing fracture [m/year],

D = dispersion coefficient [m²/year],

a_w = flow wetted surface area [m²/m³],

D_e = matrix diffusion coefficient [m²year⁻¹],

z = distance along stream direction [m],

x = penetration depth into matrix [m],

λ^n = decay rate of nuclide n [year⁻¹],

R_m^n = retardation factor for the radionuclide n in the matrix [-] (see also Equation 9-5).

R_m^p = retardation factor for the parent radionuclide p in the matrix [-].

At the boundary between fracture and matrix, i.e. for $x = 0$, the concentration in the fracture coincides with the concentration in the matrix, i.e.:

$$C_f^n(z, t) = C_m^n(z, x = 0, t).$$

The release of radionuclides from the near field into the far-field is modelled by setting the sum of advective and diffusive flow over the cross section of the fracture equal to the near-field release at the inflow boundary. Boundary conditions inside the matrix define the radionuclide flow, driven by diffusion only, to vanish. At the interface to the biosphere, the condition defines the radionuclide flow out of the fracture to be advective only; hence the dispersive flow is defined as zero.

Details of the derivation of transfer coefficients for a compartmental representation of Equation 9-18 and Equation 9-19 are given in Appendix C. Below the resulting transfer coefficients are given.

Advection

The advective transfer between two adjacent fracture compartments i and j is given by the expression:

$$TC_{ijadv} = \frac{v}{L_i} \quad \text{Equation 9-20}$$

where:

TC_{ijadv} = transfer coefficient from compartment i to compartment j [year⁻¹],

L_i = length of compartment i [m].

Dispersion

The transfer coefficient for dispersive transfer between two adjacent fracture compartments i and j is given by the expression:

$$TC_{ijdisp} = \frac{v \left(\frac{L_{tot}}{Pe} - \frac{L_i}{2} \right)}{L_i^2} \quad \text{Equation 9-21}$$

where:

TC_{ijdisp} = transfer coefficient from compartment i to compartment j [year⁻¹],

L_{tot} = total length of the flow path through the geosphere [m],

Pe = Peclet number for the fracture [-],

L_i = length of compartment¹⁰ i [m].

Matrix diffusion

Transfer coefficient for diffusion into the first matrix compartment:

$$TC_{in1diff} = \frac{2a_w D_e}{d_1} \quad \text{Equation 9-22}$$

where:

a_w = the flow wetted surface area [m²/m³],

d_1 = thickness of first matrix compartment [m],

D_e = matrix diffusion coefficient [m²year⁻¹].

Transfer coefficient for diffusion out from the first matrix compartment:

$$TC_{out1diff} = \frac{2D_e}{\phi R_m d_1^2} \quad \text{Equation 9-23}$$

where:

d_1 = thickness of first matrix compartment [m],

D_e = matrix diffusion coefficient [m²year⁻¹],

R_m = retardation in the rock matrix [-],

ϕ = matrix porosity [-].

Transfer coefficient for diffusion between two adjacent deeper matrix compartments i and j :

$$TC_{ijdiff} = \frac{2D_e}{\phi R_m d_i (d_i + d_j)} \quad \text{Equation 9-24}$$

where:

d_i = thickness of source matrix compartment [m],

d_j = thickness of target matrix compartment [m],

D_e = matrix diffusion coefficient [m²y⁻¹],

R_m = retardation in the rock matrix.

ϕ = matrix porosity [-].

9.4.4 Far-field model discretisation

Discretisation of rock matrix

The depth of the matrix compartments was chosen to increase from the fracture away into the bedrock by a constant factor adjusted so that the total depth of the rock matrix equals the maximum penetration depth.

¹⁰In the model used for SR-PSU all compartments are of the same length.

The factor can be found by solving the following equation:

$$\sum_{i=0}^{n-1} x^i d_0 = d_0 \frac{x^n - 1}{x - 1} = D_p \quad \text{Equation 9-25}$$

where:

x = incremental factor [-],

d_0 = depth of the first matrix compartment [m],

n = number of matrix compartments [-],

D_p = maximum penetration depth [m].

For $n = 20$ compartments, a maximum penetration depth D_p of 1.4 m and a depth of the first matrix compartment d_0 of 0.0001 m, Equation 9-25 gives an incremental factor $x \approx 1.5667$.

The choices of thickness of the first matrix compartment and number of compartments have been conducted by comparison of the solution of the compartment model with solutions of the semi-analytical code FARF31 (see Appendix B).

Discretisation along fractures

The advective path through fractures in the rock was divided into 20 fracture compartments of equal length. This choice is also based on comparison with results from FARF31 (see Appendix B).

As mentioned in Section 9.4.1, the F-factor was transformed to flow-wetted surface area for the radionuclide transport model. All fracture compartments were assigned the same flow-wetted surface area and travel time.

9.5 Biosphere model

The surface systems are represented by the radionuclide model for the biosphere (Saetre et al. 2013). This consists of sub-models for radionuclide transport in the (natural) ecosystems and models for the calculation of dose to humans and non-human biota.

The radionuclide transport model for the biosphere is based on the corresponding model used in the SR-Site assessment (SKB 2010a, Avila et al. 2010). The SR-Site model includes: (i) the continuous development of biosphere objects as function of shoreline displacement and succession of ecosystems, (ii) a time-dependent release of radionuclides with groundwater from the geosphere, and their distribution in a heterogeneous landscape, (iii) transport, accumulation and decay of radionuclides with different biogeochemical properties, (iv) transport of radionuclides between different parts of the landscape with water and as a result of terrestrialisation, and (v) exposure and dose calculations for future inhabitants in the landscape (SKB 2010a, Avila et al. 2010, 2013).

The SR-site model has been improved in several ways for the SR-PSU assessment. This has been done to better capture the fate of radiocarbon for more complete estimates of activity concentrations in air, soil and water. Moreover, most exposed groups for the assessment of human exposure have been defined to explicitly reflect the behaviour of self-sustained historical and present communities. In addition, the calculations of dose rates to non-human biota, previously carried out in the ERICA Tool, has been integrated into the Ecolego implementation of the model (see Saetre et al. 2013 for details). Finally, the description of landscape development in the area above the repository has been refined resulting in more precise input data for the calculation cases.

9.5.1 Biosphere objects

The location of discharge areas for groundwater from the repository is based on hydrogeological modelling (Odén et al. 2014). These discharge areas are those parts of the landscape where radionuclides from a potential release from the repository could reach the biosphere, and are referred to as biosphere objects in the present modelling of radionuclide transport and dose. Radionuclides entering a biosphere object with discharging groundwater can be retained there, but may also be

transported with surface and subsurface water to adjacent biosphere objects where they may accumulate and/or be transported further. The biosphere objects identified for SR-SU are shown in Appendix H in the **Main report**. Identification and detailed delineation of biosphere objects and associated catchment areas used in SR-PSU are described in the **Biosphere synthesis report**.

Conceptual models for radionuclide transport to, within and between biosphere objects under submerged (sea-covered) and terrestrial (land) conditions are sketched in Figure 9-22 and Figure 9-23, respectively. These models are used as a basis for modelling transport under temperate climate conditions. In addition, periglacial climate conditions where permafrost restricts groundwater flow and radionuclide transport to certain parts of the geosphere and biosphere are considered. In total, eight biosphere objects are included in the SR-PSU radionuclide transport modelling. One of these is only present in the models for periods with periglacial conditions; the modelling of temperate periods considers seven biosphere objects. However, under temperate conditions nearly the entire discharge of potentially radionuclide-containing groundwater is expected to reach one biosphere object, i.e. object 157_2.

9.5.2 Radionuclide transport model

The radionuclide transport model consists of a number of interconnected biosphere objects. Each biosphere object represents a geographical area that potentially may receive radionuclides from the repository and that undergoes a transformation due to land rise, from a marine ecosystem to a wetland ecosystem. Most biosphere objects also pass through an interconnected lake-mire stage.

To simulate the transport of radionuclides in and between the biosphere objects, a compartmental model is used (Saetre et al. 2013). This approach assumes that the distribution of radionuclides in the biosphere can be represented using a limited number of homogenous and interconnected compartments. This is a highly simplified representation of radionuclide transport in surface ecosystems. However, the effects of radionuclides on humans and non-human biota has to be assessed for releases over time scales of thousands of years and a spatial scale in the order of hectares. Thus, in this context, it is considered as reasonable to represent an ecosystem using temporally and spatially averaged conditions.

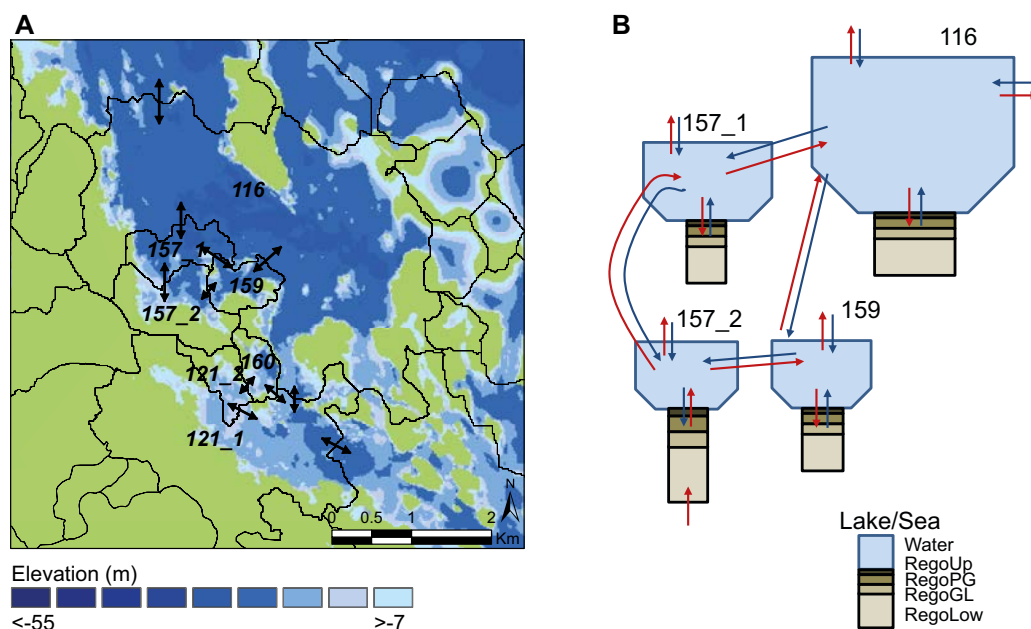


Figure 9-22. Conceptual model of discharge and dispersion of radionuclides that reach the biosphere via groundwater from the geosphere during the marine stage. *A)* Water depth and dispersion between basins at 3000 AD. Biosphere object 157_2 receives radionuclide-containing groundwater from below. All biosphere objects downstream of 157_2 receive radionuclides via surface water flow during the marine stage. *B)* Schematic sketch over the dispersion of radionuclides between regolith layers and surface waters within and between biosphere objects is shown in cross section. Red arrows show dispersion of water containing radionuclides whereas blue arrows show dispersion of water initially without radionuclides. Regolith layers are explained in table 9-1. Note that not all basins and water flows are shown in figure B.

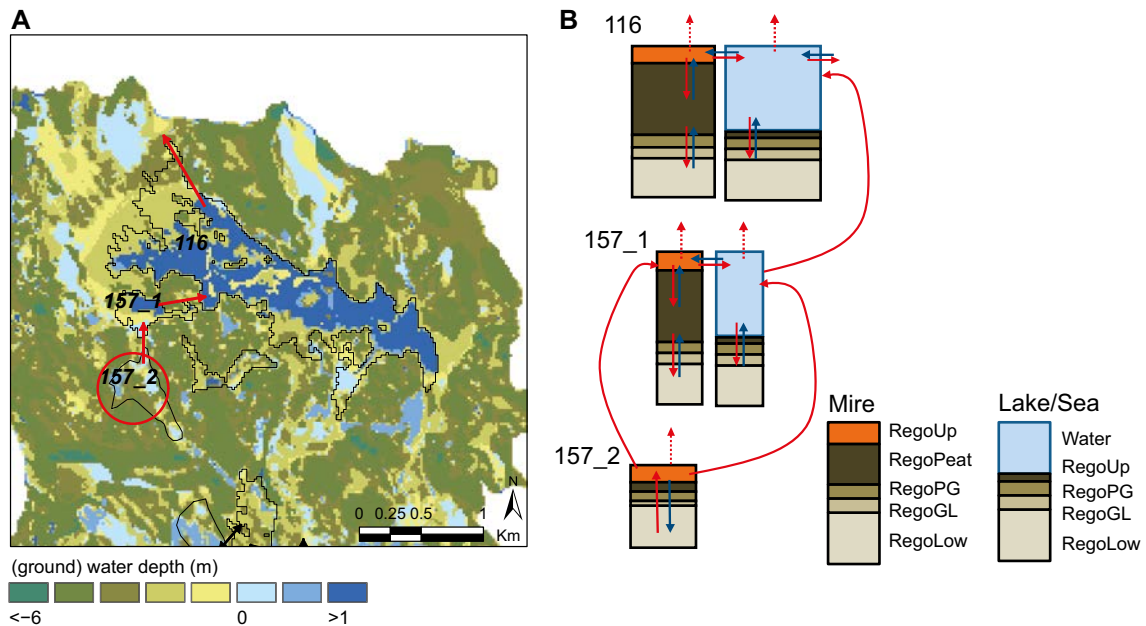


Figure 9-23. Conceptual model of discharge and dispersion of radionuclides that reach the biosphere via groundwater from the geosphere during the terrestrial stage. *A)* Ground water depth in terrestrial areas and water depths in lakes at 5000 AD. The biosphere object 157_2 that receives discharge directly is marked with a red circle. Downstream biosphere objects 157_1 and 116 receive radionuclides via surface water during the terrestrial stage. *B)* Schematic sketch over the dispersion of radionuclides between regolith layers and surface waters within and between biosphere objects is shown in cross section. Red arrows show dispersion of water containing radionuclides whereas blue arrows show dispersion of water initially without radionuclides. Regolith layers are explained in table 9-1.

Two types of ecosystems are simulated: aquatic (sea, lakes and streams) and terrestrial (mire and agricultural ecosystems). The distribution of radionuclides in aquatic ecosystems is represented by six compartments associated with regolith layers, two compartments associated with the water, and one compartment associated with aquatic primary producers (Figure 9-24, Table 9-1). Correspondingly, the distribution of radionuclides in mire ecosystems is represented by eight compartments associated with regolith layers and one compartment associated with the mire vegetation (Figure 9-24, Table 9-1). For agricultural ecosystems, a simpler model is used, which only describes the distribution of radionuclides between an organic compartment and an inorganic compartment in the upper regolith of cultivated land. (Figure 9-25, Table 9-1). The dynamic change in the radionuclide content of each compartment is related to the flows of water, solid matter and gas, and is also due to diffusion, photosynthesis, mineralisation and to radioactive decay and in-growth.

Radionuclides in the model are released to the deepest regolith layer (RegoLow) of biosphere object 157_2 and in the talik simulations to biosphere object 157_1 and 114. The other biosphere objects receive releases of radionuclides via surface water from adjacent biosphere objects. All identified biosphere objects are currently situated below sea-level. Due to shoreline displacement, these areas will in time develop from marine ecosystems to lakes and wetlands. The radionuclide transport model takes into account the natural and continuous succession of the ecosystems by allowing the characteristics of the objects (for example water and soil depth) to change over time, and by connecting aquatic and terrestrial ecosystems (Figure 9-24). The agricultural systems are modelled separately from the natural ecosystems, but taking into account accumulated inventories of radionuclides and radionuclide flows (e.g. induced by fertilising and irrigation) from the natural ecosystems as initial conditions and source terms (Figure 9-25).

The endpoints of the transport modelling are radionuclide concentrations in environmental media, that is, ground- and surface water, the various layers of the regolith (including cultivated soil), mire vegetation (for harvest) and the atmosphere. Humans, plants and animals are then assumed to come into contact with the radionuclides via these media.

Table 9-1. Brief description of compartments representing radionuclide inventories in the radionuclide transport model for the biosphere.

Model compartment	Description
Aquatic	
Water	Radionuclides in open water of sea basins, lakes and streams, including radionuclides dissolved in water and adsorbed to particulate matter.
PM _{org} *	Radionuclides stored in organic particulate matter suspended in the water column.
Prim Prod	Radionuclides stored in aquatic primary producers, including radionuclides in pelagic, microbenthic and macrobenthic primary producers.
RegoUp	Radionuclides in the upper oxic and biologically active layer of aquatic sediments, including radionuclides in pore water and adsorbed on sediment particles.
RegoUp _{org}	Radionuclides incorporated into organic particulate matter in the upper aerobic and biological active layer of aquatic sediments.
RegoPG	Radionuclides in post-glacial aquatic sediments (clay gyttja) below the biological active layer, including radionuclides in pore water and adsorbed on sediment particles.
RegoPG _{org}	Radionuclides incorporated into organic particulate matter in post-glacial aquatic sediments (clay gyttja) below the biological active layer.
RegoGL	Radionuclides in glacial clay (typically overlaid by post-glacial deposits), including radionuclides in pore water and adsorbed on sediment particles.
RegoLow	Radionuclides in till (typically overlaid by glacial clay), including radionuclides in pore water and adsorbed on sediment particles.
Terrestrial (mire)	
PrimProd	Radionuclides stored in mire vegetation biomass, including both above and below ground biomass of bryophytes, vascular plants, dwarf shrubs and trees.
RegoUp	Radionuclides in the upper oxic and biologically active layer of wetland peat (acrotelm peat), including radionuclides in pore water and adsorbed on peat.
RegoUp _{org}	Radionuclides incorporated into organic matter in the upper aerobic and biologically active layer of peat (acrotelm peat).
RegoPeat	Radionuclides in deep, permanently anoxic, wetland peat (catotelm peat), including radionuclides in pore water and adsorbed on peat.
RegoPeat _{org}	Radionuclides incorporated into organic matter in the deep, permanently anoxic wetland peat (catotelm peat).
RegoPG	Radionuclides in post-glacial sediments (clay gyttja) overlaid by wetland peat, including radionuclides in pore water and adsorbed on sediment particles.
RegoPG _{org}	Radionuclides incorporated into particulate organic matter in post-glacial sediments (clay gyttja) overlaid by wetland peat.
RegoGL	Radionuclides in glacial clay buried under wetland peat and typically overlaid by post-glacial deposits. Inventory includes radionuclides in pore water and adsorbed on sediment particles.
RegoLow	Radionuclides in till, buried under wetland peat and typically overlaid by glacial clay. Inventory includes radionuclides in pore water and adsorbed on sediment particles.
Terrestrial (agriculture)	
RegoUp	Radionuclides in the upper layer of agricultural soil (or top soil) influenced by plowing and bioturbation, and where crops primarily take up nutrients and trace elements. This layer is well drained and have a high soil biological activity. Inventory includes radionuclides in pore water and adsorbed on sediment particles.
RegoUp _{org}	Radionuclides incorporated into solid organic matter in the upper layer of agricultural soil.

* Compartment is also referred to as Water_{org} in the technical model description (Saetre et al. 2013).

The distribution of radionuclides in the landscape is simulated by linking the biosphere objects via surface water flows. Parameters that describe the characteristics of the biosphere objects (and their changes over time) and connections in the landscape have been derived from the site investigation programme and simulations of the Forsmark area (Chapters 4 and 6 in the **Main report**).

9.5.3 Exposure of humans and non-human biota

Radionuclide concentrations in soil, water, air and organisms are used to calculate the annual effective dose to humans and dose rate to non-human biota (other organisms). Dose to humans is used in the risk assessment (Chapter 10 in the **Main report**). Doses to humans and other organisms arise from external exposure (radiation from the ground, air and water), inhalation of radionuclides, and ingestion of radionuclides through food and water. Due to the evolution of the repository and of the geosphere, surface systems and climate (Chapter 6 and Sections 7.4.1–7.4.4 in the **Main report**), the concentrations of radionuclides in different environmental media in the surface systems will change over time.

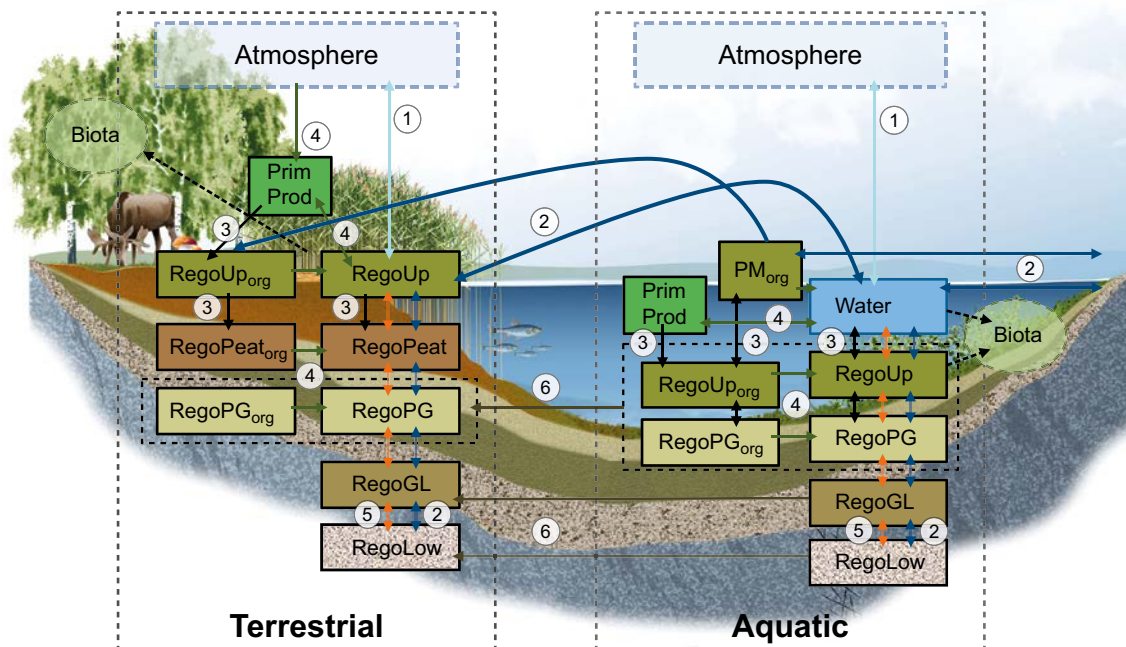


Figure 9-24. A graphical representation of the radionuclide transport model used to simulate transport and accumulation in a discharge area with two natural ecosystems (black dotted boxes). Each box corresponds to a radionuclide inventory associated with a physical compartment. Arrows represent radionuclide fluxes between compartments and fluxes into and out of the system. Radionuclide fluxes are linked to mass fluxes of gas (1, light blue), water (2, dark blue) and solid matter (3, black), to transitions between inorganic and organic forms of radionuclides (4, green), to diffusion in soil pore water (5, orange), and to ingrowth of wetland vegetation (6, green). The atmosphere serves as a source and sink of radionuclides. (Figure 3-1 in Saetre et al. 2013)

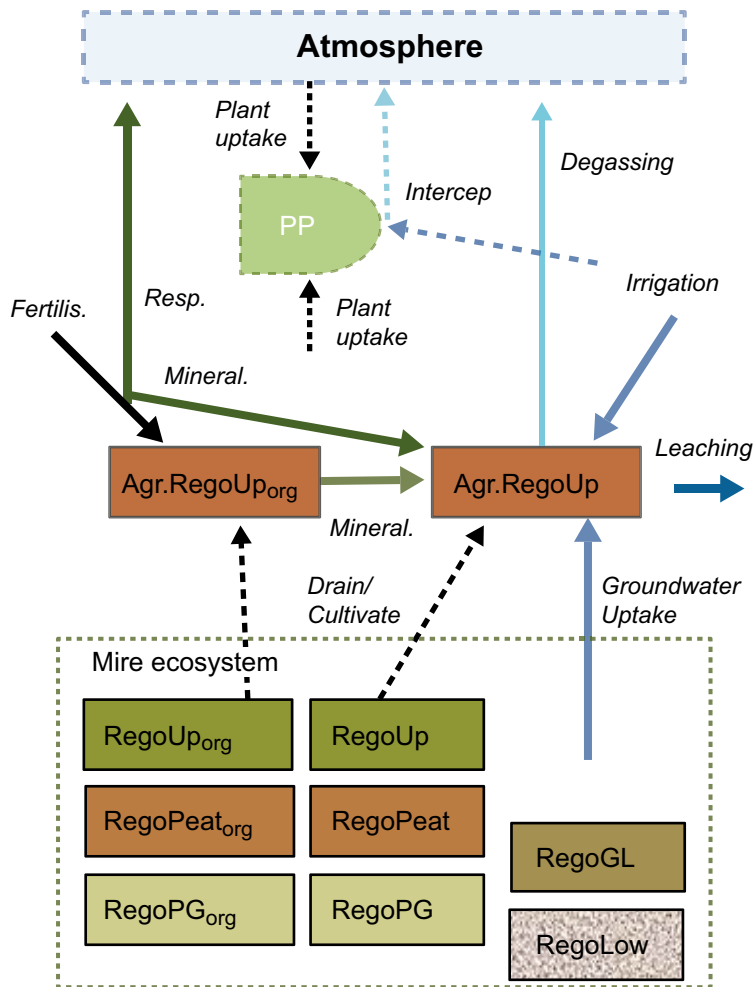


Figure 9-25. Conceptual model of transport and accumulation in cultivated soil. Three different agricultural systems are represented 1) fertilisation with hay/manure (infield-outland agriculture), 2) draining and cultivation of a lake-mire system (industrial age agriculture), and 3) cultivation of an irrigated and fertilised kitchen garden. Boxes and arrows represent radionuclide inventories and radionuclide fluxes, respectively. Dashed arrows represent radionuclide transfers that are not represented as dynamic fluxes in the soil system. Note that the mire ecosystem (green square) provides initial and boundary conditions for cultivation after drainage (see Saetre et al. 2013 for details).

Exposure of humans

In addition to the radionuclide concentrations, dose to humans depends on living habits and diet. Humans can use the land in many different ways, but the highest doses are expected if humans spend time in the land areas with the highest radionuclide concentrations, and drink water and eat food originating from these areas (Figure 9-26). Four different land-use variants have been defined to cover a range of possible future human exposure pathways. The exposed groups are credible bounding cases, reflecting land uses and habits that are reasonable and sustainable with respect to the Forsmark area as well as human physiological requirements. An analysis of exposure pathways resulted in identification of 17 quantitatively relevant exposure routes that were included in the safety analysis by inclusion in one (or more) of the four land use variants (**Biosphere synthesis report**). Figure 9-27 shows the main exposure pathways for the four variants of land use. These are also described below (comprehensive descriptions of the land-use variants and all exposure routes are given in the **Biosphere synthesis report**).

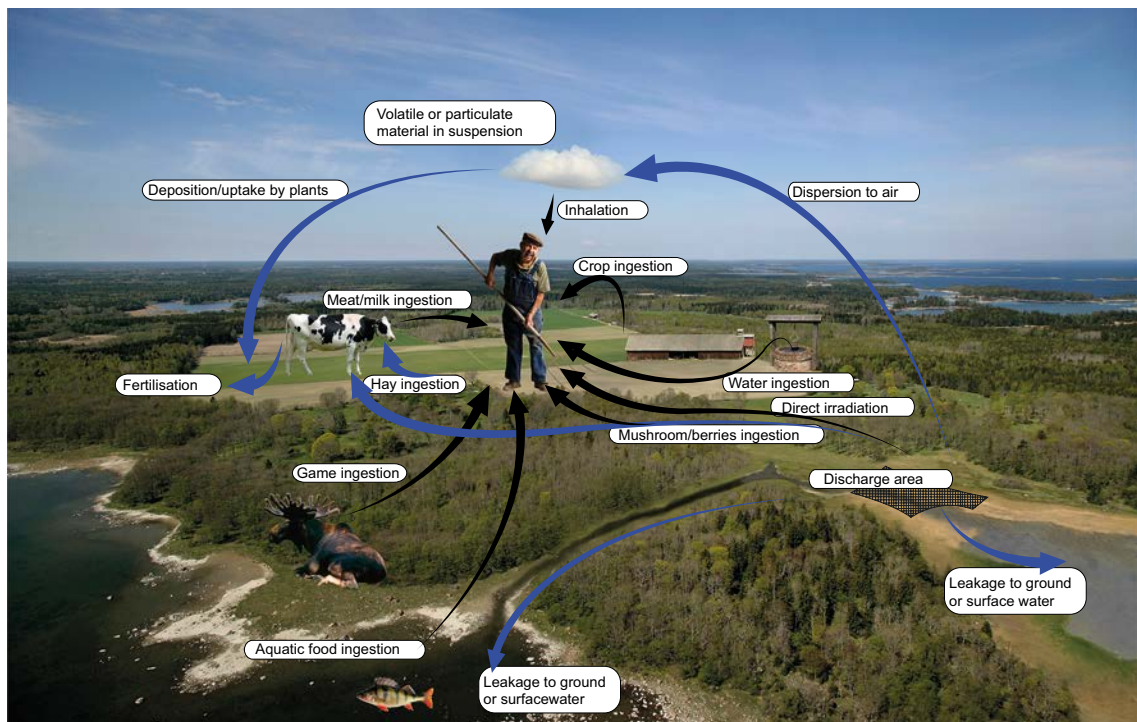


Figure 9-26. Potential exposure pathways for humans.

Hunter-gatherers (HG) – A hunter and gatherer community using the undisturbed biosphere for living space and food. The major exposure pathways are from foraging in the landscape (fishing, hunting, and collecting berries and mushrooms), and from drinking water from surface water (streams or lakes). A typical hunter-gatherer community is assumed to be made up by 30 persons that utilise a forage area of approximately 200 km².

Infield-outland farmers (IO) – Self-sustained agriculture in which infield farming of crops is dependent on nutrients from wetlands used for haymaking (outland). The major exposure pathways are consumption of meat and milk from cattle fed with wetland hay and from drinking water from either a dug well or from surface water in the biosphere object. A self-sufficient community of infield-outland farmers is assumed to be made up by 10 persons. A wetland area of 0.1 km² (10 ha) would be needed to supply winter fodder to the herd of livestock corresponding to the need of manure for infield cultivation of this group.

Drained-mire farmers (DM) – Self-sustained industrial agriculture in which wetlands are drained and used for agriculture (both crop and fodder production). The major exposure pathways are from growing food on land where radionuclides have accumulated for an extended time, and from drinking water from either a well (dug or drilled) or from surface water in the biosphere object. A self-sufficient community of drained-mire farmers is assumed to be made up by 10 persons. A wetland area of 6 ha would be needed for food production.

Garden-plot households (GP) – A type of household that is self-sustained with respect to vegetables and root crops produced through small scale horticulture. The major exposure pathways are consumption of crops from the fertilised garden plot and from using either a well (dug or drilled) or surface water for drinking and irrigation purposes. Exposure from radionuclides released when burning biofuel is also considered in this population. A garden-plot household is assumed to be made up by 5 persons and a 140 m² area garden plot is enough to support the family with vegetables and root crop.

The hunter-gatherer community uses undisturbed ecosystems, whereas the other three groups actively cultivate the land. During marine and periglacial periods, only natural ecosystems can be used for food and water supply. When the shoreline has passed, the possibility of using part of the area for agriculture and water supply (by drilling wells) increases. Wells can be drilled and mires can be drained and used for agriculture when the risk of salt water intrusion decreases, which is

estimated to be when the land is at least 1 m above sea level. In the areas that emerge early from the sea, only minor parts of the newly formed land will have the potential for cultivation due to boulder-rich regolith in the former sea and lake areas (Lindborg 2010), but, for example, in the central parts of Öregrundsgrepen, there are large areas that mainly consist of clay and sand that can be suitable for agriculture (Figure 6-18 in the **Main report**). In the smaller area north of the repository, which is of particular interest in the main scenario (due to discharge from the repository to that location, see Figure 7-3 in the **Main report**), there are small areas where agriculture might be possible.

Exposure of non-human biota

Concerning exposures of plants and animals, one challenge is to limit the number of types of organisms to be included in the analysis. This is discussed in more detail in Jaeschke et al. (2013), where a comprehensive comparison is made between species that have been identified as representative for the Forsmark region and the reference organisms that have been identified in the ERICA Project to represent organism types that can be expected to receive the highest exposures in different ecosystems (Beresford et al. 2007). As described in Saetre et al. (2013), the reference organism concept was applicable in most cases and only a few changes and additions have been made in this assessment in order to capture important site-specific aspects. For example, one small benthic limnic primary producer has been added to represent the microphytobenthos; present in thick layers of the lake sediments of many of the lakes that exist today in the Forsmark area (Andersson 2010). Two site-specific birds and a mammal that utilise aquatic as well as terrestrial habitats have also been added in order to include the combination of exposures from several ecosystem types.

The types of ecosystems and organisms included in the analysis of exposure of non-human biota are described in detail in Chapter 8.

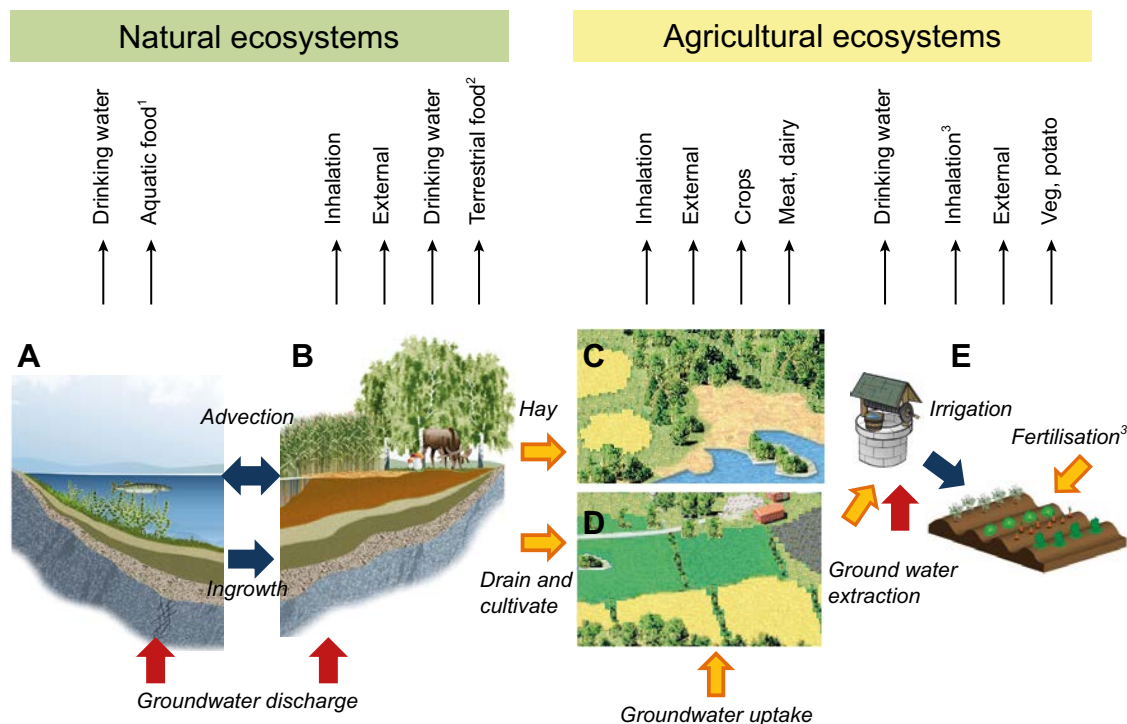


Figure 9-27. Exposure pathways included in the dose calculations for exposed populations using natural resources and/or living in biosphere objects. Hunter-gatherers use natural aquatic (A) and mire (B) ecosystems. The other three exposed populations represented different uses of arable land, namely infield-outland agriculture (C), draining and cultivating the mire (D) and small scale horticulture on a garden plot (E). Bold arrows represent input of radionuclides from the bedrock (red), from natural ecosystems or deep regolith deposits (orange), or water-bound transfer of radionuclides within the biosphere (blue). The thin arrows (top) represent exposure routes. 1 = fish and crayfish, 2 = game, berries and mushrooms, 3 = the exposure pathway inhalation and fertilisation includes radionuclides from combustion of biofuel.

10 Summary and conclusions

This report presents the results from radionuclide transport and dose calculations performed for the long-term safety assessment SR-PSU. The report presents the codes used and the results obtained from the different calculation cases. The report gives an overview of scenarios defined in Chapter 7 of the **Main report** of this safety assessment and presents the calculation cases in detail.

The results presented in this report consist of annual effective doses to a representative individual of the most exposed groups for the defined calculation cases. For the risk assessment presented in the **Main report**, these doses are converted into risk by applying a scale factor of 0.073 per Sievert given by Swedish regulation (SSM 2008:37) and by multiplying with the probability of scenario occurrence (Table 10-1 and Section 7 in the **Main report**). Demonstration of compliance with regulatory requirements is thus presented in the **Main report** whereas this report presents the radiation doses from each calculation case, without taking into account the probability of the scenario. Calculations have also been performed to assess collective doses as a required alternative safety indicator and exposure of non-human biota to assess potential radiological impacts on the environment. The dose calculations were carried out for an assessment period of 100,000 years, wherein the effects of land-uplift and climate change have been taken into account. However, for most calculation cases, the peak doses occur within a few thousand years after closure of the repository.

The presented calculation cases cover a wide range of evolutions and events that might have an impact on the performance of the repository system and the surface system with respect to long-term safety. These are ranked as realistic (for the calculation cases of the main scenario representing the reference evolution), as less probable, and finally as residual with the respective results presented in Chapters 5, 6 and 7. Residual cases illustrate the significance of individual barriers and barrier functions, exposure of humans due to intrusion into the repository, or consequences of external conditions not included in the main scenario, these cases are analyzed regardless of their probability. Hence, the obtained quantitative results from residual cases do not contribute to the assessment of total risk as presented in Chapter 10 of the **Main report**.

Peak doses from less probable cases, however, are weighted by an assumed probability of occurrence, when evaluating risk. Less probable scenarios all have a probability of occurrence below 10%. (see Table 10-1 and Section 7 in the **Main report**). In the case of the *intrusion wells scenario*, the probability is even lower, at only 8×10^{-4} or less, depending on the intruded waste vault considered. Main cases are assumed to be certain, i.e. the probability of occurrence is assumed to be one for the main cases. When implementing all calculation cases, the use of cautious assumptions with regard to uncertain processes and uncertain data makes it highly likely that the resulting doses are overestimated.

Table 10-1. Peak doses to humans, time of occurrence, most exposed group and most contributing radionuclide, in the calculation cases for the main scenario . For the early periglacial calculation case the peak dose applies to only the periglacial period (17,500-20,500AD).

Calculation case	Peak dose [μ Sv]	Year [AD]	Most exposed group	Radionuclide [%]
<i>Global warming calculation case</i>	7.7	6500	DM	Mo-93 (57.7)
<i>Timing of the releases calculation case</i>	8.2	6000	DM	Mo-93 (61.4)
<i>Early periglacial calculation case</i>	0.28	17,800	H&G	I-129 (71.7)

10.1 Calculation cases in the main scenario

Individual doses to humans

Peak annual effective doses for each calculation case in the main scenario are presented in Table 10-1. For the calculation cases in the main scenario that assess individual dose (the *global warming calculation case* (CCM_GW), the *timing of the releases calculation case* (CCM_TR) and the *early*

periglacial calculation case (CCM_EP)) the peak doses are 7.7, 8.2 and 0.28 μSv , respectively. The exposed population with the highest doses are *drained-mire farmers (DM)* in the *global warming calculation case* and the *timing of the releases calculation case*, and *hunters and gatherers (H&G)* in the *early periglacial calculation case*. During the period up to 10,000 AD, the maximum dose is found in object 157_2 and dominated by the radionuclides Mo-93 and organic C-14; these together contribute more than 75% of the peak doses in the *global warming calculation case* and the *timing of the releases calculation case*. In a subsequent period, when the highest doses are found in object 157_1, Ca-41, U-238 and Pa-231 become very important. In a final period, the maximum dose is found again in object 157_2, when Ni-59 is clearly the dominating radionuclide.

Collective doses to humans

The regulations require that collective dose is calculated and reported. In the present assessment, collective dose was calculated for two populations: 1) for the global population for C-14 releases to the atmosphere, which yielded a value of 2.5 manSv and 2) for the Baltic Sea population for radionuclide releases to the Baltic Sea and subsequent exposure of the population by ingestion of fish, which yielded a value of about 0.15 manSv, with a 96% contribution from C-14 and a 3% contribution from Ag-108m.

10.2 Calculation cases in less probable scenarios

Table 10-2 shows the results for the calculation cases in the less probable scenarios where the probability of occurrence is 10% or less.

Doses resulting from irrigation and drinking water extracted from a well drilled directly into a waste vault (the *intrusion wells calculation case*) are the highest calculated in the assessment; the highest peak mean annual dose occurs from intrusion into the 1BLA. The contribution of actinides to peak dose in the individual waste vaults is particularly high in this calculation case; their dominance is controlled by the sorption capacity that prevails in the vault. However, considering the small footprint areas of the release plume and repository, the probability for intrusion wells are very low, and greatly limit the risk.

For the *intrusion wells calculation case*, while the peak annual dose rates were significantly higher (approaching 5,000 μSv) than the doses of other calculation cases, the risk for the corresponding scenario is still below the risk limit, due to the very low probabilities, which are 8×10^{-4} and below, depending on the waste vault (see Chapter 10 in the **Main report**).

10.3 Exposure of non-human biota

Exposure of non-human biota (NHB) from radioactive contaminants has been estimated by calculating absorbed dose rates for most of the calculation cases (see Chapter 8 and Table 7-4 in the **Biosphere synthesis report**). Since all the estimated dose rates, from both deterministic calculations and the probabilistic calculations used for comparison, are well below the proposed screening value of 10 $\mu\text{Gy/h}$ (Beresford et al. 2007, Brown et al. 2008) the conclusion reached is that the repository will not affect biodiversity or sustainable use of biological resources in the Forsmark area.

10.4 Calculation cases in residual scenarios

Several residual calculation cases have been done to illustrate the dose consequences in scenarios that are unlikely to occur, but are of interest to illustrate the significance of individual barriers or the consequences of human intrusion, the consequences of an abandoned repository, or consequences due to alternative climate evolutions not included in the main scenario (see Chapter 2).

Table 10-2. Peak doses to humans, time of occurrence, most exposed group and most contributing radionuclide, in the calculation cases for the less probable scenarios.

Calculation case	Peak dose [μSv]	Year [AD]	Most exposed group	Radionuclide [%]
<i>High inventory calculation case</i>	17.7	7500	DM	Mo-93 (47.3)
<i>High flow in the bedrock calculation case</i>	9.7	6250	DM	Mo-93 (58.1)
<i>Accelerated concrete degradation calculation case</i>	10.6	5550	DM	Mo-93 (59.8)
<i>Bentonite degradation calculation case</i>	7.7	6500	DM	Mo-93 (57.7)
<i>Earthquake calculation case</i>	26.7	4550	DM	Mo-93 (71.1)
<i>High concentrations of complexing agents calculation case</i>	10.7	44,500	DM	Ni-59 (75.7)
<i>Wells downstream of the repository calculation case</i>	15.6	5000	GP	Ac-227 (21.8)
<i>Intrusion wells calculation case</i>				
<i>Silo</i>	1,406	4450	GP	C-14-org (59.9)
<i>1BMA</i>	1,474	4100	GP	Pu-240 (34.0)
<i>2BMA</i>	73	86,000	GP	Po-210 (84.4)
<i>1BTF</i>	145	3250	GP	C-14-org (36.6)
<i>2BTF</i>	194	3850	GP	Pu-240 (40.6)
<i>BRT</i>	39	3250	GP	Ag-108m (63.4)
<i>1BLA</i>	4,524	3050	GP	U-238 (30.3)
<i>2BLA</i>	923	3450	GP	Pu-239 (29.8)
<i>3BLA</i>	897	3400	GP	Pu-239 (29.4)
<i>4BLA</i>	749	3550	GP	Pu-239 (30.5)
<i>5BLA</i>	982	3550	GP	Pu-239 (30.5)

Three residual calculation cases used to illustrate the importance of the different barrier functions are:

- the *loss of barrier function calculation case – no sorption in the repository (CCR_B1)*,
- the *loss of barrier function calculation case – no sorption in the bedrock (CCR_B2)* and
- the *loss of barrier function calculation case – high water flow in the repository CCR_B3*.

The smallest effect on the annual doses among these three cases was found for the *loss of barrier function calculation case – no sorption in the bedrock*. However it is of interest to note that the relative importance of U-235 and U-238 increases in this calculation case relative to the others, due to the assumed loss of retention in the geosphere. This increased dose is mainly due to releases from 1BLA and it shows clearly the importance of the geosphere as a barrier for a waste vault without engineered barriers.

The *loss of barrier function calculation case – no sorption in the repository* and the *loss of barrier function calculation case – high water flow in the repository* show significant increases in the calculated annual doses, in both cases almost an order of magnitude higher than the *global warming calculation case*. This shows the importance of the chemical as well as the hydraulic barrier functions of the near-field in the safety concept.

10.5 Impact of parameter uncertainty

Calculations have been performed in a probabilistic manner, by means of Monte Carlo methods, to study the effects of parameter uncertainties. Figure 10-1 shows, for the peak dose of each calculation case, the mean, median, 5th percentile, 95th percentile, minimum and maximum of the distribution of annual dose as well as the methodological uncertainty (measured by the 95%-confidence interval) of the mean estimate, the result from deterministic calculations are also shown in the figure. The doses to hunters and gatherers, during the periglacial period, in the *early periglacial calculation case* (CCM_EP, third right from y-axis) have the highest uncertainty (due to the bandwidth of parameter ranges). This uncertainty does not jeopardise the demonstration of compliance, because of the low mean value (0.28 μSv) and the 95th percentile being far below the dose constraint.

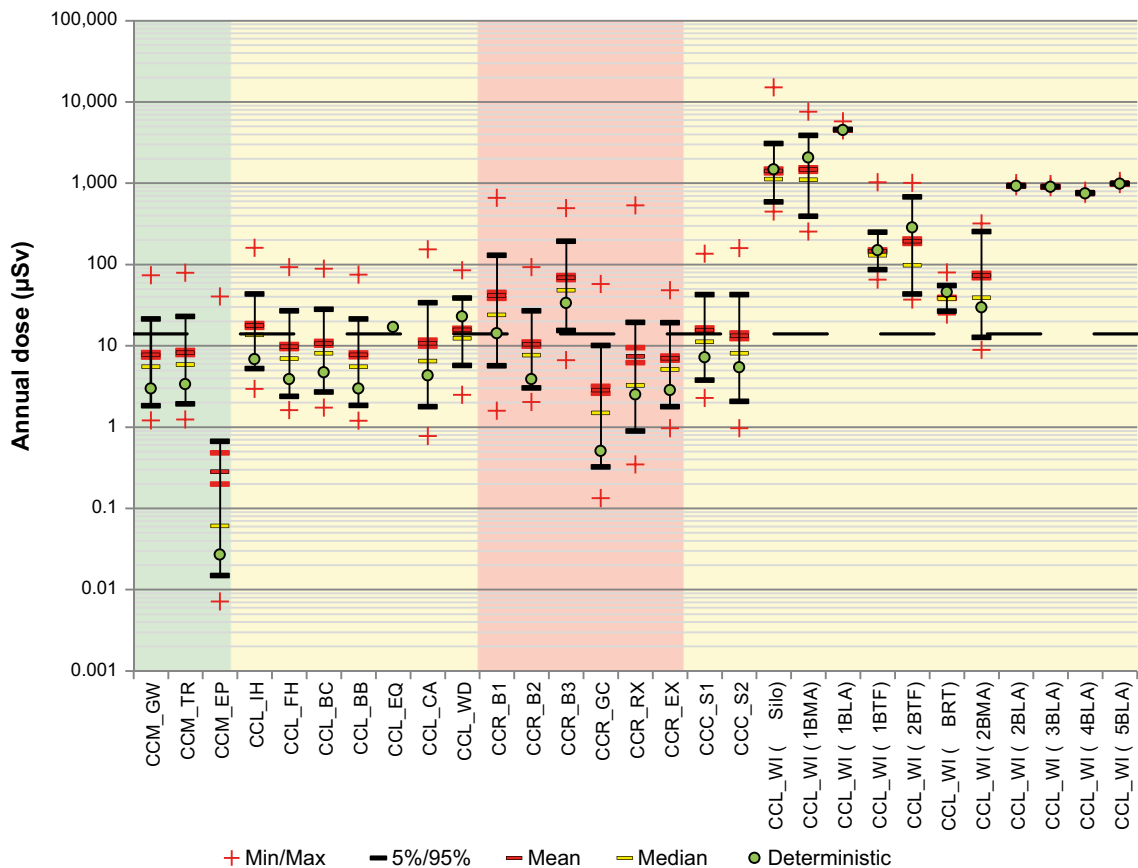


Figure 10-1. Results from all calculation cases; peak mean annual dose (red dashes with black border), deterministic result (green dot), 5 and 95 percentiles (black dashes), minimum and maximum (red crosses), uncertainty of the mean calculated with 95% confidence interval (red dashes). The background colour indicates to which scenario category the calculation case belongs; Main scenario (green), Less probable scenarios (yellow) and Residual scenarios (red).

10.6 Dose contribution from different radionuclides and waste vaults

The relative contributions to peak annual dose from the repository, from specific waste vaults or from specific radionuclides, depend on a number of factors, including: the radionuclide inventory and radiotoxicity of the wastes, the retention capacity of the different waste vaults, and the behaviour of radionuclides in the geosphere and biosphere. In addition, the relative estimates of the dose from different radionuclides or waste vaults are influenced by the degree of conservatism inherent in the assumptions made in the assessment, i.e. assumptions used to model different processes and when assigning values to model parameters. These assumptions may vary between different vaults and radionuclides depending on their (expected) relative importance. Hence, a ranking of the radionuclides in terms of their contribution to the total dose will be conditional on all the above-mentioned factors, and should be seen as valid only for this specific assessment, i.e. it does not necessarily represent the ranking of the “actual” dose contribution from individual vaults and radionuclides.

Figure 10-2 shows the contribution to the peak mean annual doses from different radionuclides. When comparing the two calculation cases for the global warming variant of the main scenario (the *global warming calculation case* (CCM_GW) and the *timing of the releases calculation case* (CCM_TR)) it can be seen that Mo-93 has a slightly larger significance in CCM_TR where the releases starts earlier than in CCM_GW. Apart from this the two calculation cases show similar characteristics, with respect to contribution from radionuclides. In the *early periglacial calculation case* (CCM_EP) on the other hand the contribution from I-129 is clearly dominating, as the peak dose measured here occurs at a much later time point, when releases of I-129 from the silo are relatively more important.

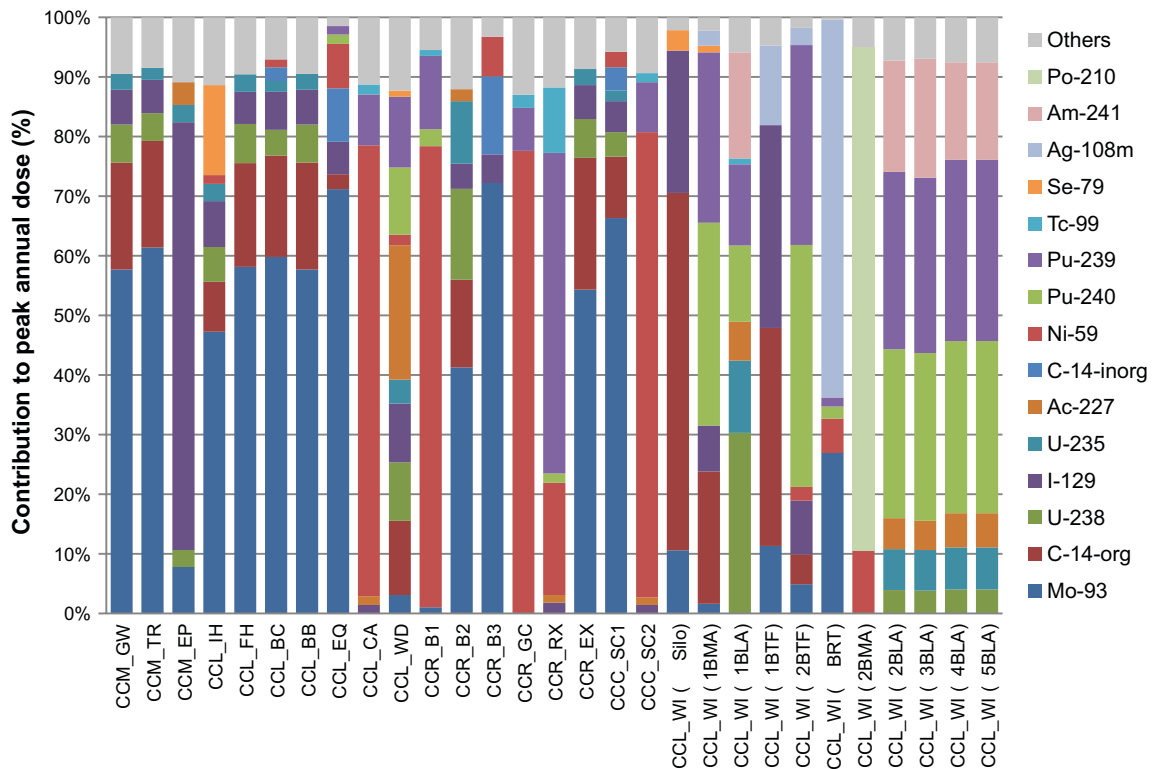


Figure 10-2. Radionuclides with largest contributions to the peak mean annual dose for all calculation cases.

Am-241 is the radionuclide with the highest initial radiotoxicity. However, most of the inventory of Am-241 is disposed in the silo and decays there. Due to the short half-life, low water flow and large sorption capacity in the silo, the dose contribution from Am-241 is insignificant in the main calculation cases.

Figure 10-3 shows the contribution to the peak mean annual doses from different waste vaults. In the two calculation cases for the global warming variant of the main scenario (the *global warming calculation case* (CCM_GW) and the *timing of the releases calculation case* (CCM_TR)) it can be seen that for 1BLA the importance would decrease with an early release, due to early release into the sea providing increased dilution and dispersion for the most dose contributing radionuclides (U-238 and U-235) in 1BLA.

The *wells downstream of the repository calculation case* (CCL_WD) shows significantly increased contributions from 1BLA. This is due to the high concentrations of U-238, U-235 and their progeny that are present in the well water, which is the dominating exposure path in this calculation case.

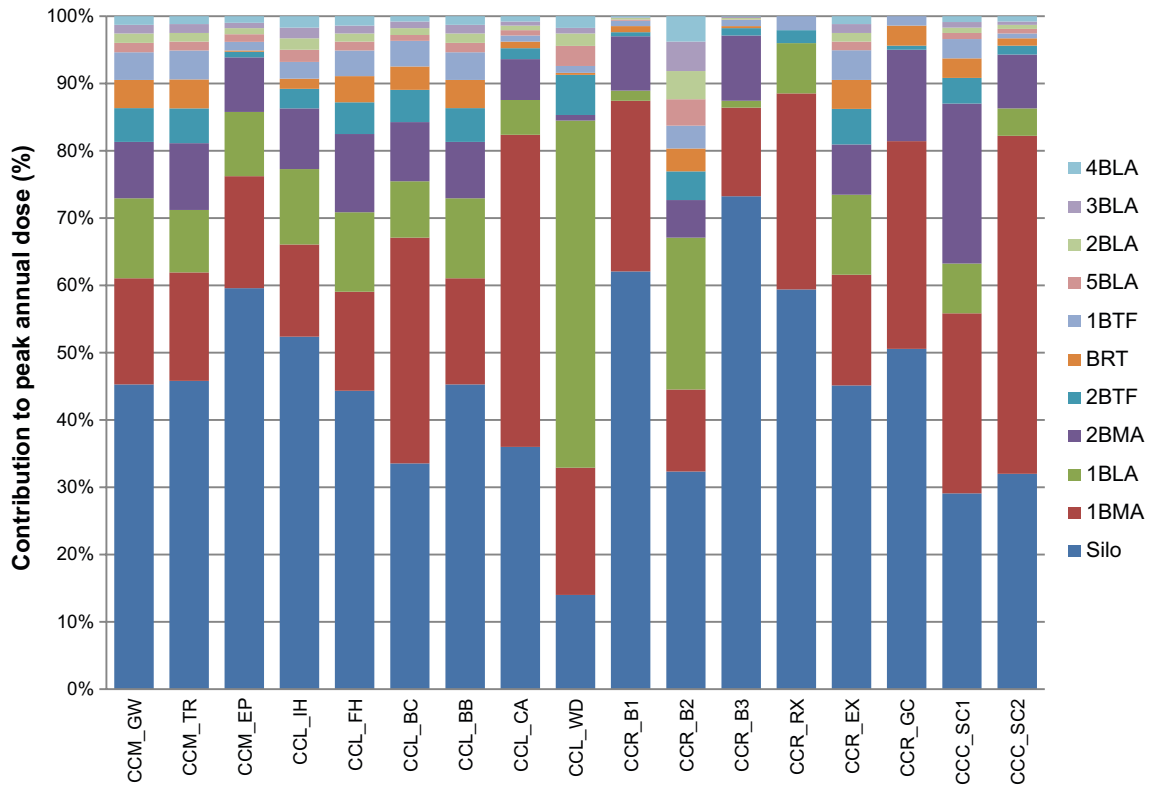


Figure 10-3. Contribution of waste vaults to the peak mean annual dose.

References

SKB's (Svensk Kärnbränslehantering AB) publications can be found at www.skb.se/publications.
References to SKB's unpublished documents are listed separately at the end of the reference list.
Unpublished documents will be submitted upon request to document@skb.se.

References with abbreviated names

Main report, 2014. Safety analysis for SFR. Long-term safety. Main report for the safety assessment SR-PSU. SKB TR-14-01, Svensk Kärnbränslehantering AB.

Barrier process report, 2014. Engineered barrier process report for the safety assessment SR-PSU. SKB TR-14-04, Svensk Kärnbränslehantering AB.

Biosphere synthesis report, 2014. Biosphere synthesis report for the safety assessment SR-PSU. SKB TR-14-06, Svensk Kärnbränslehantering AB.

Climate report, 2014. Climate and climate related issues for the safety assessment SR-PSU. SKB TR-13-05, Svensk Kärnbränslehantering AB.

Data report, 2014. Data report for the for the safety assessment SR-PSU. SKB TR-14-10, Svensk Kärnbränslehantering AB.

FEP report, 2014. FEP report for the safety assessment SR-PSU. SKB TR-14-07, Svensk Kärnbränslehantering AB.

FHA report, 2014. Handling of future human actions in the safety assessment SR-PSU. SKB TR-14-08, Svensk Kärnbränslehantering AB.

Geosphere process report, 2014. Geosphere process report for the safety assessment SR-PSU. SKB TR-14-05, Svensk Kärnbränslehantering AB.

Initial state report, 2014. Initial state report for the safety assessment SR-PSU. SKB TR-14-02, Svensk Kärnbränslehantering AB.

Input data report, 2014. Input data report for the safety assessment SR-PSU. SKB TR-14-12, Svensk Kärnbränslehantering AB.

Model summary report, 2014. Model summary report for the safety assessment SR-PSU. SKB TR-14-11, Svensk Kärnbränslehantering AB.

Waste process report, 2014. Waste form and packaging process report for the safety assessment SR-PSU. SKB TR-14-03, Svensk Kärnbränslehantering AB.

Other public references

Abarca E, Idiart A, de Vries L M, Silva O, Molinero J, von Schenk H, 2013. Flow modelling on the repository scale for the safety assessment SR-PSU. SKB TR-13-08, Svensk Kärnbränslehantering AB.

Abarca E, Silva O, Idiart A, Nardi A, Font J, Molinero J, 2014. Flow and transport modelling on the vault scale. Supporting calculations for the safety assessment SR-PSU. SKB R-14-14, Svensk Kärnbränslehantering AB.

Almkvist L, Gordon A, 2007. Low and intermediate level waste in SFR 1. Reference waste inventory 2007. SKB R-07-17, Svensk Kärnbränslehantering AB.

Andersson E (ed), 2010. The limnic ecosystems at Forsmark and Laxemar-Simpevarp. SKB TR-10-02, Svensk Kärnbränslehantering AB.

Aquilonius K (ed), 2010. The marine ecosystems at Forsmark and Laxemar-Simpevarp. SR-Site Biosphere. SKB TR-10-03, Svensk Kärnbränslehantering AB.

Avila R, Ekström P-A, Åstrand P-G, 2010. Landscape dose conversion factors used in the safety assessment SR-Site. SKB TR-10-06, Svensk Kärnbränslehantering AB.

- Avila R, Kautsky U, Ekström P-A, Åstrand P-G, Saetre P, 2013.** Model of the long-term transport and accumulation of radionuclides in future landscapes. *Ambio* 42, 497–505.
- Beresford N A, Brown J, Copplestone D, Garnier-Laplace J, Howard B, Larsson C-M, Oughton O, Pröhl G, Zinger I, 2007.** D-ERICA: An integrated approach to the assessment and management of environmental risks from ionising radiation. Description of purpose, methodology and application. A deliverable of the ERICA project (FI6RCT-2004-508847). Available at: <https://wiki.ceh.ac.uk/download/attachments/115017395/D-Erica.pdf?version=1&modificationDate=1263814127000&api=v2>
- Bergström U, Nordlinder S, Aggeryd I, 1999.** Models for dose assessments. Modules for various biosphere types SKB TR-99-14, Svensk Kärnbränslehantering AB.
- Bergström U, Avila R, Ekström P-A, de la Cruz I, 2008.** Dose assessments for SFR 1. SKB R-08-15, Svensk Kärnbränslehantering AB.
- Bosson E, Sassner M, Sabel U, Gustafsson L-G, 2010.** Modelling of present and future hydrology and solute transport at Forsmark. SR-Site Biosphere. SKB R-10-02, Svensk Kärnbränslehantering AB.
- Bosson E, Selroos J-O, Stigsson M, Gustafsson L-G, Destouni G, 2013.** Exchange and pathways of deep and shallow groundwater in different climate and permafrost conditions using the Forsmark site, Sweden, as an example catchment. *Hydrogeology Journal* 21, 225–237.
- Brown J E, Alfonso B, Avila R, Beresford N A, Copplestone D, Pröhl G, Ulanovsky A, 2008.** The ERICA Tool. *Journal of Environmental Radioactivity* 99, 1371–1383.
- Brydsten L, Strömgren M, 2010.** A coupled regolith-lake development model applied to the Forsmark site. SKB TR-10-56, Svensk Kärnbränslehantering AB.
- Brydsten L, Strömgren M, 2013.** Landscape development in the Forsmark area from the past into the future (8500 BC – 40,000 AD). SKB R-13-27, Svensk Kärnbränslehantering AB.
- Chu S Y F, Ekström L P, Firestone R B, 1999.** WWW table of radioactive isotopes. Version 2, February 1999. Available at: <http://nucleardata.nuclear.lu.se/toi/>
- Clarhäll, A, 2011.** SKB studies of the periglacial environment – report from field studies in Kangerlussuaq, Greenland 2008 and 2010. SKB P-11-05, Svensk Kärnbränslehantering AB.
- Crawford J, 2013.** Quantification of rock matrix K_d data and uncertainties for SR-PSU. SKB R-13-38, Svensk Kärnbränslehantering AB.
- DiCicio T J, Efron B, 1996.** Bootstrap confidence intervals. *Statistical Science* 11, 189–228.
- Efron B, Tibshirani R J, 1993.** An introduction to the bootstrap. New York: Chapman & Hall.
- Firestone R B, Baglin C M (ed), Chu S Y F (ed), 1998.** Table of isotopes: 1998 update. 8th ed. New York: Wiley.
- Grolander S, 2013.** Biosphere parameters used in radionuclide transport modelling and dose calculations in SR-PSU. SKB R-13-18, Svensk Kärnbränslehantering AB.
- Harrison F L, Anderson S L, 1996.** Taxonomic and development aspects of radiosensitivity. In Amiro B, Avadhanula R, Johansson G, Larsson C M, Luning M (eds). Proceedings of the International Symposium in Ionizing Radiation, Stockholm, 20–24 May 1996. Stockholm: Swedish Radiation Protection Institute (SSI), 65–88.
- Holmén J G, Stigsson M, 2001.** Modelling of future hydrogeological conditions at SFR. SKB R-01-02, Svensk Kärnbränslehantering AB.
- Holzbecher E, 2007.** Environmental modelling using Matlab. Berlin: Springer-Verlag.
- ICRP, 1991.** 1990 Recommendations of the International Commission on Radiological Protection. Oxford: Pergamon. (ICRP Publication 60; *Annals of ICRP* 21 (1–3)).
- ICRP, 2014.** Protection of the environment under different exposure situations. Oxford: Elsevier. (ICRP Publication 124; *Annals of the ICRP* 43(1)).
- Jaeschke B, Smith K, Nordén S, Alfonso B, 2013.** Assessment of risk to non-human biota from a repository for the disposal of spent nuclear fuel at Forsmark. Supplementary information. SKB TR-13-23, Svensk Kärnbränslehantering AB.

- Jörg G, Bühnemann R, Hollas S, Kivel N, Kossert K, Van Winckel S, Gostomski C L, 2010.** Preparation of radiochemically pure ⁷⁹Se and highly precise determination of its half-life. *Applied Radiation and Isotopes* 68, 2339–2351.
- Karlsson S, Bergström U, Meili M, 2001.** Models for dose assessments. Models adapted to the SFR-area, Sweden. SKB TR-01-04, Svensk Kärnbränslehantering AB.
- Keith-Roach M, Lindgren M, Källström K, 2014.** Assessment of complexing agent concentrations in SFR. SKB R-14-03, Svensk Kärnbränslehantering AB.
- Lindborg T (ed), 2010.** Landscape Forsmark – data, methodology and results for SR-Site. SKB TR-10-05, Svensk Kärnbränslehantering AB.
- Lindgren M, Pettersson M, Karlsson S, Moreno L, 2001.** Project SAFE. Radionuclide release and dose from the SFR repository. SKB R-01-18, Svensk Kärnbränslehantering AB.
- Löfgren A (ed), 2010.** The terrestrial ecosystems at Forsmark and Laxemar-Simpevarp. SR-Site Biosphere. SKB TR-10-01, Svensk Kärnbränslehantering AB.
- McKay M D, Beckman R J, Conover W J, 1979.** A comparison of three methods for selecting values of input variables in the analysis of output from a computer code. *Technometrics* 21, 239–245.
- Neretnieks I, Moreno L, 2013.** Flow and transport in fractures in concrete walls in BMA – Problem formulation and scoping calculations. SKB R-13-51, Svensk Kärnbränslehantering AB.
- Neretnieks I, Arve S, Moreno L, Rasmuson A, Zhu M, 1987.** Degradation of concrete and transport of radionuclides from SFR repository for low- and intermediate level nuclear waste. SKB SFR 87-11, Svensk Kärnbränslehantering AB.
- Norman S, Kjellbert N, 1990.** FARF31 – A far field radionuclide migration code for use with the PROPER package. SKB TR 90-01, Svensk Kärnbränslehantering AB.
- Odén M, Follin S, Öhman J, Vidstrand P, 2014.** SR-PSU Bedrock hydrogeology. Groundwater flow modelling methodology, setup and results. SKB R-13-25, Svensk Kärnbränslehantering AB.
- Saetre P, Nordén S, Keesmann S, Ekström P-A, 2013.** The biosphere model for radionuclide transport and dose assessment in SR-PSU. SKB R-13-46, Svensk Kärnbränslehantering AB.
- Schrader H, 2004.** Half-life measurements with ionization chambers – a study of systematic effects and results. *Applied Radiation and Isotopes* 60, 317–323.
- Schroeder L D, Sjoquist D L, Stephan P E, 1986.** Understanding regression analysis: an introductory guide. Beverly Hills, CA: Sage.
- SKB, 2008.** Safety analysis SFR 1. Long-term safety. SKB R-08-130, Svensk Kärnbränslehantering AB.
- SKB, 2010a.** Biosphere analyses for the safety assessment SR-Site – synthesis and summary of results. SKB TR-10-09, Svensk Kärnbränslehantering AB.
- SKB, 2010b.** Model summary report for the safety assessment SR-Site. SKB TR-10-51, Svensk Kärnbränslehantering AB.
- SKB, 2011.** Long-term safety for the final repository for spent nuclear fuel at Forsmark. Main report of the SR-Site project. SKB TR-11-01, Svensk Kärnbränslehantering AB.
- SKB, 2013.** Låg- och medelaktivt avfall i SFR. Referensinventarium för avfall 2013. SKB R-13-37, Svensk Kärnbränslehantering AB. (In Swedish.)
- SKB, 2014.** Handling of biosphere FEPs and recommendations for model development in SR-PSU. SKB R-14-02, Svensk Kärnbränslehantering AB.
- SSMFS 2008:1.** The Swedish Radiation Safety Authority’s regulations concerning safety in nuclear facilities. Stockholm: Strålsäkerhetsmyndigheten (Swedish Radiation Safety Authority).SSMFS 2008:21. The Swedish Radiation Safety Authority’s regulations concerning safety in connection with the disposal of nuclear material and nuclear waste. Stockholm: Strålsäkerhetsmyndigheten (Swedish Radiation Safety Authority).
- SSMFS 2008:37.** The Swedish Radiation Safety Authority’s regulations concerning the protection of human health and the environment in connection with the final management of spent nuclear fuel and nuclear waste. Stockholm: Strålsäkerhetsmyndigheten (Swedish Radiation Safety Authority).

Thomson G, Herben M, Lloyd P, Rose D, Smith C, Barraclough I, 2008a. Implementation of project Safe in AMBER. Verification study for SFR 1 SAR-08. SKB R-08-13, Svensk Kärnbränslehantering AB.

Thomson G, Miller A, Smith G, Jackson D, 2008b. Radionuclide release calculations for SAR-08. SKB R-08-14, Svensk Kärnbränslehantering AB.

Tröjbom M, Grolander S, Rensfeldt V, Nordén S, 2013. K_d and CR used for transport calculation in the biosphere in SR-PSU. SKB R-13-01, Svensk Kärnbränslehantering AB.

UNSCEAR, 2000. Sources and effects of ionizing radiation. Volume I. Report to the General Assembly with Scientific Annexes. United Nations Scientific Committee on the Effects of Atomic Radiation.

Werner K, Sassner M, Johansson E, 2013. Hydrology and near-surface hydrogeology at Forsmark – synthesis for the SR-PSU project. SR-PSU Biosphere. SKB R-13-19, Svensk Kärnbränslehantering AB.

Whicker F W, Schultz V, 1982. Radioecology: nuclear energy and the environment. Boca Raton, FL: CRC Press.

Åstrand P-G, Broed R, Jones J, 2005. Pandora technical description and user guide. Posiva Working Report 2005-64, Posiva Oy, Finland.

Öhman J, Follin S, 2010. Hydrogeological modelling of SFR. Model version 0.2. Site investigation SFR. SKB R-10-03, Svensk Kärnbränslehantering AB.

Unpublished documents

SKBdoc id, version	Title	Issuer, year
1412250 ver 2.0	Ansökansinventarium för mellanlagring av långlivat avfall i SFR (In Swedish.)	SKB, 2014
1427105 ver 4.0	Radionuclide inventory for application of extension of the SFR repository – Treatment of uncertainties	SKB, 2015
1481419 ver 1.0	Ny beräkning av Mo-93 i normkolli till PSU 2015-05 (In Swedish.).	SKB, 2015

Input data

This appendix relates only to near-field and far-field data. The usage and handling of data for the biosphere is described in Grolander (2013) and Saetre et al. (2013).

The main sources of data for the radionuclide transport calculations in the near-field and far-field are the **Data report** and the **Initial state report**. Data (or links to data files) used in modelling activities are compiled in the **Input data report**.

A short description of the use of the data in the modelling is presented below.

A.1 Data handling and quality assurance

The data used in the radionuclide transport modelling are stored together with relevant meta data (authorship, date of change, revision number and source) in Excel spread sheets to facilitate input, review and quality management by modellers as well as the data suppliers (subject experts). These Excel spread sheets were automatically read by the modelling tool (Ecolego). To ensure that the data in supporting documents had been interpreted and handled correctly, the subject experts reviewed the excel files before the final calculations (production runs) were conducted. Intermediate and final versions of the Excel spread sheets were stored in a revision control system with a central server based data repository using the software “Subversion” (<https://subversion.apache.org/>). This handling simplified data access and quality management including tracing of data.

A.2 Near-field data

Geometric data

Pre-processing of geometrical data was avoided as far as possible in the modelling. Hence the calculations of volumes and diffusion-lengths were done in the Ecolego model. The parameters fed into the model correspond as far as possible to the values given in the **Initial state report**.

Inventory

1–5BLA have no detailed representation of the waste packages and hence the total initial inventory of radionuclides was used in the calculation. In the BRT vault, each reactor pressure vessel was represented by an individual source term, which distinguishes induced inventories (from neutron activation) and inventories related to surface contamination.

For some near-field models (silo, 1–2BMA and 1–2BTF) the distribution of the radionuclide inventory in the vault is defined by the assignment of the number of waste packages of the given types to compartments of the waste domain. The distribution of the inventory of radionuclides was then calculated in the Ecolego model. The input data for this calculation are the number of waste packages of each type and the typical initial estimated amounts of radionuclide inventory per waste type (TIA). Hence the input data files contain the number of waste packages of each type (NRWP) and the typical initial amounts per waste type.

The radionuclide inventory in the main scenario is the best estimate inventory presented in Table A-1. TIA is given in the inventory report (SKB 2013, SKBdoc 1481419 (Mo-93)) and NRWP in Table A-1 in the **Initial state report**.

Table A-1. Best estimate radionuclide inventory [Bq] at year 2075 (Initial state report).

Nuclide	1BMA	2BMA	1BTF	2BTF	Silo	1BLA	2-5BLA	BRT	Total
H-3	8.09E+08	3.31E+12	6.82E+07	1.07E+08	8.97E+09	2.00E+08	1.94E+11		3.52E+12
Be-10	2.21E+05	2.19E+04	1.37E+04	2.48E+04	9.89E+05	6.53E+02	1.26E+03		1.27E+06
C-14 org*	1.47E+11	3.96E+09	9.84E+09	6.07E+09	7.56E+11	7.91E+07	2.25E+08		9.23E+11
C-14 inorg*	1.90E+12	1.44E+10	1.89E+11	2.69E+11	2.72E+12	4.03E+09	9.27E+08		5.10E+12
C-14 ind*		5.09E+09					1.19E+09	1.02E+10	1.65E+10
Cl-36	3.34E+08	2.02E+08	1.44E+07	1.66E+07	8.94E+08	2.17E+07	4.60E+07	7.21E+06	1.54E+09
Ca-41		1.56E+10					3.91E+09		1.95E+10
Fe-55	5.35E+10	1.05E+11	8.33E+07	1.14E+08	2.73E+12	8.78E+06	4.45E+08	1.49E+10	2.91E+12
Co-60	4.08E+11	1.99E+12	1.67E+10	2.36E+10	1.29E+13	1.03E+09	2.59E+10	1.93E+11	1.55E+13
Ni-59	2.10E+12	9.50E+11	3.31E+10	3.83E+10	6.85E+12	3.99E+09	1.15E+10	1.60E+11	1.01E+13
Ni-63	1.47E+14	9.23E+13	2.04E+12	2.27E+12	5.48E+14	3.04E+11	1.12E+12	1.44E+13	8.07E+14
Se-79	2.10E+08	7.29E+06	1.57E+07	1.54E+07	1.05E+09	4.00E+05	5.94E+06		1.31E+09
Sr-90	5.49E+11	3.60E+11	3.48E+10	5.76E+10	3.61E+12	7.42E+08	2.40E+10	2.32E+10	4.66E+12
Zr-93	3.68E+08	1.06E+09	2.29E+07	4.14E+07	4.48E+09	1.09E+06	2.95E+07	1.84E+08	6.19E+09
Nb-93m	1.73E+10	1.31E+13	1.44E+09	2.35E+09	9.33E+12	7.68E+07	1.34E+11	1.06E+12	2.36E+13
Nb-94	3.67E+09	9.12E+10	2.53E+08	4.13E+08	8.67E+10	3.14E+07	9.81E+08	7.94E+09	1.91E+11
Mo-93	1.46E+09	4.52E+09	2.56E+08	2.36E+08	1.96E+10	1.01E+08	9.01E+07	3.00E+09	2.93E+10
Tc-99	6.22E+09	1.42E+09	2.30E+09	5.45E+08	5.00E+10	1.85E+09	4.98E+08	4.49E+08	6.32E+10
Pd-107	5.25E+07	2.55E+09	3.92E+06	3.86E+06	2.75E+08	1.00E+05	1.72E+06		2.89E+09
Ag-108m	1.95E+10	4.06E+10	1.51E+09	2.21E+09	2.30E+11	1.94E+08	1.53E+09	1.62E+09	2.97E+11
Cd-113m	7.98E+08	9.32E+07	7.67E+07	6.34E+07	9.58E+09	1.96E+06	6.13E+06		1.06E+10
In-115		3.13E+05							3.13E+05
Sn-126	2.62E+07	1.75E+07	1.96E+06	1.93E+06	2.05E+08	5.00E+04	7.93E+06	7.53E+05	2.62E+08
Sb-125	4.37E+07	2.62E+08	7.47E+06	1.04E+07	1.32E+11	4.74E+05	4.46E+06	1.34E+07	1.32E+11
I-129	1.46E+08	7.67E+06	2.27E+07	1.02E+07	9.84E+08	4.35E+05	1.94E+06		1.17E+09
Cs-134	1.45E+08	2.26E+08	7.10E+04	8.86E+04	2.20E+11	1.58E+04	1.39E+06		2.20E+11
Cs-135	8.41E+08	5.33E+07	1.03E+08	1.85E+07	4.47E+09	3.07E+06	1.75E+08		5.67E+09
Cs-137	8.15E+12	8.95E+11	7.12E+11	6.22E+11	5.97E+13	1.84E+10	4.95E+11		7.05E+13
Ba-133	4.89E+07	1.43E+08	4.03E+06	6.19E+06	6.16E+08	2.20E+05	1.26E+07		8.31E+08
Pm-147	3.71E+08	4.06E+08	3.84E+06	4.57E+06	3.59E+11	3.02E+05	1.19E+06	1.37E+06	3.60E+11
Sm-151	8.26E+10	3.55E+10	6.51E+09	6.13E+09	4.63E+11	1.68E+08	5.88E+09	3.42E+08	6.00E+11
Eu-152	9.47E+07	1.33E+11	6.19E+07	6.54E+06	8.64E+08	1.02E+08	1.73E+10	5.41E+05	1.52E+11
Eu-154	2.33E+10	6.83E+09	1.98E+09	1.80E+09	5.24E+11	4.01E+07	2.67E+08	9.27E+07	5.59E+11
Eu-155	1.02E+09	3.74E+08	4.96E+07	5.83E+07	9.96E+10	1.54E+06	1.16E+07	2.40E+06	1.01E+11
Ho-166m	1.41E+09	5.22E+08	8.79E+07	1.59E+08	6.83E+09	4.18E+06	9.03E+07	7.99E+03	9.10E+09
U-232	8.85E+04	1.46E+05	1.62E+04	6.73E+03	6.20E+05	2.34E+03	9.35E+03	6.86E+03	8.96E+05
U-234	6.66E+06	3.04E+06	9.86E+05	4.55E+05	3.58E+07	1.33E+05	4.38E+05		4.75E+07
U-235	3.00E+06	7.82E+04	1.84E+07	1.12E+05	1.42E+07	2.98E+08	3.23E+08	1.49E+01	6.57E+08
U-236	2.64E+06	6.00E+06	4.02E+05	3.55E+05	1.58E+07	3.99E+04	2.06E+05	3.92E+05	2.59E+07
U-238	5.95E+06	1.23E+06	8.55E+05	8.75E+05	3.28E+07	7.33E+08	1.77E+08		9.52E+08
Np-237	2.73E+07	7.68E+06	1.07E+06	1.98E+06	5.36E+08	6.75E+04	2.61E+05	4.70E+05	5.75E+08
Pu-238	7.52E+09	4.42E+10	2.09E+09	4.56E+08	7.29E+10	3.47E+08	1.52E+09	2.72E+09	1.32E+11
Pu-239	2.77E+09	6.78E+09	4.68E+08	1.89E+08	1.70E+10	6.60E+07	2.77E+08	4.16E+08	2.80E+10
Pu-240	3.87E+09	9.21E+09	5.20E+08	2.65E+08	2.39E+10	6.74E+07	2.95E+08	5.92E+08	3.87E+10
Pu-241	2.40E+10	1.66E+11	7.30E+09	2.42E+09	3.07E+11	1.29E+09	5.74E+09	9.05E+09	5.23E+11
Pu-242	2.00E+07	5.02E+07	2.96E+06	1.37E+06	1.23E+08	3.99E+05	1.71E+06	3.11E+06	2.03E+08
Am-241	2.91E+10	4.12E+10	6.14E+09	1.83E+09	2.32E+13	5.23E+08	1.94E+09	1.99E+09	2.32E+13
Am-242m	4.46E+07	1.83E+08	7.34E+06	3.21E+06	3.22E+08	1.02E+06	4.84E+06	1.32E+07	5.79E+08
Am-243	2.02E+08	6.62E+08	3.25E+07	1.78E+07	1.60E+09	4.00E+06	1.86E+07	4.14E+07	2.57E+09
Cm-243	1.85E+07	1.03E+08	3.82E+06	4.15E+05	1.89E+08	7.58E+05	3.40E+06	6.38E+06	3.25E+08
Cm-244	6.73E+08	1.07E+10	2.68E+08	2.84E+07	9.26E+09	5.39E+07	2.80E+08	6.76E+08	2.19E+10
Cm-245	1.99E+06	1.01E+07	2.95E+05	1.36E+05	1.49E+07	3.97E+04	2.18E+05	6.83E+05	2.84E+07
Cm-246	5.27E+05	3.34E+06	7.82E+04	3.60E+04	4.29E+06	1.05E+04	6.61E+04	2.24E+05	8.58E+06
Total	1.60E+14	1.14E+14	3.06E+12	3.30E+12	6.72E+14	3.38E+11	2.05E+12	1.59E+13	9.71E+14

* C-14 has been divided into organic (org), inorganic (inorg) and induced activity (ind).

Table A-2. High radionuclide inventory [Bq] at year 2075 (calculated from the best estimate inventory including uncertainties (95th percentile) (Initial state report)).

Nuclide	1BMA	2BMA	1BTF	2BTF	Silo	1BLA	2-5BLA	BRT	Total	Ratio**
H-3	4.06E+10	2.02E+13	3.41E+09	5.38E+09	4.57E+11	1.01E+10	5.43E+11		2.12E+13	6.04
Be-10	1.11E+07	9.85E+05	6.88E+05	1.24E+06	4.98E+07	3.42E+04	2.49E+04		6.38E+07	50.2
C-14-org*	2.01E+11	7.49E+09	1.35E+10	8.31E+09	1.04E+12	1.08E+08	1.21E+09		1.27E+12	1.38
C-14-inorg*	2.60E+12	2.63E+10	2.58E+11	3.67E+11	3.75E+12	5.51E+09	4.98E+09		7.01E+12	1.37
C-14-ind*		1.76E+10					6.41E+09	1.85E+10	4.26E+10	2.59
Cl-36	6.67E+08	8.00E+08	4.81E+07	4.06E+07	3.91E+09	2.88E+07	1.13E+08	1.31E+07	5.63E+09	3.66
Ca-41		6.07E+10					1.01E+10		7.08E+10	3.63
Fe-55	2.72E+11	4.65E+11	4.17E+08	5.71E+08	1.52E+13	5.05E+07	2.64E+09	2.72E+10	1.59E+13	5.48
Co-60	4.74E+11	3.74E+12	1.71E+10	2.41E+10	2.40E+13	2.01E+09	1.66E+11	3.51E+11	2.88E+13	1.85
Ni-59	6.30E+12	2.12E+12	1.03E+11	1.16E+11	2.09E+13	1.27E+10	6.62E+10	2.91E+11	2.99E+13	2.95
Ni-63	4.40E+14	2.02E+14	6.43E+12	6.88E+12	1.67E+15	9.57E+11	6.57E+12	2.62E+13	2.36E+15	2.93
Se-79	1.05E+10	3.77E+08	7.86E+08	7.71E+08	5.30E+10	2.06E+07	5.84E+07		6.55E+10	50.2
Sr-90	7.27E+11	8.68E+11	5.14E+10	1.29E+11	5.16E+12	2.92E+09	1.80E+11	4.23E+10	7.16E+12	1.54
Zr-93	1.84E+10	3.87E+09	1.15E+09	2.07E+09	1.00E+11	5.69E+07	2.09E+08	3.36E+08	1.26E+11	20.4
Nb-93m	3.46E+11	2.50E+13	2.88E+10	4.70E+10	4.00E+13	1.66E+09	8.69E+11	1.92E+12	6.81E+13	2.88
Nb-94	1.84E+10	1.80E+11	1.27E+09	2.07E+09	3.61E+11	1.95E+08	6.15E+09	1.45E+10	5.84E+11	3.05
Mo-93	2.00E+09	8.65E+09	3.50E+08	3.22E+08	4.23E+10	1.39E+08	3.09E+08	5.46E+09	5.95E+10	2.03
Tc-99	1.22E+10	5.01E+09	8.47E+09	7.54E+08	1.97E+11	6.66E+09	3.06E+09	8.19E+08	2.34E+11	3.71
Pd-107	2.10E+09	4.72E+09	1.57E+08	1.54E+08	1.07E+10	4.14E+06	1.39E+07		1.79E+10	6.19
Ag-108m	9.74E+11	1.73E+11	7.56E+10	1.11E+11	5.09E+12	9.85E+09	8.46E+09	2.96E+09	6.44E+12	21.7
Cd-113m	4.00E+10	4.15E+09	3.85E+09	3.17E+09	5.03E+11	1.04E+08	1.79E+08		5.55E+11	52.2
In-115		8.28E+05							8.28E+05	2.65
Sn-126	1.05E+09	7.45E+07	7.87E+07	7.72E+07	5.91E+09	2.07E+06	5.58E+07	1.37E+06	7.25E+09	27.7
Sb-125	4.61E+08	1.27E+09	7.47E+07	1.04E+08	1.54E+12	5.55E+06	3.03E+07	2.45E+07	1.54E+12	11.6
I-129	3.05E+08	4.50E+07	9.17E+07	1.40E+07	3.29E+09	1.38E+06	1.45E+07		3.76E+09	3.2
Cs-134	1.93E+08	3.30E+08	8.54E+04	1.06E+05	5.85E+11	4.05E+04	9.24E+06		5.86E+11	2.66
Cs-135	1.28E+09	3.22E+08	2.46E+08	2.53E+07	9.94E+09	6.38E+06	1.21E+09		1.30E+10	2.3
Cs-137	8.35E+12	4.58E+12	8.05E+11	6.31E+11	8.99E+13	3.14E+10	3.45E+12		1.08E+14	1.53
Ba-133	9.99E+07	5.30E+08	8.09E+06	1.24E+07	1.36E+09	5.90E+05	3.33E+07		2.05E+09	2.47
Pm-147	7.63E+08	8.59E+08	7.68E+06	9.14E+06	1.18E+12	9.08E+05	5.51E+06	2.49E+06	1.18E+12	3.28
Sm-151	1.66E+11	1.36E+11	1.33E+10	1.23E+10	1.03E+12	3.97E+08	1.58E+10	6.23E+08	1.38E+12	2.29
Eu-152	2.07E+08	4.78E+11	1.24E+08	1.31E+07	2.29E+09	2.22E+08	4.57E+10	9.86E+05	5.26E+11	3.47
Eu-154	4.71E+10	1.93E+10	4.04E+09	3.61E+09	1.48E+12	1.03E+08	8.01E+08	1.69E+08	1.55E+12	2.78
Eu-155	2.07E+09	9.72E+08	1.00E+08	1.17E+08	3.17E+11	4.45E+06	3.48E+07	4.37E+06	3.20E+11	3.17
Ho-166m	2.83E+09	2.11E+09	1.78E+08	3.21E+08	1.41E+10	1.04E+07	2.39E+08	1.46E+04	1.98E+10	2.17
U-232	1.99E+05	3.46E+05	3.28E+04	1.41E+04	1.57E+06	7.61E+03	3.66E+04	1.25E+04	2.22E+06	2.48
U-234	1.47E+07	9.73E+06	2.00E+06	9.57E+05	8.44E+07	4.29E+05	1.44E+06		1.14E+08	2.39
U-235	6.29E+06	2.32E+05	3.69E+07	2.33E+05	2.98E+07	7.21E+08	1.03E+09	2.71E+01	1.82E+09	2.77
U-236	5.75E+06	1.21E+07	8.22E+05	7.44E+05	4.13E+07	1.29E+05	9.61E+05	7.14E+05	6.25E+07	2.42
U-238	1.27E+07	3.92E+06	1.76E+06	1.83E+06	7.24E+07	1.55E+09	4.47E+08		2.09E+09	2.19
Np-237	5.73E+07	1.58E+07	2.19E+06	4.18E+06	1.61E+09	2.09E+05	1.06E+06	8.57E+05	1.69E+09	2.94
Pu-238	1.30E+10	9.11E+10	3.98E+09	6.41E+08	1.78E+11	1.12E+09	6.22E+09	4.95E+09	2.99E+11	2.27
Pu-239	4.10E+09	1.49E+10	8.52E+08	2.77E+08	3.53E+10	2.12E+08	1.10E+09	7.57E+08	5.75E+10	2.06
Pu-240	5.69E+09	1.97E+10	9.20E+08	3.87E+08	4.98E+10	2.15E+08	1.23E+09	1.08E+09	7.91E+10	2.04
Pu-241	5.95E+10	3.52E+11	1.48E+10	5.08E+09	7.88E+11	4.22E+09	2.36E+10	1.65E+10	1.26E+12	2.42
Pu-242	4.40E+07	1.03E+08	6.00E+06	2.87E+06	3.12E+08	1.29E+06	7.01E+06	5.66E+06	4.82E+08	2.38
Am-241	7.46E+10	1.98E+11	5.16E+10	6.10E+09	2.81E+14	6.08E+09	2.21E+10	3.62E+09	2.81E+14	12.1
Am-242m	9.91E+07	3.62E+08	1.49E+07	6.76E+06	8.38E+08	3.32E+06	2.07E+07	2.40E+07	1.37E+09	2.36
Am-243	2.97E+08	1.32E+09	5.67E+07	2.53E+07	3.21E+09	1.28E+07	8.02E+07	7.54E+07	5.07E+09	1.97
Cm-243	3.17E+07	2.12E+08	7.57E+06	7.98E+05	4.18E+08	2.46E+06	1.40E+07	1.16E+07	6.99E+08	2.15
Cm-244	1.48E+09	2.15E+10	5.21E+08	3.74E+07	2.64E+10	1.75E+08	1.26E+09	1.23E+09	5.26E+10	2.4
Cm-245	4.37E+06	2.00E+07	5.97E+05	2.86E+05	4.15E+07	1.28E+05	1.01E+06	1.24E+06	6.91E+07	2.44
Cm-246	1.16E+06	6.50E+06	1.59E+05	7.58E+04	1.23E+07	3.41E+04	3.27E+05	4.08E+05	2.10E+07	2.45
Total	4.61E+14	2.61E+14	7.90E+12	8.36E+12	2.17E+15	1.06E+12	1.20E+13	2.89E+13	2.95E+15	3.04

* C-14 has been divided into organic (org), inorganic (inorg) and induced activity (ind).

** Ratio to the best estimate

Half-lives

In all parts of the radionuclide transport model chain (near-field, far-field and biosphere) the same data for half-lives are used as reported in the **Data report**. The range of uncertainty given for the half-lives are considered as insignificant in the context of SR-PSU modelling and the calculations are based on the best estimate values.

Table A-3. Half-lives for radionuclides with initial inventory used in SR-PSU (from Table 3-4 in the Data report). All data are taken from Firestone et al. (1998) except for a) Schrader (2004), and b) Jörg et al. (2010).

Nuclide	Half-live [years]			Nuclide	Half-live [years]		
	Best estimate	Min.	Max.		Best estimate	Min.	Max.
Ag-108m ^{a)}	438	429	447	Ni-63	100.1	98.1	102.1
Am-241	432.2	431.5	432.9	Np-237	2.144E+06	2.137E+06	2.151E+06
Am-242m	141	139	143	Pd-107	6.5E+06	6.2E+06	6.8E+06
Am-243	7,370	7,330	7,410	Pm-147	2.6234	2.6232	2.6236
Ba-133	10.51	10.46	10.56	Pu-238	87.7	87.4	88.0
Be-10	1.51E+06	1.45E+06	1.57E+06	Pu-239	24,110	24,080	24,140
C-14inorg	5,730	5,690	5,770	Pu-240	6,563	6,556	6,570
Ca-41	1.03E+05	0.99E+05	1.07E+05	Pu-241	14.35	14.25	14.45
Cd-133m	14.1	13.6	14.6	Pu-242	3.733E+05	3.721E+05	3.745E+05
Cl-36	3.01E+05	2.99E+05	3.03E+05	Ru-106	373.59 days	373.44 d	373.74 d
Cm-243	29.1	29.0	29.2	Sb-125	2.7582	2.7571	2.7593
Cm-244	18.10	18.08	18.12	Se-79 ^{b)}	3.27E+05	3.19E+05	3.35E+05
Cm-245	8,500	8,400	8,600	Sm-151	90	82	98
Cm-246	4,730	4,630	4,830	Sn-126	~ 1E+05		
Co-60	5.2714	5.2709	5.2719	Sr-90	28.78	28.74	28.82
Cs-134	2.0648	2.0638	2.0658	Tc-99	2.111E+05	2.099E+05	2.123E+05
Cs-135	2.3E+06	2.0E+06	2.6E+06	U-232	68.9	68.5	69.3
Cs-137	30.07	30.04	30.10	U-234	2.455E+05	2.449E+05	2.461E+05
Eu-152	13.537	13.531	13.543	U-235	7.038E+08	7.033E+08	7.043E+08
Eu-154	8.593	5.589	8.597	U-236	2.342E+07	2.339E+07	2.345E+07
Eu-155	4.7611	4.7598	4.7624	U-238	4.468E+09	4.465E+09	4.471E+09
Fe-55	2.73	2.70	2.76	Zr-93	1.53E+06	1.43E+06	1.63E+06
H-3	12.33	12.26	12.39				
Ho-166m	1.20E+03	1.02E+03	1.38E+03				
I-129	1.57E+07	1.53E+07	1.61E+07				
Mo-93	4.0E+03	3.2E+03	4.8E+03				
Nb-93m	16.13	15.99	16.27				
Nb-94	2.03E+04	1.87E+04	2.19E+04				
Ni-59	7.6E+04	7.1E+04	8.1E+04				

Several of the radionuclides in the **Data report** are members of decay chains. In the modelling all progeny with half-life longer than 100 days were included, hence there was a need for additional half-lives for progeny without initial inventory. These half-lives and the decay chain branching ratios were taken from <http://nucleardata.nuclear.lu.se/toi/> (Chu et al. 1999).

The half-lives for the progeny without initial inventory are listed in Table A-4. The decay chains are described in Section 3.1.2.

Inventory data used for NHB calculations.

This report is a revised edition compared to the report published in March 2015. This revised edition of the Radionuclide transport report presents results with an updated (increased) inventory of Mo-93 (SKBdoc 1481419) taken into account for doses to humans. The calculation of exposure of

non-human biota has not been updated in this revised edition as the previous calculation showed that the exposure of non-human biota is well below the screening limits, and the increased inventory of Mo-93 is not large enough to change this conclusion. The previous version of the inventory, which was used in the NHB calculations (Chapter 8), is presented in Table A-5 and Table A-6.

Table A-4. Half-lives for progeny without initial inventory.

Radionuclide	Half-life [years]
Ac-227	2.18E+01
Cm-242	4.46E-01
Pa-231	3.28E+04
Pb-210	2.23E+01
Po-210	3.79E-01
Ra-226	1.60E+03
Ra-228	5.75E+00
Th-228	1.91E+00
Th-229	7.34E+03
Th-230	7.54E+04
Th-232	1.40E+10
U-233	1.59E+05

Hydrological data

Hydrological calculations have been performed for detailed water flows inside the tunnels and silo (Abarca et al. 2013, 2014). One of the endpoints of the detailed near-field hydrological modelling is the water flow through a large number of surfaces in the near-field. These flow fields are delivered in text files to the radionuclide transport calculations. The data are then converted to the Excel spreadsheet format used by Ecolego.

The water flows are calculated as steady state values for three time points, defined by characteristic shoreline positions, and several degradation states of the barriers. Various combinations of these water flows are used in the radionuclide transport modelling, for the various scenarios (as described in Chapter 4). Linear interpolation is done between values to mimic a continuous change in the dynamic radionuclide transport model.

For the diffusion out from the silo (Section 9.3.11) the equivalent water flow, Q_{eq} , is used for representing diffusive transport out to the bedrock. The Q_{eq} values used in the calculation are presented in Appendix E in Abarca et al. (2014). Q_{eq} values for the “base case” were chosen for the whole calculation time frame.

A.3 Far-field data

Geometric data

The geometry of the geosphere is not explicitly expressed in the selected modelling approach. The required geometrical data for geosphere transport are given implicitly by the travel times and F-factors obtained by particle tracking in the hydrogeological modelling (see Section 9.4).

The locations of radionuclide releases to the biosphere are given by results from the particle tracking. This showed that a majority (on average, more than 80% – and in most cases more than 90%) of particle tracks are released into biosphere object 157_2. Hence a simplified approach was used in the modelling where the release was directed only to biosphere object 157_2. The validity of this approach was supported by results from a biosphere calculation case (Section 10.7 and 11.2 in the **Biosphere synthesis report**).

Table A-5. Best estimate radionuclide inventory [Bq], used in calculations for NHB. I.e. this is an older version of data in Table A-1.

Nuclide	1BMA	2BMA	1BTF	2BTF	Silo	1BLA	2-5BLA	BRT	Total
H-3	8.09E+08	3.31E+12	6.82E+07	1.07E+08	8.97E+09	2.00E+08	1.94E+11		3.52E+12
Be-10	2.21E+05	2.19E+04	1.37E+04	2.48E+04	9.89E+05	6.53E+02	1.26E+03		1.27E+06
C-14 org*	1.47E+11	3.96E+09	9.84E+09	6.07E+09	7.56E+11	7.91E+07	2.25E+08		9.23E+11
C-14 inorg*	1.90E+12	1.44E+10	1.89E+11	2.69E+11	2.72E+12	4.03E+09	9.27E+08		5.10E+12
C-14 ind*		5.09E+09					1.19E+09	1.02E+10	1.65E+10
Cl-36	3.34E+08	2.02E+08	1.44E+07	1.66E+07	8.94E+08	2.17E+07	4.60E+07	7.21E+06	1.54E+09
Ca-41		1.56E+10					3.91E+09		1.95E+10
Fe-55	5.35E+10	1.05E+11	8.33E+07	1.14E+08	2.73E+12	8.78E+06	4.45E+08	1.49E+10	2.91E+12
Co-60	4.08E+11	1.99E+12	1.67E+10	2.36E+10	1.29E+13	1.03E+09	2.59E+10	1.93E+11	1.55E+13
Ni-59	2.10E+12	9.50E+11	3.31E+10	3.83E+10	6.85E+12	3.99E+09	1.15E+10	1.60E+11	1.01E+13
Ni-63	1.47E+14	9.23E+13	2.04E+12	2.27E+12	5.48E+14	3.04E+11	1.12E+12	1.44E+13	8.07E+14
Se-79	2.10E+08	7.29E+06	1.57E+07	1.54E+07	1.05E+09	4.00E+05	5.94E+06		1.31E+09
Sr-90	5.49E+11	3.60E+11	3.48E+10	5.76E+10	3.61E+12	7.42E+08	2.40E+10	2.32E+10	4.66E+12
Zr-93	3.68E+08	1.06E+09	2.29E+07	4.14E+07	4.48E+09	1.09E+06	2.95E+07	1.84E+08	6.19E+09
Nb-93m	1.73E+10	1.31E+13	1.44E+09	2.35E+09	9.33E+12	7.68E+07	1.34E+11	1.06E+12	2.36E+13
Nb-94	3.67E+09	9.12E+10	2.53E+08	4.13E+08	8.67E+10	3.14E+07	9.81E+08	7.94E+09	1.91E+11
Mo-93	7.89E+08	4.24E+09	1.13E+08	1.33E+08	9.48E+09	3.80E+07	5.39E+07	3.00E+09	1.78E+10
Tc-99	6.22E+09	1.42E+09	2.30E+09	5.45E+08	5.00E+10	1.85E+09	4.98E+08	4.49E+08	6.32E+10
Pd-107	5.25E+07	2.55E+09	3.92E+06	3.86E+06	2.75E+08	1.00E+05	1.72E+06		2.89E+09
Ag-108m	1.95E+10	4.06E+10	1.51E+09	2.21E+09	2.30E+11	1.94E+08	1.53E+09	1.62E+09	2.97E+11
Cd-113m	7.98E+08	9.32E+07	7.67E+07	6.34E+07	9.58E+09	1.96E+06	6.13E+06		1.06E+10
In-115		3.13E+05							3.13E+05
Sn-126	2.62E+07	1.75E+07	1.96E+06	1.93E+06	2.05E+08	5.00E+04	7.93E+06	7.53E+05	2.62E+08
Sb-125	4.37E+07	2.62E+08	7.47E+06	1.04E+07	1.32E+11	4.74E+05	4.46E+06	1.34E+07	1.32E+11
I-129	1.46E+08	7.67E+06	2.27E+07	1.02E+07	9.84E+08	4.35E+05	1.94E+06		1.17E+09
Cs-134	1.45E+08	2.26E+08	7.10E+04	8.86E+04	2.20E+11	1.58E+04	1.39E+06		2.20E+11
Cs-135	8.41E+08	5.33E+07	1.03E+08	1.85E+07	4.47E+09	3.07E+06	1.75E+08		5.67E+09
Cs-137	8.15E+12	8.95E+11	7.12E+11	6.22E+11	5.97E+13	1.84E+10	4.95E+11		7.05E+13
Ba-133	4.89E+07	1.43E+08	4.03E+06	6.19E+06	6.16E+08	2.20E+05	1.26E+07		8.31E+08
Pm-147	3.71E+08	4.06E+08	3.84E+06	4.57E+06	3.59E+11	3.02E+05	1.19E+06	1.37E+06	3.60E+11
Sm-151	8.26E+10	3.55E+10	6.51E+09	6.13E+09	4.63E+11	1.68E+08	5.88E+09	3.42E+08	6.00E+11
Eu-152	9.47E+07	1.33E+11	6.19E+07	6.54E+06	8.64E+08	1.02E+08	1.73E+10	5.41E+05	1.52E+11
Eu-154	2.33E+10	6.83E+09	1.98E+09	1.80E+09	5.24E+11	4.01E+07	2.67E+08	9.27E+07	5.59E+11
Eu-155	1.02E+09	3.74E+08	4.96E+07	5.83E+07	9.96E+10	1.54E+06	1.16E+07	2.40E+06	1.01E+11
Ho-166m	1.41E+09	5.22E+08	8.79E+07	1.59E+08	6.83E+09	4.18E+06	9.03E+07	7.99E+03	9.10E+09
U-232	8.85E+04	1.46E+05	1.62E+04	6.73E+03	6.20E+05	2.34E+03	9.35E+03	6.86E+03	8.96E+05
U-234	6.66E+06	3.04E+06	9.86E+05	4.55E+05	3.58E+07	1.33E+05	4.38E+05		4.75E+07
U-235	3.00E+06	7.82E+04	1.84E+07	1.12E+05	1.42E+07	2.98E+08	3.23E+08	1.49E+01	6.57E+08
U-236	2.64E+06	6.00E+06	4.02E+05	3.55E+05	1.58E+07	3.99E+04	2.06E+05	3.92E+05	2.59E+07
U-238	5.95E+06	1.23E+06	8.55E+05	8.75E+05	3.28E+07	7.33E+08	1.77E+08		9.52E+08
Np-237	2.73E+07	7.68E+06	1.07E+06	1.98E+06	5.36E+08	6.75E+04	2.61E+05	4.70E+05	5.75E+08
Pu-238	7.52E+09	4.42E+10	2.09E+09	4.56E+08	7.29E+10	3.47E+08	1.52E+09	2.72E+09	1.32E+11
Pu-239	2.77E+09	6.78E+09	4.68E+08	1.89E+08	1.70E+10	6.60E+07	2.77E+08	4.16E+08	2.80E+10
Pu-240	3.87E+09	9.21E+09	5.20E+08	2.65E+08	2.39E+10	6.74E+07	2.95E+08	5.92E+08	3.87E+10
Pu-241	2.40E+10	1.66E+11	7.30E+09	2.42E+09	3.07E+11	1.29E+09	5.74E+09	9.05E+09	5.23E+11
Pu-242	2.00E+07	5.02E+07	2.96E+06	1.37E+06	1.23E+08	3.99E+05	1.71E+06	3.11E+06	2.03E+08
Am-241	2.91E+10	4.12E+10	6.14E+09	1.83E+09	2.32E+13	5.23E+08	1.94E+09	1.99E+09	2.32E+13
Am-242m	4.46E+07	1.83E+08	7.34E+06	3.21E+06	3.22E+08	1.02E+06	4.84E+06	1.32E+07	5.79E+08
Am-243	2.02E+08	6.62E+08	3.25E+07	1.78E+07	1.60E+09	4.00E+06	1.86E+07	4.14E+07	2.57E+09
Cm-243	1.85E+07	1.03E+08	3.82E+06	4.15E+05	1.89E+08	7.58E+05	3.40E+06	6.38E+06	3.25E+08
Cm-244	6.73E+08	1.07E+10	2.68E+08	2.84E+07	9.26E+09	5.39E+07	2.80E+08	6.76E+08	2.19E+10
Cm-245	1.99E+06	1.01E+07	2.95E+05	1.36E+05	1.49E+07	3.97E+04	2.18E+05	6.83E+05	2.84E+07
Cm-246	5.27E+05	3.34E+06	7.82E+04	3.60E+04	4.29E+06	1.05E+04	6.61E+04	2.24E+05	8.58E+06
Total	1.60E+14	1.14E+14	3.06E+12	3.30E+12	6.72E+14	3.38E+11	2.05E+12	1.59E+13	9.71E+14

* C-14 has been divided into organic (org), inorganic (inorg) and induced activity (ind).

Table A-6. High radionuclide inventory [Bq], used in calculations for NHB. I.e. this is an older version of data in Table A-2.

Nuclide	1BMA	2BMA	1BTF	2BTF	Silo	1BLA	2-5BLA	BRT	Total	Ratio
H-3	4.06E+10	2.02E+13	3.41E+09	5.38E+09	4.57E+11	1.01E+10	5.43E+11		2.12E+13	6.04
Be-10	1.11E+07	9.85E+05	6.88E+05	1.24E+06	4.98E+07	3.42E+04	2.49E+04		6.38E+07	50.2
C-14 org*	1.71E+11	6.90E+09	1.15E+10	7.08E+09	8.88E+11	9.38E+07	1.21E+09		1.09E+12	1.18
C-14 inorg*	2.21E+12	2.41E+10	2.20E+11	3.13E+11	3.19E+12	4.78E+09	4.98E+09		5.97E+12	1.17
C-14 ind*		1.76E+10					6.41E+09	1.85E+10	4.26E+10	2.59
Cl-36	6.67E+08	8.00E+08	4.81E+07	4.06E+07	3.91E+09	2.88E+07	1.13E+08	1.31E+07	5.63E+09	3.66
Ca-41		6.07E+10					1.01E+10		7.08E+10	3.63
Fe-55	2.72E+11	4.65E+11	4.17E+08	5.71E+08	1.52E+13	5.05E+07	2.64E+09	2.72E+10	1.59E+13	5.48
Co-60	4.74E+11	3.74E+12	1.71E+10	2.41E+10	2.40E+13	2.01E+09	1.66E+11	3.51E+11	2.88E+13	1.85
Ni-59	6.30E+12	2.12E+12	1.03E+11	1.16E+11	2.09E+13	1.27E+10	6.62E+10	2.91E+11	2.99E+13	2.95
Ni-63	4.40E+14	2.02E+14	6.43E+12	6.88E+12	1.67E+15	9.57E+11	6.57E+12	2.62E+13	2.36E+15	2.93
Se-79	1.05E+10	3.77E+08	7.86E+08	7.71E+08	5.30E+10	2.06E+07	5.84E+07		6.55E+10	50.2
Sr-90	6.62E+11	8.65E+11	4.76E+10	1.24E+11	4.76E+12	2.88E+09	1.80E+11	4.23E+10	6.68E+12	1.43
Zr-93	1.84E+10	3.87E+09	1.15E+09	2.07E+09	1.00E+11	5.69E+07	2.09E+08	3.36E+08	1.26E+11	20.4
Nb-93m	3.46E+11	2.50E+13	2.88E+10	4.70E+10	4.00E+13	1.66E+09	8.69E+11	1.92E+12	6.81E+13	2.88
Nb-94	1.84E+10	1.80E+11	1.27E+09	2.07E+09	3.61E+11	1.95E+08	6.15E+09	1.45E+10	5.84E+11	3.05
Mo-93	3.71E+09	9.80E+09	1.84E+09	1.70E+08	7.37E+10	4.72E+08	3.87E+08	5.46E+09	9.55E+10	5.36
Tc-99	1.11E+10	5.01E+09	8.30E+09	6.44E+08	1.94E+11	6.52E+09	3.06E+09	8.19E+08	2.29E+11	3.63
Pd-107	2.10E+09	4.72E+09	1.57E+08	1.54E+08	1.07E+10	4.14E+06	1.39E+07		1.79E+10	6.19
Ag-108m	9.74E+11	1.73E+11	7.56E+10	1.11E+11	5.09E+12	9.85E+09	8.46E+09	2.96E+09	6.44E+12	21.7
Cd-113m	4.00E+10	4.15E+09	3.85E+09	3.17E+09	5.03E+11	1.04E+08	1.79E+08		5.55E+11	52.2
In-115		8.28E+05							8.28E+05	2.65
Sn-126	1.05E+09	7.45E+07	7.87E+07	7.72E+07	5.91E+09	2.07E+06	5.58E+07	1.37E+06	7.25E+09	27.7
Sb-125	4.61E+08	1.27E+09	7.47E+07	1.04E+08	1.54E+12	5.55E+06	3.03E+07	2.45E+07	1.54E+12	11.6
I-129	2.81E+08	4.50E+07	9.05E+07	1.19E+07	3.18E+09	1.33E+06	1.45E+07		3.63E+09	3.09
Cs-134	1.93E+08	3.30E+08	8.54E+04	1.06E+05	5.85E+11	4.05E+04	9.24E+06		5.86E+11	2.66
Cs-135	1.13E+09	3.22E+08	2.38E+08	2.16E+07	9.40E+09	6.01E+06	1.21E+09		1.23E+10	2.18
Cs-137	8.35E+12	4.58E+12	8.05E+11	6.31E+11	8.99E+13	3.14E+10	3.45E+12		1.08E+14	1.53
Ba-133	9.99E+07	5.30E+08	8.09E+06	1.24E+07	1.36E+09	5.90E+05	3.33E+07		2.05E+09	2.47
Pm-147	7.63E+08	8.59E+08	7.68E+06	9.14E+06	1.18E+12	9.08E+05	5.51E+06	2.49E+06	1.18E+12	3.28
Sm-151	1.66E+11	1.36E+11	1.33E+10	1.23E+10	1.03E+12	3.97E+08	1.58E+10	6.23E+08	1.38E+12	2.29
Eu-152	2.07E+08	4.78E+11	1.24E+08	1.31E+07	2.29E+09	2.22E+08	4.57E+10	9.86E+05	5.26E+11	3.47
Eu-154	4.71E+10	1.93E+10	4.04E+09	3.61E+09	1.48E+12	1.03E+08	8.01E+08	1.69E+08	1.55E+12	2.78
Eu-155	2.07E+09	9.72E+08	1.00E+08	1.17E+08	3.17E+11	4.45E+06	3.48E+07	4.37E+06	3.20E+11	3.17
Ho-166m	2.83E+09	2.11E+09	1.78E+08	3.21E+08	1.41E+10	1.04E+07	2.39E+08	1.46E+04	1.98E+10	2.17
U-232	1.92E+05	3.45E+05	3.24E+04	1.37E+04	1.54E+06	7.60E+03	3.66E+04	1.25E+04	2.18E+06	2.43
U-234	1.41E+07	9.71E+06	1.97E+06	9.25E+05	8.24E+07	4.29E+05	1.44E+06		1.11E+08	2.34
U-235	6.02E+06	2.29E+05	3.69E+07	2.23E+05	2.85E+07	7.21E+08	1.03E+09	2.71E+01	1.82E+09	2.77
U-236	5.53E+06	1.21E+07	8.05E+05	7.15E+05	4.05E+07	1.29E+05	9.61E+05	7.14E+05	6.14E+07	2.37
U-238	1.22E+07	3.91E+06	1.71E+06	1.76E+06	6.99E+07	1.55E+09	4.47E+08		2.08E+09	2.19
Np-237	5.49E+07	1.58E+07	2.13E+06	4.06E+06	1.60E+09	2.08E+05	1.06E+06	8.57E+05	1.68E+09	2.92
Pu-238	1.23E+10	9.10E+10	3.95E+09	5.95E+08	1.74E+11	1.12E+09	6.22E+09	4.95E+09	2.95E+11	2.24
Pu-239	3.79E+09	1.49E+10	8.38E+08	2.59E+08	3.42E+10	2.12E+08	1.10E+09	7.57E+08	5.60E+10	2.00
Pu-240	5.26E+09	1.97E+10	9.01E+08	3.62E+08	4.82E+10	2.15E+08	1.23E+09	1.08E+09	7.70E+10	1.99
Pu-241	5.80E+10	3.51E+11	1.46E+10	4.89E+09	7.72E+11	4.22E+09	2.36E+10	1.65E+10	1.24E+12	2.38
Pu-242	4.24E+07	1.03E+08	5.93E+06	2.78E+06	3.06E+08	1.29E+06	7.01E+06	5.66E+06	4.74E+08	2.34
Am-241	7.14E+10	1.98E+11	5.15E+10	5.94E+09	2.81E+14	6.08E+09	2.21E+10	3.62E+09	2.81E+14	12.1
Am-242m	9.55E+07	3.62E+08	1.47E+07	6.53E+06	8.23E+08	3.31E+06	2.07E+07	2.40E+07	1.35E+09	2.33
Am-243	2.74E+08	1.31E+09	5.54E+07	2.35E+07	3.09E+09	1.27E+07	8.02E+07	7.54E+07	4.93E+09	1.91
Cm-243	2.99E+07	2.12E+08	7.55E+06	7.85E+05	4.07E+08	2.46E+06	1.40E+07	1.16E+07	6.85E+08	2.11
Cm-244	1.42E+09	2.15E+10	5.19E+08	3.42E+07	2.61E+10	1.75E+08	1.26E+09	1.23E+09	5.22E+10	2.38
Cm-245	4.21E+06	2.00E+07	5.90E+05	2.76E+05	4.09E+07	1.28E+05	1.01E+06	1.24E+06	6.83E+07	2.41
Cm-246	1.12E+06	6.50E+06	1.57E+05	7.32E+04	1.22E+07	3.40E+04	3.27E+05	4.08E+05	2.08E+07	2.42
Total	4.61E+14	2.61E+14	7.85E+12	8.30E+12	2.17E+15	1.06E+12	1.20E+13	2.89E+13	2.95E+15	3.04

* C-14 has been divided into organic (org), inorganic (inorg) and induced activity (ind).

Matrix porosity, density and maximum penetration depth

The radionuclide transport modelling makes use of the matrix porosity, density, and the maximum penetration depth (fracture half-spacing) to account for retention of radionuclides due to diffusion into stagnant water in the rock matrix. The value for matrix porosity (0.18%) is provided in the **Input data report**. For density, the same value as in SAR-08 was used (2,700 kg/m³, Thomson et al. 2008a). The maximum penetration depth (1.4 m) is based on the fracture intensity in the range 0.02–0.36 m⁻¹ (Öhman and Follin 2010). As a cautious assumption, the higher value was used, giving a fracture half spacing of 1.4 m. For comparison, the maximum penetration depth used in SAR-08 radionuclide transport modelling was 2 m (Thomson et al. 2008a).

Sorption coefficients

Sorption coefficients (K_d [m³/kg]) were provided in the **Data report** for four ground water types in the geosphere: Temperate saline, Early periglacial, Late periglacial and Glacial conditions (see also Crawford 2013). A cautious approach was taken in the selection of K_d values; In this approach, the minimum of the K_d values for Temperate saline, Early periglacial and Late periglacial ground water types were used in all calculation cases where the geosphere was included (except for some elements that are sensitive to pH and redox, see Table 8-7 in the **Data report** and except for Po-210, for which the value was taken to be the same as for its parent Pb-210. This was done to approximate secular equilibrium of Po-210 with Pb-210, see further discussion in the **Data report**). The K_d values for the Glacial conditions ground water type were not used. In the calculation case for glacial conditions (CCR_GC), the releases from the near-field are transported directly to the biosphere.

Figure A-1 shows the peak release from geosphere with K_d values for different ground water types. As can be seen in the graph, the releases for Glacial conditions are significantly higher for neptunium, technetium and uranium, but as mentioned above, the only calculation case with expected glacial conditions (CCR_GC) was performed without taking into account any retention in the geosphere..

Hydrogeological data

The radionuclide calculation uses results from particle tracking in the hydrogeological calculations (Odén et al. 2014). Those results are (water) travel time (t_w [y]) and the F-factor (transport resistance factor [y/m]). Water travel time is used as a parameter in the Ecolego model. The F-factor is used for the calculation of flow-wetted surface area (a_w [m²/m³]), calculated as $a_w = F/t_w$.

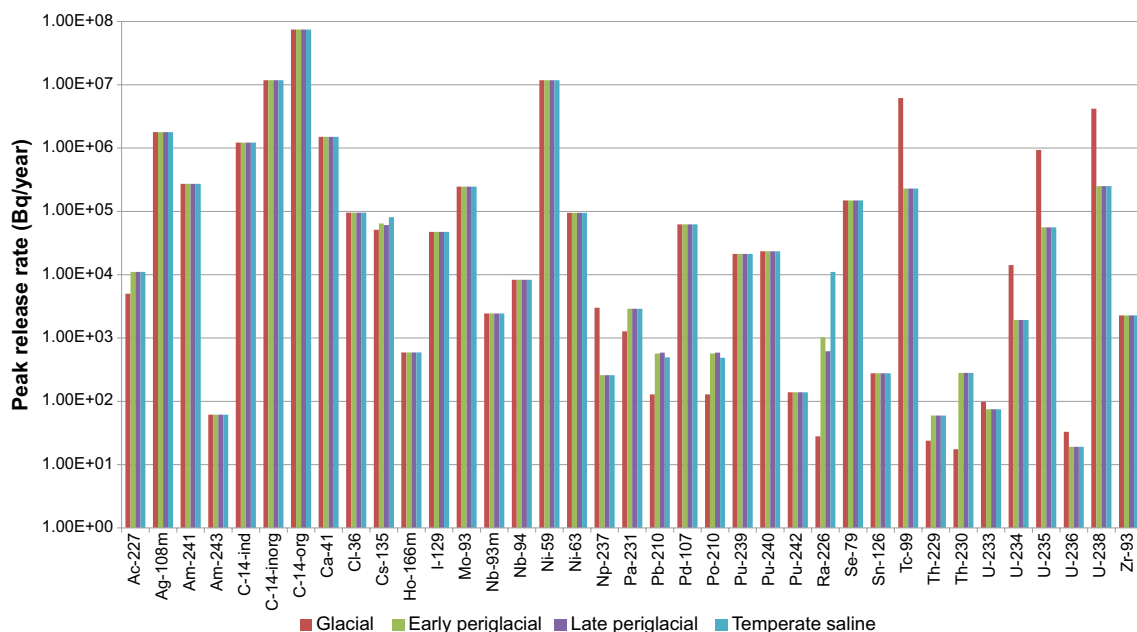


Figure A-1. Peak releases from the far-field with sets of K_d values representing different ground water types in the geosphere.

The data were delivered as text files containing results from 100,000 particle tracks each. In the deterministic calculations, the median values of these data were used. In the probabilistic calculations a subset of 100 tracks for each repository was used. These were selected randomly from the larger sets.

Figure A-2 and Figure A-3 show the travel times and flow wetted surface areas used in *global warming calculation case* (CCM_GW). Figure A-4 and Figure A-5 show the travel times and flow wetted surface areas used in *high flow in the bedrock calculation case* (CCL_FH).

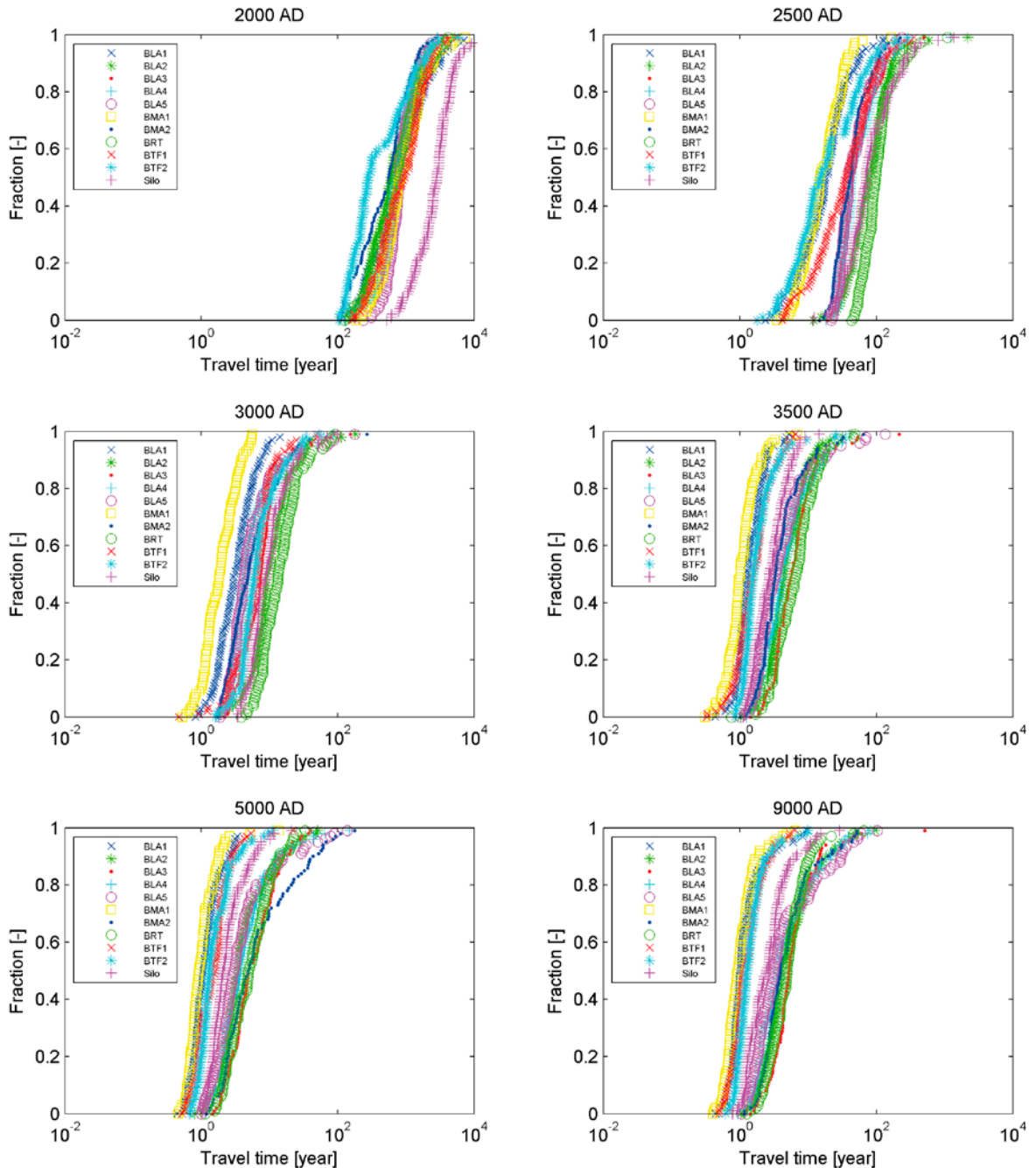


Figure A-2. Subset of 100 travel time samples (used in CCM_GW), selected from bedrock case 1 (Odén et al. 2014).

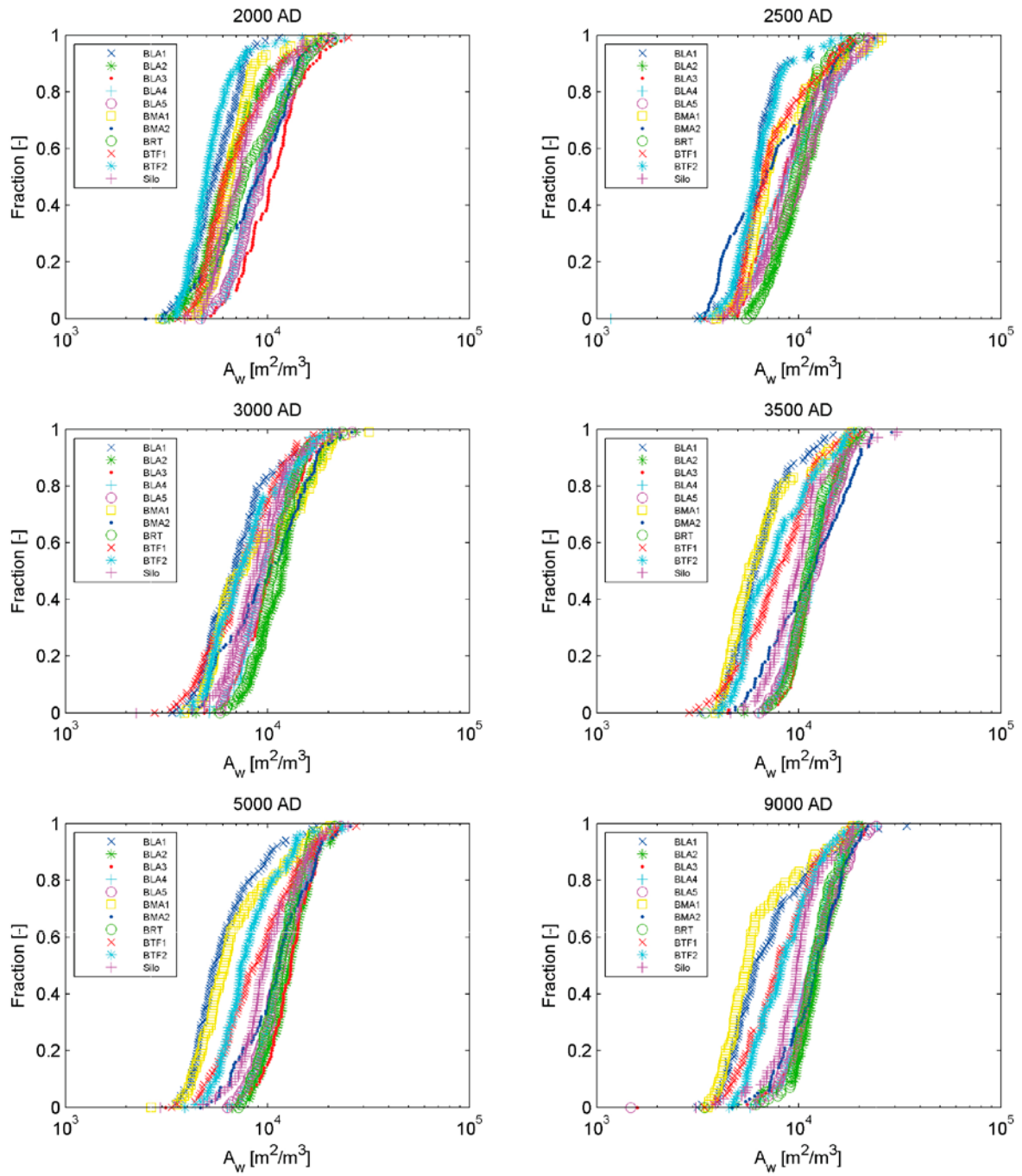


Figure A-3. Subset of 100 flow wetted area samples (used in CCM_GW), selected from the bedrock case 1 (Odén et al. 2014).

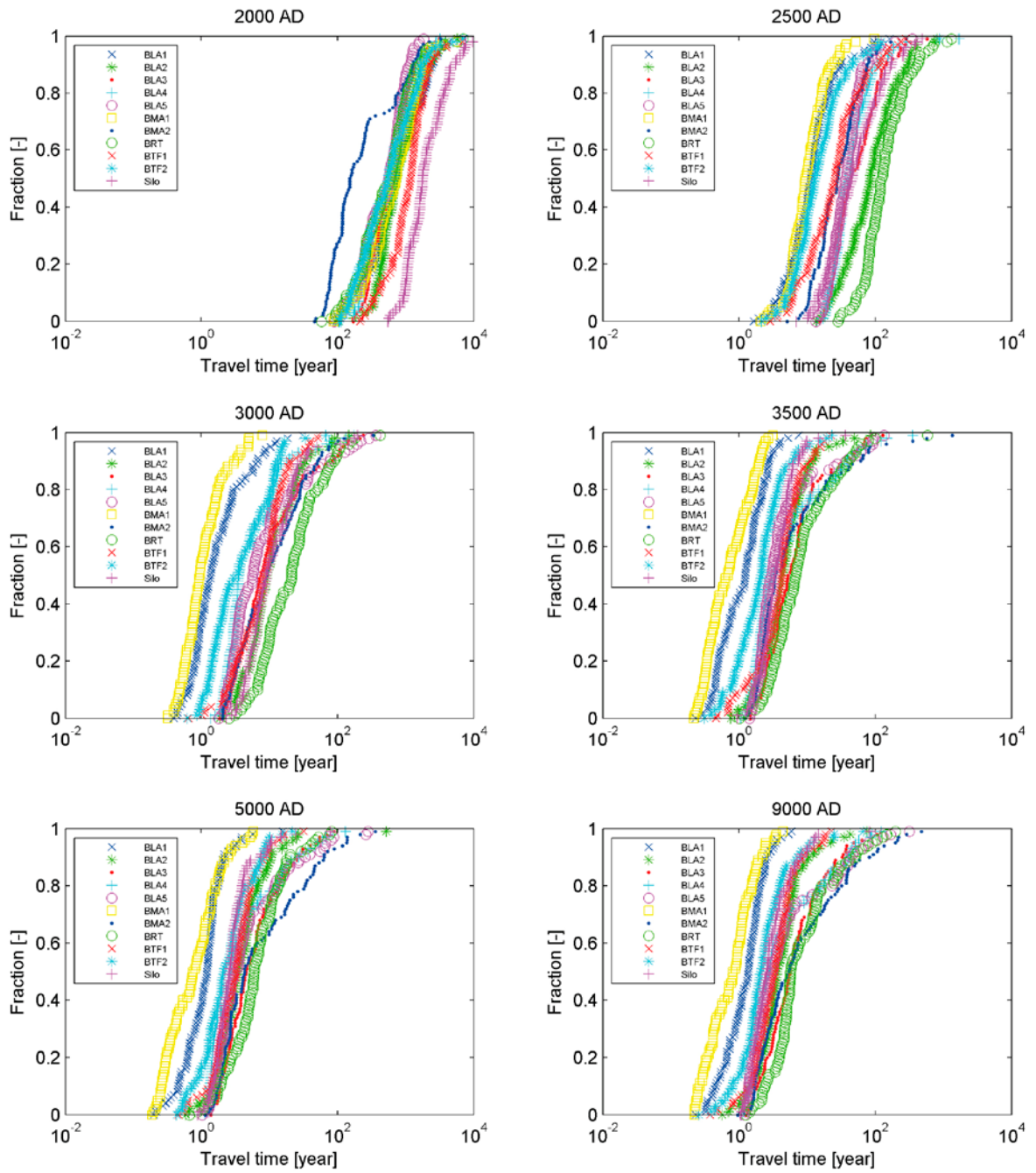


Figure A-4. Subset of 100 travel time samples (used in CCL_FH), selected from bedrock case 11. (Odén et al. 2014).

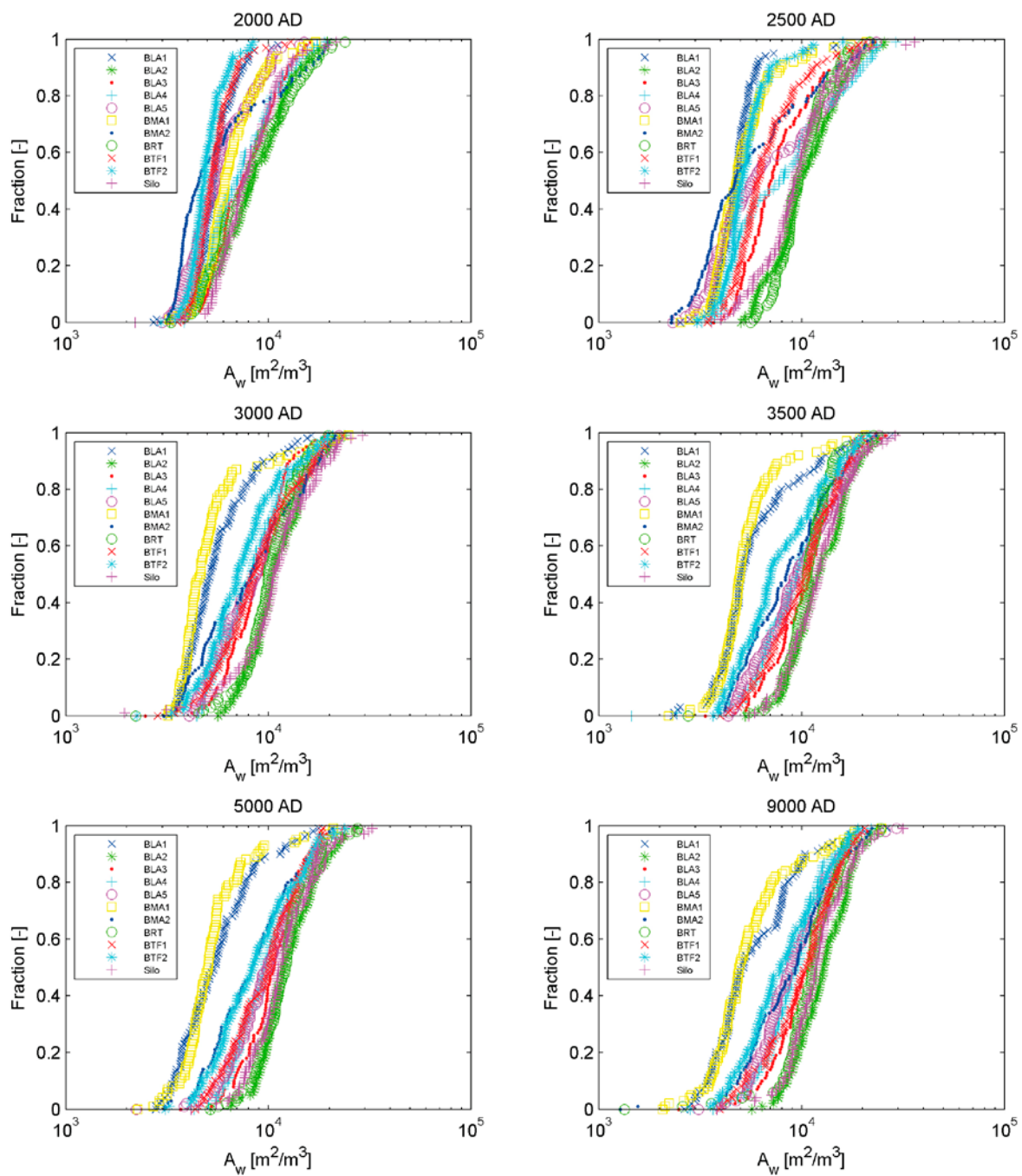


Figure A-5. Subset of 100 flow wetted area samples (used in CCL_FH), selected from bedrock case 11. (Odén et al. 2014).

Supporting calculations

This appendix presents calculations carried out for model verification, correct implementation and accuracy of the numerical tools, and the validity of simplifications done in the modelling.

B.1 Near-field models

Wall discretisation

As described in Chapter 9, the calculations in SR-PSU are performed with compartment models.

Simulation results are sensitive to the spatial resolution of engineered barriers in the near-field model, i.e. to the number of compartments used to represent transport through concrete walls.

A benchmark has been done to estimate the impact of the level of discretisation uncertainty in the obtained results. This benchmark was performed with the 1BMA model used in the SR-PSU assessment, but water flow and barrier properties (K_d , D_e) were kept constant over time to isolate the features related to the level of discretisation only.

Figure B-1 shows the release of radionuclides over time for the 1BMA model for different levels of discretisation of the outer barriers. As can be seen in the figure, the discretisation of the barrier is of significant importance for sorbing radionuclides as the peak release will be larger and earlier for a very coarse discretisation. For SR-PSU near-field models, five compartments were chosen for all barriers (floor, walls and roof). It should be noted that for some nuclides, with high K_d values, an even finer discretisation might be considered, for even more accurate results. However, a compromise has to be found between a manageable size of the compartment model and the numerical accuracy of its results.

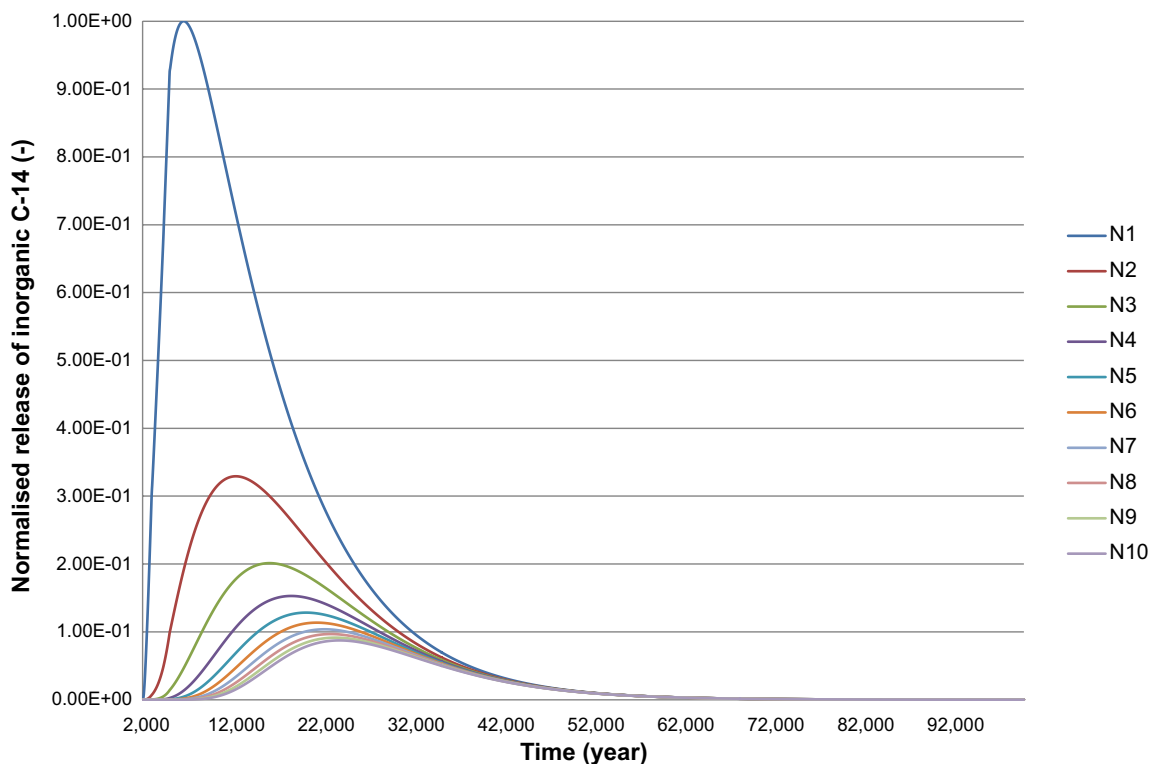


Figure B-1. Release curves for C-14 in inorganic form (sorbing). Results with 1 to 10 compartments (N1-N10) in the walls, roof and floor of the 1BMA model (normalised with respect to peak release for N1).

Solubility limits

It is expected that several nuclides will be subject to solubility limits and hence the release of some nuclides are overestimated in the calculations performed in the main calculation cases for SR-PSU. A set of calculations were performed in order to assess the effect of solubility limits on nickel. These calculations were performed with a similar model as in the SR-PSU assessment. However, as this was done early in the project a replica of the BMA model used in SAR-08 was used (Thomson et al. 2008a). Nickel was selected for this experiment due to the relevance of Ni-59 in earlier safety assessments (e.g. SAR-08) and relatively high amount of nickel present in the 1BMA vault. The mathematical approach used for calculations with solubility limits is described below.

Solubility limited transport model

Solubility limits create dependencies between the transport of all isotopes of the same chemical element if the mass inventory of all isotopes exceeds the amount which can be dissolved in a compartment. In case of nickel the radioactive isotopes Ni-59 and Ni-63 are affected.

The implementation of solubility limited transport is described in the following.

Advective transfer between compartments is expressed as:

$$Tr_{adv,ij} = \frac{q_{ij}}{Capacity_i} A_i^{nf} \quad \text{Equation B-1}$$

The diffusive transfer between compartments is expressed as:

$$Tr_{diff,ij} = \frac{1}{0.5(res_i + res_j)Capacity_i} A_i^{nf} \quad \text{Equation B-2}$$

where the quantity

A_i^{nf} : Solved or sorbed (not precipitated) amount of nuclide n in compartment i [Bq] is defined as:

$$A_i^{nf} = \begin{cases} A_i^n, & E_{conc}^n < c_{sol}^n \\ Capacity_i \cdot \lambda^n \cdot N_a \cdot \frac{A_i^{nm}}{\sum_k A_i^{km}} \cdot c_{sol}^n, & E_{conc}^n \geq c_{sol}^n \end{cases} \quad \text{Equation B-3}$$

where:

A_i^n activity of radionuclide n in compartment i [Bq],

A_i^{nm} amount of radionuclide n in compartment i [mol],

A_i^{km} amount of element k (isotope of n) in compartment i [mol],

c_{sol}^n concentration limit for element related to nuclide n [mol/m³],

E_{conc}^n element concentration related to nuclide n [mol/m³],

N_a Avogadro's number 6.022×10^{23} [mol⁻¹].

Other parts of the expressions above are defined in the same way as described in Section 9.

Solubility limited release of Ni-59

The amount of radioactive nickel in the repository alone is not large enough to give a significant effect, so in these calculations, the presence of stable nickel in the repository was also taken into account. The calculations were performed with parameter values from SAR-08 (SKB 2008). The K_d value for Ni-59 in cement was set to 0.04 m³/kg and water flow for the terrestrial period were used. In the calculation, an amount of 315 kg stable nickel in 1BMA was assumed.

Figure B-2 shows the normalised release curves for Ni-59. The green curve shows the release without the solubility limit taken into account, the red curve shows the release when the solubility limit is taken into account and sorption is not taken into account, and the blue curve shows the release when both the solubility limit and sorption were taken into account. It should be mentioned that stable nickel might not be available to the same extent as Ni-59. This was not further investigated in SR-PSU and hence the main calculations for the safety case was cautiously performed without solubility limits.

As can be seen in Figure B-2, the releases obtained for Ni-59 are likely to be very cautious when solubility limits are omitted in the calculations, as they decrease the release of Ni-59 by more than 2 orders of magnitude.

Simplified 1BMA model

A simplified version of the 1BMA model was implemented for comparison with and verification of the detailed model. In the simplified model, the whole 1BMA was modelled as one “waste section”. The same parameters as for the detailed 1BMA model were used. However, as the discretisation was simpler, the total water flow was used, instead of the detailed tunnel and waste water flow (Abarca et al. 2013). As can be seen in Figure B-3, most peak releases were overestimated by a factor of 1.5 to 2.5 with this simpler discretisation. However, this pattern might not be sure for all waste types as the simpler discretisation does not represent waste package-specific releases and retardation processes in detail for all sections in the vault. For example, in some waste sections of 1BMA there is mainly waste conditioned in bitumen, i.e. there are sections with very little sorption capacity in the waste domain. Hence, the detailed model could show a faster release of radionuclides from these sections. The detailed model used for the main calculations also took into account individual levels of complexing agents for the 15 sections of 1BMA, which may further enhance this faster-release effect. Hence, it was considered essential to use the more detailed model in the safety assessment.

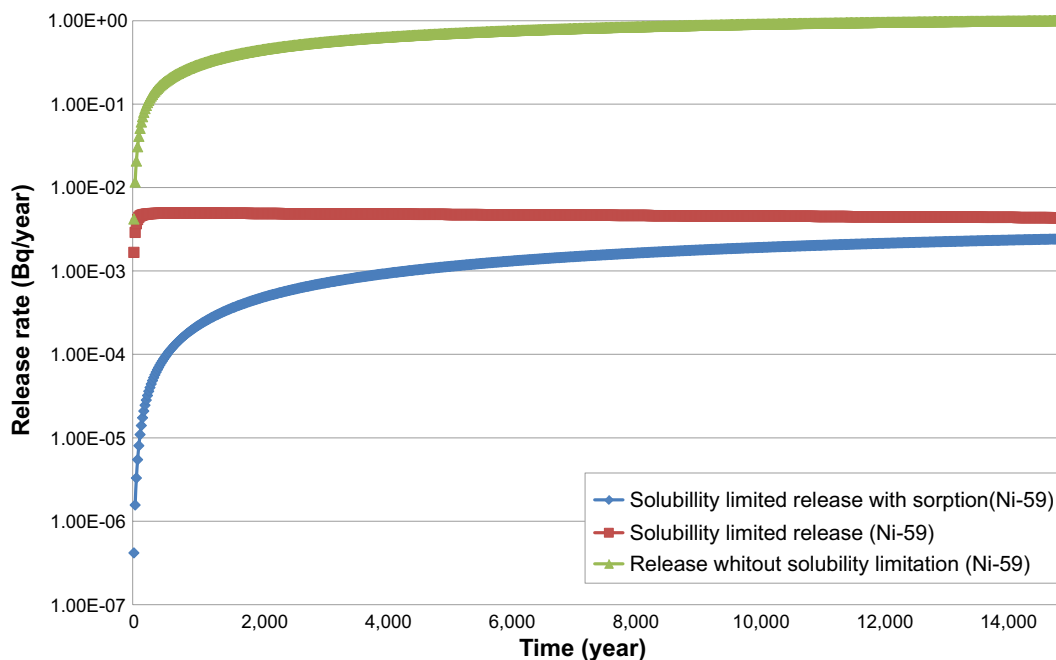


Figure B-2. Release curves for Ni-59 in the test calculation with solubility limits. The green curve shows the release without the solubility limit taken into account, the red curve shows the release when the solubility limit is taken into account and sorption is not taken into account, the blue curve shows the release when both the solubility limit and sorption were taken into account. The results are normalised with respect to the steady state release without solubility limitation. (The time window is short enough for the releases to show “steady state” behaviour. On a longer time-scale the releases would decrease due to decay and depletion of the inventory.)

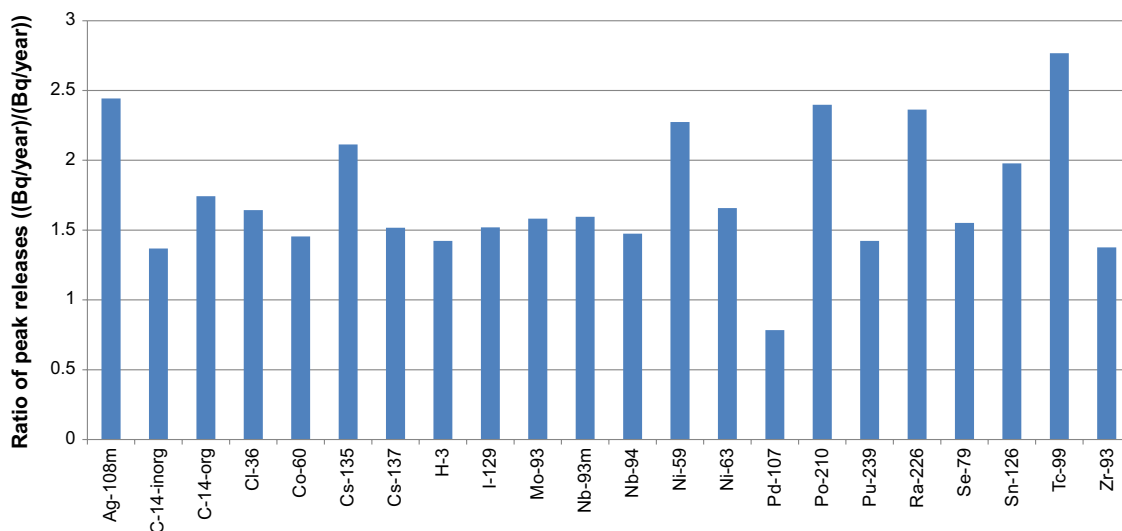


Figure B-3. Peak releases from the simplified IBMA model divided by the peak releases from the detailed IBMA model.

B.2 Far-field model

Since the Ecolego model of the far-field is implemented as a compartment model, the number of compartments used are crucial for the performance. Too many compartments would lead to long execution times and too few compartments would lead to poor spatial and temporal resolution of radionuclide transport. To find a reasonable number of compartments, the model was compared with FARF31 (Norman and Kjellbert 1990) which uses the same conceptual approach but solves the equations with a semi-analytical method. The decision to design a compartment model in Ecolego instead of using FARF31 was considered relevant, as FARF31 does not allow taking time varying water fluxes into account which is considered necessary for SR-PSU. Furthermore, having all models implemented in Ecolego simplifies the handling of the model chain.

FARF31 comparison

To evaluate the Ecolego model, a series of runs with varying number of compartments both in the fracture and for the rock matrix were used. The length of the compartments representing the rock matrix was chosen according to the scheme described in Section 9.4.4. In the comparison, the Ecolego model was used with constant values for flow-wetted surface area and travel time (as this is the only option in FARF31). The comparison was also made only for nuclide decay chains without branching (also due to limitations of the FARF31 code).

A satisfactory agreement with FARF31 was reached when the number of compartments in the Ecolego model was increased to totally 420, i.e. 20 compartments in the flow direction and 20 compartments for matrix diffusion (i.e. 20 matrix compartments for each fracture compartment, see also Figure 9-21 in Chapter 9). Figure B-4 shows the results obtained with this level of discretisation in the compartment model, compared to results from the FARF31 model. The conclusion was that a geosphere model with 420 (i.e. 20 times 21) compartments would be appropriate to use in the SR-PSU assessment.

B.3 Biosphere model

Alternative release target

As stated in Section 4.1.1, the general assumption used in this assessment is that discharge of radionuclides from the geosphere takes place only in biosphere object 157_2, i.e. this object receives the total releases of radionuclides. However, according to the hydrological modelling, a small fraction of the releases reaches other biosphere objects so, in order to investigate the impact of this simplification, a unit release simulation with different release distributions was performed during the development of the biosphere model (Section 10.7 in the **Biosphere synthesis report**). The conclusion was drawn that a release only in biosphere object 157_2 would be adequate for the purpose of the radionuclide transport and dose calculations.

A pessimistic calculation with releases in all biosphere objects was performed to confirm that the conclusions drawn in the **Biosphere synthesis report** also holds with a more realistic time-dependent release term.

This calculation was done with the maximum of calculated release fractions to all biosphere objects. i.e. the total release was more than 100% here. As can be seen in Figure B-5 none of the resulting annual doses significantly exceeds the annual doses in the *global warming calculation case*.

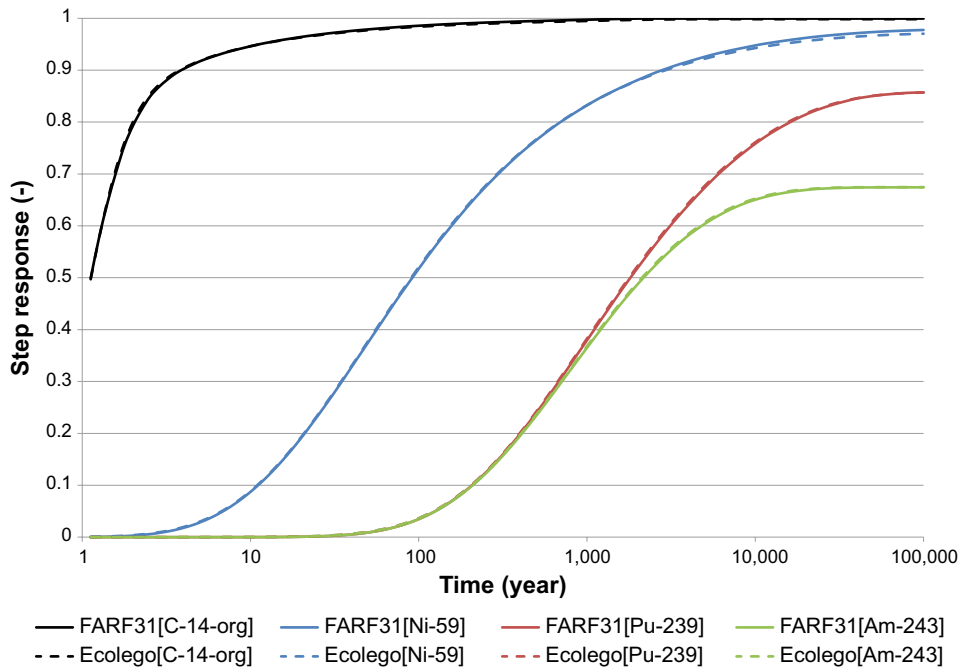


Figure B-4. Comparison of results obtained with FARF31 (solid lines) and the compartment model (dashed lines) At the 50% level on the break-through curves the ratio Ecolego-results / FARF31-results are as follows: 0.9960 for C-14-org, 1.006 for Ni-59, 1.007 for Pu-239 and 1.007 for Am-243.

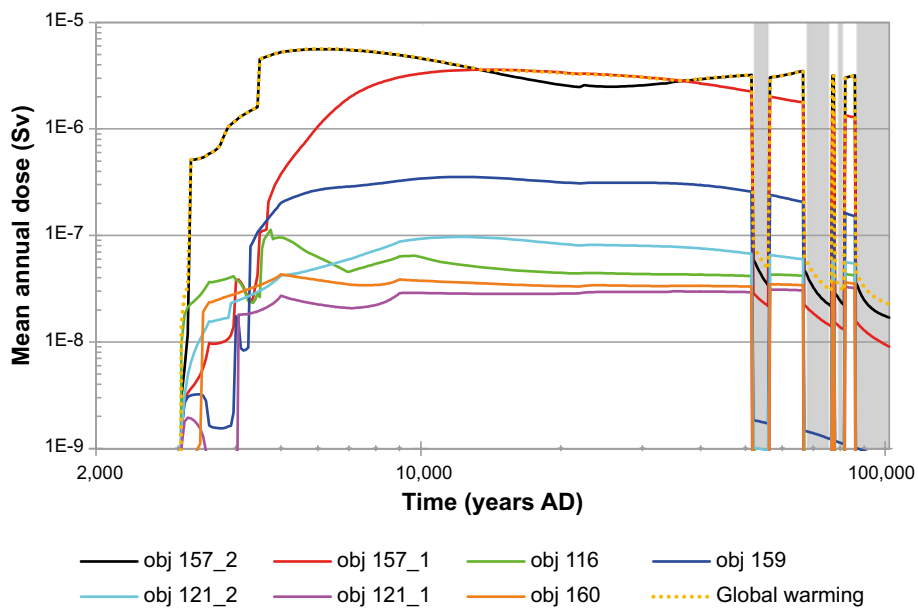


Figure B-5. Resulting annual doses in different biosphere objects with a distributed release.

Transfer coefficients for the far-field model

A compartment model implementing the same conceptual model on which FARF31 is based, was realized in the SAR-08 project (Thomson et al. 2008a). However, no justification for the used transfer coefficients was presented in Thomson et al. (2008a). This is addressed in this appendix.

The first approach to make a compartment model for advective transport in a rock fracture with dispersion and matrix diffusion would be to represent the fracture by a series of boxes, where the dimensions of box i are denoted as follows; side-length W , Length L_i , and aperture b . For each such box a stack of boxes would be set up to represent the rock matrix (see Figure C-1). The depths of the matrix boxes are denoted d_k below. The porosity of the rock matrix is denoted ϕ . The effective diffusion coefficient is denoted D_e . The capacity is denoted C . The flow-wetted surface area per m^3 water is denoted a_w .

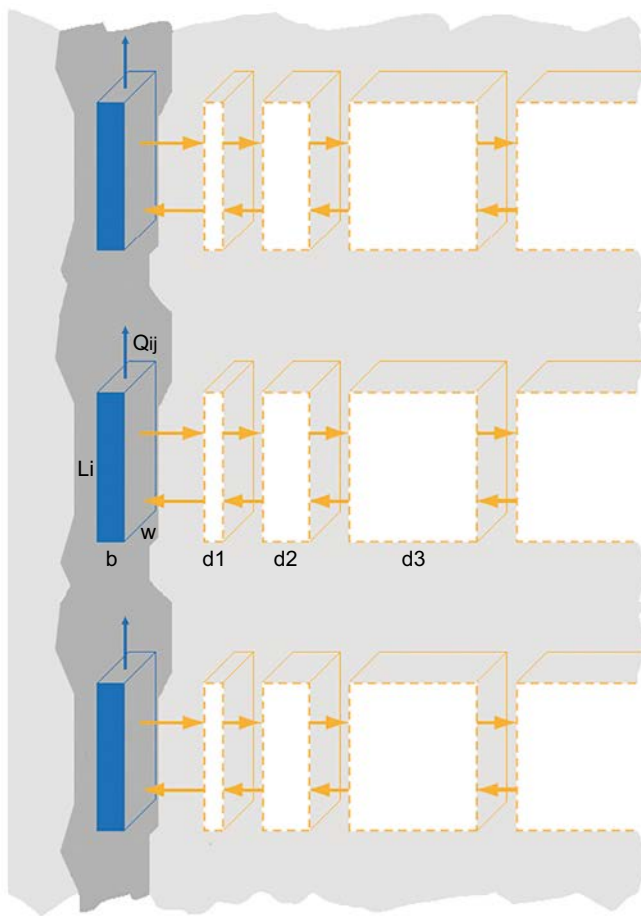


Figure C-1. Illustration of the setup of compartments for derivation of transfer coefficients for a compartment model.

Transfer coefficients for advection

$$TC_{ijadv} = \frac{Q_{ij}}{C_i} = \frac{Q_{ij}}{V_i} = \frac{vWb}{V_i} = \frac{vWb}{WbL_i} = \frac{v}{L_i} = \frac{N}{t} \quad \text{Equation C-1}$$

where:

Q_{ij} water flux [m³/year] from compartment i to j ,

v advective velocity [m/year],

W width of the compartment [m],

L_i length of the compartment [m],

b aperture [m] of the fracture/compartment,

N number of compartments [-],

t total travel time [year].

(Capacity, C , and volume, V , for the fracture compartment are equal, as there is no retardation in the fracture and the porosity for the fracture = 1).

Note: As $\frac{L}{t} = \frac{L_i N}{t}$, the expression for the TC can also be written as either v/L_i or N/t and the absolute value of L (and hence v) is not important. Hence in the model the value of L is set to 1. (v is simply considered as inverse of travel time).

Transfer coefficients for dispersion

It is noted that the transfer induced by the process of dispersion can be derived analogously to the transfer induced by diffusion, replacing the diffusion coefficient by a dispersion coefficient mathematical representation of dispersion is the same as for diffusion. The dispersion coefficient D is expressed as:

$$D = v \left(\frac{L_{tot}}{Pe} \right) \quad \text{Equation C-2}$$

where:

v advective velocity [m/y] of water in the fracture,

L_{tot} total length [m] of the geosphere flow-path,

Pe Peclet number [-].

The dispersive transfer coefficient TC_{ijdisp} from fracture compartment i to j is:

$$TC_{ijdisp} = \frac{DWb}{C_i L_i} = \frac{D}{L_i^2} = \frac{v \left(\frac{L_{tot}}{Pe} \right)}{L_i^2} \quad \text{Equation C-3}$$

The coarse spatial resolution of the compartmental structure generates dispersion. This is adjusted for by reducing the dispersion coefficient by the numerical dispersion $L_i/2$, and the final expression for the dispersion transfer coefficient can then be written as:

$$TC_{dispj} = \frac{v \left(\frac{L_{tot}}{Pe} - \frac{L_i}{2} \right)}{L_i^2} \quad \text{Equation C-4}$$

Note: As with the advective transfer (by observing that $v = \frac{L_{tot}}{t} = \frac{L_i N}{t}$) the expression for dispersion can be written independently of v and L_i .

$$TC_{dispij} = \frac{v \left(\frac{L_{tot}}{Pe} - \frac{L_i}{2} \right)}{L_i^2} = \frac{N^2}{t} \left(\frac{1}{Pe} - \frac{1}{2N} \right) \quad \text{Equation C-5}$$

Transfer coefficients for diffusion

The total flow wetted area (A_i [m²]), i.e. the common area of the compartment representing the fracture and the compartment representing the bedrock confining the fracture compartment i is:

$$A_i = 2L_i W \quad (= \text{for two sides, approximation } b \ll L_i \text{ and } W)$$

The volume (V_i [m³]) of one fracture compartment would be:

$$V_i = A_i b/2$$

The diffusive transfer coefficient $TC_{in1diff}$ from the fracture to the first rock compartment is:

$$TC_{in1diff} = \frac{2D_e A_i}{V_i d_1} = \frac{2D_e a_w}{d_1} \quad \text{Equation C-6}$$

Where D_e is the rock matrix diffusion coefficient [m²y⁻¹]

(The “porosity” for the fracture = 1, which implies $C_i = V_i$)

(The flow wetted surface area $a_w = 2/b = 2A_i/V_i$)

The diffusive transfer coefficient $TC_{out1diff}$ from the first rock compartment to the fracture is:

$$TC_{out1diff} = \frac{2D_e A_i}{C_{m1} d_1} \quad \text{Equation C-7}$$

The area can be eliminated from the expression above using the relations shown in Equation C-8 and Equation C-9.

$$C_m = V_m \phi \left(1 + \frac{K_d \rho}{\phi} \right) = V_m \phi R_m \quad \text{Equation C-8}$$

where:

C_m capacity of a rock matrix compartment

V_m volume of the rock matrix compartment.

R_m retardation factor (see Equation 9-5 in Chapter 9.)

$$a_w = \frac{2}{b} = \frac{2A_i}{V_i} \quad \text{Equation C-9}$$

where:

a_w flow wetted surface area [m²/m³],

b aperture of the fracture [m],

A_i total flow wetted surface area in one compartment [m²],

V_i volume of one compartment [m³].

Hence, diffusive transfer coefficient from the first rock compartment to the fracture can be expressed as:

$$TC_{out1diff} = \frac{2D_e}{\phi R_m d_1^2} \quad \text{Equation C-10}$$

The diffusive transfer coefficient TC_{kliff} from matrix compartment k to l :

$$TC_{kliff} = \frac{2D_e A_i}{C_{mk}(d_k + d_l)}$$

Again, the area can be eliminated from the expression by use of Equation C-8 and Equation C-9, resulting in:

$$TC_{kliff} = \frac{2D_e}{\phi R_m d_k (d_k + d_l)}$$

Transport in fractured concrete

This appendix presents the approach for modelling transport through concrete barriers. The appendix starts with a discussion of the handling of transport in fractured barriers, followed by a discussion of numerical dispersion in compartmental models for transport in porous media.

Fracture flow

A discussion on the possible future fracturing of the concrete barriers in BMA vaults can be found in Chapter 6 in the **Main report**. This appendix contains a more detailed discussion of the conditions of applicability of transport in porous media as an appropriate model for transport through the (fractured) barrier.

Advective transport through concrete barriers is modelled in two ways, either as a homogenous porous medium or as a fractured medium. The latter applies to the two BMA vaults in the far future when degradation of concrete might lead to fracturing of the concrete in the barriers and the water flow can be expected to be localised to larger fractures.

For the radionuclides transported by advection in fractures, the sorbing surface will be much smaller for large than for small fractures. This will limit the validity of a compartment model if the concrete is modelled as a homogenous medium.

Three modelling approaches will be discussed here, denoted as:

1. The *reference model*.
2. The *standard model*.
3. The *fracture model*.

The reference model is introduced only in this appendix. The *reference model* is considered to give a more correct result for fractured media than the two other modelling approaches mentioned above. The *reference model* is, in this work, only used for comparison with the *standard model*. The purpose is to find a range of water flow (governed mainly by the fracturing) where the *standard model* can be expected to give a more pessimistic result than the reference model. In this range the standard model is later used in the assessment. If this condition does not apply, the more pessimistic approach with the *fracture model* will be used.

The standard model is discussed in Chapter 9, which is transport in homogenous porous media for the migration of radionuclides through the barrier.

The fracture model is represented with an advective transfer directly from the waste domain out to the gravel backfill without taking any sorption in the concrete barrier into account.

The calculations were made without taking decay into account i.e. assuming the half-life of the radionuclide to be long in comparison with the studied time scales.

The outcome of this calculation is used to decide which of the two modelling approaches, *standard model* or *fracture model*, to apply in the assessment calculations, for each of the three degradation states of concrete used in the modelling. The three states are characterised as moderately degraded concrete ($K=10^{-7}$ m/s), severely degraded concrete ($K=10^{-5}$ m/s) and completely degraded concrete ($K=10^{-3}$ m/s).

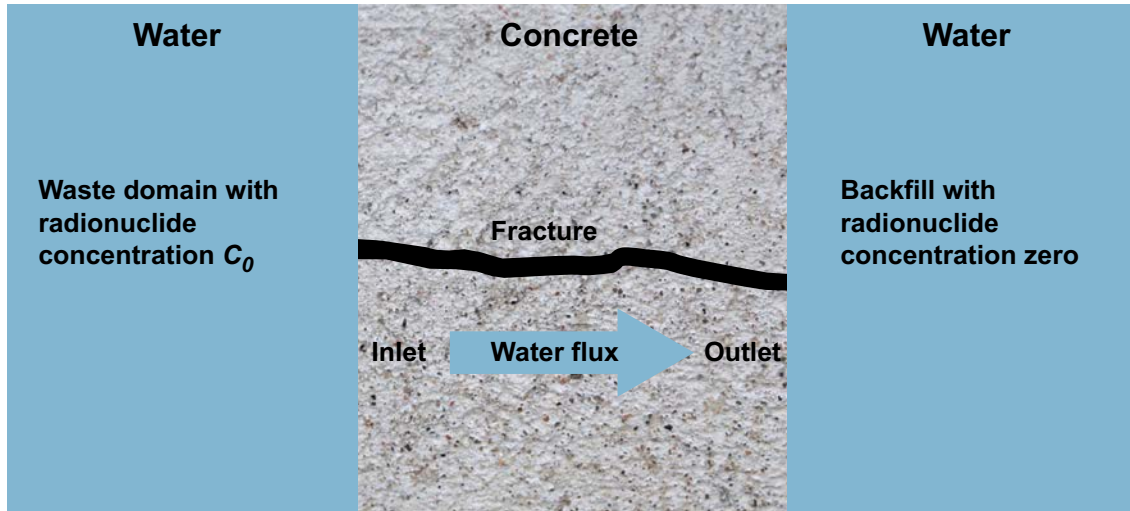


Figure D-1. Conceptual setup for the three models discussed in this appendix. On the waste side of the concrete barrier the concentration of a long lived nuclide is held constant (i.e. the inventory is not assumed to be depleted in this case). The concrete barrier is modelled in three different ways with the standard, fracture and reference models. On the outside of the barrier a zero value boundary condition is assumed.

The reference model

The reference model describes transport through fractures with a dual porosity approach, i.e. with purely advective transport in the fracture and diffusion and sorption in the matrix (Neretnieks and Moreno 2013).

A radionuclide with an initial concentration c_0 [Bq m⁻³], which is fed into the fracture, will emerge at the outlet with a concentration that varies in time t [year]. The concentration of radionuclides at the outlet of a fracture is given by Neretnieks and Moreno (2013) (However in this study the decay of the radionuclide is not taken into account, and a factor, $e^{-\lambda t}$, is deleted from Equation D-1).

$$c(t) = c_0 \operatorname{Erfc} \left(\frac{FWS MPG}{Q \sqrt{t}} \right) \quad \text{Equation D-1}$$

where:

Erfc complementary error function, $\operatorname{Erfc}(x) = 1 - \operatorname{Erf}(x) = \frac{2}{\sqrt{\pi}} \int_x^{\infty} e^{-\xi^2} d\xi$

Q water flow [m³/year],

FWS the flow-wetted (Q) surface of the fracture [m²],

MPG materials property group that accounts for the access of the pore volume and inner surfaces of the concrete on which the sorbing nuclide can attach. [m/year^{1/2}].

MPG is defined as:

$$MPG = \phi \sqrt{D_e \left(1 + \frac{K_d(1-\phi)\rho}{\phi} \right)} \quad \text{Equation D-2}$$

where:

ϕ porosity of concrete [-],

ρ particle density of concrete [kg/m³],

D_e effective diffusivity of concrete [m²/year],

K_d partitioning coefficient of concrete [m³/kg].

The standard model

For advective/diffusive transport of radionuclides through a porous barrier calculated using a compartment model, the delay of radionuclide release is shown in Equation D-8.

A radionuclide with an inflow concentration c_o [Bq] is fed into a compartment of given capacity with transfer rate $q_1 c_o$, where q_1 denotes an appropriate quantity of volumetric flow; the transfer of the radionuclide out of the compartment is determined by the radionuclide concentration c and a flow quantity q_2 so that the following balance for the radionuclide activity in the compartment holds:

$$\dot{c} = \frac{q_1 c_o - q_2 c}{Capacity} \quad \text{Equation D-3}$$

where:

q_1, q_2 volumetric flows into and out of the compartment [m^3/year],

Capacity capacity of the compartment [m^3].

Capacity is defined as:

$$Capacity = Volume(\phi + (1-\phi) K_d \rho) \quad \text{Equation D-4}$$

The differential equation is solved by

$$c(t) = \frac{q_1}{q_2} c_o \left(1 - e^{-\frac{q_2}{Capacity} t} \right) \quad \text{Equation D-5}$$

Assuming a water flow Q [Bq/m^3] through the compartment q_1 takes the following form to describe inflow driven by advection and diffusion:

$$q_1 = Q + 2 \frac{AD_e}{L} \quad \text{Equation D-6}$$

where:

L length of compartment in direction of diffusion. [m],

A cross sectional area of compartment perpendicular to direction of diffusion. [m^2],

As diffusion out of the compartment takes place both opposite and along the direction of flow q_2 takes the form

$$q_2 = Q + 4 \frac{AD_e}{L} \quad \text{Equation D-7}$$

Diffusion from downstream into the compartment is neglected in the model.

Hence, a radionuclide with initial concentration c_o will emerge at the outlet of the compartment with a concentration $c(t)$ that varies in time.

$$c(t) = c_o \left(\frac{Q + 2 \frac{AD_e}{L}}{Q + 4 \frac{AD_e}{L}} \left(1 - e^{-\frac{Q + 4 \frac{AD_e}{L}}{Capacity} t} \right) \right) \quad \text{Equation D-8}$$

where:

Q water flow through the compartment [m^3/year].

The fracture model

In the *fracture model* the outflowing concentration will be identical to the inflow concentration (i.e. $c(t) = c_o$, as the model is represented with an advective transfer directly from the waste domain out to the gravel backfill without taking any sorption in the concrete barrier into account.

Comparison of the standard and reference models

The concentration of radionuclides at the outlet will eventually reach a steady state concentration. A comparison between the times it takes to reach half the steady state concentration at the outlet of the *reference model* and the *standard model* has been used to estimate when the *standard model* overestimates the retardation of radionuclides.

The time it takes to reach half the steady state concentration at the outlet of the *reference model* is given by:

$$t_{half}^{ref} = \left(\frac{FWS MPG}{Q \cdot 0.5} \right)^2 \quad \text{Equation D-9}$$

where :

MPG defined in Equation D-2

FWS if there are 15 fractures in the concrete wall, $FWS^{11} = 15 \times 2 \times 8.4 \times 15.2$ [m²],

ϕ porosity of the concrete wall = 0.1 [-],

ρ particle density of the concrete wall = 2,529.4 [kg/m³],

D_e effective diffusivity of the concrete wall = $9.4673e-5$ [m²/year].

The time it takes to reach half the steady state concentration at the outlet of the *standard model* is given by:

$$t_{half}^{std} = \frac{Capacity}{Q + 4 \frac{AD_e}{L}} \times \ln(2) \quad \text{Equation D-10}$$

where the parameter values above are applicable for ϕ , ρ and D_e and the following geometrical parameters are valid for the concrete wall in a waste compartment in 2BMA:

Volume volume of the concrete wall = $0.5 \times 8.4 \times 15.2$ [m³],

L thickness of the concrete wall = 0.5 [m],

A : cross sectional area of the concrete wall = 8.4×15.2 [m²].

The results from the two different models are compared in figure D-2.

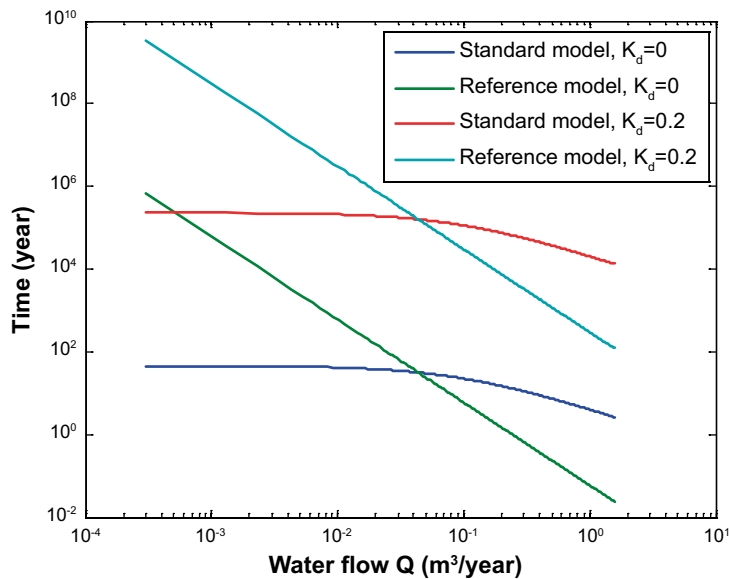


Figure D-2. The time it takes to reach half the steady state concentration at the outlet as a function of water flow rate through a fracture and a compartment for different K_d , for the reference model and the standard model.

¹¹ Numeric values applies to the concrete wall in a waste compartment in 2BMA (**Initial state report, Data report**).

At a sufficiently low flow rate, $Q < 4 \times 10^{-2}$ [m³/year], the presence of fractures will not affect the ability of the concrete wall to sorb radionuclides. The flow rates through all concrete barriers are sufficiently low for effective sorption as long as the flow barriers do not degrade severely and the flow becomes localised to a few major fractures. As shown in Abarca et al. (2013) the water flow in one section of 2BMA is about 0.02 m³/year for the moderately degraded concrete. As this is below the flow limit discussed above, it was considered to model the concrete in the barriers as a porous medium in this case. For the severely and completely degraded concrete on the other hand, the water flows were 1.58 m³/year and 7.40 m³/year and it was decided to model the barrier as a fractured medium in these cases (see also Chapter 4).

Dispersion

A compartment model, representing advective-dispersive transport through e.g. a concrete wall implies a certain degree of numerical dispersion in the modelling result. This numerical dispersion depends on the number of compartments used, and can be estimated in terms of a dispersion length as half the length that one compartment represents. Dispersion lengths for porous media are varying over several orders of magnitudes. For a transport distance of 1 m in a natural porous medium (Holzbecher 2007) reports dispersion lengths in the range of 0.001m to 0.1 m. As the available data indicates that the numerical dispersion is of the same order or higher than the real mechanical dispersion in the barriers, it was considered as not appropriate to include additional dispersion in the model.

Further it should be noted that the dispersion, as discussed above, has little, if any, effect on the main result of the radionuclide transport calculations, i.e. the estimate of the total (combined) releases from the whole repository. These releases originate from different parts of a repository with dimensions in the order of hundreds of meters, with different shapes and properties of barriers and waste packaging. The dispersive effect introduced by these factors will overshadow the issue of numerical and mechanical dispersion on the barrier thickness scale.

Result compilation

The discussion in the main text of the present report only presents results for radionuclides which contribute most to the radiotoxicity of releases or to total annual effective doses. This appendix compiles results for all radionuclides included in the calculations. The tables contain peak releases from near-field, peak releases from far-field and peak doses. For each reported release and dose value the time of occurrence is given within parentheses.

For the *wells downstream of the repository calculation case* (CCL_WD) only peak annual doses are presented. These doses are based on the assumption that 10% of the releases in the *global warming calculation case* (CCM_GW) reach a drilled well and are diluted in the volume of daily abstracted water (700 L/d).

For the *intrusion wells calculation case* (CCL_WI) the annual doses are based on the assumption that a well is drilled into a waste vault and the calculation of doses is based on the radionuclide concentrations in the backfill, which are reported instead of radionuclide release in this case. The consequences are evaluated for each vault.

All peak values (as maxima of time series) are obtained from calculation results which are output every 50 years of simulated time. Release values below 1 Bq/year are reported as "< 1 Bq/year" and annual doses below $1\text{E-}12$ Sv/year as "< $1\text{e-}12$ Sv/year". Due to the limited numerical accuracy of the simulation results, exact values below these thresholds are not meaningful.

Global warming calculation case (CCM_GW)

Table E-1. Near-field releases for CCM_GW, peak release [Bq/year] and in parentheses time of peak [1000 year AD].

Nuclide	1BMA	2BMA	1BTF	2BTF	Silo	BRT	1BLA	2-5BLA	Total
Ac-227	1.9e+02 (84)	< 1	2.9e+01 (86)	2.4e+00 (20)	1.2e+01 (86)	< 1	2.2e+04 (3)	5.2e+03 (4)	2.3e+04 (3)
Ag-108m	3.8e+05 (3)	1.4e+05 (4)	1.6e+05 (3)	7.4e+05 (3)	2.7e+04 (4)	2.0e+05 (3)	1.3e+05 (3)	6.5e+04 (3)	1.4e+06 (3)
Am-241	8.0e+01 (4)	< 1	4.8e+00 (4)	1.3e+02 (4)	< 1	6.9e+00 (4)	3.8e+05 (3)	8.8e+04 (3)	4.1e+05 (3)
Am-242m	< 1	< 1	< 1	< 1	< 1	< 1	2.5e+01 (3)	3.7e+00 (3)	2.5e+01 (3)
Am-243	9.7e+01 (7)	< 1	5.2e+00 (22)	2.8e+01 (4)	< 1	3.8e+00 (22)	1.3e+04 (3)	6.5e+03 (4)	1.4e+04 (3)
Ba-133	< 1	< 1	< 1	< 1	< 1	< 1	< 1	< 1	< 1
C-14-ind	< 1	4.5e+05 (5)	< 1	< 1	< 1	2.7e+04 (24)	< 1	4.0e+05 (4)	7.6e+05 (4)
C-14-inorg	2.5e+05 (22)	8.7e+00 (24)	1.5e+05 (12)	6.6e+05 (4)	2.1e+02 (34)	< 1	1.3e+07 (3)	3.1e+05 (4)	1.3e+07 (3)
C-14-org	2.9e+07 (4)	3.5e+05 (5)	6.3e+06 (3)	9.8e+06 (3)	5.3e+07 (5)	< 1	2.5e+05 (3)	7.5e+04 (4)	7.7e+07 (5)
Ca-41	< 1	8.0e+05 (10)	< 1	< 1	< 1	< 1	< 1	1.6e+06 (4)	1.6e+06 (4)
Cd-113m	< 1	< 1	< 1	< 1	< 1	< 1	< 1	< 1	< 1
Cl-36	4.0e+04 (4)	1.2e+04 (7)	7.0e+03 (3)	2.4e+04 (3)	3.5e+04 (6)	2.7e+02 (29)	7.6e+04 (3)	1.9e+04 (4)	1.1e+05 (3)
Cm-242	< 1	< 1	< 1	< 1	< 1	< 1	2.0e+01 (3)	3.0e+00 (3)	2.0e+01 (3)
Cm-243	< 1	< 1	< 1	< 1	< 1	< 1	< 1	< 1	< 1
Cm-244	< 1	< 1	< 1	< 1	< 1	< 1	< 1	< 1	< 1
Cm-245	< 1	< 1	< 1	< 1	< 1	< 1	1.3e+02 (3)	7.8e+01 (4)	1.5e+02 (3)
Cm-246	< 1	< 1	< 1	< 1	< 1	< 1	3.2e+01 (3)	2.1e+01 (4)	3.7e+01 (3)
Co-60	< 1	< 1	< 1	< 1	< 1	< 1	< 1	< 1	< 1
Cs-135	9.4e+04 (7)	2.4e+03 (7)	2.6e+04 (4)	1.8e+04 (3)	3.1e+04 (13)	< 1	1.1e+04 (3)	7.1e+04 (4)	1.6e+05 (4)
Cs-137	< 1	< 1	< 1	< 1	< 1	< 1	< 1	< 1	< 1
Eu-152	< 1	< 1	< 1	< 1	< 1	< 1	< 1	< 1	< 1
H-3	< 1	< 1	< 1	< 1	< 1	< 1	< 1	< 1	< 1
Ho-166m	4.5e+01 (5)	< 1	1.5e+00 (4)	7.3e+01 (4)	< 1	< 1	8.1e+03 (3)	1.5e+04 (3)	1.7e+04 (3)
I-129	2.0e+04 (22)	2.8e+02 (8)	6.8e+03 (3)	1.3e+04 (3)	2.3e+04 (6)	< 1	1.5e+03 (3)	7.9e+02 (4)	3.7e+04 (5)
Mo-93	8.1e+04 (4)	7.7e+04 (5)	7.7e+04 (3)	2.3e+05 (3)	2.5e+05 (5)	6.6e+04 (4)	3.0e+05 (3)	2.8e+04 (4)	6.2e+05 (3)
Nb-93m	1.6e+04 (24)	1.6e+03 (86)	1.1e+03 (3)	7.1e+03 (4)	7.7e+03 (62)	1.1e+03 (4)	3.0e+05 (3)	4.0e+04 (4)	3.1e+05 (3)
Nb-94	3.2e+03 (25)	5.2e+02 (67)	1.4e+02 (61)	3.3e+03 (7)	1.7e+02 (34)	1.2e+03 (67)	1.1e+05 (3)	3.8e+05 (4)	3.8e+05 (4)
Ni-59	1.4e+07 (59)	3.6e+06 (63)	2.0e+06 (4)	7.0e+06 (4)	8.2e+06 (34)	3.5e+06 (22)	1.4e+07 (3)	4.6e+06 (4)	2.2e+07 (58)
Ni-63	3.7e+02 (3)	< 1	3.5e+03 (3)	6.6e+04 (3)	< 1	1.4e+04 (3)	9.8e+05 (3)	8.7e+04 (3)	9.8e+05 (3)
Np-237	4.8e+02 (23)	2.2e+00 (86)	1.4e+00 (22)	2.4e+02 (4)	8.7e+01 (34)	< 1	5.6e+02 (3)	2.7e+02 (4)	6.7e+02 (3)
Pa-231	2.1e+01 (83)	< 1	5.6e+00 (58)	< 1	7.5e+00 (77)	< 1	2.3e+04 (3)	5.3e+03 (4)	2.4e+04 (3)
Pb-210	1.3e+02 (77)	2.2e+01 (86)	1.3e+00 (22)	2.6e+00 (22)	9.0e+00 (86)	< 1	6.1e+00 (3)	4.3e+00 (5)	1.4e+02 (77)
Pd-107	4.6e+03 (4)	1.3e+05 (6)	1.5e+02 (4)	5.5e+03 (3)	3.3e+03 (7)	< 1	3.5e+02 (3)	7.0e+02 (4)	1.4e+05 (6)
Po-210	1.1e+04 (77)	1.9e+03 (86)	1.0e+02 (22)	8.9e+01 (77)	6.8e+02 (86)	6.8e+01 (22)	6.1e+00 (3)	4.3e+00 (5)	1.2e+04 (77)
Pu-238	3.2e+00 (3)	< 1	< 1	7.2e+00 (3)	< 1	< 1	4.8e+02 (3)	4.8e+01 (3)	4.8e+02 (3)
Pu-239	2.0e+04 (5)	1.8e+02 (58)	8.0e+01 (16)	2.5e+04 (3)	2.7e+03 (35)	1.1e+02 (13)	2.3e+05 (3)	1.1e+05 (4)	2.6e+05 (3)
Pu-240	2.4e+04 (4)	3.2e+00 (57)	4.6e+01 (13)	3.2e+04 (3)	7.1e+02 (16)	1.2e+02 (4)	2.1e+05 (3)	1.0e+05 (4)	2.5e+05 (3)
Pu-241	1.5e+01 (7)	< 1	1.0e+00 (17)	1.1e+01 (13)	< 1	< 1	1.3e+02 (3)	7.8e+01 (4)	1.5e+02 (3)
Pu-242	2.2e+02 (23)	5.9e+00 (64)	1.0e+00 (32)	1.9e+02 (3)	3.7e+01 (35)	1.1e+00 (24)	1.4e+03 (3)	7.0e+02 (4)	1.7e+03 (3)
Ra-226	1.2e+03 (77)	2.5e+02 (84)	1.5e+01 (22)	6.5e+00 (22)	1.4e+02 (82)	9.0e+00 (22)	6.6e+00 (3)	4.4e+00 (5)	1.4e+03 (77)
Ra-228	< 1	< 1	< 1	< 1	< 1	< 1	< 1	< 1	< 1
Se-79	5.2e+04 (4)	9.1e+02 (5)	8.9e+03 (3)	2.8e+04 (3)	1.1e+05 (5)	< 1	1.4e+03 (3)	2.4e+03 (4)	1.5e+05 (5)
Sm-151	< 1	< 1	< 1	< 1	< 1	< 1	2.5e+02 (3)	1.9e+02 (3)	3.4e+02 (3)
Sn-126	2.2e+02 (57)	< 1	1.8e+00 (59)	1.2e+02 (5)	2.7e+01 (67)	< 1	1.8e+02 (3)	3.2e+03 (4)	3.3e+03 (4)
Sr-90	< 1	< 1	< 1	< 1	< 1	< 1	< 1	< 1	< 1
Tc-99	1.1e+05 (25)	2.1e+02 (86)	4.4e+03 (58)	7.4e+04 (4)	2.6e+04 (67)	4.0e+02 (58)	6.5e+06 (3)	2.0e+05 (4)	6.6e+06 (3)
Th-228	< 1	< 1	< 1	< 1	< 1	< 1	< 1	< 1	< 1
Th-229	6.8e+01 (84)	< 1	< 1	3.1e+00 (58)	4.5e+00 (86)	< 1	< 1	< 1	7.6e+01 (85)
Th-230	2.9e+01 (83)	< 1	< 1	2.4e+00 (22)	4.1e+00 (86)	< 1	4.5e+01 (3)	1.1e+01 (5)	4.6e+01 (3)
Th-232	< 1	< 1	< 1	< 1	< 1	< 1	< 1	< 1	< 1
U-232	< 1	< 1	< 1	< 1	< 1	< 1	< 1	< 1	< 1
U-233	9.2e+01 (56)	< 1	< 1	5.7e+00 (22)	2.1e+01 (77)	< 1	2.0e+00 (3)	2.0e+00 (5)	1.1e+02 (77)
U-234	1.2e+02 (23)	2.2e+00 (67)	< 1	6.5e+01 (4)	2.7e+01 (34)	< 1	8.6e+03 (3)	7.6e+02 (4)	8.7e+03 (3)
U-235	6.1e+01 (23)	< 1	2.5e+00 (58)	1.2e+01 (4)	6.1e+00 (34)	< 1	1.1e+06 (3)	1.3e+05 (4)	1.1e+06 (3)
U-236	3.8e+01 (23)	1.2e+00 (86)	< 1	3.9e+01 (4)	1.0e+01 (34)	< 1	1.5e+02 (3)	9.0e+01 (4)	1.8e+02 (3)
U-238	9.5e+01 (23)	< 1	< 1	9.1e+01 (4)	1.4e+01 (34)	< 1	2.6e+06 (3)	7.2e+04 (4)	2.6e+06 (3)
Zr-93	7.6e+03 (24)	5.2e+02 (86)	9.6e+01 (22)	5.9e+03 (4)	9.6e+03 (34)	2.7e+02 (22)	3.8e+03 (3)	1.2e+04 (4)	1.8e+04 (4)

Table E-2. Far-field releases for CCM_GW, peak release [Bq/year] and in parentheses time of peak [1000 year AD].

Nuclide	1BMA	2BMA	1BTF	2BTF	Silo	BRT	1BLA	2-5BLA	Total
Ac-227	1.9e+02 (85)	< 1	1.6e+01 (86)	5.1e+00 (77)	3.4e+01 (86)	< 1	1.5e+04 (5)	4.2e+03 (82)	1.5e+04 (5)
Ag-108m	3.7e+05 (3)	1.2e+05 (4)	1.4e+05 (3)	5.4e+05 (3)	2.5e+04 (4)	1.5e+05 (3)	1.2e+05 (3)	5.3e+04 (3)	1.2e+06 (3)
Am-241	1.4e+01 (5)	< 1	< 1	7.4e+00 (4)	< 1	< 1	1.9e+04 (4)	6.4e+02 (4)	2.0e+04 (4)
Am-242m	< 1	< 1	< 1	< 1	< 1	< 1	< 1	< 1	< 1
Am-243	1.8e+01 (7)	< 1	< 1	5.0e+00 (14)	< 1	< 1	1.3e+03 (4)	3.4e+02 (5)	1.3e+03 (4)
Ba-133	< 1	< 1	< 1	< 1	< 1	< 1	< 1	< 1	< 1
C-14-ind	< 1	4.0e+05 (5)	< 1	< 1	< 1	2.6e+04 (24)	< 1	3.7e+05 (4)	6.8e+05 (4)
C-14-inorg	2.5e+05 (22)	8.2e+00 (24)	1.4e+05 (12)	6.2e+05 (4)	2.1e+02 (34)	< 1	1.1e+07 (3)	2.9e+05 (4)	1.1e+07 (3)
C-14-org	2.8e+07 (4)	3.1e+05 (5)	5.7e+06 (3)	7.7e+06 (3)	5.2e+07 (5)	< 1	2.2e+05 (3)	6.9e+04 (4)	7.5e+07 (5)
Ca-41	< 1	7.8e+05 (10)	< 1	< 1	< 1	< 1	< 1	1.4e+06 (4)	1.4e+06 (4)
Cd-113m	< 1	< 1	< 1	< 1	< 1	< 1	< 1	< 1	< 1
Cl-36	4.0e+04 (4)	1.1e+04 (8)	6.8e+03 (3)	2.0e+04 (3)	3.4e+04 (6)	2.7e+02 (30)	6.9e+04 (3)	1.7e+04 (4)	1.0e+05 (3)
Cm-242	< 1	< 1	< 1	< 1	< 1	< 1	< 1	< 1	< 1
Cm-243	< 1	< 1	< 1	< 1	< 1	< 1	< 1	< 1	< 1
Cm-244	< 1	< 1	< 1	< 1	< 1	< 1	< 1	< 1	< 1
Cm-245	< 1	< 1	< 1	< 1	< 1	< 1	1.4e+01 (4)	4.1e+00 (5)	1.5e+01 (4)
Cm-246	< 1	< 1	< 1	< 1	< 1	< 1	3.3e+00 (4)	1.0e+00 (5)	3.5e+00 (4)
Co-60	< 1	< 1	< 1	< 1	< 1	< 1	< 1	< 1	< 1
Cs-135	6.6e+04 (5)	8.5e+02 (9)	1.5e+04 (4)	7.2e+03 (4)	2.2e+04 (16)	< 1	2.8e+03 (3)	2.0e+04 (5)	1.0e+05 (5)
Cs-137	< 1	< 1	< 1	< 1	< 1	< 1	< 1	< 1	< 1
Eu-152	< 1	< 1	< 1	< 1	< 1	< 1	< 1	< 1	< 1
H-3	< 1	< 1	< 1	< 1	< 1	< 1	< 1	< 1	< 1
Ho-166m	1.3e+01 (5)	< 1	< 1	8.5e+00 (4)	< 1	< 1	5.8e+02 (4)	3.3e+02 (5)	7.0e+02 (4)
I-129	2.0e+04 (22)	3.0e+02 (9)	6.7e+03 (3)	1.0e+04 (3)	2.3e+04 (6)	< 1	1.4e+03 (3)	7.2e+02 (4)	3.7e+04 (5)
Mo-93	8.0e+04 (4)	7.0e+04 (6)	7.4e+04 (3)	1.9e+05 (3)	2.5e+05 (5)	6.2e+04 (4)	2.7e+05 (3)	2.6e+04 (4)	5.4e+05 (3)
Nb-93m	1.1e+04 (28)	2.3e+02 (5)	4.0e+02 (4)	2.7e+03 (5)	1.1e+04 (50)	2.2e+02 (4)	2.0e+03 (3)	6.2e+02 (10)	2.2e+04 (32)
Nb-94	1.9e+03 (28)	4.6e+01 (67)	5.4e+01 (66)	1.3e+03 (14)	5.5e+01 (34)	2.1e+02 (67)	9.2e+03 (4)	1.3e+04 (5)	1.7e+04 (5)
Ni-59	1.2e+07 (61)	1.7e+06 (67)	8.0e+05 (4)	4.1e+06 (4)	3.5e+06 (35)	7.1e+05 (59)	3.7e+06 (3)	1.4e+06 (5)	1.6e+07 (62)
Ni-63	1.7e+02 (4)	< 1	8.6e+02 (4)	7.6e+03 (4)	< 1	3.9e+02 (4)	1.1e+05 (3)	2.4e+03 (3)	1.1e+05 (3)
Np-237	1.7e+02 (26)	< 1	< 1	3.4e+01 (9)	1.9e+01 (86)	< 1	2.4e+01 (4)	4.9e+00 (5)	2.0e+02 (26)
Pa-231	1.6e+01 (77)	< 1	2.6e+00 (86)	< 1	2.0e+00 (86)	< 1	1.9e+03 (5)	6.6e+02 (82)	1.9e+03 (5)
Pb-210	7.3e+01 (77)	4.2e+00 (86)	< 1	4.9e+00 (77)	7.6e+00 (82)	< 1	3.1e+02 (77)	7.1e+01 (82)	4.7e+02 (77)
Pd-107	4.5e+03 (4)	1.3e+05 (7)	1.5e+02 (4)	4.5e+03 (3)	3.3e+03 (7)	< 1	3.2e+02 (3)	6.4e+02 (4)	1.4e+05 (7)
Po-210	8.8e+01 (77)	4.1e+00 (86)	< 1	5.4e+00 (77)	7.2e+00 (86)	< 1	3.2e+02 (77)	6.2e+01 (82)	4.8e+02 (77)
Pu-238	< 1	< 1	< 1	< 1	< 1	< 1	5.0e+00 (3)	< 1	5.2e+00 (3)
Pu-239	1.1e+04 (5)	2.9e+01 (67)	5.1e+01 (28)	5.0e+03 (5)	1.1e+03 (38)	1.7e+01 (30)	2.3e+04 (4)	5.1e+03 (5)	3.1e+04 (4)
Pu-240	1.2e+04 (5)	< 1	1.2e+01 (16)	5.5e+03 (5)	1.7e+02 (20)	4.5e+00 (5)	2.1e+04 (4)	4.3e+03 (5)	3.0e+04 (4)
Pu-241	1.4e+00 (7)	< 1	< 1	< 1	< 1	< 1	2.2e+01 (4)	3.6e+00 (9)	2.3e+01 (4)
Pu-242	1.1e+02 (25)	1.5e+00 (86)	< 1	3.9e+01 (5)	1.8e+01 (67)	< 1	1.4e+02 (4)	3.4e+01 (5)	2.0e+02 (5)
Ra-226	1.1e+03 (77)	5.8e+01 (86)	9.7e+00 (22)	7.6e+01 (77)	1.1e+02 (82)	1.9e+00 (22)	5.4e+03 (77)	1.1e+03 (82)	7.9e+03 (77)
Ra-228	< 1	< 1	< 1	< 1	< 1	< 1	< 1	< 1	< 1
Se-79	5.2e+04 (4)	8.1e+02 (5)	8.3e+03 (3)	2.2e+04 (3)	1.0e+05 (5)	< 1	1.3e+03 (3)	2.2e+03 (4)	1.5e+05 (5)
Sm-151	< 1	< 1	< 1	< 1	< 1	< 1	1.9e+00 (3)	< 1	1.9e+00 (3)
Sn-126	1.0e+02 (63)	< 1	< 1	1.2e+01 (15)	4.1e+00 (86)	< 1	2.9e+00 (5)	1.3e+01 (16)	1.2e+02 (63)
Sr-90	< 1	< 1	< 1	< 1	< 1	< 1	< 1	< 1	< 1
Tc-99	5.5e+04 (29)	1.5e+01 (86)	1.2e+03 (61)	9.9e+03 (5)	9.1e+03 (86)	3.3e+01 (86)	3.0e+05 (4)	3.9e+03 (9)	3.0e+05 (4)
Th-228	< 1	< 1	< 1	< 1	< 1	< 1	< 1	< 1	< 1
Th-229	9.5e+01 (77)	< 1	< 1	6.3e+00 (77)	6.1e+00 (82)	< 1	< 1	< 1	1.1e+02 (77)
Th-230	2.5e+01 (77)	< 1	< 1	2.3e+00 (77)	2.7e+00 (86)	< 1	1.9e+02 (82)	4.0e+01 (82)	2.6e+02 (82)
Th-232	< 1	< 1	< 1	< 1	< 1	< 1	< 1	< 1	< 1
U-232	< 1	< 1	< 1	< 1	< 1	< 1	< 1	< 1	< 1
U-233	5.9e+01 (82)	< 1	< 1	4.2e+00 (77)	5.7e+00 (86)	< 1	< 1	< 1	6.9e+01 (82)
U-234	4.6e+01 (26)	< 1	< 1	8.2e+00 (9)	5.0e+00 (86)	< 1	5.9e+02 (5)	6.9e+01 (82)	6.1e+02 (5)
U-235	2.2e+01 (25)	< 1	1.5e+00 (86)	1.5e+00 (9)	1.3e+00 (86)	< 1	4.4e+04 (4)	2.6e+03 (10)	4.5e+04 (4)
U-236	1.6e+01 (26)	< 1	< 1	5.2e+00 (9)	2.1e+00 (86)	< 1	6.4e+00 (4)	2.0e+00 (10)	2.2e+01 (25)
U-238	3.6e+01 (26)	< 1	< 1	1.1e+01 (9)	2.9e+00 (86)	< 1	1.1e+05 (4)	1.4e+03 (10)	1.1e+05 (4)
Zr-93	4.5e+03 (26)	5.4e+01 (86)	5.0e+01 (22)	1.3e+03 (5)	4.1e+03 (86)	3.6e+01 (37)	2.8e+02 (4)	3.7e+02 (9)	7.3e+03 (28)

Table E-3. Doses for CCM_GW, peak dose [Sv/year] and in parentheses time of peak [1000 year AD].

Nuclide	1BMA	2BMA	1BTF	2BTF	Silo	BRT	1BLA	2-5BLA	Total
Total	1.8e-06 (67)	1.0e-06 (17)	4.2e-07 (5)	5.2e-07 (5)	3.6e-06 (7)	3.7e-07 (5)	1.3e-06 (24)	5.2e-07 (9)	7.7e-06 (7)
Ac-227	7.2e-10 (77)	< 1e-12	5.9e-11 (86)	3.3e-11 (44)	6.8e-11 (86)	< 1e-12	2.1e-07 (33)	9.5e-08 (57)	2.9e-07 (38)
Ag-108m	9.9e-09 (5)	4.9e-09 (5)	2.0e-09 (5)	3.8e-09 (5)	1.2e-09 (5)	2.9e-09 (5)	5.3e-10 (5)	1.4e-09 (5)	2.6e-08 (5)
Am-241	< 1e-12	< 1e-12	< 1e-12	< 1e-12	< 1e-12	< 1e-12	1.6e-10 (4)	5.8e-10 (4)	6.3e-10 (4)
Am-242m	< 1e-12	< 1e-12	< 1e-12	< 1e-12	< 1e-12	< 1e-12	< 1e-12	< 1e-12	< 1e-12
Am-243	1.4e-11 (32)	< 1e-12	1.4e-12 (29)	1.2e-11 (26)	< 1e-12	< 1e-12	2.5e-10 (15)	3.4e-10 (5)	4.9e-10 (16)
Ba-133	< 1e-12	< 1e-12	< 1e-12	< 1e-12	< 1e-12	< 1e-12	< 1e-12	< 1e-12	< 1e-12
C-14-ind	< 1e-12	1.1e-08 (5)	< 1e-12	< 1e-12	< 1e-12	7.2e-10 (24)	< 1e-12	7.8e-09 (5)	1.9e-08 (5)
C-14-inorg	6.8e-09 (23)	< 1e-12	4.1e-09 (13)	1.7e-08 (6)	5.9e-12 (34)	< 1e-12	9.0e-08 (3)	6.0e-09 (5)	9.1e-08 (3)
C-14-org	7.1e-07 (5)	8.6e-09 (5)	6.1e-08 (3)	6.4e-08 (3)	1.5e-06 (5)	< 1e-12	1.8e-09 (3)	1.5e-09 (5)	2.1e-06 (5)
Ca-41	< 1e-12	8.4e-07 (28)	< 1e-12	< 1e-12	< 1e-12	< 1e-12	< 1e-12	4.4e-07 (10)	1.0e-06 (19)
Cd-113m	< 1e-12	< 1e-12	< 1e-12	< 1e-12	< 1e-12	< 1e-12	< 1e-12	< 1e-12	< 1e-12
Cl-36	1.3e-07 (5)	3.7e-08 (8)	1.0e-08 (5)	1.1e-08 (5)	1.1e-07 (6)	8.8e-10 (30)	1.9e-08 (3)	4.8e-08 (5)	3.1e-07 (5)
Cm-242	< 1e-12	< 1e-12	< 1e-12	< 1e-12	< 1e-12	< 1e-12	< 1e-12	< 1e-12	< 1e-12
Cm-243	< 1e-12	< 1e-12	< 1e-12	< 1e-12	< 1e-12	< 1e-12	< 1e-12	< 1e-12	< 1e-12
Cm-244	< 1e-12	< 1e-12	< 1e-12	< 1e-12	< 1e-12	< 1e-12	< 1e-12	< 1e-12	< 1e-12
Cm-245	< 1e-12	< 1e-12	< 1e-12	< 1e-12	< 1e-12	< 1e-12	2.6e-12 (15)	4.2e-12 (5)	5.3e-12 (16)
Cm-246	< 1e-12	< 1e-12	< 1e-12	< 1e-12	< 1e-12	< 1e-12	< 1e-12	< 1e-12	< 1e-12
Co-60	< 1e-12	< 1e-12	< 1e-12	< 1e-12	< 1e-12	< 1e-12	< 1e-12	< 1e-12	< 1e-12
Cs-135	6.6e-07 (86)	1.9e-08 (86)	6.1e-08 (86)	1.5e-08 (86)	6.1e-07 (86)	< 1e-12	2.5e-09 (86)	9.9e-08 (86)	1.5e-06 (86)
Cs-137	< 1e-12	< 1e-12	< 1e-12	< 1e-12	< 1e-12	< 1e-12	< 1e-12	< 1e-12	< 1e-12
Eu-152	< 1e-12	< 1e-12	< 1e-12	< 1e-12	< 1e-12	< 1e-12	< 1e-12	< 1e-12	< 1e-12
H-3	< 1e-12	< 1e-12	< 1e-12	< 1e-12	< 1e-12	< 1e-12	< 1e-12	< 1e-12	< 1e-12
Ho-166m	< 1e-12	< 1e-12	< 1e-12	< 1e-12	< 1e-12	< 1e-12	< 1e-12	3.9e-12 (5)	4.4e-12 (5)
I-129	2.4e-07 (11)	8.6e-09 (27)	5.7e-08 (6)	4.1e-08 (5)	5.6e-07 (16)	< 1e-12	3.2e-09 (3)	8.2e-09 (6)	8.1e-07 (13)
Mo-93	6.6e-07 (6)	7.4e-07 (9)	3.3e-07 (5)	4.3e-07 (5)	2.3e-06 (8)	3.7e-07 (5)	2.7e-07 (5)	1.6e-07 (5)	4.5e-06 (7)
Nb-93m	2.2e-10 (6)	2.4e-10 (9)	1.1e-10 (5)	1.4e-10 (5)	7.5e-10 (8)	1.2e-10 (5)	8.8e-11 (5)	5.0e-11 (5)	1.5e-09 (7)
Nb-94	3.1e-10 (67)	2.1e-12 (86)	6.8e-12 (77)	1.4e-10 (52)	6.0e-12 (78)	2.6e-11 (77)	8.2e-11 (32)	6.3e-10 (43)	1.1e-09 (52)
Ni-59	1.3e-06 (67)	1.0e-07 (86)	4.0e-08 (35)	7.8e-08 (29)	2.9e-07 (52)	1.1e-07 (52)	1.8e-08 (15)	3.1e-08 (21)	1.8e-06 (67)
Ni-63	< 1e-12	< 1e-12	< 1e-12	< 1e-12	< 1e-12	< 1e-12	4.5e-12 (3)	1.9e-12 (3)	4.7e-12 (3)
Np-237	1.8e-09 (86)	< 1e-12	4.4e-12 (86)	3.7e-10 (86)	8.1e-11 (86)	< 1e-12	4.3e-11 (86)	3.2e-11 (86)	2.3e-09 (86)
Pa-231	1.6e-09 (86)	< 1e-12	1.4e-10 (86)	5.8e-11 (39)	8.3e-11 (86)	< 1e-12	3.9e-07 (30)	1.2e-07 (52)	4.9e-07 (34)
Pb-210	5.6e-09 (86)	4.3e-10 (67)	7.0e-11 (23)	3.8e-10 (86)	5.4e-10 (86)	1.3e-11 (23)	2.9e-08 (86)	7.5e-09 (86)	4.3e-08 (86)
Pd-107	9.9e-11 (36)	4.5e-09 (67)	1.7e-12 (30)	1.3e-11 (18)	2.1e-10 (41)	< 1e-12	< 1e-12	6.5e-12 (16)	4.7e-09 (67)
Po-210	2.0e-10 (86)	3.4e-11 (86)	2.7e-12 (22)	1.3e-11 (86)	3.0e-11 (86)	< 1e-12	9.9e-10 (86)	4.2e-10 (86)	1.6e-09 (86)
Pu-238	< 1e-12	< 1e-12	< 1e-12	< 1e-12	< 1e-12	< 1e-12	< 1e-12	< 1e-12	< 1e-12
Pu-239	1.6e-07 (57)	2.6e-10 (86)	1.1e-09 (67)	3.9e-08 (43)	2.4e-08 (77)	4.0e-10 (67)	3.2e-08 (32)	4.3e-08 (42)	2.8e-07 (52)
Pu-240	1.6e-08 (19)	< 1e-12	6.1e-11 (31)	7.9e-09 (19)	5.4e-10 (44)	2.4e-11 (28)	8.2e-09 (14)	7.0e-09 (18)	3.8e-08 (18)
Pu-241	< 1e-12	< 1e-12	< 1e-12	< 1e-12	< 1e-12	< 1e-12	< 1e-12	< 1e-12	< 1e-12
Pu-242	8.3e-09 (86)	1.3e-11 (86)	3.7e-11 (86)	1.4e-09 (86)	1.2e-09 (86)	3.7e-12 (86)	6.1e-10 (84)	1.2e-09 (86)	1.3e-08 (86)
Ra-226	3.3e-08 (86)	2.3e-09 (67)	3.6e-10 (23)	2.4e-09 (86)	3.7e-09 (86)	6.3e-11 (23)	1.8e-07 (86)	4.3e-08 (86)	2.6e-07 (86)
Ra-228	< 1e-12	< 1e-12	< 1e-12	< 1e-12	< 1e-12	< 1e-12	< 1e-12	< 1e-12	< 1e-12
Se-79	1.5e-08 (7)	3.6e-10 (11)	1.0e-09 (6)	1.5e-09 (6)	4.5e-08 (12)	< 1e-12	4.5e-11 (5)	5.2e-10 (7)	5.9e-08 (10)
Sm-151	< 1e-12	< 1e-12	< 1e-12	< 1e-12	< 1e-12	< 1e-12	< 1e-12	< 1e-12	< 1e-12
Sn-126	1.1e-10 (86)	< 1e-12	< 1e-12	1.5e-11 (78)	2.1e-12 (99)	< 1e-12	< 1e-12	1.5e-11 (78)	1.4e-10 (86)
Sr-90	< 1e-12	< 1e-12	< 1e-12	< 1e-12	< 1e-12	< 1e-12	< 1e-12	< 1e-12	< 1e-12
Tc-99	6.1e-08 (86)	2.0e-12 (86)	1.7e-09 (86)	8.7e-09 (67)	1.1e-08 (86)	2.1e-11 (86)	4.2e-08 (52)	3.3e-09 (67)	1.2e-07 (77)
Th-228	< 1e-12	< 1e-12	< 1e-12	< 1e-12	< 1e-12	< 1e-12	< 1e-12	< 1e-12	< 1e-12
Th-229	4.8e-09 (86)	< 1e-12	4.6e-12 (86)	6.1e-10 (86)	3.0e-10 (86)	< 1e-12	4.8e-11 (86)	3.6e-11 (86)	5.8e-09 (86)
Th-230	3.2e-10 (86)	< 1e-12	2.2e-12 (67)	4.0e-11 (86)	2.5e-11 (86)	< 1e-12	4.7e-09 (77)	5.5e-10 (77)	5.5e-09 (77)
Th-232	< 1e-12	< 1e-12	< 1e-12	< 1e-12	< 1e-12	< 1e-12	< 1e-12	3.4e-12 (9)	< 1e-12
U-232	< 1e-12	< 1e-12	< 1e-12	< 1e-12	< 1e-12	< 1e-12	< 1e-12	< 1e-12	< 1e-12
U-233	2.2e-09 (86)	< 1e-12	3.1e-12 (86)	2.9e-10 (86)	1.3e-10 (86)	< 1e-12	2.3e-11 (86)	2.0e-11 (86)	2.7e-09 (86)
U-234	1.4e-09 (49)	1.6e-12 (86)	5.6e-12 (52)	2.4e-10 (37)	1.6e-10 (67)	< 1e-12	3.6e-08 (49)	4.6e-09 (67)	4.3e-08 (52)
U-235	6.3e-10 (49)	< 1e-12	3.6e-11 (67)	3.5e-11 (31)	3.4e-11 (67)	< 1e-12	3.3e-07 (7)	6.4e-08 (35)	3.4e-07 (7)
U-236	4.9e-10 (49)	< 1e-12	1.2e-12 (52)	1.6e-10 (36)	5.9e-11 (67)	< 1e-12	5.4e-11 (8)	3.9e-11 (24)	7.1e-10 (48)
U-238	1.1e-09 (49)	< 1e-12	6.8e-12 (52)	3.3e-10 (36)	8.6e-11 (67)	< 1e-12	8.0e-07 (7)	3.5e-08 (35)	8.1e-07 (7)
Zr-93	8.5e-09 (86)	1.7e-11 (86)	7.4e-11 (86)	1.3e-09 (67)	8.4e-09 (86)	7.8e-11 (86)	4.6e-11 (52)	4.5e-10 (77)	1.9e-08 (86)

Timing of the releases calculation case (CCM_TR)

Table E-4. Near-field releases for CCM_TR, peak release [Bq/year] and in parentheses time of peak [1000 year AD].

Nuclide	1BMA	2BMA	1BTF	2BTF	Silo	BRT	1BLA	2-5BLA	Total
Ac-227	1.8e+02 (84)	< 1	2.9e+01 (86)	2.3e+00 (20)	1.2e+01 (86)	< 1	5.1e+03 (3)	3.9e+03 (4)	6.4e+03 (3)
Ag-108m	1.1e+06 (2)	5.5e+05 (3)	2.3e+05 (3)	8.0e+05 (2)	6.4e+04 (3)	3.7e+05 (3)	1.3e+05 (2)	1.3e+05 (3)	2.9e+06 (3)
Am-241	2.3e+02 (3)	< 1	1.2e+01 (4)	2.5e+02 (4)	< 1	1.0e+01 (4)	3.8e+05 (2)	1.7e+05 (3)	4.9e+05 (2)
Am-242m	< 1	< 1	< 1	< 1	< 1	< 1	2.9e+02 (2)	6.5e+01 (2)	3.3e+02 (2)
Am-243	1.1e+02 (7)	< 1	5.4e+00 (22)	5.5e+01 (4)	< 1	4.4e+00 (5)	5.2e+03 (3)	6.2e+03 (3)	8.9e+03 (3)
Ba-133	< 1	< 1	< 1	< 1	< 1	< 1	2.0e+00 (2)	< 1	2.0e+00 (2)
C-14-ind	< 1	4.7e+05 (4)	< 1	< 1	< 1	2.7e+04 (24)	< 1	3.9e+05 (3)	8.3e+05 (3)
C-14-inorg	2.5e+05 (22)	8.7e+00 (24)	1.6e+05 (12)	1.5e+06 (4)	2.0e+02 (34)	< 1	5.1e+06 (3)	3.0e+05 (3)	5.3e+06 (3)
C-14-org	2.9e+07 (4)	3.7e+05 (4)	4.4e+06 (3)	4.2e+06 (2)	5.3e+07 (5)	< 1	1.0e+05 (3)	7.3e+04 (3)	7.6e+07 (4)
Ca-41	< 1	8.0e+05 (10)	< 1	< 1	< 1	< 1	< 1	1.4e+06 (3)	1.4e+06 (3)
Cd-113m	< 1	< 1	< 1	< 1	< 1	< 1	2.8e+01 (2)	< 1	2.8e+01 (2)
Cl-36	4.0e+04 (4)	1.2e+04 (5)	4.9e+03 (3)	1.0e+04 (3)	3.7e+04 (5)	2.7e+02 (29)	2.9e+04 (3)	1.7e+04 (3)	9.6e+04 (5)
Cm-242	< 1	< 1	< 1	< 1	< 1	< 1	2.4e+02 (2)	5.4e+01 (2)	2.7e+02 (2)
Cm-243	< 1	< 1	< 1	< 1	< 1	< 1	3.8e+01 (2)	1.8e+00 (2)	3.9e+01 (2)
Cm-244	< 1	< 1	< 1	< 1	< 1	< 1	1.3e+03 (2)	5.8e+01 (2)	1.4e+03 (2)
Cm-245	< 1	< 1	< 1	< 1	< 1	< 1	5.2e+01 (3)	7.3e+01 (3)	9.7e+01 (3)
Cm-246	< 1	< 1	< 1	< 1	< 1	< 1	1.3e+01 (3)	2.1e+01 (3)	2.7e+01 (3)
Co-60	< 1	< 1	< 1	< 1	< 1	< 1	9.1e+03 (2)	< 1	9.1e+03 (2)
Cs-135	9.3e+04 (7)	2.7e+03 (7)	2.2e+04 (3)	8.9e+03 (3)	3.2e+04 (11)	< 1	4.2e+03 (3)	6.4e+04 (3)	1.5e+05 (4)
Cs-137	1.9e+06 (2)	8.7e+02 (2)	1.5e+05 (2)	1.1e+06 (2)	7.2e+01 (2)	< 1	9.6e+05 (2)	2.9e+05 (2)	3.8e+06 (2)
Eu-152	< 1	< 1	< 1	< 1	< 1	< 1	1.3e+03 (2)	1.9e+03 (2)	3.2e+03 (2)
H-3	4.9e+02 (2)	8.1e+03 (2)	8.5e+00 (2)	1.4e+02 (2)	< 1	< 1	2.0e+03 (2)	1.6e+04 (2)	2.7e+04 (2)
Ho-166m	6.2e+01 (4)	< 1	3.8e+00 (4)	1.1e+02 (4)	< 1	< 1	4.3e+03 (2)	1.9e+04 (3)	2.0e+04 (3)
I-129	1.9e+04 (22)	2.9e+02 (8)	4.9e+03 (3)	5.5e+03 (3)	2.3e+04 (6)	< 1	5.9e+02 (3)	7.1e+02 (3)	3.8e+04 (5)
Mo-93	8.6e+04 (3)	9.3e+04 (5)	5.7e+04 (3)	1.1e+05 (3)	2.8e+05 (5)	6.0e+04 (3)	1.3e+05 (3)	2.8e+04 (3)	5.2e+05 (4)
Nb-93m	1.5e+04 (24)	1.6e+03 (86)	7.8e+02 (3)	6.8e+03 (4)	7.7e+03 (63)	1.0e+03 (3)	1.3e+05 (3)	3.9e+04 (3)	1.5e+05 (3)
Nb-94	3.2e+03 (25)	5.2e+02 (67)	1.4e+02 (61)	3.4e+03 (7)	1.8e+02 (34)	1.2e+03 (67)	4.2e+04 (3)	3.5e+05 (3)	3.6e+05 (3)
Ni-59	1.4e+07 (59)	3.6e+06 (63)	2.2e+06 (4)	6.0e+06 (3)	8.4e+06 (34)	3.5e+06 (22)	5.4e+06 (3)	4.2e+06 (3)	2.2e+07 (58)
Ni-63	1.5e+05 (3)	2.7e+01 (3)	1.1e+05 (3)	2.1e+06 (2)	< 1	1.0e+06 (2)	6.0e+07 (2)	7.7e+06 (2)	6.6e+07 (2)
Np-237	4.8e+02 (23)	2.2e+00 (86)	1.4e+00 (22)	2.3e+02 (4)	8.5e+01 (34)	< 1	1.8e+02 (3)	2.3e+02 (3)	5.6e+02 (23)
Pa-231	2.1e+01 (83)	< 1	5.6e+00 (58)	< 1	7.4e+00 (77)	< 1	5.3e+03 (3)	4.0e+03 (4)	6.6e+03 (3)
Pb-210	1.3e+02 (77)	2.2e+01 (86)	1.3e+00 (22)	2.6e+00 (22)	9.1e+00 (86)	< 1	< 1	3.2e+00 (5)	1.4e+02 (77)
Pd-107	4.4e+03 (4)	1.4e+05 (5)	1.5e+02 (4)	2.3e+03 (3)	3.5e+03 (7)	< 1	1.4e+02 (3)	6.3e+02 (3)	1.5e+05 (5)
Po-210	1.1e+04 (77)	1.9e+03 (86)	1.0e+02 (22)	8.8e+01 (77)	6.9e+02 (86)	6.7e+01 (22)	< 1	3.2e+00 (5)	1.2e+04 (77)
Pu-238	1.2e+03 (2)	< 1	< 1	4.0e+02 (2)	< 1	4.4e+00 (2)	5.9e+04 (2)	8.1e+03 (2)	6.7e+04 (2)
Pu-239	1.9e+04 (4)	1.8e+02 (58)	8.2e+01 (15)	2.0e+04 (3)	2.7e+03 (35)	1.1e+02 (13)	8.8e+04 (3)	9.9e+04 (3)	1.7e+05 (3)
Pu-240	2.3e+04 (4)	3.2e+00 (57)	4.8e+01 (13)	2.5e+04 (3)	7.5e+02 (16)	1.2e+02 (4)	8.7e+04 (3)	9.7e+04 (3)	1.8e+05 (3)
Pu-241	3.3e+01 (2)	< 1	1.1e+00 (17)	1.1e+01 (13)	< 1	< 1	1.9e+04 (2)	7.2e+02 (2)	2.0e+04 (2)
Pu-242	2.1e+02 (23)	6.0e+00 (64)	1.0e+00 (32)	1.5e+02 (3)	3.8e+01 (35)	1.1e+00 (24)	5.4e+02 (3)	6.3e+02 (3)	1.1e+03 (3)
Ra-226	1.2e+03 (77)	2.5e+02 (84)	1.5e+01 (22)	6.3e+00 (22)	1.5e+02 (82)	8.9e+00 (22)	< 1	3.3e+00 (5)	1.4e+03 (77)
Ra-228	< 1	< 1	< 1	< 1	< 1	< 1	< 1	< 1	< 1
Se-79	4.8e+04 (4)	8.9e+02 (5)	5.6e+03 (3)	1.1e+04 (2)	1.0e+05 (5)	< 1	5.4e+02 (3)	2.2e+03 (3)	1.4e+05 (5)
Sm-151	1.2e+01 (2)	< 1	< 1	1.5e+00 (3)	< 1	< 1	2.9e+04 (2)	3.3e+04 (2)	5.8e+04 (2)
Sn-126	2.2e+02 (57)	< 1	1.8e+00 (59)	1.1e+02 (4)	2.7e+01 (67)	< 1	6.8e+01 (3)	2.9e+03 (3)	3.0e+03 (3)
Sr-90	4.1e+01 (2)	< 1	1.4e+00 (2)	9.9e+01 (2)	< 1	3.1e+02 (2)	3.7e+04 (2)	1.3e+04 (2)	4.7e+04 (2)
Tc-99	1.1e+05 (25)	2.1e+02 (86)	4.4e+03 (58)	7.3e+04 (4)	2.6e+04 (67)	4.0e+02 (58)	2.5e+06 (3)	1.8e+05 (3)	2.6e+06 (3)
Th-228	< 1	< 1	< 1	< 1	< 1	< 1	< 1	< 1	< 1
Th-229	6.8e+01 (85)	< 1	< 1	3.1e+00 (58)	4.5e+00 (86)	< 1	< 1	< 1	7.5e+01 (85)
Th-230	2.8e+01 (83)	< 1	< 1	2.3e+00 (58)	4.0e+00 (86)	< 1	7.9e+00 (3)	8.6e+00 (5)	3.4e+01 (84)
Th-232	< 1	< 1	< 1	< 1	< 1	< 1	< 1	< 1	< 1
U-232	< 1	< 1	< 1	< 1	< 1	< 1	< 1	< 1	< 1
U-233	9.2e+01 (56)	< 1	< 1	5.6e+00 (22)	2.1e+01 (77)	< 1	< 1	1.5e+00 (5)	1.1e+02 (77)
U-234	1.2e+02 (23)	2.2e+00 (66)	< 1	6.2e+01 (4)	2.7e+01 (34)	< 1	2.1e+03 (3)	6.0e+02 (4)	2.4e+03 (3)
U-235	6.0e+01 (23)	< 1	2.5e+00 (58)	1.1e+01 (4)	6.2e+00 (34)	< 1	4.0e+05 (3)	1.2e+05 (3)	4.6e+05 (3)
U-236	3.8e+01 (23)	1.2e+00 (86)	< 1	3.7e+01 (4)	1.0e+01 (34)	< 1	5.6e+01 (3)	7.9e+01 (3)	1.3e+02 (3)
U-238	9.4e+01 (23)	< 1	< 1	8.7e+01 (4)	1.5e+01 (34)	< 1	1.0e+06 (3)	6.5e+04 (3)	1.0e+06 (3)
Zr-93	7.5e+03 (24)	5.2e+02 (86)	9.6e+01 (22)	5.7e+03 (4)	9.7e+03 (34)	2.7e+02 (22)	1.5e+03 (3)	1.1e+04 (3)	1.7e+04 (4)

Table E-5. Far-field releases for CCM_TR, peak release [Bq/year] and in parentheses time of peak [1000 year AD].

Nuclide	1BMA	2BMA	1BTF	2BTF	Silo	BRT	1BLA	2-5BLA	Total
Ac-227	1.9e+02 (85)	< 1	1.7e+01 (86)	5.1e+00 (77)	3.5e+01 (86)	< 1	1.3e+04 (5)	4.1e+03 (82)	1.3e+04 (5)
Ag-108m	2.2e+06 (3)	6.6e+05 (3)	2.4e+05 (3)	1.4e+06 (3)	7.8e+04 (3)	3.8e+05 (3)	2.8e+05 (3)	1.6e+05 (3)	4.3e+06 (3)
Am-241	4.3e+01 (4)	< 1	< 1	1.3e+01 (4)	< 1	< 1	1.1e+04 (3)	1.2e+03 (4)	1.3e+04 (4)
Am-242m	< 1	< 1	< 1	< 1	< 1	< 1	< 1	< 1	< 1
Am-243	2.1e+01 (8)	< 1	< 1	8.5e+00 (5)	< 1	< 1	7.6e+02 (4)	3.4e+02 (5)	8.7e+02 (4)
Ba-133	< 1	< 1	< 1	< 1	< 1	< 1	< 1	< 1	< 1
C-14-ind	< 1	5.2e+05 (3)	< 1	< 1	< 1	2.6e+04 (24)	< 1	5.3e+05 (3)	1.1e+06 (3)
C-14-inorg	2.4e+05 (22)	8.1e+00 (24)	1.5e+05 (12)	1.5e+06 (4)	1.9e+02 (34)	< 1	1.2e+07 (3)	4.2e+05 (3)	1.2e+07 (3)
C-14-org	3.2e+07 (3)	4.1e+05 (3)	6.2e+06 (3)	8.9e+06 (3)	5.2e+07 (5)	< 1	2.2e+05 (3)	1.0e+05 (3)	7.6e+07 (4)
Ca-41	< 1	7.8e+05 (10)	< 1	< 1	< 1	< 1	< 1	2.0e+06 (3)	2.0e+06 (3)
Cd-113m	< 1	< 1	< 1	< 1	< 1	< 1	< 1	< 1	< 1
Cl-36	4.0e+04 (4)	1.1e+04 (6)	7.2e+03 (3)	2.1e+04 (3)	3.6e+04 (5)	2.7e+02 (30)	6.6e+04 (3)	2.3e+04 (3)	1.3e+05 (3)
Cm-242	< 1	< 1	< 1	< 1	< 1	< 1	< 1	< 1	< 1
Cm-243	< 1	< 1	< 1	< 1	< 1	< 1	< 1	< 1	< 1
Cm-244	< 1	< 1	< 1	< 1	< 1	< 1	< 1	< 1	< 1
Cm-245	< 1	< 1	< 1	< 1	< 1	< 1	8.0e+00 (4)	4.2e+00 (5)	9.6e+00 (4)
Cm-246	< 1	< 1	< 1	< 1	< 1	< 1	1.9e+00 (4)	1.0e+00 (5)	2.4e+00 (4)
Co-60	< 1	< 1	< 1	< 1	< 1	< 1	< 1	< 1	< 1
Cs-135	7.1e+04 (5)	9.5e+02 (9)	1.8e+04 (4)	6.2e+03 (4)	2.2e+04 (15)	< 1	1.9e+03 (3)	1.9e+04 (5)	1.1e+05 (5)
Cs-137	7.2e+00 (3)	< 1	< 1	2.8e+01 (3)	< 1	< 1	3.0e+00 (3)	< 1	3.9e+01 (3)
Eu-152	< 1	< 1	< 1	< 1	< 1	< 1	< 1	< 1	< 1
H-3	< 1	1.4e+00 (2)	< 1	< 1	< 1	< 1	< 1	< 1	1.5e+00 (2)
Ho-166m	2.0e+01 (5)	< 1	< 1	1.5e+01 (4)	< 1	< 1	3.4e+02 (4)	3.5e+02 (5)	6.3e+02 (4)
I-129	1.9e+04 (22)	2.9e+02 (9)	7.0e+03 (3)	9.6e+03 (3)	2.3e+04 (6)	< 1	1.4e+03 (3)	9.9e+02 (3)	3.8e+04 (5)
Mo-93	1.4e+05 (3)	8.3e+04 (5)	7.9e+04 (3)	2.2e+05 (3)	2.7e+05 (5)	7.7e+04 (3)	2.8e+05 (3)	3.9e+04 (3)	6.8e+05 (3)
Nb-93m	1.1e+04 (28)	2.9e+02 (5)	5.3e+02 (3)	2.9e+03 (5)	1.1e+04 (48)	2.7e+02 (3)	1.3e+03 (3)	6.0e+02 (9)	2.2e+04 (31)
Nb-94	1.9e+03 (28)	4.6e+01 (67)	5.4e+01 (66)	1.3e+03 (9)	6.8e+01 (34)	2.1e+02 (67)	5.6e+03 (4)	1.4e+04 (5)	1.8e+04 (5)
Ni-59	1.2e+07 (61)	1.7e+06 (67)	1.0e+06 (4)	5.2e+06 (4)	3.5e+06 (34)	7.3e+05 (5)	2.7e+06 (3)	1.3e+06 (5)	1.6e+07 (62)
Ni-63	2.4e+04 (3)	2.7e+00 (3)	6.0e+03 (3)	9.7e+04 (3)	< 1	1.5e+03 (3)	7.1e+05 (3)	4.5e+04 (3)	8.2e+05 (3)
Np-237	1.7e+02 (26)	< 1	< 1	3.5e+01 (9)	1.9e+01 (86)	< 1	1.5e+01 (4)	5.1e+00 (5)	2.0e+02 (26)
Pa-231	1.6e+01 (77)	< 1	2.6e+00 (86)	< 1	2.0e+00 (86)	< 1	1.6e+03 (5)	6.6e+02 (82)	1.7e+03 (10)
Pb-210	7.3e+01 (77)	4.2e+00 (86)	< 1	4.9e+00 (77)	7.5e+00 (82)	< 1	3.4e+02 (77)	7.1e+01 (82)	5.0e+02 (77)
Pd-107	5.8e+03 (3)	1.3e+05 (6)	1.5e+02 (4)	4.7e+03 (3)	3.5e+03 (7)	< 1	2.9e+02 (3)	8.9e+02 (3)	1.4e+05 (6)
Po-210	8.7e+01 (77)	4.1e+00 (86)	< 1	5.4e+00 (77)	7.2e+00 (86)	< 1	3.5e+02 (77)	6.1e+01 (82)	5.1e+02 (77)
Pu-238	2.5e+00 (3)	< 1	< 1	< 1	< 1	< 1	3.3e+01 (3)	1.0e+00 (3)	3.3e+01 (3)
Pu-239	1.2e+04 (5)	2.9e+01 (67)	5.1e+01 (28)	5.2e+03 (5)	1.1e+03 (38)	1.7e+01 (30)	1.3e+04 (4)	5.2e+03 (5)	2.8e+04 (5)
Pu-240	1.3e+04 (5)	< 1	1.3e+01 (16)	5.7e+03 (5)	1.8e+02 (20)	5.5e+00 (5)	1.2e+04 (4)	4.4e+03 (5)	2.8e+04 (5)
Pu-241	1.7e+00 (7)	< 1	< 1	< 1	< 1	< 1	1.5e+01 (4)	3.6e+00 (5)	1.7e+01 (5)
Pu-242	1.1e+02 (25)	1.5e+00 (86)	< 1	4.0e+01 (5)	1.8e+01 (67)	< 1	8.2e+01 (4)	3.5e+01 (5)	2.1e+02 (5)
Ra-226	1.1e+03 (77)	5.8e+01 (86)	9.7e+00 (22)	7.6e+01 (77)	1.1e+02 (82)	1.9e+00 (22)	5.8e+03 (77)	1.1e+03 (82)	8.3e+03 (77)
Ra-228	< 1	< 1	< 1	< 1	< 1	< 1	< 1	< 1	< 1
Se-79	6.3e+04 (3)	8.3e+02 (3)	7.9e+03 (3)	2.4e+04 (3)	1.0e+05 (5)	< 1	1.3e+03 (3)	3.1e+03 (3)	1.4e+05 (5)
Sm-151	< 1	< 1	< 1	< 1	< 1	< 1	5.2e+00 (3)	1.2e+00 (3)	6.2e+00 (3)
Sn-126	1.0e+02 (63)	< 1	< 1	1.2e+01 (15)	4.1e+00 (86)	< 1	2.3e+00 (5)	1.3e+01 (17)	1.2e+02 (63)
Sr-90	< 1	< 1	< 1	1.6e+00 (3)	< 1	< 1	2.4e+00 (3)	< 1	4.2e+00 (3)
Tc-99	5.4e+04 (29)	1.5e+01 (86)	1.2e+03 (61)	1.1e+04 (5)	9.2e+03 (86)	3.3e+01 (86)	1.9e+05 (4)	3.8e+03 (9)	1.9e+05 (4)
Th-228	< 1	< 1	< 1	< 1	< 1	< 1	< 1	< 1	< 1
Th-229	9.5e+01 (77)	< 1	< 1	6.3e+00 (77)	6.2e+00 (82)	< 1	< 1	< 1	1.1e+02 (77)
Th-230	2.5e+01 (77)	< 1	< 1	2.3e+00 (77)	2.7e+00 (86)	< 1	2.0e+02 (82)	4.0e+01 (82)	2.7e+02 (82)
Th-232	< 1	< 1	< 1	< 1	< 1	< 1	< 1	< 1	< 1
U-232	< 1	< 1	< 1	< 1	< 1	< 1	< 1	< 1	< 1
U-233	5.9e+01 (82)	< 1	< 1	4.2e+00 (77)	5.7e+00 (86)	< 1	< 1	< 1	6.9e+01 (82)
U-234	4.6e+01 (26)	< 1	< 1	8.3e+00 (9)	5.0e+00 (86)	< 1	5.2e+02 (5)	6.9e+01 (82)	5.4e+02 (9)
U-235	2.2e+01 (25)	< 1	1.5e+00 (86)	1.5e+00 (9)	1.3e+00 (86)	< 1	2.8e+04 (4)	2.5e+03 (10)	2.8e+04 (4)
U-236	1.5e+01 (26)	< 1	< 1	5.2e+00 (9)	2.1e+00 (86)	< 1	4.0e+00 (4)	2.0e+00 (10)	2.1e+01 (26)
U-238	3.6e+01 (26)	< 1	< 1	1.2e+01 (9)	2.9e+00 (86)	< 1	6.9e+04 (4)	1.4e+03 (10)	6.9e+04 (4)
Zr-93	4.4e+03 (26)	5.4e+01 (86)	5.0e+01 (22)	1.4e+03 (5)	4.1e+03 (86)	3.6e+01 (37)	1.7e+02 (4)	3.6e+02 (9)	7.3e+03 (27)

Table E-6. Doses for CCM_TR, peak dose [Sv/year] and in parentheses time of peak [1000 year AD].

Nuclide	1BMA	2BMA	1BTF	2BTF	Silo	BRT	1BLA	2-5BLA	Total
Total	1.8e-06 (67)	1.0e-06 (16)	4.3e-07 (5)	5.4e-07 (5)	3.8e-06 (7)	3.9e-07 (5)	1.2e-06 (26)	5.2e-07 (9)	8.2e-06 (6)
Ac-227	7.2e-10 (77)	< 1e-12	5.9e-11 (86)	3.3e-11 (44)	6.9e-11 (86)	< 1e-12	2.0e-07 (34)	9.5e-08 (57)	2.8e-07 (39)
Ag-108m	1.7e-08 (5)	1.2e-08 (5)	2.3e-09 (5)	4.5e-09 (5)	2.5e-09 (5)	3.4e-09 (5)	5.9e-10 (5)	2.0e-09 (5)	4.4e-08 (5)
Am-241	< 1e-12	< 1e-12	< 1e-12	< 1e-12	< 1e-12	< 1e-12	1.2e-10 (4)	1.2e-09 (4)	1.2e-09 (4)
Am-242m	< 1e-12	< 1e-12	< 1e-12	< 1e-12	< 1e-12	< 1e-12	< 1e-12	< 1e-12	< 1e-12
Am-243	1.5e-11 (30)	< 1e-12	1.5e-12 (28)	1.3e-11 (25)	< 1e-12	< 1e-12	2.1e-10 (15)	3.6e-10 (5)	4.6e-10 (17)
Ba-133	< 1e-12	< 1e-12	< 1e-12	< 1e-12	< 1e-12	< 1e-12	< 1e-12	< 1e-12	< 1e-12
C-14-ind	< 1e-12	1.2e-08 (5)	< 1e-12	< 1e-12	< 1e-12	7.2e-10 (24)	< 1e-12	6.2e-09 (5)	1.8e-08 (5)
C-14-inorg	6.7e-09 (23)	< 1e-12	4.3e-09 (13)	2.1e-08 (5)	5.8e-12 (34)	< 1e-12	1.1e-08 (3)	4.8e-09 (5)	2.8e-08 (5)
C-14-org	5.8e-07 (5)	9.2e-09 (5)	3.7e-08 (5)	2.3e-08 (5)	1.5e-06 (5)	< 1e-12	2.3e-10 (3)	1.2e-09 (5)	2.1e-06 (5)
Ca-41	< 1e-12	8.4e-07 (28)	< 1e-12	< 1e-12	< 1e-12	< 1e-12	< 1e-12	4.5e-07 (9)	1.0e-06 (19)
Cd-113m	< 1e-12	< 1e-12	< 1e-12	< 1e-12	< 1e-12	< 1e-12	< 1e-12	< 1e-12	< 1e-12
Cl-36	1.2e-07 (5)	3.6e-08 (8)	8.6e-09 (5)	9.9e-09 (5)	1.1e-07 (5)	8.8e-10 (30)	4.6e-09 (3)	3.8e-08 (5)	3.1e-07 (5)
Cm-242	< 1e-12	< 1e-12	< 1e-12	< 1e-12	< 1e-12	< 1e-12	< 1e-12	< 1e-12	< 1e-12
Cm-243	< 1e-12	< 1e-12	< 1e-12	< 1e-12	< 1e-12	< 1e-12	< 1e-12	< 1e-12	< 1e-12
Cm-244	< 1e-12	< 1e-12	< 1e-12	< 1e-12	< 1e-12	< 1e-12	< 1e-12	< 1e-12	< 1e-12
Cm-245	< 1e-12	< 1e-12	< 1e-12	< 1e-12	< 1e-12	< 1e-12	2.1e-12 (15)	4.3e-12 (5)	5.0e-12 (16)
Cm-246	< 1e-12	< 1e-12	< 1e-12	< 1e-12	< 1e-12	< 1e-12	< 1e-12	< 1e-12	< 1e-12
Co-60	< 1e-12	< 1e-12	< 1e-12	< 1e-12	< 1e-12	< 1e-12	< 1e-12	< 1e-12	< 1e-12
Cs-135	6.6e-07 (86)	2.0e-08 (86)	6.0e-08 (86)	1.5e-08 (86)	6.2e-07 (86)	< 1e-12	2.4e-09 (86)	9.8e-08 (86)	1.5e-06 (86)
Cs-137	< 1e-12	< 1e-12	< 1e-12	< 1e-12	< 1e-12	< 1e-12	< 1e-12	< 1e-12	< 1e-12
Eu-152	< 1e-12	< 1e-12	< 1e-12	< 1e-12	< 1e-12	< 1e-12	< 1e-12	< 1e-12	< 1e-12
H-3	< 1e-12	< 1e-12	< 1e-12	< 1e-12	< 1e-12	< 1e-12	< 1e-12	< 1e-12	< 1e-12
Ho-166m	< 1e-12	< 1e-12	< 1e-12	< 1e-12	< 1e-12	< 1e-12	< 1e-12	4.2e-12 (5)	4.6e-12 (5)
I-129	2.3e-07 (10)	8.3e-09 (27)	5.4e-08 (6)	3.9e-08 (5)	5.6e-07 (16)	< 1e-12	3.1e-09 (3)	7.8e-09 (5)	8.1e-07 (12)
Mo-93	7.6e-07 (6)	8.5e-07 (8)	3.4e-07 (5)	4.5e-07 (5)	2.5e-06 (7)	3.8e-07 (5)	2.7e-07 (5)	1.7e-07 (5)	5.1e-06 (6)
Nb-93m	2.6e-10 (6)	2.8e-10 (8)	1.1e-10 (5)	1.4e-10 (5)	8.3e-10 (7)	1.2e-10 (5)	8.8e-11 (5)	5.3e-11 (5)	1.7e-09 (6)
Nb-94	3.1e-10 (67)	2.1e-12 (86)	6.8e-12 (77)	1.4e-10 (52)	7.9e-12 (77)	2.7e-11 (77)	7.4e-11 (33)	6.3e-10 (43)	1.1e-09 (52)
Ni-59	1.3e-06 (67)	1.0e-07 (86)	4.1e-08 (34)	7.9e-08 (28)	2.9e-07 (52)	1.1e-07 (52)	1.7e-08 (16)	3.1e-08 (21)	1.8e-06 (67)
Ni-63	< 1e-12	< 1e-12	< 1e-12	1.8e-12 (3)	< 1e-12	< 1e-12	7.5e-12 (3)	1.1e-11 (3)	1.4e-11 (3)
Np-237	1.8e-09 (86)	< 1e-12	4.4e-12 (86)	3.7e-10 (86)	8.5e-11 (86)	< 1e-12	4.0e-11 (86)	3.1e-11 (86)	2.3e-09 (86)
Pa-231	1.6e-09 (86)	< 1e-12	1.4e-10 (86)	5.8e-11 (38)	8.4e-11 (86)	< 1e-12	3.6e-07 (32)	1.2e-07 (52)	4.7e-07 (36)
Pb-210	5.6e-09 (86)	4.3e-10 (67)	7.0e-11 (23)	3.8e-10 (86)	5.5e-10 (86)	1.3e-11 (23)	3.1e-08 (86)	7.5e-09 (86)	4.6e-08 (86)
Pd-107	9.8e-11 (36)	4.4e-09 (67)	1.7e-12 (29)	1.4e-11 (17)	2.1e-10 (41)	< 1e-12	< 1e-12	6.5e-12 (15)	4.6e-09 (67)
Po-210	2.0e-10 (86)	3.3e-11 (86)	2.7e-12 (22)	1.3e-11 (86)	3.0e-11 (86)	< 1e-12	1.1e-09 (86)	4.2e-10 (86)	1.7e-09 (86)
Pu-238	< 1e-12	< 1e-12	< 1e-12	< 1e-12	< 1e-12	< 1e-12	< 1e-12	< 1e-12	< 1e-12
Pu-239	1.7e-07 (57)	2.6e-10 (86)	1.1e-09 (66)	3.9e-08 (43)	2.5e-08 (77)	4.0e-10 (67)	2.9e-08 (33)	4.3e-08 (42)	2.8e-07 (52)
Pu-240	1.7e-08 (19)	< 1e-12	6.3e-11 (30)	8.0e-09 (18)	5.6e-10 (43)	2.5e-11 (28)	7.0e-09 (15)	7.1e-09 (18)	3.9e-08 (18)
Pu-241	< 1e-12	< 1e-12	< 1e-12	< 1e-12	< 1e-12	< 1e-12	< 1e-12	< 1e-12	< 1e-12
Pu-242	8.3e-09 (86)	1.3e-11 (86)	3.7e-11 (86)	1.4e-09 (86)	1.2e-09 (86)	3.8e-12 (86)	5.8e-10 (86)	1.2e-09 (86)	1.3e-08 (86)
Ra-226	3.3e-08 (86)	2.3e-09 (67)	3.6e-10 (23)	2.4e-09 (86)	3.7e-09 (86)	6.3e-11 (23)	1.9e-07 (86)	4.3e-08 (86)	2.8e-07 (86)
Ra-228	< 1e-12	< 1e-12	< 1e-12	< 1e-12	< 1e-12	< 1e-12	< 1e-12	< 1e-12	< 1e-12
Se-79	1.5e-08 (7)	3.6e-10 (9)	1.0e-09 (5)	1.6e-09 (5)	4.5e-08 (11)	< 1e-12	4.9e-11 (5)	5.3e-10 (6)	5.9e-08 (10)
Sm-151	< 1e-12	< 1e-12	< 1e-12	< 1e-12	< 1e-12	< 1e-12	< 1e-12	< 1e-12	< 1e-12
Sn-126	1.1e-10 (86)	< 1e-12	< 1e-12	1.5e-11 (78)	2.2e-12 (98)	< 1e-12	< 1e-12	1.5e-11 (78)	1.4e-10 (86)
Sr-90	< 1e-12	< 1e-12	< 1e-12	< 1e-12	< 1e-12	< 1e-12	< 1e-12	< 1e-12	< 1e-12
Tc-99	6.1e-08 (78)	2.0e-12 (86)	1.7e-09 (86)	8.7e-09 (67)	1.1e-08 (86)	2.1e-11 (86)	4.0e-08 (52)	3.3e-09 (67)	1.2e-07 (77)
Th-228	< 1e-12	< 1e-12	< 1e-12	< 1e-12	< 1e-12	< 1e-12	< 1e-12	< 1e-12	< 1e-12
Th-229	4.8e-09 (86)	< 1e-12	4.7e-12 (86)	6.1e-10 (86)	3.1e-10 (86)	< 1e-12	4.4e-11 (86)	3.5e-11 (86)	5.8e-09 (86)
Th-230	3.2e-10 (86)	< 1e-12	2.2e-12 (67)	4.0e-11 (86)	2.6e-11 (86)	< 1e-12	4.6e-09 (77)	5.5e-10 (77)	5.4e-09 (77)
Th-232	< 1e-12	< 1e-12	< 1e-12	< 1e-12	< 1e-12	< 1e-12	< 1e-12	< 1e-12	< 1e-12
U-232	< 1e-12	< 1e-12	< 1e-12	< 1e-12	< 1e-12	< 1e-12	< 1e-12	< 1e-12	< 1e-12
U-233	2.2e-09 (86)	< 1e-12	3.1e-12 (86)	2.9e-10 (86)	1.4e-10 (86)	< 1e-12	2.1e-11 (86)	2.0e-11 (86)	2.7e-09 (86)
U-234	1.4e-09 (48)	1.6e-12 (86)	5.6e-12 (52)	2.4e-10 (36)	1.6e-10 (67)	< 1e-12	3.6e-08 (52)	4.6e-09 (67)	4.2e-08 (52)
U-235	6.3e-10 (49)	< 1e-12	3.6e-11 (67)	3.6e-11 (31)	3.5e-11 (67)	< 1e-12	2.7e-07 (8)	6.3e-08 (35)	2.9e-07 (8)
U-236	4.9e-10 (49)	< 1e-12	1.2e-12 (52)	1.6e-10 (36)	5.9e-11 (67)	< 1e-12	4.5e-11 (8)	3.7e-11 (24)	7.1e-10 (48)
U-238	1.0e-09 (49)	< 1e-12	6.8e-12 (52)	3.3e-10 (36)	8.7e-11 (67)	< 1e-12	6.6e-07 (8)	3.5e-08 (35)	6.7e-07 (8)
Zr-93	8.5e-09 (86)	1.7e-11 (86)	7.5e-11 (86)	1.3e-09 (67)	8.5e-09 (86)	7.9e-11 (86)	4.3e-11 (57)	4.5e-10 (77)	1.9e-08 (86)

High inventory calculation case (CCL_IH)

Table E-7. Near-field releases for CCL_IH, peak release [Bq/year] and in parentheses time of peak [1000 year AD].

Nuclide	1BMA	2BMA	1BTF	2BTF	Silo	BRT	1BLA	2-5BLA	Total
Ac-227	3.9e+02 (84)	< 1	5.8e+01 (86)	5.0e+00 (19)	2.6e+01 (86)	< 1	5.4e+04 (3)	1.7e+04 (4)	5.6e+04 (3)
Ag-108m	1.9e+07 (3)	6.1e+05 (4)	8.0e+06 (3)	3.7e+07 (3)	6.0e+05 (4)	2.0e+05 (3)	6.7e+06 (3)	3.6e+05 (3)	6.1e+07 (3)
Am-241	2.0e+02 (4)	< 1	3.9e+01 (4)	4.3e+02 (4)	< 1	1.3e+01 (4)	4.1e+06 (3)	9.4e+05 (3)	4.4e+06 (3)
Am-242m	< 1	< 1	< 1	< 1	< 1	< 1	8.0e+01 (3)	1.6e+01 (3)	8.0e+01 (3)
Am-243	1.4e+02 (7)	< 1	9.1e+00 (22)	4.0e+01 (4)	< 1	6.8e+00 (22)	4.1e+04 (3)	2.8e+04 (4)	4.8e+04 (3)
Ba-133	< 1	< 1	< 1	< 1	< 1	< 1	< 1	< 1	< 1
C-14-ind	< 1	1.5e+06 (5)	< 1	< 1	< 1	5.0e+04 (24)	< 1	2.1e+06 (4)	3.3e+06 (4)
C-14-inorg	3.5e+05 (22)	1.6e+01 (24)	2.0e+05 (12)	9.0e+05 (4)	2.9e+02 (34)	< 1	1.7e+07 (3)	1.7e+06 (4)	1.8e+07 (3)
C-14-org	3.9e+07 (4)	6.6e+05 (5)	8.6e+06 (3)	1.3e+07 (3)	7.3e+07 (5)	< 1	3.4e+05 (3)	4.0e+05 (4)	1.1e+08 (5)
Ca-41	< 1	3.1e+06 (10)	< 1	< 1	< 1	< 1	< 1	4.1e+06 (4)	4.1e+06 (4)
Cd-113m	< 1	< 1	< 1	< 1	< 1	< 1	< 1	< 1	< 1
Cl-36	8.0e+04 (4)	4.6e+04 (7)	2.4e+04 (3)	5.9e+04 (3)	1.5e+05 (6)	4.9e+02 (29)	1.0e+05 (3)	4.6e+04 (4)	3.1e+05 (5)
Cm-242	< 1	< 1	< 1	< 1	< 1	< 1	6.6e+01 (3)	1.3e+01 (3)	6.6e+01 (3)
Cm-243	< 1	< 1	< 1	< 1	< 1	< 1	< 1	< 1	< 1
Cm-244	< 1	< 1	< 1	< 1	< 1	< 1	< 1	< 1	< 1
Cm-245	1.5e+00 (7)	< 1	< 1	< 1	< 1	< 1	4.2e+02 (3)	3.6e+02 (4)	5.2e+02 (3)
Cm-246	< 1	< 1	< 1	< 1	< 1	< 1	1.0e+02 (3)	1.0e+02 (4)	1.4e+02 (3)
Co-60	< 1	< 1	< 1	< 1	< 1	< 1	< 1	< 1	< 1
Cs-135	1.4e+05 (7)	1.5e+04 (7)	6.2e+04 (4)	2.4e+04 (3)	7.0e+04 (13)	< 1	2.3e+04 (3)	4.9e+05 (4)	6.4e+05 (4)
Cs-137	< 1	< 1	< 1	< 1	< 1	< 1	< 1	< 1	< 1
Eu-152	< 1	< 1	< 1	< 1	< 1	< 1	< 1	< 1	< 1
H-3	< 1	< 1	< 1	< 1	< 1	< 1	< 1	< 1	< 1
Ho-166m	9.0e+01 (5)	< 1	3.1e+00 (4)	1.5e+02 (4)	< 1	< 1	2.0e+04 (3)	4.0e+04 (3)	4.5e+04 (3)
I-129	4.2e+04 (22)	1.7e+03 (8)	2.7e+04 (3)	1.8e+04 (3)	7.7e+04 (6)	< 1	4.9e+03 (3)	5.9e+03 (4)	1.1e+05 (5)
Mo-93	1.1e+05 (4)	1.5e+05 (5)	1.0e+05 (3)	3.2e+05 (3)	5.4e+05 (5)	6.6e+04 (4)	4.1e+05 (3)	9.5e+04 (4)	9.3e+05 (5)
Nb-93m	7.8e+05 (24)	5.7e+03 (86)	1.1e+04 (18)	3.4e+05 (5)	1.7e+05 (62)	1.1e+03 (4)	6.1e+05 (3)	1.8e+05 (4)	9.3e+05 (24)
Nb-94	1.6e+04 (25)	1.0e+03 (67)	7.3e+02 (61)	1.7e+04 (7)	7.2e+02 (34)	1.3e+03 (67)	6.6e+05 (3)	2.4e+06 (4)	2.4e+06 (4)
Ni-59	4.1e+07 (59)	7.9e+06 (63)	6.2e+06 (4)	2.1e+07 (4)	2.5e+07 (34)	3.8e+06 (58)	4.4e+07 (3)	2.7e+07 (4)	6.1e+07 (3)
Ni-63	1.1e+03 (3)	< 1	1.1e+04 (3)	2.0e+05 (3)	< 1	1.4e+04 (3)	3.1e+06 (3)	5.1e+05 (3)	3.1e+06 (3)
Np-237	1.0e+03 (23)	7.3e+00 (86)	5.0e+00 (22)	5.6e+02 (4)	4.2e+02 (34)	1.3e+00 (22)	4.3e+03 (3)	2.2e+03 (4)	4.8e+03 (3)
Pa-231	4.3e+01 (83)	< 1	1.1e+01 (58)	2.0e+00 (22)	1.6e+01 (77)	< 1	5.6e+04 (3)	1.7e+04 (4)	5.8e+04 (3)
Pb-210	2.7e+02 (77)	4.9e+01 (86)	2.5e+00 (22)	5.1e+00 (22)	2.2e+01 (86)	1.4e+00 (22)	1.4e+01 (3)	1.4e+01 (5)	3.0e+02 (77)
Pd-107	1.8e+05 (4)	2.5e+05 (6)	6.2e+03 (4)	2.2e+05 (3)	1.3e+05 (7)	< 1	1.5e+04 (3)	5.7e+03 (4)	5.2e+05 (6)
Po-210	2.2e+04 (77)	4.3e+03 (86)	2.0e+02 (22)	1.7e+02 (77)	1.6e+03 (86)	1.2e+02 (22)	1.4e+01 (3)	1.4e+01 (5)	2.4e+04 (77)
Pu-238	5.8e+00 (3)	< 1	< 1	1.2e+01 (3)	< 1	< 1	1.6e+03 (3)	2.0e+02 (3)	1.6e+03 (3)
Pu-239	3.0e+04 (5)	3.9e+02 (58)	1.5e+02 (16)	3.7e+04 (3)	5.6e+03 (35)	2.0e+02 (13)	7.3e+05 (3)	4.3e+05 (4)	8.4e+05 (3)
Pu-240	3.5e+04 (4)	6.9e+00 (57)	8.2e+01 (13)	4.6e+04 (3)	1.5e+03 (16)	2.2e+02 (4)	6.8e+05 (3)	4.2e+05 (4)	8.1e+05 (3)
Pu-241	3.2e+01 (7)	< 1	2.1e+00 (17)	2.2e+01 (13)	< 1	< 1	4.2e+02 (3)	3.6e+02 (4)	5.2e+02 (3)
Pu-242	4.9e+02 (23)	1.2e+01 (64)	2.1e+00 (32)	3.9e+02 (3)	9.4e+01 (35)	1.9e+00 (24)	4.5e+03 (3)	2.8e+03 (4)	5.5e+03 (3)
Ra-226	2.5e+03 (77)	5.6e+02 (84)	3.0e+01 (22)	1.2e+01 (22)	3.5e+02 (82)	1.6e+01 (22)	1.6e+01 (3)	1.4e+01 (5)	3.0e+03 (77)
Ra-228	< 1	< 1	< 1	< 1	< 1	< 1	< 1	< 1	< 1
Se-79	2.6e+06 (4)	4.7e+04 (5)	4.4e+05 (3)	1.4e+06 (3)	5.3e+06 (5)	< 1	7.3e+04 (3)	2.4e+04 (4)	7.6e+06 (5)
Sm-151	< 1	< 1	< 1	< 1	< 1	< 1	5.9e+02 (3)	5.2e+02 (3)	8.5e+02 (3)
Sn-126	8.8e+03 (57)	2.9e+00 (61)	7.0e+01 (59)	4.8e+03 (5)	7.8e+02 (67)	< 1	7.2e+03 (3)	2.2e+04 (4)	2.9e+04 (4)
Sr-90	< 1	< 1	< 1	< 1	< 1	< 1	< 1	< 1	< 1
Tc-99	2.1e+05 (25)	7.5e+02 (86)	1.6e+04 (58)	1.0e+05 (4)	1.0e+05 (67)	6.7e+02 (58)	2.3e+07 (3)	1.2e+06 (4)	2.4e+07 (3)
Th-228	< 1	< 1	< 1	< 1	< 1	< 1	< 1	< 1	< 1
Th-229	1.5e+02 (84)	< 1	< 1	7.1e+00 (58)	2.1e+01 (86)	< 1	< 1	1.7e+00 (5)	1.8e+02 (85)
Th-230	5.9e+01 (83)	< 1	< 1	4.6e+00 (22)	9.7e+00 (86)	< 1	1.0e+02 (3)	3.7e+01 (5)	1.1e+02 (3)
Th-232	< 1	< 1	< 1	< 1	< 1	< 1	< 1	< 1	< 1
U-232	< 1	< 1	< 1	< 1	< 1	< 1	< 1	< 1	< 1
U-233	2.0e+02 (56)	2.9e+00 (77)	1.3e+00 (77)	1.3e+01 (22)	9.7e+01 (77)	< 1	1.4e+01 (3)	1.6e+01 (5)	2.9e+02 (77)
U-234	2.4e+02 (23)	4.9e+00 (67)	1.1e+00 (65)	1.2e+02 (4)	6.4e+01 (34)	< 1	1.9e+04 (3)	2.4e+03 (4)	2.0e+04 (3)
U-235	1.3e+02 (23)	< 1	5.1e+00 (58)	2.4e+01 (4)	1.3e+01 (34)	< 1	2.5e+06 (3)	4.2e+05 (4)	2.6e+06 (3)
U-236	7.4e+01 (23)	2.4e+00 (86)	< 1	8.0e+01 (4)	2.5e+01 (34)	< 1	4.8e+02 (3)	4.1e+02 (4)	6.3e+02 (3)
U-238	2.0e+02 (23)	< 1	1.4e+00 (29)	1.9e+02 (4)	3.2e+01 (34)	< 1	5.5e+06 (3)	1.8e+05 (4)	5.5e+06 (3)
Zr-93	3.8e+05 (24)	1.9e+03 (86)	4.8e+03 (22)	3.0e+05 (4)	2.1e+05 (34)	2.7e+02 (22)	2.0e+05 (3)	8.5e+04 (4)	5.4e+05 (24)

Table E-8. Far-field releases for CCL_IH, peak release [Bq/year] and in parentheses time of peak [1000 year AD].

Nuclide	1BMA	2BMA	1BTF	2BTF	Silo	BRT	1BLA	2-5BLA	Total
Ac-227	4.0e+02 (85)	< 1	3.3e+01 (86)	1.1e+01 (77)	7.3e+01 (86)	< 1	3.6e+04 (5)	1.3e+04 (82)	3.8e+04 (5)
Ag-108m	1.9e+07 (3)	5.1e+05 (4)	7.0e+06 (3)	2.7e+07 (3)	5.6e+05 (4)	1.5e+05 (3)	6.0e+06 (3)	2.9e+05 (3)	5.3e+07 (3)
Am-241	3.7e+01 (5)	< 1	< 1	2.4e+01 (4)	< 1	< 1	2.1e+05 (4)	6.8e+03 (4)	2.2e+05 (4)
Am-242m	< 1	< 1	< 1	< 1	< 1	< 1	1.4e+00 (3)	< 1	1.4e+00 (3)
Am-243	2.7e+01 (7)	< 1	1.5e+00 (17)	7.1e+00 (14)	< 1	< 1	4.1e+03 (4)	1.4e+03 (5)	4.3e+03 (4)
Ba-133	< 1	< 1	< 1	< 1	< 1	< 1	< 1	< 1	< 1
C-14-ind	< 1	1.4e+06 (5)	< 1	< 1	< 1	4.7e+04 (24)	< 1	2.0e+06 (4)	3.0e+06 (4)
C-14-inorg	3.4e+05 (22)	1.5e+01 (24)	2.0e+05 (12)	8.5e+05 (4)	2.9e+02 (34)	< 1	1.6e+07 (3)	1.5e+06 (4)	1.6e+07 (3)
C-14-org	3.9e+07 (4)	5.8e+05 (5)	7.8e+06 (3)	1.1e+07 (3)	7.2e+07 (5)	< 1	3.1e+05 (3)	3.7e+05 (4)	1.0e+08 (5)
Ca-41	< 1	3.0e+06 (10)	< 1	< 1	< 1	< 1	< 1	3.7e+06 (4)	3.7e+06 (4)
Cd-113m	< 1	< 1	< 1	< 1	< 1	< 1	< 1	< 1	< 1
Cl-36	8.0e+04 (4)	4.5e+04 (8)	2.3e+04 (3)	5.0e+04 (3)	1.5e+05 (6)	4.8e+02 (30)	9.2e+04 (3)	4.2e+04 (4)	3.0e+05 (5)
Cm-242	< 1	< 1	< 1	< 1	< 1	< 1	1.4e+00 (3)	< 1	1.4e+00 (3)
Cm-243	< 1	< 1	< 1	< 1	< 1	< 1	< 1	< 1	< 1
Cm-244	< 1	< 1	< 1	< 1	< 1	< 1	< 1	< 1	< 1
Cm-245	< 1	< 1	< 1	< 1	< 1	< 1	4.5e+01 (4)	1.9e+01 (5)	4.8e+01 (4)
Cm-246	< 1	< 1	< 1	< 1	< 1	< 1	1.1e+01 (4)	5.0e+00 (5)	1.2e+01 (4)
Co-60	< 1	< 1	< 1	< 1	< 1	< 1	< 1	< 1	< 1
Cs-135	1.0e+05 (5)	5.1e+03 (9)	3.6e+04 (4)	9.9e+03 (4)	4.8e+04 (16)	< 1	5.7e+03 (3)	1.4e+05 (5)	2.8e+05 (5)
Cs-137	< 1	< 1	< 1	< 1	< 1	< 1	< 1	< 1	< 1
Eu-152	< 1	< 1	< 1	< 1	< 1	< 1	< 1	< 1	< 1
H-3	< 1	< 1	< 1	< 1	< 1	< 1	< 1	< 1	< 1
Ho-166m	2.6e+01 (5)	< 1	< 1	1.7e+01 (4)	< 1	< 1	1.5e+03 (4)	8.8e+02 (5)	1.8e+03 (4)
I-129	4.1e+04 (22)	1.7e+03 (9)	2.7e+04 (3)	1.4e+04 (3)	7.6e+04 (6)	< 1	4.4e+03 (3)	5.4e+03 (4)	1.1e+05 (5)
Mo-93	1.1e+05 (4)	1.3e+05 (6)	1.0e+05 (3)	2.6e+05 (3)	5.3e+05 (5)	6.3e+04 (4)	3.7e+05 (3)	8.8e+04 (4)	9.0e+05 (5)
Nb-93m	5.7e+05 (28)	4.3e+02 (5)	5.3e+03 (22)	1.3e+05 (5)	2.5e+05 (50)	2.3e+02 (4)	2.6e+04 (4)	4.4e+03 (10)	8.2e+05 (29)
Nb-94	9.6e+03 (28)	9.0e+01 (67)	2.7e+02 (66)	6.4e+03 (14)	2.5e+02 (34)	2.2e+02 (67)	5.7e+04 (4)	8.4e+04 (5)	1.1e+05 (5)
Ni-59	3.7e+07 (61)	3.8e+06 (67)	2.5e+06 (4)	1.2e+07 (4)	1.1e+07 (35)	9.2e+05 (59)	1.2e+07 (3)	7.8e+06 (5)	4.6e+07 (62)
Ni-63	5.2e+02 (4)	< 1	2.7e+03 (4)	2.3e+04 (4)	< 1	3.9e+02 (4)	3.4e+05 (3)	1.4e+04 (3)	3.5e+05 (3)
Np-237	3.6e+02 (26)	< 1	2.5e+00 (86)	7.9e+01 (9)	8.8e+01 (86)	< 1	1.9e+02 (4)	4.0e+01 (5)	4.7e+02 (26)
Pa-231	3.2e+01 (77)	< 1	5.2e+00 (86)	1.2e+00 (77)	4.2e+00 (86)	< 1	4.5e+03 (5)	2.1e+03 (82)	4.8e+03 (5)
Pb-210	1.5e+02 (77)	9.5e+00 (86)	1.8e+00 (22)	9.6e+00 (77)	1.8e+01 (82)	< 1	6.6e+02 (77)	1.8e+02 (82)	1.0e+03 (77)
Pd-107	1.8e+05 (4)	2.4e+05 (7)	6.1e+03 (4)	1.8e+05 (3)	1.3e+05 (7)	< 1	1.3e+04 (3)	5.1e+03 (4)	5.0e+05 (6)
Po-210	1.8e+02 (77)	9.2e+00 (86)	1.7e+00 (22)	1.0e+01 (77)	1.7e+01 (86)	< 1	6.8e+02 (77)	1.6e+02 (82)	1.0e+03 (77)
Pu-238	< 1	< 1	< 1	< 1	< 1	< 1	1.6e+01 (3)	< 1	1.7e+01 (3)
Pu-239	1.6e+04 (5)	6.4e+01 (67)	9.2e+01 (28)	7.3e+03 (5)	2.2e+03 (38)	3.1e+01 (30)	7.4e+04 (4)	2.0e+04 (5)	8.9e+04 (4)
Pu-240	1.8e+04 (5)	< 1	2.2e+01 (16)	8.1e+03 (5)	3.6e+02 (20)	8.2e+00 (5)	6.7e+04 (4)	1.8e+04 (5)	8.4e+04 (4)
Pu-241	3.2e+00 (7)	< 1	< 1	< 1	< 1	< 1	7.2e+01 (4)	1.7e+01 (9)	7.6e+01 (4)
Pu-242	2.5e+02 (25)	3.0e+00 (86)	1.5e+00 (39)	8.2e+01 (5)	4.5e+01 (67)	< 1	4.7e+02 (4)	1.4e+02 (5)	6.1e+02 (4)
Ra-226	2.2e+03 (77)	1.3e+02 (86)	1.9e+01 (22)	1.5e+02 (77)	2.5e+02 (82)	3.4e+00 (22)	1.1e+04 (77)	2.9e+03 (82)	1.7e+04 (77)
Ra-228	< 1	< 1	< 1	< 1	< 1	< 1	< 1	< 1	< 1
Se-79	2.6e+06 (4)	4.2e+04 (5)	4.2e+05 (3)	1.1e+06 (3)	5.2e+06 (5)	< 1	6.6e+04 (3)	2.1e+04 (4)	7.5e+06 (5)
Sm-151	< 1	< 1	< 1	< 1	< 1	< 1	4.4e+00 (3)	< 1	4.6e+00 (3)
Sn-126	4.1e+03 (63)	< 1	2.5e+01 (67)	4.7e+02 (15)	1.2e+02 (86)	< 1	1.2e+02 (5)	9.0e+01 (16)	4.5e+03 (63)
Sr-90	< 1	< 1	< 1	< 1	< 1	< 1	< 1	< 1	< 1
Tc-99	1.1e+05 (29)	5.4e+01 (86)	4.6e+03 (61)	1.4e+04 (5)	3.6e+04 (86)	5.5e+01 (86)	1.1e+06 (4)	2.4e+04 (9)	1.1e+06 (4)
Th-228	< 1	< 1	< 1	< 1	< 1	< 1	< 1	< 1	< 1
Th-229	2.1e+02 (77)	< 1	1.2e+00 (77)	1.5e+01 (77)	2.9e+01 (82)	< 1	1.6e+00 (77)	5.0e+00 (82)	2.6e+02 (77)
Th-230	5.2e+01 (77)	< 1	< 1	4.5e+00 (77)	6.4e+00 (86)	< 1	4.0e+02 (82)	1.0e+02 (82)	5.7e+02 (82)
Th-232	< 1	< 1	< 1	< 1	< 1	< 1	< 1	< 1	< 1
U-232	< 1	< 1	< 1	< 1	< 1	< 1	< 1	< 1	< 1
U-233	1.3e+02 (82)	< 1	< 1	9.6e+00 (77)	2.7e+01 (86)	< 1	1.6e+00 (9)	4.7e+00 (82)	1.7e+02 (82)
U-234	9.4e+01 (26)	< 1	< 1	1.6e+01 (9)	1.2e+01 (86)	< 1	1.3e+03 (5)	1.8e+02 (82)	1.3e+03 (5)
U-235	4.7e+01 (25)	< 1	2.9e+00 (86)	3.1e+00 (9)	2.7e+00 (86)	< 1	1.1e+05 (4)	8.2e+03 (10)	1.1e+05 (4)
U-236	3.1e+01 (26)	< 1	< 1	1.0e+01 (9)	5.1e+00 (86)	< 1	2.1e+01 (4)	9.2e+00 (10)	4.6e+01 (25)
U-238	7.7e+01 (26)	< 1	< 1	2.4e+01 (9)	6.4e+00 (86)	< 1	2.3e+05 (4)	3.6e+03 (10)	2.3e+05 (4)
Zr-93	2.2e+05 (26)	2.0e+02 (86)	2.5e+03 (22)	6.7e+04 (5)	9.1e+04 (86)	3.6e+01 (37)	1.4e+04 (4)	2.6e+03 (9)	2.9e+05 (27)

Table E-9. Doses for CCL_IH, peak dose [Sv/year] and in parentheses time of peak [1000 year AD].

Nuclide	1BMA	2BMA	1BTF	2BTF	Silo	BRT	1BLA	2-5BLA	Total
Total	5.1e-06 (67)	3.5e-06 (28)	7.9e-07 (5)	8.2e-07 (5)	9.3e-06 (8)	3.8e-07 (5)	3.1e-06 (25)	1.4e-06 (9)	1.8e-05 (8)
Ac-227	1.5e-09 (77)	< 1e-12	1.3e-10 (86)	9.3e-11 (52)	1.5e-10 (86)	< 1e-12	5.1e-07 (33)	3.0e-07 (57)	7.7e-07 (39)
Ag-108m	5.0e-07 (5)	2.1e-08 (5)	9.9e-08 (5)	1.9e-07 (5)	2.7e-08 (5)	2.9e-09 (5)	2.7e-08 (5)	7.8e-09 (5)	8.6e-07 (5)
Am-241	< 1e-12	< 1e-12	< 1e-12	< 1e-12	< 1e-12	< 1e-12	1.7e-09 (4)	6.2e-09 (4)	6.8e-09 (4)
Am-242m	< 1e-12	< 1e-12	< 1e-12	< 1e-12	< 1e-12	< 1e-12	< 1e-12	< 1e-12	< 1e-12
Am-243	2.1e-11 (32)	< 1e-12	2.6e-12 (29)	1.7e-11 (26)	< 1e-12	< 1e-12	7.9e-10 (15)	1.5e-09 (5)	1.8e-09 (16)
Ba-133	< 1e-12	< 1e-12	< 1e-12	< 1e-12	< 1e-12	< 1e-12	< 1e-12	< 1e-12	< 1e-12
C-14-ind	< 1e-12	3.8e-08 (5)	< 1e-12	< 1e-12	< 1e-12	1.3e-09 (24)	< 1e-12	4.2e-08 (5)	7.9e-08 (5)
C-14-inorg	9.2e-09 (23)	< 1e-12	5.6e-09 (13)	2.4e-08 (6)	8.4e-12 (34)	< 1e-12	1.2e-07 (3)	3.2e-08 (5)	1.3e-07 (3)
C-14-org	9.7e-07 (5)	1.6e-08 (5)	8.3e-08 (3)	8.7e-08 (3)	2.0e-06 (5)	< 1e-12	2.4e-09 (3)	7.9e-09 (5)	2.9e-06 (5)
Ca-41	< 1e-12	3.3e-06 (28)	< 1e-12	< 1e-12	< 1e-12	< 1e-12	< 1e-12	1.1e-06 (10)	3.6e-06 (27)
Cd-113m	< 1e-12	< 1e-12	< 1e-12	< 1e-12	< 1e-12	< 1e-12	< 1e-12	< 1e-12	< 1e-12
Cl-36	2.5e-07 (5)	1.5e-07 (8)	3.4e-08 (5)	2.7e-08 (5)	4.7e-07 (6)	1.6e-09 (30)	2.5e-08 (3)	1.2e-07 (5)	9.6e-07 (5)
Cm-242	< 1e-12	< 1e-12	< 1e-12	< 1e-12	< 1e-12	< 1e-12	< 1e-12	< 1e-12	< 1e-12
Cm-243	< 1e-12	< 1e-12	< 1e-12	< 1e-12	< 1e-12	< 1e-12	< 1e-12	< 1e-12	< 1e-12
Cm-244	< 1e-12	< 1e-12	< 1e-12	< 1e-12	< 1e-12	< 1e-12	< 1e-12	< 1e-12	< 1e-12
Cm-245	< 1e-12	< 1e-12	< 1e-12	< 1e-12	< 1e-12	< 1e-12	9.2e-12 (16)	2.1e-11 (5)	2.8e-11 (18)
Cm-246	< 1e-12	< 1e-12	< 1e-12	< 1e-12	< 1e-12	< 1e-12	1.0e-12 (10)	5.2e-12 (5)	5.6e-12 (5)
Co-60	< 1e-12	< 1e-12	< 1e-12	< 1e-12	< 1e-12	< 1e-12	< 1e-12	< 1e-12	< 1e-12
Cs-135	1.0e-06 (86)	1.2e-07 (86)	1.5e-07 (86)	2.0e-08 (86)	1.3e-06 (86)	< 1e-12	5.3e-09 (86)	6.8e-07 (86)	3.3e-06 (86)
Cs-137	< 1e-12	< 1e-12	< 1e-12	< 1e-12	< 1e-12	< 1e-12	< 1e-12	< 1e-12	< 1e-12
Eu-152	< 1e-12	< 1e-12	< 1e-12	< 1e-12	< 1e-12	< 1e-12	< 1e-12	< 1e-12	< 1e-12
H-3	< 1e-12	< 1e-12	< 1e-12	< 1e-12	< 1e-12	< 1e-12	< 1e-12	< 1e-12	< 1e-12
Ho-166m	< 1e-12	< 1e-12	< 1e-12	< 1e-12	< 1e-12	< 1e-12	1.6e-12 (6)	1.0e-11 (5)	1.2e-11 (5)
I-129	4.9e-07 (11)	5.0e-08 (27)	2.3e-07 (6)	5.6e-08 (5)	1.9e-06 (16)	< 1e-12	1.0e-08 (3)	6.2e-08 (6)	2.5e-06 (14)
Mo-93	9.1e-07 (6)	1.4e-06 (9)	4.6e-07 (5)	5.9e-07 (5)	4.9e-06 (8)	3.8e-07 (5)	3.8e-07 (5)	5.4e-07 (5)	8.4e-06 (7)
Nb-93m	4.6e-09 (86)	4.6e-10 (9)	1.5e-10 (5)	6.7e-10 (77)	2.0e-09 (86)	1.2e-10 (5)	1.2e-10 (5)	1.7e-10 (5)	7.4e-09 (86)
Nb-94	1.5e-09 (67)	4.2e-12 (86)	3.5e-11 (77)	7.1e-10 (52)	2.6e-11 (78)	2.7e-11 (77)	5.1e-10 (32)	4.0e-09 (43)	6.3e-09 (51)
Ni-59	3.9e-06 (67)	2.2e-07 (86)	1.3e-07 (35)	2.3e-07 (29)	8.8e-07 (52)	1.3e-07 (67)	5.7e-08 (15)	1.8e-07 (21)	5.3e-06 (67)
Ni-63	< 1e-12	< 1e-12	< 1e-12	1.2e-12 (4)	< 1e-12	< 1e-12	1.4e-11 (3)	1.1e-11 (3)	1.5e-11 (3)
Np-237	3.9e-09 (86)	< 1e-12	2.6e-11 (86)	8.4e-10 (86)	3.9e-10 (86)	< 1e-12	3.9e-10 (86)	3.9e-10 (86)	5.9e-09 (86)
Pa-231	3.4e-09 (86)	< 1e-12	3.1e-10 (86)	1.6e-10 (47)	2.0e-10 (86)	< 1e-12	9.4e-07 (30)	3.9e-07 (52)	1.3e-06 (35)
Pb-210	1.2e-08 (86)	9.7e-10 (67)	1.4e-10 (23)	8.2e-10 (86)	1.3e-09 (86)	2.5e-11 (23)	6.2e-08 (86)	2.0e-08 (86)	9.5e-08 (86)
Pd-107	4.0e-09 (36)	8.3e-09 (67)	6.7e-11 (31)	5.3e-10 (18)	8.3e-09 (41)	< 1e-12	1.5e-11 (14)	5.2e-11 (16)	2.0e-08 (42)
Po-210	4.2e-10 (86)	7.6e-11 (86)	5.4e-12 (22)	2.7e-11 (86)	7.3e-11 (86)	1.6e-12 (6)	2.1e-09 (86)	1.1e-09 (86)	3.5e-09 (86)
Pu-238	< 1e-12	< 1e-12	< 1e-12	< 1e-12	< 1e-12	< 1e-12	< 1e-12	< 1e-12	< 1e-12
Pu-239	2.4e-07 (57)	5.7e-10 (86)	1.9e-09 (67)	5.7e-08 (43)	5.0e-08 (77)	7.3e-10 (67)	1.0e-07 (32)	1.7e-07 (42)	5.8e-07 (52)
Pu-240	2.4e-08 (19)	1.8e-12 (67)	1.1e-10 (31)	1.2e-08 (19)	1.1e-09 (44)	4.4e-11 (28)	2.6e-08 (14)	2.9e-08 (18)	8.8e-08 (18)
Pu-241	< 1e-12	< 1e-12	< 1e-12	< 1e-12	< 1e-12	< 1e-12	< 1e-12	< 1e-12	1.2e-12 (17)
Pu-242	1.8e-08 (86)	2.9e-11 (86)	9.5e-11 (86)	2.8e-09 (86)	3.0e-09 (86)	2.7e-11 (86)	2.0e-09 (86)	5.1e-09 (86)	3.1e-08 (86)
Ra-226	6.7e-08 (86)	5.3e-09 (67)	7.2e-10 (23)	5.1e-09 (86)	9.0e-09 (86)	1.2e-10 (23)	3.8e-07 (86)	1.1e-07 (86)	5.8e-07 (86)
Ra-228	< 1e-12	< 1e-12	< 1e-12	< 1e-12	< 1e-12	< 1e-12	< 1e-12	< 1e-12	< 1e-12
Se-79	7.4e-07 (7)	1.8e-08 (11)	5.1e-08 (6)	7.7e-08 (6)	2.3e-06 (12)	< 1e-12	2.3e-09 (5)	5.2e-09 (7)	3.0e-06 (10)
Sm-151	< 1e-12	< 1e-12	< 1e-12	< 1e-12	< 1e-12	< 1e-12	< 1e-12	< 1e-12	< 1e-12
Sn-126	4.4e-09 (86)	< 1e-12	1.8e-11 (98)	6.0e-10 (78)	6.7e-11 (98)	< 1e-12	3.0e-11 (58)	1.1e-10 (78)	5.2e-09 (86)
Sr-90	< 1e-12	< 1e-12	< 1e-12	< 1e-12	< 1e-12	< 1e-12	< 1e-12	< 1e-12	< 1e-12
Tc-99	1.2e-07 (78)	8.2e-12 (86)	6.1e-09 (86)	1.2e-08 (67)	4.2e-08 (86)	3.3e-11 (86)	1.5e-07 (52)	2.1e-08 (67)	3.3e-07 (77)
Th-228	< 1e-12	< 1e-12	< 1e-12	< 1e-12	< 1e-12	< 1e-12	< 1e-12	< 1e-12	< 1e-12
Th-229	1.0e-08 (86)	< 1e-12	6.1e-11 (86)	1.4e-09 (86)	1.4e-09 (86)	< 1e-12	4.8e-10 (86)	6.0e-10 (86)	1.4e-08 (86)
Th-230	6.6e-10 (86)	< 1e-12	5.2e-12 (67)	8.6e-11 (86)	6.5e-11 (86)	< 1e-12	1.0e-08 (77)	1.4e-09 (86)	1.2e-08 (77)
Th-232	< 1e-12	< 1e-12	< 1e-12	< 1e-12	1.9e-12 (5)	< 1e-12	< 1e-12	1.1e-12 (4)	< 1e-12
U-232	< 1e-12	< 1e-12	< 1e-12	< 1e-12	< 1e-12	< 1e-12	< 1e-12	< 1e-12	< 1e-12
U-233	4.8e-09 (86)	< 1e-12	2.5e-11 (86)	6.8e-10 (86)	6.6e-10 (86)	< 1e-12	2.3e-10 (86)	3.4e-10 (86)	6.7e-09 (86)
U-234	2.8e-09 (49)	4.5e-12 (86)	1.7e-11 (67)	4.7e-10 (37)	3.9e-10 (67)	1.5e-12 (24)	7.7e-08 (49)	1.2e-08 (67)	9.2e-08 (52)
U-235	1.3e-09 (49)	< 1e-12	7.8e-11 (67)	8.7e-11 (36)	7.7e-11 (67)	< 1e-12	8.0e-07 (7)	2.0e-07 (35)	8.3e-07 (7)
U-236	9.5e-10 (49)	< 1e-12	5.1e-12 (52)	3.1e-10 (36)	1.5e-10 (67)	< 1e-12	1.8e-10 (8)	2.5e-10 (34)	1.7e-09 (47)
U-238	2.2e-09 (49)	< 1e-12	2.2e-11 (67)	6.9e-10 (36)	1.9e-10 (67)	< 1e-12	1.7e-06 (7)	8.9e-08 (35)	1.7e-06 (7)
Zr-93	4.3e-07 (86)	6.3e-11 (86)	3.7e-09 (86)	6.4e-08 (67)	1.9e-07 (86)	7.8e-11 (86)	2.4e-09 (52)	3.2e-09 (77)	6.9e-07 (86)

High flow in the bedrock calculation case (CCL_FH)

Table E-10. Near-field releases for CCL_FH, peak release [Bq/year] and in parentheses time of peak [1000 year AD].

Nuclide	1BMA	2BMA	1BTF	2BTF	Silo	BRT	1BLA	2-5BLA	Total
Ac-227	3.0e+02 (24)	1.8e+00 (86)	5.5e+01 (86)	2.9e+00 (12)	1.6e+01 (86)	< 1	3.6e+04 (3)	7.4e+03 (3)	3.9e+04 (3)
Ag-108m	6.0e+05 (3)	4.3e+05 (4)	3.0e+05 (3)	1.4e+06 (3)	4.2e+04 (4)	6.0e+05 (3)	2.4e+05 (3)	1.9e+05 (3)	2.9e+06 (3)
Am-241	1.9e+02 (4)	< 1	2.0e+01 (4)	8.9e+02 (4)	< 1	4.0e+01 (4)	6.8e+05 (3)	2.5e+05 (3)	7.5e+05 (3)
Am-242m	< 1	< 1	< 1	< 1	< 1	< 1	4.5e+01 (3)	1.3e+01 (3)	4.5e+01 (3)
Am-243	2.1e+02 (7)	1.0e+00 (59)	1.3e+01 (22)	1.9e+02 (4)	< 1	1.8e+01 (22)	2.2e+04 (3)	1.4e+04 (3)	2.7e+04 (3)
Ba-133	< 1	< 1	< 1	< 1	< 1	< 1	< 1	< 1	< 1
C-14-ind	< 1	8.3e+05 (4)	< 1	< 1	< 1	3.2e+04 (23)	< 1	8.6e+05 (3)	1.5e+06 (3)
C-14-inorg	8.1e+05 (22)	5.8e+01 (23)	2.7e+05 (12)	3.3e+06 (4)	3.2e+02 (33)	< 1	2.1e+07 (3)	6.7e+05 (3)	2.1e+07 (3)
C-14-org	3.9e+07 (4)	6.4e+05 (4)	1.1e+07 (3)	1.9e+07 (3)	6.5e+07 (5)	< 1	4.2e+05 (3)	1.6e+05 (3)	9.1e+07 (4)
Ca-41	< 1	1.3e+06 (8)	< 1	< 1	< 1	< 1	< 1	3.3e+06 (3)	3.3e+06 (3)
Cd-113m	< 1	< 1	< 1	< 1	< 1	< 1	< 1	< 1	< 1
Cl-36	4.8e+04 (4)	1.9e+04 (5)	1.2e+04 (3)	5.1e+04 (3)	4.4e+04 (5)	2.7e+02 (25)	1.3e+05 (3)	3.9e+04 (3)	2.1e+05 (3)
Cm-242	< 1	< 1	< 1	< 1	< 1	< 1	3.7e+01 (3)	1.1e+01 (3)	3.7e+01 (3)
Cm-243	< 1	< 1	< 1	< 1	< 1	< 1	< 1	< 1	< 1
Cm-244	< 1	< 1	< 1	< 1	< 1	< 1	< 1	< 1	< 1
Cm-245	1.5e+00 (7)	< 1	< 1	1.2e+00 (4)	< 1	< 1	2.2e+02 (3)	1.7e+02 (3)	2.8e+02 (3)
Cm-246	< 1	< 1	< 1	< 1	< 1	< 1	5.4e+01 (3)	4.6e+01 (3)	7.4e+01 (3)
Co-60	< 1	< 1	< 1	< 1	< 1	< 1	< 1	< 1	< 1
Cs-135	1.1e+05 (7)	5.9e+03 (7)	4.3e+04 (3)	4.0e+04 (3)	4.0e+04 (10)	< 1	1.8e+04 (3)	1.5e+05 (3)	2.6e+05 (3)
Cs-137	< 1	< 1	< 1	< 1	< 1	< 1	< 1	< 1	< 1
Eu-152	< 1	< 1	< 1	< 1	< 1	< 1	< 1	< 1	< 1
H-3	< 1	< 1	< 1	< 1	< 1	< 1	< 1	< 1	< 1
Ho-166m	8.6e+01 (5)	< 1	7.8e+00 (4)	3.6e+02 (4)	< 1	< 1	1.4e+04 (3)	3.7e+04 (3)	4.1e+04 (3)
I-129	3.0e+04 (22)	4.7e+02 (23)	1.1e+04 (3)	2.8e+04 (3)	2.9e+04 (6)	< 1	2.6e+03 (3)	1.6e+03 (3)	4.7e+04 (22)
Mo-93	1.0e+05 (4)	1.5e+05 (5)	1.3e+05 (3)	5.1e+05 (3)	3.3e+05 (5)	1.6e+05 (3)	5.1e+05 (3)	6.1e+04 (3)	1.2e+06 (3)
Nb-93m	3.2e+04 (23)	7.9e+03 (84)	1.8e+03 (3)	1.2e+04 (4)	9.5e+03 (49)	2.6e+03 (3)	5.1e+05 (3)	8.6e+04 (3)	5.3e+05 (3)
Nb-94	8.9e+03 (24)	3.6e+03 (64)	2.5e+02 (60)	8.5e+03 (5)	2.5e+02 (34)	4.1e+03 (63)	1.8e+05 (3)	7.9e+05 (3)	8.2e+05 (3)
Ni-59	2.9e+07 (57)	1.5e+07 (58)	3.7e+06 (4)	1.5e+07 (3)	1.2e+07 (34)	9.9e+06 (4)	2.4e+07 (3)	9.6e+06 (3)	4.9e+07 (58)
Ni-63	7.3e+02 (3)	< 1	1.2e+04 (3)	2.8e+05 (3)	< 1	7.1e+04 (3)	1.8e+06 (3)	3.4e+05 (3)	1.8e+06 (3)
Np-237	1.3e+03 (22)	1.0e+01 (67)	2.2e+00 (22)	4.1e+02 (4)	1.2e+02 (34)	1.6e+00 (22)	9.4e+02 (3)	5.3e+02 (3)	1.4e+03 (22)
Pa-231	4.1e+01 (23)	< 1	1.1e+01 (58)	1.2e+00 (22)	1.0e+01 (77)	< 1	3.7e+04 (3)	7.6e+03 (3)	4.0e+04 (3)
Pb-210	2.2e+02 (77)	1.0e+02 (82)	1.9e+00 (22)	3.1e+00 (4)	1.2e+01 (86)	1.9e+00 (22)	9.7e+00 (3)	3.3e+00 (4)	2.9e+02 (77)
Pd-107	5.5e+03 (4)	2.2e+05 (5)	2.4e+02 (4)	1.2e+04 (3)	4.2e+03 (6)	< 1	5.9e+02 (3)	1.4e+03 (3)	2.3e+05 (5)
Po-210	1.8e+04 (77)	8.8e+03 (82)	1.5e+02 (22)	9.2e+01 (22)	9.1e+02 (86)	1.6e+02 (22)	9.7e+00 (3)	3.3e+00 (4)	2.4e+04 (77)
Pu-238	6.0e+00 (3)	< 1	< 1	2.7e+01 (3)	< 1	< 1	8.6e+02 (3)	1.9e+02 (3)	8.6e+02 (3)
Pu-239	4.4e+04 (22)	8.7e+02 (57)	1.5e+02 (12)	5.3e+04 (3)	3.7e+03 (35)	2.8e+02 (12)	3.8e+05 (3)	2.2e+05 (3)	5.0e+05 (3)
Pu-240	3.2e+04 (4)	1.9e+01 (23)	9.0e+01 (12)	6.8e+04 (3)	1.1e+03 (16)	3.2e+02 (4)	3.6e+05 (3)	2.2e+05 (3)	5.0e+05 (3)
Pu-241	2.4e+01 (7)	1.7e+00 (63)	2.3e+00 (15)	3.2e+01 (4)	< 1	< 1	2.2e+02 (3)	1.7e+02 (3)	2.9e+02 (3)
Pu-242	5.3e+02 (22)	2.8e+01 (59)	1.8e+00 (27)	3.9e+02 (3)	5.0e+01 (35)	2.8e+00 (23)	2.4e+03 (3)	1.4e+03 (3)	3.2e+03 (3)
Ra-226	1.7e+03 (77)	1.0e+03 (82)	2.3e+01 (22)	6.6e+00 (22)	2.0e+02 (82)	1.9e+01 (22)	1.0e+01 (3)	3.4e+00 (4)	2.6e+03 (77)
Ra-228	< 1	< 1	< 1	< 1	< 1	< 1	< 1	< 1	< 1
Se-79	6.8e+04 (4)	1.5e+03 (4)	1.5e+04 (3)	5.5e+04 (3)	1.3e+05 (5)	< 1	2.4e+03 (3)	5.0e+03 (3)	1.8e+05 (5)
Sm-151	< 1	< 1	< 1	< 1	< 1	< 1	4.5e+02 (3)	7.6e+02 (3)	9.9e+02 (3)
Sn-126	5.1e+02 (22)	3.3e+00 (59)	2.9e+00 (59)	2.2e+02 (4)	3.5e+01 (67)	< 1	3.0e+02 (3)	6.6e+03 (3)	6.8e+03 (3)
Sr-90	< 1	< 1	< 1	< 1	< 1	< 1	< 1	< 1	< 1
Tc-99	2.7e+05 (23)	1.5e+03 (86)	8.2e+03 (22)	1.4e+05 (4)	3.5e+04 (64)	1.8e+03 (58)	1.1e+07 (3)	4.2e+05 (3)	1.1e+07 (3)
Th-228	< 1	< 1	< 1	< 1	< 1	< 1	< 1	< 1	< 1
Th-229	1.4e+02 (83)	< 1	< 1	3.3e+00 (58)	6.2e+00 (86)	< 1	< 1	< 1	1.5e+02 (83)
Th-230	4.5e+01 (82)	2.7e+00 (86)	< 1	2.9e+00 (22)	5.6e+00 (86)	< 1	7.2e+01 (3)	1.3e+01 (4)	7.7e+01 (3)
Th-232	< 1	< 1	< 1	< 1	< 1	< 1	< 1	< 1	< 1
U-232	< 1	< 1	< 1	< 1	< 1	< 1	< 1	< 1	< 1
U-233	1.6e+02 (22)	3.7e+00 (77)	< 1	6.7e+00 (22)	2.6e+01 (77)	< 1	3.2e+00 (3)	2.5e+00 (4)	1.6e+02 (22)
U-234	3.0e+02 (22)	1.0e+01 (61)	< 1	1.2e+02 (4)	3.3e+01 (34)	< 1	1.4e+04 (3)	1.4e+03 (3)	1.4e+04 (3)
U-235	1.6e+02 (22)	< 1	4.8e+00 (86)	2.2e+01 (4)	7.6e+00 (34)	< 1	1.8e+06 (3)	2.7e+05 (3)	1.8e+06 (3)
U-236	9.3e+01 (22)	5.5e+00 (64)	< 1	7.4e+01 (4)	1.3e+01 (34)	< 1	2.5e+02 (3)	1.8e+02 (3)	3.6e+02 (3)
U-238	2.4e+02 (22)	< 1	1.2e+00 (26)	1.7e+02 (4)	1.8e+01 (34)	< 1	4.4e+06 (3)	1.5e+05 (3)	4.4e+06 (3)
Zr-93	1.8e+04 (23)	2.6e+03 (85)	1.5e+02 (22)	1.1e+04 (4)	1.4e+04 (34)	9.7e+02 (22)	6.5e+03 (3)	2.5e+04 (3)	3.6e+04 (3)

Intrusion wells calculation case (CCL_WI)

Table E-11. Far-field releases for CCL_FH, peak release [Bq/year] and in parentheses time of peak [1000 year AD].

Nuclide	1BMA	2BMA	1BTF	2BTF	Silo	BRT	1BLA	2-5BLA	Total
Ac-227	2.8e+02 (84)	< 1	1.7e+01 (86)	3.5e+00 (25)	4.7e+01 (86)	< 1	1.4e+04 (5)	6.4e+03 (82)	1.6e+04 (5)
Ag-108m	5.9e+05 (3)	4.1e+05 (4)	2.2e+05 (3)	1.2e+06 (3)	3.7e+04 (4)	3.1e+05 (3)	2.0e+05 (3)	1.3e+05 (3)	2.1e+06 (3)
Am-241	5.6e+01 (4)	< 1	< 1	1.7e+01 (4)	< 1	< 1	5.6e+04 (3)	4.3e+03 (4)	5.7e+04 (3)
Am-242m	< 1	< 1	< 1	< 1	< 1	< 1	2.9e+00 (3)	< 1	2.9e+00 (3)
Am-243	5.3e+01 (7)	< 1	1.1e+00 (17)	1.3e+01 (9)	< 1	< 1	2.1e+03 (3)	5.2e+02 (5)	2.1e+03 (3)
Ba-133	< 1	< 1	< 1	< 1	< 1	< 1	< 1	< 1	< 1
C-14-ind	< 1	7.1e+05 (4)	< 1	< 1	< 1	2.8e+04 (23)	< 1	8.0e+05 (4)	1.5e+06 (4)
C-14-inorg	7.9e+05 (22)	5.0e+01 (23)	2.6e+05 (12)	3.1e+06 (4)	3.2e+02 (33)	< 1	1.9e+07 (3)	6.2e+05 (4)	1.9e+07 (3)
C-14-org	3.9e+07 (4)	5.6e+05 (5)	8.4e+06 (3)	1.6e+07 (3)	6.3e+07 (5)	< 1	3.8e+05 (3)	1.5e+05 (4)	8.8e+07 (4)
Ca-41	< 1	1.2e+06 (9)	< 1	< 1	< 1	< 1	< 1	3.1e+06 (4)	3.1e+06 (4)
Cd-113m	< 1	< 1	< 1	< 1	< 1	< 1	< 1	< 1	< 1
Cl-36	4.8e+04 (4)	1.9e+04 (5)	9.7e+03 (3)	4.3e+04 (3)	4.3e+04 (5)	2.6e+02 (29)	1.2e+05 (3)	3.7e+04 (4)	1.8e+05 (3)
Cm-242	< 1	< 1	< 1	< 1	< 1	< 1	1.8e+00 (3)	< 1	1.8e+00 (3)
Cm-243	< 1	< 1	< 1	< 1	< 1	< 1	< 1	< 1	< 1
Cm-244	< 1	< 1	< 1	< 1	< 1	< 1	< 1	< 1	< 1
Cm-245	< 1	< 1	< 1	< 1	< 1	< 1	2.0e+01 (3)	6.9e+00 (5)	2.1e+01 (3)
Cm-246	< 1	< 1	< 1	< 1	< 1	< 1	5.0e+00 (3)	1.7e+00 (5)	5.1e+00 (3)
Co-60	< 1	< 1	< 1	< 1	< 1	< 1	< 1	< 1	< 1
Cs-135	9.7e+04 (5)	1.8e+03 (9)	1.1e+04 (4)	9.0e+03 (4)	2.4e+04 (15)	< 1	5.7e+03 (3)	2.7e+04 (4)	1.4e+05 (5)
Cs-137	< 1	< 1	< 1	< 1	< 1	< 1	< 1	< 1	< 1
Eu-152	< 1	< 1	< 1	< 1	< 1	< 1	< 1	< 1	< 1
H-3	< 1	< 1	< 1	< 1	< 1	< 1	< 1	< 1	< 1
Ho-166m	4.2e+01 (5)	< 1	< 1	6.3e+01 (4)	< 1	< 1	1.2e+03 (3)	1.0e+03 (4)	1.7e+03 (4)
I-129	2.9e+04 (22)	4.3e+02 (8)	9.5e+03 (3)	2.2e+04 (3)	2.8e+04 (6)	< 1	2.3e+03 (3)	1.6e+03 (4)	4.6e+04 (22)
Mo-93	1.0e+05 (4)	1.3e+05 (5)	1.1e+05 (3)	4.1e+05 (3)	3.1e+05 (5)	1.4e+05 (4)	4.6e+05 (3)	5.6e+04 (4)	9.5e+05 (3)
Nb-93m	1.8e+04 (24)	8.9e+02 (86)	4.4e+02 (3)	4.9e+03 (9)	1.2e+04 (86)	5.6e+02 (4)	1.3e+04 (3)	9.9e+02 (9)	2.6e+04 (25)
Nb-94	6.0e+03 (26)	8.2e+02 (67)	5.1e+01 (61)	2.6e+03 (9)	8.6e+01 (34)	2.6e+02 (67)	1.4e+04 (3)	2.7e+04 (5)	3.2e+04 (5)
Ni-59	2.5e+07 (58)	5.8e+06 (61)	7.9e+05 (5)	7.0e+06 (4)	4.4e+06 (35)	1.2e+06 (5)	7.4e+06 (3)	2.0e+06 (4)	3.3e+07 (59)
Ni-63	4.5e+02 (4)	< 1	9.4e+02 (4)	4.6e+04 (3)	< 1	1.6e+03 (4)	3.8e+05 (3)	1.5e+04 (3)	4.0e+05 (3)
Np-237	4.4e+02 (23)	1.5e+00 (86)	< 1	5.0e+01 (5)	1.9e+01 (86)	< 1	4.5e+01 (3)	8.2e+00 (9)	4.7e+02 (23)
Pa-231	2.5e+01 (83)	< 1	2.4e+00 (86)	< 1	2.3e+00 (86)	< 1	2.3e+03 (4)	7.3e+02 (82)	2.3e+03 (4)
Pb-210	1.4e+02 (77)	2.3e+01 (85)	< 1	3.8e+00 (77)	6.8e+00 (86)	< 1	2.6e+02 (77)	8.3e+01 (82)	5.0e+02 (77)
Pd-107	5.5e+03 (4)	2.3e+05 (5)	2.3e+02 (4)	9.6e+03 (3)	4.1e+03 (7)	< 1	5.4e+02 (3)	1.4e+03 (4)	2.4e+05 (5)
Po-210	1.9e+02 (77)	2.3e+01 (84)	< 1	4.2e+00 (77)	7.8e+00 (86)	< 1	2.9e+02 (77)	8.1e+01 (77)	5.8e+02 (77)
Pu-238	< 1	< 1	< 1	< 1	< 1	< 1	4.9e+01 (3)	< 1	5.0e+01 (3)
Pu-239	2.2e+04 (23)	1.2e+02 (67)	4.7e+01 (29)	6.4e+03 (4)	1.2e+03 (36)	3.7e+01 (30)	3.7e+04 (3)	1.1e+04 (5)	4.9e+04 (4)
Pu-240	1.9e+04 (5)	1.8e+00 (25)	1.6e+01 (14)	7.9e+03 (4)	2.3e+02 (19)	8.9e+00 (15)	3.5e+04 (3)	8.9e+03 (5)	5.0e+04 (4)
Pu-241	4.3e+00 (5)	< 1	< 1	< 1	< 1	< 1	4.0e+01 (4)	8.6e+00 (5)	4.5e+01 (4)
Pu-242	2.7e+02 (23)	5.4e+00 (86)	< 1	4.9e+01 (5)	1.9e+01 (67)	< 1	2.3e+02 (3)	7.0e+01 (5)	3.3e+02 (4)
Ra-226	1.6e+03 (77)	2.3e+02 (84)	8.2e+00 (22)	6.1e+01 (77)	1.2e+02 (82)	3.1e+00 (22)	4.8e+03 (77)	1.5e+03 (77)	8.2e+03 (77)
Ra-228	< 1	< 1	< 1	< 1	< 1	< 1	< 1	< 1	< 1
Se-79	6.7e+04 (4)	1.4e+03 (5)	1.2e+04 (3)	4.7e+04 (3)	1.3e+05 (5)	< 1	2.2e+03 (3)	4.7e+03 (4)	1.7e+05 (5)
Sm-151	< 1	< 1	< 1	< 1	< 1	< 1	2.4e+01 (3)	1.7e+00 (3)	2.4e+01 (3)
Sn-126	2.0e+02 (28)	< 1	< 1	1.5e+01 (10)	3.5e+00 (86)	< 1	5.5e+00 (4)	2.8e+01 (12)	2.4e+02 (28)
Sr-90	< 1	< 1	< 1	< 1	< 1	< 1	< 1	< 1	< 1
Tc-99	1.3e+05 (25)	2.5e+02 (86)	1.0e+03 (59)	1.4e+04 (5)	8.0e+03 (86)	9.5e+01 (86)	5.3e+05 (4)	7.7e+03 (5)	5.3e+05 (4)
Th-228	< 1	< 1	< 1	< 1	< 1	< 1	< 1	< 1	< 1
Th-229	1.1e+02 (82)	< 1	< 1	3.7e+00 (77)	7.4e+00 (77)	< 1	< 1	< 1	1.3e+02 (82)
Th-230	3.7e+01 (83)	< 1	< 1	1.6e+00 (77)	3.4e+00 (82)	< 1	1.7e+02 (77)	4.5e+01 (82)	2.6e+02 (82)
Th-232	< 1	< 1	< 1	< 1	< 1	< 1	< 1	< 1	< 1
U-232	< 1	< 1	< 1	< 1	< 1	< 1	< 1	< 1	< 1
U-233	6.7e+01 (77)	< 1	< 1	3.2e+00 (77)	6.0e+00 (86)	< 1	< 1	< 1	7.6e+01 (82)
U-234	1.0e+02 (24)	< 1	< 1	1.1e+01 (9)	5.4e+00 (86)	< 1	1.0e+03 (4)	6.9e+01 (82)	1.0e+03 (4)
U-235	5.0e+01 (23)	< 1	1.3e+00 (86)	1.9e+00 (9)	1.3e+00 (86)	< 1	9.0e+04 (4)	4.9e+03 (5)	8.8e+04 (4)
U-236	3.3e+01 (24)	< 1	< 1	6.7e+00 (9)	2.2e+00 (86)	< 1	1.3e+01 (4)	3.5e+00 (5)	3.9e+01 (24)
U-238	8.0e+01 (24)	< 1	< 1	1.5e+01 (9)	3.1e+00 (86)	< 1	2.2e+05 (4)	2.7e+03 (5)	2.1e+05 (4)
Zr-93	9.6e+03 (24)	5.8e+02 (86)	3.9e+01 (23)	1.8e+03 (5)	4.3e+03 (86)	6.7e+01 (34)	4.5e+02 (4)	6.6e+02 (5)	1.2e+04 (24)

Table E-12. Doses for CCL_FH, peak dose [Sv/year] and in parentheses time of peak [1000 year AD].

Nuclide	1BMA	2BMA	1BTF	2BTF	Silo	BRT	1BLA	2-5BLA	Total
Total	3.3e-06 (67)	1.4e-06 (14)	5.1e-07 (5)	6.7e-07 (5)	4.5e-06 (7)	5.1e-07 (5)	1.5e-06 (7)	5.5e-07 (8)	9.7e-06 (6)
Ac-227	1.2e-09 (86)	1.1e-12 (86)	3.9e-11 (86)	3.9e-11 (43)	8.8e-11 (86)	< 1e-12	2.3e-07 (30)	1.1e-07 (57)	3.3e-07 (35)
Ag-108m	1.4e-08 (5)	1.1e-08 (5)	2.4e-09 (5)	4.8e-09 (5)	1.8e-09 (5)	4.3e-09 (3)	5.0e-10 (5)	2.5e-09 (5)	4.0e-08 (5)
Am-241	1.1e-12 (5)	< 1e-12	< 1e-12	< 1e-12	< 1e-12	< 1e-12	3.2e-10 (4)	4.1e-09 (4)	4.2e-09 (4)
Am-242m	< 1e-12	< 1e-12	< 1e-12	< 1e-12	< 1e-12	< 1e-12	< 1e-12	< 1e-12	< 1e-12
Am-243	3.4e-11 (35)	< 1e-12	3.0e-12 (29)	2.1e-11 (25)	< 1e-12	2.4e-12 (25)	2.8e-10 (14)	5.9e-10 (5)	6.5e-10 (5)
Ba-133	< 1e-12	< 1e-12	< 1e-12	< 1e-12	< 1e-12	< 1e-12	< 1e-12	< 1e-12	< 1e-12
C-14-ind	< 1e-12	1.9e-08 (5)	< 1e-12	< 1e-12	< 1e-12	7.7e-10 (23)	< 1e-12	7.0e-09 (5)	2.6e-08 (5)
C-14-inorg	2.1e-08 (23)	1.4e-12 (24)	7.1e-09 (13)	4.4e-08 (5)	9.0e-12 (34)	< 1e-12	8.5e-08 (3)	5.4e-09 (5)	9.0e-08 (3)
C-14-org	7.3e-07 (5)	1.5e-08 (5)	8.6e-08 (3)	6.5e-08 (3)	1.8e-06 (5)	< 1e-12	1.7e-09 (3)	1.3e-09 (5)	2.5e-06 (5)
Ca-41	< 1e-12	1.0e-06 (26)	< 1e-12	< 1e-12	< 1e-12	< 1e-12	< 1e-12	4.6e-07 (9)	1.2e-06 (18)
Cd-113m	< 1e-12	< 1e-12	< 1e-12	< 1e-12	< 1e-12	< 1e-12	< 1e-12	< 1e-12	< 1e-12
Cl-36	1.5e-07 (5)	6.1e-08 (5)	1.1e-08 (5)	1.1e-08 (5)	1.3e-07 (5)	8.8e-10 (29)	2.3e-08 (3)	4.4e-08 (5)	3.7e-07 (5)
Cm-242	< 1e-12	< 1e-12	< 1e-12	< 1e-12	< 1e-12	< 1e-12	< 1e-12	< 1e-12	< 1e-12
Cm-243	< 1e-12	< 1e-12	< 1e-12	< 1e-12	< 1e-12	< 1e-12	< 1e-12	< 1e-12	< 1e-12
Cm-244	< 1e-12	< 1e-12	< 1e-12	< 1e-12	< 1e-12	< 1e-12	< 1e-12	< 1e-12	< 1e-12
Cm-245	< 1e-12	< 1e-12	< 1e-12	< 1e-12	< 1e-12	< 1e-12	3.1e-12 (14)	7.7e-12 (5)	8.4e-12 (5)
Cm-246	< 1e-12	< 1e-12	< 1e-12	< 1e-12	< 1e-12	< 1e-12	< 1e-12	1.6e-12 (5)	1.7e-12 (5)
Co-60	< 1e-12	< 1e-12	< 1e-12	< 1e-12	< 1e-12	< 1e-12	< 1e-12	< 1e-12	< 1e-12
Cs-135	7.1e-07 (86)	1.8e-08 (86)	4.5e-08 (86)	1.4e-08 (86)	7.3e-07 (86)	< 1e-12	2.6e-09 (86)	1.0e-07 (86)	1.6e-06 (86)
Cs-137	< 1e-12	< 1e-12	< 1e-12	< 1e-12	< 1e-12	< 1e-12	< 1e-12	< 1e-12	< 1e-12
Eu-152	< 1e-12	< 1e-12	< 1e-12	< 1e-12	< 1e-12	< 1e-12	< 1e-12	< 1e-12	< 1e-12
H-3	< 1e-12	< 1e-12	< 1e-12	< 1e-12	< 1e-12	< 1e-12	< 1e-12	< 1e-12	< 1e-12
Ho-166m	< 1e-12	< 1e-12	< 1e-12	< 1e-12	< 1e-12	< 1e-12	< 1e-12	1.2e-11 (4)	1.2e-11 (4)
I-129	2.7e-07 (10)	1.1e-08 (25)	6.9e-08 (5)	5.2e-08 (5)	6.9e-07 (15)	< 1e-12	3.6e-09 (3)	1.0e-08 (5)	9.6e-07 (12)
Mo-93	8.1e-07 (6)	1.2e-06 (8)	4.1e-07 (5)	5.5e-07 (5)	2.8e-06 (8)	5.0e-07 (5)	2.5e-07 (5)	2.1e-07 (5)	5.7e-06 (7)
Nb-93m	2.7e-10 (6)	4.0e-10 (8)	1.3e-10 (5)	1.8e-10 (5)	9.4e-10 (8)	1.6e-10 (5)	8.0e-11 (5)	6.8e-11 (5)	1.9e-09 (7)
Nb-94	7.5e-10 (67)	6.2e-11 (86)	7.5e-12 (77)	2.0e-10 (49)	8.6e-12 (77)	3.8e-11 (77)	8.8e-11 (31)	8.1e-10 (40)	1.8e-09 (52)
Ni-59	2.6e-06 (67)	3.6e-07 (86)	4.2e-08 (34)	9.3e-08 (28)	3.8e-07 (52)	1.6e-07 (52)	1.9e-08 (15)	3.3e-08 (20)	3.5e-06 (67)
Ni-63	< 1e-12	< 1e-12	< 1e-12	2.1e-12 (3)	< 1e-12	1.4e-12 (4)	1.1e-11 (3)	9.1e-12 (3)	1.3e-11 (3)
Np-237	3.1e-09 (86)	1.9e-12 (86)	4.3e-12 (86)	3.4e-10 (86)	8.0e-11 (86)	< 1e-12	4.5e-11 (86)	4.7e-11 (86)	3.6e-09 (86)
Pa-231	2.7e-09 (86)	< 1e-12	9.5e-11 (86)	6.3e-11 (39)	8.1e-11 (86)	< 1e-12	4.3e-07 (28)	1.4e-07 (48)	5.6e-07 (32)
Pb-210	7.7e-09 (86)	1.2e-09 (67)	5.5e-11 (23)	3.2e-10 (86)	6.7e-10 (86)	2.1e-11 (24)	2.9e-08 (86)	7.9e-09 (86)	4.1e-08 (86)
Pd-107	1.2e-10 (34)	5.8e-09 (40)	2.4e-12 (29)	1.4e-11 (15)	2.5e-10 (41)	< 1e-12	< 1e-12	6.5e-12 (15)	6.2e-09 (40)
Po-210	2.8e-10 (86)	1.8e-10 (86)	2.3e-12 (22)	1.1e-11 (86)	3.4e-11 (86)	1.2e-12 (22)	8.7e-10 (86)	4.7e-10 (82)	1.7e-09 (86)
Pu-238	< 1e-12	< 1e-12	< 1e-12	< 1e-12	< 1e-12	< 1e-12	< 1e-12	< 1e-12	< 1e-12
Pu-239	2.8e-07 (57)	1.2e-09 (86)	1.5e-09 (64)	4.8e-08 (42)	2.3e-08 (77)	6.0e-10 (67)	3.4e-08 (31)	5.0e-08 (39)	4.1e-07 (52)
Pu-240	2.5e-08 (19)	5.9e-12 (41)	9.8e-11 (29)	1.0e-08 (18)	6.2e-10 (37)	3.5e-11 (27)	9.1e-09 (14)	1.2e-08 (5)	5.3e-08 (18)
Pu-241	< 1e-12	< 1e-12	< 1e-12	< 1e-12	< 1e-12	< 1e-12	< 1e-12	< 1e-12	< 1e-12
Pu-242	1.3e-08 (86)	7.2e-11 (86)	6.1e-11 (86)	1.6e-09 (86)	1.1e-09 (86)	2.3e-11 (86)	6.3e-10 (83)	1.3e-09 (86)	1.8e-08 (86)
Ra-226	5.0e-08 (86)	8.2e-09 (67)	3.3e-10 (23)	2.0e-09 (86)	4.1e-09 (86)	1.2e-10 (23)	1.5e-07 (86)	4.9e-08 (86)	2.6e-07 (86)
Ra-228	< 1e-12	< 1e-12	< 1e-12	< 1e-12	< 1e-12	< 1e-12	< 1e-12	< 1e-12	< 1e-12
Se-79	1.6e-08 (7)	4.3e-10 (8)	1.1e-09 (5)	1.7e-09 (5)	5.3e-08 (11)	< 1e-12	4.2e-11 (5)	6.2e-10 (6)	6.8e-08 (10)
Sm-151	< 1e-12	< 1e-12	< 1e-12	< 1e-12	< 1e-12	< 1e-12	< 1e-12	< 1e-12	< 1e-12
Sn-126	2.1e-10 (86)	< 1e-12	< 1e-12	1.4e-11 (77)	2.2e-12 (86)	< 1e-12	< 1e-12	2.6e-11 (77)	2.5e-10 (86)
Sr-90	< 1e-12	< 1e-12	< 1e-12	< 1e-12	< 1e-12	< 1e-12	< 1e-12	< 1e-12	< 1e-12
Tc-99	9.7e-08 (77)	6.0e-11 (86)	1.5e-09 (86)	7.9e-09 (66)	8.0e-09 (86)	5.3e-11 (86)	4.6e-08 (49)	4.3e-09 (67)	1.6e-07 (67)
Th-228	< 1e-12	< 1e-12	< 1e-12	< 1e-12	< 1e-12	< 1e-12	< 1e-12	< 1e-12	< 1e-12
Th-229	6.7e-09 (86)	4.5e-12 (86)	4.4e-12 (86)	6.1e-10 (86)	2.9e-10 (86)	< 1e-12	5.1e-11 (86)	4.8e-11 (86)	7.7e-09 (86)
Th-230	5.9e-10 (86)	1.7e-12 (86)	< 1e-12	4.0e-11 (67)	3.1e-11 (86)	< 1e-12	5.5e-09 (77)	6.0e-10 (86)	6.3e-09 (77)
Th-232	< 1e-12	< 1e-12	< 1e-12	< 1e-12	< 1e-12	< 1e-12	< 1e-12	< 1e-12	< 1e-12
U-232	< 1e-12	< 1e-12	< 1e-12	< 1e-12	< 1e-12	< 1e-12	< 1e-12	< 1e-12	< 1e-12
U-233	3.0e-09 (86)	6.0e-12 (86)	3.0e-12 (86)	2.9e-10 (86)	1.5e-10 (86)	< 1e-12	2.4e-11 (86)	2.5e-11 (86)	3.5e-09 (86)
U-234	2.0e-09 (42)	2.5e-11 (86)	5.5e-12 (67)	2.6e-10 (35)	1.5e-10 (67)	< 1e-12	3.8e-08 (45)	4.6e-09 (67)	4.4e-08 (48)
U-235	9.0e-10 (42)	< 1e-12	4.2e-11 (67)	4.1e-11 (32)	3.1e-11 (67)	< 1e-12	3.9e-07 (6)	7.0e-08 (29)	4.2e-07 (7)
U-236	7.0e-10 (43)	1.1e-11 (86)	1.9e-12 (52)	1.7e-10 (35)	5.5e-11 (67)	< 1e-12	6.3e-11 (7)	5.3e-11 (13)	9.4e-10 (42)
U-238	1.5e-09 (43)	1.3e-12 (86)	6.5e-12 (52)	3.5e-10 (35)	7.8e-11 (67)	< 1e-12	9.6e-07 (6)	3.9e-08 (29)	9.8e-07 (7)
Zr-93	1.2e-08 (78)	2.7e-10 (86)	7.2e-11 (86)	1.3e-09 (67)	7.6e-09 (86)	1.6e-10 (86)	4.8e-11 (51)	5.8e-10 (77)	2.1e-08 (86)

Accelerated concrete degradation calculation case (CCL_BC)

Table E-13. Near-field releases for CCL_BC, peak release [Bq/year] and in parentheses time of peak [1000 year AD].

Nuclide	1BMA	2BMA	1BTF	2BTF	Silo	BRT	1BLA	2-5BLA	Total
Ac-227	1.5e+02 (84)	< 1	2.9e+01 (86)	2.0e+00 (12)	1.3e+01 (67)	< 1	2.2e+04 (3)	5.2e+03 (4)	2.3e+04 (3)
Ag-108m	2.5e+06 (3)	3.0e+05 (4)	1.5e+05 (3)	7.5e+05 (3)	3.2e+04 (4)	2.0e+05 (3)	1.3e+05 (3)	6.5e+04 (3)	3.7e+06 (3)
Am-241	1.2e+03 (4)	< 1	3.5e+01 (4)	3.4e+02 (4)	< 1	6.9e+00 (4)	3.8e+05 (3)	8.8e+04 (3)	4.1e+05 (3)
Am-242m	< 1	< 1	< 1	< 1	< 1	< 1	2.5e+01 (3)	3.7e+00 (3)	2.5e+01 (3)
Am-243	7.1e+02 (7)	3.4e+00 (27)	7.3e+00 (22)	7.5e+01 (4)	< 1	3.8e+00 (22)	1.3e+04 (3)	6.5e+03 (4)	1.4e+04 (3)
Ba-133	< 1	< 1	< 1	< 1	< 1	< 1	< 1	< 1	< 1
C-14-ind	< 1	6.9e+05 (5)	< 1	< 1	< 1	2.7e+04 (24)	< 1	4.0e+05 (4)	1.0e+06 (4)
C-14-inorg	8.0e+06 (5)	3.3e+02 (23)	2.4e+05 (7)	3.0e+06 (4)	8.0e+02 (31)	< 1	1.3e+07 (3)	3.1e+05 (4)	1.6e+07 (3)
C-14-org	7.5e+07 (3)	5.3e+05 (5)	5.3e+06 (3)	9.8e+06 (3)	5.6e+07 (5)	< 1	2.5e+05 (3)	7.5e+04 (4)	9.6e+07 (4)
Ca-41	< 1	1.4e+06 (9)	< 1	< 1	< 1	< 1	< 1	1.6e+06 (4)	1.6e+06 (4)
Cd-113m	< 1	< 1	< 1	< 1	< 1	< 1	< 1	< 1	< 1
Cl-36	1.1e+05 (3)	2.1e+04 (6)	6.7e+03 (3)	2.6e+04 (3)	4.0e+04 (5)	2.7e+02 (29)	7.6e+04 (3)	1.9e+04 (4)	2.0e+05 (3)
Cm-242	< 1	< 1	< 1	< 1	< 1	< 1	2.0e+01 (3)	3.0e+00 (3)	2.0e+01 (3)
Cm-243	< 1	< 1	< 1	< 1	< 1	< 1	< 1	< 1	< 1
Cm-244	< 1	< 1	< 1	< 1	< 1	< 1	< 1	< 1	< 1
Cm-245	6.3e+00 (7)	< 1	< 1	< 1	< 1	< 1	1.3e+02 (3)	7.8e+01 (4)	1.5e+02 (3)
Cm-246	1.2e+00 (7)	< 1	< 1	< 1	< 1	< 1	3.2e+01 (3)	2.1e+01 (4)	3.7e+01 (3)
Co-60	< 1	< 1	< 1	< 1	< 1	< 1	< 1	< 1	< 1
Cs-135	1.8e+05 (5)	4.2e+03 (7)	2.4e+04 (3)	1.8e+04 (3)	2.9e+04 (10)	< 1	1.1e+04 (3)	7.1e+04 (4)	2.7e+05 (4)
Cs-137	< 1	< 1	< 1	< 1	< 1	< 1	< 1	< 1	< 1
Eu-152	< 1	< 1	< 1	< 1	< 1	< 1	< 1	< 1	< 1
H-3	< 1	< 1	< 1	< 1	< 1	< 1	< 1	< 1	< 1
Ho-166m	5.6e+02 (4)	< 1	7.4e+00 (4)	1.6e+02 (4)	< 1	< 1	8.1e+03 (3)	1.5e+04 (3)	1.7e+04 (3)
I-129	4.3e+04 (3)	5.3e+02 (7)	6.8e+03 (3)	1.4e+04 (3)	2.6e+04 (6)	< 1	1.5e+03 (3)	7.9e+02 (4)	6.2e+04 (3)
Mo-93	4.6e+05 (3)	1.5e+05 (5)	7.8e+04 (3)	2.5e+05 (3)	3.0e+05 (5)	6.6e+04 (4)	3.0e+05 (3)	2.8e+04 (4)	1.1e+06 (3)
Nb-93m	3.6e+04 (5)	2.5e+03 (5)	1.0e+03 (3)	7.2e+03 (4)	7.8e+03 (52)	1.1e+03 (4)	3.0e+05 (3)	4.0e+04 (4)	3.2e+05 (3)
Nb-94	1.3e+04 (7)	1.7e+03 (35)	1.4e+02 (61)	4.9e+03 (6)	3.1e+02 (34)	1.2e+03 (67)	1.1e+05 (3)	3.8e+05 (4)	3.8e+05 (4)
Ni-59	5.4e+07 (7)	4.7e+06 (30)	2.4e+06 (4)	8.8e+06 (3)	1.0e+07 (34)	3.5e+06 (22)	1.4e+07 (3)	4.6e+06 (4)	5.8e+07 (7)
Ni-63	6.5e+05 (3)	2.0e+00 (4)	9.3e+03 (3)	1.2e+05 (3)	< 1	1.4e+04 (3)	9.8e+05 (3)	8.7e+04 (3)	1.4e+06 (3)
Np-237	7.0e+02 (7)	2.2e+00 (67)	1.5e+00 (22)	3.0e+02 (4)	1.1e+02 (34)	< 1	5.6e+02 (3)	2.7e+02 (4)	1.2e+03 (4)
Pa-231	1.7e+01 (83)	< 1	5.7e+00 (58)	< 1	8.3e+00 (77)	< 1	2.3e+04 (3)	5.3e+03 (4)	2.4e+04 (3)
Pb-210	1.1e+02 (77)	2.2e+01 (86)	1.2e+00 (22)	2.4e+00 (22)	9.2e+00 (86)	< 1	6.1e+00 (3)	4.3e+00 (5)	1.2e+02 (77)
Pd-107	1.7e+04 (3)	2.4e+05 (6)	2.1e+02 (4)	5.8e+03 (3)	3.3e+03 (7)	< 1	3.5e+02 (3)	7.0e+02 (4)	2.5e+05 (6)
Po-210	8.7e+03 (77)	1.9e+03 (86)	9.2e+01 (22)	8.4e+01 (77)	7.0e+02 (86)	6.8e+01 (22)	6.1e+00 (3)	4.3e+00 (5)	9.9e+03 (77)
Pu-238	3.2e+01 (3)	< 1	< 1	1.3e+01 (3)	< 1	< 1	4.8e+02 (3)	4.8e+01 (3)	4.8e+02 (3)
Pu-239	6.3e+04 (3)	4.7e+02 (24)	9.9e+01 (14)	3.4e+04 (3)	3.2e+03 (35)	1.1e+02 (13)	2.3e+05 (3)	1.1e+05 (4)	3.2e+05 (3)
Pu-240	7.9e+04 (3)	1.2e+02 (23)	7.1e+01 (8)	4.4e+04 (3)	9.8e+02 (16)	1.2e+02 (4)	2.1e+05 (3)	1.0e+05 (4)	3.3e+05 (3)
Pu-241	1.0e+02 (6)	3.8e+00 (30)	1.5e+00 (13)	1.7e+01 (7)	< 1	< 1	1.3e+02 (3)	7.8e+01 (4)	1.6e+02 (3)
Pu-242	4.7e+02 (3)	6.3e+00 (29)	1.0e+00 (30)	2.6e+02 (3)	4.3e+01 (35)	1.1e+00 (24)	1.4e+03 (3)	7.0e+02 (4)	2.1e+03 (3)
Ra-226	9.9e+02 (77)	2.5e+02 (84)	1.5e+01 (22)	5.5e+00 (22)	1.6e+02 (82)	9.0e+00 (22)	6.6e+00 (3)	4.4e+00 (5)	1.3e+03 (77)
Ra-228	< 1	< 1	< 1	< 1	< 1	< 1	< 1	< 1	< 1
Se-79	1.7e+05 (3)	1.4e+03 (5)	8.0e+03 (3)	2.8e+04 (3)	1.1e+05 (5)	< 1	1.4e+03 (3)	2.4e+03 (4)	2.1e+05 (3)
Sm-151	2.7e+00 (3)	< 1	< 1	< 1	< 1	< 1	2.5e+02 (3)	1.9e+02 (3)	3.4e+02 (3)
Sn-126	3.5e+02 (4)	< 1	1.7e+00 (59)	1.6e+02 (4)	3.1e+01 (52)	< 1	1.8e+02 (3)	3.2e+03 (4)	3.7e+03 (4)
Sr-90	< 1	< 1	< 1	< 1	< 1	< 1	< 1	< 1	< 1
Tc-99	3.4e+05 (7)	3.3e+02 (67)	4.9e+03 (22)	8.3e+04 (4)	2.6e+04 (46)	4.0e+02 (58)	6.5e+06 (3)	2.0e+05 (4)	6.6e+06 (3)
Th-228	< 1	< 1	< 1	< 1	< 1	< 1	< 1	< 1	< 1
Th-229	5.7e+01 (86)	< 1	< 1	3.0e+00 (58)	5.0e+00 (86)	< 1	< 1	< 1	6.4e+01 (86)
Th-230	2.3e+01 (84)	< 1	< 1	2.2e+00 (58)	4.4e+00 (86)	< 1	4.5e+01 (3)	1.1e+01 (5)	4.6e+01 (3)
Th-232	< 1	< 1	< 1	< 1	< 1	< 1	< 1	< 1	< 1
U-232	< 1	< 1	< 1	< 1	< 1	< 1	< 1	< 1	< 1
U-233	4.7e+01 (22)	< 1	< 1	5.0e+00 (22)	2.1e+01 (77)	< 1	2.0e+00 (3)	2.0e+00 (5)	7.2e+01 (77)
U-234	1.7e+02 (7)	2.4e+00 (32)	< 1	8.4e+01 (4)	3.0e+01 (34)	< 1	8.6e+03 (3)	7.6e+02 (4)	8.8e+03 (3)
U-235	9.1e+01 (7)	< 1	2.6e+00 (58)	1.5e+01 (4)	7.4e+00 (34)	< 1	1.1e+06 (3)	1.3e+05 (4)	1.1e+06 (3)
U-236	4.5e+01 (7)	1.2e+00 (86)	< 1	5.0e+01 (4)	1.2e+01 (34)	< 1	1.5e+02 (3)	9.0e+01 (4)	2.2e+02 (3)
U-238	1.4e+02 (7)	< 1	< 1	1.2e+02 (4)	1.7e+01 (34)	< 1	2.6e+06 (3)	7.2e+04 (4)	2.6e+06 (3)
Zr-93	1.8e+04 (7)	6.4e+02 (86)	9.6e+01 (22)	6.7e+03 (4)	1.0e+04 (34)	2.7e+02 (22)	3.8e+03 (3)	1.2e+04 (4)	3.0e+04 (4)

Table E-14. Far-field releases for CCL_BC, peak release [Bq/year] and in parentheses time of peak [1000 year AD].

Nuclide	1BMA	2BMA	1BTF	2BTF	Silo	BRT	1BLA	2-5BLA	Total
Ac-227	1.7e+02 (86)	< 1	1.7e+01 (86)	5.0e+00 (77)	3.7e+01 (86)	< 1	1.5e+04 (5)	4.2e+03 (82)	1.5e+04 (5)
Ag-108m	2.4e+06 (3)	2.7e+05 (4)	1.3e+05 (3)	5.4e+05 (3)	3.0e+04 (4)	1.5e+05 (3)	1.2e+05 (3)	5.3e+04 (3)	3.3e+06 (3)
Am-241	1.9e+02 (4)	< 1	< 1	1.6e+01 (4)	< 1	< 1	1.9e+04 (4)	6.4e+02 (4)	2.0e+04 (4)
Am-242m	< 1	< 1	< 1	< 1	< 1	< 1	< 1	< 1	< 1
Am-243	1.1e+02 (7)	< 1	1.3e+00 (13)	1.1e+01 (5)	< 1	< 1	1.3e+03 (4)	3.4e+02 (5)	1.3e+03 (4)
Ba-133	< 1	< 1	< 1	< 1	< 1	< 1	< 1	< 1	< 1
C-14-ind	< 1	6.1e+05 (5)	< 1	< 1	< 1	2.6e+04 (24)	< 1	3.7e+05 (4)	9.1e+05 (4)
C-14-inorg	7.9e+06 (5)	3.1e+02 (23)	2.4e+05 (7)	2.9e+06 (4)	7.9e+02 (31)	< 1	1.1e+07 (3)	2.9e+05 (4)	1.5e+07 (3)
C-14-org	7.1e+07 (3)	4.7e+05 (5)	4.8e+06 (3)	7.6e+06 (3)	5.5e+07 (5)	< 1	2.2e+05 (3)	6.9e+04 (4)	9.5e+07 (4)
Ca-41	< 1	1.4e+06 (9)	< 1	< 1	< 1	< 1	< 1	1.4e+06 (4)	1.5e+06 (9)
Cd-113m	< 1	< 1	< 1	< 1	< 1	< 1	< 1	< 1	< 1
Cl-36	1.0e+05 (3)	1.9e+04 (6)	6.3e+03 (3)	2.1e+04 (3)	3.9e+04 (5)	2.7e+02 (30)	6.9e+04 (3)	1.7e+04 (4)	1.9e+05 (3)
Cm-242	< 1	< 1	< 1	< 1	< 1	< 1	< 1	< 1	< 1
Cm-243	< 1	< 1	< 1	< 1	< 1	< 1	< 1	< 1	< 1
Cm-244	< 1	< 1	< 1	< 1	< 1	< 1	< 1	< 1	< 1
Cm-245	2.2e+00 (7)	< 1	< 1	< 1	< 1	< 1	1.4e+01 (4)	4.1e+00 (5)	1.5e+01 (4)
Cm-246	< 1	< 1	< 1	< 1	< 1	< 1	3.3e+00 (4)	1.0e+00 (5)	3.6e+00 (4)
Co-60	< 1	< 1	< 1	< 1	< 1	< 1	< 1	< 1	< 1
Cs-135	1.5e+05 (5)	1.4e+03 (9)	1.4e+04 (4)	7.2e+03 (4)	1.9e+04 (14)	< 1	2.8e+03 (3)	2.0e+04 (5)	1.9e+05 (5)
Cs-137	< 1	< 1	< 1	< 1	< 1	< 1	< 1	< 1	< 1
Eu-152	< 1	< 1	< 1	< 1	< 1	< 1	< 1	< 1	< 1
H-3	< 1	< 1	< 1	< 1	< 1	< 1	< 1	< 1	< 1
Ho-166m	1.8e+02 (5)	< 1	1.4e+00 (4)	1.7e+01 (4)	< 1	< 1	5.8e+02 (4)	3.3e+02 (5)	7.9e+02 (4)
I-129	4.2e+04 (3)	5.3e+02 (8)	6.6e+03 (3)	1.2e+04 (3)	2.5e+04 (6)	< 1	1.4e+03 (3)	7.2e+02 (4)	5.9e+04 (3)
Mo-93	4.5e+05 (3)	1.4e+05 (6)	7.5e+04 (3)	2.1e+05 (3)	2.9e+05 (5)	6.2e+04 (4)	2.7e+05 (3)	2.6e+04 (4)	9.7e+05 (3)
Nb-93m	2.3e+04 (9)	4.6e+02 (5)	3.8e+02 (4)	3.0e+03 (5)	1.1e+04 (44)	2.2e+02 (4)	2.0e+03 (3)	6.2e+02 (10)	2.8e+04 (9)
Nb-94	5.2e+03 (9)	2.4e+02 (50)	5.4e+01 (65)	1.8e+03 (9)	1.2e+02 (34)	2.1e+02 (67)	9.2e+03 (4)	1.3e+04 (5)	2.1e+04 (5)
Ni-59	3.8e+07 (5)	2.4e+06 (40)	1.2e+06 (4)	5.6e+06 (4)	4.2e+06 (34)	7.1e+05 (59)	3.7e+06 (3)	1.4e+06 (5)	4.3e+07 (5)
Ni-63	1.5e+05 (3)	< 1	1.7e+03 (4)	1.0e+04 (4)	< 1	3.9e+02 (4)	1.1e+05 (3)	2.4e+03 (3)	2.5e+05 (3)
Np-237	2.8e+02 (9)	< 1	< 1	4.0e+01 (9)	2.0e+01 (86)	< 1	2.4e+01 (4)	4.9e+00 (5)	3.3e+02 (9)
Pa-231	1.2e+01 (86)	< 1	2.6e+00 (86)	< 1	2.2e+00 (86)	< 1	1.9e+03 (5)	6.6e+02 (82)	1.9e+03 (5)
Pb-210	6.2e+01 (77)	4.4e+00 (86)	< 1	4.8e+00 (77)	9.0e+00 (82)	< 1	3.1e+02 (77)	7.1e+01 (82)	4.6e+02 (77)
Pd-107	1.7e+04 (3)	2.2e+05 (6)	2.0e+02 (4)	4.8e+03 (3)	3.3e+03 (7)	< 1	3.2e+02 (3)	6.4e+02 (4)	2.3e+05 (6)
Po-210	7.6e+01 (77)	4.2e+00 (86)	< 1	5.3e+00 (77)	8.0e+00 (82)	< 1	3.2e+02 (77)	6.2e+01 (82)	4.7e+02 (77)
Pu-238	1.3e+00 (3)	< 1	< 1	< 1	< 1	< 1	5.0e+00 (3)	< 1	6.5e+00 (3)
Pu-239	3.4e+04 (5)	8.1e+01 (40)	5.6e+01 (27)	6.0e+03 (5)	1.2e+03 (37)	1.7e+01 (30)	2.3e+04 (4)	5.1e+03 (5)	5.2e+04 (5)
Pu-240	3.7e+04 (5)	1.1e+01 (28)	2.0e+01 (13)	6.6e+03 (5)	2.3e+02 (19)	4.5e+00 (5)	2.1e+04 (4)	4.3e+03 (5)	5.4e+04 (5)
Pu-241	8.9e+00 (7)	< 1	< 1	< 1	< 1	< 1	2.2e+01 (4)	3.6e+00 (9)	2.5e+01 (4)
Pu-242	2.6e+02 (5)	2.2e+00 (86)	< 1	4.7e+01 (5)	1.9e+01 (48)	< 1	1.4e+02 (4)	3.4e+01 (5)	3.9e+02 (5)
Ra-226	9.7e+02 (77)	6.0e+01 (86)	9.4e+00 (22)	7.5e+01 (77)	1.3e+02 (82)	1.9e+00 (22)	5.4e+03 (77)	1.1e+03 (82)	7.8e+03 (77)
Ra-228	< 1	< 1	< 1	< 1	< 1	< 1	< 1	< 1	< 1
Se-79	1.6e+05 (3)	1.2e+03 (5)	7.4e+03 (3)	2.2e+04 (3)	1.1e+05 (5)	< 1	1.3e+03 (3)	2.2e+03 (4)	1.9e+05 (3)
Sm-151	< 1	< 1	< 1	< 1	< 1	< 1	1.9e+00 (3)	< 1	2.1e+00 (3)
Sn-126	1.6e+02 (30)	< 1	< 1	1.3e+01 (11)	5.5e+00 (86)	< 1	2.9e+00 (5)	1.3e+01 (16)	1.8e+02 (30)
Sr-90	< 1	< 1	< 1	< 1	< 1	< 1	< 1	< 1	< 1
Tc-99	9.3e+04 (9)	5.3e+01 (86)	1.3e+03 (60)	1.1e+04 (5)	9.3e+03 (67)	3.3e+01 (86)	3.0e+05 (4)	3.9e+03 (9)	3.1e+05 (4)
Th-228	< 1	< 1	< 1	< 1	< 1	< 1	< 1	< 1	< 1
Th-229	6.8e+01 (77)	< 1	< 1	6.2e+00 (77)	7.5e+00 (82)	< 1	< 1	< 1	8.3e+01 (77)
Th-230	2.0e+01 (77)	< 1	< 1	2.3e+00 (77)	3.2e+00 (82)	< 1	1.9e+02 (82)	4.0e+01 (82)	2.6e+02 (82)
Th-232	< 1	< 1	< 1	< 1	< 1	< 1	< 1	< 1	< 1
U-232	< 1	< 1	< 1	< 1	< 1	< 1	< 1	< 1	< 1
U-233	4.0e+01 (82)	< 1	< 1	4.1e+00 (77)	6.6e+00 (86)	< 1	< 1	< 1	5.1e+01 (82)
U-234	6.7e+01 (9)	< 1	< 1	9.4e+00 (9)	5.6e+00 (86)	< 1	5.9e+02 (5)	6.9e+01 (82)	6.5e+02 (5)
U-235	3.2e+01 (9)	< 1	1.5e+00 (86)	1.7e+00 (9)	1.5e+00 (86)	< 1	4.4e+04 (4)	2.6e+03 (10)	4.5e+04 (4)
U-236	1.9e+01 (9)	< 1	< 1	5.9e+00 (9)	2.3e+00 (86)	< 1	6.4e+00 (4)	2.0e+00 (10)	2.8e+01 (9)
U-238	5.3e+01 (9)	< 1	< 1	1.3e+01 (9)	3.3e+00 (86)	< 1	1.1e+05 (4)	1.4e+03 (10)	1.1e+05 (4)
Zr-93	9.3e+03 (9)	1.4e+02 (86)	5.2e+01 (22)	1.5e+03 (5)	4.1e+03 (86)	3.6e+01 (37)	2.8e+02 (4)	3.7e+02 (9)	1.1e+04 (9)

Table E-15. Doses for CCL_BC, peak dose [Sv/year] and in parentheses time of peak [1000 year AD].

Nuclide	1BMA	2BMA	1BTF	2BTF	Silo	BRT	1BLA	2-5BLA	Total
Total	4.2e-06 (5)	1.7e-06 (15)	4.3e-07 (5)	5.6e-07 (5)	3.9e-06 (7)	3.7e-07 (5)	1.3e-06 (24)	5.2e-07 (9)	1.1e-05 (6)
Ac-227	8.7e-10 (57)	< 1e-12	6.5e-11 (86)	3.4e-11 (43)	8.2e-11 (86)	< 1e-12	2.1e-07 (33)	9.5e-08 (57)	2.9e-07 (38)
Ag-108m	2.9e-08 (5)	9.5e-09 (5)	1.8e-09 (5)	3.8e-09 (5)	1.4e-09 (5)	2.9e-09 (5)	5.3e-10 (5)	1.4e-09 (5)	4.9e-08 (5)
Am-241	3.7e-12 (5)	< 1e-12	< 1e-12	< 1e-12	< 1e-12	< 1e-12	1.6e-10 (4)	5.8e-10 (4)	6.3e-10 (4)
Am-242m	< 1e-12	< 1e-12	< 1e-12	< 1e-12	< 1e-12	< 1e-12	< 1e-12	< 1e-12	< 1e-12
Am-243	8.0e-11 (21)	1.2e-12 (46)	2.4e-12 (27)	1.7e-11 (24)	< 1e-12	< 1e-12	2.5e-10 (15)	3.4e-10 (5)	5.5e-10 (17)
Ba-133	< 1e-12	< 1e-12	< 1e-12	< 1e-12	< 1e-12	< 1e-12	< 1e-12	< 1e-12	< 1e-12
C-14-ind	< 1e-12	1.7e-08 (5)	< 1e-12	< 1e-12	< 1e-12	7.2e-10 (24)	< 1e-12	7.8e-09 (5)	2.5e-08 (5)
C-14-inorg	2.2e-07 (5)	8.7e-12 (24)	6.9e-09 (7)	3.8e-08 (5)	2.4e-11 (31)	< 1e-12	9.0e-08 (3)	6.0e-09 (5)	2.7e-07 (5)
C-14-org	1.1e-06 (5)	1.3e-08 (5)	5.1e-08 (3)	6.1e-08 (3)	1.5e-06 (5)	< 1e-12	1.8e-09 (3)	1.5e-09 (5)	2.6e-06 (5)
Ca-41	< 1e-12	1.1e-06 (19)	< 1e-12	< 1e-12	< 1e-12	< 1e-12	< 1e-12	4.4e-07 (10)	1.4e-06 (18)
Cd-113m	< 1e-12	< 1e-12	< 1e-12	< 1e-12	< 1e-12	< 1e-12	< 1e-12	< 1e-12	< 1e-12
Cl-36	2.8e-07 (5)	6.2e-08 (7)	1.0e-08 (5)	1.1e-08 (5)	1.2e-07 (5)	8.8e-10 (30)	1.9e-08 (3)	4.8e-08 (5)	4.9e-07 (5)
Cm-242	< 1e-12	< 1e-12	< 1e-12	< 1e-12	< 1e-12	< 1e-12	< 1e-12	< 1e-12	< 1e-12
Cm-243	< 1e-12	< 1e-12	< 1e-12	< 1e-12	< 1e-12	< 1e-12	< 1e-12	< 1e-12	< 1e-12
Cm-244	< 1e-12	< 1e-12	< 1e-12	< 1e-12	< 1e-12	< 1e-12	< 1e-12	< 1e-12	< 1e-12
Cm-245	1.0e-12 (18)	< 1e-12	< 1e-12	< 1e-12	< 1e-12	< 1e-12	2.6e-12 (15)	4.2e-12 (5)	6.3e-12 (16)
Cm-246	< 1e-12	< 1e-12	< 1e-12	< 1e-12	< 1e-12	< 1e-12	< 1e-12	< 1e-12	< 1e-12
Co-60	< 1e-12	< 1e-12	< 1e-12	< 1e-12	< 1e-12	< 1e-12	< 1e-12	< 1e-12	< 1e-12
Cs-135	7.0e-07 (86)	2.2e-08 (86)	6.1e-08 (86)	1.5e-08 (86)	5.6e-07 (86)	< 1e-12	2.5e-09 (86)	9.9e-08 (86)	1.5e-06 (86)
Cs-137	< 1e-12	< 1e-12	< 1e-12	< 1e-12	< 1e-12	< 1e-12	< 1e-12	< 1e-12	< 1e-12
Eu-152	< 1e-12	< 1e-12	< 1e-12	< 1e-12	< 1e-12	< 1e-12	< 1e-12	< 1e-12	< 1e-12
H-3	< 1e-12	< 1e-12	< 1e-12	< 1e-12	< 1e-12	< 1e-12	< 1e-12	< 1e-12	< 1e-12
Ho-166m	< 1e-12	< 1e-12	< 1e-12	< 1e-12	< 1e-12	< 1e-12	< 1e-12	3.9e-12 (5)	4.6e-12 (5)
I-129	4.7e-07 (6)	1.2e-08 (13)	5.7e-08 (6)	4.2e-08 (5)	5.8e-07 (15)	< 1e-12	3.2e-09 (3)	8.2e-09 (6)	1.0e-06 (8)
Mo-93	2.3e-06 (5)	1.4e-06 (8)	3.3e-07 (5)	4.4e-07 (5)	2.6e-06 (8)	3.7e-07 (5)	2.7e-07 (5)	1.6e-07 (5)	6.7e-06 (6)
Nb-93m	7.6e-10 (5)	4.5e-10 (8)	1.1e-10 (5)	1.4e-10 (5)	8.5e-10 (7)	1.2e-10 (5)	8.8e-11 (5)	5.0e-11 (5)	2.2e-09 (6)
Nb-94	7.3e-10 (57)	3.7e-11 (78)	7.9e-12 (67)	1.6e-10 (51)	1.5e-11 (77)	2.6e-11 (77)	8.2e-11 (32)	6.3e-10 (43)	1.6e-09 (52)
Ni-59	2.5e-06 (52)	3.1e-07 (67)	4.1e-08 (33)	8.2e-08 (26)	3.5e-07 (52)	1.1e-07 (52)	1.8e-08 (15)	3.1e-08 (21)	3.3e-06 (52)
Ni-63	7.0e-12 (3)	< 1e-12	< 1e-12	< 1e-12	< 1e-12	< 1e-12	4.5e-12 (3)	1.9e-12 (3)	1.2e-11 (3)
Np-237	2.8e-09 (86)	1.4e-12 (86)	5.1e-12 (86)	3.8e-10 (86)	1.1e-10 (86)	< 1e-12	4.3e-11 (86)	3.2e-11 (86)	3.3e-09 (86)
Pa-231	1.8e-09 (77)	< 1e-12	1.5e-10 (86)	6.0e-11 (37)	1.1e-10 (86)	< 1e-12	3.9e-07 (30)	1.2e-07 (52)	4.9e-07 (34)
Pb-210	5.7e-09 (86)	4.5e-10 (67)	6.8e-11 (23)	3.8e-10 (86)	6.5e-10 (86)	1.3e-11 (23)	2.9e-08 (86)	7.5e-09 (86)	4.3e-08 (86)
Pd-107	1.5e-10 (16)	6.4e-09 (36)	1.8e-12 (28)	1.3e-11 (17)	2.0e-10 (39)	< 1e-12	< 1e-12	6.5e-12 (16)	6.7e-09 (36)
Po-210	2.0e-10 (86)	3.5e-11 (86)	2.6e-12 (22)	1.3e-11 (86)	3.5e-11 (86)	< 1e-12	9.9e-10 (86)	4.2e-10 (86)	1.6e-09 (86)
Pu-238	< 1e-12	< 1e-12	< 1e-12	< 1e-12	< 1e-12	< 1e-12	< 1e-12	< 1e-12	< 1e-12
Pu-239	3.1e-07 (51)	2.0e-09 (77)	1.3e-09 (60)	4.1e-08 (42)	2.7e-08 (77)	4.0e-10 (67)	3.2e-08 (32)	4.3e-08 (42)	4.3e-07 (50)
Pu-240	4.9e-08 (19)	4.5e-11 (43)	9.9e-11 (27)	9.0e-09 (18)	7.0e-10 (41)	2.4e-11 (28)	8.2e-09 (14)	7.0e-09 (18)	7.2e-08 (18)
Pu-241	< 1e-12	< 1e-12	< 1e-12	< 1e-12	< 1e-12	< 1e-12	< 1e-12	< 1e-12	< 1e-12
Pu-242	1.2e-08 (86)	1.2e-10 (86)	4.4e-11 (86)	1.4e-09 (86)	1.3e-09 (86)	3.7e-12 (86)	6.1e-10 (84)	1.2e-09 (86)	1.7e-08 (86)
Ra-226	3.3e-08 (86)	2.4e-09 (67)	3.5e-10 (23)	2.4e-09 (86)	4.4e-09 (86)	6.3e-11 (23)	1.8e-07 (86)	4.3e-08 (86)	2.6e-07 (86)
Ra-228	< 1e-12	< 1e-12	< 1e-12	< 1e-12	< 1e-12	< 1e-12	< 1e-12	< 1e-12	< 1e-12
Se-79	2.3e-08 (6)	4.7e-10 (9)	9.9e-10 (6)	1.5e-09 (6)	4.4e-08 (11)	< 1e-12	4.5e-11 (5)	5.2e-10 (7)	5.8e-08 (8)
Sm-151	< 1e-12	< 1e-12	< 1e-12	< 1e-12	< 1e-12	< 1e-12	< 1e-12	< 1e-12	< 1e-12
Sn-126	1.8e-10 (86)	< 1e-12	< 1e-12	1.5e-11 (78)	3.5e-12 (97)	< 1e-12	< 1e-12	1.5e-11 (78)	2.1e-10 (86)
Sr-90	< 1e-12	< 1e-12	< 1e-12	< 1e-12	< 1e-12	< 1e-12	< 1e-12	< 1e-12	< 1e-12
Tc-99	8.4e-08 (67)	3.9e-11 (86)	1.8e-09 (86)	8.6e-09 (67)	1.2e-08 (86)	2.1e-11 (86)	4.2e-08 (52)	3.3e-09 (67)	1.5e-07 (67)
Th-228	< 1e-12	< 1e-12	< 1e-12	< 1e-12	< 1e-12	< 1e-12	< 1e-12	< 1e-12	< 1e-12
Th-229	5.6e-09 (86)	< 1e-12	5.5e-12 (86)	6.2e-10 (86)	3.8e-10 (86)	< 1e-12	4.8e-11 (86)	3.6e-11 (86)	6.7e-09 (86)
Th-230	3.8e-10 (86)	< 1e-12	2.3e-12 (67)	4.0e-11 (86)	3.3e-11 (86)	< 1e-12	4.7e-09 (77)	5.5e-10 (77)	5.5e-09 (77)
Th-232	< 1e-12	< 1e-12	< 1e-12	< 1e-12	< 1e-12	< 1e-12	< 1e-12	3.4e-12 (9)	< 1e-12
U-232	< 1e-12	< 1e-12	< 1e-12	< 1e-12	< 1e-12	< 1e-12	< 1e-12	< 1e-12	< 1e-12
U-233	2.5e-09 (86)	< 1e-12	3.4e-12 (86)	3.0e-10 (86)	1.7e-10 (86)	< 1e-12	2.3e-11 (86)	2.0e-11 (86)	3.0e-09 (86)
U-234	1.8e-09 (38)	6.8e-12 (77)	6.3e-12 (52)	2.5e-10 (35)	1.9e-10 (67)	< 1e-12	3.6e-08 (49)	4.6e-09 (67)	4.3e-08 (52)
U-235	7.9e-10 (38)	< 1e-12	4.1e-11 (67)	3.6e-11 (30)	4.4e-11 (67)	< 1e-12	3.3e-07 (7)	6.4e-08 (35)	3.4e-07 (7)
U-236	6.3e-10 (40)	3.0e-12 (86)	1.3e-12 (49)	1.6e-10 (35)	7.0e-11 (67)	< 1e-12	5.4e-11 (8)	3.9e-11 (24)	8.7e-10 (40)
U-238	1.4e-09 (38)	< 1e-12	7.4e-12 (52)	3.3e-10 (35)	1.0e-10 (67)	< 1e-12	8.0e-07 (7)	3.5e-08 (35)	8.1e-07 (7)
Zr-93	1.1e-08 (77)	1.7e-10 (86)	8.4e-11 (78)	1.3e-09 (67)	8.9e-09 (86)	7.8e-11 (86)	4.6e-11 (52)	4.5e-10 (77)	2.2e-08 (86)

Bentonite degradation calculation case (CCL_BB)

Table E-16. Near-field releases for CCL_BB, peak release [Bq/year] and in parentheses time of peak [1000 year AD].

Nuclide	1BMA	2BMA	1BTF	2BTF	Silo	BRT	1BLA	2-5BLA	Total
Ac-227	1.6e+02 (28)	< 1	1.6e+01 (86)	2.4e+00 (12)	1.9e+01 (67)	< 1	2.2e+04 (3)	5.2e+03 (4)	2.3e+04 (3)
Ag-108m	3.8e+05 (3)	1.4e+05 (4)	1.6e+05 (3)	7.4e+05 (3)	2.7e+04 (4)	2.0e+05 (3)	1.3e+05 (3)	6.5e+04 (3)	1.4e+06 (3)
Am-241	8.0e+01 (4)	< 1	4.8e+00 (4)	1.3e+02 (4)	< 1	6.9e+00 (4)	3.8e+05 (3)	8.8e+04 (3)	4.1e+05 (3)
Am-242m	< 1	< 1	< 1	< 1	< 1	< 1	2.5e+01 (3)	3.7e+00 (3)	2.5e+01 (3)
Am-243	9.7e+01 (7)	< 1	3.9e+00 (22)	2.8e+01 (4)	< 1	3.3e+00 (5)	1.3e+04 (3)	6.5e+03 (4)	1.4e+04 (3)
Ba-133	< 1	< 1	< 1	< 1	< 1	< 1	< 1	< 1	< 1
C-14-ind	< 1	4.5e+05 (5)	< 1	< 1	< 1	2.7e+04 (24)	< 1	4.0e+05 (4)	7.6e+05 (4)
C-14-inorg	2.6e+05 (22)	8.7e+00 (24)	1.6e+05 (12)	6.6e+05 (4)	3.0e+03 (34)	< 1	1.3e+07 (3)	3.1e+05 (4)	1.3e+07 (3)
C-14-org	2.9e+07 (4)	3.5e+05 (5)	6.3e+06 (3)	9.8e+06 (3)	5.3e+07 (5)	< 1	2.5e+05 (3)	7.5e+04 (4)	7.7e+07 (5)
Ca-41	< 1	8.0e+05 (10)	< 1	< 1	< 1	< 1	< 1	1.6e+06 (4)	1.6e+06 (4)
Cd-113m	< 1	< 1	< 1	< 1	< 1	< 1	< 1	< 1	< 1
Cl-36	4.0e+04 (4)	1.2e+04 (7)	7.0e+03 (3)	2.4e+04 (3)	4.8e+04 (21)	2.7e+02 (29)	7.6e+04 (3)	1.9e+04 (4)	1.1e+05 (3)
Cm-242	< 1	< 1	< 1	< 1	< 1	< 1	2.0e+01 (3)	3.0e+00 (3)	2.0e+01 (3)
Cm-243	< 1	< 1	< 1	< 1	< 1	< 1	< 1	< 1	< 1
Cm-244	< 1	< 1	< 1	< 1	< 1	< 1	< 1	< 1	< 1
Cm-245	< 1	< 1	< 1	< 1	< 1	< 1	1.3e+02 (3)	7.8e+01 (4)	1.5e+02 (3)
Cm-246	< 1	< 1	< 1	< 1	< 1	< 1	3.2e+01 (3)	2.1e+01 (4)	3.7e+01 (3)
Co-60	< 1	< 1	< 1	< 1	< 1	< 1	< 1	< 1	< 1
Cs-135	9.4e+04 (7)	2.4e+03 (7)	2.6e+04 (4)	1.8e+04 (3)	5.3e+04 (34)	< 1	1.1e+04 (3)	7.1e+04 (4)	1.6e+05 (4)
Cs-137	< 1	< 1	< 1	< 1	< 1	< 1	< 1	< 1	< 1
Eu-152	< 1	< 1	< 1	< 1	< 1	< 1	< 1	< 1	< 1
H-3	< 1	< 1	< 1	< 1	< 1	< 1	< 1	< 1	< 1
Ho-166m	4.5e+01 (5)	< 1	1.5e+00 (4)	7.3e+01 (4)	< 1	< 1	8.1e+03 (3)	1.5e+04 (3)	1.7e+04 (3)
I-129	2.6e+04 (22)	3.0e+02 (24)	6.8e+03 (3)	1.3e+04 (3)	4.8e+04 (21)	< 1	1.5e+03 (3)	7.9e+02 (4)	5.9e+04 (22)
Mo-93	8.1e+04 (4)	7.7e+04 (5)	7.7e+04 (3)	2.3e+05 (3)	2.5e+05 (5)	6.6e+04 (4)	3.0e+05 (3)	2.8e+04 (4)	6.2e+05 (3)
Nb-93m	1.7e+04 (24)	1.6e+03 (86)	1.1e+03 (3)	7.1e+03 (4)	1.3e+04 (45)	1.1e+03 (4)	3.0e+05 (3)	4.0e+04 (4)	3.1e+05 (3)
Nb-94	3.2e+03 (25)	5.2e+02 (67)	1.2e+02 (61)	3.3e+03 (7)	2.2e+03 (34)	1.2e+03 (67)	1.1e+05 (3)	3.8e+05 (4)	3.8e+05 (4)
Ni-59	1.0e+07 (23)	3.6e+06 (63)	2.0e+06 (4)	7.0e+06 (4)	2.1e+07 (34)	3.6e+06 (22)	1.4e+07 (3)	4.6e+06 (4)	3.0e+07 (34)
Ni-63	3.7e+02 (3)	< 1	3.5e+03 (3)	6.6e+04 (3)	< 1	1.4e+04 (3)	9.8e+05 (3)	8.7e+04 (3)	9.8e+05 (3)
Np-237	5.2e+02 (23)	2.2e+00 (86)	1.4e+00 (22)	2.4e+02 (4)	2.0e+02 (34)	< 1	5.6e+02 (3)	2.7e+02 (4)	6.7e+02 (3)
Pa-231	1.8e+01 (26)	< 1	3.0e+00 (58)	< 1	6.3e+01 (77)	< 1	2.3e+04 (3)	5.3e+03 (4)	2.4e+04 (3)
Pb-210	4.3e+01 (77)	2.2e+01 (86)	1.0e+00 (21)	1.7e+00 (12)	4.7e+01 (77)	< 1	6.1e+00 (3)	4.3e+00 (5)	9.6e+01 (77)
Pd-107	4.6e+03 (4)	1.3e+05 (6)	1.5e+02 (4)	5.5e+03 (3)	4.7e+03 (21)	< 1	3.5e+02 (3)	7.0e+02 (4)	1.4e+05 (6)
Po-210	3.4e+03 (77)	1.9e+03 (86)	8.5e+01 (21)	1.0e+02 (77)	3.3e+03 (77)	7.1e+01 (22)	6.1e+00 (3)	4.3e+00 (5)	7.2e+03 (82)
Pu-238	3.2e+00 (3)	< 1	< 1	7.2e+00 (3)	< 1	< 1	4.8e+02 (3)	4.8e+01 (3)	4.8e+02 (3)
Pu-239	2.0e+04 (5)	1.8e+02 (58)	8.1e+01 (13)	2.5e+04 (3)	8.2e+03 (35)	1.1e+02 (13)	2.3e+05 (3)	1.1e+05 (4)	2.6e+05 (3)
Pu-240	2.4e+04 (4)	3.2e+00 (57)	4.9e+01 (12)	3.2e+04 (3)	1.1e+03 (27)	1.2e+02 (4)	2.1e+05 (3)	1.0e+05 (4)	2.5e+05 (3)
Pu-241	1.5e+01 (7)	< 1	1.1e+00 (17)	8.9e+00 (9)	< 1	< 1	1.3e+02 (3)	7.8e+01 (4)	1.5e+02 (3)
Pu-242	2.3e+02 (23)	5.9e+00 (64)	< 1	1.9e+02 (3)	1.2e+02 (44)	1.1e+00 (24)	1.4e+03 (3)	7.0e+02 (4)	1.7e+03 (3)
Ra-226	3.6e+02 (77)	2.5e+02 (84)	1.3e+01 (21)	8.4e+00 (21)	1.5e+03 (77)	9.9e+00 (22)	6.6e+00 (3)	4.4e+00 (5)	2.0e+03 (77)
Ra-228	< 1	< 1	< 1	< 1	< 1	< 1	< 1	< 1	< 1
Se-79	5.2e+04 (4)	9.1e+02 (5)	8.9e+03 (3)	2.8e+04 (3)	1.1e+05 (5)	< 1	1.4e+03 (3)	2.4e+03 (4)	1.5e+05 (5)
Sm-151	< 1	< 1	< 1	< 1	< 1	< 1	2.5e+02 (3)	1.9e+02 (3)	3.4e+02 (3)
Sn-126	2.2e+02 (23)	< 1	1.7e+00 (59)	1.2e+02 (5)	1.0e+02 (67)	< 1	1.8e+02 (3)	3.2e+03 (4)	3.3e+03 (4)
Sr-90	< 1	< 1	< 1	< 1	< 1	< 1	< 1	< 1	< 1
Tc-99	1.2e+05 (25)	2.1e+02 (86)	3.0e+03 (58)	7.4e+04 (4)	1.4e+05 (35)	4.0e+02 (58)	6.5e+06 (3)	2.0e+05 (4)	6.6e+06 (3)
Th-228	< 1	< 1	< 1	< 1	< 1	< 1	< 1	< 1	< 1
Th-229	3.0e+01 (52)	< 1	< 1	2.1e+00 (58)	4.2e+01 (86)	< 1	< 1	< 1	7.2e+01 (86)
Th-230	1.6e+01 (35)	< 1	< 1	1.8e+00 (58)	2.8e+01 (86)	< 1	4.5e+01 (3)	1.1e+01 (5)	4.6e+01 (3)
Th-232	< 1	< 1	< 1	< 1	< 1	< 1	< 1	< 1	< 1
U-232	< 1	< 1	< 1	< 1	< 1	< 1	< 1	< 1	< 1
U-233	6.6e+01 (22)	< 1	< 1	4.1e+00 (58)	6.5e+01 (82)	< 1	2.0e+00 (3)	2.0e+00 (5)	1.2e+02 (82)
U-234	1.3e+02 (23)	2.2e+00 (66)	< 1	6.5e+01 (4)	6.9e+01 (34)	< 1	8.6e+03 (3)	7.6e+02 (4)	8.7e+03 (3)
U-235	6.5e+01 (22)	< 1	1.4e+00 (58)	1.2e+01 (4)	1.5e+01 (34)	< 1	1.1e+06 (3)	1.3e+05 (4)	1.1e+06 (3)
U-236	4.0e+01 (23)	1.2e+00 (86)	< 1	3.9e+01 (4)	2.6e+01 (34)	< 1	1.5e+02 (3)	9.0e+01 (4)	1.8e+02 (3)
U-238	1.0e+02 (23)	< 1	< 1	9.1e+01 (4)	3.7e+01 (34)	< 1	2.6e+06 (3)	7.2e+04 (4)	2.6e+06 (3)
Zr-93	8.4e+03 (24)	5.1e+02 (86)	8.7e+01 (22)	5.9e+03 (4)	5.7e+04 (34)	2.3e+02 (22)	3.8e+03 (3)	1.2e+04 (4)	6.2e+04 (34)

Table E-17. Far-field releases for CCL_BB, peak release [Bq/year] and in parentheses time of peak [1000 year AD].

Nuclide	1BMA	2BMA	1BTF	2BTF	Silo	BRT	1BLA	2-5BLA	Total
Ac-227	1.6e+02 (41)	< 1	8.5e+00 (86)	4.5e+00 (82)	1.6e+02 (86)	< 1	1.5e+04 (5)	4.3e+03 (82)	1.5e+04 (5)
Ag-108m	3.7e+05 (3)	1.2e+05 (4)	1.4e+05 (3)	5.4e+05 (3)	2.5e+04 (4)	1.5e+05 (3)	1.2e+05 (3)	5.3e+04 (3)	1.2e+06 (3)
Am-241	1.4e+01 (5)	< 1	< 1	7.4e+00 (4)	< 1	< 1	1.9e+04 (4)	6.4e+02 (4)	2.0e+04 (4)
Am-242m	< 1	< 1	< 1	< 1	< 1	< 1	< 1	< 1	< 1
Am-243	1.8e+01 (7)	< 1	< 1	4.9e+00 (5)	< 1	< 1	1.3e+03 (4)	3.4e+02 (5)	1.3e+03 (4)
Ba-133	< 1	< 1	< 1	< 1	< 1	< 1	< 1	< 1	< 1
C-14-ind	< 1	4.0e+05 (5)	< 1	< 1	< 1	2.6e+04 (24)	< 1	3.7e+05 (4)	6.8e+05 (4)
C-14-inorg	2.5e+05 (22)	8.2e+00 (24)	1.6e+05 (12)	6.2e+05 (4)	2.9e+03 (34)	< 1	1.1e+07 (3)	2.9e+05 (4)	1.1e+07 (3)
C-14-org	2.8e+07 (4)	3.1e+05 (5)	5.7e+06 (3)	7.7e+06 (3)	5.2e+07 (5)	< 1	2.2e+05 (3)	6.9e+04 (4)	7.5e+07 (5)
Ca-41	< 1	7.8e+05 (10)	< 1	< 1	< 1	< 1	< 1	1.4e+06 (4)	1.4e+06 (4)
Cd-113m	< 1	< 1	< 1	< 1	< 1	< 1	< 1	< 1	< 1
Cl-36	4.0e+04 (4)	1.1e+04 (8)	6.8e+03 (3)	2.0e+04 (3)	4.5e+04 (21)	2.7e+02 (30)	6.9e+04 (3)	1.7e+04 (4)	1.0e+05 (3)
Cm-242	< 1	< 1	< 1	< 1	< 1	< 1	< 1	< 1	< 1
Cm-243	< 1	< 1	< 1	< 1	< 1	< 1	< 1	< 1	< 1
Cm-244	< 1	< 1	< 1	< 1	< 1	< 1	< 1	< 1	< 1
Cm-245	< 1	< 1	< 1	< 1	< 1	< 1	1.4e+01 (4)	4.1e+00 (5)	1.5e+01 (4)
Cm-246	< 1	< 1	< 1	< 1	< 1	< 1	3.3e+00 (4)	1.0e+00 (5)	3.5e+00 (4)
Co-60	< 1	< 1	< 1	< 1	< 1	< 1	< 1	< 1	< 1
Cs-135	6.6e+04 (5)	8.5e+02 (9)	1.5e+04 (4)	7.2e+03 (4)	3.3e+04 (25)	< 1	2.8e+03 (3)	2.0e+04 (5)	1.0e+05 (5)
Cs-137	< 1	< 1	< 1	< 1	< 1	< 1	< 1	< 1	< 1
Eu-152	< 1	< 1	< 1	< 1	< 1	< 1	< 1	< 1	< 1
H-3	< 1	< 1	< 1	< 1	< 1	< 1	< 1	< 1	< 1
Ho-166m	1.3e+01 (5)	< 1	< 1	8.5e+00 (4)	< 1	< 1	5.8e+02 (4)	3.3e+02 (5)	7.0e+02 (4)
I-129	2.5e+04 (22)	3.0e+02 (9)	6.7e+03 (3)	1.0e+04 (3)	4.6e+04 (21)	< 1	1.4e+03 (3)	7.2e+02 (4)	5.9e+04 (22)
Mo-93	8.0e+04 (4)	7.0e+04 (6)	7.4e+04 (3)	1.9e+05 (3)	2.5e+05 (5)	6.2e+04 (4)	2.7e+05 (3)	2.6e+04 (4)	5.4e+05 (3)
Nb-93m	1.2e+04 (27)	2.3e+02 (5)	4.0e+02 (4)	2.7e+03 (5)	2.9e+04 (38)	2.2e+02 (4)	2.0e+03 (3)	6.2e+02 (10)	4.0e+04 (37)
Nb-94	1.9e+03 (28)	4.6e+01 (67)	4.6e+01 (65)	1.3e+03 (9)	6.3e+02 (52)	2.0e+02 (67)	9.2e+03 (4)	1.3e+04 (5)	1.7e+04 (5)
Ni-59	8.6e+06 (25)	1.7e+06 (67)	8.0e+05 (4)	4.1e+06 (4)	1.1e+07 (35)	7.3e+05 (59)	3.7e+06 (3)	1.4e+06 (5)	1.9e+07 (35)
Ni-63	1.7e+02 (4)	< 1	8.6e+02 (4)	7.6e+03 (4)	< 1	3.9e+02 (4)	1.1e+05 (3)	2.4e+03 (3)	1.1e+05 (3)
Np-237	1.7e+02 (26)	< 1	< 1	3.4e+01 (9)	6.1e+01 (86)	< 1	2.4e+01 (4)	4.9e+00 (5)	2.0e+02 (26)
Pa-231	1.1e+01 (56)	< 1	1.4e+00 (86)	< 1	9.9e+00 (86)	< 1	1.9e+03 (5)	6.8e+02 (82)	1.9e+03 (5)
Pb-210	3.3e+01 (77)	4.2e+00 (86)	< 1	4.4e+00 (77)	4.2e+01 (82)	< 1	3.3e+02 (77)	7.2e+01 (82)	4.8e+02 (77)
Pd-107	4.5e+03 (4)	1.3e+05 (7)	1.5e+02 (4)	4.5e+03 (3)	4.6e+03 (21)	< 1	3.2e+02 (3)	6.4e+02 (4)	1.4e+05 (7)
Po-210	4.0e+01 (77)	4.1e+00 (86)	< 1	4.7e+00 (77)	3.8e+01 (82)	< 1	3.4e+02 (77)	6.3e+01 (82)	4.8e+02 (77)
Pu-238	< 1	< 1	< 1	< 1	< 1	< 1	5.0e+00 (3)	< 1	5.2e+00 (3)
Pu-239	1.1e+04 (5)	2.9e+01 (67)	4.5e+01 (28)	5.0e+03 (5)	3.1e+03 (41)	1.6e+01 (31)	2.3e+04 (4)	5.1e+03 (5)	3.1e+04 (4)
Pu-240	1.2e+04 (5)	< 1	1.3e+01 (16)	5.5e+03 (5)	2.7e+02 (30)	6.6e+00 (18)	2.1e+04 (4)	4.3e+03 (5)	3.0e+04 (4)
Pu-241	1.4e+00 (7)	< 1	< 1	< 1	< 1	< 1	2.2e+01 (4)	3.6e+00 (9)	2.3e+01 (4)
Pu-242	1.2e+02 (24)	1.5e+00 (86)	< 1	3.9e+01 (5)	5.8e+01 (67)	< 1	1.4e+02 (4)	3.4e+01 (5)	2.0e+02 (5)
Ra-226	5.2e+02 (77)	5.8e+01 (86)	7.3e+00 (22)	6.8e+01 (77)	6.1e+02 (82)	1.6e+00 (22)	5.6e+03 (77)	1.2e+03 (82)	8.0e+03 (77)
Ra-228	< 1	< 1	< 1	< 1	< 1	< 1	< 1	< 1	< 1
Se-79	5.2e+04 (4)	8.1e+02 (5)	8.3e+03 (3)	2.2e+04 (3)	1.0e+05 (5)	< 1	1.3e+03 (3)	2.2e+03 (4)	1.5e+05 (5)
Sm-151	< 1	< 1	< 1	< 1	< 1	< 1	1.9e+00 (3)	< 1	1.9e+00 (3)
Sn-126	8.8e+01 (34)	< 1	< 1	1.1e+01 (12)	1.7e+01 (86)	< 1	2.9e+00 (5)	2.4e+01 (18)	1.1e+02 (37)
Sr-90	< 1	< 1	< 1	< 1	< 1	< 1	< 1	< 1	< 1
Tc-99	5.8e+04 (29)	1.5e+01 (86)	8.8e+02 (60)	9.9e+03 (5)	3.7e+04 (66)	3.2e+01 (86)	3.0e+05 (4)	3.9e+03 (9)	3.0e+05 (4)
Th-228	< 1	< 1	< 1	< 1	< 1	< 1	< 1	< 1	< 1
Th-229	5.8e+01 (77)	< 1	< 1	6.2e+00 (77)	2.2e+01 (82)	< 1	< 1	< 1	8.7e+01 (77)
Th-230	1.5e+01 (56)	< 1	< 1	2.1e+00 (77)	1.3e+01 (86)	< 1	2.0e+02 (82)	4.1e+01 (82)	2.7e+02 (82)
Th-232	< 1	< 1	< 1	< 1	< 1	< 1	< 1	< 1	< 1
U-232	< 1	< 1	< 1	< 1	< 1	< 1	< 1	< 1	< 1
U-233	3.6e+01 (82)	< 1	< 1	4.1e+00 (77)	1.8e+01 (86)	< 1	< 1	< 1	5.7e+01 (82)
U-234	4.8e+01 (25)	< 1	< 1	8.2e+00 (9)	1.7e+01 (86)	< 1	5.9e+02 (5)	7.2e+01 (82)	6.1e+02 (5)
U-235	2.3e+01 (25)	< 1	< 1	1.5e+00 (9)	3.9e+00 (86)	< 1	4.4e+04 (4)	2.6e+03 (10)	4.5e+04 (4)
U-236	1.6e+01 (26)	< 1	< 1	5.2e+00 (9)	6.9e+00 (86)	< 1	6.4e+00 (4)	2.0e+00 (10)	2.2e+01 (26)
U-238	3.7e+01 (25)	< 1	< 1	1.1e+01 (9)	9.4e+00 (86)	< 1	1.1e+05 (4)	1.4e+03 (10)	1.1e+05 (4)
Zr-93	4.8e+03 (26)	5.4e+01 (86)	4.0e+01 (22)	1.3e+03 (5)	1.1e+04 (39)	3.0e+01 (39)	2.8e+02 (4)	3.7e+02 (9)	1.4e+04 (38)

Table E-18. Doses for CCL_BB, peak dose [Sv/year] and in parentheses time of peak [1000 year AD].

Nuclide	1BMA	2BMA	1BTF	2BTF	Silo	BRT	1BLA	2-5BLA	Total
Total	1.5e-06 (67)	1.0e-06 (17)	4.2e-07 (5)	5.2e-07 (5)	3.6e-06 (7)	3.7e-07 (5)	1.3e-06 (20)	5.2e-07 (9)	7.7e-06 (7)
Ac-227	6.6e-10 (67)	< 1e-12	2.6e-11 (86)	2.5e-11 (45)	3.7e-10 (86)	< 1e-12	2.0e-07 (33)	9.5e-08 (57)	2.8e-07 (39)
Ag-108m	9.9e-09 (5)	4.9e-09 (5)	2.0e-09 (5)	3.8e-09 (5)	1.2e-09 (5)	2.9e-09 (5)	5.3e-10 (5)	1.4e-09 (5)	2.6e-08 (5)
Am-241	< 1e-12	< 1e-12	< 1e-12	< 1e-12	< 1e-12	< 1e-12	1.6e-10 (4)	5.8e-10 (4)	6.3e-10 (4)
Am-242m	< 1e-12	< 1e-12	< 1e-12	< 1e-12	< 1e-12	< 1e-12	< 1e-12	< 1e-12	< 1e-12
Am-243	1.3e-11 (33)	< 1e-12	< 1e-12	8.5e-12 (22)	< 1e-12	< 1e-12	2.5e-10 (15)	3.4e-10 (5)	4.9e-10 (16)
Ba-133	< 1e-12	< 1e-12	< 1e-12	< 1e-12	< 1e-12	< 1e-12	< 1e-12	< 1e-12	< 1e-12
C-14-ind	< 1e-12	1.1e-08 (5)	< 1e-12	< 1e-12	< 1e-12	7.2e-10 (24)	< 1e-12	7.8e-09 (5)	1.9e-08 (5)
C-14-inorg	6.9e-09 (23)	< 1e-12	4.4e-09 (13)	1.7e-08 (6)	8.5e-11 (34)	< 1e-12	9.0e-08 (3)	6.0e-09 (5)	9.1e-08 (3)
C-14-org	7.1e-07 (5)	8.6e-09 (5)	6.1e-08 (3)	6.4e-08 (3)	1.5e-06 (5)	< 1e-12	1.8e-09 (3)	1.5e-09 (5)	2.1e-06 (5)
Ca-41	< 1e-12	8.2e-07 (30)	< 1e-12	< 1e-12	< 1e-12	< 1e-12	< 1e-12	4.4e-07 (10)	9.9e-07 (17)
Cd-113m	< 1e-12	< 1e-12	< 1e-12	< 1e-12	< 1e-12	< 1e-12	< 1e-12	< 1e-12	< 1e-12
Cl-36	1.3e-07 (5)	3.7e-08 (8)	1.0e-08 (5)	1.1e-08 (5)	1.3e-07 (21)	8.8e-10 (30)	1.9e-08 (3)	4.8e-08 (5)	3.1e-07 (5)
Cm-242	< 1e-12	< 1e-12	< 1e-12	< 1e-12	< 1e-12	< 1e-12	< 1e-12	< 1e-12	< 1e-12
Cm-243	< 1e-12	< 1e-12	< 1e-12	< 1e-12	< 1e-12	< 1e-12	< 1e-12	< 1e-12	< 1e-12
Cm-244	< 1e-12	< 1e-12	< 1e-12	< 1e-12	< 1e-12	< 1e-12	< 1e-12	< 1e-12	< 1e-12
Cm-245	< 1e-12	< 1e-12	< 1e-12	< 1e-12	< 1e-12	< 1e-12	2.6e-12 (15)	4.2e-12 (5)	5.3e-12 (16)
Cm-246	< 1e-12	< 1e-12	< 1e-12	< 1e-12	< 1e-12	< 1e-12	< 1e-12	< 1e-12	< 1e-12
Co-60	< 1e-12	< 1e-12	< 1e-12	< 1e-12	< 1e-12	< 1e-12	< 1e-12	< 1e-12	< 1e-12
Cs-135	6.5e-07 (86)	1.8e-08 (86)	5.9e-08 (86)	1.5e-08 (86)	7.5e-07 (86)	< 1e-12	2.5e-09 (86)	9.7e-08 (86)	1.6e-06 (86)
Cs-137	< 1e-12	< 1e-12	< 1e-12	< 1e-12	< 1e-12	< 1e-12	< 1e-12	< 1e-12	< 1e-12
Eu-152	< 1e-12	< 1e-12	< 1e-12	< 1e-12	< 1e-12	< 1e-12	< 1e-12	< 1e-12	< 1e-12
H-3	< 1e-12	< 1e-12	< 1e-12	< 1e-12	< 1e-12	< 1e-12	< 1e-12	< 1e-12	< 1e-12
Ho-166m	< 1e-12	< 1e-12	< 1e-12	< 1e-12	< 1e-12	< 1e-12	< 1e-12	3.9e-12 (5)	4.4e-12 (5)
I-129	2.5e-07 (24)	9.0e-09 (28)	5.7e-08 (6)	4.1e-08 (5)	8.6e-07 (26)	< 1e-12	3.2e-09 (3)	8.2e-09 (6)	1.1e-06 (25)
Mo-93	6.6e-07 (6)	7.4e-07 (9)	3.3e-07 (5)	4.3e-07 (5)	2.3e-06 (8)	3.7e-07 (5)	2.7e-07 (5)	1.6e-07 (5)	4.5e-06 (7)
Nb-93m	2.2e-10 (6)	2.4e-10 (9)	1.1e-10 (5)	1.4e-10 (5)	7.6e-10 (8)	1.2e-10 (5)	8.8e-11 (5)	5.0e-11 (5)	1.5e-09 (7)
Nb-94	2.9e-10 (67)	2.1e-12 (86)	5.7e-12 (77)	9.4e-11 (52)	7.3e-11 (78)	2.3e-11 (78)	8.1e-11 (32)	6.0e-10 (44)	1.1e-09 (52)
Ni-59	1.0e-06 (52)	1.0e-07 (86)	3.1e-08 (35)	6.4e-08 (20)	8.5e-07 (52)	1.0e-07 (67)	1.8e-08 (15)	3.1e-08 (20)	2.1e-06 (67)
Ni-63	< 1e-12	< 1e-12	< 1e-12	< 1e-12	< 1e-12	< 1e-12	4.5e-12 (3)	1.9e-12 (3)	4.7e-12 (3)
Np-237	1.6e-09 (86)	< 1e-12	3.4e-12 (86)	3.1e-10 (86)	2.6e-10 (86)	< 1e-12	4.3e-11 (86)	3.1e-11 (86)	2.3e-09 (86)
Pa-231	1.4e-09 (77)	< 1e-12	6.5e-11 (86)	4.4e-11 (39)	5.2e-10 (86)	< 1e-12	3.7e-07 (31)	1.2e-07 (52)	4.7e-07 (37)
Pb-210	3.7e-09 (86)	4.3e-10 (67)	3.1e-11 (17)	3.0e-10 (86)	2.9e-09 (86)	4.2e-12 (52)	3.0e-08 (86)	7.6e-09 (86)	4.5e-08 (86)
Pd-107	9.9e-11 (37)	4.5e-09 (67)	1.3e-12 (30)	1.3e-11 (17)	3.0e-10 (43)	< 1e-12	< 1e-12	6.5e-12 (16)	4.8e-09 (67)
Po-210	1.3e-10 (86)	3.3e-11 (86)	1.3e-12 (17)	1.1e-11 (86)	1.5e-10 (86)	< 1e-12	1.0e-09 (86)	4.3e-10 (86)	1.7e-09 (86)
Pu-238	< 1e-12	< 1e-12	< 1e-12	< 1e-12	< 1e-12	< 1e-12	< 1e-12	< 1e-12	< 1e-12
Pu-239	1.6e-07 (57)	2.6e-10 (86)	8.7e-10 (67)	3.3e-08 (43)	6.7e-08 (77)	3.6e-10 (67)	3.1e-08 (32)	4.1e-08 (43)	3.0e-07 (58)
Pu-240	1.6e-08 (17)	< 1e-12	4.8e-11 (32)	7.6e-09 (17)	1.1e-09 (50)	1.9e-11 (28)	8.2e-09 (14)	6.9e-09 (17)	3.8e-08 (17)
Pu-241	< 1e-12	< 1e-12	< 1e-12	< 1e-12	< 1e-12	< 1e-12	< 1e-12	< 1e-12	< 1e-12
Pu-242	7.4e-09 (86)	1.3e-11 (86)	2.8e-11 (86)	1.2e-09 (86)	3.3e-09 (86)	3.0e-12 (86)	6.0e-10 (84)	1.2e-09 (86)	1.4e-08 (86)
Ra-226	2.2e-08 (86)	2.3e-09 (67)	1.6e-10 (17)	1.9e-09 (86)	2.0e-08 (86)	3.1e-11 (17)	1.9e-07 (86)	4.4e-08 (86)	2.8e-07 (86)
Ra-228	< 1e-12	< 1e-12	< 1e-12	< 1e-12	< 1e-12	< 1e-12	< 1e-12	< 1e-12	< 1e-12
Se-79	1.5e-08 (7)	3.6e-10 (11)	1.0e-09 (6)	1.5e-09 (6)	4.5e-08 (12)	< 1e-12	4.5e-11 (5)	5.2e-10 (7)	5.9e-08 (10)
Sm-151	< 1e-12	< 1e-12	< 1e-12	< 1e-12	< 1e-12	< 1e-12	< 1e-12	< 1e-12	< 1e-12
Sn-126	9.7e-11 (86)	< 1e-12	< 1e-12	1.2e-11 (86)	9.4e-12 (98)	< 1e-12	< 1e-12	1.4e-11 (86)	1.3e-10 (86)
Sr-90	< 1e-12	< 1e-12	< 1e-12	< 1e-12	< 1e-12	< 1e-12	< 1e-12	< 1e-12	< 1e-12
Tc-99	5.9e-08 (77)	2.0e-12 (86)	1.1e-09 (86)	7.4e-09 (67)	4.6e-08 (86)	2.0e-11 (86)	4.1e-08 (52)	3.3e-09 (77)	1.5e-07 (86)
Th-228	< 1e-12	< 1e-12	< 1e-12	< 1e-12	< 1e-12	< 1e-12	< 1e-12	< 1e-12	< 1e-12
Th-229	4.0e-09 (86)	< 1e-12	3.7e-12 (86)	5.3e-10 (86)	9.7e-10 (86)	< 1e-12	4.8e-11 (86)	3.5e-11 (86)	5.6e-09 (86)
Th-230	2.7e-10 (86)	< 1e-12	1.6e-12 (67)	3.3e-11 (86)	1.1e-10 (86)	< 1e-12	4.7e-09 (77)	5.5e-10 (86)	5.5e-09 (77)
Th-232	< 1e-12	< 1e-12	< 1e-12	< 1e-12	< 1e-12	< 1e-12	< 1e-12	3.4e-12 (9)	< 1e-12
U-232	< 1e-12	< 1e-12	< 1e-12	< 1e-12	< 1e-12	< 1e-12	< 1e-12	< 1e-12	< 1e-12
U-233	1.8e-09 (67)	< 1e-12	2.5e-12 (86)	2.5e-10 (86)	4.4e-10 (86)	< 1e-12	2.3e-11 (86)	2.0e-11 (86)	2.5e-09 (86)
U-234	1.4e-09 (49)	1.6e-12 (86)	4.1e-12 (52)	2.0e-10 (41)	5.0e-10 (67)	< 1e-12	3.7e-08 (52)	4.7e-09 (67)	4.3e-08 (52)
U-235	6.3e-10 (50)	< 1e-12	1.5e-11 (67)	2.9e-11 (13)	1.1e-10 (67)	< 1e-12	3.3e-07 (7)	6.1e-08 (40)	3.4e-07 (7)
U-236	4.8e-10 (50)	< 1e-12	< 1e-12	1.3e-10 (40)	1.9e-10 (67)	< 1e-12	5.4e-11 (8)	3.5e-11 (25)	7.7e-10 (52)
U-238	1.0e-09 (50)	< 1e-12	5.5e-12 (52)	2.7e-10 (40)	2.6e-10 (67)	< 1e-12	8.0e-07 (7)	3.4e-08 (40)	8.1e-07 (7)
Zr-93	8.0e-09 (86)	1.7e-11 (86)	6.0e-11 (86)	1.1e-09 (67)	2.3e-08 (86)	6.4e-11 (86)	4.5e-11 (52)	4.5e-10 (77)	3.3e-08 (86)

High concentrations of complexing agents calculation case (CCL_CA)

Table E-19. Near-field releases for CCL_CA, peak release [Bq/year] and in parentheses time of peak [1000 year AD].

Nuclide	1BMA	2BMA	1BTF	2BTF	Silo	BRT	1BLA	2-5BLA	Total
Ac-227	1.3e+02 (83)	1.3e+00 (86)	1.6e+02 (86)	1.9e+00 (6)	3.0e+01 (67)	< 1	2.2e+04 (3)	5.2e+03 (4)	2.3e+04 (3)
Ag-108m	1.6e+06 (3)	2.2e+05 (4)	1.7e+05 (3)	7.7e+05 (3)	1.8e+05 (4)	2.0e+05 (3)	1.3e+05 (3)	6.5e+04 (3)	2.7e+06 (3)
Am-241	4.0e+03 (4)	< 1	4.4e+02 (4)	2.5e+03 (4)	< 1	6.9e+00 (4)	3.8e+05 (3)	8.8e+04 (3)	4.1e+05 (3)
Am-242m	< 1	< 1	< 1	< 1	< 1	< 1	2.5e+01 (3)	3.7e+00 (3)	2.5e+01 (3)
Am-243	2.5e+03 (7)	1.5e+00 (61)	7.2e+01 (4)	5.5e+02 (4)	1.5e+00 (34)	3.8e+00 (22)	1.3e+04 (3)	6.5e+03 (4)	1.4e+04 (3)
Ba-133	< 1	< 1	< 1	< 1	< 1	< 1	< 1	< 1	< 1
C-14-ind	< 1	4.5e+05 (5)	< 1	< 1	< 1	2.7e+04 (24)	< 1	4.0e+05 (4)	7.6e+05 (4)
C-14-inorg	7.9e+05 (7)	8.7e+00 (24)	1.5e+05 (12)	6.6e+05 (4)	1.8e+02 (34)	< 1	1.3e+07 (3)	3.1e+05 (4)	1.3e+07 (3)
C-14-org	4.2e+07 (3)	3.5e+05 (5)	6.3e+06 (3)	9.8e+06 (3)	5.3e+07 (5)	< 1	2.5e+05 (3)	7.5e+04 (4)	8.0e+07 (4)
Ca-41	< 1	8.0e+05 (10)	< 1	< 1	< 1	< 1	< 1	1.6e+06 (4)	1.6e+06 (4)
Cd-113m	< 1	< 1	< 1	< 1	< 1	< 1	< 1	< 1	< 1
Cl-36	6.5e+04 (3)	1.2e+04 (7)	7.0e+03 (3)	2.4e+04 (3)	3.5e+04 (6)	2.7e+02 (29)	7.6e+04 (3)	1.9e+04 (4)	1.6e+05 (3)
Cm-242	< 1	< 1	< 1	< 1	< 1	< 1	2.0e+01 (3)	3.0e+00 (3)	2.0e+01 (3)
Cm-243	< 1	< 1	< 1	< 1	< 1	< 1	< 1	< 1	< 1
Cm-244	< 1	< 1	< 1	< 1	< 1	< 1	< 1	< 1	< 1
Cm-245	2.0e+01 (7)	< 1	< 1	3.0e+00 (4)	< 1	< 1	1.3e+02 (3)	7.8e+01 (4)	1.5e+02 (3)
Cm-246	3.8e+00 (7)	< 1	< 1	< 1	< 1	< 1	3.2e+01 (3)	2.1e+01 (4)	3.7e+01 (3)
Co-60	< 1	< 1	< 1	< 1	< 1	< 1	< 1	< 1	< 1
Cs-135	1.1e+05 (4)	2.4e+03 (7)	2.6e+04 (4)	1.8e+04 (3)	3.1e+04 (13)	< 1	1.1e+04 (3)	7.1e+04 (4)	2.1e+05 (4)
Cs-137	< 1	< 1	< 1	< 1	< 1	< 1	< 1	< 1	< 1
Eu-152	< 1	< 1	< 1	< 1	< 1	< 1	< 1	< 1	< 1
H-3	< 1	< 1	< 1	< 1	< 1	< 1	< 1	< 1	< 1
Ho-166m	2.0e+03 (4)	< 1	9.6e+01 (4)	1.1e+03 (4)	< 1	< 1	8.1e+03 (3)	1.5e+04 (3)	1.8e+04 (3)
I-129	2.4e+04 (3)	2.8e+02 (8)	6.8e+03 (3)	1.3e+04 (3)	2.3e+04 (6)	< 1	1.5e+03 (3)	7.9e+02 (4)	4.6e+04 (5)
Mo-93	2.6e+05 (3)	7.7e+04 (5)	7.7e+04 (3)	2.3e+05 (3)	2.5e+05 (5)	6.6e+04 (4)	3.0e+05 (3)	2.8e+04 (4)	8.1e+05 (3)
Nb-93m	5.1e+04 (5)	6.4e+03 (86)	1.1e+03 (3)	1.1e+04 (4)	2.3e+04 (18)	1.1e+03 (4)	3.0e+05 (3)	4.0e+04 (4)	3.2e+05 (3)
Nb-94	6.3e+04 (7)	5.2e+03 (67)	8.8e+02 (22)	2.0e+04 (5)	8.4e+03 (34)	1.2e+03 (67)	1.1e+05 (3)	3.8e+05 (4)	4.1e+05 (4)
Ni-59	1.6e+08 (7)	1.3e+07 (58)	7.6e+06 (4)	2.4e+07 (3)	6.3e+07 (34)	3.5e+06 (22)	1.4e+07 (3)	4.6e+06 (4)	2.0e+08 (7)
Ni-63	1.2e+06 (3)	4.8e+02 (3)	6.4e+04 (3)	6.6e+05 (3)	2.7e+02 (4)	1.4e+04 (3)	9.8e+05 (3)	8.7e+04 (3)	2.5e+06 (3)
Np-237	1.7e+03 (4)	2.3e+01 (86)	9.2e+00 (22)	7.3e+02 (4)	9.2e+02 (34)	< 1	5.6e+02 (3)	2.7e+02 (4)	2.7e+03 (3)
Pa-231	1.6e+01 (82)	< 1	3.3e+01 (58)	< 1	6.4e+01 (77)	< 1	2.3e+04 (3)	5.3e+03 (4)	2.4e+04 (3)
Pb-210	1.0e+02 (82)	6.1e+01 (83)	3.1e+00 (82)	1.9e+00 (4)	6.9e+01 (77)	< 1	6.1e+00 (3)	4.3e+00 (5)	2.0e+02 (82)
Pd-107	1.8e+04 (3)	2.8e+05 (5)	7.0e+02 (3)	6.8e+03 (3)	1.4e+04 (5)	< 1	3.5e+02 (3)	7.0e+02 (4)	3.0e+05 (5)
Po-210	8.4e+03 (77)	5.4e+03 (83)	2.5e+02 (77)	4.5e+01 (18)	2.6e+03 (77)	6.8e+01 (22)	6.1e+00 (3)	4.3e+00 (5)	1.4e+04 (82)
Pu-238	9.7e+01 (3)	< 1	< 1	6.1e+01 (3)	< 1	< 1	4.8e+02 (3)	4.8e+01 (3)	5.2e+02 (3)
Pu-239	1.9e+05 (3)	2.0e+03 (58)	1.1e+03 (12)	1.1e+05 (3)	4.5e+04 (10)	1.1e+02 (13)	2.3e+05 (3)	1.1e+05 (4)	5.0e+05 (3)
Pu-240	2.4e+05 (3)	3.7e+01 (57)	7.9e+02 (5)	1.4e+05 (3)	3.6e+04 (8)	1.2e+02 (4)	2.1e+05 (3)	1.0e+05 (4)	5.6e+05 (3)
Pu-241	3.9e+02 (6)	2.5e+00 (63)	1.2e+01 (9)	1.0e+02 (4)	< 1	< 1	1.3e+02 (3)	7.8e+01 (4)	5.2e+02 (5)
Pu-242	1.4e+03 (3)	6.7e+01 (61)	9.6e+00 (23)	8.1e+02 (3)	3.4e+02 (15)	1.1e+00 (24)	1.4e+03 (3)	7.0e+02 (4)	3.4e+03 (3)
Ra-226	9.4e+02 (77)	7.2e+02 (82)	3.3e+01 (22)	4.3e+00 (17)	9.3e+02 (77)	9.0e+00 (22)	6.6e+00 (3)	4.4e+00 (5)	2.3e+03 (82)
Ra-228	< 1	< 1	< 1	< 1	< 1	< 1	< 1	< 1	< 1
Se-79	9.9e+04 (3)	9.1e+02 (5)	8.9e+03 (3)	2.8e+04 (3)	1.1e+05 (5)	< 1	1.4e+03 (3)	2.4e+03 (4)	1.5e+05 (4)
Sm-151	3.5e+00 (3)	< 1	< 1	3.4e+00 (3)	< 1	< 1	2.5e+02 (3)	1.9e+02 (3)	3.4e+02 (3)
Sn-126	1.6e+03 (4)	6.9e+00 (62)	9.1e+00 (23)	6.5e+02 (3)	4.8e+02 (35)	< 1	1.8e+02 (3)	3.2e+03 (4)	5.3e+03 (4)
Sr-90	< 1	< 1	< 1	< 1	< 1	< 1	< 1	< 1	< 1
Tc-99	4.6e+05 (7)	1.9e+03 (86)	2.8e+04 (22)	1.5e+05 (3)	3.0e+05 (34)	4.0e+02 (58)	6.5e+06 (3)	2.0e+05 (4)	6.7e+06 (3)
Th-228	< 1	< 1	< 1	< 1	< 1	< 1	< 1	< 1	< 1
Th-229	8.8e+01 (83)	1.0e+00 (86)	< 1	1.1e+00 (22)	6.1e+01 (86)	< 1	< 1	< 1	1.5e+02 (83)
Th-230	2.6e+01 (82)	3.6e+00 (86)	2.0e+00 (58)	1.8e+00 (22)	4.4e+01 (86)	< 1	4.5e+01 (3)	1.1e+01 (5)	7.4e+01 (82)
Th-232	< 1	< 1	< 1	< 1	< 1	< 1	< 1	< 1	< 1
U-232	< 1	< 1	< 1	< 1	< 1	< 1	< 1	< 1	< 1
U-233	6.9e+01 (77)	9.4e+00 (77)	1.4e+00 (82)	6.0e+00 (4)	1.2e+02 (77)	< 1	2.0e+00 (3)	2.0e+00 (5)	2.0e+02 (77)
U-234	5.6e+02 (4)	2.4e+01 (63)	5.1e+00 (23)	2.3e+02 (3)	1.9e+02 (34)	< 1	8.6e+03 (3)	7.6e+02 (4)	8.9e+03 (3)
U-235	2.7e+02 (3)	< 1	2.9e+01 (26)	4.2e+01 (3)	4.7e+01 (34)	< 1	1.1e+06 (3)	1.3e+05 (4)	1.1e+06 (3)
U-236	1.4e+02 (4)	1.3e+01 (65)	2.3e+00 (23)	1.4e+02 (3)	7.5e+01 (34)	< 1	1.5e+02 (3)	9.0e+01 (4)	4.0e+02 (3)
U-238	4.6e+02 (4)	1.8e+00 (65)	5.5e+00 (23)	3.3e+02 (3)	1.1e+02 (34)	< 1	2.6e+06 (3)	7.2e+04 (4)	2.6e+06 (3)
Zr-93	2.5e+04 (5)	2.7e+03 (86)	3.5e+02 (8)	1.1e+04 (3)	5.4e+04 (34)	2.7e+02 (22)	3.8e+03 (3)	1.2e+04 (4)	5.7e+04 (34)

Table E-20. Far-field releases for CCL_CA, peak release [Bq/year] and in parentheses time of peak [1000 year AD].

Nuclide	1BMA	2BMA	1BTF	2BTF	Silo	BRT	1BLA	2-5BLA	Total
Ac-227	1.6e+02 (84)	< 1	1.4e+02 (77)	5.3e+00 (25)	2.8e+02 (86)	< 1	1.5e+04 (5)	4.2e+03 (82)	1.5e+04 (5)
Ag-108m	1.5e+06 (3)	1.9e+05 (4)	1.5e+05 (3)	5.6e+05 (3)	1.7e+05 (4)	1.5e+05 (3)	1.2e+05 (3)	5.3e+04 (3)	2.4e+06 (3)
Am-241	6.2e+02 (4)	< 1	1.2e+01 (5)	1.4e+02 (4)	< 1	< 1	1.9e+04 (4)	6.4e+02 (4)	2.0e+04 (4)
Am-242m	< 1	< 1	< 1	< 1	< 1	< 1	< 1	< 1	< 1
Am-243	4.3e+02 (7)	< 1	1.4e+01 (9)	7.3e+01 (5)	< 1	< 1	1.3e+03 (4)	3.4e+02 (5)	1.4e+03 (4)
Ba-133	< 1	< 1	< 1	< 1	< 1	< 1	< 1	< 1	< 1
C-14-ind	< 1	4.0e+05 (5)	< 1	< 1	< 1	2.6e+04 (24)	< 1	3.7e+05 (4)	6.8e+05 (4)
C-14-inorg	7.8e+05 (7)	8.1e+00 (24)	1.4e+05 (12)	6.2e+05 (4)	1.8e+02 (34)	< 1	1.1e+07 (3)	2.9e+05 (4)	1.1e+07 (3)
C-14-org	4.1e+07 (3)	3.1e+05 (5)	5.7e+06 (3)	7.7e+06 (3)	5.2e+07 (5)	< 1	2.2e+05 (3)	6.9e+04 (4)	7.9e+07 (4)
Ca-41	< 1	7.8e+05 (10)	< 1	< 1	< 1	< 1	< 1	1.4e+06 (4)	1.4e+06 (4)
Cd-113m	< 1	< 1	< 1	< 1	< 1	< 1	< 1	< 1	< 1
Cl-36	6.4e+04 (3)	1.1e+04 (8)	6.8e+03 (3)	2.0e+04 (3)	3.4e+04 (6)	2.7e+02 (30)	6.9e+04 (3)	1.7e+04 (4)	1.5e+05 (3)
Cm-242	< 1	< 1	< 1	< 1	< 1	< 1	< 1	< 1	< 1
Cm-243	< 1	< 1	< 1	< 1	< 1	< 1	< 1	< 1	< 1
Cm-244	< 1	< 1	< 1	< 1	< 1	< 1	< 1	< 1	< 1
Cm-245	6.9e+00 (7)	< 1	< 1	< 1	< 1	< 1	1.4e+01 (4)	4.1e+00 (5)	1.5e+01 (4)
Cm-246	1.3e+00 (7)	< 1	< 1	< 1	< 1	< 1	3.3e+00 (4)	1.0e+00 (5)	3.6e+00 (4)
Co-60	< 1	< 1	< 1	< 1	< 1	< 1	< 1	< 1	< 1
Cs-135	9.0e+04 (5)	8.5e+02 (9)	1.5e+04 (4)	7.2e+03 (4)	2.2e+04 (16)	< 1	2.8e+03 (3)	2.0e+04 (5)	1.3e+05 (5)
Cs-137	< 1	< 1	< 1	< 1	< 1	< 1	< 1	< 1	< 1
Eu-152	< 1	< 1	< 1	< 1	< 1	< 1	< 1	< 1	< 1
H-3	< 1	< 1	< 1	< 1	< 1	< 1	< 1	< 1	< 1
Ho-166m	6.8e+02 (5)	< 1	1.6e+01 (4)	1.2e+02 (4)	< 1	< 1	5.8e+02 (4)	3.3e+02 (5)	1.2e+03 (5)
I-129	2.4e+04 (3)	3.0e+02 (9)	6.7e+03 (3)	1.0e+04 (3)	2.3e+04 (6)	< 1	1.4e+03 (3)	7.2e+02 (4)	4.5e+04 (5)
Mo-93	2.6e+05 (3)	7.0e+04 (6)	7.4e+04 (3)	1.9e+05 (3)	2.5e+05 (5)	6.2e+04 (4)	2.7e+05 (3)	2.6e+04 (4)	7.3e+05 (3)
Nb-93m	2.5e+04 (9)	5.6e+02 (86)	4.3e+02 (18)	4.2e+03 (5)	5.2e+04 (37)	2.2e+02 (4)	2.0e+03 (3)	6.2e+02 (10)	6.0e+04 (37)
Nb-94	2.2e+04 (9)	4.8e+02 (67)	3.3e+02 (16)	5.1e+03 (6)	3.0e+03 (35)	2.1e+02 (67)	9.2e+03 (4)	1.3e+04 (5)	4.0e+04 (9)
Ni-59	1.1e+08 (5)	6.6e+06 (61)	3.9e+06 (4)	1.3e+07 (4)	2.9e+07 (34)	7.1e+05 (59)	3.7e+06 (3)	1.4e+06 (5)	1.2e+08 (5)
Ni-63	2.9e+05 (3)	5.6e+01 (4)	7.4e+03 (4)	3.8e+04 (3)	3.6e+01 (4)	3.9e+02 (4)	1.1e+05 (3)	2.4e+03 (3)	4.2e+05 (3)
Np-237	5.7e+02 (9)	1.9e+00 (86)	4.0e+00 (26)	7.4e+01 (5)	1.6e+02 (61)	< 1	2.4e+01 (4)	4.9e+00 (5)	6.6e+02 (9)
Pa-231	1.3e+01 (82)	< 1	1.9e+01 (77)	< 1	1.9e+01 (86)	< 1	1.9e+03 (5)	6.6e+02 (82)	1.9e+03 (5)
Pb-210	7.0e+01 (77)	1.2e+01 (86)	2.8e+00 (77)	4.3e+00 (77)	8.2e+01 (77)	< 1	3.1e+02 (77)	7.1e+01 (82)	5.5e+02 (77)
Pd-107	1.8e+04 (3)	2.5e+05 (6)	7.2e+02 (4)	5.5e+03 (3)	1.4e+04 (5)	< 1	3.2e+02 (3)	6.4e+02 (4)	2.7e+05 (5)
Po-210	8.5e+01 (77)	1.2e+01 (86)	3.4e+00 (77)	4.6e+00 (77)	7.9e+01 (77)	< 1	3.2e+02 (77)	6.2e+01 (82)	5.6e+02 (77)
Pu-238	4.1e+00 (3)	< 1	< 1	< 1	< 1	< 1	5.0e+00 (3)	< 1	9.3e+00 (3)
Pu-239	9.0e+04 (5)	3.4e+02 (67)	5.3e+02 (23)	1.1e+04 (5)	1.4e+04 (18)	1.7e+01 (30)	2.3e+04 (4)	5.1e+03 (5)	1.1e+05 (5)
Pu-240	9.9e+04 (5)	4.1e+00 (30)	2.2e+02 (9)	1.3e+04 (4)	7.8e+03 (11)	4.5e+00 (5)	2.1e+04 (4)	4.3e+03 (5)	1.2e+05 (5)
Pu-241	2.9e+01 (7)	< 1	< 1	2.6e+00 (5)	< 1	< 1	2.2e+01 (4)	3.6e+00 (9)	4.5e+01 (5)
Pu-242	7.0e+02 (5)	1.6e+01 (86)	6.3e+00 (24)	8.7e+01 (5)	1.5e+02 (37)	< 1	1.4e+02 (4)	3.4e+01 (5)	8.7e+02 (5)
Ra-226	1.0e+03 (77)	1.6e+02 (86)	4.4e+01 (77)	6.9e+01 (77)	1.3e+03 (77)	1.9e+00 (22)	5.4e+03 (77)	1.1e+03 (82)	9.0e+03 (77)
Ra-228	< 1	< 1	< 1	< 1	< 1	< 1	< 1	< 1	< 1
Se-79	9.5e+04 (3)	8.1e+02 (5)	8.3e+03 (3)	2.2e+04 (3)	1.0e+05 (5)	< 1	1.3e+03 (3)	2.2e+03 (4)	1.5e+05 (4)
Sm-151	< 1	< 1	< 1	< 1	< 1	< 1	1.9e+00 (3)	< 1	2.1e+00 (3)
Sn-126	3.2e+02 (9)	< 1	2.5e+00 (65)	2.6e+01 (10)	6.9e+01 (52)	< 1	2.9e+00 (5)	1.3e+01 (16)	3.6e+02 (9)
Sr-90	< 1	< 1	< 1	< 1	< 1	< 1	< 1	< 1	< 1
Tc-99	1.2e+05 (9)	1.5e+02 (86)	6.7e+03 (23)	1.6e+04 (5)	7.6e+04 (44)	3.3e+01 (86)	3.0e+05 (4)	3.9e+03 (9)	3.2e+05 (4)
Th-228	< 1	< 1	< 1	< 1	< 1	< 1	< 1	< 1	< 1
Th-229	8.5e+01 (77)	< 1	1.6e+00 (77)	4.4e+00 (77)	7.1e+01 (82)	< 1	< 1	< 1	1.6e+02 (82)
Th-230	2.4e+01 (82)	< 1	1.3e+00 (77)	1.8e+00 (77)	3.4e+01 (82)	< 1	1.9e+02 (82)	4.0e+01 (82)	3.0e+02 (82)
Th-232	< 1	< 1	< 1	< 1	< 1	< 1	< 1	< 1	< 1
U-232	< 1	< 1	< 1	< 1	< 1	< 1	< 1	< 1	< 1
U-233	5.1e+01 (82)	< 1	1.2e+00 (77)	3.2e+00 (77)	5.8e+01 (82)	< 1	< 1	< 1	1.1e+02 (82)
U-234	1.6e+02 (5)	1.7e+00 (86)	2.4e+00 (26)	2.0e+01 (5)	4.9e+01 (49)	< 1	5.9e+02 (5)	6.9e+01 (82)	7.8e+02 (5)
U-235	7.6e+01 (5)	< 1	1.7e+01 (64)	3.6e+00 (5)	1.2e+01 (82)	< 1	4.4e+04 (4)	2.6e+03 (10)	4.5e+04 (4)
U-236	4.5e+01 (9)	< 1	1.0e+00 (25)	1.2e+01 (5)	1.9e+01 (61)	< 1	6.4e+00 (4)	2.0e+00 (10)	6.1e+01 (9)
U-238	1.3e+02 (5)	< 1	2.4e+00 (25)	2.8e+01 (5)	2.8e+01 (64)	< 1	1.1e+05 (4)	1.4e+03 (10)	1.1e+05 (4)
Zr-93	1.1e+04 (5)	4.0e+02 (86)	1.8e+02 (16)	2.0e+03 (5)	1.9e+04 (39)	3.6e+01 (37)	2.8e+02 (4)	3.7e+02 (9)	2.2e+04 (38)

Table E-21. Doses for CCL_CA, peak dose [Sv/year] and in parentheses time of peak [1000 year AD].

Nuclide	1BMA	2BMA	1BTF	2BTF	Silo	BRT	1BLA	2-5BLA	Total
Total	5.0e-06 (44)	1.0e-06 (17)	4.3e-07 (5)	5.3e-07 (5)	3.9e-06 (46)	3.7e-07 (5)	1.3e-06 (24)	5.2e-07 (9)	1.1e-05 (45)
Ac-227	1.2e-09 (46)	< 1e-12	7.3e-10 (86)	5.5e-11 (38)	8.7e-10 (86)	< 1e-12	2.1e-07 (33)	9.5e-08 (57)	2.9e-07 (38)
Ag-108m	2.1e-08 (5)	6.9e-09 (5)	2.1e-09 (5)	3.9e-09 (5)	7.6e-09 (5)	2.9e-09 (5)	5.3e-10 (5)	1.4e-09 (5)	4.5e-08 (5)
Am-241	1.3e-11 (5)	< 1e-12	< 1e-12	3.4e-12 (5)	< 1e-12	< 1e-12	1.6e-10 (4)	5.8e-10 (4)	6.3e-10 (4)
Am-242m	< 1e-12	< 1e-12	< 1e-12	< 1e-12	< 1e-12	< 1e-12	< 1e-12	< 1e-12	< 1e-12
Am-243	3.5e-10 (21)	< 1e-12	2.3e-11 (28)	7.8e-11 (22)	< 1e-12	< 1e-12	2.5e-10 (15)	3.4e-10 (5)	8.9e-10 (19)
Ba-133	< 1e-12	< 1e-12	< 1e-12	< 1e-12	< 1e-12	< 1e-12	< 1e-12	< 1e-12	< 1e-12
C-14-ind	< 1e-12	1.1e-08 (5)	< 1e-12	< 1e-12	< 1e-12	7.2e-10 (24)	< 1e-12	7.8e-09 (5)	1.9e-08 (5)
C-14-inorg	2.3e-08 (7)	< 1e-12	4.1e-09 (13)	1.7e-08 (6)	5.6e-12 (34)	< 1e-12	9.0e-08 (3)	6.0e-09 (5)	9.1e-08 (3)
C-14-org	8.0e-07 (5)	8.6e-09 (5)	6.1e-08 (3)	6.4e-08 (3)	1.5e-06 (5)	< 1e-12	1.8e-09 (3)	1.5e-09 (5)	2.2e-06 (5)
Ca-41	< 1e-12	8.4e-07 (28)	< 1e-12	< 1e-12	< 1e-12	< 1e-12	< 1e-12	4.4e-07 (10)	1.0e-06 (19)
Cd-113m	< 1e-12	< 1e-12	< 1e-12	< 1e-12	< 1e-12	< 1e-12	< 1e-12	< 1e-12	< 1e-12
Cl-36	1.9e-07 (5)	3.7e-08 (8)	1.0e-08 (5)	1.1e-08 (5)	1.1e-07 (6)	8.8e-10 (30)	1.9e-08 (3)	4.8e-08 (5)	3.6e-07 (5)
Cm-242	< 1e-12	< 1e-12	< 1e-12	< 1e-12	< 1e-12	< 1e-12	< 1e-12	< 1e-12	< 1e-12
Cm-243	< 1e-12	< 1e-12	< 1e-12	< 1e-12	< 1e-12	< 1e-12	< 1e-12	< 1e-12	< 1e-12
Cm-244	< 1e-12	< 1e-12	< 1e-12	< 1e-12	< 1e-12	< 1e-12	< 1e-12	< 1e-12	< 1e-12
Cm-245	5.3e-12 (20)	< 1e-12	< 1e-12	< 1e-12	< 1e-12	< 1e-12	2.6e-12 (15)	4.2e-12 (5)	1.1e-11 (18)
Cm-246	< 1e-12	< 1e-12	< 1e-12	< 1e-12	< 1e-12	< 1e-12	< 1e-12	< 1e-12	< 1e-12
Co-60	< 1e-12	< 1e-12	< 1e-12	< 1e-12	< 1e-12	< 1e-12	< 1e-12	< 1e-12	< 1e-12
Cs-135	6.7e-07 (86)	1.9e-08 (86)	6.1e-08 (86)	1.5e-08 (86)	6.1e-07 (86)	< 1e-12	2.5e-09 (86)	9.9e-08 (86)	1.5e-06 (86)
Cs-137	< 1e-12	< 1e-12	< 1e-12	< 1e-12	< 1e-12	< 1e-12	< 1e-12	< 1e-12	< 1e-12
Eu-152	< 1e-12	< 1e-12	< 1e-12	< 1e-12	< 1e-12	< 1e-12	< 1e-12	< 1e-12	< 1e-12
H-3	< 1e-12	< 1e-12	< 1e-12	< 1e-12	< 1e-12	< 1e-12	< 1e-12	< 1e-12	< 1e-12
Ho-166m	2.0e-12 (8)	< 1e-12	< 1e-12	< 1e-12	< 1e-12	< 1e-12	< 1e-12	3.9e-12 (5)	5.1e-12 (5)
I-129	3.3e-07 (8)	8.6e-09 (27)	5.7e-08 (6)	4.1e-08 (5)	5.6e-07 (16)	< 1e-12	3.2e-09 (3)	8.2e-09 (6)	8.5e-07 (9)
Mo-93	1.6e-06 (5)	7.4e-07 (9)	3.3e-07 (5)	4.3e-07 (5)	2.3e-06 (8)	3.7e-07 (5)	2.7e-07 (5)	1.6e-07 (5)	5.2e-06 (6)
Nb-93m	5.2e-10 (5)	2.4e-10 (9)	1.1e-10 (5)	1.4e-10 (5)	7.6e-10 (8)	1.2e-10 (5)	8.8e-11 (5)	5.0e-11 (5)	1.7e-09 (6)
Nb-94	1.7e-09 (51)	2.7e-11 (86)	4.6e-11 (57)	3.7e-10 (47)	4.4e-10 (77)	2.6e-11 (77)	8.2e-11 (32)	6.3e-10 (43)	3.1e-09 (52)
Ni-59	4.2e-06 (44)	6.5e-07 (67)	8.6e-08 (23)	1.4e-07 (22)	3.2e-06 (44)	1.1e-07 (52)	1.8e-08 (15)	3.1e-08 (21)	8.1e-06 (45)
Ni-63	1.4e-11 (3)	< 1e-12	< 1e-12	2.1e-12 (3)	< 1e-12	< 1e-12	4.5e-12 (3)	1.9e-12 (3)	2.0e-11 (3)
Np-237	3.9e-09 (86)	2.3e-12 (86)	5.5e-11 (86)	5.0e-10 (86)	1.6e-09 (86)	< 1e-12	4.3e-11 (86)	3.2e-11 (86)	6.1e-09 (86)
Pa-231	2.3e-09 (41)	< 1e-12	1.6e-09 (86)	1.0e-10 (35)	1.5e-09 (86)	< 1e-12	3.9e-07 (30)	1.2e-07 (52)	5.0e-07 (34)
Pb-210	6.5e-09 (86)	1.1e-09 (67)	2.5e-10 (86)	3.9e-10 (86)	6.2e-09 (86)	1.3e-11 (23)	2.9e-08 (86)	7.5e-09 (86)	5.1e-08 (86)
Pd-107	1.4e-10 (16)	7.0e-09 (31)	5.2e-12 (25)	1.4e-11 (15)	5.5e-10 (34)	< 1e-12	< 1e-12	6.5e-12 (16)	7.7e-09 (31)
Po-210	2.3e-10 (86)	1.0e-10 (86)	9.6e-12 (86)	1.3e-11 (86)	2.8e-10 (86)	< 1e-12	9.9e-10 (86)	4.2e-10 (86)	1.9e-09 (86)
Pu-238	< 1e-12	< 1e-12	< 1e-12	< 1e-12	< 1e-12	< 1e-12	< 1e-12	< 1e-12	< 1e-12
Pu-239	5.2e-07 (41)	3.1e-09 (86)	1.1e-08 (57)	5.8e-08 (38)	3.2e-07 (65)	4.0e-10 (67)	3.2e-08 (32)	4.3e-08 (42)	9.2e-07 (50)
Pu-240	1.2e-07 (17)	1.5e-11 (67)	9.8e-10 (25)	1.5e-08 (17)	2.2e-08 (28)	2.4e-11 (28)	8.2e-09 (14)	7.0e-09 (18)	1.7e-07 (18)
Pu-241	< 1e-12	< 1e-12	< 1e-12	< 1e-12	< 1e-12	< 1e-12	< 1e-12	< 1e-12	< 1e-12
Pu-242	1.7e-08 (86)	1.9e-10 (86)	4.4e-10 (86)	1.7e-09 (86)	1.3e-08 (86)	3.7e-12 (86)	6.1e-10 (84)	1.2e-09 (86)	3.5e-08 (86)
Ra-226	3.9e-08 (86)	6.4e-09 (67)	1.5e-09 (86)	2.5e-09 (86)	4.0e-08 (86)	6.3e-11 (23)	1.8e-07 (86)	4.3e-08 (86)	3.1e-07 (86)
Ra-228	< 1e-12	< 1e-12	< 1e-12	< 1e-12	< 1e-12	< 1e-12	< 1e-12	< 1e-12	< 1e-12
Se-79	1.7e-08 (6)	3.6e-10 (11)	1.0e-09 (6)	1.5e-09 (6)	4.5e-08 (12)	< 1e-12	4.5e-11 (5)	5.2e-10 (7)	5.9e-08 (10)
Sm-151	< 1e-12	< 1e-12	< 1e-12	< 1e-12	< 1e-12	< 1e-12	< 1e-12	< 1e-12	< 1e-12
Sn-126	2.5e-10 (67)	< 1e-12	2.9e-12 (86)	2.1e-11 (67)	6.9e-11 (86)	< 1e-12	< 1e-12	1.5e-11 (78)	3.5e-10 (77)
Sr-90	< 1e-12	< 1e-12	< 1e-12	< 1e-12	< 1e-12	< 1e-12	< 1e-12	< 1e-12	< 1e-12
Tc-99	7.8e-08 (67)	3.7e-11 (86)	9.1e-09 (86)	9.3e-09 (67)	1.2e-07 (86)	2.1e-11 (86)	4.2e-08 (52)	3.3e-09 (67)	2.5e-07 (77)
Th-228	< 1e-12	< 1e-12	< 1e-12	< 1e-12	< 1e-12	< 1e-12	< 1e-12	< 1e-12	< 1e-12
Th-229	7.2e-09 (86)	3.3e-12 (86)	1.1e-10 (86)	7.2e-10 (86)	4.3e-09 (86)	< 1e-12	4.8e-11 (86)	3.6e-11 (86)	1.2e-08 (86)
Th-230	4.7e-10 (86)	1.9e-12 (86)	1.9e-11 (86)	4.4e-11 (67)	4.4e-10 (86)	< 1e-12	4.7e-09 (77)	5.5e-10 (77)	5.8e-09 (77)
Th-232	< 1e-12	< 1e-12	1.0e-12 (7)	< 1e-12	< 1e-12	< 1e-12	< 1e-12	3.4e-12 (9)	< 1e-12
U-232	< 1e-12	< 1e-12	< 1e-12	< 1e-12	< 1e-12	< 1e-12	< 1e-12	< 1e-12	< 1e-12
U-233	3.3e-09 (86)	2.3e-12 (86)	4.4e-11 (86)	3.5e-10 (86)	1.9e-09 (86)	< 1e-12	2.3e-11 (86)	2.0e-11 (86)	5.7e-09 (86)
U-234	2.7e-09 (12)	3.1e-11 (86)	8.6e-11 (52)	3.4e-10 (11)	1.9e-09 (67)	< 1e-12	3.6e-08 (49)	4.6e-09 (67)	4.5e-08 (52)
U-235	1.2e-09 (12)	< 1e-12	6.3e-10 (67)	6.0e-11 (11)	4.8e-10 (67)	< 1e-12	3.3e-07 (7)	6.4e-08 (35)	3.4e-07 (7)
U-236	9.7e-10 (30)	1.0e-11 (86)	2.7e-11 (50)	2.2e-10 (28)	7.4e-10 (67)	< 1e-12	5.4e-11 (8)	3.9e-11 (24)	1.7e-09 (51)
U-238	2.0e-09 (12)	1.5e-12 (86)	7.5e-11 (52)	4.7e-10 (11)	1.1e-09 (67)	< 1e-12	8.0e-07 (7)	3.5e-08 (35)	8.1e-07 (7)
Zr-93	1.1e-08 (77)	2.4e-10 (86)	2.8e-10 (77)	1.5e-09 (67)	5.4e-08 (86)	7.8e-11 (86)	4.6e-11 (52)	4.5e-10 (77)	6.7e-08 (86)

Wells downstream of the repository calculation case (CCL_WD)

Table E-22. Doses for CCL_WD, peak dose [Sv/year] and in parentheses time of peak [1000 year AD].

Nuclide	1BMA	2BMA	1BTF	2BTF	Silo	BRT	1BLA	2-5BLA	Total
Total	2.8e-06 (5)	1.3e-07 (4)	5.0e-07 (3)	1.1e-06 (3)	2.1e-06 (5)	1.6e-07 (3)	9.3e-06 (4)	1.7e-06 (82)	1.5e-05 (5)
Ac-227	6.8e-08 (86)	< 1e-12	5.7e-09 (86)	1.7e-09 (82)	1.1e-08 (86)	< 1e-12	5.1e-06 (5)	1.4e-06 (82)	5.3e-06 (5)
Ag-108m	2.6e-07 (3)	8.4e-08 (4)	9.8e-08 (3)	3.7e-07 (3)	1.4e-08 (4)	1.0e-07 (3)	8.2e-08 (3)	3.7e-08 (3)	8.2e-07 (3)
Am-241	8.3e-10 (5)	< 1e-12	3.9e-12 (5)	4.3e-10 (4)	< 1e-12	< 1e-12	1.1e-06 (4)	3.6e-08 (4)	1.1e-06 (4)
Am-242m	< 1e-12	< 1e-12	< 1e-12	< 1e-12	< 1e-12	< 1e-12	1.8e-11 (3)	< 1e-12	1.8e-11 (3)
Am-243	1.1e-09 (8)	< 1e-12	4.5e-11 (17)	2.9e-10 (14)	< 1e-12	1.2e-11 (19)	7.5e-08 (4)	1.9e-08 (5)	7.7e-08 (4)
Ba-133	< 1e-12	< 1e-12	< 1e-12	< 1e-12	< 1e-12	< 1e-12	< 1e-12	< 1e-12	< 1e-12
C-14-ind	< 1e-12	1.1e-08 (5)	< 1e-12	< 1e-12	< 1e-12	7.2e-10 (24)	< 1e-12	1.0e-08 (4)	1.9e-08 (4)
C-14-inorg	6.7e-09 (23)	< 1e-12	4.0e-09 (13)	1.8e-08 (4)	4.7e-12 (34)	< 1e-12	3.2e-07 (3)	8.1e-09 (4)	3.2e-07 (3)
C-14-org	8.0e-07 (4)	8.5e-09 (5)	1.6e-07 (3)	2.2e-07 (3)	1.3e-06 (5)	< 1e-12	6.3e-09 (3)	2.0e-09 (4)	2.0e-06 (4)
Ca-41	< 1e-12	4.8e-08 (10)	< 1e-12	< 1e-12	< 1e-12	< 1e-12	< 1e-12	8.8e-08 (4)	8.9e-08 (4)
Cd-113m	< 1e-12	< 1e-12	< 1e-12	< 1e-12	< 1e-12	< 1e-12	< 1e-12	< 1e-12	< 1e-12
Cl-36	3.3e-08 (4)	9.6e-09 (8)	5.6e-09 (3)	1.7e-08 (3)	2.6e-08 (6)	2.2e-10 (30)	5.7e-08 (3)	1.4e-08 (4)	8.6e-08 (3)
Cm-242	< 1e-12	< 1e-12	< 1e-12	< 1e-12	< 1e-12	< 1e-12	1.3e-12 (3)	< 1e-12	1.3e-12 (3)
Cm-243	< 1e-12	< 1e-12	< 1e-12	< 1e-12	< 1e-12	< 1e-12	< 1e-12	< 1e-12	< 1e-12
Cm-244	< 1e-12	< 1e-12	< 1e-12	< 1e-12	< 1e-12	< 1e-12	< 1e-12	< 1e-12	< 1e-12
Cm-245	1.4e-11 (7)	< 1e-12	< 1e-12	3.0e-12 (5)	< 1e-12	< 1e-12	8.4e-10 (4)	2.4e-10 (5)	8.7e-10 (4)
Cm-246	1.9e-12 (7)	< 1e-12	< 1e-12	< 1e-12	< 1e-12	< 1e-12	2.0e-10 (4)	4.7e-11 (5)	2.0e-10 (4)
Co-60	< 1e-12	< 1e-12	< 1e-12	< 1e-12	< 1e-12	< 1e-12	< 1e-12	< 1e-12	< 1e-12
Cs-135	3.9e-08 (5)	5.0e-10 (9)	8.8e-09 (4)	4.2e-09 (4)	1.1e-08 (16)	< 1e-12	1.6e-09 (3)	1.2e-08 (5)	6.0e-08 (5)
Cs-137	< 1e-12	< 1e-12	< 1e-12	< 1e-12	< 1e-12	< 1e-12	< 1e-12	< 1e-12	< 1e-12
Eu-152	< 1e-12	< 1e-12	< 1e-12	< 1e-12	< 1e-12	< 1e-12	< 1e-12	< 1e-12	< 1e-12
H-3	< 1e-12	< 1e-12	< 1e-12	< 1e-12	< 1e-12	< 1e-12	< 1e-12	< 1e-12	< 1e-12
Ho-166m	8.0e-12 (5)	< 1e-12	< 1e-12	5.2e-12 (4)	< 1e-12	< 1e-12	3.6e-10 (4)	2.2e-10 (5)	4.4e-10 (4)
I-129	3.6e-07 (5)	9.4e-09 (9)	2.1e-07 (3)	3.3e-07 (3)	6.5e-07 (6)	< 1e-12	4.4e-08 (3)	2.3e-08 (4)	1.1e-06 (5)
Mo-93	4.4e-08 (4)	7.0e-08 (6)	3.9e-08 (3)	1.1e-07 (3)	1.2e-07 (5)	6.7e-08 (4)	1.1e-07 (3)	1.7e-08 (4)	2.9e-07 (5)
Nb-93m	4.0e-10 (28)	7.4e-12 (5)	6.7e-12 (4)	9.3e-11 (5)	3.5e-10 (44)	7.8e-12 (4)	2.7e-11 (3)	2.1e-11 (10)	7.1e-10 (31)
Nb-94	1.0e-09 (28)	2.3e-11 (67)	2.9e-11 (66)	6.7e-10 (14)	1.8e-11 (67)	1.1e-10 (67)	4.9e-09 (4)	7.2e-09 (5)	9.3e-09 (5)
Ni-59	2.3e-07 (62)	3.2e-08 (67)	1.5e-08 (4)	7.7e-08 (4)	5.5e-08 (35)	1.3e-08 (59)	7.0e-08 (3)	2.5e-08 (5)	2.9e-07 (62)
Ni-63	7.6e-12 (4)	< 1e-12	3.8e-11 (4)	3.4e-10 (4)	< 1e-12	1.7e-11 (4)	4.7e-09 (3)	1.0e-10 (3)	4.9e-09 (3)
Np-237	5.4e-09 (26)	2.8e-12 (86)	1.3e-11 (43)	1.1e-09 (9)	5.4e-10 (86)	< 1e-12	7.8e-10 (4)	1.6e-10 (5)	6.4e-09 (26)
Pa-231	3.0e-09 (77)	< 1e-12	4.9e-10 (86)	4.3e-11 (82)	3.1e-10 (86)	< 1e-12	3.8e-07 (5)	1.3e-07 (82)	4.0e-07 (5)
Pb-210	1.2e-08 (77)	9.0e-10 (86)	1.5e-10 (22)	4.7e-10 (77)	1.2e-09 (86)	1.2e-11 (22)	4.0e-08 (82)	1.2e-08 (82)	6.5e-08 (82)
Pd-107	5.0e-11 (4)	1.4e-09 (7)	1.7e-12 (4)	4.9e-11 (3)	3.2e-11 (7)	< 1e-12	3.5e-12 (3)	7.0e-12 (4)	1.5e-09 (7)
Po-210	2.0e-08 (77)	1.4e-09 (86)	2.3e-10 (22)	8.3e-10 (77)	2.1e-09 (86)	8.7e-12 (22)	6.0e-08 (82)	1.7e-08 (82)	1.0e-07 (82)
Pu-238	7.8e-12 (3)	< 1e-12	< 1e-12	1.4e-12 (3)	< 1e-12	< 1e-12	3.3e-10 (3)	2.5e-12 (3)	3.4e-10 (3)
Pu-239	8.0e-07 (5)	2.1e-09 (67)	3.6e-09 (29)	3.6e-07 (5)	6.7e-08 (39)	1.2e-09 (30)	1.7e-06 (4)	3.7e-07 (5)	2.2e-06 (4)
Pu-240	8.9e-07 (5)	1.6e-11 (60)	8.8e-10 (17)	4.0e-07 (5)	1.1e-08 (20)	3.2e-10 (5)	1.5e-06 (4)	3.1e-07 (5)	2.1e-06 (4)
Pu-241	1.9e-12 (7)	< 1e-12	< 1e-12	< 1e-12	< 1e-12	< 1e-12	3.1e-11 (4)	4.5e-12 (9)	3.2e-11 (4)
Pu-242	7.8e-09 (25)	9.1e-11 (86)	4.0e-11 (38)	2.7e-09 (5)	1.1e-09 (67)	1.1e-11 (52)	1.0e-08 (4)	2.4e-09 (5)	1.4e-08 (5)
Ra-226	6.2e-08 (77)	5.4e-09 (86)	8.8e-10 (22)	3.2e-09 (77)	7.5e-09 (86)	1.5e-10 (22)	2.6e-07 (82)	8.1e-08 (82)	4.1e-07 (82)
Ra-228	< 1e-12	< 1e-12	< 1e-12	< 1e-12	< 1e-12	< 1e-12	< 1e-12	< 1e-12	< 1e-12
Se-79	4.4e-08 (4)	6.8e-10 (5)	7.0e-09 (3)	1.9e-08 (3)	7.8e-08 (5)	< 1e-12	1.1e-09 (3)	1.8e-09 (4)	1.2e-07 (5)
Sm-151	< 1e-12	< 1e-12	< 1e-12	< 1e-12	< 1e-12	< 1e-12	< 1e-12	< 1e-12	< 1e-12
Sn-126	1.5e-10 (63)	< 1e-12	< 1e-12	1.8e-11 (16)	5.0e-12 (86)	< 1e-12	4.2e-12 (5)	1.9e-11 (16)	1.8e-10 (63)
Sr-90	< 1e-12	< 1e-12	< 1e-12	< 1e-12	< 1e-12	< 1e-12	< 1e-12	< 1e-12	< 1e-12
Tc-99	1.1e-08 (29)	2.8e-12 (86)	2.4e-10 (61)	1.9e-09 (5)	1.5e-09 (86)	6.3e-12 (86)	5.8e-08 (4)	7.4e-10 (9)	5.8e-08 (4)
Th-228	< 1e-12	< 1e-12	< 1e-12	< 1e-12	< 1e-12	< 1e-12	< 1e-12	< 1e-12	< 1e-12
Th-229	1.3e-08 (77)	< 1e-12	1.4e-11 (77)	9.8e-10 (77)	8.8e-10 (82)	< 1e-12	6.7e-12 (77)	2.5e-11 (82)	1.5e-08 (77)
Th-230	1.4e-09 (77)	< 1e-12	2.3e-12 (86)	1.2e-10 (77)	1.3e-10 (86)	< 1e-12	1.1e-08 (82)	2.4e-09 (82)	1.5e-08 (82)
Th-232	< 1e-12	< 1e-12	< 1e-12	< 1e-12	< 1e-12	< 1e-12	< 1e-12	< 1e-12	< 1e-12
U-232	< 1e-12	< 1e-12	< 1e-12	< 1e-12	< 1e-12	< 1e-12	< 1e-12	< 1e-12	< 1e-12
U-233	8.6e-10 (82)	< 1e-12	< 1e-12	5.7e-11 (82)	7.0e-11 (86)	< 1e-12	< 1e-12	< 1e-12	9.8e-10 (82)
U-234	6.5e-10 (26)	1.1e-12 (86)	2.1e-12 (49)	1.2e-10 (9)	6.0e-11 (86)	< 1e-12	8.5e-09 (5)	9.8e-10 (82)	9.0e-09 (5)
U-235	3.1e-10 (26)	< 1e-12	1.8e-11 (58)	1.8e-11 (9)	1.3e-11 (86)	< 1e-12	6.1e-07 (4)	3.6e-08 (10)	6.1e-07 (4)
U-236	2.1e-10 (26)	< 1e-12	< 1e-12	6.9e-11 (9)	2.2e-11 (86)	< 1e-12	8.6e-11 (4)	2.2e-11 (10)	2.7e-10 (26)
U-238	5.1e-10 (26)	< 1e-12	2.4e-12 (37)	1.6e-10 (9)	3.3e-11 (86)	< 1e-12	1.5e-06 (4)	2.0e-08 (10)	1.5e-06 (4)
Zr-93	1.4e-09 (26)	1.7e-11 (86)	1.6e-11 (22)	4.3e-10 (5)	1.1e-09 (86)	1.1e-11 (38)	8.8e-11 (4)	1.2e-10 (9)	2.2e-09 (27)

Intrusion wells calculation case (CCL_WI)

Table E-23. Concentration in backfill for CCL_WI (SFR1), peak concentration [Bq/m³] and in parentheses time of peak [1000 year AD].

Nuclide	1BMA	1BTF	2BTF	Silo	1BLA
Ac-227	3.6e+00 (87)	6.1e+00 (87)	< 1	3.7e+00 (87)	3.3e+02 (3)
Ag-108m	4.7e+04 (3)	1.3e+04 (3)	1.7e+04 (3)	9.9e+03 (4)	6.9e+03 (2)
Am-241	3.5e+00 (4)	< 1	< 1	< 1	1.9e+04 (2)
Am-242m	< 1	< 1	< 1	< 1	3.6e+01 (2)
Am-243	3.5e+00 (7)	< 1	< 1	< 1	1.9e+02 (3)
Ba-133	< 1	< 1	< 1	< 1	7.8e+00 (2)
C-14-ind	< 1	< 1	< 1	< 1	< 1
C-14-inorg	1.2e+03 (22)	1.9e+03 (24)	3.5e+03 (23)	4.3e+01 (34)	1.8e+05 (3)
C-14-org	4.6e+06 (4)	7.5e+05 (3)	2.6e+05 (3)	1.2e+07 (4)	3.6e+03 (3)
Ca-41	< 1	< 1	< 1	< 1	< 1
Cd-113m	< 1	< 1	< 1	< 1	7.0e+01 (2)
Cl-36	7.0e+03 (5)	6.9e+02 (3)	6.0e+02 (3)	7.4e+03 (5)	1.1e+03 (3)
Cm-242	< 1	< 1	< 1	< 1	2.4e+01 (2)
Cm-243	< 1	< 1	< 1	< 1	2.7e+01 (2)
Cm-244	< 1	< 1	< 1	< 1	1.9e+03 (2)
Cm-245	< 1	< 1	< 1	< 1	1.9e+00 (3)
Cm-246	< 1	< 1	< 1	< 1	< 1
Co-60	< 1	< 1	< 1	< 1	3.7e+04 (2)
Cs-135	1.1e+04 (7)	3.2e+03 (4)	4.5e+02 (4)	7.5e+03 (10)	1.6e+02 (3)
Cs-137	< 1	< 1	< 1	< 1	6.5e+05 (2)
Eu-152	< 1	< 1	< 1	< 1	3.6e+03 (2)
H-3	< 1	< 1	< 1	< 1	7.1e+03 (2)
Ho-166m	1.7e+00 (5)	< 1	< 1	< 1	1.5e+02 (2)
I-129	1.9e+03 (6)	6.4e+02 (3)	2.9e+02 (3)	4.7e+03 (5)	2.3e+01 (3)
Mo-93	9.6e+03 (5)	6.1e+03 (3)	5.1e+03 (3)	5.7e+04 (5)	4.4e+03 (3)
Nb-93m	4.7e+02 (7)	8.8e+01 (3)	1.8e+02 (5)	1.9e+03 (62)	4.5e+03 (3)
Nb-94	9.2e+01 (25)	4.6e+00 (63)	5.3e+01 (59)	3.4e+01 (34)	1.6e+03 (3)
Ni-59	6.3e+05 (7)	5.2e+04 (4)	9.7e+04 (4)	2.3e+06 (34)	2.1e+05 (3)
Ni-63	1.7e+01 (4)	7.0e+01 (3)	3.7e+02 (3)	< 1	1.1e+07 (2)
Np-237	1.8e+01 (7)	< 1	3.1e+00 (22)	2.4e+01 (34)	8.3e+00 (3)
Pa-231	< 1	< 1	< 1	< 1	3.4e+02 (3)
Pb-210	2.0e+00 (94)	< 1	< 1	1.8e+00 (86)	< 1
Pd-107	6.3e+02 (5)	3.8e+00 (4)	1.3e+02 (3)	8.7e+02 (6)	5.2e+00 (3)
Po-210	1.7e+02 (94)	9.0e+00 (22)	2.3e+01 (96)	1.6e+02 (86)	< 1
Pu-238	< 1	< 1	< 1	< 1	1.2e+04 (2)
Pu-239	2.3e+03 (4)	2.5e+00 (36)	3.6e+02 (4)	7.3e+02 (35)	3.3e+03 (3)
Pu-240	2.7e+03 (4)	< 1	4.3e+02 (4)	2.0e+02 (16)	3.1e+03 (3)
Pu-241	< 1	< 1	< 1	< 1	4.6e+04 (2)
Pu-242	1.7e+01 (4)	< 1	2.7e+00 (4)	1.0e+01 (35)	2.1e+01 (3)
Ra-226	2.7e+01 (95)	1.4e+00 (22)	3.6e+00 (56)	2.5e+01 (86)	< 1
Ra-228	< 1	< 1	< 1	< 1	< 1
Se-79	7.9e+03 (5)	6.5e+02 (3)	7.6e+02 (3)	2.2e+04 (4)	2.1e+01 (3)
Sm-151	< 1	< 1	< 1	< 1	6.0e+03 (2)
Sn-126	1.0e+01 (23)	< 1	2.4e+00 (22)	6.8e+00 (67)	2.6e+00 (3)
Sr-90	< 1	< 1	< 1	< 1	2.6e+04 (2)
Tc-99	2.5e+03 (25)	3.6e+02 (58)	1.2e+03 (22)	3.9e+03 (52)	9.6e+04 (3)
Th-228	< 1	< 1	< 1	< 1	< 1
Th-229	1.1e+00 (85)	< 1	< 1	< 1	< 1
Th-230	< 1	< 1	< 1	< 1	< 1
Th-232	< 1	< 1	< 1	< 1	< 1
U-232	< 1	< 1	< 1	< 1	< 1
U-233	1.8e+00 (56)	< 1	< 1	7.6e+00 (102)	< 1
U-234	4.7e+00 (7)	< 1	< 1	7.2e+00 (34)	1.3e+02 (3)
U-235	1.8e+00 (7)	< 1	< 1	1.7e+00 (34)	1.5e+04 (3)
U-236	1.8e+00 (22)	< 1	< 1	2.7e+00 (34)	2.2e+00 (3)
U-238	3.2e+00 (7)	< 1	1.3e+00 (22)	3.9e+00 (34)	3.8e+04 (3)
Zr-93	1.9e+02 (24)	2.6e+00 (22)	8.5e+01 (6)	9.1e+02 (51)	5.6e+01 (3)

Table E-24. Doses for CCL_WI (SFR1), peak dose [Sv/year] and in parentheses time of peak [1000 year AD].

Nuclide	1BMA	1BTF	2BTF	Silo	1BLA
Total	1.5e-03 (4)	1.4e-04 (3)	1.9e-04 (4)	1.3e-03 (4)	1.6e-02 (2)
Ac-227	2.2e-06 (85)	2.8e-06 (86)	2.1e-08 (22)	3.1e-06 (86)	2.9e-04 (3)
Ag-108m	8.4e-05 (3)	2.2e-05 (3)	3.1e-05 (3)	1.8e-05 (4)	1.2e-05 (2)
Am-241	5.1e-07 (4)	1.5e-08 (4)	6.4e-08 (4)	< 1e-12	2.7e-03 (2)
Am-242m	< 1e-12	< 1e-12	< 1e-12	< 1e-12	5.1e-06 (2)
Am-243	5.0e-07 (7)	< 1e-12	7.5e-09 (4)	< 1e-12	2.8e-05 (3)
Ba-133	< 1e-12	< 1e-12	< 1e-12	< 1e-12	9.0e-09 (2)
C-14-ind	< 1e-12	< 1e-12	< 1e-12	< 1e-12	< 1e-12
C-14-inorg	7.9e-08 (23)	1.4e-07 (25)	2.6e-07 (24)	3.1e-09 (34)	1.3e-05 (3)
C-14-org	3.3e-04 (4)	5.4e-05 (3)	1.9e-05 (3)	8.7e-04 (4)	2.6e-07 (3)
Ca-41	< 1e-12	< 1e-12	< 1e-12	< 1e-12	< 1e-12
Cd-113m	< 1e-12	< 1e-12	< 1e-12	< 1e-12	1.4e-06 (2)
Cl-36	1.5e-05 (5)	1.5e-06 (3)	1.3e-06 (3)	1.6e-05 (5)	2.4e-06 (3)
Cm-242	< 1e-12	< 1e-12	< 1e-12	< 1e-12	2.2e-07 (2)
Cm-243	< 1e-12	< 1e-12	< 1e-12	< 1e-12	3.0e-06 (2)
Cm-244	< 1e-12	< 1e-12	< 1e-12	< 1e-12	1.7e-04 (2)
Cm-245	2.7e-09 (7)	< 1e-12	< 1e-12	< 1e-12	2.9e-07 (3)
Cm-246	< 1e-12	< 1e-12	< 1e-12	< 1e-12	< 1e-12
Co-60	< 1e-12	< 1e-12	< 1e-12	< 1e-12	9.4e-05 (2)
Cs-135	1.6e-05 (7)	4.9e-06 (4)	6.7e-07 (4)	1.1e-05 (10)	2.4e-07 (3)
Cs-137	< 1e-12	< 1e-12	< 1e-12	< 1e-12	6.4e-03 (2)
Eu-152	< 1e-12	< 1e-12	< 1e-12	< 1e-12	3.8e-06 (2)
H-3	< 1e-12	< 1e-12	< 1e-12	< 1e-12	9.5e-08 (2)
Ho-166m	2.5e-09 (5)	1.7e-11 (4)	3.4e-10 (4)	< 1e-12	2.3e-07 (2)
I-129	1.5e-04 (6)	5.2e-05 (3)	2.3e-05 (3)	3.8e-04 (5)	1.8e-06 (3)
Mo-93	1.5e-05 (5)	7.2e-06 (3)	7.9e-06 (3)	7.5e-05 (5)	4.5e-06 (3)
Nb-93m	3.8e-08 (9)	3.4e-09 (3)	1.6e-08 (6)	1.7e-07 (62)	2.4e-07 (2)
Nb-94	1.2e-07 (25)	6.0e-09 (63)	7.1e-08 (59)	4.7e-08 (34)	2.1e-06 (3)
Ni-59	3.0e-05 (7)	2.5e-06 (4)	4.6e-06 (4)	7.5e-05 (35)	9.8e-06 (3)
Ni-63	1.9e-09 (4)	7.9e-09 (3)	4.2e-08 (3)	< 1e-12	1.2e-03 (2)
Np-237	1.5e-06 (7)	< 1e-12	2.3e-07 (23)	1.5e-06 (35)	6.8e-07 (3)
Pa-231	1.6e-08 (78)	2.1e-07 (86)	< 1e-12	1.0e-07 (86)	1.8e-04 (3)
Pb-210	6.5e-07 (77)	1.1e-08 (86)	< 1e-12	8.8e-07 (86)	< 1e-12
Pd-107	1.8e-08 (5)	1.0e-10 (4)	3.7e-09 (3)	2.4e-08 (6)	1.5e-10 (3)
Po-210	1.0e-04 (82)	7.8e-06 (22)	5.4e-06 (77)	1.4e-04 (86)	< 1e-12
Pu-238	1.3e-08 (3)	< 1e-12	< 1e-12	< 1e-12	2.1e-03 (2)
Pu-239	4.2e-04 (4)	4.3e-07 (35)	6.6e-05 (4)	1.3e-04 (35)	6.1e-04 (3)
Pu-240	5.0e-04 (4)	8.5e-08 (17)	7.9e-05 (4)	3.7e-05 (16)	5.8e-04 (3)
Pu-241	1.6e-09 (7)	< 1e-12	< 1e-12	< 1e-12	1.7e-04 (2)
Pu-242	3.1e-06 (4)	< 1e-12	4.6e-07 (4)	1.7e-06 (35)	3.7e-06 (3)
Ra-226	3.1e-06 (82)	2.7e-07 (22)	1.2e-08 (22)	6.0e-06 (86)	< 1e-12
Ra-228	< 1e-12	< 1e-12	< 1e-12	< 1e-12	< 1e-12
Se-79	1.7e-05 (5)	1.4e-06 (3)	1.6e-06 (3)	4.8e-05 (4)	4.5e-08 (3)
Sm-151	< 1e-12	< 1e-12	< 1e-12	< 1e-12	4.3e-07 (2)
Sn-126	3.8e-08 (23)	< 1e-12	8.4e-09 (23)	2.6e-08 (67)	9.9e-09 (3)
Sr-90	< 1e-12	< 1e-12	< 1e-12	< 1e-12	6.5e-04 (2)
Tc-99	1.2e-06 (25)	9.5e-08 (59)	4.1e-07 (23)	1.9e-06 (52)	4.7e-05 (3)
Th-228	< 1e-12	< 1e-12	< 1e-12	< 1e-12	< 1e-12
Th-229	4.2e-07 (85)	< 1e-12	2.9e-08 (59)	1.2e-07 (86)	< 1e-12
Th-230	2.8e-08 (83)	< 1e-12	6.2e-09 (59)	5.8e-08 (86)	< 1e-12
Th-232	< 1e-12	< 1e-12	< 1e-12	< 1e-12	< 1e-12
U-232	< 1e-12	< 1e-12	< 1e-12	< 1e-12	< 1e-12
U-233	5.8e-08 (57)	< 1e-12	5.7e-09 (59)	1.8e-07 (77)	< 1e-12
U-234	1.7e-07 (7)	< 1e-12	2.7e-08 (23)	1.9e-07 (35)	4.6e-06 (3)
U-235	5.7e-08 (7)	6.5e-09 (58)	1.6e-09 (23)	4.0e-08 (35)	5.5e-04 (3)
U-236	5.5e-08 (23)	< 1e-12	1.5e-08 (23)	6.6e-08 (35)	7.6e-08 (3)
U-238	1.1e-07 (7)	< 1e-12	3.9e-08 (23)	1.0e-07 (35)	1.4e-03 (3)
Zr-93	1.5e-07 (24)	2.0e-09 (22)	7.0e-08 (6)	7.4e-07 (51)	4.6e-08 (3)

Table E-25. Concentration in backfill for CCL_WI (SFR3), peak concentration [Bq/m³] and in parentheses time of peak [1000 year AD].

Nuclide	2BMA	BRT	2BLA	3BLA	4BLA	5BLA
Ac-227	< 1	< 1	6.1e+01 (4)	5.7e+01 (4)	5.9e+01 (4)	7.4e+01 (4)
Ag-108m	8.3e+03 (4)	1.4e+04 (3)	1.0e+03 (3)	1.0e+03 (3)	7.4e+02 (3)	9.9e+02 (3)
Am-241	< 1	< 1	1.4e+03 (3)	1.4e+03 (3)	1.0e+03 (3)	1.4e+03 (3)
Am-242m	< 1	< 1	< 1	< 1	< 1	< 1
Am-243	< 1	< 1	9.1e+01 (4)	8.8e+01 (3)	7.5e+01 (4)	9.8e+01 (4)
Ba-133	< 1	< 1	< 1	< 1	< 1	< 1
C-14-ind	2.7e+04 (5)	1.2e+03 (24)	5.6e+03 (4)	5.4e+03 (3)	4.6e+03 (4)	6.1e+03 (4)
C-14-inorg	< 1	< 1	4.4e+03 (4)	4.2e+03 (3)	3.6e+03 (4)	4.7e+03 (4)
C-14-org	2.1e+04 (5)	< 1	1.1e+03 (4)	1.0e+03 (3)	8.7e+02 (4)	1.1e+03 (4)
Ca-41	4.6e+04 (10)	< 1	2.2e+04 (4)	2.1e+04 (3)	1.8e+04 (4)	2.4e+04 (4)
Cd-113m	< 1	< 1	< 1	< 1	< 1	< 1
Cl-36	6.9e+02 (7)	1.2e+01 (29)	2.6e+02 (4)	2.5e+02 (3)	2.2e+02 (4)	2.8e+02 (4)
Cm-242	< 1	< 1	< 1	< 1	< 1	< 1
Cm-243	< 1	< 1	< 1	< 1	< 1	< 1
Cm-244	< 1	< 1	< 1	< 1	< 1	< 1
Cm-245	< 1	< 1	1.1e+00 (4)	1.0e+00 (3)	< 1	1.2e+00 (4)
Cm-246	< 1	< 1	< 1	< 1	< 1	< 1
Co-60	< 1	< 1	< 1	< 1	< 1	< 1
Cs-135	1.2e+02 (7)	< 1	9.9e+02 (4)	9.5e+02 (3)	8.3e+02 (4)	1.1e+03 (4)
Cs-137	< 1	< 1	< 1	< 1	< 1	< 1
Eu-152	< 1	< 1	< 1	< 1	< 1	< 1
H-3	< 1	< 1	< 1	< 1	< 1	< 1
Ho-166m	< 1	< 1	2.2e+02 (3)	2.2e+02 (3)	1.7e+02 (3)	2.3e+02 (3)
I-129	2.0e+01 (25)	< 1	1.1e+01 (4)	1.0e+01 (3)	9.2e+00 (4)	1.2e+01 (4)
Mo-93	4.3e+03 (6)	4.3e+03 (3)	3.9e+02 (3)	3.8e+02 (3)	3.2e+02 (4)	4.2e+02 (4)
Nb-93m	7.3e+01 (5)	7.1e+01 (3)	5.6e+02 (4)	5.4e+02 (3)	4.6e+02 (4)	6.0e+02 (4)
Nb-94	1.2e+01 (67)	5.4e+01 (67)	5.3e+03 (4)	5.1e+03 (3)	4.4e+03 (4)	5.7e+03 (4)
Ni-59	1.8e+05 (67)	1.6e+05 (22)	6.4e+04 (4)	6.2e+04 (3)	5.4e+04 (4)	7.0e+04 (4)
Ni-63	< 1	1.0e+03 (3)	1.4e+03 (3)	1.5e+03 (3)	9.8e+02 (3)	1.3e+03 (3)
Np-237	< 1	< 1	3.7e+00 (4)	3.5e+00 (4)	3.1e+00 (4)	4.0e+00 (4)
Pa-231	< 1	< 1	6.3e+01 (4)	5.8e+01 (4)	6.0e+01 (4)	7.5e+01 (4)
Pb-210	< 1	< 1	< 1	< 1	< 1	< 1
Pd-107	7.9e+03 (7)	< 1	9.7e+00 (4)	9.3e+00 (3)	8.2e+00 (4)	1.1e+01 (4)
Po-210	7.0e+01 (86)	3.0e+00 (22)	< 1	< 1	< 1	< 1
Pu-238	< 1	< 1	< 1	< 1	< 1	< 1
Pu-239	7.4e+00 (60)	5.6e+00 (4)	1.5e+03 (4)	1.4e+03 (3)	1.3e+03 (4)	1.6e+03 (4)
Pu-240	< 1	6.8e+00 (4)	1.4e+03 (4)	1.4e+03 (3)	1.2e+03 (4)	1.5e+03 (4)
Pu-241	< 1	< 1	1.1e+00 (4)	1.0e+00 (3)	< 1	1.2e+00 (4)
Pu-242	< 1	< 1	9.6e+00 (4)	9.2e+00 (3)	8.1e+00 (4)	1.1e+01 (4)
Ra-226	1.1e+01 (86)	< 1	< 1	< 1	< 1	< 1
Ra-228	< 1	< 1	< 1	< 1	< 1	< 1
Se-79	5.4e+01 (5)	< 1	3.3e+01 (4)	3.2e+01 (3)	2.8e+01 (4)	3.6e+01 (4)
Sm-151	< 1	< 1	3.2e+00 (3)	3.3e+00 (3)	2.2e+00 (3)	3.0e+00 (3)
Sn-126	< 1	< 1	4.4e+01 (4)	4.2e+01 (3)	3.7e+01 (4)	4.8e+01 (4)
Sr-90	< 1	< 1	< 1	< 1	< 1	< 1
Tc-99	5.0e+00 (87)	1.8e+01 (58)	2.8e+03 (4)	2.7e+03 (3)	2.3e+03 (4)	3.0e+03 (4)
Th-228	< 1	< 1	< 1	< 1	< 1	< 1
Th-229	< 1	< 1	< 1	< 1	< 1	< 1
Th-230	< 1	< 1	< 1	< 1	< 1	< 1
Th-232	< 1	< 1	< 1	< 1	< 1	< 1
U-232	< 1	< 1	< 1	< 1	< 1	< 1
U-233	< 1	< 1	< 1	< 1	< 1	< 1
U-234	< 1	< 1	9.9e+00 (4)	9.4e+00 (4)	8.8e+00 (4)	1.1e+01 (4)
U-235	< 1	< 1	1.8e+03 (4)	1.7e+03 (3)	1.5e+03 (4)	2.0e+03 (4)
U-236	< 1	< 1	1.2e+00 (4)	1.2e+00 (4)	1.0e+00 (4)	1.4e+00 (4)
U-238	< 1	< 1	1.0e+03 (4)	9.6e+02 (3)	8.4e+02 (4)	1.1e+03 (4)
Zr-93	1.5e+01 (87)	1.2e+01 (22)	1.7e+02 (4)	1.6e+02 (3)	1.4e+02 (4)	1.8e+02 (4)

Table E-26. Doses for CCL_WI (SFR3), peak dose [Sv/year] and in parentheses time of peak [1000 year AD].

Nuclide	2BMA	BRT	2BLA	3BLA	4BLA	5BLA
Total	7.3e-05 (86)	3.9e-05 (3)	9.2e-04 (3)	9.0e-04 (3)	7.5e-04 (4)	9.8e-04 (4)
Ac-227	< 1e-12	< 1e-12	5.5e-05 (4)	5.1e-05 (4)	5.2e-05 (4)	6.6e-05 (4)
Ag-108m	1.5e-05 (4)	2.5e-05 (3)	1.8e-06 (3)	1.8e-06 (3)	1.3e-06 (3)	1.8e-06 (3)
Am-241	< 1e-12	4.5e-08 (4)	2.0e-04 (3)	2.0e-04 (3)	1.5e-04 (3)	2.0e-04 (3)
Am-242m	< 1e-12	< 1e-12	< 1e-12	< 1e-12	< 1e-12	< 1e-12
Am-243	< 1e-12	1.5e-08 (4)	1.3e-05 (4)	1.3e-05 (3)	1.1e-05 (4)	1.5e-05 (4)
Ba-133	< 1e-12	< 1e-12	< 1e-12	< 1e-12	< 1e-12	< 1e-12
C-14-ind	2.0e-06 (5)	8.6e-08 (24)	4.0e-07 (4)	3.9e-07 (3)	3.3e-07 (4)	4.4e-07 (4)
C-14-inorg	3.4e-11 (24)	< 1e-12	3.1e-07 (4)	3.0e-07 (3)	2.6e-07 (4)	3.4e-07 (4)
C-14-org	1.5e-06 (5)	< 1e-12	7.6e-08 (4)	7.3e-08 (3)	6.3e-08 (4)	8.2e-08 (4)
Ca-41	7.3e-06 (10)	< 1e-12	3.4e-06 (4)	3.3e-06 (3)	2.9e-06 (4)	3.8e-06 (4)
Cd-113m	< 1e-12	< 1e-12	< 1e-12	< 1e-12	< 1e-12	< 1e-12
Cl-36	1.5e-06 (7)	2.5e-08 (29)	5.5e-07 (4)	5.2e-07 (3)	4.6e-07 (4)	6.0e-07 (4)
Cm-242	< 1e-12	< 1e-12	< 1e-12	< 1e-12	< 1e-12	< 1e-12
Cm-243	< 1e-12	< 1e-12	< 1e-12	< 1e-12	< 1e-12	< 1e-12
Cm-244	< 1e-12	< 1e-12	< 1e-12	< 1e-12	< 1e-12	< 1e-12
Cm-245	< 1e-12	< 1e-12	1.7e-07 (4)	1.6e-07 (3)	< 1e-12	1.8e-07 (4)
Cm-246	< 1e-12	< 1e-12	< 1e-12	< 1e-12	< 1e-12	< 1e-12
Co-60	< 1e-12	< 1e-12	< 1e-12	< 1e-12	< 1e-12	< 1e-12
Cs-135	1.8e-07 (7)	< 1e-12	1.5e-06 (4)	1.4e-06 (3)	1.2e-06 (4)	1.6e-06 (4)
Cs-137	< 1e-12	< 1e-12	< 1e-12	< 1e-12	< 1e-12	< 1e-12
Eu-152	< 1e-12	< 1e-12	< 1e-12	< 1e-12	< 1e-12	< 1e-12
H-3	< 1e-12	< 1e-12	< 1e-12	< 1e-12	< 1e-12	< 1e-12
Ho-166m	< 1e-12	< 1e-12	3.5e-07 (3)	3.4e-07 (3)	2.7e-07 (3)	3.6e-07 (3)
I-129	1.7e-06 (25)	< 1e-12	8.9e-07 (4)	8.5e-07 (3)	7.4e-07 (4)	9.7e-07 (4)
Mo-93	1.1e-05 (6)	1.2e-05 (3)	6.4e-07 (3)	6.2e-07 (3)	5.3e-07 (4)	6.9e-07 (4)
Nb-93m	6.0e-09 (5)	6.3e-09 (3)	3.6e-08 (4)	3.4e-08 (3)	2.9e-08 (4)	3.8e-08 (4)
Nb-94	1.6e-08 (67)	7.3e-08 (67)	7.1e-06 (4)	6.8e-06 (3)	5.9e-06 (4)	7.7e-06 (4)
Ni-59	8.7e-06 (67)	6.8e-06 (4)	3.1e-06 (4)	2.9e-06 (3)	2.6e-06 (4)	3.3e-06 (4)
Ni-63	< 1e-12	1.2e-07 (3)	1.6e-07 (3)	1.7e-07 (3)	1.1e-07 (3)	1.5e-07 (3)
Np-237	< 1e-12	< 1e-12	3.0e-07 (4)	2.9e-07 (4)	2.6e-07 (4)	3.3e-07 (4)
Pa-231	< 1e-12	< 1e-12	3.3e-05 (4)	3.1e-05 (4)	3.2e-05 (4)	3.9e-05 (4)
Pb-210	3.3e-07 (86)	< 1e-12	< 1e-12	< 1e-12	< 1e-12	< 1e-12
Pd-107	2.2e-07 (7)	< 1e-12	2.7e-10 (4)	2.6e-10 (3)	2.3e-10 (4)	3.0e-10 (4)
Po-210	6.2e-05 (86)	2.4e-06 (22)	< 1e-12	< 1e-12	< 1e-12	< 1e-12
Pu-238	< 1e-12	< 1e-12	< 1e-12	< 1e-12	< 1e-12	< 1e-12
Pu-239	1.3e-06 (60)	1.0e-06 (4)	2.8e-04 (4)	2.7e-04 (3)	2.3e-04 (4)	3.0e-04 (4)
Pu-240	2.1e-08 (25)	1.2e-06 (4)	2.6e-04 (4)	2.5e-04 (3)	2.2e-04 (4)	2.8e-04 (4)
Pu-241	< 1e-12	< 1e-12	3.9e-09 (4)	3.8e-09 (3)	< 1e-12	4.3e-09 (4)
Pu-242	1.7e-08 (67)	< 1e-12	1.7e-06 (4)	1.6e-06 (3)	1.4e-06 (4)	1.9e-06 (4)
Ra-226	2.5e-06 (86)	2.8e-08 (22)	< 1e-12	< 1e-12	< 1e-12	< 1e-12
Ra-228	< 1e-12	< 1e-12	< 1e-12	< 1e-12	< 1e-12	< 1e-12
Se-79	1.2e-07 (5)	< 1e-12	7.2e-08 (4)	6.9e-08 (3)	6.1e-08 (4)	7.9e-08 (4)
Sm-151	< 1e-12	< 1e-12	2.3e-10 (3)	2.4e-10 (3)	1.6e-10 (3)	2.2e-10 (3)
Sn-126	< 1e-12	< 1e-12	1.7e-07 (4)	1.6e-07 (3)	1.4e-07 (4)	1.9e-07 (4)
Sr-90	< 1e-12	< 1e-12	< 1e-12	< 1e-12	< 1e-12	< 1e-12
Tc-99	2.4e-09 (86)	8.4e-09 (59)	1.4e-06 (4)	1.3e-06 (3)	1.2e-06 (4)	1.5e-06 (4)
Th-228	< 1e-12	< 1e-12	< 1e-12	< 1e-12	< 1e-12	< 1e-12
Th-229	< 1e-12	< 1e-12	< 1e-12	< 1e-12	< 1e-12	< 1e-12
Th-230	< 1e-12	< 1e-12	< 1e-12	< 1e-12	< 1e-12	< 1e-12
Th-232	< 1e-12	< 1e-12	< 1e-12	< 1e-12	< 1e-12	< 1e-12
U-232	< 1e-12	< 1e-12	< 1e-12	< 1e-12	< 1e-12	< 1e-12
U-233	< 1e-12	< 1e-12	< 1e-12	< 1e-12	< 1e-12	< 1e-12
U-234	< 1e-12	< 1e-12	3.6e-07 (4)	3.4e-07 (4)	3.2e-07 (4)	4.1e-07 (4)
U-235	< 1e-12	< 1e-12	6.4e-05 (4)	6.2e-05 (3)	5.4e-05 (4)	7.0e-05 (4)
U-236	< 1e-12	< 1e-12	4.3e-08 (4)	4.1e-08 (4)	3.6e-08 (4)	4.7e-08 (4)
U-238	< 1e-12	< 1e-12	3.6e-05 (4)	3.4e-05 (3)	3.0e-05 (4)	3.9e-05 (4)
Zr-93	1.2e-08 (86)	9.2e-09 (23)	1.4e-07 (4)	1.3e-07 (3)	1.1e-07 (4)	1.5e-07 (4)

Scenario combination 1 calculation case (CCC_SC1)

Table E-27. Near-field releases for CCC_SC1, peak release [Bq/year] and in parentheses time of peak [1000 year AD].

Nuclide	1BMA	2BMA	1BTF	2BTF	Silo	BRT	1BLA	2-5BLA	Total
Ac-227	2.3e+02 (83)	1.8e+00 (86)	5.5e+01 (86)	2.4e+00 (5)	1.7e+01 (67)	<1	3.6e+04 (3)	7.4e+03 (3)	3.9e+04 (3)
Ag-108m	6.8e+06 (3)	1.9e+06 (3)	2.9e+05 (3)	1.5e+06 (3)	4.8e+04 (4)	6.0e+05 (3)	2.4e+05 (3)	1.9e+05 (3)	1.0e+07 (3)
Am-241	5.6e+03 (3)	1.3e+00 (5)	1.1e+02 (4)	1.6e+03 (4)	<1	4.0e+01 (4)	6.8e+05 (3)	2.5e+05 (3)	7.5e+05 (3)
Am-242m	<1	<1	<1	<1	<1	<1	4.5e+01 (3)	1.3e+01 (3)	4.5e+01 (3)
Am-243	1.8e+03 (7)	2.5e+01 (25)	1.9e+01 (4)	3.5e+02 (4)	<1	1.8e+01 (22)	2.2e+04 (3)	1.4e+04 (3)	2.7e+04 (3)
Ba-133	<1	<1	<1	<1	<1	<1	<1	<1	<1
C-14-ind	<1	2.2e+06 (3)	<1	<1	<1	3.2e+04 (23)	<1	8.6e+05 (3)	3.1e+06 (3)
C-14-inorg	2.2e+07 (5)	1.7e+03 (23)	6.4e+05 (4)	8.6e+06 (4)	1.2e+03 (30)	<1	2.1e+07 (3)	6.7e+05 (3)	3.5e+07 (3)
C-14-org	1.9e+08 (3)	1.7e+06 (3)	9.5e+06 (3)	1.9e+07 (3)	6.8e+07 (5)	<1	4.2e+05 (3)	1.6e+05 (3)	2.2e+08 (3)
Ca-41	<1	4.4e+06 (7)	<1	<1	<1	<1	<1	3.3e+06 (3)	4.5e+06 (7)
Cd-113m	<1	<1	<1	<1	<1	<1	<1	<1	<1
Cl-36	2.6e+05 (3)	5.4e+04 (4)	1.2e+04 (3)	5.4e+04 (3)	4.9e+04 (5)	2.7e+02 (25)	1.3e+05 (3)	3.9e+04 (3)	4.6e+05 (3)
Cm-242	<1	<1	<1	<1	<1	<1	3.7e+01 (3)	1.1e+01 (3)	3.7e+01 (3)
Cm-243	<1	<1	<1	<1	<1	<1	<1	<1	<1
Cm-244	<1	<1	<1	<1	<1	<1	<1	<1	<1
Cm-245	1.6e+01 (7)	<1	<1	1.9e+00 (4)	<1	<1	2.2e+02 (3)	1.7e+02 (3)	2.8e+02 (3)
Cm-246	3.0e+00 (7)	<1	<1	<1	<1	<1	5.4e+01 (3)	4.6e+01 (3)	7.4e+01 (3)
Co-60	<1	<1	<1	<1	<1	<1	<1	<1	<1
Cs-135	3.9e+05 (3)	1.0e+04 (7)	4.1e+04 (3)	4.2e+04 (3)	3.7e+04 (9)	<1	1.8e+04 (3)	1.5e+05 (3)	6.0e+05 (3)
Cs-137	<1	<1	<1	<1	<1	<1	<1	<1	<1
Eu-152	<1	<1	<1	<1	<1	<1	<1	<1	<1
H-3	<1	<1	<1	<1	<1	<1	<1	<1	<1
Ho-166m	2.0e+03 (4)	<1	2.6e+01 (4)	6.1e+02 (4)	<1	<1	1.4e+04 (3)	3.7e+04 (3)	4.2e+04 (3)
I-129	1.1e+05 (3)	1.5e+03 (5)	1.2e+04 (3)	3.2e+04 (3)	3.2e+04 (5)	<1	2.6e+03 (3)	1.6e+03 (3)	1.5e+05 (3)
Mo-93	1.2e+06 (3)	5.2e+05 (4)	1.4e+05 (3)	5.8e+05 (3)	3.8e+05 (5)	1.6e+05 (3)	5.1e+05 (3)	6.1e+04 (3)	2.4e+06 (3)
Nb-93m	7.3e+04 (5)	8.3e+03 (4)	1.7e+03 (3)	1.2e+04 (4)	9.7e+03 (47)	2.6e+03 (3)	5.1e+05 (3)	8.6e+04 (3)	5.5e+05 (3)
Nb-94	4.0e+04 (7)	1.1e+04 (30)	2.7e+02 (22)	1.3e+04 (5)	4.3e+02 (34)	4.1e+03 (63)	1.8e+05 (3)	7.9e+05 (3)	8.3e+05 (3)
Ni-59	1.0e+08 (5)	2.1e+07 (24)	4.1e+06 (4)	1.9e+07 (3)	1.3e+07 (34)	9.9e+06 (4)	2.4e+07 (3)	9.6e+06 (3)	1.2e+08 (3)
Ni-63	2.6e+06 (3)	3.6e+01 (4)	2.6e+04 (3)	4.9e+05 (3)	<1	7.1e+04 (3)	1.8e+06 (3)	3.4e+05 (3)	4.3e+06 (3)
Np-237	1.4e+03 (7)	1.0e+01 (37)	2.4e+00 (22)	5.0e+02 (4)	1.5e+02 (34)	1.6e+00 (22)	9.4e+02 (3)	5.3e+02 (3)	2.7e+03 (3)
Pa-231	2.8e+01 (82)	<1	1.1e+01 (58)	1.0e+00 (22)	1.1e+01 (77)	<1	3.7e+04 (3)	7.6e+03 (3)	4.0e+04 (3)
Pb-210	1.5e+02 (77)	9.9e+01 (82)	1.8e+00 (22)	3.0e+00 (4)	1.2e+01 (86)	1.9e+00 (22)	9.7e+00 (3)	3.3e+00 (4)	2.2e+02 (82)
Pd-107	4.2e+04 (3)	6.3e+05 (4)	3.1e+02 (4)	1.3e+04 (3)	4.2e+03 (6)	<1	5.9e+02 (3)	1.4e+03 (3)	6.4e+05 (4)
Po-210	1.2e+04 (77)	8.6e+03 (82)	1.4e+02 (22)	8.3e+01 (22)	9.2e+02 (86)	1.6e+02 (22)	9.7e+00 (3)	3.3e+00 (4)	1.8e+04 (82)
Pu-238	1.2e+02 (3)	<1	<1	4.3e+01 (3)	<1	<1	8.6e+02 (3)	1.9e+02 (3)	9.0e+02 (3)
Pu-239	1.7e+05 (3)	2.3e+03 (23)	1.8e+02 (13)	7.6e+04 (3)	4.1e+03 (35)	2.8e+02 (12)	3.8e+05 (3)	2.2e+05 (3)	6.9e+05 (3)
Pu-240	2.1e+05 (3)	6.0e+02 (23)	1.5e+02 (7)	9.8e+04 (3)	1.4e+03 (15)	3.2e+02 (4)	3.6e+05 (3)	2.2e+05 (3)	7.3e+05 (3)
Pu-241	2.6e+02 (5)	2.7e+01 (29)	3.5e+00 (11)	5.9e+01 (4)	<1	<1	2.2e+02 (3)	1.7e+02 (3)	3.7e+02 (3)
Pu-242	1.2e+03 (3)	3.0e+01 (25)	1.8e+00 (26)	5.7e+02 (3)	5.5e+01 (35)	2.8e+00 (23)	2.4e+03 (3)	1.4e+03 (3)	4.6e+03 (3)
Ra-226	1.2e+03 (77)	1.0e+03 (82)	2.2e+01 (22)	5.5e+00 (22)	2.2e+02 (77)	1.9e+01 (22)	1.0e+01 (3)	3.4e+00 (4)	2.2e+03 (77)
Ra-228	<1	<1	<1	<1	<1	<1	<1	<1	<1
Se-79	4.3e+05 (3)	3.7e+03 (3)	1.4e+04 (3)	5.4e+04 (3)	1.4e+05 (5)	<1	2.4e+03 (3)	5.0e+03 (3)	5.0e+05 (3)
Sm-151	1.7e+01 (3)	<1	<1	<1	<1	<1	4.5e+02 (3)	7.6e+02 (3)	1.0e+03 (3)
Sn-126	9.5e+02 (3)	4.2e+00 (25)	2.8e+00 (59)	3.1e+02 (3)	3.9e+01 (52)	<1	3.0e+02 (3)	6.6e+03 (3)	7.9e+03 (3)
Sr-90	<1	<1	<1	<1	<1	<1	<1	<1	<1
Tc-99	8.6e+05 (7)	1.9e+03 (52)	1.0e+04 (22)	1.5e+05 (4)	3.5e+04 (41)	1.8e+03 (58)	1.1e+07 (3)	4.2e+05 (3)	1.1e+07 (3)
Th-228	<1	<1	<1	<1	<1	<1	<1	<1	<1
Th-229	1.2e+02 (83)	<1	<1	3.1e+00 (58)	6.9e+00 (86)	<1	<1	<1	1.3e+02 (83)
Th-230	3.5e+01 (83)	2.9e+00 (86)	<1	2.5e+00 (22)	6.0e+00 (86)	<1	7.2e+01 (3)	1.3e+01 (4)	7.7e+01 (3)
Th-232	<1	<1	<1	<1	<1	<1	<1	<1	<1
U-232	<1	<1	<1	<1	<1	<1	<1	<1	<1
U-233	5.8e+01 (22)	3.8e+00 (77)	<1	5.7e+00 (22)	2.6e+01 (77)	<1	3.2e+00 (3)	2.5e+00 (4)	8.1e+01 (77)
U-234	4.2e+02 (3)	1.1e+01 (27)	<1	1.5e+02 (4)	3.7e+01 (34)	<1	1.4e+04 (3)	1.4e+03 (3)	1.5e+04 (3)
U-235	2.0e+02 (3)	<1	4.9e+00 (58)	2.7e+01 (4)	9.0e+00 (34)	<1	1.8e+06 (3)	2.7e+05 (3)	1.8e+06 (3)
U-236	1.0e+02 (3)	5.3e+00 (35)	<1	9.0e+01 (4)	1.4e+01 (34)	<1	2.5e+02 (3)	1.8e+02 (3)	4.8e+02 (3)
U-238	3.3e+02 (3)	<1	1.2e+00 (25)	2.1e+02 (4)	2.0e+01 (34)	<1	4.4e+06 (3)	1.5e+05 (3)	4.4e+06 (3)
Zr-93	3.8e+04 (5)	2.7e+03 (40)	1.7e+02 (9)	1.1e+04 (4)	1.4e+04 (34)	9.7e+02 (22)	6.5e+03 (3)	2.5e+04 (3)	5.8e+04 (4)

Table E-28. Far-field releases for CCC_SC1, peak release [Bq/year] and in parentheses time of peak [1000 year AD].

Nuclide	1BMA	2BMA	1BTF	2BTF	Silo	BRT	1BLA	2-5BLA	Total
Ac-227	2.3e+02 (84)	< 1	1.8e+01 (86)	3.4e+00 (25)	4.9e+01 (86)	< 1	1.4e+04 (5)	6.4e+03 (82)	1.6e+04 (5)
Ag-108m	6.5e+06 (3)	1.6e+06 (4)	2.1e+05 (3)	1.3e+06 (3)	4.2e+04 (4)	3.1e+05 (3)	2.0e+05 (3)	1.3e+05 (3)	8.5e+06 (3)
Am-241	1.6e+03 (4)	< 1	1.7e+00 (4)	3.6e+01 (4)	< 1	< 1	5.6e+04 (3)	4.3e+03 (4)	5.7e+04 (3)
Am-242m	< 1	< 1	< 1	< 1	< 1	< 1	2.9e+00 (3)	< 1	2.9e+00 (3)
Am-243	4.0e+02 (7)	6.1e+00 (28)	1.7e+00 (13)	2.3e+01 (5)	< 1	< 1	2.1e+03 (3)	5.2e+02 (5)	2.1e+03 (3)
Ba-133	< 1	< 1	< 1	< 1	< 1	< 1	< 1	< 1	< 1
C-14-ind	< 1	2.2e+06 (4)	< 1	< 1	< 1	2.8e+04 (23)	< 1	8.0e+05 (4)	3.0e+06 (4)
C-14-inorg	2.1e+07 (5)	1.5e+03 (23)	5.5e+05 (4)	8.2e+06 (4)	1.2e+03 (30)	< 1	1.9e+07 (3)	6.2e+05 (4)	3.3e+07 (3)
C-14-org	1.8e+08 (3)	1.7e+06 (4)	7.3e+06 (3)	1.7e+07 (3)	6.6e+07 (5)	< 1	3.8e+05 (3)	1.5e+05 (4)	2.0e+08 (3)
Ca-41	< 1	3.6e+06 (8)	< 1	< 1	< 1	< 1	< 1	3.1e+06 (4)	3.6e+06 (8)
Cd-113m	< 1	< 1	< 1	< 1	< 1	< 1	< 1	< 1	< 1
Cl-36	2.6e+05 (3)	5.2e+04 (5)	9.3e+03 (3)	4.6e+04 (3)	4.8e+04 (5)	2.6e+02 (29)	1.2e+05 (3)	3.7e+04 (4)	4.2e+05 (3)
Cm-242	< 1	< 1	< 1	< 1	< 1	< 1	1.8e+00 (3)	< 1	1.8e+00 (3)
Cm-243	< 1	< 1	< 1	< 1	< 1	< 1	< 1	< 1	< 1
Cm-244	< 1	< 1	< 1	< 1	< 1	< 1	< 1	< 1	< 1
Cm-245	5.4e+00 (7)	< 1	< 1	< 1	< 1	< 1	2.0e+01 (3)	6.9e+00 (5)	2.1e+01 (3)
Cm-246	1.0e+00 (7)	< 1	< 1	< 1	< 1	< 1	5.0e+00 (3)	1.7e+00 (5)	5.1e+00 (3)
Co-60	< 1	< 1	< 1	< 1	< 1	< 1	< 1	< 1	< 1
Cs-135	3.3e+05 (4)	3.3e+03 (5)	1.1e+04 (4)	9.1e+03 (4)	2.2e+04 (9)	< 1	5.7e+03 (3)	2.7e+04 (4)	3.8e+05 (4)
Cs-137	< 1	< 1	< 1	< 1	< 1	< 1	< 1	< 1	< 1
Eu-152	< 1	< 1	< 1	< 1	< 1	< 1	< 1	< 1	< 1
H-3	< 1	< 1	< 1	< 1	< 1	< 1	< 1	< 1	< 1
Ho-166m	8.7e+02 (5)	< 1	1.4e+00 (4)	1.1e+02 (4)	< 1	< 1	1.2e+03 (3)	1.0e+03 (4)	2.4e+03 (4)
I-129	1.1e+05 (3)	1.5e+03 (5)	9.7e+03 (3)	2.6e+04 (3)	3.1e+04 (5)	< 1	2.3e+03 (3)	1.6e+03 (4)	1.4e+05 (3)
Mo-93	1.2e+06 (3)	4.6e+05 (5)	1.1e+05 (3)	4.7e+05 (3)	3.6e+05 (5)	1.4e+05 (4)	4.6e+05 (3)	5.6e+04 (4)	2.1e+06 (3)
Nb-93m	5.0e+04 (5)	2.5e+03 (5)	4.6e+02 (3)	5.2e+03 (9)	1.2e+04 (86)	5.6e+02 (4)	1.3e+04 (3)	9.9e+02 (9)	5.8e+04 (5)
Nb-94	1.6e+04 (9)	2.7e+03 (38)	5.3e+01 (25)	3.3e+03 (9)	1.2e+02 (34)	2.6e+02 (67)	1.4e+04 (3)	2.7e+04 (5)	4.6e+04 (5)
Ni-59	8.5e+07 (5)	8.1e+06 (27)	1.0e+06 (5)	8.4e+06 (4)	5.0e+06 (35)	1.2e+06 (5)	7.4e+06 (3)	2.0e+06 (4)	9.1e+07 (5)
Ni-63	1.1e+06 (3)	2.8e+00 (4)	1.6e+03 (4)	7.5e+04 (3)	< 1	1.6e+03 (4)	3.8e+05 (3)	1.5e+04 (3)	1.4e+06 (3)
Np-237	7.1e+02 (5)	2.4e+00 (86)	< 1	5.9e+01 (5)	2.1e+01 (86)	< 1	4.5e+01 (3)	8.2e+00 (9)	7.8e+02 (5)
Pa-231	2.0e+01 (83)	< 1	2.4e+00 (86)	< 1	2.6e+00 (86)	< 1	2.3e+03 (4)	7.3e+02 (82)	2.3e+03 (4)
Pb-210	1.0e+02 (77)	2.3e+01 (85)	< 1	3.8e+00 (77)	7.3e+00 (86)	< 1	2.6e+02 (77)	8.3e+01 (82)	4.6e+02 (77)
Pd-107	4.1e+04 (3)	6.6e+05 (5)	2.9e+02 (4)	1.1e+04 (3)	4.1e+03 (6)	< 1	5.4e+02 (3)	1.4e+03 (4)	6.8e+05 (5)
Po-210	1.4e+02 (77)	2.4e+01 (84)	< 1	4.1e+00 (77)	8.3e+00 (86)	< 1	2.9e+02 (77)	8.1e+01 (77)	5.3e+02 (77)
Pu-238	1.5e+01 (3)	< 1	< 1	< 1	< 1	< 1	4.9e+01 (3)	< 1	5.9e+01 (3)
Pu-239	8.0e+04 (5)	3.1e+02 (33)	5.1e+01 (28)	8.2e+03 (4)	1.3e+03 (36)	3.7e+01 (30)	3.7e+04 (3)	1.1e+04 (5)	1.1e+05 (4)
Pu-240	8.8e+04 (5)	5.7e+01 (25)	3.0e+01 (9)	1.0e+04 (4)	3.1e+02 (18)	8.9e+00 (15)	3.5e+04 (3)	8.9e+03 (5)	1.2e+05 (4)
Pu-241	4.7e+01 (5)	< 1	< 1	< 1	< 1	< 1	4.0e+01 (4)	8.6e+00 (5)	7.1e+01 (5)
Pu-242	6.2e+02 (5)	7.1e+00 (86)	< 1	6.1e+01 (4)	2.0e+01 (52)	< 1	2.3e+02 (3)	7.0e+01 (5)	7.9e+02 (5)
Ra-226	1.2e+03 (77)	2.3e+02 (84)	8.0e+00 (22)	6.0e+01 (77)	1.4e+02 (82)	3.1e+00 (22)	4.8e+03 (77)	1.5e+03 (77)	7.8e+03 (77)
Ra-228	< 1	< 1	< 1	< 1	< 1	< 1	< 1	< 1	< 1
Se-79	4.1e+05 (3)	3.8e+03 (4)	1.1e+04 (3)	4.8e+04 (3)	1.3e+05 (5)	< 1	2.2e+03 (3)	4.7e+03 (4)	4.7e+05 (3)
Sm-151	2.9e+00 (3)	< 1	< 1	< 1	< 1	< 1	2.4e+01 (3)	1.7e+00 (3)	2.5e+01 (3)
Sn-126	3.3e+02 (9)	< 1	< 1	1.7e+01 (10)	4.5e+00 (67)	< 1	5.5e+00 (4)	2.8e+01 (12)	3.8e+02 (9)
Sr-90	< 1	< 1	< 1	< 1	< 1	< 1	< 1	< 1	< 1
Tc-99	2.6e+05 (7)	4.4e+02 (86)	1.0e+03 (59)	1.5e+04 (5)	8.2e+03 (86)	9.5e+01 (86)	5.3e+05 (4)	7.7e+03 (5)	5.8e+05 (4)
Th-228	< 1	< 1	< 1	< 1	< 1	< 1	< 1	< 1	< 1
Th-229	9.0e+01 (84)	< 1	< 1	3.6e+00 (77)	8.6e+00 (77)	< 1	< 1	< 1	1.0e+02 (84)
Th-230	2.9e+01 (83)	1.0e+00 (82)	< 1	1.6e+00 (77)	3.9e+00 (82)	< 1	1.7e+02 (77)	4.5e+01 (82)	2.5e+02 (82)
Th-232	< 1	< 1	< 1	< 1	< 1	< 1	< 1	< 1	< 1
U-232	< 1	< 1	< 1	< 1	< 1	< 1	< 1	< 1	< 1
U-233	4.0e+01 (82)	< 1	< 1	3.1e+00 (77)	6.9e+00 (86)	< 1	< 1	< 1	5.1e+01 (82)
U-234	1.9e+02 (5)	1.5e+00 (86)	< 1	1.2e+01 (5)	6.0e+00 (86)	< 1	1.0e+03 (4)	6.9e+01 (82)	1.1e+03 (4)
U-235	9.0e+01 (5)	< 1	1.4e+00 (86)	2.2e+00 (5)	1.5e+00 (86)	< 1	9.0e+04 (4)	4.9e+03 (5)	8.8e+04 (4)
U-236	4.9e+01 (5)	< 1	< 1	7.5e+00 (5)	2.5e+00 (86)	< 1	1.3e+01 (4)	3.5e+00 (5)	6.4e+01 (5)
U-238	1.5e+02 (5)	< 1	< 1	1.7e+01 (5)	3.5e+00 (86)	< 1	2.2e+05 (4)	2.7e+03 (5)	2.2e+05 (4)
Zr-93	2.5e+04 (5)	7.1e+02 (86)	4.1e+01 (23)	1.9e+03 (5)	4.2e+03 (86)	6.7e+01 (34)	4.5e+02 (4)	6.6e+02 (5)	2.8e+04 (5)

Table E-29. Doses for CCC_SC1, peak dose [Sv/year] and in parentheses time of peak [1000 year AD].

Nuclide	1BMA	2BMA	1BTF	2BTF	Silo	BRT	1BLA	2-5BLA	Total
Total	5.3e-06 (5)	3.9e-06 (6)	5.3e-07 (5)	7.3e-07 (5)	4.8e-06 (7)	5.1e-07 (5)	1.5e-06 (7)	5.5e-07 (8)	1.6e-05 (6)
Ac-227	1.2e-09 (67)	2.6e-12 (86)	4.4e-11 (86)	3.9e-11 (42)	1.0e-10 (86)	< 1e-12	2.3e-07 (30)	1.1e-07 (57)	3.3e-07 (35)
Ag-108m	4.3e-08 (5)	3.7e-08 (5)	2.3e-09 (5)	4.8e-09 (5)	1.9e-09 (5)	4.3e-09 (3)	5.0e-10 (5)	2.5e-09 (5)	9.4e-08 (5)
Am-241	2.6e-11 (5)	< 1e-12	< 1e-12	< 1e-12	< 1e-12	< 1e-12	3.2e-10 (4)	4.1e-09 (4)	4.2e-09 (4)
Am-242m	< 1e-12	< 1e-12	< 1e-12	< 1e-12	< 1e-12	< 1e-12	< 1e-12	< 1e-12	< 1e-12
Am-243	2.5e-10 (19)	1.5e-11 (41)	4.6e-12 (27)	2.9e-11 (24)	< 1e-12	2.4e-12 (25)	2.8e-10 (14)	5.9e-10 (5)	8.6e-10 (17)
Ba-133	< 1e-12	< 1e-12	< 1e-12	< 1e-12	< 1e-12	< 1e-12	< 1e-12	< 1e-12	< 1e-12
C-14-ind	< 1e-12	3.2e-08 (5)	< 1e-12	< 1e-12	< 1e-12	7.7e-10 (23)	< 1e-12	7.0e-09 (5)	3.9e-08 (5)
C-14-inorg	6.1e-07 (5)	4.1e-11 (23)	1.5e-08 (6)	9.1e-08 (4)	3.4e-11 (30)	< 1e-12	8.5e-08 (3)	5.4e-09 (5)	7.1e-07 (5)
C-14-org	1.4e-06 (3)	2.5e-08 (5)	7.5e-08 (3)	6.0e-08 (3)	1.9e-06 (5)	< 1e-12	1.7e-09 (3)	1.3e-09 (5)	2.4e-06 (5)
Ca-41	< 1e-12	1.5e-06 (15)	< 1e-12	< 1e-12	< 1e-12	< 1e-12	< 1e-12	4.6e-07 (9)	1.9e-06 (14)
Cd-113m	< 1e-12	< 1e-12	< 1e-12	< 1e-12	< 1e-12	< 1e-12	< 1e-12	< 1e-12	< 1e-12
Cl-36	3.6e-07 (5)	1.7e-07 (5)	1.1e-08 (5)	1.1e-08 (5)	1.5e-07 (5)	8.8e-10 (29)	2.3e-08 (3)	4.4e-08 (5)	7.1e-07 (5)
Cm-242	< 1e-12	< 1e-12	< 1e-12	< 1e-12	< 1e-12	< 1e-12	< 1e-12	< 1e-12	< 1e-12
Cm-243	< 1e-12	< 1e-12	< 1e-12	< 1e-12	< 1e-12	< 1e-12	< 1e-12	< 1e-12	< 1e-12
Cm-244	< 1e-12	< 1e-12	< 1e-12	< 1e-12	< 1e-12	< 1e-12	< 1e-12	< 1e-12	< 1e-12
Cm-245	3.4e-12 (18)	< 1e-12	< 1e-12	< 1e-12	< 1e-12	< 1e-12	3.1e-12 (14)	7.7e-12 (5)	1.1e-11 (17)
Cm-246	< 1e-12	< 1e-12	< 1e-12	< 1e-12	< 1e-12	< 1e-12	< 1e-12	1.6e-12 (5)	1.8e-12 (5)
Co-60	< 1e-12	< 1e-12	< 1e-12	< 1e-12	< 1e-12	< 1e-12	< 1e-12	< 1e-12	< 1e-12
Cs-135	7.5e-07 (86)	2.4e-08 (86)	4.5e-08 (86)	1.4e-08 (86)	6.4e-07 (86)	< 1e-12	2.6e-09 (86)	1.0e-07 (86)	1.6e-06 (86)
Cs-137	< 1e-12	< 1e-12	< 1e-12	< 1e-12	< 1e-12	< 1e-12	< 1e-12	< 1e-12	< 1e-12
Eu-152	< 1e-12	< 1e-12	< 1e-12	< 1e-12	< 1e-12	< 1e-12	< 1e-12	< 1e-12	< 1e-12
H-3	< 1e-12	< 1e-12	< 1e-12	< 1e-12	< 1e-12	< 1e-12	< 1e-12	< 1e-12	< 1e-12
Ho-166m	2.4e-12 (7)	< 1e-12	< 1e-12	< 1e-12	< 1e-12	< 1e-12	< 1e-12	1.2e-11 (4)	1.2e-11 (4)
I-129	6.4e-07 (5)	2.2e-08 (8)	6.9e-08 (5)	5.2e-08 (5)	7.0e-07 (14)	< 1e-12	3.6e-09 (3)	1.0e-08 (5)	1.1e-06 (8)
Mo-93	3.2e-06 (5)	3.7e-06 (6)	4.1e-07 (5)	5.6e-07 (5)	3.2e-06 (8)	5.0e-07 (5)	2.5e-07 (5)	2.1e-07 (5)	1.0e-05 (6)
Nb-93m	1.0e-09 (5)	1.2e-09 (6)	1.3e-10 (5)	1.8e-10 (5)	1.0e-09 (7)	1.6e-10 (5)	8.0e-11 (5)	6.8e-11 (5)	3.4e-09 (6)
Nb-94	1.8e-09 (52)	5.6e-10 (77)	8.6e-12 (67)	2.2e-10 (47)	1.4e-11 (77)	3.8e-11 (77)	8.8e-11 (31)	8.1e-10 (40)	3.3e-09 (52)
Ni-59	4.3e-06 (44)	8.4e-07 (52)	4.3e-08 (32)	9.8e-08 (25)	4.4e-07 (52)	1.6e-07 (52)	1.9e-08 (15)	3.3e-08 (20)	5.8e-06 (47)
Ni-63	4.4e-11 (3)	< 1e-12	< 1e-12	3.1e-12 (3)	< 1e-12	1.4e-12 (4)	1.1e-11 (3)	9.1e-12 (3)	5.7e-11 (3)
Np-237	4.3e-09 (86)	1.3e-11 (86)	5.1e-12 (86)	3.5e-10 (86)	1.1e-10 (86)	< 1e-12	4.5e-11 (86)	4.7e-11 (86)	4.9e-09 (86)
Pa-231	2.6e-09 (67)	1.1e-12 (86)	1.0e-10 (86)	6.4e-11 (37)	1.1e-10 (86)	< 1e-12	4.3e-07 (28)	1.4e-07 (48)	5.6e-07 (32)
Pb-210	7.2e-09 (86)	1.2e-09 (67)	5.4e-11 (23)	3.2e-10 (86)	7.7e-10 (86)	2.1e-11 (24)	2.9e-08 (86)	7.9e-09 (86)	4.1e-08 (86)
Pd-107	1.6e-10 (15)	8.0e-09 (19)	2.6e-12 (27)	1.4e-11 (15)	2.3e-10 (39)	< 1e-12	< 1e-12	6.5e-12 (15)	8.3e-09 (19)
Po-210	2.5e-10 (86)	1.9e-10 (86)	2.3e-12 (22)	1.1e-11 (86)	3.8e-11 (86)	1.2e-12 (22)	8.7e-10 (86)	4.7e-10 (82)	1.7e-09 (86)
Pu-238	< 1e-12	< 1e-12	< 1e-12	< 1e-12	< 1e-12	< 1e-12	< 1e-12	< 1e-12	< 1e-12
Pu-239	5.4e-07 (44)	7.0e-09 (67)	1.8e-09 (58)	5.1e-08 (41)	2.6e-08 (77)	6.0e-10 (67)	3.4e-08 (31)	5.0e-08 (39)	6.9e-07 (44)
Pu-240	1.1e-07 (18)	2.1e-10 (39)	1.5e-10 (26)	1.2e-08 (17)	8.3e-10 (35)	3.5e-11 (27)	9.1e-09 (14)	1.2e-08 (5)	1.4e-07 (18)
Pu-241	< 1e-12	< 1e-12	< 1e-12	< 1e-12	< 1e-12	< 1e-12	< 1e-12	< 1e-12	< 1e-12
Pu-242	1.8e-08 (86)	4.1e-10 (86)	7.1e-11 (86)	1.6e-09 (86)	1.3e-09 (86)	2.3e-11 (86)	6.3e-10 (83)	1.3e-09 (86)	2.4e-08 (86)
Ra-226	4.7e-08 (86)	8.7e-09 (67)	3.3e-10 (23)	2.0e-09 (86)	4.7e-09 (86)	1.2e-10 (23)	1.5e-07 (86)	4.9e-08 (86)	2.6e-07 (86)
Ra-228	< 1e-12	< 1e-12	< 1e-12	< 1e-12	< 1e-12	< 1e-12	< 1e-12	< 1e-12	< 1e-12
Se-79	2.4e-08 (5)	6.7e-10 (6)	1.1e-09 (5)	1.7e-09 (5)	5.2e-08 (10)	< 1e-12	4.2e-11 (5)	6.2e-10 (6)	6.5e-08 (9)
Sm-151	< 1e-12	< 1e-12	< 1e-12	< 1e-12	< 1e-12	< 1e-12	< 1e-12	< 1e-12	< 1e-12
Sn-126	3.0e-10 (77)	< 1e-12	< 1e-12	1.4e-11 (77)	3.2e-12 (86)	< 1e-12	< 1e-12	2.6e-11 (77)	3.4e-10 (77)
Sr-90	< 1e-12	< 1e-12	< 1e-12	< 1e-12	< 1e-12	< 1e-12	< 1e-12	< 1e-12	< 1e-12
Tc-99	1.2e-07 (57)	4.3e-10 (86)	1.6e-09 (86)	7.9e-09 (65)	9.1e-09 (86)	5.3e-11 (86)	4.6e-08 (49)	4.3e-09 (67)	1.9e-07 (58)
Th-228	< 1e-12	< 1e-12	< 1e-12	< 1e-12	< 1e-12	< 1e-12	< 1e-12	< 1e-12	< 1e-12
Th-229	7.3e-09 (86)	4.4e-11 (86)	5.4e-12 (86)	6.1e-10 (86)	3.7e-10 (86)	< 1e-12	5.1e-11 (86)	4.8e-11 (86)	8.4e-09 (86)
Th-230	6.2e-10 (86)	8.4e-12 (86)	< 1e-12	3.9e-11 (67)	3.7e-11 (86)	< 1e-12	5.5e-09 (77)	6.0e-10 (86)	6.3e-09 (77)
Th-232	< 1e-12	< 1e-12	1.1e-12 (5)	< 1e-12	< 1e-12	< 1e-12	< 1e-12	< 1e-12	< 1e-12
U-232	< 1e-12	< 1e-12	< 1e-12	< 1e-12	< 1e-12	< 1e-12	< 1e-12	< 1e-12	< 1e-12
U-233	3.2e-09 (86)	1.9e-11 (86)	3.2e-12 (86)	2.9e-10 (86)	1.8e-10 (86)	< 1e-12	2.4e-11 (86)	2.5e-11 (86)	3.7e-09 (86)
U-234	2.4e-09 (11)	8.3e-11 (67)	6.3e-12 (52)	2.6e-10 (34)	1.8e-10 (67)	< 1e-12	3.8e-08 (45)	4.6e-09 (67)	4.5e-08 (48)
U-235	1.1e-09 (11)	< 1e-12	4.7e-11 (67)	4.1e-11 (31)	4.0e-11 (67)	< 1e-12	3.9e-07 (6)	7.0e-08 (29)	4.2e-07 (7)
U-236	8.9e-10 (35)	4.0e-11 (67)	2.0e-12 (52)	1.7e-10 (34)	6.6e-11 (67)	< 1e-12	6.3e-11 (7)	5.3e-11 (13)	1.1e-09 (35)
U-238	1.8e-09 (11)	4.1e-12 (77)	7.3e-12 (51)	3.5e-10 (34)	9.6e-11 (67)	< 1e-12	9.6e-07 (6)	3.9e-08 (29)	9.8e-07 (7)
Zr-93	1.4e-08 (62)	1.4e-09 (86)	8.1e-11 (86)	1.3e-09 (67)	8.0e-09 (86)	1.6e-10 (86)	4.8e-11 (51)	5.8e-10 (77)	2.4e-08 (86)

Scenario combination 2 calculation case (CCC_SC2)

Table E-30. Near-field releases for CCC_SC2, peak release [Bq/year] and in parentheses time of peak [1000 year AD].

Nuclide	1BMA	2BMA	1BTF	2BTF	Silo	BRT	1BLA	2-5BLA	Total
Ac-227	1.9e+02 (82)	6.9e+00 (86)	2.5e+02 (86)	2.7e+00 (5)	3.5e+01 (67)	< 1	3.6e+04 (3)	7.4e+03 (3)	3.9e+04 (3)
Ag-108m	4.3e+06 (3)	6.5e+05 (3)	3.2e+05 (3)	1.4e+06 (3)	2.7e+05 (4)	6.0e+05 (3)	2.4e+05 (3)	1.9e+05 (3)	6.9e+06 (3)
Am-241	2.1e+04 (4)	< 1	1.3e+03 (4)	6.6e+03 (3)	< 1	4.0e+01 (4)	6.8e+05 (3)	2.5e+05 (3)	7.5e+05 (3)
Am-242m	< 1	< 1	< 1	< 1	< 1	< 1	4.5e+01 (3)	1.3e+01 (3)	4.5e+01 (3)
Am-243	5.1e+03 (7)	1.0e+01 (59)	2.1e+02 (4)	1.4e+03 (4)	2.6e+00 (34)	1.8e+01 (22)	2.2e+04 (3)	1.4e+04 (3)	2.7e+04 (3)
Ba-133	< 1	< 1	< 1	< 1	< 1	< 1	< 1	< 1	< 1
C-14-ind	< 1	8.3e+05 (4)	< 1	< 1	< 1	3.2e+04 (23)	< 1	8.6e+05 (3)	1.5e+06 (3)
C-14-inorg	7.2e+06 (7)	5.8e+01 (23)	2.7e+05 (12)	3.3e+06 (4)	3.0e+02 (33)	< 1	2.1e+07 (3)	6.7e+05 (3)	2.1e+07 (3)
C-14-org	1.0e+08 (3)	6.4e+05 (4)	1.1e+07 (3)	1.9e+07 (3)	6.5e+07 (5)	< 1	4.2e+05 (3)	1.6e+05 (3)	1.3e+08 (3)
Ca-41	< 1	1.3e+06 (8)	< 1	< 1	< 1	< 1	< 1	3.3e+06 (3)	3.3e+06 (3)
Cd-113m	< 1	< 1	< 1	< 1	< 1	< 1	< 1	< 1	< 1
Cl-36	1.5e+05 (3)	1.9e+04 (5)	1.2e+04 (3)	5.1e+04 (3)	4.4e+04 (5)	2.7e+02 (25)	1.3e+05 (3)	3.9e+04 (3)	3.4e+05 (3)
Cm-242	< 1	< 1	< 1	< 1	< 1	< 1	3.7e+01 (3)	1.1e+01 (3)	3.7e+01 (3)
Cm-243	< 1	< 1	< 1	< 1	< 1	< 1	< 1	< 1	< 1
Cm-244	< 1	< 1	< 1	< 1	< 1	< 1	< 1	< 1	< 1
Cm-245	4.5e+01 (7)	< 1	1.4e+00 (4)	7.6e+00 (4)	< 1	< 1	2.2e+02 (3)	1.7e+02 (3)	2.9e+02 (3)
Cm-246	8.5e+00 (7)	< 1	< 1	1.8e+00 (4)	< 1	< 1	5.4e+01 (3)	4.6e+01 (3)	7.5e+01 (3)
Co-60	< 1	< 1	< 1	< 1	< 1	< 1	< 1	< 1	< 1
Cs-135	2.3e+05 (3)	5.9e+03 (7)	4.3e+04 (3)	4.0e+04 (3)	4.0e+04 (10)	< 1	1.8e+04 (3)	1.5e+05 (3)	4.4e+05 (3)
Cs-137	< 1	< 1	< 1	< 1	< 1	< 1	< 1	< 1	< 1
Eu-152	< 1	< 1	< 1	< 1	< 1	< 1	< 1	< 1	< 1
H-3	< 1	< 1	< 1	< 1	< 1	< 1	< 1	< 1	< 1
Ho-166m	7.3e+03 (4)	< 1	2.4e+02 (4)	2.8e+03 (3)	< 1	< 1	1.4e+04 (3)	3.7e+04 (3)	4.6e+04 (3)
I-129	5.6e+04 (3)	4.7e+02 (23)	1.1e+04 (3)	2.8e+04 (3)	2.9e+04 (6)	< 1	2.6e+03 (3)	1.6e+03 (3)	8.9e+04 (3)
Mo-93	6.4e+05 (3)	1.5e+05 (5)	1.3e+05 (3)	5.1e+05 (3)	3.3e+05 (5)	1.6e+05 (3)	5.1e+05 (3)	6.1e+04 (3)	1.8e+06 (3)
Nb-93m	9.4e+04 (4)	2.1e+04 (64)	1.8e+03 (3)	2.1e+04 (3)	3.1e+04 (15)	2.6e+03 (3)	5.1e+05 (3)	8.6e+04 (3)	5.6e+05 (3)
Nb-94	1.7e+05 (7)	3.2e+04 (62)	1.5e+03 (22)	4.5e+04 (4)	1.3e+04 (34)	4.1e+03 (63)	1.8e+05 (3)	7.9e+05 (3)	8.7e+05 (3)
Ni-59	2.4e+08 (4)	4.0e+07 (7)	1.1e+07 (4)	5.2e+07 (3)	7.3e+07 (34)	9.9e+06 (4)	2.4e+07 (3)	9.6e+06 (3)	2.8e+08 (4)
Ni-63	5.3e+06 (3)	2.6e+03 (3)	1.6e+05 (3)	2.1e+06 (3)	5.8e+02 (4)	7.1e+04 (3)	1.8e+06 (3)	3.4e+05 (3)	9.1e+06 (3)
Np-237	4.1e+03 (3)	9.9e+01 (60)	1.3e+01 (12)	1.6e+03 (3)	1.1e+03 (34)	1.6e+00 (22)	9.4e+02 (3)	5.3e+02 (3)	6.5e+03 (3)
Pa-231	2.6e+01 (77)	< 1	5.3e+01 (58)	1.4e+00 (4)	8.6e+01 (77)	< 1	3.7e+04 (3)	7.6e+03 (3)	4.0e+04 (3)
Pb-210	1.5e+02 (77)	2.6e+02 (77)	4.6e+00 (77)	2.3e+00 (4)	9.1e+01 (77)	1.9e+00 (22)	9.7e+00 (3)	3.3e+00 (4)	4.9e+02 (77)
Pd-107	4.6e+04 (3)	4.5e+05 (4)	1.1e+03 (3)	1.4e+04 (3)	1.8e+04 (5)	< 1	5.9e+02 (3)	1.4e+03 (3)	4.8e+05 (4)
Po-210	1.2e+04 (77)	2.3e+04 (77)	3.8e+02 (77)	3.6e+01 (10)	3.3e+03 (77)	1.6e+02 (22)	9.7e+00 (3)	3.3e+00 (4)	3.8e+04 (77)
Pu-238	3.9e+02 (3)	< 1	< 1	1.9e+02 (3)	< 1	< 1	8.6e+02 (3)	1.9e+02 (3)	1.3e+03 (3)
Pu-239	4.7e+05 (3)	9.5e+03 (57)	1.7e+03 (12)	2.4e+05 (3)	5.8e+04 (9)	2.8e+02 (12)	3.8e+05 (3)	2.2e+05 (3)	1.1e+06 (3)
Pu-240	5.9e+05 (3)	2.1e+02 (23)	1.5e+03 (4)	3.0e+05 (3)	5.0e+04 (8)	3.2e+02 (4)	3.6e+05 (3)	2.2e+05 (3)	1.3e+06 (3)
Pu-241	1.0e+03 (5)	1.7e+01 (61)	2.4e+01 (8)	2.6e+02 (4)	< 1	< 1	2.2e+02 (3)	1.7e+02 (3)	1.3e+03 (5)
Pu-242	3.4e+03 (3)	3.0e+02 (58)	1.5e+01 (22)	1.8e+03 (3)	4.2e+02 (14)	2.8e+00 (23)	2.4e+03 (3)	1.4e+03 (3)	7.8e+03 (3)
Ra-226	1.1e+03 (77)	2.8e+03 (77)	4.9e+01 (77)	3.2e+00 (4)	1.2e+03 (77)	1.9e+01 (22)	1.0e+01 (3)	3.4e+00 (4)	5.0e+03 (77)
Ra-228	< 1	< 1	< 1	< 1	< 1	< 1	< 1	< 1	< 1
Se-79	2.5e+05 (3)	1.5e+03 (4)	1.5e+04 (3)	5.5e+04 (3)	1.3e+05 (5)	< 1	2.4e+03 (3)	5.0e+03 (3)	3.2e+05 (3)
Sm-151	3.4e+01 (3)	< 1	< 1	1.7e+01 (3)	< 1	< 1	4.5e+02 (3)	7.6e+02 (3)	1.0e+03 (3)
Sn-126	4.1e+03 (3)	3.3e+01 (59)	1.3e+01 (22)	1.4e+03 (3)	5.9e+02 (34)	< 1	3.0e+02 (3)	6.6e+03 (3)	1.2e+04 (3)
Sr-90	< 1	< 1	< 1	< 1	< 1	< 1	< 1	< 1	< 1
Tc-99	7.7e+05 (7)	9.1e+03 (66)	5.1e+04 (22)	3.4e+05 (3)	4.0e+05 (34)	1.8e+03 (58)	1.1e+07 (3)	4.2e+05 (3)	1.1e+07 (3)
Th-228	< 1	< 1	< 1	< 1	< 1	< 1	< 1	< 1	< 1
Th-229	1.8e+02 (77)	7.2e+00 (86)	1.6e+00 (58)	< 1	8.2e+01 (86)	< 1	< 1	< 1	2.7e+02 (77)
Th-230	4.2e+01 (77)	2.1e+01 (86)	3.3e+00 (58)	2.9e+00 (4)	5.8e+01 (86)	< 1	7.2e+01 (3)	1.3e+01 (4)	1.2e+02 (82)
Th-232	< 1	< 1	< 1	< 1	< 1	< 1	< 1	< 1	< 1
U-232	< 1	< 1	< 1	< 1	< 1	< 1	< 1	< 1	< 1
U-233	8.8e+01 (77)	3.4e+01 (77)	2.0e+00 (58)	8.7e+00 (3)	1.4e+02 (77)	< 1	3.2e+00 (3)	2.5e+00 (4)	2.7e+02 (77)
U-234	1.4e+03 (3)	1.1e+02 (58)	8.4e+00 (23)	5.0e+02 (3)	2.3e+02 (34)	< 1	1.4e+04 (3)	1.4e+03 (3)	1.6e+04 (3)
U-235	6.8e+02 (3)	1.8e+00 (58)	5.3e+01 (12)	9.0e+01 (3)	5.6e+01 (34)	< 1	1.8e+06 (3)	2.7e+05 (3)	1.8e+06 (3)
U-236	3.4e+02 (3)	5.6e+01 (58)	3.7e+00 (22)	2.9e+02 (3)	8.8e+01 (34)	< 1	2.5e+02 (3)	1.8e+02 (3)	9.1e+02 (3)
U-238	1.2e+03 (3)	8.1e+00 (58)	8.5e+00 (22)	7.1e+02 (3)	1.3e+02 (34)	< 1	4.4e+06 (3)	1.5e+05 (3)	4.4e+06 (3)
Zr-93	4.8e+04 (4)	9.2e+03 (62)	6.4e+02 (6)	2.4e+04 (3)	6.9e+04 (34)	9.7e+02 (22)	6.5e+03 (3)	2.5e+04 (3)	8.5e+04 (3)

Table E-31. Far-field releases for CCC_SC2, peak release [Bq/year] and in parentheses time of peak [1000 year AD].

Nuclide	1BMA	2BMA	1BTF	2BTF	Silo	BRT	1BLA	2-5BLA	Total
Ac-227	2.1e+02 (83)	1.5e+00 (86)	1.2e+02 (86)	3.4e+00 (17)	3.1e+02 (86)	< 1	1.4e+04 (5)	6.4e+03 (82)	1.6e+04 (5)
Ag-108m	4.2e+06 (3)	5.9e+05 (4)	2.3e+05 (3)	1.3e+06 (3)	2.4e+05 (4)	3.1e+05 (3)	2.0e+05 (3)	1.3e+05 (3)	5.9e+06 (3)
Am-241	6.2e+03 (4)	< 1	2.6e+01 (4)	3.6e+02 (4)	< 1	< 1	5.6e+04 (3)	4.3e+03 (4)	5.7e+04 (3)
Am-242m	< 1	< 1	< 1	< 1	< 1	< 1	2.9e+00 (3)	< 1	2.9e+00 (3)
Am-243	1.4e+03 (7)	2.4e+00 (61)	1.4e+01 (9)	1.2e+02 (5)	< 1	< 1	2.1e+03 (3)	5.2e+02 (5)	2.2e+03 (4)
Ba-133	< 1	< 1	< 1	< 1	< 1	< 1	< 1	< 1	< 1
C-14-ind	< 1	7.1e+05 (4)	< 1	< 1	< 1	2.8e+04 (23)	< 1	8.0e+05 (4)	1.5e+06 (4)
C-14-inorg	7.2e+06 (7)	5.0e+01 (23)	2.6e+05 (12)	3.1e+06 (4)	3.0e+02 (33)	< 1	1.9e+07 (3)	6.2e+05 (4)	1.9e+07 (3)
C-14-org	1.0e+08 (3)	5.6e+05 (5)	8.4e+06 (3)	1.6e+07 (3)	6.3e+07 (5)	< 1	3.8e+05 (3)	1.5e+05 (4)	1.2e+08 (3)
Ca-41	< 1	1.2e+06 (9)	< 1	< 1	< 1	< 1	< 1	3.1e+06 (4)	3.1e+06 (4)
Cd-113m	< 1	< 1	< 1	< 1	< 1	< 1	< 1	< 1	< 1
Cl-36	1.5e+05 (3)	1.9e+04 (5)	9.7e+03 (3)	4.3e+04 (3)	4.3e+04 (5)	2.6e+02 (29)	1.2e+05 (3)	3.7e+04 (4)	3.0e+05 (3)
Cm-242	< 1	< 1	< 1	< 1	< 1	< 1	1.8e+00 (3)	< 1	1.8e+00 (3)
Cm-243	< 1	< 1	< 1	< 1	< 1	< 1	< 1	< 1	< 1
Cm-244	< 1	< 1	< 1	< 1	< 1	< 1	< 1	< 1	< 1
Cm-245	1.6e+01 (7)	< 1	< 1	1.3e+00 (4)	< 1	< 1	2.0e+01 (3)	6.9e+00 (5)	2.6e+01 (5)
Cm-246	3.3e+00 (5)	< 1	< 1	< 1	< 1	< 1	5.0e+00 (3)	1.7e+00 (5)	6.2e+00 (4)
Co-60	< 1	< 1	< 1	< 1	< 1	< 1	< 1	< 1	< 1
Cs-135	1.9e+05 (4)	1.8e+03 (9)	1.1e+04 (4)	9.0e+03 (4)	2.4e+04 (15)	< 1	5.7e+03 (3)	2.7e+04 (4)	2.4e+05 (4)
Cs-137	< 1	< 1	< 1	< 1	< 1	< 1	< 1	< 1	< 1
Eu-152	< 1	< 1	< 1	< 1	< 1	< 1	< 1	< 1	< 1
H-3	< 1	< 1	< 1	< 1	< 1	< 1	< 1	< 1	< 1
Ho-166m	3.1e+03 (5)	< 1	1.2e+01 (4)	6.0e+02 (4)	< 1	< 1	1.2e+03 (3)	1.0e+03 (4)	4.3e+03 (4)
I-129	5.5e+04 (3)	4.3e+02 (8)	9.5e+03 (3)	2.2e+04 (3)	2.8e+04 (6)	< 1	2.3e+03 (3)	1.6e+03 (4)	8.2e+04 (3)
Mo-93	6.3e+05 (3)	1.3e+05 (5)	1.1e+05 (3)	4.1e+05 (3)	3.1e+05 (5)	1.4e+05 (4)	4.6e+05 (3)	5.6e+04 (4)	1.5e+06 (3)
Nb-93m	5.9e+04 (5)	3.8e+03 (86)	4.4e+02 (3)	5.8e+03 (9)	4.6e+04 (44)	5.6e+02 (4)	1.3e+04 (3)	9.9e+02 (9)	6.6e+04 (5)
Nb-94	6.1e+04 (5)	6.5e+03 (67)	2.9e+02 (16)	8.2e+03 (5)	3.1e+03 (34)	2.6e+02 (67)	1.4e+04 (3)	2.7e+04 (5)	9.8e+04 (5)
Ni-59	1.9e+08 (4)	8.4e+06 (58)	3.2e+06 (4)	1.4e+07 (4)	3.0e+07 (35)	1.2e+06 (5)	7.4e+06 (3)	2.0e+06 (4)	2.1e+08 (4)
Ni-63	2.2e+06 (3)	2.1e+02 (4)	7.4e+03 (3)	2.8e+05 (3)	4.8e+01 (4)	1.6e+03 (4)	3.8e+05 (3)	1.5e+04 (3)	2.7e+06 (3)
Np-237	1.4e+03 (5)	1.4e+01 (86)	3.1e+00 (28)	1.0e+02 (5)	1.5e+02 (65)	< 1	4.5e+01 (3)	8.2e+00 (9)	1.5e+03 (5)
Pa-231	1.9e+01 (82)	< 1	1.5e+01 (86)	< 1	2.0e+01 (86)	< 1	2.3e+03 (4)	7.3e+02 (82)	2.3e+03 (4)
Pb-210	1.0e+02 (77)	5.1e+01 (83)	2.7e+00 (77)	3.0e+00 (77)	6.1e+01 (82)	< 1	2.6e+02 (77)	8.3e+01 (82)	5.3e+02 (77)
Pd-107	4.4e+04 (3)	4.7e+05 (5)	9.8e+02 (3)	1.2e+04 (3)	1.7e+04 (5)	< 1	5.4e+02 (3)	1.4e+03 (4)	5.0e+05 (5)
Po-210	1.3e+02 (77)	4.6e+01 (83)	2.8e+00 (77)	3.0e+00 (77)	8.0e+01 (77)	< 1	2.9e+02 (77)	8.1e+01 (77)	6.0e+02 (77)
Pu-238	4.6e+01 (3)	< 1	< 1	2.8e+00 (3)	< 1	< 1	4.9e+01 (3)	< 1	9.1e+01 (3)
Pu-239	1.8e+05 (4)	1.1e+03 (63)	4.0e+02 (24)	1.8e+04 (4)	1.4e+04 (17)	3.7e+01 (30)	3.7e+04 (3)	1.1e+04 (5)	2.4e+05 (4)
Pu-240	2.3e+05 (4)	2.1e+01 (26)	2.4e+02 (9)	2.3e+04 (4)	8.7e+03 (10)	8.9e+00 (15)	3.5e+04 (3)	8.9e+03 (5)	2.8e+05 (4)
Pu-241	1.5e+02 (5)	< 1	< 1	4.1e+00 (5)	< 1	< 1	4.0e+01 (4)	8.6e+00 (5)	1.8e+02 (5)
Pu-242	1.4e+03 (4)	4.7e+01 (86)	4.9e+00 (26)	1.4e+02 (4)	1.5e+02 (38)	< 1	2.3e+02 (3)	7.0e+01 (5)	1.7e+03 (4)
Ra-226	1.2e+03 (77)	5.1e+02 (83)	4.5e+01 (77)	5.1e+01 (77)	1.4e+03 (77)	3.1e+00 (22)	4.8e+03 (77)	1.5e+03 (77)	9.3e+03 (77)
Ra-228	< 1	< 1	< 1	< 1	< 1	< 1	< 1	< 1	< 1
Se-79	2.4e+05 (3)	1.4e+03 (5)	1.2e+04 (3)	4.7e+04 (3)	1.3e+05 (5)	< 1	2.2e+03 (3)	4.7e+03 (4)	2.9e+05 (3)
Sm-151	6.8e+00 (3)	< 1	< 1	< 1	< 1	< 1	2.4e+01 (3)	1.7e+00 (3)	2.5e+01 (3)
Sn-126	8.4e+02 (5)	2.3e+00 (86)	1.3e+00 (33)	2.9e+01 (9)	5.5e+01 (67)	< 1	5.5e+00 (4)	2.8e+01 (12)	8.8e+02 (5)
Sr-90	< 1	< 1	< 1	< 1	< 1	< 1	< 1	< 1	< 1
Tc-99	2.8e+05 (5)	1.5e+03 (86)	5.5e+03 (23)	2.0e+04 (5)	6.7e+04 (52)	9.5e+01 (86)	5.3e+05 (4)	7.7e+03 (5)	6.6e+05 (4)
Th-228	< 1	< 1	< 1	< 1	< 1	< 1	< 1	< 1	< 1
Th-229	1.2e+02 (82)	3.5e+00 (82)	1.2e+00 (77)	2.6e+00 (77)	7.6e+01 (82)	< 1	< 1	< 1	2.1e+02 (82)
Th-230	3.4e+01 (82)	4.7e+00 (86)	1.1e+00 (77)	1.3e+00 (77)	3.9e+01 (82)	< 1	1.7e+02 (77)	4.5e+01 (82)	3.0e+02 (82)
Th-232	< 1	< 1	< 1	< 1	< 1	< 1	< 1	< 1	< 1
U-232	< 1	< 1	< 1	< 1	< 1	< 1	< 1	< 1	< 1
U-233	6.4e+01 (77)	3.4e+00 (86)	1.1e+00 (82)	2.4e+00 (82)	5.4e+01 (82)	< 1	< 1	< 1	1.2e+02 (82)
U-234	4.0e+02 (5)	9.1e+00 (86)	1.8e+00 (67)	2.3e+01 (5)	4.9e+01 (67)	< 1	1.0e+03 (4)	6.9e+01 (82)	1.4e+03 (4)
U-235	1.9e+02 (4)	< 1	1.5e+01 (86)	4.2e+00 (5)	1.3e+01 (86)	< 1	9.0e+04 (4)	4.9e+03 (5)	8.8e+04 (4)
U-236	1.1e+02 (5)	5.1e+00 (86)	< 1	1.4e+01 (5)	2.0e+01 (86)	< 1	1.3e+01 (4)	3.5e+00 (5)	1.3e+02 (5)
U-238	3.2e+02 (4)	< 1	1.5e+00 (25)	3.3e+01 (5)	2.8e+01 (86)	< 1	2.2e+05 (4)	2.7e+03 (5)	2.2e+05 (4)
Zr-93	3.0e+04 (5)	1.9e+03 (86)	1.2e+02 (17)	2.3e+03 (5)	1.9e+04 (43)	6.7e+01 (34)	4.5e+02 (4)	6.6e+02 (5)	3.3e+04 (5)

Table E-32. Doses for CCC_SC2, peak dose [Sv/year] and in parentheses time of peak [1000 year AD].

Nuclide	1BMA	2BMA	1BTF	2BTF	Silo	BRT	1BLA	2-5BLA	Total
Total	6.7e-06 (37)	1.4e-06 (14)	5.1e-07 (5)	6.8e-07 (5)	4.5e-06 (7)	5.1e-07 (5)	1.5e-06 (7)	5.5e-07 (8)	1.3e-05 (40)
Ac-227	1.5e-09 (39)	1.0e-11 (86)	5.1e-10 (86)	5.0e-11 (35)	9.9e-10 (86)	< 1e-12	2.3e-07 (30)	1.1e-07 (57)	3.3e-07 (35)
Ag-108m	3.1e-08 (5)	1.5e-08 (5)	2.5e-09 (5)	4.9e-09 (5)	1.1e-08 (5)	4.3e-09 (3)	5.0e-10 (5)	2.5e-09 (5)	6.8e-08 (5)
Am-241	1.0e-10 (5)	< 1e-12	< 1e-12	6.2e-12 (5)	< 1e-12	< 1e-12	3.2e-10 (4)	4.1e-09 (4)	4.2e-09 (4)
Am-242m	< 1e-12	< 1e-12	< 1e-12	< 1e-12	< 1e-12	< 1e-12	< 1e-12	< 1e-12	< 1e-12
Am-243	9.9e-10 (19)	7.2e-12 (63)	3.0e-11 (27)	1.0e-10 (22)	< 1e-12	2.4e-12 (25)	2.8e-10 (14)	5.9e-10 (5)	1.7e-09 (18)
Ba-133	< 1e-12	< 1e-12	< 1e-12	< 1e-12	< 1e-12	< 1e-12	< 1e-12	< 1e-12	< 1e-12
C-14-ind	< 1e-12	1.9e-08 (5)	< 1e-12	< 1e-12	< 1e-12	7.7e-10 (23)	< 1e-12	7.0e-09 (5)	2.6e-08 (5)
C-14-inorg	2.0e-07 (7)	1.4e-12 (24)	7.1e-09 (13)	4.4e-08 (5)	8.7e-12 (34)	< 1e-12	8.5e-08 (3)	5.4e-09 (5)	2.5e-07 (7)
C-14-org	8.1e-07 (3)	1.5e-08 (5)	8.6e-08 (3)	6.5e-08 (3)	1.8e-06 (5)	< 1e-12	1.7e-09 (3)	1.3e-09 (5)	2.4e-06 (5)
Ca-41	< 1e-12	1.0e-06 (26)	< 1e-12	< 1e-12	< 1e-12	< 1e-12	< 1e-12	4.6e-07 (9)	1.2e-06 (18)
Cd-113m	< 1e-12	< 1e-12	< 1e-12	< 1e-12	< 1e-12	< 1e-12	< 1e-12	< 1e-12	< 1e-12
Cl-36	2.1e-07 (5)	6.1e-08 (5)	1.1e-08 (5)	1.1e-08 (5)	1.3e-07 (5)	8.8e-10 (29)	2.3e-08 (3)	4.4e-08 (5)	4.3e-07 (5)
Cm-242	< 1e-12	< 1e-12	< 1e-12	< 1e-12	< 1e-12	< 1e-12	< 1e-12	< 1e-12	< 1e-12
Cm-243	< 1e-12	< 1e-12	< 1e-12	< 1e-12	< 1e-12	< 1e-12	< 1e-12	< 1e-12	< 1e-12
Cm-244	< 1e-12	< 1e-12	< 1e-12	< 1e-12	< 1e-12	< 1e-12	< 1e-12	< 1e-12	< 1e-12
Cm-245	1.4e-11 (19)	< 1e-12	< 1e-12	< 1e-12	< 1e-12	< 1e-12	3.1e-12 (14)	7.7e-12 (5)	2.2e-11 (18)
Cm-246	1.3e-12 (12)	< 1e-12	< 1e-12	< 1e-12	< 1e-12	< 1e-12	< 1e-12	1.6e-12 (5)	1.9e-12 (12)
Co-60	< 1e-12	< 1e-12	< 1e-12	< 1e-12	< 1e-12	< 1e-12	< 1e-12	< 1e-12	< 1e-12
Cs-135	7.3e-07 (86)	1.8e-08 (86)	4.5e-08 (86)	1.4e-08 (86)	7.3e-07 (86)	< 1e-12	2.6e-09 (86)	1.0e-07 (86)	1.6e-06 (86)
Cs-137	< 1e-12	< 1e-12	< 1e-12	< 1e-12	< 1e-12	< 1e-12	< 1e-12	< 1e-12	< 1e-12
Eu-152	< 1e-12	< 1e-12	< 1e-12	< 1e-12	< 1e-12	< 1e-12	< 1e-12	< 1e-12	< 1e-12
H-3	< 1e-12	< 1e-12	< 1e-12	< 1e-12	< 1e-12	< 1e-12	< 1e-12	< 1e-12	< 1e-12
Ho-166m	8.5e-12 (7)	< 1e-12	< 1e-12	< 1e-12	< 1e-12	< 1e-12	< 1e-12	1.2e-11 (4)	1.3e-11 (5)
I-129	4.2e-07 (5)	1.1e-08 (25)	6.9e-08 (5)	5.2e-08 (5)	6.9e-07 (15)	< 1e-12	3.6e-09 (3)	1.0e-08 (5)	9.8e-07 (9)
Mo-93	2.3e-06 (5)	1.2e-06 (8)	4.1e-07 (5)	5.5e-07 (5)	2.8e-06 (8)	5.0e-07 (5)	2.5e-07 (5)	2.1e-07 (5)	6.7e-06 (6)
Nb-93m	7.5e-10 (5)	4.0e-10 (8)	1.3e-10 (5)	1.8e-10 (5)	9.4e-10 (8)	1.6e-10 (5)	8.0e-11 (5)	6.8e-11 (5)	2.2e-09 (6)
Nb-94	3.3e-09 (46)	6.6e-10 (86)	4.0e-11 (57)	4.4e-10 (43)	4.2e-10 (77)	3.8e-11 (77)	8.8e-11 (31)	8.1e-10 (40)	5.1e-09 (50)
Ni-59	5.6e-06 (37)	1.0e-06 (67)	7.5e-08 (23)	1.4e-07 (19)	3.7e-06 (44)	1.6e-07 (52)	1.9e-08 (15)	3.3e-08 (20)	1.0e-05 (41)
Ni-63	9.3e-11 (3)	< 1e-12	< 1e-12	1.0e-11 (3)	< 1e-12	1.4e-12 (4)	1.1e-11 (3)	9.1e-12 (3)	1.1e-10 (3)
Np-237	5.6e-09 (86)	2.6e-11 (86)	4.1e-11 (86)	4.2e-10 (86)	1.5e-09 (86)	< 1e-12	4.5e-11 (86)	4.7e-11 (86)	7.6e-09 (86)
Pa-231	2.9e-09 (35)	2.7e-12 (86)	1.2e-09 (86)	8.6e-11 (33)	1.4e-09 (86)	< 1e-12	4.3e-07 (28)	1.4e-07 (48)	5.6e-07 (32)
Pb-210	7.8e-09 (86)	2.4e-09 (67)	2.3e-10 (86)	2.9e-10 (67)	6.8e-09 (86)	2.1e-11 (24)	2.9e-08 (86)	7.9e-09 (86)	4.9e-08 (86)
Pd-107	1.5e-10 (15)	7.8e-09 (27)	6.3e-12 (23)	1.4e-11 (14)	6.2e-10 (31)	< 1e-12	< 1e-12	6.5e-12 (15)	8.5e-09 (27)
Po-210	2.7e-10 (86)	3.5e-10 (86)	9.5e-12 (86)	1.0e-11 (86)	3.1e-10 (86)	1.2e-12 (22)	8.7e-10 (86)	4.7e-10 (82)	2.1e-09 (86)
Pu-238	< 1e-12	< 1e-12	< 1e-12	< 1e-12	< 1e-12	< 1e-12	< 1e-12	< 1e-12	< 1e-12
Pu-239	7.7e-07 (37)	1.3e-08 (86)	1.3e-08 (57)	6.5e-08 (36)	2.9e-07 (67)	6.0e-10 (67)	3.4e-08 (31)	5.0e-08 (39)	1.1e-06 (44)
Pu-240	2.2e-07 (16)	7.2e-11 (41)	1.1e-09 (25)	1.8e-08 (16)	2.0e-08 (27)	3.5e-11 (27)	9.1e-09 (14)	1.2e-08 (5)	2.7e-07 (17)
Pu-241	< 1e-12	< 1e-12	< 1e-12	< 1e-12	< 1e-12	< 1e-12	< 1e-12	< 1e-12	< 1e-12
Pu-242	2.3e-08 (86)	8.1e-10 (86)	5.2e-10 (86)	1.8e-09 (86)	1.2e-08 (86)	2.3e-11 (86)	6.3e-10 (83)	1.3e-09 (86)	4.0e-08 (86)
Ra-226	5.1e-08 (86)	1.7e-08 (86)	1.4e-09 (86)	1.9e-09 (67)	4.4e-08 (86)	1.2e-10 (23)	1.5e-07 (86)	4.9e-08 (86)	3.2e-07 (86)
Ra-228	< 1e-12	< 1e-12	< 1e-12	< 1e-12	< 1e-12	< 1e-12	< 1e-12	< 1e-12	< 1e-12
Se-79	1.9e-08 (6)	4.3e-10 (8)	1.1e-09 (5)	1.7e-09 (5)	5.3e-08 (11)	< 1e-12	4.2e-11 (5)	6.2e-10 (6)	6.7e-08 (9)
Sm-151	< 1e-12	< 1e-12	< 1e-12	< 1e-12	< 1e-12	< 1e-12	< 1e-12	< 1e-12	< 1e-12
Sn-126	3.4e-10 (66)	< 1e-12	1.5e-12 (86)	1.7e-11 (67)	6.2e-11 (86)	< 1e-12	< 1e-12	2.6e-11 (77)	4.4e-10 (67)
Sr-90	< 1e-12	< 1e-12	< 1e-12	< 1e-12	< 1e-12	< 1e-12	< 1e-12	< 1e-12	< 1e-12
Tc-99	1.2e-07 (67)	5.9e-10 (86)	7.1e-09 (86)	8.1e-09 (62)	1.0e-07 (86)	5.3e-11 (86)	4.6e-08 (49)	4.3e-09 (67)	2.7e-07 (77)
Th-228	< 1e-12	< 1e-12	< 1e-12	< 1e-12	< 1e-12	< 1e-12	< 1e-12	< 1e-12	< 1e-12
Th-229	9.6e-09 (86)	1.1e-10 (86)	6.4e-11 (86)	6.3e-10 (86)	3.9e-09 (86)	< 1e-12	5.1e-11 (86)	4.8e-11 (86)	1.4e-08 (86)
Th-230	6.7e-10 (86)	2.1e-11 (86)	1.1e-11 (86)	3.9e-11 (49)	4.6e-10 (86)	< 1e-12	5.5e-09 (77)	6.0e-10 (86)	6.6e-09 (77)
Th-232	< 1e-12	< 1e-12	< 1e-12	< 1e-12	< 1e-12	< 1e-12	< 1e-12	< 1e-12	< 1e-12
U-232	< 1e-12	< 1e-12	< 1e-12	< 1e-12	< 1e-12	< 1e-12	< 1e-12	< 1e-12	< 1e-12
U-233	4.2e-09 (86)	8.9e-11 (86)	3.5e-11 (86)	3.0e-10 (86)	1.8e-09 (86)	< 1e-12	2.4e-11 (86)	2.5e-11 (86)	6.4e-09 (86)
U-234	4.4e-09 (9)	2.7e-10 (67)	7.2e-11 (52)	3.1e-10 (7)	1.8e-09 (67)	< 1e-12	3.8e-08 (45)	4.6e-09 (67)	4.6e-08 (50)
U-235	1.9e-09 (9)	3.5e-12 (86)	5.8e-10 (67)	5.4e-11 (7)	4.4e-10 (67)	< 1e-12	3.9e-07 (6)	7.0e-08 (29)	4.2e-07 (7)
U-236	1.4e-09 (10)	1.4e-10 (86)	2.4e-11 (52)	2.0e-10 (26)	6.8e-10 (67)	< 1e-12	6.3e-11 (7)	5.3e-11 (13)	1.8e-09 (41)
U-238	3.3e-09 (9)	1.9e-11 (86)	5.7e-11 (52)	4.2e-10 (7)	9.9e-10 (67)	< 1e-12	9.6e-07 (6)	3.9e-08 (29)	9.8e-07 (7)
Zr-93	1.4e-08 (67)	1.9e-09 (86)	2.5e-10 (78)	1.3e-09 (65)	4.6e-08 (86)	1.6e-10 (86)	4.8e-11 (51)	5.8e-10 (77)	6.3e-08 (86)

Loss of barrier function calculation case – no sorption in the repository (CCR_B1)

Table E-33. Near-field releases for CCR_B1, peak release [Bq/year] and in parentheses time of peak [1000 year AD].

Nuclide	1BMA	2BMA	1BTF	2BTF	Silo	BRT	1BLA	2-5BLA	Total
Ac-227	3.5e+01 (5)	< 1	2.5e+02 (3)	4.4e+00 (3)	1.4e+02 (10)	< 1	2.2e+04 (3)	5.2e+03 (4)	2.3e+04 (3)
Ag-108m	5.1e+05 (3)	2.3e+05 (4)	1.7e+05 (3)	7.7e+05 (3)	7.2e+05 (4)	2.7e+05 (3)	1.3e+05 (3)	6.5e+04 (3)	1.8e+06 (3)
Am-241	7.1e+05 (3)	2.6e+05 (4)	6.4e+05 (3)	6.5e+05 (3)	5.2e+05 (4)	3.7e+05 (3)	3.8e+05 (3)	8.8e+04 (3)	2.6e+06 (3)
Am-242m	2.4e+01 (3)	1.1e+01 (3)	2.0e+01 (3)	3.4e+01 (3)	8.7e+00 (3)	4.9e+01 (3)	2.5e+01 (3)	3.7e+00 (3)	1.4e+02 (3)
Am-243	4.2e+04 (4)	6.3e+04 (5)	1.9e+04 (3)	3.0e+04 (3)	1.2e+05 (5)	4.2e+04 (3)	1.3e+04 (3)	6.5e+03 (4)	2.3e+05 (5)
Ba-133	< 1	< 1	< 1	< 1	< 1	< 1	< 1	< 1	< 1
C-14-ind	< 1	4.5e+05 (5)	< 1	< 1	< 1	2.7e+04 (24)	< 1	4.0e+05 (4)	7.6e+05 (4)
C-14-inorg	4.2e+08 (4)	1.3e+06 (5)	1.3e+08 (3)	4.3e+08 (3)	1.9e+08 (5)	< 1	1.3e+07 (3)	3.1e+05 (4)	8.5e+08 (3)
C-14-org	2.9e+07 (4)	3.5e+05 (5)	6.3e+06 (3)	9.8e+06 (3)	5.3e+07 (5)	< 1	2.5e+05 (3)	7.5e+04 (4)	7.7e+07 (5)
Ca-41	< 1	1.9e+06 (5)	< 1	< 1	< 1	< 1	< 1	1.6e+06 (4)	3.0e+06 (4)
Cd-113m	< 1	< 1	< 1	< 1	< 1	< 1	< 1	< 1	< 1
Cl-36	8.1e+04 (4)	2.5e+04 (5)	1.0e+04 (3)	3.0e+04 (3)	9.0e+04 (5)	2.7e+02 (26)	7.6e+04 (3)	1.9e+04 (4)	2.0e+05 (5)
Cm-242	2.0e+01 (3)	8.9e+00 (3)	1.6e+01 (3)	2.8e+01 (3)	7.1e+00 (3)	4.1e+01 (3)	2.0e+01 (3)	3.0e+00 (3)	1.2e+02 (3)
Cm-243	< 1	< 1	< 1	< 1	< 1	< 1	< 1	< 1	< 1
Cm-244	< 1	< 1	< 1	< 1	< 1	< 1	< 1	< 1	< 1
Cm-245	4.2e+02 (4)	9.9e+02 (5)	1.7e+02 (3)	2.3e+02 (3)	1.2e+03 (5)	< 1	1.3e+02 (3)	7.8e+01 (4)	2.6e+03 (5)
Cm-246	9.8e+01 (4)	2.7e+02 (5)	4.2e+01 (3)	5.7e+01 (3)	2.8e+02 (5)	< 1	3.2e+01 (3)	2.1e+01 (4)	6.5e+02 (5)
Co-60	< 1	< 1	< 1	< 1	< 1	< 1	< 1	< 1	< 1
Cs-135	2.1e+05 (4)	6.7e+03 (5)	5.7e+04 (3)	3.4e+04 (3)	4.5e+05 (5)	< 1	1.1e+04 (3)	7.1e+04 (4)	6.8e+05 (5)
Cs-137	< 1	< 1	< 1	< 1	< 1	< 1	< 1	< 1	< 1
Eu-152	< 1	< 1	< 1	< 1	< 1	< 1	< 1	< 1	< 1
H-3	< 1	< 1	< 1	< 1	< 1	< 1	< 1	< 1	< 1
Ho-166m	1.3e+05 (3)	1.6e+04 (4)	3.4e+04 (3)	1.6e+05 (3)	1.4e+05 (4)	4.4e+00 (3)	8.1e+03 (3)	1.5e+04 (3)	3.1e+05 (4)
I-129	3.7e+04 (4)	9.6e+02 (5)	1.3e+04 (3)	1.9e+04 (3)	1.0e+05 (5)	< 1	1.5e+03 (3)	7.9e+02 (4)	1.3e+05 (5)
Mo-93	2.9e+05 (4)	3.4e+05 (5)	1.4e+05 (3)	3.6e+05 (3)	1.2e+06 (5)	2.1e+05 (3)	3.0e+05 (3)	2.8e+04 (4)	1.8e+06 (5)
Nb-93m	3.7e+05 (4)	4.7e+05 (5)	1.6e+05 (3)	4.4e+05 (3)	1.6e+06 (5)	4.2e+05 (3)	3.0e+05 (3)	4.0e+04 (4)	2.4e+06 (5)
Nb-94	8.6e+05 (4)	1.0e+07 (5)	1.8e+05 (3)	7.3e+05 (3)	7.9e+06 (5)	7.9e+06 (3)	1.1e+05 (3)	3.8e+05 (4)	1.9e+07 (5)
Ni-59	5.1e+08 (4)	1.2e+08 (5)	2.3e+07 (3)	7.0e+07 (3)	6.8e+08 (5)	1.2e+08 (3)	1.4e+07 (3)	4.6e+06 (4)	1.2e+09 (5)
Ni-63	6.5e+06 (3)	4.5e+05 (3)	6.5e+05 (3)	2.9e+06 (3)	1.2e+06 (3)	4.3e+06 (3)	9.8e+05 (3)	8.7e+04 (3)	1.5e+07 (3)
Np-237	8.6e+03 (4)	2.1e+03 (5)	1.4e+03 (3)	4.2e+03 (3)	1.8e+04 (5)	9.9e+02 (3)	5.6e+02 (3)	2.7e+02 (4)	2.7e+04 (5)
Pa-231	3.5e+01 (5)	< 1	2.5e+02 (3)	4.5e+00 (3)	1.4e+02 (10)	< 1	2.3e+04 (3)	5.3e+03 (4)	2.4e+04 (3)
Pb-210	2.4e+01 (7)	5.7e+01 (10)	2.8e+00 (5)	1.9e+00 (3)	2.1e+02 (12)	2.8e+00 (4)	6.1e+00 (3)	4.3e+00 (5)	2.8e+02 (11)
Pd-107	1.3e+04 (4)	3.2e+05 (5)	2.2e+03 (3)	7.1e+03 (3)	2.8e+04 (5)	< 1	3.5e+02 (3)	7.0e+02 (4)	3.6e+05 (5)
Po-210	2.4e+01 (7)	5.7e+01 (10)	2.8e+00 (5)	1.9e+00 (3)	2.1e+02 (12)	2.8e+00 (4)	6.1e+00 (3)	4.3e+00 (5)	2.8e+02 (11)
Pu-238	2.4e+02 (3)	8.8e+01 (3)	2.8e+02 (3)	2.8e+02 (3)	6.3e+01 (3)	4.9e+02 (3)	4.8e+02 (3)	4.8e+01 (3)	1.6e+03 (3)
Pu-239	6.6e+05 (4)	7.9e+05 (5)	2.8e+05 (3)	3.4e+05 (3)	1.6e+06 (5)	4.6e+05 (3)	2.3e+05 (3)	1.1e+05 (4)	3.0e+06 (5)
Pu-240	7.8e+05 (4)	8.5e+05 (5)	2.9e+05 (3)	4.4e+05 (3)	1.8e+06 (5)	5.9e+05 (3)	2.1e+05 (3)	1.0e+05 (4)	3.4e+06 (4)
Pu-241	4.2e+02 (4)	1.0e+03 (5)	1.7e+02 (3)	2.3e+02 (3)	1.2e+03 (5)	< 1	1.3e+02 (3)	7.8e+01 (4)	2.6e+03 (5)
Pu-242	5.0e+03 (4)	6.3e+03 (5)	1.9e+03 (3)	2.5e+03 (3)	1.0e+04 (5)	3.5e+03 (3)	1.4e+03 (3)	7.0e+02 (4)	2.1e+04 (5)
Ra-226	2.5e+01 (7)	5.7e+01 (10)	2.9e+00 (5)	2.0e+00 (3)	2.1e+02 (12)	2.9e+00 (4)	6.6e+00 (3)	4.4e+00 (5)	2.8e+02 (11)
Ra-228	< 1	< 1	< 1	< 1	< 1	< 1	< 1	< 1	< 1
Se-79	5.2e+04 (4)	9.1e+02 (5)	8.9e+03 (3)	2.8e+04 (3)	1.1e+05 (5)	< 1	1.4e+03 (3)	2.4e+03 (4)	1.5e+05 (5)
Sm-151	2.4e+03 (3)	6.8e+01 (3)	6.5e+02 (3)	3.4e+03 (3)	3.6e+02 (3)	5.9e+01 (3)	2.5e+02 (3)	1.9e+02 (3)	6.7e+03 (3)
Sn-126	6.5e+03 (4)	2.1e+03 (5)	1.1e+03 (3)	3.5e+03 (3)	2.0e+04 (5)	8.5e+02 (3)	1.8e+02 (3)	3.2e+03 (4)	3.0e+04 (5)
Sr-90	< 1	< 1	< 1	< 1	< 1	< 1	< 1	< 1	< 1
Tc-99	1.5e+06 (4)	1.8e+05 (5)	1.3e+06 (3)	1.0e+06 (3)	5.0e+06 (5)	6.1e+04 (3)	6.5e+06 (3)	2.0e+05 (4)	9.1e+06 (3)
Th-228	< 1	< 1	< 1	< 1	< 1	< 1	< 1	< 1	< 1
Th-229	1.3e+01 (8)	1.1e+01 (13)	< 1	< 1	1.3e+02 (12)	< 1	< 1	< 1	1.5e+02 (12)
Th-230	4.9e+01 (5)	8.2e+01 (8)	1.1e+01 (3)	1.1e+01 (3)	2.7e+02 (10)	1.2e+01 (3)	4.5e+01 (3)	1.1e+01 (5)	3.8e+02 (9)
Th-232	< 1	< 1	< 1	< 1	< 1	< 1	< 1	< 1	< 1
U-232	< 1	< 1	< 1	< 1	< 1	< 1	< 1	< 1	< 1
U-233	8.0e+01 (5)	3.5e+01 (9)	6.0e+00 (3)	1.8e+01 (3)	3.7e+02 (11)	4.8e+00 (3)	2.0e+00 (3)	2.0e+00 (5)	4.4e+02 (10)
U-234	2.4e+03 (4)	2.4e+03 (5)	1.1e+03 (3)	1.1e+03 (3)	6.3e+03 (5)	1.1e+03 (3)	8.6e+03 (3)	7.6e+02 (4)	1.2e+04 (3)
U-235	8.0e+02 (4)	1.2e+01 (5)	1.1e+04 (3)	2.0e+02 (3)	1.4e+03 (5)	< 1	1.1e+06 (3)	1.3e+05 (4)	1.1e+06 (3)
U-236	7.1e+02 (4)	8.4e+02 (5)	2.7e+02 (3)	6.7e+02 (3)	1.8e+03 (5)	4.7e+02 (3)	1.5e+02 (3)	9.0e+01 (4)	3.4e+03 (5)
U-238	1.5e+03 (4)	1.5e+02 (5)	6.0e+02 (3)	1.6e+03 (3)	3.3e+03 (5)	< 1	2.6e+06 (3)	7.2e+04 (4)	2.6e+06 (3)
Zr-93	9.2e+04 (4)	1.3e+05 (5)	1.7e+04 (3)	7.6e+04 (3)	4.5e+05 (5)	2.1e+05 (3)	3.8e+03 (3)	1.2e+04 (4)	6.8e+05 (5)

Table E-34. Far-field releases for CCR_B1, peak release [Bq/year] and in parentheses time of peak [1000 year AD].

Nuclide	1BMA	2BMA	1BTF	2BTF	Silo	BRT	1BLA	2-5BLA	Total
Ac-227	2.1e+02 (10)	3.1e+00 (82)	7.9e+02 (9)	5.2e+00 (11)	5.6e+02 (31)	< 1	1.5e+04 (5)	4.2e+03 (82)	1.6e+04 (5)
Ag-108m	4.9e+05 (3)	2.1e+05 (4)	1.5e+05 (3)	5.6e+05 (3)	6.8e+05 (4)	1.9e+05 (3)	1.2e+05 (3)	5.3e+04 (3)	1.7e+06 (4)
Am-241	1.7e+05 (4)	3.9e+03 (4)	5.3e+04 (4)	1.9e+04 (4)	2.0e+04 (4)	1.8e+03 (4)	1.9e+04 (4)	6.4e+02 (4)	2.8e+05 (4)
Am-242m	1.7e+00 (4)	< 1	< 1	< 1	< 1	< 1	< 1	< 1	2.9e+00 (4)
Am-243	1.6e+04 (5)	4.8e+03 (9)	2.8e+03 (4)	1.8e+03 (4)	1.9e+04 (9)	7.8e+02 (5)	1.3e+03 (4)	3.4e+02 (5)	4.0e+04 (5)
Ba-133	< 1	< 1	< 1	< 1	< 1	< 1	< 1	< 1	< 1
C-14-ind	< 1	4.0e+05 (5)	< 1	< 1	< 1	2.6e+04 (24)	< 1	3.7e+05 (4)	6.8e+05 (4)
C-14-inorg	4.2e+08 (4)	1.1e+06 (5)	1.2e+08 (3)	3.4e+08 (3)	1.9e+08 (5)	< 1	1.1e+07 (3)	2.9e+05 (4)	7.7e+08 (3)
C-14-org	2.8e+07 (4)	3.1e+05 (5)	5.7e+06 (3)	7.7e+06 (3)	5.2e+07 (5)	< 1	2.2e+05 (3)	6.9e+04 (4)	7.5e+07 (5)
Ca-41	< 1	1.7e+06 (5)	< 1	< 1	< 1	< 1	< 1	1.4e+06 (4)	2.8e+06 (4)
Cd-113m	< 1	< 1	< 1	< 1	< 1	< 1	< 1	< 1	< 1
Cl-36	8.0e+04 (4)	2.3e+04 (5)	9.4e+03 (3)	2.4e+04 (3)	8.8e+04 (5)	2.7e+02 (28)	6.9e+04 (3)	1.7e+04 (4)	1.9e+05 (5)
Cm-242	2.1e+00 (4)	< 1	< 1	< 1	< 1	< 1	< 1	< 1	3.1e+00 (4)
Cm-243	< 1	< 1	< 1	< 1	< 1	< 1	< 1	< 1	< 1
Cm-244	< 1	< 1	< 1	< 1	< 1	< 1	< 1	< 1	< 1
Cm-245	1.8e+02 (5)	8.5e+01 (9)	2.5e+01 (4)	1.3e+01 (4)	1.9e+02 (9)	< 1	1.4e+01 (4)	4.1e+00 (5)	4.1e+02 (5)
Cm-246	3.9e+01 (5)	1.8e+01 (9)	5.9e+00 (4)	3.2e+00 (4)	3.5e+01 (9)	< 1	3.3e+00 (4)	1.0e+00 (5)	9.4e+01 (5)
Co-60	< 1	< 1	< 1	< 1	< 1	< 1	< 1	< 1	< 1
Cs-135	1.5e+05 (4)	2.5e+03 (9)	3.0e+04 (4)	9.0e+03 (4)	2.5e+05 (9)	< 1	2.8e+03 (3)	2.0e+04 (5)	3.9e+05 (5)
Cs-137	< 1	< 1	< 1	< 1	< 1	< 1	< 1	< 1	< 1
Eu-152	< 1	< 1	< 1	< 1	< 1	< 1	< 1	< 1	< 1
H-3	< 1	< 1	< 1	< 1	< 1	< 1	< 1	< 1	< 1
Ho-166m	3.6e+04 (4)	7.9e+02 (5)	4.2e+03 (4)	7.5e+03 (4)	1.3e+04 (5)	< 1	5.8e+02 (4)	3.3e+02 (5)	4.9e+04 (4)
I-129	3.7e+04 (4)	8.6e+02 (5)	1.2e+04 (3)	1.5e+04 (3)	9.7e+04 (5)	< 1	1.4e+03 (3)	7.2e+02 (4)	1.3e+05 (5)
Mo-93	2.9e+05 (4)	3.0e+05 (5)	1.3e+05 (3)	2.8e+05 (3)	1.2e+06 (5)	1.7e+05 (3)	2.7e+05 (3)	2.6e+04 (4)	1.7e+06 (5)
Nb-93m	8.9e+04 (5)	1.3e+04 (16)	5.6e+03 (4)	8.6e+03 (5)	1.8e+05 (12)	2.6e+03 (5)	2.0e+03 (3)	6.2e+02 (10)	2.4e+05 (10)
Nb-94	3.5e+05 (5)	6.8e+05 (11)	2.5e+04 (4)	3.9e+04 (5)	1.5e+06 (9)	1.2e+05 (5)	9.2e+03 (4)	1.3e+04 (5)	2.4e+06 (9)
Ni-59	3.8e+08 (4)	4.7e+07 (9)	1.3e+07 (4)	1.9e+07 (4)	3.5e+08 (9)	1.4e+07 (4)	3.7e+06 (3)	1.4e+06 (5)	7.4e+08 (5)
Ni-63	1.5e+06 (3)	2.5e+04 (4)	5.7e+04 (3)	1.4e+05 (3)	1.0e+05 (4)	4.2e+04 (4)	1.1e+05 (3)	2.4e+03 (3)	1.8e+06 (3)
Np-237	2.6e+03 (5)	8.4e+01 (14)	1.1e+02 (5)	1.4e+02 (5)	2.2e+03 (14)	5.6e+00 (9)	2.4e+01 (4)	4.9e+00 (5)	3.7e+03 (9)
Pa-231	2.4e+01 (9)	< 1	8.7e+01 (9)	< 1	5.3e+01 (25)	< 1	1.9e+03 (5)	6.6e+02 (82)	2.0e+03 (5)
Pb-210	3.2e+01 (77)	6.9e+01 (77)	6.4e+00 (77)	3.7e+00 (77)	3.6e+02 (77)	2.8e+00 (77)	3.1e+02 (77)	7.1e+01 (82)	8.6e+02 (77)
Pd-107	1.3e+04 (4)	2.8e+05 (5)	2.1e+03 (3)	5.6e+03 (3)	2.7e+04 (5)	< 1	3.2e+02 (3)	6.4e+02 (4)	3.2e+05 (5)
Po-210	3.4e+01 (77)	6.7e+01 (77)	6.9e+00 (77)	3.7e+00 (77)	3.8e+02 (77)	3.0e+00 (77)	3.2e+02 (77)	6.2e+01 (82)	8.8e+02 (77)
Pu-238	1.1e+01 (3)	< 1	2.6e+00 (4)	1.0e+00 (4)	< 1	< 1	5.0e+00 (3)	< 1	1.8e+01 (3)
Pu-239	2.9e+05 (5)	6.6e+04 (10)	4.6e+04 (4)	2.3e+04 (4)	3.4e+05 (9)	1.1e+04 (5)	2.3e+04 (4)	5.1e+03 (5)	6.1e+05 (5)
Pu-240	3.2e+05 (5)	5.0e+04 (9)	4.7e+04 (4)	2.8e+04 (4)	2.8e+05 (9)	1.2e+04 (5)	2.1e+04 (4)	4.3e+03 (5)	6.6e+05 (5)
Pu-241	4.5e+02 (5)	1.3e+02 (11)	4.7e+01 (5)	3.1e+01 (5)	4.8e+02 (11)	< 1	2.2e+01 (4)	3.6e+00 (9)	1.0e+03 (9)
Pu-242	2.3e+03 (5)	6.0e+02 (11)	3.1e+02 (4)	1.7e+02 (4)	2.4e+03 (9)	8.5e+01 (5)	1.4e+02 (4)	3.4e+01 (5)	4.4e+03 (5)
Ra-226	5.6e+02 (77)	1.1e+03 (77)	1.1e+02 (77)	6.2e+01 (77)	6.1e+03 (77)	5.5e+01 (77)	5.4e+03 (77)	1.1e+03 (82)	1.5e+04 (77)
Ra-228	< 1	< 1	< 1	< 1	< 1	< 1	< 1	< 1	< 1
Se-79	5.2e+04 (4)	8.1e+02 (5)	8.3e+03 (3)	2.2e+04 (3)	1.0e+05 (5)	< 1	1.3e+03 (3)	2.2e+03 (4)	1.5e+05 (5)
Sm-151	7.4e+01 (3)	< 1	5.5e+00 (4)	6.7e+00 (3)	2.1e+00 (4)	< 1	1.9e+00 (3)	< 1	8.6e+01 (3)
Sn-126	1.1e+03 (9)	2.7e+01 (22)	3.3e+01 (9)	3.8e+01 (9)	1.1e+03 (20)	< 1	2.9e+00 (5)	1.3e+01 (16)	1.6e+03 (13)
Sr-90	< 1	< 1	< 1	< 1	< 1	< 1	< 1	< 1	< 1
Tc-99	4.3e+05 (5)	7.1e+03 (16)	1.1e+05 (5)	3.4e+04 (5)	6.4e+05 (12)	1.6e+03 (47)	3.0e+05 (4)	3.9e+03 (9)	1.1e+06 (9)
Th-228	< 1	< 1	< 1	< 1	< 1	< 1	< 1	< 1	< 1
Th-229	3.7e+01 (77)	1.6e+01 (82)	2.6e+00 (77)	3.5e+00 (82)	2.9e+02 (82)	< 1	< 1	< 1	3.5e+02 (82)
Th-230	3.4e+01 (9)	2.7e+01 (82)	3.8e+00 (9)	1.6e+00 (77)	1.4e+02 (82)	1.3e+00 (82)	1.9e+02 (82)	4.0e+01 (82)	4.3e+02 (82)
Th-232	< 1	< 1	< 1	< 1	< 1	< 1	< 1	< 1	< 1
U-232	< 1	< 1	< 1	< 1	< 1	< 1	< 1	< 1	< 1
U-233	5.8e+01 (9)	1.5e+01 (77)	2.3e+00 (9)	2.8e+00 (77)	2.3e+02 (82)	< 1	< 1	< 1	2.8e+02 (82)
U-234	6.6e+02 (5)	9.3e+01 (15)	8.9e+01 (5)	3.9e+01 (5)	8.0e+02 (13)	5.8e+00 (5)	5.9e+02 (5)	6.9e+01 (82)	1.8e+03 (9)
U-235	2.2e+02 (5)	< 1	8.9e+02 (5)	7.0e+00 (5)	1.9e+02 (13)	< 1	4.4e+04 (4)	2.6e+03 (10)	4.6e+04 (4)
U-236	2.0e+02 (5)	4.0e+01 (16)	2.3e+01 (5)	2.3e+01 (5)	2.6e+02 (13)	2.7e+00 (11)	6.4e+00 (4)	2.0e+00 (10)	4.4e+02 (10)
U-238	4.3e+02 (5)	6.2e+00 (15)	4.9e+01 (5)	5.5e+01 (5)	4.3e+02 (13)	< 1	1.1e+05 (4)	1.4e+03 (10)	1.1e+05 (4)
Zr-93	3.9e+04 (5)	9.5e+03 (12)	2.0e+03 (5)	4.0e+03 (5)	9.0e+04 (11)	1.8e+03 (5)	2.8e+02 (4)	3.7e+02 (9)	1.2e+05 (9)

Table E-35. Doses for CCR_B1, peak dose [Sv/year] and in parentheses time of peak [1000 year AD].

Nuclide	1BMA	2BMA	1BTF	2BTF	Silo	BRT	1BLA	2-5BLA	Total
Total	1.2e-05 (5)	3.6e-06 (8)	1.5e-06 (5)	2.9e-06 (3)	2.6e-05 (28)	6.6e-07 (5)	1.3e-06 (24)	5.2e-07 (9)	4.1e-05 (25)
Ac-227	2.4e-09 (34)	8.7e-11 (66)	8.8e-09 (37)	6.2e-11 (32)	5.9e-09 (52)	2.0e-12 (67)	2.1e-07 (33)	9.5e-08 (57)	3.1e-07 (38)
Ag-108m	1.3e-08 (5)	7.2e-09 (5)	2.1e-09 (5)	3.9e-09 (5)	2.8e-08 (5)	3.2e-09 (5)	5.3e-10 (5)	1.4e-09 (5)	5.8e-08 (5)
Am-241	2.0e-09 (5)	4.5e-09 (4)	1.2e-09 (4)	2.2e-10 (4)	2.3e-09 (4)	2.0e-09 (4)	1.6e-10 (4)	5.8e-10 (4)	1.0e-08 (4)
Am-242m	< 1e-12	< 1e-12	< 1e-12	< 1e-12	< 1e-12	< 1e-12	< 1e-12	< 1e-12	< 1e-12
Am-243	1.1e-08 (17)	6.5e-09 (9)	1.3e-09 (17)	8.3e-10 (16)	2.4e-08 (23)	9.2e-10 (5)	2.5e-10 (15)	3.4e-10 (5)	4.4e-08 (21)
Ba-133	< 1e-12	< 1e-12	< 1e-12	< 1e-12	< 1e-12	< 1e-12	< 1e-12	< 1e-12	< 1e-12
C-14-ind	< 1e-12	1.1e-08 (5)	< 1e-12	< 1e-12	< 1e-12	7.2e-10 (24)	< 1e-12	7.8e-09 (5)	1.9e-08 (5)
C-14-inorg	9.0e-06 (5)	3.2e-08 (5)	1.2e-06 (3)	2.8e-06 (3)	5.2e-06 (5)	< 1e-12	9.0e-08 (3)	6.0e-09 (5)	1.6e-05 (5)
C-14-org	7.1e-07 (5)	8.6e-09 (5)	6.1e-08 (3)	6.4e-08 (3)	1.5e-06 (5)	< 1e-12	1.8e-09 (3)	1.5e-09 (5)	2.1e-06 (5)
Ca-41	< 1e-12	1.3e-06 (15)	< 1e-12	< 1e-12	< 1e-12	< 1e-12	< 1e-12	4.4e-07 (10)	1.6e-06 (14)
Cd-113m	< 1e-12	< 1e-12	< 1e-12	< 1e-12	< 1e-12	< 1e-12	< 1e-12	< 1e-12	< 1e-12
Cl-36	2.5e-07 (5)	7.5e-08 (5)	1.0e-08 (5)	1.1e-08 (5)	2.9e-07 (5)	8.8e-10 (28)	1.9e-08 (3)	4.8e-08 (5)	6.4e-07 (5)
Cm-242	< 1e-12	< 1e-12	< 1e-12	< 1e-12	< 1e-12	< 1e-12	< 1e-12	< 1e-12	< 1e-12
Cm-243	< 1e-12	< 1e-12	< 1e-12	< 1e-12	< 1e-12	< 1e-12	< 1e-12	< 1e-12	< 1e-12
Cm-244	< 1e-12	< 1e-12	< 1e-12	< 1e-12	< 1e-12	< 1e-12	< 1e-12	< 1e-12	< 1e-12
Cm-245	1.5e-10 (18)	1.4e-10 (24)	1.5e-11 (17)	8.6e-12 (17)	3.2e-10 (24)	< 1e-12	2.6e-12 (15)	4.2e-12 (5)	6.1e-10 (23)
Cm-246	1.6e-11 (13)	2.5e-11 (9)	1.6e-12 (12)	< 1e-12	2.8e-11 (17)	< 1e-12	< 1e-12	< 1e-12	5.9e-11 (15)
Co-60	< 1e-12	< 1e-12	< 1e-12	< 1e-12	< 1e-12	< 1e-12	< 1e-12	< 1e-12	< 1e-12
Cs-135	7.1e-07 (86)	2.7e-08 (86)	6.3e-08 (86)	1.5e-08 (86)	2.9e-06 (86)	< 1e-12	2.5e-09 (86)	9.9e-08 (86)	3.8e-06 (86)
Cs-137	< 1e-12	< 1e-12	< 1e-12	< 1e-12	< 1e-12	< 1e-12	< 1e-12	< 1e-12	< 1e-12
Eu-152	< 1e-12	< 1e-12	< 1e-12	< 1e-12	< 1e-12	< 1e-12	< 1e-12	< 1e-12	< 1e-12
H-3	< 1e-12	< 1e-12	< 1e-12	< 1e-12	< 1e-12	< 1e-12	< 1e-12	< 1e-12	< 1e-12
Ho-166m	1.0e-10 (7)	9.8e-12 (5)	6.0e-12 (6)	1.3e-11 (6)	4.1e-11 (8)	< 1e-12	< 1e-12	3.9e-12 (5)	1.6e-10 (7)
I-129	5.0e-07 (7)	1.9e-08 (9)	7.5e-08 (5)	4.7e-08 (5)	2.1e-06 (10)	< 1e-12	3.2e-09 (3)	8.2e-09 (6)	2.6e-06 (9)
Mo-93	1.9e-06 (6)	2.8e-06 (7)	4.6e-07 (5)	5.2e-07 (5)	9.9e-06 (7)	6.0e-07 (5)	2.7e-07 (5)	1.6e-07 (5)	1.5e-05 (7)
Nb-93m	6.1e-10 (6)	8.7e-10 (7)	1.5e-10 (5)	1.6e-10 (5)	3.1e-09 (7)	1.9e-10 (5)	8.8e-11 (5)	5.0e-11 (5)	4.9e-09 (7)
Nb-94	9.8e-09 (34)	5.0e-08 (48)	4.5e-10 (35)	8.5e-10 (36)	9.2e-08 (45)	4.4e-09 (45)	8.2e-11 (32)	6.3e-10 (43)	1.6e-07 (45)
Ni-59	9.5e-06 (18)	2.2e-06 (28)	1.2e-07 (17)	1.6e-07 (17)	2.1e-05 (27)	2.9e-07 (21)	1.8e-08 (15)	3.1e-08 (21)	3.2e-05 (25)
Ni-63	7.4e-11 (3)	2.2e-11 (4)	2.9e-12 (3)	6.5e-12 (3)	9.1e-12 (4)	3.7e-11 (4)	4.5e-12 (3)	1.9e-12 (3)	9.2e-11 (3)
Np-237	9.1e-09 (86)	9.8e-10 (86)	4.4e-10 (86)	5.2e-10 (86)	2.2e-08 (86)	5.9e-11 (86)	4.3e-11 (86)	3.2e-11 (86)	3.3e-08 (86)
Pa-231	4.7e-09 (32)	1.2e-10 (61)	1.6e-08 (33)	1.1e-10 (30)	9.6e-09 (52)	3.8e-12 (65)	3.9e-07 (30)	1.2e-07 (52)	5.2e-07 (35)
Pb-210	5.2e-09 (52)	7.9e-09 (86)	8.0e-10 (67)	3.5e-10 (67)	3.8e-08 (86)	3.3e-10 (86)	2.9e-08 (86)	7.5e-09 (86)	8.8e-08 (86)
Pd-107	1.9e-10 (18)	8.4e-09 (23)	9.2e-12 (14)	1.4e-11 (15)	8.7e-10 (25)	< 1e-12	< 1e-12	6.5e-12 (16)	9.5e-09 (23)
Po-210	1.5e-10 (67)	4.5e-10 (77)	2.4e-11 (86)	1.2e-11 (86)	1.3e-09 (86)	1.9e-11 (82)	9.9e-10 (86)	4.2e-10 (86)	3.2e-09 (86)
Pu-238	< 1e-12	< 1e-12	< 1e-12	< 1e-12	< 1e-12	< 1e-12	< 1e-12	< 1e-12	1.1e-12 (4)
Pu-239	1.3e-06 (33)	8.7e-07 (49)	1.6e-07 (34)	6.7e-08 (34)	4.3e-06 (44)	5.0e-08 (43)	3.2e-08 (32)	4.3e-08 (42)	6.8e-06 (42)
Pu-240	4.0e-07 (16)	1.2e-07 (22)	3.9e-08 (16)	2.0e-08 (15)	7.4e-07 (22)	1.7e-08 (5)	8.2e-09 (14)	7.0e-09 (18)	1.3e-06 (20)
Pu-241	5.6e-12 (18)	6.3e-12 (21)	< 1e-12	< 1e-12	1.4e-11 (24)	< 1e-12	< 1e-12	< 1e-12	2.6e-11 (22)
Pu-242	3.2e-08 (86)	3.4e-08 (86)	3.6e-09 (86)	1.8e-09 (86)	1.1e-07 (86)	1.8e-09 (86)	6.1e-10 (84)	1.2e-09 (86)	1.9e-07 (86)
Ra-226	3.2e-08 (52)	4.9e-08 (86)	5.0e-09 (67)	2.3e-09 (86)	2.4e-07 (86)	2.1e-09 (86)	1.8e-07 (86)	4.3e-08 (86)	5.5e-07 (86)
Ra-228	< 1e-12	< 1e-12	< 1e-12	< 1e-12	< 1e-12	< 1e-12	< 1e-12	< 1e-12	< 1e-12
Se-79	1.5e-08 (7)	3.6e-10 (11)	1.0e-09 (6)	1.5e-09 (6)	4.5e-08 (12)	< 1e-12	4.5e-11 (5)	5.2e-10 (7)	5.9e-08 (10)
Sm-151	< 1e-12	< 1e-12	< 1e-12	< 1e-12	< 1e-12	< 1e-12	< 1e-12	< 1e-12	< 1e-12
Sn-126	4.2e-10 (57)	3.7e-11 (86)	1.4e-11 (67)	2.2e-11 (67)	1.1e-09 (77)	1.1e-12 (78)	< 1e-12	1.5e-11 (78)	1.6e-09 (77)
Sr-90	< 1e-12	< 1e-12	< 1e-12	< 1e-12	< 1e-12	< 1e-12	< 1e-12	< 1e-12	< 1e-12
Tc-99	1.5e-07 (52)	9.0e-09 (77)	3.5e-08 (57)	1.0e-08 (57)	6.2e-07 (67)	1.6e-09 (86)	4.2e-08 (52)	3.3e-09 (67)	8.6e-07 (67)
Th-228	< 1e-12	< 1e-12	< 1e-12	< 1e-12	< 1e-12	< 1e-12	< 1e-12	< 1e-12	< 1e-12
Th-229	1.3e-08 (86)	1.7e-09 (86)	6.0e-10 (86)	7.2e-10 (86)	3.7e-08 (86)	7.2e-11 (86)	4.8e-11 (86)	3.6e-11 (86)	5.3e-08 (86)
Th-230	8.2e-10 (29)	6.2e-10 (86)	9.9e-11 (52)	4.2e-11 (67)	4.0e-09 (86)	2.6e-11 (86)	4.7e-09 (77)	5.5e-10 (77)	8.7e-09 (86)
Th-232	< 1e-12	< 1e-12	< 1e-12	< 1e-12	< 1e-12	< 1e-12	< 1e-12	3.4e-12 (9)	< 1e-12
U-232	< 1e-12	< 1e-12	< 1e-12	< 1e-12	< 1e-12	< 1e-12	< 1e-12	< 1e-12	< 1e-12
U-233	5.9e-09 (86)	1.0e-09 (86)	2.7e-10 (86)	3.5e-10 (86)	1.8e-08 (86)	5.0e-11 (86)	2.3e-11 (86)	2.0e-11 (86)	2.5e-08 (86)
U-234	9.1e-09 (11)	3.0e-09 (46)	9.7e-10 (12)	4.9e-10 (9)	1.9e-08 (36)	1.7e-10 (34)	3.6e-08 (49)	4.6e-09 (67)	6.7e-08 (40)
U-235	2.9e-09 (11)	5.3e-11 (52)	1.0e-08 (12)	8.6e-11 (9)	4.5e-09 (37)	1.7e-12 (57)	3.3e-07 (7)	6.4e-08 (35)	3.5e-07 (7)
U-236	3.3e-09 (11)	1.5e-09 (48)	2.9e-10 (12)	3.0e-10 (9)	7.0e-09 (37)	1.1e-10 (36)	5.4e-11 (8)	3.9e-11 (24)	1.1e-08 (34)
U-238	5.7e-09 (11)	2.2e-10 (50)	4.8e-10 (11)	6.6e-10 (9)	1.0e-08 (37)	< 1e-12	8.0e-07 (7)	3.5e-08 (35)	8.1e-07 (7)
Zr-93	1.6e-08 (52)	1.8e-08 (77)	7.1e-10 (57)	1.6e-09 (60)	1.3e-07 (77)	2.9e-09 (77)	4.6e-11 (52)	4.5e-10 (77)	1.6e-07 (77)

Loss of barrier function calculation case – no sorption in the bedrock (CCR_B2)

Table E-36. Far-field releases for CCR_B2, peak release [Bq/year] and in parentheses time of peak [1000 year AD].

Nuclide	1BMA	2BMA	1BTF	2BTF	Silo	BRT	1BLA	2-5BLA	Total
Ac-227	1.7e+02 (84)	< 1	2.6e+01 (86)	2.1e+00 (12)	1.1e+01 (86)	< 1	2.0e+04 (3)	5.1e+03 (5)	2.1e+04 (3)
Ag-108m	3.7e+05 (3)	1.2e+05 (4)	1.4e+05 (3)	5.4e+05 (3)	2.5e+04 (4)	1.5e+05 (3)	1.2e+05 (3)	5.3e+04 (3)	1.2e+06 (3)
Am-241	7.8e+01 (4)	< 1	4.6e+00 (4)	9.6e+01 (4)	< 1	4.8e+00 (4)	3.3e+05 (3)	7.2e+04 (3)	3.5e+05 (3)
Am-242m	< 1	< 1	< 1	< 1	< 1	< 1	1.9e+01 (3)	2.5e+00 (3)	2.0e+01 (3)
Am-243	8.0e+01 (7)	< 1	3.9e+00 (22)	2.2e+01 (4)	< 1	3.2e+00 (22)	1.2e+04 (3)	6.0e+03 (4)	1.2e+04 (3)
Ba-133	< 1	< 1	< 1	< 1	< 1	< 1	< 1	< 1	< 1
C-14-ind	< 1	4.0e+05 (5)	< 1	< 1	< 1	2.6e+04 (24)	< 1	3.7e+05 (4)	6.8e+05 (4)
C-14-inorg	2.5e+05 (22)	8.1e+00 (24)	1.4e+05 (12)	6.2e+05 (4)	1.8e+02 (34)	< 1	1.1e+07 (3)	2.9e+05 (4)	1.1e+07 (3)
C-14-org	2.8e+07 (4)	3.1e+05 (5)	5.7e+06 (3)	7.7e+06 (3)	5.2e+07 (5)	< 1	2.2e+05 (3)	6.9e+04 (4)	7.5e+07 (5)
Ca-41	< 1	7.8e+05 (10)	< 1	< 1	< 1	< 1	< 1	1.4e+06 (4)	1.4e+06 (4)
Cd-113m	< 1	< 1	< 1	< 1	< 1	< 1	< 1	< 1	< 1
Cl-36	4.0e+04 (4)	1.1e+04 (8)	6.8e+03 (3)	2.0e+04 (3)	3.4e+04 (6)	2.7e+02 (30)	6.9e+04 (3)	1.7e+04 (4)	1.0e+05 (3)
Cm-242	< 1	< 1	< 1	< 1	< 1	< 1	1.5e+01 (3)	2.1e+00 (3)	1.6e+01 (3)
Cm-243	< 1	< 1	< 1	< 1	< 1	< 1	< 1	< 1	< 1
Cm-244	< 1	< 1	< 1	< 1	< 1	< 1	< 1	< 1	< 1
Cm-245	< 1	< 1	< 1	< 1	< 1	< 1	1.2e+02 (3)	7.1e+01 (4)	1.3e+02 (3)
Cm-246	< 1	< 1	< 1	< 1	< 1	< 1	2.9e+01 (3)	2.0e+01 (4)	3.2e+01 (3)
Co-60	< 1	< 1	< 1	< 1	< 1	< 1	< 1	< 1	< 1
Cs-135	8.7e+04 (7)	2.2e+03 (7)	2.6e+04 (4)	1.5e+04 (3)	3.1e+04 (13)	< 1	9.8e+03 (3)	6.5e+04 (4)	1.6e+05 (4)
Cs-137	< 1	< 1	< 1	< 1	< 1	< 1	< 1	< 1	< 1
Eu-152	< 1	< 1	< 1	< 1	< 1	< 1	< 1	< 1	< 1
H-3	< 1	< 1	< 1	< 1	< 1	< 1	< 1	< 1	< 1
Ho-166m	4.4e+01 (5)	< 1	1.5e+00 (4)	6.8e+01 (4)	< 1	< 1	7.3e+03 (3)	1.4e+04 (4)	1.5e+04 (4)
I-129	2.0e+04 (22)	3.0e+02 (9)	6.7e+03 (3)	1.0e+04 (3)	2.3e+04 (6)	< 1	1.4e+03 (3)	7.2e+02 (4)	3.7e+04 (5)
Mo-93	8.0e+04 (4)	7.0e+04 (6)	7.4e+04 (3)	1.9e+05 (3)	2.5e+05 (5)	6.2e+04 (4)	2.7e+05 (3)	2.6e+04 (4)	5.4e+05 (3)
Nb-93m	1.5e+04 (24)	4.0e+04 (6)	2.5e+04 (3)	7.8e+04 (3)	6.8e+04 (6)	3.4e+04 (3)	2.7e+05 (3)	3.7e+04 (4)	3.6e+05 (3)
Nb-94	3.1e+03 (25)	5.1e+02 (67)	1.4e+02 (61)	3.3e+03 (7)	1.7e+02 (34)	1.2e+03 (67)	9.7e+04 (3)	3.5e+05 (4)	3.6e+05 (4)
Ni-59	1.4e+07 (59)	3.5e+06 (63)	1.7e+06 (4)	7.1e+06 (4)	7.4e+06 (34)	2.7e+06 (22)	1.3e+07 (3)	4.2e+06 (4)	2.1e+07 (58)
Ni-63	3.6e+02 (3)	< 1	3.0e+03 (3)	5.4e+04 (3)	< 1	8.0e+03 (3)	6.8e+05 (3)	5.6e+04 (3)	7.2e+05 (3)
Np-237	4.8e+02 (23)	2.2e+00 (86)	1.2e+00 (22)	2.2e+02 (4)	7.7e+01 (34)	< 1	5.1e+02 (3)	2.5e+02 (4)	6.1e+02 (3)
Pa-231	2.1e+01 (83)	< 1	5.4e+00 (58)	< 1	7.3e+00 (77)	< 1	2.1e+04 (3)	5.2e+03 (5)	2.1e+04 (3)
Pb-210	2.1e+02 (77)	1.0e+02 (86)	2.9e+00 (22)	3.1e+00 (22)	3.7e+01 (86)	3.9e+00 (22)	5.9e+00 (3)	4.4e+00 (5)	2.7e+02 (82)
Pd-107	4.5e+03 (4)	1.3e+05 (7)	1.5e+02 (4)	4.5e+03 (3)	3.3e+03 (7)	< 1	3.2e+02 (3)	6.4e+02 (4)	1.4e+05 (7)
Po-210	1.9e+03 (77)	1.2e+02 (86)	1.4e+01 (22)	9.4e+00 (22)	5.6e+01 (86)	4.1e+00 (22)	5.9e+00 (3)	4.4e+00 (5)	2.0e+03 (77)
Pu-238	2.8e+00 (3)	< 1	< 1	5.6e+00 (3)	< 1	< 1	3.2e+02 (3)	3.0e+01 (3)	3.4e+02 (3)
Pu-239	2.0e+04 (5)	1.7e+02 (59)	8.0e+01 (16)	2.5e+04 (3)	2.7e+03 (35)	1.0e+02 (13)	2.1e+05 (3)	9.8e+04 (4)	2.3e+05 (3)
Pu-240	2.3e+04 (4)	3.1e+00 (57)	4.6e+01 (13)	3.1e+04 (3)	7.1e+02 (17)	1.1e+02 (4)	1.9e+05 (3)	9.3e+04 (4)	2.3e+05 (3)
Pu-241	1.3e+01 (7)	< 1	< 1	8.7e+00 (13)	< 1	< 1	1.2e+02 (3)	7.1e+01 (4)	1.3e+02 (3)
Pu-242	2.2e+02 (23)	5.9e+00 (66)	1.0e+00 (32)	1.8e+02 (3)	3.7e+01 (35)	1.1e+00 (23)	1.3e+03 (3)	6.3e+02 (4)	1.5e+03 (3)
Ra-226	1.2e+03 (77)	2.3e+02 (84)	1.5e+01 (22)	6.4e+00 (22)	1.3e+02 (86)	8.4e+00 (22)	6.4e+00 (3)	4.5e+00 (5)	1.4e+03 (77)
Ra-228	< 1	< 1	< 1	< 1	< 1	< 1	< 1	< 1	< 1
Se-79	5.2e+04 (4)	8.1e+02 (5)	8.3e+03 (3)	2.2e+04 (3)	1.0e+05 (5)	< 1	1.3e+03 (3)	2.2e+03 (4)	1.5e+05 (5)
Sm-151	< 1	< 1	< 1	< 1	< 1	< 1	1.6e+02 (3)	1.2e+02 (3)	2.4e+02 (3)
Sn-126	2.2e+02 (57)	< 1	1.7e+00 (59)	1.2e+02 (5)	2.7e+01 (67)	< 1	1.6e+02 (3)	2.9e+03 (4)	3.0e+03 (4)
Sr-90	< 1	< 1	< 1	< 1	< 1	< 1	< 1	< 1	< 1
Tc-99	1.1e+05 (25)	2.1e+02 (86)	3.7e+03 (58)	6.9e+04 (4)	2.6e+04 (67)	3.7e+02 (59)	5.9e+06 (3)	1.8e+05 (4)	5.9e+06 (3)
Th-228	< 1	< 1	< 1	< 1	< 1	< 1	< 1	< 1	< 1
Th-229	6.8e+01 (84)	< 1	< 1	2.9e+00 (58)	4.6e+00 (86)	< 1	< 1	< 1	7.6e+01 (85)
Th-230	2.9e+01 (83)	< 1	< 1	2.1e+00 (58)	4.0e+00 (86)	< 1	4.2e+01 (3)	1.2e+01 (5)	4.3e+01 (3)
Th-232	< 1	< 1	< 1	< 1	< 1	< 1	< 1	< 1	< 1
U-232	< 1	< 1	< 1	< 1	< 1	< 1	< 1	< 1	< 1
U-233	9.1e+01 (56)	< 1	< 1	5.5e+00 (22)	2.0e+01 (77)	< 1	1.8e+00 (3)	2.0e+00 (5)	1.1e+02 (77)
U-234	1.2e+02 (23)	2.2e+00 (67)	< 1	6.4e+01 (4)	2.5e+01 (34)	< 1	7.8e+03 (3)	7.1e+02 (4)	7.8e+03 (3)
U-235	6.0e+01 (23)	< 1	2.5e+00 (58)	1.1e+01 (4)	5.7e+00 (34)	< 1	9.5e+05 (3)	1.2e+05 (4)	9.7e+05 (3)
U-236	3.8e+01 (23)	1.2e+00 (86)	< 1	3.8e+01 (4)	9.4e+00 (34)	< 1	1.3e+02 (3)	8.2e+01 (4)	1.6e+02 (3)
U-238	9.4e+01 (23)	< 1	< 1	9.0e+01 (4)	1.3e+01 (34)	< 1	2.3e+06 (3)	6.6e+04 (4)	2.4e+06 (3)
Zr-93	7.6e+03 (24)	5.1e+02 (86)	9.1e+01 (22)	5.7e+03 (4)	8.7e+03 (34)	2.5e+02 (22)	3.5e+03 (3)	1.1e+04 (4)	1.8e+04 (4)

Table E-37. Doses for CCR_B2, peak dose [Sv/year] and in parentheses time of peak [1000 year AD].

Nuclide	1BMA	2BMA	1BTF	2BTF	Silo	BRT	1BLA	2-5BLA	Total
Total	2.1e-06 (67)	1.0e-06 (17)	4.3e-07 (5)	5.3e-07 (5)	3.6e-06 (7)	3.8e-07 (5)	3.8e-06 (5)	2.2e-06 (17)	1.0e-05 (6)
Ac-227	1.0e-09 (67)	< 1e-12	1.6e-10 (86)	8.2e-11 (39)	2.3e-10 (86)	< 1e-12	3.1e-07 (22)	3.9e-07 (23)	7.0e-07 (23)
Ag-108m	9.9e-09 (5)	4.9e-09 (5)	2.0e-09 (5)	3.8e-09 (5)	1.2e-09 (5)	2.9e-09 (5)	5.3e-10 (5)	1.4e-09 (5)	2.6e-08 (5)
Am-241	1.5e-12 (5)	< 1e-12	< 1e-12	1.6e-12 (4)	< 1e-12	5.3e-12 (4)	1.4e-09 (3)	8.7e-08 (3)	8.7e-08 (3)
Am-242m	< 1e-12	< 1e-12	< 1e-12	< 1e-12	< 1e-12	< 1e-12	< 1e-12	< 1e-12	< 1e-12
Am-243	2.3e-11 (31)	< 1e-12	5.0e-12 (27)	2.7e-11 (25)	< 1e-12	7.6e-12 (23)	4.9e-10 (12)	7.2e-09 (4)	7.2e-09 (4)
Ba-133	< 1e-12	< 1e-12	< 1e-12	< 1e-12	< 1e-12	< 1e-12	< 1e-12	< 1e-12	< 1e-12
C-14-ind	< 1e-12	1.1e-08 (5)	< 1e-12	< 1e-12	< 1e-12	7.2e-10 (24)	< 1e-12	7.8e-09 (5)	1.9e-08 (5)
C-14-inorg	6.8e-09 (23)	< 1e-12	4.1e-09 (13)	1.7e-08 (6)	5.5e-12 (34)	< 1e-12	9.0e-08 (3)	6.0e-09 (5)	9.1e-08 (3)
C-14-org	7.1e-07 (5)	8.6e-09 (5)	6.1e-08 (3)	6.4e-08 (3)	1.5e-06 (5)	< 1e-12	1.8e-09 (3)	1.5e-09 (5)	2.1e-06 (5)
Ca-41	< 1e-12	8.4e-07 (28)	< 1e-12	< 1e-12	< 1e-12	< 1e-12	< 1e-12	4.4e-07 (10)	1.0e-06 (19)
Cd-113m	< 1e-12	< 1e-12	< 1e-12	< 1e-12	< 1e-12	< 1e-12	< 1e-12	< 1e-12	< 1e-12
Cl-36	1.3e-07 (5)	3.7e-08 (8)	1.0e-08 (5)	1.1e-08 (5)	1.1e-07 (6)	8.8e-10 (30)	1.9e-08 (3)	4.8e-08 (5)	3.1e-07 (5)
Cm-242	< 1e-12	< 1e-12	< 1e-12	< 1e-12	< 1e-12	< 1e-12	< 1e-12	< 1e-12	< 1e-12
Cm-243	< 1e-12	< 1e-12	< 1e-12	< 1e-12	< 1e-12	< 1e-12	< 1e-12	< 1e-12	< 1e-12
Cm-244	< 1e-12	< 1e-12	< 1e-12	< 1e-12	< 1e-12	< 1e-12	< 1e-12	< 1e-12	< 1e-12
Cm-245	< 1e-12	< 1e-12	< 1e-12	< 1e-12	< 1e-12	< 1e-12	5.3e-12 (14)	9.0e-11 (4)	9.0e-11 (4)
Cm-246	< 1e-12	< 1e-12	< 1e-12	< 1e-12	< 1e-12	< 1e-12	< 1e-12	2.5e-11 (4)	2.5e-11 (4)
Co-60	< 1e-12	< 1e-12	< 1e-12	< 1e-12	< 1e-12	< 1e-12	< 1e-12	< 1e-12	< 1e-12
Cs-135	7.1e-07 (86)	3.6e-08 (86)	6.7e-08 (86)	1.7e-08 (86)	8.5e-07 (86)	< 1e-12	2.7e-09 (86)	1.6e-07 (86)	1.8e-06 (86)
Cs-137	< 1e-12	< 1e-12	< 1e-12	< 1e-12	< 1e-12	< 1e-12	< 1e-12	< 1e-12	< 1e-12
Eu-152	< 1e-12	< 1e-12	< 1e-12	< 1e-12	< 1e-12	< 1e-12	< 1e-12	< 1e-12	< 1e-12
H-3	< 1e-12	< 1e-12	< 1e-12	< 1e-12	< 1e-12	< 1e-12	< 1e-12	< 1e-12	< 1e-12
Ho-166m	< 1e-12	< 1e-12	< 1e-12	< 1e-12	< 1e-12	< 1e-12	2.1e-12 (5)	1.8e-10 (4)	1.8e-10 (4)
I-129	2.4e-07 (11)	8.6e-09 (27)	5.7e-08 (6)	4.1e-08 (5)	5.6e-07 (16)	< 1e-12	3.2e-09 (3)	8.2e-09 (6)	8.1e-07 (13)
Mo-93	6.6e-07 (6)	7.4e-07 (9)	3.3e-07 (5)	4.3e-07 (5)	2.3e-06 (8)	3.7e-07 (5)	2.7e-07 (5)	1.6e-07 (5)	4.5e-06 (7)
Nb-93m	2.2e-10 (6)	2.5e-10 (8)	1.1e-10 (5)	1.4e-10 (5)	7.5e-10 (8)	1.2e-10 (5)	8.8e-11 (5)	5.9e-11 (5)	1.5e-09 (7)
Nb-94	4.5e-10 (67)	3.7e-11 (86)	1.2e-11 (77)	2.8e-10 (46)	1.6e-11 (78)	1.3e-10 (77)	1.3e-10 (27)	4.1e-09 (28)	4.7e-09 (32)
Ni-59	1.5e-06 (67)	2.3e-07 (86)	4.6e-08 (32)	9.0e-08 (26)	4.0e-07 (52)	1.8e-07 (52)	2.0e-08 (13)	6.1e-08 (15)	2.3e-06 (67)
Ni-63	< 1e-12	< 1e-12	< 1e-12	2.6e-12 (3)	< 1e-12	7.1e-12 (3)	1.8e-11 (3)	4.9e-11 (3)	5.7e-11 (3)
Np-237	3.1e-09 (86)	4.7e-12 (86)	1.0e-11 (86)	6.7e-10 (86)	4.3e-10 (86)	1.4e-12 (86)	6.5e-11 (86)	2.6e-10 (86)	4.5e-09 (86)
Pa-231	2.3e-09 (86)	< 1e-12	4.5e-10 (86)	1.5e-10 (34)	4.8e-10 (86)	< 1e-12	6.3e-07 (20)	8.3e-07 (21)	1.5e-06 (21)
Pb-210	6.2e-09 (86)	1.8e-09 (67)	9.5e-11 (23)	2.8e-10 (48)	9.9e-10 (67)	6.3e-11 (22)	2.6e-08 (67)	7.8e-09 (62)	3.7e-08 (67)
Pd-107	9.9e-11 (36)	4.5e-09 (67)	1.7e-12 (30)	1.3e-11 (18)	2.1e-10 (41)	< 1e-12	< 1e-12	6.5e-12 (16)	4.7e-09 (67)
Po-210	2.2e-10 (86)	8.0e-10 (86)	4.7e-12 (22)	5.7e-12 (67)	6.0e-11 (86)	2.7e-11 (22)	9.9e-11 (67)	3.0e-11 (63)	9.6e-10 (86)
Pu-238	< 1e-12	< 1e-12	< 1e-12	< 1e-12	< 1e-12	< 1e-12	< 1e-12	3.9e-11 (3)	3.9e-11 (3)
Pu-239	2.3e-07 (52)	1.7e-09 (86)	1.6e-09 (67)	6.9e-08 (39)	4.9e-08 (67)	1.9e-09 (57)	4.5e-08 (27)	1.9e-07 (28)	5.2e-07 (46)
Pu-240	2.8e-08 (18)	7.5e-12 (67)	1.2e-10 (27)	1.8e-08 (16)	1.7e-09 (35)	2.5e-10 (23)	1.5e-08 (12)	1.4e-07 (4)	1.4e-07 (4)
Pu-241	< 1e-12	< 1e-12	< 1e-12	< 1e-12	< 1e-12	< 1e-12	< 1e-12	2.1e-12 (4)	2.1e-12 (4)
Pu-242	1.1e-08 (86)	9.9e-11 (86)	6.7e-11 (86)	2.1e-09 (86)	2.3e-09 (86)	7.2e-11 (86)	7.2e-10 (77)	3.3e-09 (78)	2.0e-08 (86)
Ra-226	3.9e-08 (86)	9.0e-09 (67)	5.9e-10 (22)	1.6e-09 (67)	6.6e-09 (86)	3.4e-10 (23)	1.1e-07 (78)	3.2e-08 (77)	1.5e-07 (86)
Ra-228	< 1e-12	< 1e-12	< 1e-12	< 1e-12	< 1e-12	< 1e-12	< 1e-12	< 1e-12	< 1e-12
Se-79	1.5e-08 (7)	3.6e-10 (11)	1.0e-09 (6)	1.5e-09 (6)	4.5e-08 (12)	< 1e-12	4.5e-11 (5)	5.2e-10 (7)	5.9e-08 (10)
Sm-151	< 1e-12	< 1e-12	< 1e-12	< 1e-12	< 1e-12	< 1e-12	< 1e-12	< 1e-12	< 1e-12
Sn-126	2.1e-10 (86)	< 1e-12	< 1e-12	3.8e-11 (67)	2.1e-11 (86)	< 1e-12	1.4e-12 (38)	2.3e-10 (40)	4.5e-10 (77)
Sr-90	< 1e-12	< 1e-12	< 1e-12	< 1e-12	< 1e-12	< 1e-12	< 1e-12	< 1e-12	< 1e-12
Tc-99	9.7e-08 (77)	5.7e-11 (86)	3.4e-09 (86)	1.6e-08 (52)	3.7e-08 (86)	2.9e-10 (86)	6.4e-08 (36)	1.8e-08 (38)	2.1e-07 (77)
Th-228	< 1e-12	< 1e-12	< 1e-12	< 1e-12	< 1e-12	< 1e-12	< 1e-12	< 1e-12	< 1e-12
Th-229	6.9e-09 (86)	1.2e-11 (86)	2.0e-11 (86)	1.0e-09 (86)	1.6e-09 (86)	1.5e-12 (86)	7.9e-11 (86)	3.2e-10 (86)	9.9e-09 (86)
Th-230	4.6e-10 (86)	2.6e-12 (86)	4.3e-12 (62)	6.0e-11 (40)	1.3e-10 (77)	2.2e-12 (61)	5.1e-09 (67)	1.6e-09 (66)	7.1e-09 (67)
Th-232	< 1e-12	< 1e-12	2.4e-12 (9)	< 1e-12	1.0e-12 (10)	< 1e-12	< 1e-12	2.0e-12 (7)	< 1e-12
U-232	< 1e-12	< 1e-12	< 1e-12	< 1e-12	< 1e-12	< 1e-12	< 1e-12	< 1e-12	< 1e-12
U-233	3.1e-09 (86)	8.2e-12 (86)	8.3e-12 (86)	4.4e-10 (86)	5.5e-10 (86)	1.2e-12 (86)	3.5e-11 (86)	1.4e-10 (86)	4.3e-09 (86)
U-234	1.9e-09 (40)	4.1e-11 (67)	1.3e-11 (52)	5.6e-10 (7)	6.4e-10 (67)	5.1e-12 (52)	3.7e-08 (29)	1.2e-08 (25)	5.1e-08 (31)
U-235	9.0e-10 (40)	< 1e-12	6.4e-11 (67)	9.8e-11 (7)	1.5e-10 (67)	< 1e-12	1.0e-06 (5)	9.5e-07 (7)	1.8e-06 (6)
U-236	6.9e-10 (40)	1.8e-11 (67)	4.1e-12 (44)	3.3e-10 (8)	2.4e-10 (67)	1.9e-12 (52)	1.5e-10 (5)	6.8e-10 (7)	1.3e-09 (37)
U-238	1.5e-09 (40)	< 1e-12	1.6e-11 (51)	7.6e-10 (7)	3.5e-10 (67)	< 1e-12	2.5e-06 (5)	5.1e-07 (7)	2.9e-06 (5)
Zr-93	1.1e-08 (86)	1.9e-10 (86)	1.1e-10 (77)	1.8e-09 (52)	2.1e-08 (86)	3.6e-10 (86)	5.7e-11 (41)	1.6e-09 (42)	3.5e-08 (86)

Loss of barrier function calculation case – high water flow in the repository (CCR_B3)

Table E-38. Near-field releases* for CCR_B3, peak release [Bq/year] and in parentheses time of peak [1000 year AD].

Nuclide	1BMA	2BMA	1BTF	2BTF	Silo	BRT	1BLA	2-5BLA	Total
Ac-227	2.1e+02 (16)	< 1	7.1e+02 (61)	6.9e+00 (4)	6.8e+00 (3)	< 1	5.7e+04 (3)	9.5e+03 (4)	5.7e+04 (3)
Ag-108m	1.4e+07 (3)	1.6e+06 (4)	9.3e+05 (3)	2.6e+06 (3)	3.2e+08 (3)	5.8e+04 (4)	3.3e+05 (3)	4.8e+04 (4)	3.4e+08 (3)
Am-241	3.0e+04 (4)	8.3e+00 (5)	2.8e+04 (3)	1.8e+04 (3)	2.0e+03 (5)	2.2e+00 (4)	9.5e+05 (3)	6.5e+04 (4)	9.8e+05 (3)
Am-242m	< 1	< 1	1.1e+00 (3)	< 1	< 1	< 1	5.3e+01 (3)	< 1	5.4e+01 (3)
Am-243	1.9e+04 (7)	1.3e+02 (7)	3.6e+03 (4)	2.8e+03 (4)	7.9e+03 (9)	2.9e+00 (22)	3.3e+04 (3)	9.9e+03 (4)	3.4e+04 (3)
Ba-133	< 1	< 1	< 1	< 1	< 1	< 1	< 1	< 1	< 1
C-14-ind	< 1	2.9e+06 (4)	< 1	< 1	< 1	2.7e+04 (24)	< 1	6.0e+05 (4)	3.5e+06 (4)
C-14-inorg	1.4e+08 (5)	6.0e+03 (7)	9.9e+07 (3)	7.7e+07 (3)	3.0e+08 (3)	< 1	3.2e+07 (3)	4.7e+05 (4)	4.8e+08 (3)
C-14-org	4.5e+08 (3)	2.3e+06 (4)	4.2e+07 (3)	3.4e+07 (3)	1.9e+08 (3)	< 1	6.3e+05 (3)	1.1e+05 (4)	7.2e+08 (3)
Ca-41	< 1	6.8e+06 (5)	< 1	< 1	< 1	< 1	< 1	2.5e+06 (4)	8.4e+06 (5)
Cd-113m	< 1	< 1	< 1	< 1	< 1	< 1	< 1	< 1	< 1
Cl-36	2.9e+06 (3)	1.4e+05 (4)	6.9e+04 (3)	1.0e+05 (3)	1.5e+06 (3)	2.7e+02 (29)	1.9e+05 (3)	3.0e+04 (4)	4.8e+06 (3)
Cm-242	< 1	< 1	2.9e+00 (3)	1.7e+00 (3)	< 1	< 1	4.4e+01 (3)	< 1	4.7e+01 (3)
Cm-243	< 1	< 1	< 1	< 1	< 1	< 1	< 1	< 1	< 1
Cm-244	< 1	< 1	< 1	< 1	< 1	< 1	< 1	< 1	< 1
Cm-245	1.1e+02 (7)	4.9e+00 (7)	2.3e+01 (4)	1.7e+01 (4)	6.7e+01 (12)	< 1	3.3e+02 (3)	1.2e+02 (4)	3.5e+02 (3)
Cm-246	2.1e+01 (7)	1.2e+00 (7)	5.4e+00 (4)	3.9e+00 (4)	1.1e+01 (10)	< 1	8.1e+01 (3)	3.2e+01 (4)	8.7e+01 (3)
Co-60	< 1	< 1	< 1	< 1	< 1	< 1	< 1	< 1	< 1
Cs-135	6.9e+06 (3)	1.4e+04 (5)	5.2e+05 (3)	1.2e+05 (3)	4.0e+07 (3)	< 1	2.8e+04 (3)	1.1e+05 (4)	4.7e+07 (3)
Cs-137	1.9e+00 (3)	< 1	< 1	< 1	1.7e+01 (3)	< 1	< 1	< 1	1.9e+01 (3)
Eu-152	< 1	< 1	< 1	< 1	< 1	< 1	< 1	< 1	< 1
H-3	< 1	< 1	< 1	< 1	< 1	< 1	< 1	< 1	< 1
Ho-166m	1.1e+04 (4)	6.4e+00 (7)	6.8e+03 (3)	5.8e+03 (3)	3.3e+04 (4)	< 1	2.1e+04 (3)	1.8e+04 (4)	7.1e+04 (4)
I-129	1.6e+06 (3)	5.1e+03 (4)	9.2e+04 (3)	5.8e+04 (3)	4.2e+06 (3)	< 1	3.9e+03 (3)	1.3e+03 (4)	6.0e+06 (3)
Mo-93	1.1e+07 (3)	1.9e+06 (4)	8.7e+05 (3)	1.1e+06 (3)	6.8e+07 (3)	5.9e+04 (4)	7.6e+05 (3)	4.1e+04 (4)	8.1e+07 (3)
Nb-93m	2.4e+05 (3)	3.1e+04 (4)	1.6e+04 (3)	7.4e+04 (3)	4.1e+06 (3)	9.4e+02 (4)	7.7e+05 (3)	6.0e+04 (4)	5.2e+06 (3)
Nb-94	1.1e+05 (9)	6.1e+03 (43)	1.2e+04 (4)	7.1e+04 (4)	6.7e+06 (4)	1.1e+03 (67)	2.7e+05 (3)	6.0e+05 (4)	7.2e+06 (4)
Ni-59	2.7e+09 (3)	1.8e+08 (7)	7.9e+07 (3)	9.1e+07 (3)	1.2e+10 (3)	3.6e+06 (22)	3.6e+07 (3)	7.4e+06 (4)	1.4e+10 (3)
Ni-63	4.5e+07 (3)	1.3e+03 (4)	3.2e+06 (3)	3.8e+06 (3)	4.6e+08 (3)	8.9e+02 (3)	1.9e+06 (3)	1.4e+04 (3)	4.9e+08 (3)
Np-237	3.3e+03 (3)	1.5e+01 (86)	5.9e+01 (4)	3.0e+03 (3)	7.6e+04 (3)	< 1	1.4e+03 (3)	4.4e+02 (4)	7.8e+04 (3)
Pa-231	2.6e+01 (7)	< 1	1.2e+02 (59)	1.5e+00 (4)	5.2e+02 (3)	< 1	5.9e+04 (3)	9.7e+03 (4)	5.9e+04 (3)
Pb-210	2.6e+02 (77)	7.1e+01 (83)	8.9e+00 (77)	2.2e+00 (4)	6.8e+02 (5)	< 1	1.5e+01 (3)	6.7e+00 (5)	7.2e+02 (5)
Pd-107	3.5e+05 (3)	1.7e+06 (4)	6.8e+03 (3)	2.3e+04 (3)	1.7e+06 (3)	< 1	9.0e+02 (3)	1.1e+03 (4)	2.1e+06 (3)
Po-210	2.2e+04 (77)	6.5e+03 (83)	6.8e+02 (77)	1.8e+02 (4)	6.2e+04 (6)	6.0e+01 (22)	1.5e+01 (3)	6.7e+00 (5)	6.3e+04 (6)
Pu-238	4.6e+02 (3)	< 1	7.9e+00 (3)	2.7e+02 (3)	1.1e+04 (3)	< 1	9.0e+02 (3)	7.2e+00 (3)	1.1e+04 (3)
Pu-239	5.2e+05 (3)	1.9e+03 (32)	1.3e+04 (3)	3.1e+05 (3)	1.6e+07 (3)	1.1e+02 (13)	5.8e+05 (3)	1.7e+05 (4)	1.6e+07 (3)
Pu-240	6.6e+05 (3)	4.7e+02 (19)	1.6e+04 (3)	4.0e+05 (3)	2.0e+07 (3)	9.4e+01 (5)	5.4e+05 (3)	1.5e+05 (4)	2.1e+07 (3)
Pu-241	1.5e+03 (6)	8.4e+01 (7)	1.2e+02 (4)	3.9e+02 (3)	1.0e+04 (10)	< 1	3.3e+02 (3)	1.2e+02 (4)	1.1e+04 (10)
Pu-242	3.9e+03 (3)	4.0e+01 (67)	9.6e+01 (3)	2.3e+03 (3)	9.2e+04 (3)	1.1e+00 (24)	3.6e+03 (3)	1.1e+03 (4)	9.8e+04 (3)
Ra-226	1.9e+03 (77)	9.3e+02 (83)	8.1e+01 (77)	4.8e+00 (4)	3.2e+02 (34)	8.2e+00 (22)	1.7e+01 (3)	6.9e+00 (5)	2.6e+03 (77)
Ra-228	< 1	< 1	< 1	< 1	< 1	< 1	< 1	< 1	< 1
Se-79	6.2e+05 (3)	5.2e+03 (4)	3.4e+04 (3)	9.7e+04 (3)	2.7e+05 (3)	< 1	3.6e+03 (3)	3.9e+03 (4)	1.0e+06 (3)
Sm-151	4.3e+01 (3)	< 1	1.7e+02 (3)	8.9e+01 (3)	9.9e+00 (3)	< 1	4.6e+02 (3)	2.7e+01 (3)	7.3e+02 (3)
Sn-126	3.4e+03 (4)	1.1e+00 (86)	4.7e+01 (4)	2.2e+03 (3)	7.9e+04 (4)	< 1	4.5e+02 (3)	5.1e+03 (4)	8.6e+04 (4)
Sr-90	< 1	< 1	< 1	< 1	< 1	< 1	< 1	< 1	< 1
Tc-99	1.2e+06 (7)	2.2e+03 (67)	1.3e+05 (4)	4.4e+05 (3)	1.1e+08 (3)	3.1e+02 (58)	1.7e+07 (3)	3.2e+05 (4)	1.1e+08 (3)
Th-228	< 1	< 1	< 1	< 1	< 1	< 1	< 1	< 1	< 1
Th-229	8.4e+01 (83)	< 1	4.0e+00 (58)	< 1	4.8e+01 (6)	< 1	< 1	< 1	9.6e+01 (82)
Th-230	3.2e+01 (7)	1.7e+00 (86)	6.6e+00 (58)	4.5e+00 (4)	4.0e+02 (3)	< 1	1.1e+02 (3)	2.0e+01 (4)	4.1e+02 (3)
Th-232	< 1	< 1	< 1	< 1	< 1	< 1	< 1	< 1	< 1
U-232	< 1	< 1	< 1	< 1	< 1	< 1	< 1	< 1	< 1
U-233	5.6e+01 (77)	5.9e+00 (77)	2.7e+00 (58)	1.4e+01 (3)	5.0e+02 (3)	< 1	5.2e+00 (3)	3.6e+00 (4)	5.4e+02 (3)
U-234	9.8e+02 (3)	1.4e+01 (67)	2.7e+01 (4)	8.3e+02 (3)	3.8e+04 (3)	< 1	2.2e+04 (3)	1.3e+03 (4)	5.3e+04 (3)
U-235	4.6e+02 (3)	< 1	1.1e+02 (25)	1.5e+02 (3)	7.7e+03 (3)	< 1	2.7e+06 (3)	2.1e+05 (4)	2.7e+06 (3)
U-236	2.2e+02 (3)	7.9e+00 (86)	1.4e+01 (4)	4.9e+02 (3)	1.0e+04 (3)	< 1	3.8e+02 (3)	1.5e+02 (4)	1.1e+04 (3)
U-238	7.7e+02 (3)	1.1e+00 (86)	4.1e+01 (4)	1.2e+03 (3)	1.9e+04 (3)	< 1	6.6e+06 (3)	1.2e+05 (4)	6.6e+06 (3)
Zr-93	8.7e+04 (3)	2.9e+03 (45)	5.8e+03 (3)	4.9e+04 (3)	1.8e+07 (3)	2.2e+02 (22)	9.8e+03 (3)	1.9e+04 (4)	1.8e+07 (3)

* Due to the very high water flow in this calculation case the peak release from the near-field occurs for non-sorbing radionuclides before the first output of simulation results after 50 years of simulated time. This holds for example for C-14-org. As the near-field and far-field models are directly coupled in the modelling without data loss this artefact is not assumed to affect the final result.

Table E-39. Far-field releases for CCR_B3, peak release [Bq/year] and in parentheses time of peak [1000 year AD].

Nuclide	1BMA	2BMA	1BTF	2BTF	Silo	BRT	1BLA	2-5BLA	Total
Ac-227	2.1e+02 (19)	< 1	4.8e+02 (22)	5.3e+00 (16)	5.3e+02 (26)	< 1	1.4e+04 (5)	4.1e+03 (82)	1.5e+04 (5)
Ag-108m	2.2e+07 (3)	1.3e+06 (4)	1.4e+06 (3)	2.8e+06 (3)	2.2e+08 (3)	4.8e+04 (4)	4.0e+05 (3)	4.0e+04 (4)	2.5e+08 (3)
Am-241	3.6e+03 (4)	< 1	1.4e+03 (4)	9.2e+02 (4)	4.5e+01 (5)	< 1	2.3e+04 (3)	5.5e+02 (5)	2.3e+04 (3)
Am-242m	< 1	< 1	< 1	< 1	< 1	< 1	1.1e+00 (3)	< 1	1.1e+00 (3)
Am-243	2.5e+03 (7)	5.6e+00 (12)	1.9e+02 (5)	1.9e+02 (5)	1.4e+03 (16)	< 1	1.0e+03 (4)	4.4e+02 (5)	3.3e+03 (7)
Ba-133	< 1	< 1	< 1	< 1	< 1	< 1	< 1	< 1	< 1
C-14-ind	< 1	2.5e+06 (4)	< 1	< 1	< 1	2.6e+04 (24)	< 1	5.4e+05 (4)	3.0e+06 (4)
C-14-inorg	1.4e+08 (5)	5.3e+03 (7)	8.6e+07 (3)	6.3e+07 (3)	3.0e+08 (4)	< 1	3.8e+07 (3)	4.2e+05 (4)	4.8e+08 (4)
C-14-org	7.3e+08 (3)	1.9e+06 (4)	5.8e+07 (3)	3.7e+07 (3)	2.6e+09 (3)	< 1	7.5e+05 (3)	1.0e+05 (4)	3.4e+09 (3)
Ca-41	< 1	5.9e+06 (5)	< 1	< 1	< 1	< 1	< 1	2.3e+06 (4)	7.4e+06 (5)
Cd-113m	< 1	< 1	< 1	< 1	< 1	< 1	< 1	< 1	< 1
Cl-36	3.4e+06 (3)	1.2e+05 (4)	8.5e+04 (3)	1.0e+05 (3)	5.1e+06 (3)	2.7e+02 (30)	2.3e+05 (3)	2.7e+04 (4)	9.0e+06 (3)
Cm-242	< 1	< 1	< 1	< 1	< 1	< 1	1.1e+00 (3)	< 1	1.1e+00 (3)
Cm-243	< 1	< 1	< 1	< 1	< 1	< 1	< 1	< 1	< 1
Cm-244	< 1	< 1	< 1	< 1	< 1	< 1	< 1	< 1	< 1
Cm-245	4.3e+01 (7)	< 1	2.3e+00 (4)	1.7e+00 (5)	1.6e+01 (15)	< 1	1.1e+01 (4)	5.5e+00 (5)	5.0e+01 (7)
Cm-246	8.1e+00 (7)	< 1	< 1	< 1	2.1e+00 (13)	< 1	2.7e+00 (4)	1.4e+00 (5)	9.6e+00 (7)
Co-60	< 1	< 1	< 1	< 1	< 1	< 1	< 1	< 1	< 1
Cs-135	1.2e+06 (3)	3.3e+03 (5)	5.0e+04 (4)	1.3e+04 (4)	2.1e+06 (4)	< 1	5.8e+03 (3)	2.8e+04 (5)	2.6e+06 (4)
Cs-137	< 1	< 1	< 1	< 1	< 1	< 1	< 1	< 1	< 1
Eu-152	< 1	< 1	< 1	< 1	< 1	< 1	< 1	< 1	< 1
H-3	< 1	< 1	< 1	< 1	< 1	< 1	< 1	< 1	< 1
Ho-166m	3.0e+03 (4)	< 1	1.3e+03 (4)	6.8e+02 (4)	2.5e+03 (5)	< 1	5.0e+02 (3)	4.4e+02 (5)	6.4e+03 (5)
I-129	1.6e+06 (3)	4.4e+03 (4)	1.0e+05 (3)	5.9e+04 (3)	6.8e+06 (3)	< 1	4.7e+03 (3)	1.1e+03 (4)	8.6e+06 (3)
Mo-93	1.2e+07 (3)	1.6e+06 (4)	1.0e+06 (3)	1.1e+06 (3)	1.0e+08 (3)	5.5e+04 (5)	9.1e+05 (3)	3.6e+04 (4)	1.2e+08 (3)
Nb-93m	6.9e+04 (5)	5.5e+03 (4)	6.4e+03 (3)	8.3e+03 (5)	5.5e+05 (3)	1.9e+02 (5)	8.5e+03 (3)	6.2e+02 (9)	6.4e+05 (3)
Nb-94	6.7e+04 (9)	9.3e+02 (52)	2.4e+03 (9)	1.1e+04 (5)	1.0e+06 (9)	1.8e+02 (67)	7.7e+03 (4)	1.7e+04 (5)	1.1e+06 (9)
Ni-59	1.6e+09 (4)	4.2e+07 (9)	1.8e+07 (4)	2.5e+07 (4)	2.5e+09 (4)	7.5e+05 (59)	8.9e+06 (3)	1.9e+06 (5)	4.1e+09 (4)
Ni-63	1.3e+07 (3)	1.0e+02 (4)	3.1e+05 (3)	1.8e+05 (3)	1.4e+07 (3)	5.0e+01 (4)	4.7e+05 (3)	7.1e+02 (4)	2.7e+07 (3)
Np-237	8.1e+02 (9)	2.5e+00 (86)	1.3e+01 (9)	1.1e+02 (5)	2.8e+03 (5)	< 1	2.1e+01 (4)	6.1e+00 (5)	3.6e+03 (5)
Pa-231	1.6e+01 (18)	< 1	6.7e+01 (77)	< 1	4.9e+01 (22)	< 1	1.8e+03 (5)	6.6e+02 (82)	1.9e+03 (5)
Pb-210	1.3e+02 (77)	1.6e+01 (86)	7.2e+00 (77)	3.9e+00 (77)	3.4e+02 (77)	< 1	3.2e+02 (77)	7.1e+01 (82)	8.7e+02 (77)
Pd-107	3.5e+05 (3)	1.5e+06 (4)	7.2e+03 (3)	2.4e+04 (3)	2.2e+06 (3)	< 1	1.1e+03 (3)	1.0e+03 (4)	2.6e+06 (3)
Po-210	1.6e+02 (77)	1.5e+01 (86)	9.0e+00 (77)	4.1e+00 (77)	3.4e+02 (77)	< 1	3.3e+02 (77)	6.1e+01 (82)	9.1e+02 (77)
Pu-238	1.6e+01 (3)	< 1	< 1	< 1	9.3e+00 (4)	< 1	1.5e+01 (3)	< 1	3.2e+01 (3)
Pu-239	1.6e+05 (5)	5.1e+02 (42)	2.5e+03 (5)	2.0e+04 (4)	8.3e+05 (5)	1.7e+01 (30)	1.8e+04 (4)	6.7e+03 (5)	1.0e+06 (5)
Pu-240	1.7e+05 (4)	7.9e+01 (23)	2.8e+03 (4)	2.4e+04 (4)	9.2e+05 (5)	4.1e+00 (15)	1.6e+04 (4)	5.7e+03 (5)	1.1e+06 (5)
Pu-241	1.9e+02 (6)	< 1	5.6e+00 (5)	5.7e+00 (5)	9.7e+01 (20)	< 1	2.0e+01 (4)	4.1e+00 (5)	2.2e+02 (5)
Pu-242	1.2e+03 (5)	1.5e+01 (86)	1.9e+01 (5)	1.5e+02 (4)	5.2e+03 (5)	< 1	1.1e+02 (4)	4.5e+01 (5)	6.7e+03 (5)
Ra-226	1.9e+03 (77)	2.1e+02 (85)	1.1e+02 (77)	6.5e+01 (77)	5.8e+03 (77)	1.7e+00 (22)	5.5e+03 (77)	1.1e+03 (82)	1.5e+04 (77)
Ra-228	< 1	< 1	< 1	< 1	< 1	< 1	< 1	< 1	< 1
Se-79	1.0e+06 (3)	4.5e+03 (4)	5.5e+04 (3)	1.0e+05 (3)	4.2e+06 (3)	< 1	4.3e+03 (3)	3.5e+03 (4)	5.4e+06 (3)
Sm-151	6.4e+00 (4)	< 1	1.7e+00 (3)	< 1	< 1	< 1	6.4e+00 (3)	< 1	9.2e+00 (4)
Sn-126	4.7e+02 (9)	< 1	7.4e+00 (10)	3.3e+01 (9)	1.3e+03 (14)	< 1	2.8e+00 (5)	1.3e+01 (16)	1.7e+03 (13)
Sr-90	< 1	< 1	< 1	< 1	< 1	< 1	< 1	< 1	< 1
Tc-99	3.2e+05 (8)	3.4e+02 (86)	2.3e+04 (9)	3.4e+04 (5)	1.4e+06 (5)	2.7e+01 (86)	2.7e+05 (4)	3.8e+03 (9)	1.9e+06 (5)
Th-228	< 1	< 1	< 1	< 1	< 1	< 1	< 1	< 1	< 1
Th-229	9.6e+01 (77)	< 1	3.3e+00 (77)	3.8e+00 (77)	2.7e+02 (82)	< 1	< 1	< 1	3.8e+02 (82)
Th-230	3.0e+01 (82)	< 1	3.3e+00 (77)	1.7e+00 (77)	1.4e+02 (82)	< 1	1.9e+02 (82)	4.0e+01 (82)	4.1e+02 (82)
Th-232	< 1	< 1	< 1	< 1	< 1	< 1	< 1	< 1	< 1
U-232	< 1	< 1	< 1	< 1	< 1	< 1	< 1	< 1	< 1
U-233	5.9e+01 (82)	< 1	2.4e+00 (77)	2.9e+00 (77)	2.2e+02 (82)	< 1	< 1	< 1	2.9e+02 (82)
U-234	2.0e+02 (9)	1.6e+00 (86)	6.5e+00 (26)	2.9e+01 (5)	1.4e+03 (5)	< 1	5.7e+02 (5)	6.9e+01 (82)	2.2e+03 (5)
U-235	8.3e+01 (9)	< 1	5.8e+01 (30)	5.2e+00 (5)	3.2e+02 (5)	< 1	3.8e+04 (4)	2.6e+03 (5)	3.9e+04 (4)
U-236	6.7e+01 (9)	< 1	2.5e+00 (24)	1.7e+01 (5)	3.9e+02 (5)	< 1	5.5e+00 (4)	2.0e+00 (10)	4.7e+02 (5)
U-238	1.5e+02 (9)	< 1	6.2e+00 (9)	4.0e+01 (5)	7.2e+02 (5)	< 1	9.4e+04 (4)	1.4e+03 (5)	9.5e+04 (4)
Zr-93	3.2e+04 (5)	7.6e+02 (86)	9.1e+02 (5)	3.8e+03 (5)	1.5e+05 (5)	3.4e+01 (43)	2.4e+02 (4)	3.7e+02 (9)	1.9e+05 (5)

Table E-40. Doses for CCR_B3, peak dose [Sv/year] and in parentheses time of peak [1000 year AD].

Nuclide	1BMA	2BMA	1BTF	2BTF	Silo	BRT	1BLA	2-5BLA	Total
Total	1.1e-05 (15)	1.0e-05 (6)	9.6e-07 (3)	8.0e-07 (3)	5.1e-05 (5)	3.5e-07 (6)	1.3e-06 (25)	5.5e-07 (8)	6.9e-05 (5)
Ac-227	1.6e-09 (48)	1.7e-12 (86)	2.8e-09 (86)	5.7e-11 (35)	5.9e-09 (52)	< 1e-12	2.1e-07 (33)	9.6e-08 (57)	3.0e-07 (38)
Ag-108m	2.4e-08 (5)	4.2e-08 (5)	1.9e-09 (5)	4.6e-09 (5)	5.9e-07 (5)	1.7e-09 (5)	3.8e-10 (5)	1.5e-09 (5)	6.5e-07 (5)
Am-241	7.1e-11 (5)	3.6e-12 (26)	3.3e-11 (4)	1.4e-11 (5)	3.9e-11 (33)	< 1e-12	1.6e-10 (4)	5.7e-10 (5)	7.1e-10 (5)
Am-242m	< 1e-12	< 1e-12	< 1e-12	< 1e-12	< 1e-12	< 1e-12	< 1e-12	< 1e-12	< 1e-12
Am-243	1.5e-09 (21)	1.8e-11 (37)	1.7e-10 (20)	1.4e-10 (20)	2.5e-09 (30)	< 1e-12	2.4e-10 (15)	4.6e-10 (5)	4.3e-09 (26)
Ba-133	< 1e-12	< 1e-12	< 1e-12	< 1e-12	< 1e-12	< 1e-12	< 1e-12	< 1e-12	< 1e-12
C-14-ind	< 1e-12	5.2e-08 (5)	< 1e-12	< 1e-12	< 1e-12	7.2e-10 (24)	< 1e-12	1.3e-08 (5)	6.6e-08 (5)
C-14-inorg	3.9e-06 (5)	1.5e-10 (7)	7.9e-07 (3)	6.4e-07 (3)	5.0e-06 (5)	< 1e-12	2.0e-08 (3)	1.0e-08 (5)	9.3e-06 (5)
C-14-org	4.7e-07 (3)	4.0e-08 (5)	4.5e-08 (3)	5.0e-08 (3)	4.1e-06 (3)	< 1e-12	4.0e-10 (3)	2.5e-09 (5)	4.6e-06 (3)
Ca-41	< 1e-12	1.8e-06 (10)	< 1e-12	< 1e-12	< 1e-12	< 1e-12	< 1e-12	4.6e-07 (9)	2.3e-06 (10)
Cd-113m	< 1e-12	< 1e-12	< 1e-12	< 1e-12	< 1e-12	< 1e-12	< 1e-12	< 1e-12	< 1e-12
Cl-36	1.8e-07 (3)	3.8e-07 (5)	7.5e-09 (3)	1.2e-08 (3)	4.2e-07 (3)	8.8e-10 (30)	9.9e-09 (3)	8.3e-08 (5)	6.2e-07 (3)
Cm-242	< 1e-12	< 1e-12	< 1e-12	< 1e-12	< 1e-12	< 1e-12	< 1e-12	< 1e-12	< 1e-12
Cm-243	< 1e-12	< 1e-12	< 1e-12	< 1e-12	< 1e-12	< 1e-12	< 1e-12	< 1e-12	< 1e-12
Cm-244	< 1e-12	< 1e-12	< 1e-12	< 1e-12	< 1e-12	< 1e-12	< 1e-12	< 1e-12	< 1e-12
Cm-245	2.4e-11 (22)	< 1e-12	1.9e-12 (19)	1.2e-12 (17)	4.7e-11 (36)	< 1e-12	2.5e-12 (15)	5.9e-12 (5)	7.1e-11 (31)
Cm-246	2.2e-12 (14)	< 1e-12	< 1e-12	< 1e-12	2.1e-12 (25)	< 1e-12	< 1e-12	1.3e-12 (5)	3.9e-12 (19)
Co-60	< 1e-12	< 1e-12	< 1e-12	< 1e-12	< 1e-12	< 1e-12	< 1e-12	< 1e-12	< 1e-12
Cs-135	7.1e-07 (86)	2.7e-08 (86)	6.1e-08 (86)	1.5e-08 (86)	3.1e-06 (86)	< 1e-12	2.5e-09 (86)	9.9e-08 (86)	4.0e-06 (86)
Cs-137	< 1e-12	< 1e-12	< 1e-12	< 1e-12	< 1e-12	< 1e-12	< 1e-12	< 1e-12	< 1e-12
Eu-152	< 1e-12	< 1e-12	< 1e-12	< 1e-12	< 1e-12	< 1e-12	< 1e-12	< 1e-12	< 1e-12
H-3	< 1e-12	< 1e-12	< 1e-12	< 1e-12	< 1e-12	< 1e-12	< 1e-12	< 1e-12	< 1e-12
Ho-166m	8.7e-12 (7)	< 1e-12	1.4e-12 (6)	1.3e-12 (7)	6.6e-12 (8)	< 1e-12	< 1e-12	5.3e-12 (5)	1.9e-11 (7)
I-129	1.2e-06 (3)	4.2e-08 (6)	1.0e-07 (3)	6.7e-08 (3)	5.9e-06 (3)	< 1e-12	2.9e-09 (3)	1.1e-08 (5)	7.3e-06 (3)
Mo-93	3.0e-06 (5)	9.4e-06 (6)	4.1e-07 (5)	5.2e-07 (5)	4.0e-05 (5)	3.5e-07 (6)	1.9e-07 (5)	2.0e-07 (5)	5.0e-05 (5)
Nb-93m	9.4e-10 (5)	3.0e-09 (6)	1.3e-10 (5)	1.7e-10 (5)	1.2e-08 (5)	1.1e-10 (6)	5.8e-11 (5)	6.5e-11 (5)	1.6e-08 (5)
Nb-94	4.5e-09 (44)	2.1e-10 (78)	1.5e-10 (45)	4.9e-10 (44)	6.5e-08 (49)	2.4e-11 (77)	8.0e-11 (33)	6.4e-10 (43)	7.1e-08 (49)
Ni-59	9.9e-06 (15)	1.8e-06 (30)	1.1e-07 (17)	1.6e-07 (18)	2.5e-05 (18)	1.1e-07 (52)	1.8e-08 (15)	3.2e-08 (21)	3.6e-05 (18)
Ni-63	6.1e-10 (3)	< 1e-12	1.1e-11 (3)	8.1e-12 (3)	1.3e-09 (3)	< 1e-12	9.1e-12 (3)	< 1e-12	1.4e-09 (3)
Np-237	6.1e-09 (86)	1.2e-11 (86)	1.6e-10 (86)	5.1e-10 (86)	2.3e-08 (86)	< 1e-12	4.2e-11 (86)	3.2e-11 (86)	3.0e-08 (86)
Pa-231	3.2e-09 (42)	1.9e-12 (86)	6.7e-09 (86)	1.0e-10 (32)	9.6e-09 (51)	< 1e-12	3.8e-07 (31)	1.2e-07 (52)	5.0e-07 (35)
Pb-210	8.7e-09 (86)	1.5e-09 (67)	7.4e-10 (86)	3.8e-10 (67)	3.6e-08 (86)	1.2e-11 (23)	2.9e-08 (86)	7.5e-09 (86)	8.4e-08 (86)
Pd-107	1.8e-10 (14)	9.6e-09 (15)	7.1e-12 (16)	1.1e-11 (14)	8.9e-10 (14)	< 1e-12	< 1e-12	6.5e-12 (15)	1.1e-08 (15)
Po-210	2.7e-10 (86)	1.3e-10 (86)	2.5e-11 (86)	1.2e-11 (86)	1.3e-09 (86)	< 1e-12	1.0e-09 (86)	4.2e-10 (86)	3.0e-09 (86)
Pu-238	< 1e-12	< 1e-12	< 1e-12	< 1e-12	1.2e-12 (4)	< 1e-12	< 1e-12	< 1e-12	1.2e-12 (4)
Pu-239	8.5e-07 (38)	1.1e-08 (77)	3.5e-08 (50)	6.3e-08 (36)	4.7e-06 (40)	4.0e-10 (67)	3.1e-08 (32)	4.3e-08 (42)	5.7e-06 (40)
Pu-240	2.2e-07 (17)	2.5e-10 (38)	4.9e-09 (20)	1.9e-08 (15)	1.1e-06 (18)	2.4e-11 (28)	7.9e-09 (14)	7.2e-09 (18)	1.4e-06 (18)
Pu-241	< 1e-12	< 1e-12	< 1e-12	< 1e-12	1.6e-12 (33)	< 1e-12	< 1e-12	< 1e-12	2.6e-12 (28)
Pu-242	2.5e-08 (86)	6.7e-10 (86)	1.3e-09 (86)	1.7e-09 (86)	1.2e-07 (86)	3.9e-12 (86)	6.0e-10 (84)	1.2e-09 (86)	1.5e-07 (86)
Ra-226	5.1e-08 (86)	8.4e-09 (67)	4.3e-09 (86)	2.4e-09 (86)	2.3e-07 (86)	5.7e-11 (23)	1.8e-07 (86)	4.3e-08 (86)	5.2e-07 (86)
Ra-228	< 1e-12	< 1e-12	< 1e-12	< 1e-12	< 1e-12	< 1e-12	< 1e-12	< 1e-12	< 1e-12
Se-79	9.7e-09 (5)	7.5e-10 (6)	6.0e-10 (5)	1.3e-09 (5)	5.9e-08 (5)	< 1e-12	3.2e-11 (5)	6.2e-10 (6)	7.1e-08 (5)
Sm-151	< 1e-12	< 1e-12	< 1e-12	< 1e-12	< 1e-12	< 1e-12	< 1e-12	< 1e-12	< 1e-12
Sn-126	3.3e-10 (67)	< 1e-12	7.1e-12 (78)	2.2e-11 (67)	1.2e-09 (77)	< 1e-12	< 1e-12	1.5e-11 (78)	1.5e-09 (77)
Sr-90	< 1e-12	< 1e-12	< 1e-12	< 1e-12	< 1e-12	< 1e-12	< 1e-12	< 1e-12	< 1e-12
Tc-99	1.4e-07 (57)	3.0e-10 (86)	2.6e-08 (77)	1.0e-08 (57)	6.2e-07 (67)	1.8e-11 (86)	4.2e-08 (52)	3.4e-09 (67)	8.4e-07 (64)
Th-228	< 1e-12	< 1e-12	< 1e-12	< 1e-12	< 1e-12	< 1e-12	< 1e-12	< 1e-12	< 1e-12
Th-229	1.1e-08 (86)	1.4e-11 (86)	2.8e-10 (86)	7.2e-10 (86)	3.8e-08 (86)	< 1e-12	4.7e-11 (86)	3.6e-11 (86)	5.0e-08 (86)
Th-230	7.5e-10 (86)	4.0e-12 (86)	5.9e-11 (86)	4.4e-11 (67)	3.9e-09 (86)	< 1e-12	4.7e-09 (77)	5.5e-10 (77)	8.0e-09 (86)
Th-232	< 1e-12	< 1e-12	< 1e-12	< 1e-12	< 1e-12	< 1e-12	< 1e-12	1.0e-12 (6)	< 1e-12
U-232	< 1e-12	< 1e-12	< 1e-12	< 1e-12	< 1e-12	< 1e-12	< 1e-12	< 1e-12	< 1e-12
U-233	4.8e-09 (86)	1.2e-11 (86)	1.2e-10 (86)	3.5e-10 (86)	1.8e-08 (86)	< 1e-12	2.2e-11 (86)	2.0e-11 (86)	2.3e-08 (86)
U-234	4.2e-09 (28)	5.5e-11 (77)	2.4e-10 (51)	4.2e-10 (9)	1.9e-08 (29)	< 1e-12	3.6e-08 (50)	4.6e-09 (67)	6.2e-08 (42)
U-235	1.6e-09 (26)	< 1e-12	2.2e-09 (52)	7.4e-11 (9)	4.6e-09 (31)	< 1e-12	3.1e-07 (7)	6.4e-08 (35)	3.3e-07 (7)
U-236	1.7e-09 (29)	2.8e-11 (86)	8.1e-11 (45)	2.7e-10 (10)	7.2e-09 (31)	< 1e-12	5.2e-11 (8)	3.8e-11 (23)	9.3e-09 (30)
U-238	2.9e-09 (27)	3.3e-12 (86)	1.6e-10 (40)	5.7e-10 (9)	1.0e-08 (31)	< 1e-12	7.7e-07 (7)	3.5e-08 (35)	7.8e-07 (7)
Zr-93	1.6e-08 (57)	1.4e-09 (86)	5.1e-10 (67)	1.6e-09 (60)	1.3e-07 (67)	7.4e-11 (86)	4.5e-11 (52)	4.6e-10 (77)	1.5e-07 (67)

Changed repository redox conditions in SFR 1 calculation case (CCR_RX)

Table E-41. Doses for CCR_RX, peak dose [Sv/year] and in parentheses time of peak [1000 year AD].

Nuclide	1BMA	1BTF	2BTF	Silo	1BLA	Total
Total	2.3e-06 (67)	4.3e-07 (5)	5.3e-07 (5)	4.4e-06 (51)	1.3e-06 (24)	7.4e-06 (52)
Ac-227	7.1e-10 (86)	2.4e-11 (86)	3.0e-11 (36)	5.7e-10 (67)	2.1e-07 (33)	2.1e-07 (33)
Ag-108m	1.0e-08 (5)	2.0e-09 (5)	3.8e-09 (5)	1.2e-09 (5)	5.3e-10 (5)	1.7e-08 (5)
Am-241	< 1e-12	< 1e-12	< 1e-12	< 1e-12	1.6e-10 (4)	1.6e-10 (4)
Am-242m	< 1e-12	< 1e-12	< 1e-12	< 1e-12	< 1e-12	< 1e-12
Am-243	1.6e-11 (22)	2.3e-12 (29)	1.3e-11 (27)	< 1e-12	2.5e-10 (15)	2.7e-10 (16)
Ba-133	< 1e-12	< 1e-12	< 1e-12	< 1e-12	< 1e-12	< 1e-12
C-14-ind	< 1e-12	< 1e-12	< 1e-12	< 1e-12	< 1e-12	< 1e-12
C-14-inorg	6.6e-09 (23)	4.0e-09 (13)	1.7e-08 (6)	4.9e-12 (34)	9.0e-08 (3)	9.0e-08 (3)
C-14-org	7.1e-07 (5)	6.1e-08 (3)	6.4e-08 (3)	1.4e-06 (5)	1.8e-09 (3)	2.1e-06 (5)
Ca-41	< 1e-12	< 1e-12	< 1e-12	< 1e-12	< 1e-12	< 1e-12
Cd-113m	< 1e-12	< 1e-12	< 1e-12	< 1e-12	< 1e-12	< 1e-12
Cl-36	1.3e-07 (5)	1.0e-08 (5)	1.1e-08 (5)	1.1e-07 (6)	1.9e-08 (3)	2.5e-07 (5)
Cm-242	< 1e-12	< 1e-12	< 1e-12	< 1e-12	< 1e-12	< 1e-12
Cm-243	< 1e-12	< 1e-12	< 1e-12	< 1e-12	< 1e-12	< 1e-12
Cm-244	< 1e-12	< 1e-12	< 1e-12	< 1e-12	< 1e-12	< 1e-12
Cm-245	< 1e-12	< 1e-12	< 1e-12	< 1e-12	2.6e-12 (15)	2.7e-12 (15)
Cm-246	< 1e-12	< 1e-12	< 1e-12	< 1e-12	< 1e-12	< 1e-12
Co-60	< 1e-12	< 1e-12	< 1e-12	< 1e-12	< 1e-12	< 1e-12
Cs-135	6.7e-07 (86)	6.2e-08 (86)	1.5e-08 (86)	5.6e-07 (86)	2.5e-09 (86)	1.3e-06 (86)
Cs-137	< 1e-12	< 1e-12	< 1e-12	< 1e-12	< 1e-12	< 1e-12
Eu-152	< 1e-12	< 1e-12	< 1e-12	< 1e-12	< 1e-12	< 1e-12
H-3	< 1e-12	< 1e-12	< 1e-12	< 1e-12	< 1e-12	< 1e-12
Ho-166m	< 1e-12	< 1e-12	< 1e-12	< 1e-12	< 1e-12	< 1e-12
I-129	2.5e-07 (10)	5.7e-08 (6)	4.1e-08 (5)	6.5e-07 (16)	3.2e-09 (3)	9.0e-07 (13)
Mo-93	6.8e-07 (6)	3.4e-07 (5)	4.4e-07 (5)	2.3e-06 (8)	2.7e-07 (5)	3.5e-06 (7)
Nb-93m	2.1e-10 (6)	1.1e-10 (5)	1.4e-10 (5)	7.0e-10 (8)	8.8e-11 (5)	1.1e-09 (7)
Nb-94	2.5e-10 (67)	6.2e-12 (77)	1.4e-10 (52)	6.7e-12 (77)	8.2e-11 (32)	4.4e-10 (67)
Ni-59	1.3e-06 (67)	4.0e-08 (35)	7.7e-08 (29)	3.0e-07 (52)	1.8e-08 (15)	1.6e-06 (67)
Ni-63	< 1e-12	< 1e-12	< 1e-12	< 1e-12	4.5e-12 (3)	4.6e-12 (3)
Np-237	7.3e-09 (86)	2.9e-10 (86)	5.2e-10 (86)	2.0e-08 (86)	4.3e-11 (86)	2.8e-08 (86)
Pa-231	1.6e-09 (86)	8.0e-11 (86)	6.0e-11 (34)	1.1e-09 (67)	3.9e-07 (30)	3.9e-07 (31)
Pb-210	4.6e-09 (86)	5.1e-11 (23)	3.1e-10 (86)	2.6e-09 (86)	2.9e-08 (86)	3.6e-08 (86)
Pd-107	9.8e-11 (37)	1.7e-12 (29)	1.3e-11 (18)	2.1e-10 (41)	< 1e-12	3.2e-10 (39)
Po-210	1.8e-10 (86)	2.8e-12 (22)	1.1e-11 (86)	1.2e-10 (86)	9.9e-10 (86)	1.3e-09 (86)
Pu-238	< 1e-12	< 1e-12	< 1e-12	< 1e-12	< 1e-12	< 1e-12
Pu-239	8.1e-07 (42)	6.9e-08 (48)	6.8e-08 (35)	3.1e-06 (49)	3.2e-08 (32)	4.0e-06 (48)
Pu-240	1.9e-07 (17)	9.3e-09 (21)	2.0e-08 (16)	4.3e-07 (23)	8.2e-09 (14)	6.3e-07 (21)
Pu-241	< 1e-12	< 1e-12	< 1e-12	< 1e-12	< 1e-12	< 1e-12
Pu-242	2.8e-08 (86)	2.4e-09 (86)	1.8e-09 (86)	9.5e-08 (86)	6.1e-10 (84)	1.3e-07 (86)
Ra-226	3.1e-08 (86)	3.8e-10 (23)	2.2e-09 (86)	2.0e-08 (86)	1.8e-07 (86)	2.3e-07 (86)
Ra-228	< 1e-12	< 1e-12	< 1e-12	< 1e-12	< 1e-12	< 1e-12
Se-79	1.1e-08 (9)	8.8e-10 (6)	1.5e-09 (6)	3.4e-08 (13)	4.5e-11 (5)	4.4e-08 (12)
Sm-151	< 1e-12	< 1e-12	< 1e-12	< 1e-12	< 1e-12	< 1e-12
Sn-126	1.1e-10 (86)	< 1e-12	1.5e-11 (78)	2.3e-12 (98)	< 1e-12	1.2e-10 (86)
Sr-90	< 1e-12	< 1e-12	< 1e-12	< 1e-12	< 1e-12	< 1e-12
Tc-99	1.5e-07 (52)	3.6e-08 (57)	1.1e-08 (57)	6.2e-07 (67)	4.2e-08 (52)	8.5e-07 (67)
Th-228	< 1e-12	< 1e-12	< 1e-12	< 1e-12	< 1e-12	< 1e-12
Th-229	1.1e-08 (86)	3.9e-10 (86)	7.4e-10 (86)	3.2e-08 (86)	4.8e-11 (86)	4.4e-08 (86)
Th-230	3.2e-10 (86)	< 1e-12	3.7e-11 (86)	3.0e-10 (86)	4.7e-09 (77)	5.2e-09 (77)
Th-232	< 1e-12	< 1e-12	< 1e-12	< 1e-12	< 1e-12	< 1e-12
U-232	< 1e-12	< 1e-12	< 1e-12	< 1e-12	< 1e-12	< 1e-12
U-233	4.8e-09 (86)	1.6e-10 (86)	3.3e-10 (86)	1.2e-08 (86)	2.3e-11 (86)	1.7e-08 (86)
U-234	1.3e-09 (67)	< 1e-12	2.0e-10 (37)	1.5e-09 (52)	3.6e-08 (49)	3.9e-08 (50)
U-235	6.1e-10 (67)	3.1e-12 (67)	2.8e-11 (27)	4.4e-10 (52)	3.3e-07 (7)	3.3e-07 (7)
U-236	5.9e-10 (41)	1.1e-11 (32)	1.4e-10 (32)	1.1e-09 (44)	5.4e-11 (8)	1.8e-09 (43)
U-238	1.0e-09 (67)	< 1e-12	2.6e-10 (35)	8.2e-10 (52)	8.0e-07 (7)	8.0e-07 (7)
Zr-93	8.4e-09 (86)	7.1e-11 (86)	1.3e-09 (67)	7.8e-09 (86)	4.6e-11 (52)	1.8e-08 (86)

Extended global warming calculation case (CCR_EX)

Table E-42. Near-field releases for CCR_EX, peak release [Bq/year] and in parentheses time of peak [1000 year AD].

Nuclide	1BMA	2BMA	1BTF	2BTF	Silo	BRT	1BLA	2-5BLA	Total
Ac-227	1.6e+02 (57)	< 1	3.6e+01 (102)	2.4e+00 (20)	1.7e+01 (102)	< 1	2.2e+04 (3)	5.2e+03 (4)	2.3e+04 (3)
Ag-108m	3.8e+05 (3)	1.4e+05 (4)	1.6e+05 (3)	7.4e+05 (3)	2.7e+04 (4)	2.0e+05 (3)	1.3e+05 (3)	6.5e+04 (3)	1.4e+06 (3)
Am-241	8.0e+01 (4)	< 1	4.8e+00 (4)	1.3e+02 (4)	< 1	6.9e+00 (4)	3.8e+05 (3)	8.8e+04 (3)	4.1e+05 (3)
Am-242m	< 1	< 1	< 1	< 1	< 1	< 1	2.5e+01 (3)	3.7e+00 (3)	2.5e+01 (3)
Am-243	9.7e+01 (7)	< 1	5.2e+00 (22)	2.8e+01 (4)	< 1	3.8e+00 (22)	1.3e+04 (3)	6.5e+03 (4)	1.4e+04 (3)
Ba-133	< 1	< 1	< 1	< 1	< 1	< 1	< 1	< 1	< 1
C-14-ind	< 1	4.5e+05 (5)	< 1	< 1	< 1	2.7e+04 (24)	< 1	4.0e+05 (4)	7.6e+05 (4)
C-14-inorg	2.5e+05 (22)	8.8e+00 (53)	1.5e+05 (12)	6.6e+05 (4)	2.0e+02 (34)	< 1	1.3e+07 (3)	3.1e+05 (4)	1.3e+07 (3)
C-14-org	2.9e+07 (4)	3.5e+05 (5)	6.3e+06 (3)	9.8e+06 (3)	5.3e+07 (5)	< 1	2.5e+05 (3)	7.5e+04 (4)	7.7e+07 (5)
Ca-41	< 1	8.0e+05 (10)	< 1	< 1	< 1	< 1	< 1	1.6e+06 (4)	1.6e+06 (4)
Cd-113m	< 1	< 1	< 1	< 1	< 1	< 1	< 1	< 1	< 1
Cl-36	4.0e+04 (4)	1.2e+04 (7)	7.0e+03 (3)	2.4e+04 (3)	3.5e+04 (6)	2.7e+02 (29)	7.6e+04 (3)	1.9e+04 (4)	1.1e+05 (3)
Cm-242	< 1	< 1	< 1	< 1	< 1	< 1	2.0e+01 (3)	3.0e+00 (3)	2.0e+01 (3)
Cm-243	< 1	< 1	< 1	< 1	< 1	< 1	< 1	< 1	< 1
Cm-244	< 1	< 1	< 1	< 1	< 1	< 1	< 1	< 1	< 1
Cm-245	< 1	< 1	< 1	< 1	< 1	< 1	1.3e+02 (3)	7.8e+01 (4)	1.5e+02 (3)
Cm-246	< 1	< 1	< 1	< 1	< 1	< 1	3.2e+01 (3)	2.1e+01 (4)	3.7e+01 (3)
Co-60	< 1	< 1	< 1	< 1	< 1	< 1	< 1	< 1	< 1
Cs-135	9.4e+04 (7)	2.4e+03 (7)	2.6e+04 (4)	1.8e+04 (3)	3.1e+04 (13)	< 1	1.1e+04 (3)	7.1e+04 (4)	1.6e+05 (4)
Cs-137	< 1	< 1	< 1	< 1	< 1	< 1	< 1	< 1	< 1
Eu-152	< 1	< 1	< 1	< 1	< 1	< 1	< 1	< 1	< 1
H-3	< 1	< 1	< 1	< 1	< 1	< 1	< 1	< 1	< 1
Ho-166m	4.5e+01 (5)	< 1	1.5e+00 (4)	7.3e+01 (4)	< 1	< 1	8.1e+03 (3)	1.5e+04 (3)	1.7e+04 (3)
I-129	2.0e+04 (22)	2.8e+02 (8)	6.8e+03 (3)	1.3e+04 (3)	2.3e+04 (6)	< 1	1.5e+03 (3)	7.9e+02 (4)	3.7e+04 (5)
Mo-93	8.1e+04 (4)	7.7e+04 (5)	7.7e+04 (3)	2.3e+05 (3)	2.5e+05 (5)	6.6e+04 (4)	3.0e+05 (3)	2.8e+04 (4)	6.2e+05 (3)
Nb-93m	1.6e+04 (24)	2.0e+03 (102)	1.1e+03 (3)	7.1e+03 (4)	7.8e+03 (57)	1.1e+03 (4)	3.0e+05 (3)	4.0e+04 (4)	3.1e+05 (3)
Nb-94	3.2e+03 (25)	6.0e+02 (65)	1.4e+02 (61)	3.3e+03 (7)	1.4e+02 (72)	1.2e+03 (66)	1.1e+05 (3)	3.8e+05 (4)	3.8e+05 (4)
Ni-59	1.4e+07 (55)	3.7e+06 (59)	2.0e+06 (4)	7.0e+06 (4)	8.2e+06 (34)	3.5e+06 (22)	1.4e+07 (3)	4.6e+06 (4)	2.2e+07 (58)
Ni-63	3.7e+02 (3)	< 1	3.5e+03 (3)	6.6e+04 (3)	< 1	1.4e+04 (3)	9.8e+05 (3)	8.7e+04 (3)	9.8e+05 (3)
Np-237	4.8e+02 (23)	2.3e+00 (102)	1.4e+00 (22)	2.4e+02 (4)	8.5e+01 (34)	< 1	5.6e+02 (3)	2.7e+02 (4)	6.7e+02 (3)
Pa-231	1.9e+01 (55)	< 1	6.0e+00 (58)	< 1	8.4e+00 (102)	< 1	2.3e+04 (3)	5.3e+03 (4)	2.4e+04 (3)
Pb-210	5.2e+01 (89)	2.4e+01 (102)	1.3e+00 (22)	2.6e+00 (22)	1.2e+01 (102)	< 1	6.1e+00 (3)	4.3e+00 (5)	8.9e+01 (102)
Pd-107	4.6e+03 (4)	1.3e+05 (6)	1.5e+02 (4)	5.5e+03 (3)	3.3e+03 (7)	< 1	3.5e+02 (3)	7.0e+02 (4)	1.4e+05 (6)
Po-210	4.1e+03 (90)	2.1e+03 (102)	1.0e+02 (22)	8.2e+01 (22)	9.1e+02 (102)	6.8e+01 (22)	6.1e+00 (3)	4.3e+00 (5)	7.2e+03 (102)
Pu-238	3.2e+00 (3)	< 1	< 1	7.2e+00 (3)	< 1	< 1	4.8e+02 (3)	4.8e+01 (3)	4.8e+02 (3)
Pu-239	2.0e+04 (5)	2.0e+02 (54)	8.0e+01 (16)	2.5e+04 (3)	2.7e+03 (35)	1.1e+02 (13)	2.3e+05 (3)	1.1e+05 (4)	2.6e+05 (3)
Pu-240	2.4e+04 (4)	4.9e+00 (53)	4.6e+01 (13)	3.2e+04 (3)	7.2e+02 (17)	1.2e+02 (4)	2.1e+05 (3)	1.0e+05 (4)	2.5e+05 (3)
Pu-241	1.5e+01 (7)	< 1	1.0e+00 (17)	1.1e+01 (13)	< 1	< 1	1.3e+02 (3)	7.8e+01 (4)	1.5e+02 (3)
Pu-242	2.2e+02 (23)	6.0e+00 (60)	1.0e+00 (32)	1.9e+02 (3)	3.7e+01 (35)	1.1e+00 (24)	1.4e+03 (3)	7.0e+02 (4)	1.7e+03 (3)
Ra-226	3.7e+02 (96)	2.7e+02 (102)	1.5e+01 (22)	6.5e+00 (22)	1.8e+02 (102)	9.0e+00 (22)	6.6e+00 (3)	4.4e+00 (5)	8.4e+02 (102)
Ra-228	< 1	< 1	< 1	< 1	< 1	< 1	< 1	< 1	< 1
Se-79	5.2e+04 (4)	9.1e+02 (5)	8.9e+03 (3)	2.8e+04 (3)	1.1e+05 (5)	< 1	1.4e+03 (3)	2.4e+03 (4)	1.5e+05 (5)
Sm-151	< 1	< 1	< 1	< 1	< 1	< 1	2.5e+02 (3)	1.9e+02 (3)	3.4e+02 (3)
Sn-126	2.3e+02 (53)	< 1	1.7e+00 (59)	1.2e+02 (5)	2.9e+01 (73)	< 1	1.8e+02 (3)	3.2e+03 (4)	3.3e+03 (4)
Sr-90	< 1	< 1	< 1	< 1	< 1	< 1	< 1	< 1	< 1
Tc-99	1.1e+05 (25)	3.2e+02 (102)	4.4e+03 (58)	7.4e+04 (4)	2.6e+04 (63)	4.5e+02 (58)	6.5e+06 (3)	2.0e+05 (4)	6.6e+06 (3)
Th-228	< 1	< 1	< 1	< 1	< 1	< 1	< 1	< 1	< 1
Th-229	5.4e+01 (102)	< 1	< 1	3.1e+00 (58)	7.0e+00 (102)	< 1	< 1	< 1	6.3e+01 (102)
Th-230	2.4e+01 (57)	< 1	< 1	2.4e+00 (22)	5.9e+00 (102)	< 1	4.5e+01 (3)	1.1e+01 (5)	4.6e+01 (3)
Th-232	< 1	< 1	< 1	< 1	< 1	< 1	< 1	< 1	< 1
U-232	< 1	< 1	< 1	< 1	< 1	< 1	< 1	< 1	< 1
U-233	7.6e+01 (53)	< 1	< 1	5.7e+00 (22)	2.1e+01 (102)	< 1	2.0e+00 (3)	2.0e+00 (5)	8.8e+01 (53)
U-234	1.2e+02 (23)	2.2e+00 (63)	< 1	6.5e+01 (4)	2.7e+01 (34)	< 1	8.6e+03 (3)	7.6e+02 (4)	8.7e+03 (3)
U-235	6.1e+01 (23)	< 1	2.8e+00 (102)	1.2e+01 (4)	6.2e+00 (34)	< 1	1.1e+06 (3)	1.3e+05 (4)	1.1e+06 (3)
U-236	3.8e+01 (23)	1.2e+00 (102)	< 1	3.9e+01 (4)	1.0e+01 (34)	< 1	1.5e+02 (3)	9.0e+01 (4)	1.8e+02 (3)
U-238	9.5e+01 (23)	< 1	< 1	9.1e+01 (4)	1.4e+01 (34)	< 1	2.6e+06 (3)	7.2e+04 (4)	2.6e+06 (3)
Zr-93	7.6e+03 (24)	6.5e+02 (102)	9.6e+01 (22)	5.9e+03 (4)	9.7e+03 (34)	2.7e+02 (22)	3.8e+03 (3)	1.2e+04 (4)	1.8e+04 (4)

Table E-43. Far-field releases for CCR_EX, peak release [Bq/year] and in parentheses time of peak [1000 year AD].

Nuclide	1BMA	2BMA	1BTF	2BTF	Silo	BRT	1BLA	2-5BLA	Total
Ac-227	1.7e+02 (61)	< 1	2.2e+01 (102)	5.0e+00 (28)	6.1e+01 (102)	< 1	1.5e+04 (5)	3.9e+03 (44)	1.5e+04 (5)
Ag-108m	3.7e+05 (3)	1.2e+05 (4)	1.4e+05 (3)	5.4e+05 (3)	2.5e+04 (4)	1.5e+05 (3)	1.2e+05 (3)	5.3e+04 (3)	1.2e+06 (3)
Am-241	1.4e+01 (5)	< 1	< 1	7.4e+00 (4)	< 1	< 1	1.9e+04 (4)	6.4e+02 (4)	2.0e+04 (4)
Am-242m	< 1	< 1	< 1	< 1	< 1	< 1	< 1	< 1	< 1
Am-243	1.8e+01 (7)	< 1	< 1	5.0e+00 (14)	< 1	< 1	1.3e+03 (4)	3.4e+02 (5)	1.3e+03 (4)
Ba-133	< 1	< 1	< 1	< 1	< 1	< 1	< 1	< 1	< 1
C-14-ind	< 1	4.0e+05 (5)	< 1	< 1	< 1	2.6e+04 (24)	< 1	3.7e+05 (4)	6.8e+05 (4)
C-14-inorg	2.5e+05 (22)	8.2e+00 (53)	1.4e+05 (12)	6.2e+05 (4)	2.0e+02 (34)	< 1	1.1e+07 (3)	2.9e+05 (4)	1.1e+07 (3)
C-14-org	2.8e+07 (4)	3.1e+05 (5)	5.7e+06 (3)	7.7e+06 (3)	5.2e+07 (5)	< 1	2.2e+05 (3)	6.9e+04 (4)	7.5e+07 (5)
Ca-41	< 1	7.8e+05 (10)	< 1	< 1	< 1	< 1	< 1	1.4e+06 (4)	1.4e+06 (4)
Cd-113m	< 1	< 1	< 1	< 1	< 1	< 1	< 1	< 1	< 1
Cl-36	4.0e+04 (4)	1.1e+04 (8)	6.8e+03 (3)	2.0e+04 (3)	3.4e+04 (6)	2.7e+02 (30)	6.9e+04 (3)	1.7e+04 (4)	1.0e+05 (3)
Cm-242	< 1	< 1	< 1	< 1	< 1	< 1	< 1	< 1	< 1
Cm-243	< 1	< 1	< 1	< 1	< 1	< 1	< 1	< 1	< 1
Cm-244	< 1	< 1	< 1	< 1	< 1	< 1	< 1	< 1	< 1
Cm-245	< 1	< 1	< 1	< 1	< 1	< 1	1.4e+01 (4)	4.1e+00 (5)	1.5e+01 (4)
Cm-246	< 1	< 1	< 1	< 1	< 1	< 1	3.3e+00 (4)	1.0e+00 (5)	3.5e+00 (4)
Co-60	< 1	< 1	< 1	< 1	< 1	< 1	< 1	< 1	< 1
Cs-135	6.6e+04 (5)	8.5e+02 (9)	1.5e+04 (4)	7.2e+03 (4)	2.2e+04 (16)	< 1	2.8e+03 (3)	2.0e+04 (5)	1.0e+05 (5)
Cs-137	< 1	< 1	< 1	< 1	< 1	< 1	< 1	< 1	< 1
Eu-152	< 1	< 1	< 1	< 1	< 1	< 1	< 1	< 1	< 1
H-3	< 1	< 1	< 1	< 1	< 1	< 1	< 1	< 1	< 1
Ho-166m	1.3e+01 (5)	< 1	< 1	8.5e+00 (4)	< 1	< 1	5.8e+02 (4)	3.3e+02 (5)	7.0e+02 (4)
I-129	2.0e+04 (22)	3.0e+02 (9)	6.7e+03 (3)	1.0e+04 (3)	2.3e+04 (6)	< 1	1.4e+03 (3)	7.2e+02 (4)	3.7e+04 (5)
Mo-93	8.0e+04 (4)	7.0e+04 (6)	7.4e+04 (3)	1.9e+05 (3)	2.5e+05 (5)	6.2e+04 (4)	2.7e+05 (3)	2.6e+04 (4)	5.4e+05 (3)
Nb-93m	1.1e+04 (28)	2.6e+02 (102)	4.0e+02 (4)	2.7e+03 (5)	1.1e+04 (60)	2.2e+02 (4)	2.0e+03 (3)	6.2e+02 (10)	2.2e+04 (31)
Nb-94	1.9e+03 (28)	8.8e+01 (80)	5.4e+01 (65)	1.3e+03 (14)	6.2e+01 (78)	2.3e+02 (73)	9.2e+03 (4)	1.3e+04 (5)	1.7e+04 (5)
Ni-59	1.3e+07 (57)	1.8e+06 (69)	8.0e+05 (4)	4.1e+06 (4)	3.4e+06 (34)	6.9e+05 (59)	3.7e+06 (3)	1.4e+06 (5)	1.7e+07 (59)
Ni-63	1.7e+02 (4)	< 1	8.6e+02 (4)	7.6e+03 (4)	< 1	3.9e+02 (4)	1.1e+05 (3)	2.4e+03 (3)	1.1e+05 (3)
Np-237	1.7e+02 (26)	< 1	< 1	3.4e+01 (9)	2.3e+01 (102)	< 1	2.4e+01 (4)	4.9e+00 (5)	2.0e+02 (26)
Pa-231	1.3e+01 (60)	< 1	3.4e+00 (102)	< 1	3.1e+00 (102)	< 1	1.9e+03 (5)	5.6e+02 (41)	1.9e+03 (5)
Pb-210	3.3e+01 (102)	4.9e+00 (102)	< 1	1.1e+00 (84)	9.9e+00 (102)	< 1	1.1e+02 (102)	4.2e+01 (102)	2.0e+02 (102)
Pd-107	4.5e+03 (4)	1.3e+05 (7)	1.5e+02 (4)	4.5e+03 (3)	3.3e+03 (7)	< 1	3.2e+02 (3)	6.4e+02 (4)	1.4e+05 (7)
Po-210	3.7e+01 (102)	4.7e+00 (102)	< 1	1.3e+00 (90)	9.9e+00 (102)	< 1	1.0e+02 (102)	4.0e+01 (102)	2.0e+02 (102)
Pu-238	< 1	< 1	< 1	< 1	< 1	< 1	5.0e+00 (3)	< 1	5.2e+00 (3)
Pu-239	1.1e+04 (5)	3.5e+01 (69)	5.1e+01 (28)	5.0e+03 (5)	1.0e+03 (38)	1.7e+01 (30)	2.3e+04 (4)	5.1e+03 (5)	3.1e+04 (4)
Pu-240	1.2e+04 (5)	< 1	1.2e+01 (16)	5.5e+03 (5)	1.7e+02 (20)	4.5e+00 (5)	2.1e+04 (4)	4.3e+03 (5)	3.0e+04 (4)
Pu-241	1.4e+00 (7)	< 1	< 1	< 1	< 1	< 1	2.2e+01 (4)	3.6e+00 (9)	2.3e+01 (4)
Pu-242	1.1e+02 (25)	2.2e+00 (102)	< 1	3.9e+01 (5)	1.8e+01 (70)	< 1	1.4e+02 (4)	3.4e+01 (5)	2.0e+02 (5)
Ra-226	3.9e+02 (102)	6.6e+01 (102)	9.7e+00 (22)	1.8e+01 (102)	1.3e+02 (102)	1.9e+00 (22)	1.7e+03 (102)	6.5e+02 (102)	3.0e+03 (102)
Ra-228	< 1	< 1	< 1	< 1	< 1	< 1	< 1	< 1	< 1
Se-79	5.2e+04 (4)	8.1e+02 (5)	8.3e+03 (3)	2.2e+04 (3)	1.0e+05 (5)	< 1	1.3e+03 (3)	2.2e+03 (4)	1.5e+05 (5)
Sm-151	< 1	< 1	< 1	< 1	< 1	< 1	1.9e+00 (3)	< 1	1.9e+00 (3)
Sn-126	1.1e+02 (59)	< 1	< 1	1.2e+01 (15)	6.6e+00 (102)	< 1	2.9e+00 (5)	1.3e+01 (16)	1.2e+02 (59)
Sr-90	< 1	< 1	< 1	< 1	< 1	< 1	< 1	< 1	< 1
Tc-99	5.5e+04 (29)	5.4e+01 (102)	1.3e+03 (61)	9.9e+03 (5)	1.1e+04 (102)	5.7e+01 (102)	3.0e+05 (4)	3.9e+03 (9)	3.0e+05 (4)
Th-228	< 1	< 1	< 1	< 1	< 1	< 1	< 1	< 1	< 1
Th-229	5.1e+01 (102)	< 1	< 1	3.0e+00 (69)	9.4e+00 (102)	< 1	< 1	< 1	6.5e+01 (102)
Th-230	1.9e+01 (63)	< 1	< 1	1.4e+00 (62)	4.1e+00 (102)	< 1	1.0e+02 (102)	3.2e+01 (102)	1.6e+02 (102)
Th-232	< 1	< 1	< 1	< 1	< 1	< 1	< 1	< 1	< 1
U-232	< 1	< 1	< 1	< 1	< 1	< 1	< 1	< 1	< 1
U-233	4.2e+01 (56)	< 1	< 1	2.7e+00 (62)	8.3e+00 (102)	< 1	< 1	< 1	4.8e+01 (57)
U-234	4.6e+01 (26)	< 1	< 1	8.2e+00 (9)	6.5e+00 (102)	< 1	5.9e+02 (5)	5.6e+01 (71)	6.1e+02 (5)
U-235	2.2e+01 (25)	< 1	1.8e+00 (102)	1.5e+00 (9)	1.7e+00 (102)	< 1	4.4e+04 (4)	2.6e+03 (10)	4.5e+04 (4)
U-236	1.6e+01 (26)	< 1	< 1	5.2e+00 (9)	2.7e+00 (102)	< 1	6.4e+00 (4)	2.0e+00 (10)	2.1e+01 (26)
U-238	3.6e+01 (26)	< 1	< 1	1.1e+01 (9)	3.9e+00 (102)	< 1	1.1e+05 (4)	1.4e+03 (10)	1.1e+05 (4)
Zr-93	4.5e+03 (26)	1.5e+02 (102)	5.0e+01 (22)	1.3e+03 (5)	4.2e+03 (86)	3.6e+01 (37)	2.8e+02 (4)	3.7e+02 (9)	7.3e+03 (27)

Table E-44. Doses for CCR_EX, max value Sv/year and time of peak [1000 year AD].

Nuclide	1BMA	2BMA	1BTF	2BTF	Silo	BRT	1BLA	2-5BLA	Total
Total	2.3e-06 (84)	7.4e-07 (10)	3.6e-07 (6)	4.2e-07 (6)	3.2e-06 (7)	3.2e-07 (6)	1.2e-06 (29)	3.5e-07 (6)	7.0e-06 (6)
Ac-227	9.6e-10 (102)	< 1e-12	1.5e-10 (102)	3.4e-11 (49)	1.7e-10 (102)	< 1e-12	2.0e-07 (36)	9.3e-08 (61)	2.8e-07 (41)
Ag-108m	3.1e-09 (5)	2.0e-09 (6)	4.6e-10 (5)	8.3e-10 (5)	5.9e-10 (6)	6.8e-10 (5)	8.9e-11 (5)	4.1e-10 (5)	8.0e-09 (5)
Am-241	< 1e-12	< 1e-12	< 1e-12	< 1e-12	< 1e-12	< 1e-12	1.2e-10 (4)	5.2e-10 (4)	5.6e-10 (4)
Am-242m	< 1e-12	< 1e-12	< 1e-12	< 1e-12	< 1e-12	< 1e-12	< 1e-12	< 1e-12	< 1e-12
Am-243	1.4e-11 (32)	< 1e-12	1.4e-12 (29)	1.1e-11 (26)	< 1e-12	< 1e-12	2.4e-10 (15)	3.4e-10 (5)	4.8e-10 (16)
Ba-133	< 1e-12	< 1e-12	< 1e-12	< 1e-12	< 1e-12	< 1e-12	< 1e-12	< 1e-12	< 1e-12
C-14-ind	< 1e-12	1.1e-08 (6)	< 1e-12	< 1e-12	< 1e-12	7.3e-10 (24)	< 1e-12	4.1e-09 (6)	1.5e-08 (6)
C-14-inorg	6.9e-09 (23)	< 1e-12	4.2e-09 (13)	1.8e-08 (6)	5.9e-12 (34)	< 1e-12	2.0e-09 (3)	3.2e-09 (6)	2.2e-08 (23)
C-14-org	4.5e-07 (6)	8.3e-09 (6)	2.2e-08 (6)	1.2e-08 (6)	1.4e-06 (6)	< 1e-12	3.9e-11 (3)	7.8e-10 (6)	1.8e-06 (6)
Ca-41	< 1e-12	4.9e-07 (29)	< 1e-12	< 1e-12	< 1e-12	< 1e-12	< 1e-12	2.3e-07 (12)	5.9e-07 (21)
Cd-113m	< 1e-12	< 1e-12	< 1e-12	< 1e-12	< 1e-12	< 1e-12	< 1e-12	< 1e-12	< 1e-12
Cl-36	9.8e-08 (6)	3.3e-08 (8)	4.9e-09 (6)	5.5e-09 (6)	9.6e-08 (6)	7.8e-10 (30)	4.2e-10 (4)	2.5e-08 (6)	2.6e-07 (6)
Cm-242	< 1e-12	< 1e-12	< 1e-12	< 1e-12	< 1e-12	< 1e-12	< 1e-12	< 1e-12	< 1e-12
Cm-243	< 1e-12	< 1e-12	< 1e-12	< 1e-12	< 1e-12	< 1e-12	< 1e-12	< 1e-12	< 1e-12
Cm-244	< 1e-12	< 1e-12	< 1e-12	< 1e-12	< 1e-12	< 1e-12	< 1e-12	< 1e-12	< 1e-12
Cm-245	< 1e-12	< 1e-12	< 1e-12	< 1e-12	< 1e-12	< 1e-12	2.5e-12 (15)	4.2e-12 (5)	5.2e-12 (16)
Cm-246	< 1e-12	< 1e-12	< 1e-12	< 1e-12	< 1e-12	< 1e-12	< 1e-12	< 1e-12	< 1e-12
Co-60	< 1e-12	< 1e-12	< 1e-12	< 1e-12	< 1e-12	< 1e-12	< 1e-12	< 1e-12	< 1e-12
Cs-135	3.0e-07 (102)	1.1e-08 (102)	2.8e-08 (102)	6.8e-09 (102)	3.3e-07 (102)	< 1e-12	1.1e-09 (102)	4.8e-08 (102)	7.3e-07 (102)
Cs-137	< 1e-12	< 1e-12	< 1e-12	< 1e-12	< 1e-12	< 1e-12	< 1e-12	< 1e-12	< 1e-12
Eu-152	< 1e-12	< 1e-12	< 1e-12	< 1e-12	< 1e-12	< 1e-12	< 1e-12	< 1e-12	< 1e-12
H-3	< 1e-12	< 1e-12	< 1e-12	< 1e-12	< 1e-12	< 1e-12	< 1e-12	< 1e-12	< 1e-12
Ho-166m	< 1e-12	< 1e-12	< 1e-12	< 1e-12	< 1e-12	< 1e-12	2.3e-12 (4)	3.9e-12 (5)	4.0e-12 (5)
I-129	1.3e-07 (6)	3.3e-09 (26)	4.4e-08 (6)	3.6e-08 (4)	2.5e-07 (14)	< 1e-12	2.1e-09 (4)	6.5e-09 (6)	4.1e-07 (6)
Mo-93	5.7e-07 (6)	6.3e-07 (9)	2.8e-07 (6)	3.5e-07 (6)	1.9e-06 (8)	3.2e-07 (6)	1.7e-07 (6)	1.4e-07 (6)	3.9e-06 (7)
Nb-93m	1.9e-10 (6)	1.9e-10 (8)	8.7e-11 (6)	1.1e-10 (6)	6.1e-10 (7)	9.9e-11 (6)	5.2e-11 (6)	4.1e-11 (6)	1.2e-09 (7)
Nb-94	3.5e-10 (79)	1.7e-11 (102)	9.4e-12 (95)	1.4e-10 (53)	1.4e-11 (102)	4.5e-11 (102)	8.0e-11 (32)	6.2e-10 (42)	1.1e-09 (52)
Ni-59	1.8e-06 (84)	2.7e-07 (102)	3.7e-08 (34)	7.2e-08 (28)	2.8e-07 (61)	1.1e-07 (67)	1.7e-08 (15)	2.9e-08 (21)	2.4e-06 (84)
Ni-63	< 1e-12	< 1e-12	< 1e-12	< 1e-12	< 1e-12	< 1e-12	< 1e-12	< 1e-12	< 1e-12
Np-237	2.5e-09 (102)	1.2e-12 (102)	7.0e-12 (102)	4.2e-10 (102)	2.1e-10 (102)	< 1e-12	4.1e-11 (102)	3.1e-11 (102)	3.2e-09 (102)
Pa-231	2.3e-09 (102)	< 1e-12	3.8e-10 (102)	5.8e-11 (42)	2.4e-10 (102)	< 1e-12	3.6e-07 (37)	1.2e-07 (102)	4.7e-07 (41)
Pb-210	6.7e-09 (102)	5.5e-10 (102)	6.4e-11 (23)	3.8e-10 (102)	1.1e-09 (102)	1.2e-11 (23)	5.1e-08 (102)	9.8e-09 (102)	6.2e-08 (102)
Pd-107	9.1e-11 (36)	4.4e-09 (66)	1.5e-12 (29)	1.2e-11 (17)	1.9e-10 (40)	< 1e-12	< 1e-12	6.0e-12 (15)	4.7e-09 (66)
Po-210	2.5e-10 (102)	4.2e-11 (102)	3.1e-12 (7)	1.4e-11 (102)	5.7e-11 (102)	< 1e-12	1.2e-09 (102)	5.2e-10 (102)	2.0e-09 (102)
Pu-238	< 1e-12	< 1e-12	< 1e-12	< 1e-12	< 1e-12	< 1e-12	< 1e-12	< 1e-12	< 1e-12
Pu-239	1.7e-07 (64)	9.9e-10 (102)	1.1e-09 (69)	3.8e-08 (42)	2.9e-08 (87)	4.3e-10 (80)	3.1e-08 (31)	4.2e-08 (42)	2.8e-07 (57)
Pu-240	1.6e-08 (19)	1.2e-12 (70)	6.1e-11 (31)	7.8e-09 (19)	5.2e-10 (44)	2.4e-11 (28)	7.9e-09 (14)	7.0e-09 (18)	3.8e-08 (18)
Pu-241	< 1e-12	< 1e-12	< 1e-12	< 1e-12	< 1e-12	< 1e-12	< 1e-12	< 1e-12	< 1e-12
Pu-242	1.1e-08 (102)	9.2e-11 (102)	5.5e-11 (102)	1.4e-09 (102)	2.1e-09 (102)	1.2e-11 (102)	5.6e-10 (79)	1.2e-09 (101)	1.6e-08 (102)
Ra-226	4.3e-08 (102)	3.2e-09 (102)	3.5e-10 (23)	2.7e-09 (102)	7.9e-09 (102)	7.0e-11 (102)	2.2e-07 (102)	6.2e-08 (102)	3.4e-07 (102)
Ra-228	< 1e-12	< 1e-12	< 1e-12	< 1e-12	< 1e-12	< 1e-12	< 1e-12	< 1e-12	< 1e-12
Se-79	1.4e-08 (7)	3.2e-10 (10)	9.9e-10 (6)	1.5e-09 (6)	4.1e-08 (11)	< 1e-12	4.1e-11 (6)	5.0e-10 (6)	5.4e-08 (10)
Sm-151	< 1e-12	< 1e-12	< 1e-12	< 1e-12	< 1e-12	< 1e-12	< 1e-12	< 1e-12	< 1e-12
Sn-126	1.4e-10 (102)	< 1e-12	< 1e-12	1.5e-11 (96)	5.4e-12 (102)	< 1e-12	< 1e-12	1.5e-11 (102)	1.8e-10 (102)
Sr-90	< 1e-12	< 1e-12	< 1e-12	< 1e-12	< 1e-12	< 1e-12	< 1e-12	< 1e-12	< 1e-12
Tc-99	6.7e-08 (96)	3.6e-11 (102)	2.5e-09 (102)	8.4e-09 (76)	2.1e-08 (102)	6.1e-11 (102)	3.9e-08 (50)	3.3e-09 (85)	1.3e-07 (101)
Th-228	< 1e-12	< 1e-12	< 1e-12	< 1e-12	< 1e-12	< 1e-12	< 1e-12	< 1e-12	< 1e-12
Th-229	8.8e-09 (102)	< 1e-12	1.1e-11 (102)	9.6e-10 (102)	1.2e-09 (102)	< 1e-12	6.0e-11 (102)	4.9e-11 (102)	1.1e-08 (102)
Th-230	4.9e-10 (102)	< 1e-12	2.4e-12 (76)	4.5e-11 (102)	6.3e-11 (102)	< 1e-12	7.3e-09 (102)	1.0e-09 (102)	8.7e-09 (102)
Th-232	< 1e-12	< 1e-12	< 1e-12	< 1e-12	< 1e-12	< 1e-12	< 1e-12	< 1e-12	< 1e-12
U-232	< 1e-12	< 1e-12	< 1e-12	< 1e-12	< 1e-12	< 1e-12	< 1e-12	< 1e-12	< 1e-12
U-233	3.1e-09 (102)	1.3e-12 (102)	5.4e-12 (102)	3.5e-10 (102)	3.5e-10 (102)	< 1e-12	2.2e-11 (102)	2.0e-11 (102)	3.8e-09 (102)
U-234	1.4e-09 (69)	7.4e-12 (102)	6.0e-12 (66)	2.2e-10 (38)	2.8e-10 (102)	< 1e-12	3.3e-08 (60)	4.9e-09 (102)	3.9e-08 (67)
U-235	6.3e-10 (69)	< 1e-12	5.7e-11 (102)	3.1e-11 (32)	6.5e-11 (102)	< 1e-12	2.9e-07 (7)	5.3e-08 (36)	3.0e-07 (7)
U-236	4.9e-10 (71)	3.4e-12 (102)	1.4e-12 (53)	1.4e-10 (37)	1.1e-10 (102)	< 1e-12	4.8e-11 (7)	3.2e-11 (23)	6.8e-10 (71)
U-238	1.1e-09 (70)	< 1e-12	6.7e-12 (60)	2.9e-10 (37)	1.6e-10 (102)	< 1e-12	7.2e-07 (7)	3.0e-08 (36)	7.3e-07 (7)
Zr-93	9.4e-09 (102)	1.7e-10 (102)	8.1e-11 (102)	1.2e-09 (78)	1.4e-08 (102)	1.1e-10 (102)	4.3e-11 (52)	4.6e-10 (96)	2.5e-08 (102)

Sensitivity analysis

This appendix presents results for sensitivity analysis for five selected radionuclides and endpoints in the *global warming calculation case*. The aim of the analysis was to identify individual parameters with a strong influence on dose from individual radionuclides to future human inhabitants. A similar analysis of biosphere parameters, using a constant release rate, is presented in the **Biosphere synthesis report** (Section 10.9)

In the dose calculations several hundred parameters have been varied according to pre-specified probability density functions (**Data report** and Grolander 2013). Due to the numerous parameters, and endpoints that vary dynamically in time (doses from different radionuclides to different exposed groups in various biosphere objects), this sensitivity analysis is focused on the time for the peak average dose. Thus for each of four dose contributing radionuclides, parameters with a strong influence on the calculated dose *to a specific exposed group in a certain area at a specific point in time* have been identified. The metric used in the sensitivity analysis was the standardised regression coefficients of first-order effects (SRC, Schroeder et al. 1986). This coefficient indicates both the direction of the effects of a parameter on the endpoint, and its importance (in terms of explained variation). The identified parameters thus tend to have both had a clear influence on end results (typically a proportional effect) and a PDF spanning a large variation. For each radionuclide, the three most influential parameters (in terms of explained dose variation) are presented in tornado plots.

As most of the underlying relationships were expected to be multiplicative, the sensitivity analysis was carried out on logarithmic scales. The effect of variation in retention parameters, e.g. K_d for cement, influences both the timing of peak releases and the level of the peak. This means that the results have to be interpreted with care, as the analyses were performed at a fixed point in time.

Mo-93

Mo-93 is a radionuclide with a half-life of 4,000 years. It has relatively high mobility in both near-field and far-field, hence the releases are most significant in the first part of the assessment period. The sources of release of Mo-93 are mainly silo, 1BLA, BRT, 2BMA, 2BTF and 1BMA.

The peak of the average dose from exposure of Mo-93 occurs at 6950 AD for a *drained mire farmer* community in biosphere object 157_2. Variation in identified parameters together explained 93% of the examined dose variation. Of the three most important parameters, one was from the near field model, whereas the other two were from the biosphere model (Table F-1).

The dose decreased with an increasing sorption of Mo-93 in cement (Figure F-1). This effect was expected as Mo-93 has a relatively short half-life, and thus an increased retention by sorption in the barriers will result in less activity reaching the surface due to radioactive decay in the barriers.

Table F-1. Description of sensitive parameters shown in Figure F-1.

Name	Description	Probability density function
cR_agri_cereal[Mo]	Represents the uptake of molybdenum from the soil into cereal grains growing in agricultural fields.	PDF: Log-normal GM = 1.23 GSD = 3.178 Unit [kgdw/kgC]
NF.KdDS1[Mo][Cement]	Represents the distribution constant for cement paste, for degradation state 1.	PDF: Log-triangular Min = 0.0003 Max = 0.033 Mode = 0.003 Unit [m ³ /kg]
kD_regoPG[Mo]	Distribution constant for post glacial clay	PDF: Log-normal GM = 3.29 GSD = 5.47 Unit [m ³ /kgDW]

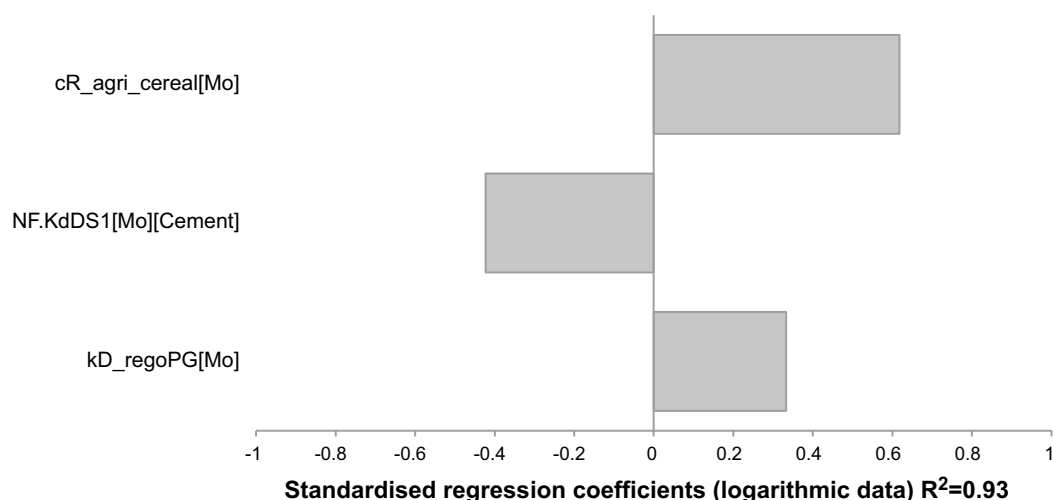


Figure F-1. Parameter sensitivity at peak average exposure of Mo-93 (Drained-mire farmer in biosphere object 157_2 at 6900 AD). Values are shown for the **global warming calculation case (CCM_GW)** in the main scenario.

The dominating exposure pathway for the selected endpoint was consumption of cereals. Consequently it was not surprising that variation in the parameter describing plant uptake for cereal (CR_agri_cereal) was important for dose variation. As CR determines the radionuclide concentration in crops (given the soil concentration), dose increased with this parameter. Similarly, sorption in post-glacial clay gyttja (Kd_regoPG), which is mixed into the cultivated soil when the mire is drained, increased soil concentrations and the annual dose (Figure F-1, Table F-1)

Organic C-14

C-14 is a radionuclide with a half-life of 5,730 years. It occurs in organic compounds (referred to as C-14-org) and is in that form very mobile in the both near-field and far-field, hence the releases are most significant in the first part of the assessment period. The organic compounds are assumed to be in the form of low molecular compounds, and thus they are expected to be transformed to CO₂ in the biosphere. The sources to the release of C-14-org are mainly the silo and 1BMA.

The peak of the average dose from exposure of C-14-org occurs at 4750 AD for a *hunter and gatherer* community in biosphere object 157_2. Variation in identified parameters together explained 97% of the examined dose variation. The three most important parameters were from the biosphere model (Table F-2), indicate that biosphere parameters are essentially controlling the uncertainty of dose due to exposure of C-14-org at the examined time point. This is due to the fact that organic C-14 is not retained by sorption in neither the near- nor the far-field.

Table F-2. Description of sensitive parameters shown in Figure F-2.

Name	Description	Probability density function
f_H2CO3_ter	Fraction of dissolved inorganic carbon in peat in the form of CO ₂ /H ₂ CO ₃	PDF: Uniform Min = 0.03 Max = 0.96 Unit [-]
f_H2CO3_lake	Fraction of dissolved inorganic carbon in lake water in the form of CO ₂ /H ₂ CO ₃	PDF: Normal Mean = 0.035 SD = 0.065 Unit [-]
conc_DIC_lake	Concentration of dissolved inorganic carbon in lake water	PDF: Normal Mean = 0.021 SD = 0.01 Unit [kgC/m ³]

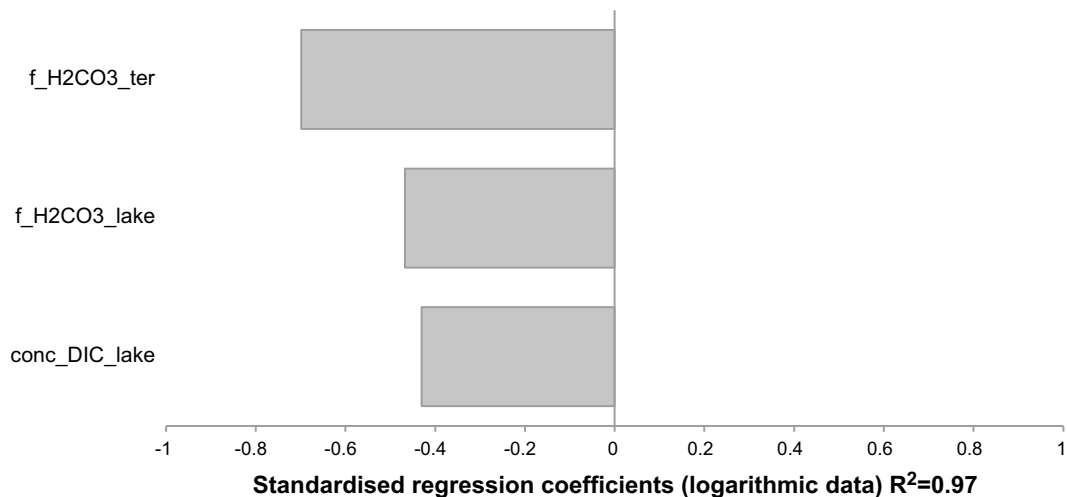


Figure F-2. Parameter sensitivity at peak average exposure of C-14-org (Hunter and gatherer in biosphere object 157_2 at 4750 AD). Values are shown for the **global warming calculation case (CCM_GW)** in the main scenario.

The dominating exposure pathway at the time for maximum dose is consumption of fish. The parameter contributing most to uncertainty in dose at that time is the fraction of dissolved inorganic carbon in peat in the form of CO₂/H₂CO₃ (f_H2CO3_ter). This parameter is a measure of the part of the C-14 reaching the mire via groundwater which will degas to the atmosphere. C-14 that has not degassed will enter the freshwater system via surface and/or near-surface groundwater recharge and is therefore the input of radiocarbon to this ecosystem. A large relative range is used for this parameter (0.03–0.96) and since a higher value leads to a lower C-14 input and thus a lower dose this parameter has a negative SRC. Other parameters influencing the uncertainty are the fraction of dissolved (uncontaminated) inorganic carbon in lake water in the form of CO₂/H₂CO₃ (f_H2CO3_lake) and the water concentration of (uncontaminated) dissolved inorganic carbon (conc_DIC_lake). These two parameters are negatively correlated with dose since higher parameter values lead to larger dilution of radiocarbon in the lake ecosystem.

CI-36

Cl-36 is a radionuclide with long half-life (301,000 years). It has relatively high mobility in both near-field and far-field, hence the releases are most significant in the first part of the assessment period. The sources of release of Cl-36 are mainly silo, 1BLA and 1BMA.

The peak of the average dose from exposure of Cl-36 occurs at 5000 AD for a *drained mire farmer* community in biosphere object 157_2. Variation in identified parameters together explained 94% of the examined dose variation. Of the three most important parameters, one was from the repository model, whereas the other two were from the biosphere model (Table F-3).

The dose decreased with an increasing sorption of Cl-36 in cement (KdDS) (Figure F-3). This effect was partly due to a smoothing of the release peak, and partly due to the fact that high K_d values delayed the release to the biosphere beyond the time point of the peak of the average dose.

The dominating exposure pathway at maximum dose was consumption of milk. Thus, it was not surprising that the parameter contributing most to the uncertainty in dose was CR for fodder

(CR_agri_fodder). A high CR is associated with a high plant uptake of Cl-36 from soil, and consequently a high Cl-36 concentration the fodder for dairy cows. Similarly, an increased transfer coefficients for milk, (TC_milk) also resulted in a higher dose to the most exposed group. This parameters accounted for the transfer of Cl-36 in fodder to dairy products, and consequently a high transfer was associated with a high concentration in human food.

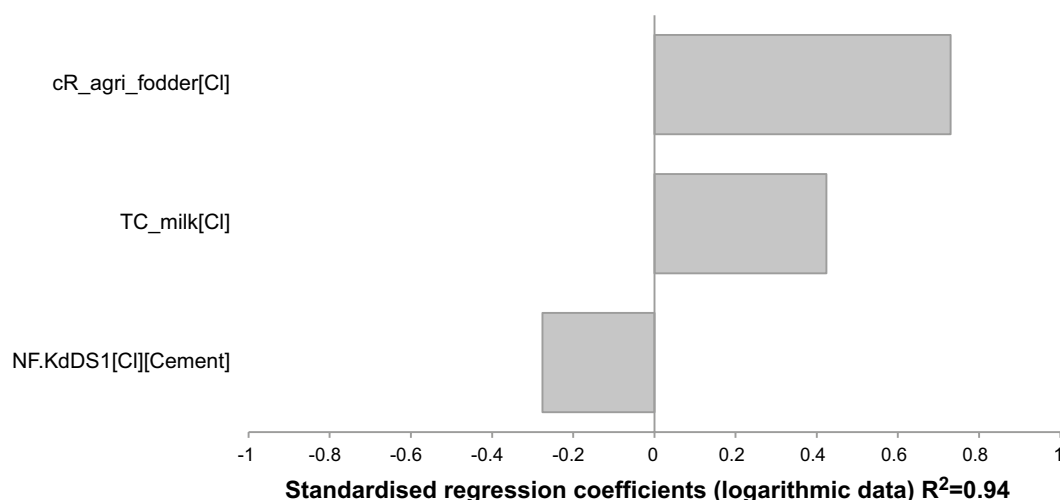


Figure F-3. Parameter sensitivity at peak average exposure of Cl-36 (Drained-mire farmer in biosphere object 157_2 at 5000 AD). Values are shown for the **global warming calculation case (CCM_GW)** in the main scenario.

Table F-3 Description of sensitive parameters shown in Figure F-3.

Name	Description	Probability density function
cR_agri_fodder[Cl]	Concentration ratio between soil and fodder	PDF: Log-normal GM = 389 GSD = 4.0 Unit [kgdw/kgC]
TC_milk[Cl]	Transfer coefficient from intake of radionuclides in fodder and water to dairy products	PDF: Log-normal GM = 0.0054 GSD = 4.0 Unit [d/l]
NF.KdDS1[Cl][Cement]	Represents the distribution constant for cement paste, for degradation state 1.	PDF: Log-triangular Min = 0.0002 Max = 0.01 Mode = 0.001 Unit [m ³ /kg]

Ni-59

Ni-59 is a radionuclide with a half-life of 76,000 years. It is relatively immobile; hence the releases are relatively constant over the whole assessment period, as the inventory is not significantly depleted.

The sources of release to the biosphere of Ni-59 are mainly from waste vaults 1BMA, silo, 1BLA and 2BTF. Ni-59 is long-lived and sorbs strongly in regolith layers in the biosphere, and therefore most of the released Ni-59 will continuously accumulate in till (Regolow) and glacial clay (RegoGL).

The peak of the average dose from exposure of Ni-59 occurs at the end of the temperate period at 66,500 AD for a *drained mire farmer* community in biosphere object 157_2. Variation in identified parameters together explained 93% of the examined dose variation. Of the three most important parameters, one was from the repository model, whereas the other two were from the biosphere model (Table F-4).

The dose decreased with an increasing sorption of Ni-59 in cement (Figure F-4). This effect was expected, as an increased sorption in the near field will delay the release of Ni-93 to the geosphere and the surface ecosystems. Thus a delayed release results in less accumulation of Ni-59 in regolith layers.

The dominating exposure pathway at 66,500 AD was consumption of meat. Consequently, it was not surprising that the dose to the most exposed group increased with an increase transfer efficiency of radionuclides from fodder to meat (TC_meat) (Figure F-4). Increased sorption in glacial clay (RegoGL), resulted in increased concentrations of Ni-59 in this layer. As glacial clay was mixed into the cultivated soil (when the mire was drained), increased soil concentrations in soil and fodder consumed by cattle resulted to elevated dose of the most exposed group.

Table F-4 Description of sensitive parameters shown in Figure F-4.

Name	Description	Probability density function
kD_regoGL[Ni]	Distribution constant for glacial clay	PDF: Log-normal GM = 17 GSD = 3.0 Unit [m ³ /kgDW]
TC_meat[Ni]	Transfer coefficient from intake of radionuclides in fodder and water to beef	PDF: Log-normal GM = 0.16 GSD = 4.0 Unit [d/kgFW]
NF.KdDS2[Ni] [Cement]	Represents the distribution constant for cement paste, for degradation state 2.	PDF: Log-triangular Min = 0.08 Max = 2 Mode = 0.2 Unit =[m ³ /kg]

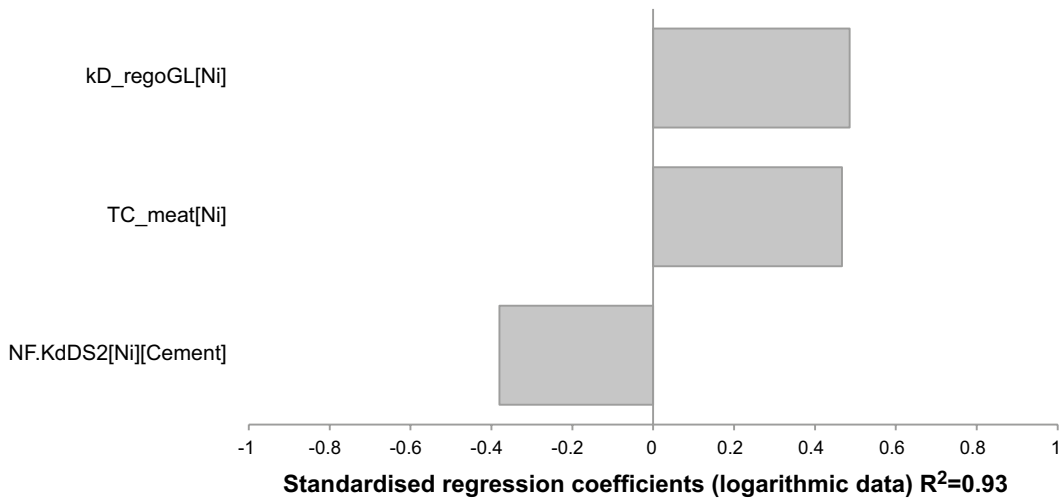


Figure F-4. Parameter sensitivity at peak average exposure of Ni-59 (Drained-mire farmer in biosphere object 157_2 at 66,500 AD). Values are shown for the **global warming calculation case (CCM_GW)** in the main scenario.

Glossary

This appendix contains explanations of terms and abbreviations used in the report.

Term/abbreviation	Description
Advection	Transport of a dissolved substance by the bulk flow of water.
AMBER	Compartmental modelling code used in the previous (SAR-08) assessment for SFR
Annual dose	Used in this report to denote yearly effective dose to an exposed group.
BCC	Biosphere calculation case.
Biosphere object	A part of the landscape that potentially will receive radionuclides released from the repository (see also "Object 157_1" and "Object 157_2" in this glossary).
BLA	Vault for low-level waste.
BMA	Vault for intermediate-level waste.
BRT	Vault for reactor pressure vessels.
BTF	Vault for concrete tanks.
Calculation case (or CC)	A calculation case provides a parameterised model chain for the quantitative assessment of a scenario. Several calculation cases can be needed to fully assess one scenario.
Control volume	Entities of the 3D-domain of the hydrological near-field model used to derive the water balance of the specified volume, for which flows across surfaces of the control volume are determined. Compartments of the near-field radionuclide transport model correspond with control volumes of the hydrological model or with fractions of them.
DM	Drained-mire farmers. DM refers to a self-sustained industrial agriculture in which wetlands are drained and used for agriculture (both crop and fodder production). It is one of four land use variants considered in SR-PSU for assessment of the most exposed group.
Ecolgo	Compartmental modelling code used for radionuclide transport calculations in this assessment
Effective dose	Effective dose or effective dose equivalent is a measure of dose designed to reflect the risk associated with the dose. It is calculated as the weighted sum of the dose equivalents in the different tissues of the body.
Exposed group	Four different hypothetical communities that utilize the Forsmark area in different ways have been used in this assessment (DM, IO, HG and GP). These groups are credible bounding cases for relevant exposure pathways, and reflect land use and habits that are reasonable and sustainable.
GP	Garden-plot households. GP refers to a type of household that is self-sustained with respect to vegetables and root crops produced through small scale horticulture. It is one of four land use variants considered in SR-PSU for assessment of the most exposed group.
FARF31	Semi-analytic modelling code for modelling of radionuclide transport in the far-field. The compartment model used for modelling transport in the far-field in this assessment is based on the same conceptual model as FARF31.
HG	Hunter-gatherers. HG refers to a community that uses the undisturbed surface ecosystems as living space and to obtain food. It is one of four land use variants considered in SR-PSU for assessment of the most exposed group.
IO	Infield-outland farmers. IO refers to a self-sustained agriculture in which infield farming of crops is dependent on nutrients from wetlands for haymaking (outland). It is one of four land use variants considered in SR-PSU for assessment of the most exposed group.
Mean annual dose	The arithmetic mean value of the calculated annual dose (in a probabilistic assessment).
Most exposed group	In this report the term most exposed group is used to denote the one of the four, DM, IO, HG and GP that receives the largest dose in a certain calculation case (sometimes defined at a certain time point).
NHB	Non-human biota
Kd	Partitioning coefficient for sorption [L3/M]. Partitioning coefficient is defined as the ratio between the element concentrations in the solid and liquid phases.
Object 157_1	The biosphere object 157_1 is a present sea basin with an average depth of 11 meters and a maximum depth of 16.5 meters. At 4500 AD the future lake will be isolated. The total isolation process takes about 400 years. The mean depth of the lake at isolation will be 2 meters with a maximum depth of 3 meters. During the next period of 1,200 years, the lake slowly undergoes sediment accumulation and ingrowth of vegetation. At 5700 AD the lake becomes infilled and only a small stream passes through the object area, draining the 157 catchment and the upstream area of 157_2. Almost the whole object area will be useful for agricultural practices.

Term/abbreviation	Description
Object 157_2	The biosphere object 157_2 is at present below sea level (average depth 5.8 and maximum depth 13.5 meters). The object area will have no future lake and the succession from a marine to a terrestrial ecosystem will take place without a lake stage. The starting point of the transition from a marine to a terrestrial ecosystem is in 3000 AD and the total area becomes land at 4500 AD. Hydrological modelling shows an area with high water levels in the upper soil and a wetland will form after the sea has withdrawn due to shoreline displacement. The object drains down to object 157_1 in the surface water flow network. According to the regolith development modelling, 25% of the wetland area could be used for agricultural purposes.
Peak dose	In this report, peak dose (or peak annual dose) denotes the maximum (over time) of the annual dose.
Peak release	In this report, peak release denotes the maximum (over time) for the releases of activity or radiotoxicity (from the near-field or from the far-field).
Periglacial climate domain	Regions that contain permafrost without the presence of an ice sheet.
PSU	Project SFR Extension.
RN	Radionuclide.
RPV	Reactor pressure vessel.
SAFE	Long-term safety assessment for SFR reported to the regulatory authorities in 2001.
SAR	Safety Analysis Report.
SAR-08	Long-term safety assessment for SFR reported to the regulatory authorities in 2008.
Scenario	Scenarios are used to describe future potential evolutions of the repository (see also Section 2.2)
SFR	Repository in Forsmark for low-and intermediate-level radioactive waste.
SKB	Swedish Nuclear Fuel and Waste Management Company.
Sorption	In this report, the term is used to designate all processes by which a dissolved species is retained at a solid surface.
SSM	Swedish Radiation Safety Authority.
SR-PSU	This long-term safety assessment (Safety Report – Project SFR Extension).
Temperate climate domain	Region without permafrost or the presence of ice sheets. It is dominated by a temperate climate in a broad sense, with cold winters and either cold or warm summers. Within the temperate domain, the site of SFR may also at times be submerged by the sea.
Waste form	The physical and chemical form of the waste after treatment and/or conditioning.
Waste package	The waste (form) and its packaging.
Waste type	In order to systematically classify the wastes, different waste types have been defined and a code system developed.
Waste vault (or vault)	Part of repository where waste is stored.
Weichselian glacial cycle	The last 120,000 year long glacial cycle in north-eastern Europe.